Water content and geochemistry of the Cenozoic basalts in SE China : implications for enrichment in the mantle source of intra-plate basalts

Shaochen Liu

Université de Lorraine and
University of Science and Technology of China

THÈSE DE DOCTORAT

Water content and geochemistry of the Cenozoic basalts in SE China: implications for enrichment in the mantle source of intra-plate basalts

Author's Name: Shaochen LIU

Speciality: Geosciences

Supervisors: Prof. Etienne DELOULE, Prof. Qunke XIA

Date: Mar. 22th, 2017

Composition du Jury:

M. Etienne DELOULE DR CNRS, CRPG, CNRS-Université de Lorraine, FRANCE Directeur de thèse

M. QunKe XIA Professeur - Zhejiang University, Hangzhou, CHINE Directeur de thèse

M. Jannick INGRIN DR - CNRS, UMET, CNRS-Université Lille 1, FRANCE, Rapporteur

M. Yigang XU Professeur - Guangzhou Institute of Geochemistry, Guangzhou, CHINE, Rapporteur

Mme Qin WANG Professeur - Nanjing University, Nanjing, CHINE, Examinateur

Mme Liping QIN Professeur - University of Science and Technology of China, Hefei, CHINE, Examinateur

Acknowledgements:

The first and greatest gratitude should go to my thesis supervisors, Prof. Qunke Xia and Prof. Etienne Deloule. During past years, Prof. Xia and Prof. Etienne Deloule gave me so many concerns and guide not only on my research but also on my life.

It is so lucky for me to work together with intelligent and enthusiastic supervisors, Prof. Xia and Prof. Deloule. Prof. Xia`s famous and humorous pet phrase “from data to model” has always reminded the most basic method and attitude to do natural science and encouraged me to follow the most serious principle every day since we met nine years ago. I also appreciate the profound knowledge and kindness of Prof. Deloule, who help me so much when I studied in CRPG, France.

Those professors and experts have instructed me large numbers of geological knowledge and skills when I studied in USTC: Yongfei Zheng, Jiangfeng Chen, Zhi Xie, Fukun Chen, Xiaoyong Yang, Yilin Xiao, Fang Huang and so on. I appreciate their solid professional knowledge and kindly help for me.

I give my sincerely gratitude to Prof. Qicheng Fan providing the samples from Hainan to complete my study and research. My communication with Dr. Huaiyu He, Dr. Xinmin Zhou, Dr. Andrey A. Gurenko, Dr. Franz Weis, and Dr Jannick Ingrin are productive and impressive me so much. Their constructive suggestions gave me so much inspiration to finish this work.

I would like to thank Jiangling Xu and Mrs. Min Feng for their help in EPMA analysis; Miss Xiao and Mr. Jianfeng He for their help in TIMS analysis; Prof. Honglin Yuan and Assistant Prof. Hong Zhang in Northwest University for their help in ICP-MS analysis. Laurie Reisberg, Christiane Parmentier, Nordine Bouden, Johan Villeneuve, Aimeryc Schumacher and Catherine Zimmermann should also be thanked for their generous help and patient teaching on measurements by ion microprobe and TIMS/MC-ICP-MS in CRPG-CNRS. In addition, Xiaoyan Gu were my first teacher for FTIR analysis. I also appreciate Pei Li, Yantao Hao, and Jia Liu, for the discussion of scientific issues with them always inspired me.

The editorial work by Pei Li, Jia Liu, Suofei Dong, Hongluo Zhang and Mr. Markhand are much helpful to complete this thesis. I also enjoy the work and life together with other members in our group, Bo Zhao, Peipei Zhang, Guicai Yang, Yaping Zhang, Ling Liu, Jia Liu, Huan Chen, Zubing Jia, Zhenzhen Tian, Zizhen Wang, Haoran

Yu, Piaoyi Wang, and Hui Chen.

Finally yet most importantly, I would like to give my unfeignedly gratitude to my parents for their kindness in raising and educating me. I also would like to thank my wife, who always supports me and tolerates my defects.

Abstract:

The origin and genesis of intra-plate basalts, especially continental basalts, have been studied extensively but still are debated hotly during past several decades. The enriched geochemical characteristics of intra-plate basalts are usually suggested to be closely associated with the recycled crustal materials. The eastern China is an ideal area to decipher the effect and contributions of different recycled components in basalt source, where the Cenozoic basalts are widespread distributed. However, existing evidence for the Cenozoic basalts in eastern China failed to figure out clearly the source of the enriched components and their genesis. Previous studies have proposed several candidates inducing enrichment in the mantle source of eastern China basalts: a) the recycled subducted oceanic crusts and sediments, originated from ancient subduction events (e.g., Paleo-Tethyan, Paleo-Asian or Izanagi plate subductions) and present subduction event (i.e., Pacific subduction); b) the delaminated thicken lower continental crust and lithospheric mantle in Mesozoic; and c) the re-enriched continental lithosphere.

The eastern China has undergone multiple subduction of oceanic plates since Mesozoic. In addition, geophysical studies have discovered plume structures in the mantle beneath the Changbaishan volcanic area in northeast China and the Hainan volcanic area in the most southern part of eastern China, respectively. Therefore, the complex geological history of eastern China offers an opportunity to conduct comparative studies on basalts from distinct geological backgrounds. In SE China, a stagnant Pacific slab exists in the mantle transition zone (MTZ) beneath the northern part (e.g, Zhejiang and Jiangxi provinces), a plume structure was found in the lower mantle beneath the southern part (e.g., South Guangdong and Hainan provinces), and neither stagnant slab nor plume has been discovered in the middle part (e.g., Fujian province). Therefore, the Cenozoic intra-plate basalts in SE China have three kinds of geological backgrounds.

H_2O and Ce have similar partition coefficients between mantle minerals and melt. Because their ratios remain unchanged through partial melting and crystal fractionation, the H_2O/Ce ratios of melts contain information regarding the mantle source. Recycled components have H_2O/Ce ratios that are distinguishable from mantle components. Therefore, in combination with other trace elements ratios (e.g., Ba/Th, Nb/La, Ce/Pb),

H_2O/Ce ratios in basalts may serve as an index for identifying various components within mantle source. In addition, due to distinct oxygen isotope compositions between normal mantle and recycled crustal materials that acquired abnormal oxygen isotopic ratios by interacting with surface water, $\delta^{18}O$ values can be used to recognize recycled materials. Several studies have reported H_2O content and $\delta^{18}O$ values in the Cenozoic basalts from NCC and successfully traced recycled oceanic materials in the mantle source combining with other elemental and isotopic compositions, however, such systematic investigations on the SE China basalts are lacking.

To decipher the relationship between the possible recycled components and the geochemical heterogeneities of the SE China basalts that formed on distinct geological backgrounds, the major and trace element contents and Sr-Nd-Pb isotopic compositions of the Cenozoic basalts from Zhejiang, Fujian and Hainan provinces have been measured. In particular, we recovered the H_2O contents of the "initial" magmas based on the H_2O contents of the clinopyroxene (cpx) phenocrysts and the partition coefficients of H_2O between cpx and basaltic melts. Moreover, the oxygen isotope compositions of the cpx phenocrysts have been determined. The results of the Cenozoic basalts from three regions in SE China have given the new insight of the enrichment composition and the genesis of Cenozoic basalts in SE China:

1) Zhejiang Cenozoic basalts erupted in two stages, 20-27Ma and after 11Ma, respectively, with distinct geochemical features. The H_2O contents of the Zhejiang basalts range from 1.3 to 2.6 (wt. %), falling within the range of the H_2O contents of back-arc basin (BABs) or island arc basalts (IABs). The older basalts have more alkaline, lower Si and Al contents, higher trace element concentrations, La/Yb, Ce/Pb and Nb/La ratios, lower H_2O/Ce and Ba/Th ratios, and stronger negative K, Pb, Zr, Hf and Ti anomalies than the younger ones. The younger basalts are less alkaline and have higher Si and Al contents; lower trace element concentrations; lower La/Yb, Ce/Pb and Nb/La ratios; higher H_2O/Ce and Ba/Th ratios. The co-relationships between Ba/La, H_2O/Ce, Nb/La, Ce/Pb and Ba/Th ratios in two groups of Zhejiang Cenozoic basalts indicate that a component of recycled dehydrated oceanic basalt is needed in the source of the older rocks, along with the depleted mantle component. Meanwhile, additional recycled dehydrated sediments together with recycled dehydrated oceanic basalts are required to serve as the enrichment components in the source of the younger rocks. The change of the recycled oceanic materials over time in the mantle source of Zhejiang Cenozoic basalts require a continuous supply of the recycled materials, demonstrating

the recycled oceanic components originated from the Pacific slab, which is the only subducted plate since 100 Ma in the Zhejiang region. Therefore, the recycled oceanic materials are likely to be provided by the stagnant Pacific slab, which has been revealed in the Zhejiang region by the geophysical evidence of the seismic image in the MTZ.

2) Fujian Cenozoic basaltic rocks erupted after 10Ma and have similar trace element patterns to Zhejiang Cenozoic basalts. All the Fujian samples have strong negative Th, U, and Pb anomalies in the extended trace element pattern. Unlike the basalts, the diabases have very weak or no negative K, Zr, Hf, and Ti anomalies in the extended trace element pattern. Fujian Cenozoic basalts have more radiogenic Sr, Nd, and Pb isotopic data than Zhejiang Cenozoic basalts. Unsimilar to Zhejiang, Fujian samples from three areas have heterogeneous H_2O contents. The estimated H_2O contents of initial basaltic melts for the Shiheng (SH) basalts range from 1.3 to 2.4 (wt. %) that is within the H_2O contents range of BABBs and IABs; the Bailin (BL) diabases have "fake" basaltic melt water contents from 1.9 to 2.1 (wt. %), due to the later H re-equilibrium of the cpx phenocrysts; and the Mingxi (MX) basalts have lower initial H_2O contents (0.3-0.5 wt. %), when the H-loss are excluded. The higher $\delta^{18}O$ values of the cpx phenocryst from Fujian Cenozoic basalts than the normal mantle are observed, suggesting the recycled materials from the surface of earth in their mantle source. The highest $\delta^{18}O$ values are found in the cpx phenocrysts with the intermediate ratios of Si/Al and Ca/Al and the relationship between Mg# and $\delta^{18}O$, suggesting a mixture of two kinds of magma. Fujian Cenozoic basalts display similar relationships between the ratios of Ba/La, Nb/La, Ce/Pb, and Ba/Th to Zhejiang Cenozoic basalts, indicating that the components of recycled dehydrated oceanic crusts and sediments are also needed in their mantle source along with the depleted mantle component. The heterogeneity of H_2O contents in Fujian Cenozoic basalts may be the result of different degree of recycled materials dehydration or the heterogeneity of the mantle. Because of the fuzzy existence of the subducted slab beneath the Fujian region in the seismic image, the pronounced recycled oceanic materials are likely distributed in the upper mantle, most likely the residue of the previous subducted slab sunk to the lower mantle.

3) Relative to Fujian and Zhejiang Cenozoic basalts, Hainan Cenozoic basalts have complex trace element patterns, including HIMUs-like and EM-like characters. These differences indicate Hainan Cenozoic basalts have more heterogeneous mantle source than Zhejiang and Fujian Cenozoic basalts. Considering the more enriched Sr, Nd, and Pb isotopic ratios, and higher $\delta^{18}O$ values of the cpx phenocrysts in Hainan Cenozoic

basalts than those of the normal mantle, the recycled materials are also required in the mantle source. The Li isotopic data of the some basalts suggests the cpx phenocryst have undergone Li diffusion after crystallization. Some of Hainan Cenozoic basalts are almost dry, due to intense H-loss. H_2O content the basalts from Leihuling (LH), Dayang (DY) and Fujitian (FJT) areas are 2.7 wt. %, 1.3 wt. %, and 2.6 wt. %, respectively. The coexistence of high and low $\delta^{18}O$ cpx phenocrysts observed in the LH basalts, combined with their trace element composition, the recycled upper oceanic crust components are dominantly required in the LH basalts, while limited recycled lower oceanic gabbro components were also involved. The mixture of DMM, recycled oceanic sediments, and crusts most likely resulted in the DY and FJT basalts. These recycled materials should not be very old and are most likely caught by upwelling plume from the deep mantle.

Overall, the SE China Cenozoic basalts with different geological backgrounds have involved the recycled oceanic materials in their mantle source. The H_2O contents of the Cenozoic basalts in SE China are generally as enriched as in BABBs and IABs, although the basalts have various range of Sr-Nd-Pb radiogenic ratios, and discrepant trace element characteristics, implying various proportions of different compositions and the mantle heterogeneity. The recycled oceanic materials have different existential state and locations, when the geological history of SE China are considered. The subducted Pacific slab most likely effect the composition of mantle in SE China.

Key words:

water content;
continental basalts;
recycled oceanic crust;
recycled oceanic sediments;
Southeast China.

Catalogue

Chapter 1 Introduction

1.1 Intra-plate basalts

Mafic rocks usually develop in the most active or weakest regions on the earth, such as at active plate margins, hot spots, and deep faults. Mid Ocean Ridge Basalts (MORBs) and Island Arc Basalts (IABs) are the most important representatives of the basalts forming at the active plate margins. The intra-plate basalts being different from MORBs and IABs erupt in the inner regions of the continental or oceanic plates. The intra-plate basalts consist of “continental intra-plate basalts”, “continental rift basalts” (CRBs), “continental flood basalts” (CFBs) and “oceanic island basalts” (OIBs). The CFBs and OIBs are often associated with mantle plumes (such as Siberian, Yellow Stone, Tarim, and Hawaii), whereas, the CRBs are located above the lithospheric deep rifts (such as East African rift). Meanwhile, the continental intra-plate basalts usually occur at broader active continental regions (such as East Asia). Due to fast ascent, the continental intra-plate basalts, particularly xenolith-bearing alkali basalts, avoid significant crustal contaminations. Therefore, the compositions of these basalts are considered to be able to represent the mantle source, making them one of the most important windows to observe the deep earth. However, despite intensive studies of several decades, the origin of the enriched components in the mantle source and the genesis of intra-plate basalts remain poorly constrained.

1.1.1 The source of intra-plate basalts

Because basalts are produced directly by partial melting of the mantle rocks, they can be used to deduce the composition information of the mantle source where from they are inherited. High-pressure experiments and observation of natural samples are the most important and effective methods to determine the relationship between the compositions of basalts and their source. After numerous researches, the divergences of the source properties for intra-plate basalts are mainly on the lithologies, geochemical characteristics, and the enrichment origin of the mantle source rocks, as well as, how these geochemical characteristics are produced. A number of high-pressure melting experiments on peridotites and other rocks have been conducted during last 30

years to study the geochemical lithologies and compositions of the mantle source for various basalts (Baker and Stolper, 1994; Falloon and Danyushevsky, 2000; Hirose and Kushiro, 1993; Laporte et al., 2004; Schwab and Johnston, 2001; Walter, 1998; Wasylenki et al., 2003). Following the result of these melting experiments, the source lithologies of the intra-plate basalts may involve pyroxenites, eclogites (along with carbonated eclogites), as well as hornblendites, beside these the peridotites are also conventionally considered (Petermann and Hirschmann, 2003; Sobolev et al., 2005, 2007; Dasgupta et al., 2010; Niu et al., 2011; Putirka et al., 2011). Meanwhile, the existence of non-peridotite components is recognized by some natural samples from Hawaii OIBs (Sobolev et al., 2007; Sobolev et al., 2005). The geochemical compositions, heterogeneity, and the origin of enrichment the in the mantle source of the intra-plate basalts has remained the subject of interest for geoscientists in the past decades. The studies of trace elements and Sr-Nd-Pb about MORBs and OIBs revealed the primary understanding of the geochemical compositions and heterogeneity for the mantle (Hofmann and White, 1982; Zindler and Hart, 1986; Sun and McDonough, 1989). The chemical composition of MORBs are relatively homogeneous. Comparing to MORBs, the intra-plate basalts, especially OIBs, display various geochemical characteristics (Workman et al., 2004; Zindler et al., 1984). Zindler and Hart, (1986) defined the four end mantle members on the basis of the Sr-Nd-Pb composition of OIBs to explain the composition variation of the mantle: (a) depleted MORBs mantle (DMM) has the most depleted $^{87}Sr/^{86}Sr$ and $^{143}Nd/^{144}Nd$; (b) enriched mantle type I (EM I) has enriched $^{87}Sr/^{86}Sr$ and $^{143}Nd/^{144}Nd$, but depleted Pb radiogenic isotope; (b) enriched mantle type II (EM II) also has enriched $^{87}Sr/^{86}Sr$ and $^{143}Nd/^{144}Nd$, as well as Pb radiogenic isotope; and (d) high-μ (HIMU) has extremely enriched Pb radiogenic isotope, but moderately depleted to a little enriched $^{87}Sr/^{86}Sr$ and $^{143}Nd/^{144}Nd$. Every mantle end-member also has unique trace element characteristics: (a) DMM is incompatible-element-depleted; (b) EM I and EM II have enriched incompatible elements; and (c) HIMU contains higher Nb and Ta than other incompatible elements. Most oceanic basalts lie within the tetrahedron delineated by the four mantle end-members (Hart et al., 1992). The clarification on the origin of enrichments in the mantle always is the important research topic for geochemists. One widely accepted opinion involves recycled oceanic materials, to explain the genesis of the enriched composition in the mantle source of OIBs and some continental intra-plate basalts. Growing numbers of experimental and natural observations in the past decades have demonstrated that the

recycled materials can provide the enriched mantle components for intra-plate basalt genesis (Hofmann and White, 1982; Hirschmann and Stopler, 1996; Stracke et al., 2005; Willbold and Stracke, 2006; Jackson et al., 2007; Dasgupta et al., 2010). Nevertheless, these recycled materials have various lithologies and complicated petrogenesis. The recycled oceanic materials are subsumed at subduction zones, where the oceanic lithosphere consisting of pelagic sediments, altered oceanic crust and oceanic lithospheric mantle sink back into the convecting mantle and enter into the mantle source at different oceanic structures (Hofmann and White, 1982; Hirschmann and Stopler, 1996; Stracke et al., 2005; Willbold and Stracke, 2006; Jackson et al., 2007; Dasgupta et al., 2010). These subducted oceanic materials can be recycled to the shallow upper mantle again from the mantle transition zone (MTZ) or even the core-mantle boundary (Hofmann and White, 1982; Hirschmann and Stopler, 1996; Herzberg, 2011). However, some researchers believe that the enriched geochemical compositions of the OIBs originate from the mineral veins (like amphiboles) metasomatized by the infiltration of mantle melts derived by small degree of partial melting in the lithospheric mantle (Halliday et al., 1990; Niu and O'Hara, 2003; Pilet et al., 2008). The origin of the enriched composition in the mantle source of the continental intra-plate basalts is more complex than that of the OIBs, due to existence of old and thickened continental lithospheric mantle (DePaolo and Daley, 2000). On one hand, Wang et al. (2008) and Liu et al. (2008) suggested that the continent lithospheric mantle could serve as the mantle source of the intra-plate basalts as in some Mesozoic basalts in eastern China. The thick continental lithospheric mantle can be re-enriched and metasomatized by mantle derived fluids or melts (DePaolo and Daley, 2000). On the other hand, the thickened lower continental crust and lithospheric mantle enter into convective mantle by lithospheric delamination as observed from some Cenozoic intra-plate basalts in the North China Craton (Xu et al., 2004; Zeng et al., 2011). Therefore, identifying the contribution of each individual recycled material enriched in the mantle sources of intra-plate basalts is a grand challenge, which could offer a new insight and constraint to understand the origin of the enrichments in the mantle sources of the intra-plate basalts (Castillo, 2015; Dixon et al., 2002; Hofmann, 1988; Jackson et al., 2007; Kuritani et al., 2011; Sakuyama et al., 2013; Sobolev et al., 2007; Sobolev et al., 2005; Workman et al., 2004; Xu et al., 2012a; Zindler et al., 1984).

1.1.2 Cenozoic alkali basalt in SE China

Chapter 1

Cenozoic sodic alkali basalt is one of the dominant types of basalt among the continental intra-plate basalts in East Asia. Cenozoic intra-plate basalts in eastern China as a part of "Pacific Ring of Fire", are widely distributed along the eastern coast of Eurasian Plate (Fig. 1-1), from the north part of Russia to the South China Sea (SCS). There are four main regions of Cenozoic intra-plate basalts in China: NE China, the North China Craton (NCC), SE China and the SCS, all of four have their own unique geological history (Zou et al., 2000; Choi et al., 2006). The geochemical abundance of Cenozoic intra-plate basalts in east China have been studied in the past decades. These basalts generally have OIBs-like trace element patterns and are enriched in incompatible elements, as well as moderately depleted to enriched Sr-Nd isotopic compositions (Fan and Hooper, 1991; Ho et al., 2003; Kuritani et al., 2011; Li et al., 2015; Sakuyama et al., 2013; Tang et al., 2006; Xu et al., 2012a; Zhou and Armstrong, 1982; Zou et al., 2000). The radiogenic $^{206}Pb/^{204}Pb$ vs $^{87}Sr/^{86}Sr$ and $^{143}Nd/^{144}Nd$ isotope ratios of the Cenozoic intra-plate basalts in eastern China reveal prominent variations with latitude from the north to the south in the mantle sources: DMM to EM I components in the northern part (with some HIMU-like basalts in NE China), DMM to EM II components in the southern part, and a mixture of DMM, EM I and EM II in the central part (Choi et al., 2006; Xu et al., 2012a; Zou et al., 2000). Therefore, Cenozoic basalts in eastern China provide a showcase for studying the origin of enriched components in the sources of intra-plate basalts. The enriched components have been locally identified as recycled oceanic materials (Chen et al., 2015; Kuritani et al., 2011; Li et al., 2015; Liu et al., 2015b; Sakuyama et al., 2013; Wang et al., 2011; Xu et al., 2012a; Xu et al., 2012b; Zhang et al., 2009). Xu et al. (2012a) and Sakuyama et al. (2013) interpreted the enriched materials as young recycled oceanic crust, based on HIMU-like trace element patterns and weakly radioactive Sr-Nd-Pb isotopic ratios in Shuangliao NE China and in Shandong the NCC. Meanwhile, due to the presence of a stagnant subducted Pacific slab in the MTZ, (440-660 km) beneath eastern China (Huang and Zhao, 2006; Li and van der Hilst, 2010; Wei et al., 2012; Zhao and Ohtani, 2009) (Fig. 1-2), these recycled oceanic materials could be linked to subduction of the Pacific oceanic plate. Some researchers have instinctively linked the enrichment to the subduction of the Pacific plate (ancient and/or present). Liu et al. (2015b) and Chen et al. (2015) have recognized recycled pelagic sediment components in the source of basalts from Taihang in the NCC, and in Shuangliao in NE China based on their

relatively high water contents.

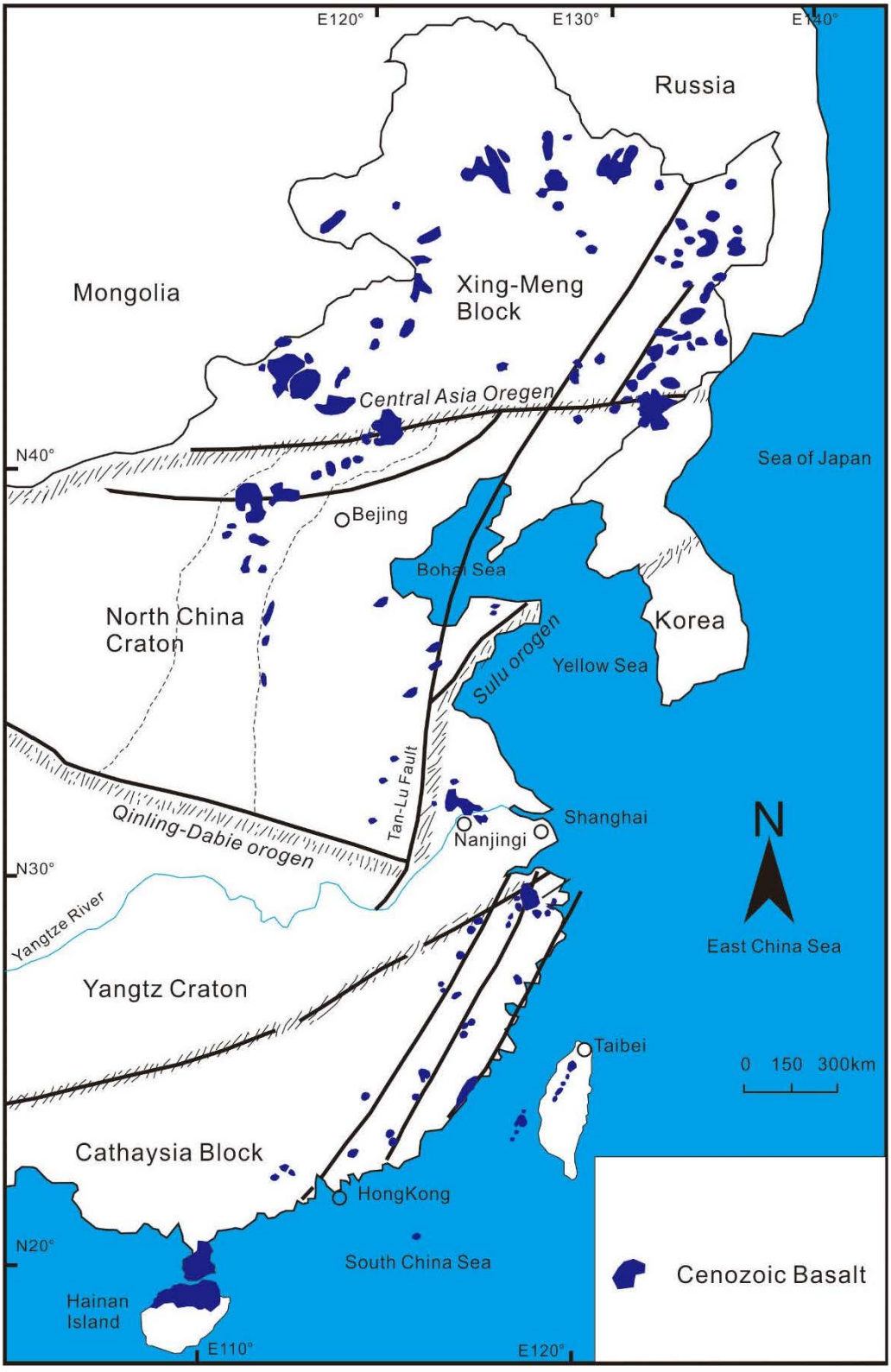

Fig. 1-1 The locations of Cenozoic basalts in East China.

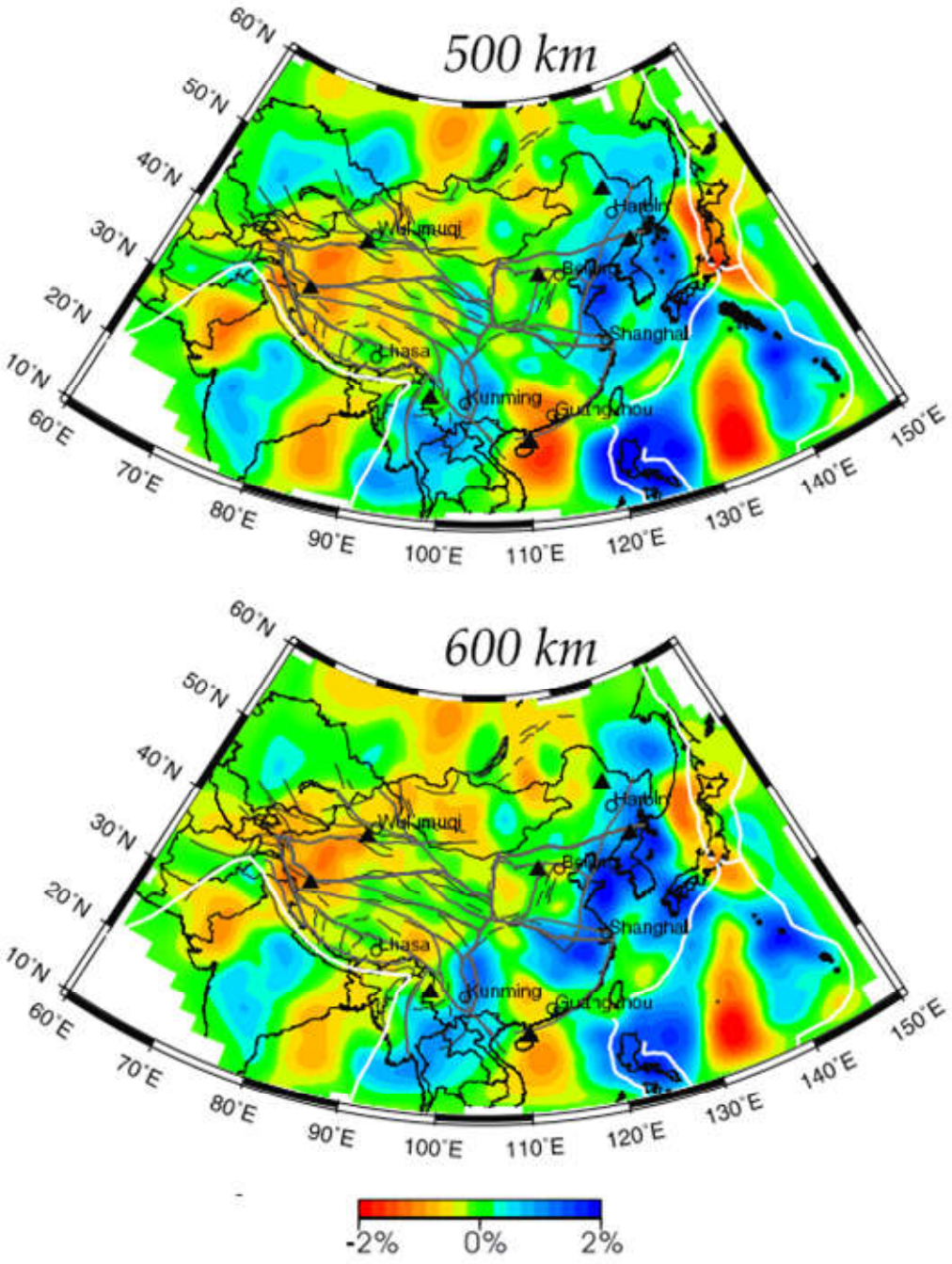

Fig. 1-2

Fig. 1-3 Image slice of P wave velocity perturbations in East China at MTZ depth (in percent from the average velocity) from Huang and Zhao (2006). Red and blue colors denote low and high velocities, respectively.

1.2 H_2O in nominally anhydrous minerals and basaltic magma

Hydrogen is a chemically active element in nature. It usually loses an electron and exists as proton with positive charge (H^+), such as H_2O, -OH. When hydrogen is under reduced conditions, it usually exists as CH_4 or H_2. Hydrogen can also be present in hydrated fluids or hydrous melts in the crevices of minerals, when water contents exceed the storage capacity of host minerals. Hydrogen can be bound with oxygen and be stored in hydrous minerals, such as phlogopite and hornblende, which have hydrogen in its chemical formula. Meanwhile, hydrogen can also enter into the defects of crystalline lattices of nominally anhydrous minerals (NAMs) as impurities, such as olivine (ol) and pyroxene. The NAMs can store up to thousands of ppm of H_2O, as the form of -OH. Different forms of "water" can be transformed from one to another between fluid/melts, hydrous minerals, and the NAMs depending on the chemical and physical conditions around.

The physical and chemical properties of minerals and rocks in the mantle are remarkably effected when even limited amount of water exists, such as electrical conductivity (e.g., Karato, 1990; Huang et al., 2005; Wang et al., 2006; Yoshino et al., 2006; Yoshino and Katsura, 2013), ionic diffusivities (e.g., Wang et al., 2004; Hier-Majumder et al., 2005a and b; Demouchy et al., 2007; Costa and Chakraborty, 2008; Otsuka and Karato, 2015), rheology (e.g., Mackwell et al., 1985; Karato et al., 1986, 2015; Karato and Wu, 1993; Chen et al., 1998; Mei and Kohlstedt, 2000a, 2000b; Dixon et al., 2004; Hier-Majumder et al., 2005a; Karato, 2010a, 2010b; Manthilake et al., 2013), seismic velocity (e.g., Karato and Jung, 1998; Jung and Karato, 2001; Falus et al., 2008; Karato et al., 2008), and the temperature and pressure of partial melting (e.g., Hirth and Kohlstedt, 1996; Gaetani and Grove, 1998; Asimow and Langmuir, 2003; Hirschmann et al., 2009; Green et al., 2010, 2014; Kelley et al., 2010; Tenner et al., 2012a). Water is also a fundamental factor in the evolution process of Earth, e.g. the stability of the craton, the generation of magma, the enrichment and migration of elements, and the movement of plates. Therefore, the research of the existence form and content of water in deep mantle, is one of the most important point to answer the question of petrology, geochemistry, geophysics, and geodynamics of the Earth evolution.

Water is an important influence factor for the generation and evolution of basaltic magma, because water can decrease the melting temperature and pressure, increase the

depth of starting melting, decrease the viscosity of magma and increase the ascending velocity of basaltic melting. The water content of basaltic magma have the potential to distinguish different geological structures, where the basalts are produced from. The basaltic magma produced from different geological structures have different water contents: (i) MORBs, about 0.1 to 0.3 wt. % (Asimow et al., 2004; Danyushevsky et al., 2000; Dixon et al., 1988; Michael, 1988, 1995; Sobolev and Chaussidon, 1996; Saal et al., 2002; Simons et al., 2002); (ii) OIBs, about 0.3 to 1.0 wt.% (Dixon et al., 1997; Dixon and Clague, 2001; Nichols et al., 1999; Simons et al., 2002; Wallace, 1998); (iii) the back-arc basin basalts (BABBs), about 0.2 to 2.0 wt.% (Danyushevsky et al., 1993; Hochstaedter et al., 1990; Stolper and Newman, 1994); (iv) island arc magmas (IABs), about 2.0 to 8.0 wt.% (Dobson et al., 1995; Sisson and Layne, 1993; Wallace, 2005; as shown in Fig. 1-3). The subducted oceanic slabs are believed to be able to carry large amount of water into deep mantle (Niu 2005; Garth and Rietbrock, 2014; Shaw et al., 2012). Because H_2O and Ce usually have similar behaviors during the magma process of partially melting and fractional crystallization, and the H_2O/Ce ratios of basalts can remain its primitive values in mantle source (Dixon et al., 2001 and 2004). The H_2O/Ce ratios of basalts have the potential to represent the H_2O/Ce ratios of the mantle sources for basalts and to identify the contribution of each different recycled material to the enriched components in the mantle source for basalts (Dixon et al., 2002; Michael, 1995; Shaw et al., 2012). Different recycled components have distinct H_2O/Ce ratios and are distinguishable from mantle components: (i) The H_2O/Ce ratios of GLOSS can be up to 1200 (Plank and Langmuir, 1998), while the H_2O/Ce of sub-marine basaltic glasses in the Minus basin is up to 903, with δD values down to -126 and $^3He/^4He$ ratios up to 15 R/RA (Shaw et al., 2012). This recycled signature of subducted hydrous oceanic sediments can be preserved in the mantle longer than 1Gyr (Shaw et al., 2012); (ii) the H_2O/Ce ratios of dehydrated recycled oceanic crust (ROC) are approximately 100; (iii) the H_2O/Ce ratios of DMM are about 200; and (iv) the H_2O/Ce ratios of EM are closed to 100 (Dixon et al., 2002).

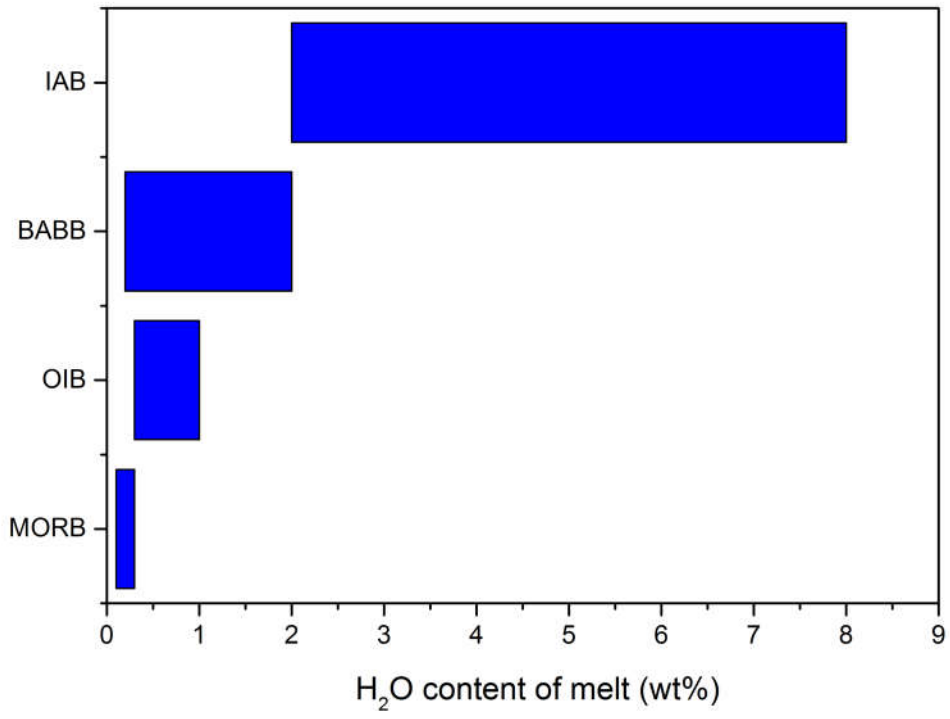

Fig. 1-4 The ranges of H_2O content for OIBs, MORBs, BABBs and IABs (Dixon et al. (2004) and the references therein).

1.3 Lithium and Oxygen isotopes

1.3.1 Lithium isotopes

The Lithium (Li) isotope could play an efficient role in distinguishing the contributions of different recycled materials to the enriched components in the mantle source of basalts and to trace hydrogen re-equilibrium of cpx phenocrysts after crystallization, due to the similar diffusion rate, respectively. Lithium belongs to the alkali metal group and has 2 isotopes: ^{6}Li and ^{7}Li. Both of them are stable isotopes with natural isotopic abundances of 7.52% and 92.48% in nature, respectively. Lithium is easy to lose an electron to form a monovalent cation, like other alkali metals. Therefore, Li is very active, and has no pure metal substance in nature. All the Li combines with other anions as crystals (such as triphane), or enters into the crystalline lattices defects as impurities (such as olivine), or is dissolved in solution (such as sea water). The mass

difference between ^{6}Li and ^{7}Li relative to the mass of the element is about 16%. Therefore, the mass fractionation of the Lithium isotope is easy to be observed in nature. A change of 25% of $^{6}Li/^{7}Li$ ratio were observed after the Li-solutions percolate through a zeolite column (Taylor and Urey, 1938). Thus, considerable fractionation of ^{6}Li and ^{7}Li can be expected in geochemical processes, such as rock weathering and mantle metasomatism. Meanwhile, different reservoirs in the nature have large Li isotopic variation (Fig. 1-4, Tomascak, 2004), which can be used to distinguish the origin of the enrichment in mantle source. The Li isotopic composition is usually expressed as:

$\delta^{7}Li = [(^{7}Li/^{6}Li)_{sample}/(^{7}Li/^{6}Li)_{L\text{-}SVEC}-1]\times1000$,

where L-SVEC is the Li_2CO_3 international standard with the $^{7}Li/^{6}Li$ ratio of 12.0192 (Flesch et al., 1973).

The residence time of Li, as a conservative element, is about one million year in the ocean (Misra and Froelich, 2012). The Li in the ocean is consumed by (a) low temperature removal of Li into oceanic basalts; (b) deposited Li in the marine sediments, which return into deep earth at subduction zones as subducted oceanic sediments and crusts. The Li in the ocean is supplied by inputs of (a) dissolved Li from rivers (average $\delta^{7}Li$ +23‰, Huh et al. 1998); (b) high-temperature hydrothermal fluids around ocean ridges; (c) re-dissolved Li from oceanic basalts and marine sediments. The oceanic Li can be considered as dynamic equilibrium. Mantle-derived basalts have a relatively uniform composition with $\delta^{7}Li$ values of +4 ± 2‰ (Tomaszak 2004). However, the continental crust generally has a lighter Li isotope composition than the upper mantle from which it was derived (Teng et al. 2004). Therefore, Li isotope is considered to be used as a tracer to identify the existence of recycled material in the mantle (e.g. Moriguti and Nakamura 1998; Leeman et al. 2004). Unfortunately, some arc lavas display normal $\delta^{7}Li$ values, being indistinguishable from MORBs, because Li is decoupled from other fluid mobile elements and is partitioned into Mg-silicates (pyroxene, olivine) in the mantle (Tomascak et al. 2002).

Lithium diffuses rapidly in silicate minerals with $D=1.0\times10^{-15}$ to 5×10^{-10} at 1100 °C (Vlastelic et al., 2009, Parkinson et al. 2007). In addition, the diffusivity of ^{6}Li is faster than ^{7}Li in both melts and minerals (Richter et al., 2003, 2014). Theoretical calculation shows that the Li content and Li isotope will change in a few days by Li diffusion under ~1100 °C and the change will exist for several years (Fig. 1-5, Li et al., 2012; Jeffcoate et al., 2007; Parkinson et al., 2007). The abundance of peridotite xenoliths entrained in most of the small isolated alkali basalts in eastern China required rapid magma ascent

and cooling (O'Reilly and Griffin, 2010). This suggests that the Li isotopic profiles of cpx phenocrysts in such basalts can preserve the information of Li diffusion of cpx phenocryst during the magma ascent and cooling after eruption, which can be used to deduce the magma evolution. Detailed Li diffusive profiles in mineral grains are also considered as a candidate for high-resolution geo-speedometer for timescales as short as a few to hundreds of days (Jeffcoate et al., 2007; Parkinson et al., 2007). Meanwhile, because the Li and H diffuse very fast in minerals, at given high diffusion rate of H in cpx at 900°C, ($D=10^{-10}$~$10^{-10.5}$ m^2/s, Hercule and Ingrin, 1999; Ingrin and Blanchard, 2006; Ingrin and Skogby, 2000; Woods et al., 2000), detailed Li diffusive profiles of cpx phenocrysts measured by SIMS combined with the profiles of -OH measured by FTIR can be used to identify whether H diffusion took place or not, during the subsequent ascent of the basaltic melts.

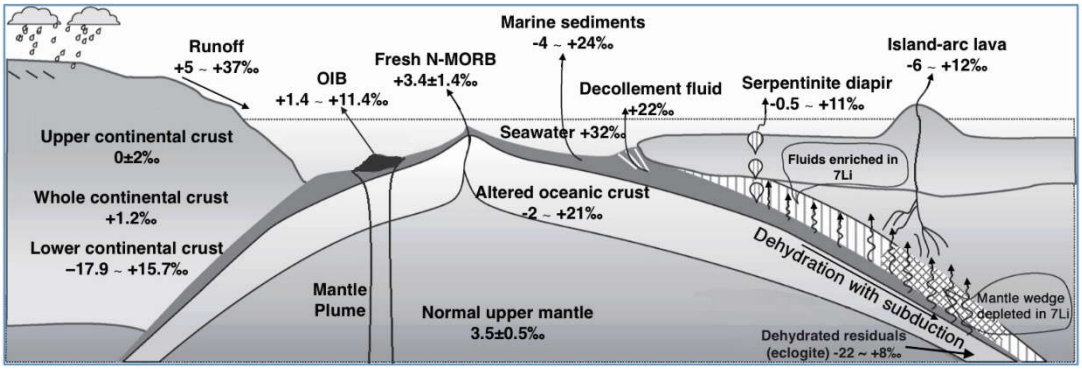

Fig. 1-5 Li isotopic compositions of Earth reservoirs, modified from Tang et al. (2010) expressed in ^{7}Li values. The data are from: seawater (Chan and Edmond, 1988; You and Chan, 1996), river water (Huh et al., 1998, 2001; Millot et al., 2010; Dellinger et al., 2015), arc lavas (Moriguti and Nakamura, 1998; Tomascak et al., 2002; Chan et al., 2002a; Agostini et a., 2008; Košler et al., 2009), Fresh N-MORB (Tomascak et al., 2008), OIB (Tomascak et al., 1999; Chan and Frey, 2003; Kobayashi et al., 2004; Ryan and Kyle, 2004; Nishio et al., 2005; Jeffcoate et al., 2007; Chan et al., 2009), altered oceanic crust (Chan et al., 1992, 2002b), marine sediments (Chan et al., 1994, 2006; Chan and Kastner, 2000; Bouman et al., 2004), upper continental crust (Teng et al., 2004), lower continental crust (Teng et al., 2008), normal upper mantle (Von Strandmann et al., 2011), eclogite (Zack et al., 2003; Marschall et al., 2007; Penniston-Dorland et al., 2010).

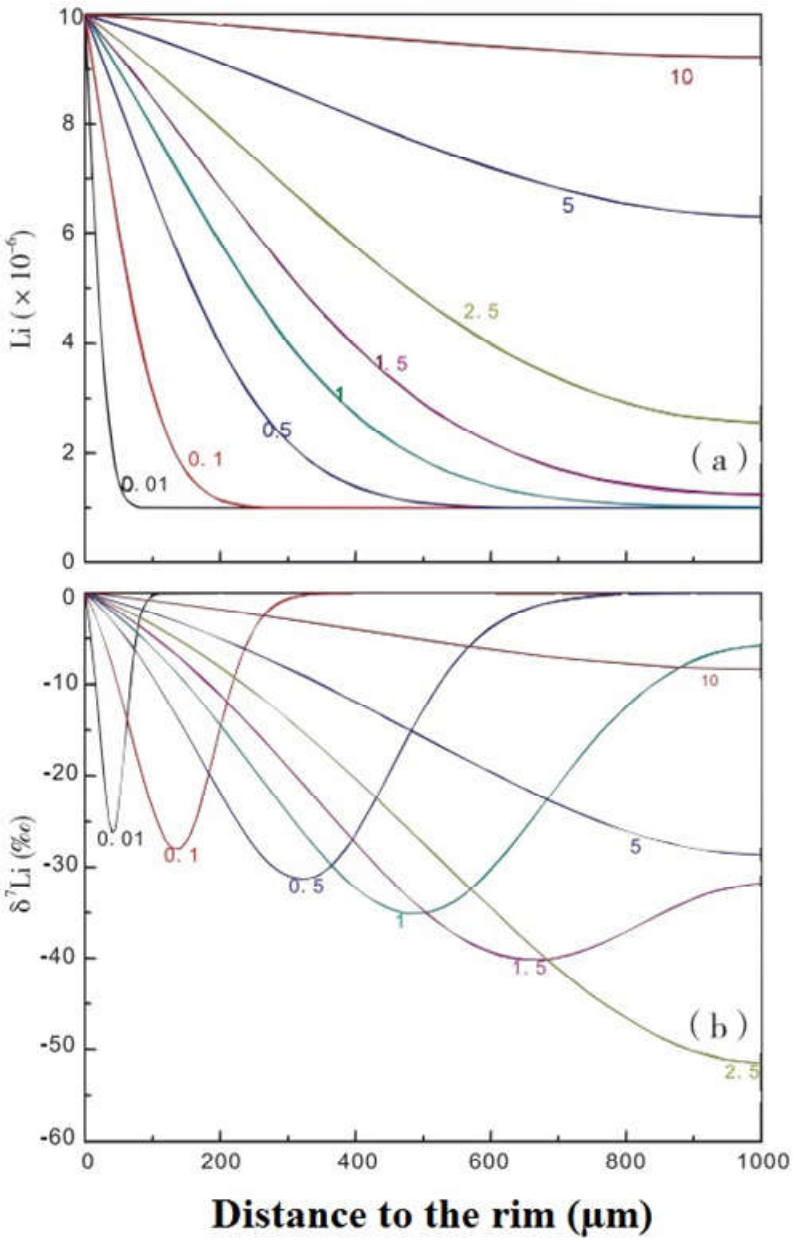

Fig. 1-6 The Li content and Li isotope change with time by diffusion (Li et al., 2012). (a) The evolution of Li content with time; (b) the evolution of δ^7Li with time. The numbers on the straight lines are durations in years.

1.3.2 Oxygen isotopes

Oxygen (O) is the most abundant element on Earth. It can be present as molecules in the air and as a compounds with other elements. The metal oxides usually have wide thermal stability over large range of temperature. Oxygen has three stable isotopes, i.e.

^{16}O, ^{17}O and ^{18}O, these isotopes are some of the most important isotopes known to be used to trace the circulation of materials between the deep mantle and the shallow layers of Earth. The oxygen isotopes traditionally are displayed in two different δ-scales: $\delta^{18}O_{(VSMOW)}$ and $\delta^{18}O_{(VPDB)}$. The δ-scales of $\delta^{18}O_{(VSMOW)}$ are used in this thesis. The mantle rocks (if are represented by MORBs) have narrow but homogeneous oxygen isotope ($\delta^{18}O$ ~5.7±0.2 ‰) (Fig. 1-6a, Eiler et al., 2001). The continental crust and oceanic materials generally have a wider range of oxygen isotope than that of the upper mantle. The isotope fractionation of oxygen is controlled by the strength of chemical bonds and the equilibrium temperature of exchanging. Large fractionation of oxygen isotopes occur at low temperature and between two phases with distinct chemical compositions, such as water-rock exchange reaction. It is known that oxygen isotopes have small fractionation during igneous differentiation processes at high temperature. The pristine continental and fresh MORBs should not have large O isotope fractionation compared to the mantle source. Therefore, the various oxygen isotope of continental crust and oceanic crust materials must have been modified by secondary processes, such as low temperature water-rock reaction. The recycled materials often undergo low-temperature processes, and they usually have non-mantle-like $\delta^{18}O$ values, such as the lower continental crust, oceanic sediments and altered oceanic crust. The recycled pelagic sediments and delaminated lower continental crust have high $\delta^{18}O$. The shallow oceanic basalts have higher $\delta^{18}O$ values than the normal mantle because of low temperature water-rock reaction with sea water. Nevertheless, the lower gabbros have slight lower $\delta^{18}O$ than normal mantle values due to high-temperature hydrothermal reaction (Fig. 1-6c). The contributions of subducted pelagic sediments and related fluids to subduction-related lavas can also be constrained by the variations of oxygen isotope (Eiler et al. 2000; Dorendorf et al. 2000, Zheng et al., 2012). The non-mantle-like $\delta^{18}O$ values in basalts can be used to indicate the existence and origin of these recycled materials, if combined with other geochemical data. The variation of $\delta^{18}O$ is larger than 5‰ among more than 2000 fresh basalts and glasses in the Neogene volcanic rocks all over the world, suggesting significant oxygen isotope heterogeneities in the mantle sources of the basalts (Harmon and Hoefs, 1995).

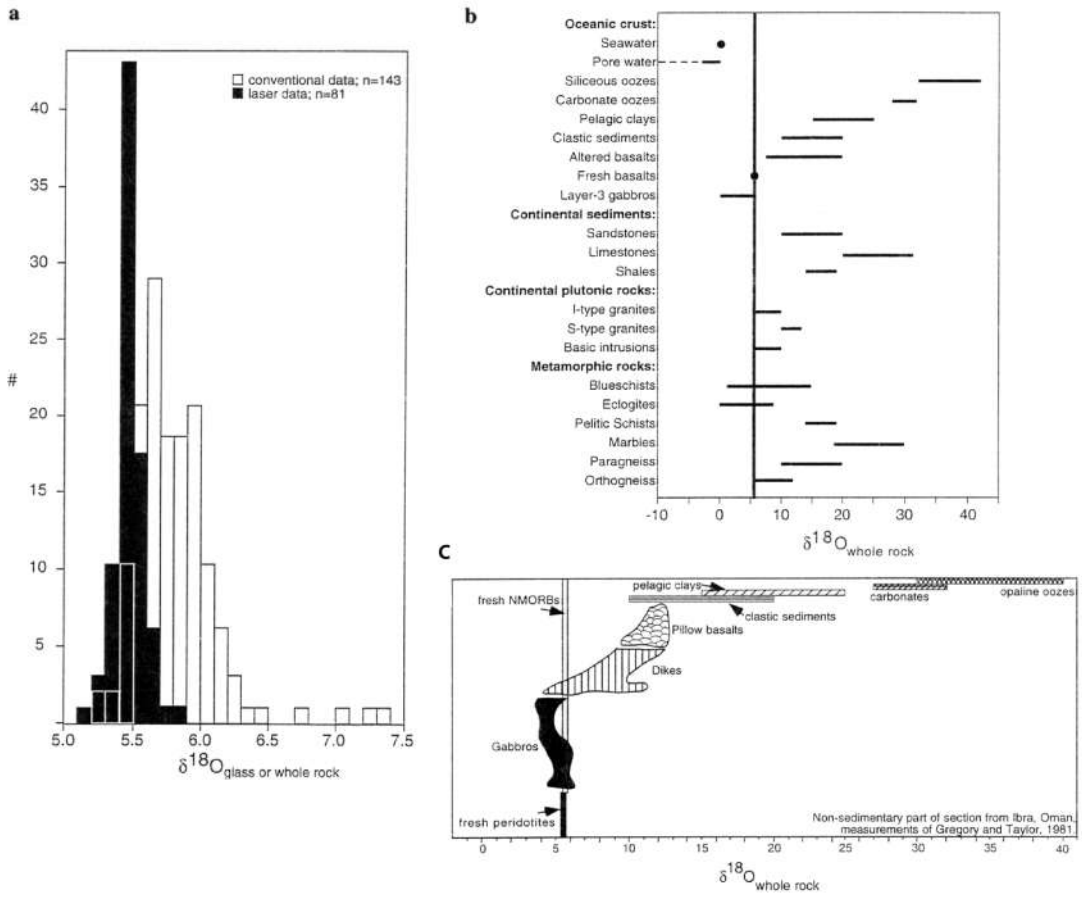

Fig. 1-7 Oxygen isotope compositions of MORBs glasses and whole-rocks. (Eiler, 2001. Fig. 9 in its book. Unfilled boxes are data collected using conventional (resistance heated) fluorination methods between 1966 and 1993; filled boxes are data collected only on glass using laser-based methods. Data sources are listed in the original text); b. The main composition of Oxygen in different geological units in Earth (Eiler, 2001. Fig. 7 in its book. Data sources are listed in the original text.); c. The idealized $\delta^{18}O$ of altered, sediment-covered oceanic crust (Eiler, 2001. Fig. 7 in its book, based on Gregory and Taylor's (1981) study of the Ibra section of the Oman ophiolite and marine sediments data sources are listed in the original text).

1.4 Objectives of this work

The objectives of the present study are to decipher the origin of enriched compositions in the mantle sources of Cenozoic basalts in SE China through:

(1) The water content distribution of the upper mantle in SE China during Cenozoic. Comparison of the water contents of Cenozoic basalts at different locations in SE China, as well as those of the peridotite xenoliths entrained by Cenozoic basalts do not only help us to understand the water content distribution of the upper mantle, including upper lithosphere and lower convective asthenosphere, but also provide a typical case to study the relationship between the water contents and the geochemical composition in the mantle source of Cenozoic basalts in SE China.

(2) The characteristics of trace element ratios combined with O isotope in the mantle source of Cenozoic basalts in SE China. These distinctively useful index have been identified to trace the source process, because the unique geochemical characteristics in each enriched composition are believed not to be fractionated during mantle partial melting and crystallization during magma evolution, representing the mantle source. These characteristics can be used to determine the contributions of each kinds of recycled materials to enriched mantle source in Cenozoic basalts in, SE China.

(3) The temporal and spatial variation of the enriched compositions in the mantle source of Cenozoic basalts in SE China. Comparison of the temporal and spatial variation of the enriched compositions in the mantle source with different geological backgrounds besides providing the new information and restriction to decipher the origin of these enrichment of Cenozoic basalts in SE China can also reveal the indispensable clues to determine the influence of important geological events and recover the geological history, if any.

Chapter 2 Geological background and Samples

The eastern part of China continent has mainly three tectonic units of Cenozoic basalts: NE China block, the NCC, and SE China. The NE China consists of a group of blocks, mainly including, Erguna, Xingkai, Songnen, Jiamusi, Longgang, Khanka, and so on. These small blocks have their individual geological histories, and are assemble in early Mesozoic. The NCC is one of the oldest cratons in the world, containing the crust as old as 3.8Ga (Liu et al., 1992). The lithosphere under eastern part of China is one of the best example to study the lithosphere thinning in the world (Windley et al., 2010). Based on a series of studies on peridotite xenoliths, xenocrysts and mineral inclusions in diamonds from mid-Ordovician kimberlites, a typical cratonic lithospheric mantle with high thickness of 200km and low surface geothermal current value of 40 mW/m^2 until mid-Ordovician in the NCC is revealed. Recent geophysical seismic wave map discovered the root of old, cold and thickened lithosphere replaced by a hot (60–80 mW/m^2) and thin (80–60 km) lithospheric mantle during the late Mesozoic (Griffin et al., 1998; Huang and Zhao, 2006; Menzies et al., 2007; Menzies et al., 1993). The South China consists of the Yangtze Craton and SE China block (or the Southeast China fold belt, i.e., the Cathaysia block or the Cathaysia fold belt) and has been focus of many recent studies in relation to global tectonics, especially the Rodinia supercontinent history (e.g. Li et al., 2009; Li et al., 2010; Yao et al., 2011; Wang et al., 2013). The SE China lies on the southeastern continental margin of Asian plate, separated from the Yangtze Craton by the Jiangshan-Shaoxing fault zones. The oldest age recorded in SE China crust is 3.76 Ga from zircons in the Mesozoic granites of the central SE China block (Yu et al., 2007). In general, the most of ancient metamorphic basement of SE China is a series of complexes in the southwestern and northern Zhejiang region with the age of 1.8-2.0 Ga (Xiang et al., 2008; Yu et al., 2009). Towards the northeast fold belt resulted from an early Paleozoic orogeny, occupying almost whole SE China block more than 300,000 km^2 (Faure et al., 2009). During Neoproterozoic, the continental crust in SE China had experienced a sequence of continental reworking and growth events (Li et al., 2003a; Li et al., 2003b; Wang et al., 2006; Wu et al., 2006; Zhou et al., 2002a; Zhou et al., 2006; Zhou et al., 2002b). The basement of SE China has reworked in the early Paleozoic, on a large scale of anatexis and emplacement in Silurian (Faure et al., 2009; Charvet et al., 2010). Recent tectonic studies on SE China Fold Belt regard it as an intra-continental orogeny (Faure et al.,

2009; Li et al., 2010; Charvet et al., 2010). Although the South China is not the typical thinning region like the NCC, during Mesozoic in traditional opinion, Li et al. (2009) show the evidence of coeval lithospheric extension and thinning in Yangtze craton. The deep Tan-Lu fault may trigger over-thickened lithosphere delamination and Archean lithospheric mantle replacement (Huang et al., 2008; Zheng et al., 1998). Its lithospheric mantle may have experienced a thinning process during Mesozoic, as recorded by the NCC (Ho et al., 2003; Wu et al., 2003; Xu et al., 2000; Xu et al., 2002). Meanwhile, previous studies have suggested that SE China block has undergone several subduction events of the Izanagi plate, the Paleo-Tethyan plate, and the present Pacific plate (Müller et al., 2008; Windley et al., 2010). Meanwhile, the geophysical data has displayed the presence of a stagnant subducted Pacific slab in MTZ, beneath the northeastern part of China as shown in Fig. 2-1, (Huang and Zhao, 2006; Li and van der Hilst, 2010; Wei et al., 2012; Zhao and Ohtani, 2009). Mesozoic basalts is SE China have both IABs-like and OIBs-like trace element patterns (Chen et al., 2008; Wang et al., 2008; Xie et al., 2001), but dominant Cenozoic basalts have OIBs-like trace element patterns.

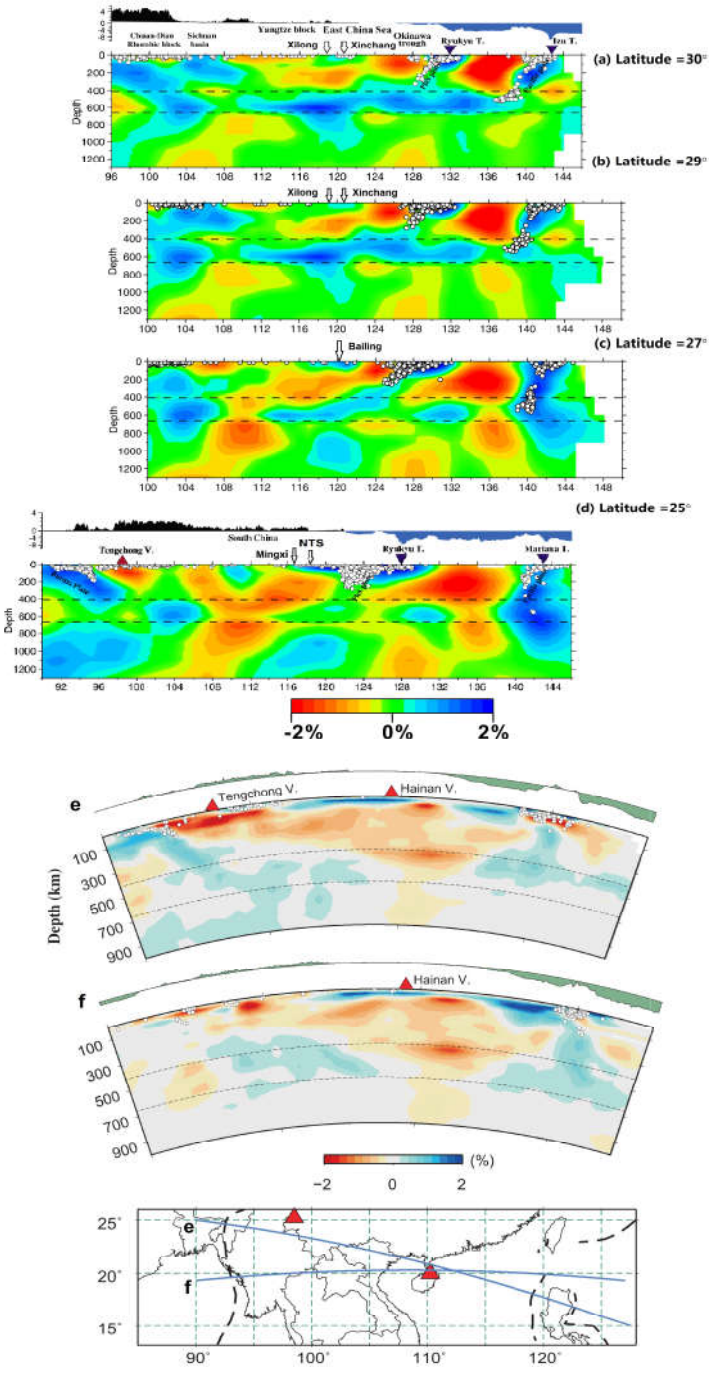

Fig. 2-1 Vertical cross section of P wave velocity perturbations along latitude N 30°, N 29°, N 27°, N 25° and at Hainan island (modified from Huang and Zhao (2006) and Wei et al. (2012)). Red and blue colors denote low and high velocities, respectively. The latitude of Xilong and Xinchang (GP and SC) are in the range of N 29° to 29.5°. The latitude of Mingxi (MX and SH) and Bailing are close to N 26.4° and N 27.2°. The latitude of Niutoushan (NTS) are close to N 25°.

2.1 Basalt locations and Samples

The SE China was in an extensional tectonic setting since Cenozoic (Ma and Wu, 1987). Cenozoic basaltic volcanism in SE China occurred dispersive at small-scale and mainly controlled by a series of northeast-southwest trending fault systems (). The earliest basaltic volcanos in Early Tertiary (38–64 Ma) had only been restricted in the central and western Guangdong province (Zhu et al., 2004). Only a few basaltic pipes have been found in the eastern Guangdong province, the Zhejiang Inner volcanic belt, the coast of Fujian, and the northern part of Hainan Island, during 34.3-16.3 Ma (Ho et al., 2003). Miocene to Pliocene (after 17 Ma, dominantly younger than 6 Ma) basalts are widespread in SE China (Zhu et al., 2004; Ho et al., 2003). The detailed information of locations of Cenozoic basalts in SE China is listed in Table 2-1.

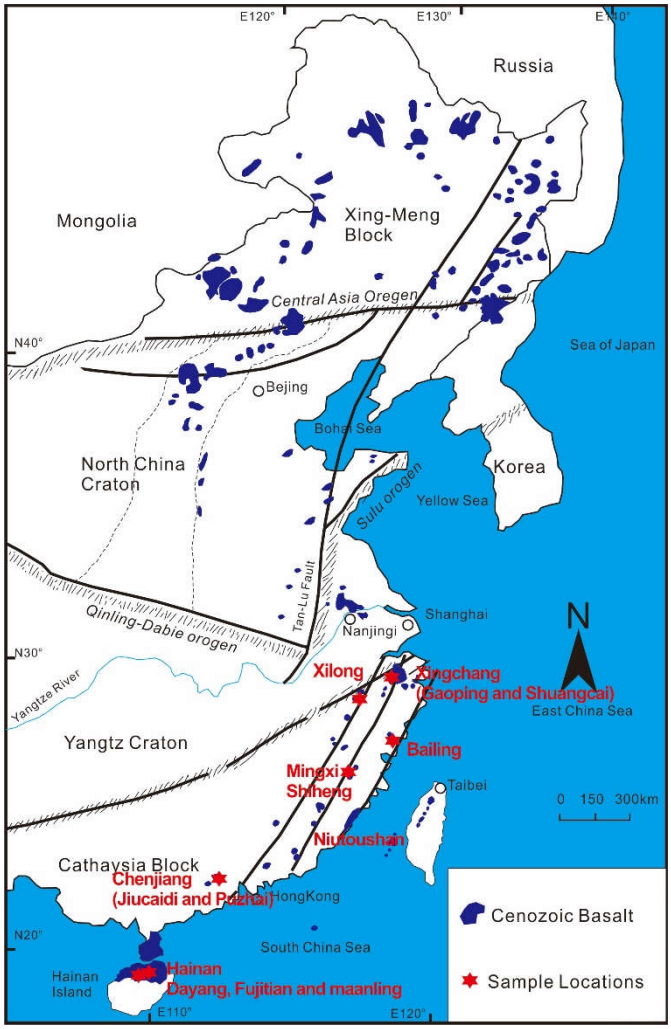

Fig. 2-2 Simplified tectonic units and distribution of the Cenozoic basalts in eastern China and the location of the basalt samples in Southeast China.

2.1.1 Cenozoic alkali basalts in the Zhejiang region

The age of Cenozoic basaltic volcanism of the Zhejiang region in the northeastern part of the Southeast China block can be divided into two stages (Ho et al., 2003): (1) stage 1: ca. 26-17 Ma, composed primarily of basanites; and (2) stage 2: after 11 Ma, composed mainly of alkali olivine basalts, olivine tholeiites, quartz tholeiites and a small amount of basanites. Our samples were collected from Xilong (XL) and Xinchang (including the Shuangcai (SC) and Gaoping (GP) volcanoes). The sample locations are shown in Fig. 2-2 and 2-3. The samples from XL are basanites, and those from SC are alkali olivine basalt. The GP samples are transitional rocks, from basanites to alkali olivine basalts. The XL and GP basalts have caught some mantle xenoliths, including spinel lherzolites, spinel harzburgites and garnet lherzolites. The XL basanites contain approximately 6 vol. % ol and <4 vol. % cpx phenocrysts. The GP basaltic rocks contain <3 vol. % ol, <2 vol. % cpx and <3 vol. % plagioclase (pl). The SC alkali olivine basalts contain 10-15 vol. % cpx and <2 vol. % ol and pl. The cpx phenocryst grains in the XL and GP basaltic rocks are normally <1 mm in size, but those in the SC samples are up to 3 mm. The Ar-Ar ages of the XL basanites range from 23 to 27 Ma associating them with stage 1 volcanism, and those of the GP and SC samples are from 5 to 10 Ma associating them with stage 2 volcanism (Ho et al., 2003). The stagnant subducted slabs of Pacific plate in the MTZ are revealed by geophysical evidence beneath Zhejiang region, as shown in Fig. 2-1a and b.

Fig. 2-3 The detailed locations of the basalt samples in the Zhejiang region.

2.1.2 Cenozoic alkali basalts and diabases in the Fujian region

The Fujian region lies at latitude from N23.6° to N27.2°, longitude from E115.8° to E120.5°, in the center part of SE China block (Fig. 2-2 and Fig. 2-4). Our samples of Cenozoic basalts and diabases in Fujian region are collected from Mingxi (MX), Shiheng (SH), Bailin (BL) and Niutoushan (NTS). The stagnant subducted slab of Pacific plate in the MTZ are obscure on the seismic waves maps beneath Bailin in Fig. 2-1 c, but disappear at the latitude of MX and NTS. The samples from NTS are transitional rocks from alkali olivine basalts to sub-alkali basalts, the samples from SH range from basanites into alkali olivine basalts, all the MX samples are basanites while, the BL samples are diabases. All the Fujian basaltic rocks, except the SH basalts, have caught mantle xenoliths, including spinel lherzolites, spinel harzburgites, and garnet lherzolites (only in the MX basalts). Only some broken small xenocrysts are found in the SH basalts. The NTS samples have the oldest age from 17.1 to 14.9 Ma among the Fujian basaltic rocks, while the MX samples are 1.2-2.2 Ma and the SH samples are 2.95 Ma, respectively (Ho et al., 2003). The BL diabases have intruded into a Pleistocene layer, implying their age younger than Pleistocene. The NTS basalts are commonly in aphanic texture, without any phenocrysts. The xenocrysts are broken from xenoliths and jumble in the matrix of MX basanites, including ol, orthopyroxene (opx) and cpx. Some xenocryst grains rim have reacted with hosting melts and grew new phenocrysts around them. MX basalts contain about 4-7 vol. % ol and 5-8 vol. % cpx phenocrysts, except xenocrysts, but it is hard to find pl. The phenocrysts in the SH basaltic rocks are smaller than those in the MX basalts. The SH basalts contain about 1 vol. % ol about 2 vol. % cpx, some of which grew around some xenocrysts, and <0.5 vol. % very fine feldspar, despite a few small xenocrysts. The cpx phenocryst grains in the MX and SH basaltic rocks are normally less than 1 mm and 0.3 mm in size, respectively. The ol phenocryst grains range from 0.1 to 1 mm and are less than 0.2 mm in size, respectively. The diabases have diabasic texture and contain about 15-20 vol. % glass and fine crystals as matrix and about 5% metallic oxide. All the ol, cpx and pl phenocrysts have very fine crystallinity. The ol and cpx phenocrysts are euhedral and surrounded by pl phenocrysts, certifying the crystallization of ol and cpx as earlier than pl. Moreover, some small ol are captured by cpx, suggesting an earlier crystallization of ol than cpx. The diameters of porphyritic cpx coarse-grain can be bigger than 0.5 cm, and the strip pl and granular ol phenocrysts are relatively smaller.

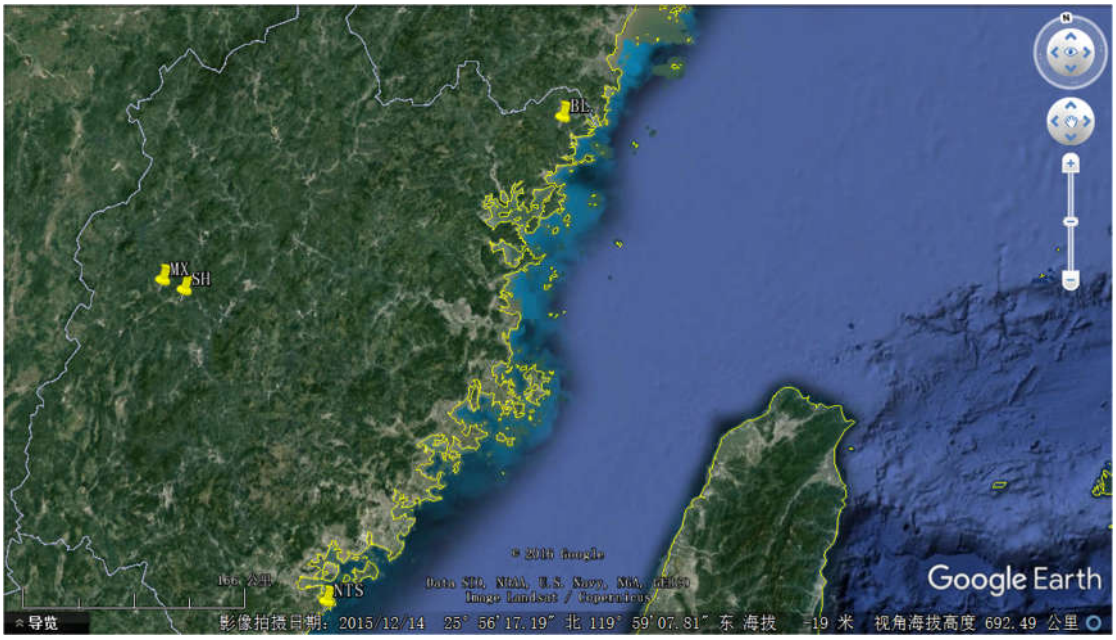

Fig. 2-4 The google earth imagery showing the sample locations of the basalt samples in the Fujian region.

2.1.3 Cenozoic basalts in the Hainan Island

Hainan Island lies in the southern-most part of China continent, located at the northern edge of the South China Sea Basin. The mantle "plume" structure in upper mantle are revealed on the seismic wave map beneath Hainan region in Fig. 2-1e and f. Cenozoic volcano in Hainan Island started to erupt since 28.4 Ma at the peak time of about Pleistocene (1.8–0.012 Ma) which gradually died down in the Holocene (Ho et al., 2000; Fan et al., 2004). The Hainan basalts have OIBs-like incompatible element distributions, Dupal-like Pb isotopic signatures and depleted Sr-Nd isotopic compositions. Some early studies suggested that the Hainan basalts were mostly produced in the posterior stage of South China Sea Basin extension, whose intense time of eruption activity is the Pleistocene and Holocene (Flower et al., 1992; Ho et al., 2000, 2003). Seven basalts samples are from the studies of Zou and Fan (2010), located in the northern part of the Hainan Island; including two Holocene samples from Maanling (ML), four Holocene samples from Leihuling (LH), and one Pleistocene sample from Sanjiaoyuan (SJY) as shown in Fig. 2-5. The ML samples are olivine tholeiites, the LH samples are mostly alkali olivine basalts (AOBs), and the SJY sample is olivine tholeiite. The ML, LH and SJY cpx phenocrysts are all euhedral or subhedral crystal aggregation. The SJY sample is relatively more compacted than other samples, and has about 5 vol. %

ol phenocrysts ranging from 0.5 to 1mm in size and 2 vol. % cpx phenocrysts about 0.5mm in size. The LH and ML samples have vesicular texture with enriched bubble and have a little ol and cpx phenocrysts.

There are 9 and 10 samples were collected from two locations of the Dayang (DY) and Fujitian (FJT), respectively, lying in the east part of the Hainan Island around Penglai city. They erupted in Holocene (Wang et al., 2012), like ML and LH. All the DY and FJT samples are AOBs and carry large number of mantle peridotite xenoliths. The FJT samples also entrained some cpx megacrysts. A little cpx megacrysts and peridotite xenoliths is relative wet analyzed by Zhang et al. (2010). Typical columnar joint structure are found in the DY basalts. The DY samples have less than 3 vol. % ol phenocrysts ranging from 0.5 to 2 mm in size and less than 1 vol. % cpx phenocrysts mostly smaller than 0.3 mm in size. Meanwhile, a few ol and cpx xenocrysts, even tiny xenoliths separated from broken peridotite xenocrysts were caught in the matrix, with reacting rim. The FJT samples have not only mantle peridotite xenoliths/xenocryst but also have very a few xenocrysts with low Mg# and TiO_2, suggesting their origin may be the shallow layers of the earth (crust). The FJT basalts have very a little ol and cpx phenocrysts. The slight secondary alteration along the cracks of rocks are observed in some FJT samples. The FJT samples have less than 3 vol. % ol phenocrysts smaller than 1.5 mm in size and less than 1 vol. % cpx phenocrysts mostly smaller than 0.5 mm in size.

Fig. 2-5 The google earth imagery showing the sample locations of the basalt samples in the Hainan Island.

Table 2-1 The sample locations and numbers of Cenozoic basalts from the SE China

Location		Samples No.	GPS	Rock type	Age	Xeno
Zhejiang	Xilong	XL-1	N 29° 3'46.00"	Basanite	23.7-26.4Ma [a]	Yes
		XL-2	E 118°58'52.40"	Basanite		Yes
		XL-3		Basanite		Yes
		XL-4		Basanite		Yes
		XL-5		Basanite		Yes
		XL-6		Basanite		Yes
		XL-7		Basanite		Yes
		XL-8		Basanite		Yes
		XL-9		Basanite		Yes
		XL-10		Basanite		Yes
		XL-11		Basanite		Yes
		XL-12		Basanite		Yes
		XL-13		Basanite		Yes
	Gaoping (Xinchang)	GP-1	N 29° 3'46.00"	Basanite	4.7-5.3Ma [a]	Yes
		GP-2	E 118°58'52.40"	Basanite		Yes
		GP-3		Basanite		Yes
		GP-4		AOB [d]		Yes
		GP-5		AOB		Yes
		GP-6		Basanite		Yes
		GP-7		AOB		Yes
	Shuangcai (Xinchang)	SC-1	N 29°20'9.40"	AOB	8.4-9.3Ma [a]	No
		SC-2	E 120°51'15.10"	AOB		No
		SC-3		AOB		No
		SC-4		AOB		No
		SC-5		AOB		No
Fujian	Mingxi	MX-1	N 26°25'22.71"	Basanite	1.2-2.2 Ma [a]	Yes
		MX-2	E 117° 7'7.09"	Basanite		Yes
		MX-3		Basanite		Yes
		MX-4		Basanite		Yes
		MX-5		Basanite		Yes
		MX-6		Basanite		Yes
		MX-7		Basanite		Yes
		MX-8	N 26°24'21.25"	Basanite		Yes
		MX-9	E 117° 7'6.08"	Basanite		Yes
		MX-10		Basanite		Yes
		MX-11		Basanite		Yes

Table 2-1 continuted

		MX-12		Basanite		Yes
	Shenghe	SH-1	N 26°20'37"	AOB	2.95 Ma [a]	Yes
		SH-2	E 117°16'12.2"	AOB		Yes
		SH-3		AOB		Yes
		SH-4		Basanite		Yes
		SH-5		Basanite		Yes
	Bailin	BL-3	N 27° 9'38.43"	Diabase	Pleistocene	Yes
		BL-4	E 120°10'4.44"	Diabase		Yes
		BL-5		Diabase		Yes
		BL-6		Diabase		Yes
		BL-7		Diabase		Yes
		BL-8		Diabase		Yes
		BL-9		Diabase		Yes
		BL-10		Diabase		Yes
		BL-11		Diabase		Yes
	Niutoushan	NTS-4	N 24°13'12.60"	Tholeiite	17.1-14.9 Ma [a]	No
		NTS-5	E 118° 2'26.80"	Tholeiite		No
		NTS-6		Tholeiite		No
Hainan	Maanling	HN9901		OT [e]	~9ka [b]	No
		HN9902		OT		No
	Leihuling	HN9907		AOB	~9ka [b]	No
		HN9908		AOB		No
		HN9910		AOB		No
		HN9912		AOB		No
	Sanjiaoyuan	HN9914		OT	65-77ka [b]	No
	Dayang	DY-1	N 19°30'16.83"	AOB	Holocene	Yes
		DY-2	E 110°32'3.00"	AOB	3.1-4.4 Ma [c]	Yes
		DY-3		AOB		Yes
		DY-4		AOB		Yes
		DY-5		AOB		Yes
		DY-6		AOB		Yes
		DY-7		AOB		Yes
		DY-8		AOB		Yes
		DY-9		AOB		Yes

Table 2-1 continuted

Fujitian	FJT-1	N 19°33'22.40"	AOB	Holocene	Yes
	FJT-2	E 110°30'36.58"	AOB	3.1-4.4 Ma [c]	Yes
	FJT-3		AOB		Yes
	FJT-4		AOB		Yes
	FJT-5		AOB		Yes
	FJT-6		AOB		Yes
	FJT-7		AOB		Yes
	FJT-8		AOB		Yes
	FJT-9		AOB		Yes
	FJT-10		AOB		Yes

a	The age is from Ho et al., 2003
b	The age is from Zou et al., 2010
c	The age is from Wang et al., 2012
d	alkali olivine basalt
e	olivine tholeiite

Chapter 3 Analytical protocols

3.1 Sample preparations

The fresh samples were chosen for geochemical analysis. Some parts of basalt samples were sawed into slabs. The chips of 1-2 cm in size were prepared from the central parts of the basalt samples. The chips were cleaned using distilled water, dried at 110°C for 6 hours, and then crushed into powder of ~200mesh size in an agate mortar for bulk rock analysis. Meanwhile, the doubly polished thin sections were prepared, for the in situ analyses of the phenocrysts, by Fourier transform infrared spectroscopy (FTIR), electron microprobe (EMP), and secondary ion mass spectrometry (SIMS) investigation. The doubly polished thin sections are controlled in thicknesses between 0.05 and 0.12 mm depending on the diameter of the cpx phenocrysts. For each unknown basalt sample, several cpx phenocryst grains were chosen for isotopic SIMS analysis after FTIR and EMP analysis, which show no-OH IR bands of hydrous minerals. The selected cpx grains are poked down from the doubly polished thin sections for SIMS, after the analyses of FTIR and EMP. Two cpx megacryst fragments are chosen as the standard materials to monitor the instrument drift of SIMS during analysis. Then these cpx grains were mounted in epoxy resin and polished to expose their interior, with standard procedures abrasive paper, in order from 9μ to 0.1μ. Then, the slices were washed by ethanol in ultrasonic cleaners and were coated with gold for analysis.

3.2 Analytical protocols

Realizing the aim of this thesis, much concern was paid to the technological approach in measuring the water contents of magma and the geochemical composition of the basalts. In this thesis; the water contents, chemical compositions, and Li as well as O isotope of cpx phenocrysts from the 9 Cenozoic alkali basalts in SE China were measured by FTIR and EPMA. The XRF (X-ray Fluorescence), ICP-MS (Inductively Coupled Plasma Mass Spectrometry), and TIMS (Thermal Ionization Mass Spectrometry) are used to analyze the bulk rock powders to get the composition of major elements, trace elements, and Sr-Nd and Pb isotope of Cenozoic basalts from 10 locations in SE China. For the precise and accurate analysis of Lithium and Oxygen isotope, the in-situ SIMS and appropriated standards are applied for cpx phenocrysts.

3.2.1 Major and trace element concentrations of the bulk rocks

Bulk rock major element concentrations of all samples except nine samples (six samples from XL in the Zhejiang region (XL-6 to -11, and XL-13), and three samples from NTS (NTS-4, -5, and -6) in the Fujian region) were determined at the Public Experiment Center at the University of Science and Technology of China (USTC) using XRF. Loss-on-ignition (LOI) was determined before XRF analysis. Analytical precision was better than ±5%, estimated from repeated analyses of GSR-3 (Chinese reference material, basalt standard).

For trace element analysis, sample powders (~50 mg) were dissolved with mixed acid (1:1 concentrated HF: HNO_3) in high-pressure Teflon bombs for 48 hours at ~190°C. Then, the solution was dried on a hot plate, and the residues were again dissolved in concentrated HNO_3. Finally, the solution was dried and then diluted to 80 g with 2% HNO_3 for analysis. The solution was analyzed using an Agilent 7500a ICP-MS instrument at the State Key Laboratory of Continental Dynamics at Northwest University, China. The precision of the measured trace element concentration was better than 5% for the repeatedly analyzed USGS standards, BCR-2, BHVO-2, AGV-2 and Chinese reference material, GSR-1.

Major and trace element concentrations of nine samples including six samples from XL in Zhejiang(XL-6 to -11, and XL-13), and three samples from NTS (NTS-4, -5 and -6) were measured at the ALS Company in Guangzhou, China, using the same methods and with the same analytical precision.

3.2.2 Sr-Nd-Pb isotopic compositions of the bulk rocks

Sr–Nd–Pb isotopic analyses (except all the XL samples, SC-1, BL-6, BL -7, BL-9, BL-11 and MX-11) were carried on Finnigan MAT-262 thermal ionization mass spectrometer (TIMS) at the Key Laboratory of Crust-Mantle Materials and Environments, Chinese Academy of Sciences (CMME-CAS) in USTC. Sample powders (~ 100 mg) were dissolved with a mixture of $HClO_4$-HF for 7 days in Teflon screw-crap beakers at 120°C. Finally, the solution was dried and then re-dissolved in HCl to prepare for element separation. Pb was leached from the solution and purified twice, first using AGI-X8 resin. Then, Sr was separated from the solution through a cation-exchange column filled with Bio-Rad resin. HDEHP resin was used to separate Nd from the remaining solution. During analyses, the $^{87}Sr/^{86}Sr$ ratios of the NBS987 standard were 0.710251 ± 0.000018 (2σ) and the $^{143}Nd/^{144}Nd$ ratios of the La Jolla

standard were 0.511870 ± 0.000016 (2σ). An NBS981 standard solution was repeatedly measured to correct the mass fractionation of the Pb isotope. Further details of the analytical techniques used for the Sr and Nd isotopes are given in Chen et al. (2002). The reported Sr and Nd isotopic ratios were normalized to $^{86}Sr/^{88}Sr = 0.1194$ and $^{146}Nd/^{144}Nd = 0.7219$ (Thirlwall, 1991), respectively.

Sr and Nd isotopic compositions of all the XL samples, SC-1, BL-6, BL -7, BL-9, BL-11 and MX-11 were measured on a Thermo TRITON *Plus* TIMS and on a Neptune plus, MC-ICP-MS NEPTUNE *Plus* with an Aridus II Desolvating Nebulizer System to enhance the sensitivity, respectively, at CRPG (Centre de Recherches Petrographiques et Geochimiques) in Nancy, France. Approximately 100 mg of sample powder was digested with a mixture of HF-HNO_3-$HClO_4$ (a few drops) in a screw-top Teflon beaker for 3 days at 130°C and then evaporated to dryness. The residues were re-dissolved with HCl (6 N) at 110°C for 2 days and were evaporated again and then re-dissolved in HCl (2.5 N) before an approximately 10% solution was loaded on Sr. Spec cation-exchange resin to separate Sr. Sr was then eluted from the resin and purified twice. The TRU. Spec resins were used to separate LREEs from the rest of the solution, and Nd was then eluted using LN. Spec resins. The measured $^{87}Sr/^{86}Sr$ ratios were corrected for mass fractionation by normalization to a $^{86}Sr/^{88}Sr$ ratio of 0.1194. The average value of the $^{87}Sr/^{86}Sr$ ratios in the NBS 987 standard analysis during the last 3 years was 0.710255 ± 0.000032 (2σ, n = 111) in CRPG. $^{143}Nd/^{144}Nd$ ratios were normalized to a $^{146}Nd/^{144}Nd$ ratio of 0.7219 to correct for mass fractionation. Both the JNdi-1 and La Jolla standards were used to control the reproducibility and accuracy of the measurements during each session. Average values of $^{143}Nd/^{144}Nd$ of the JNdi-1 and La Jolla standards during the last 3 years were 0.512082 ± 0.000027 and 0.511831 ± 0.000028 (2σ), respectively. The $^{143}Nd/^{144}Nd$ ratios were corrected relative to 0.511852, which is the accepted value of the La Jolla standard.

3.2.3 Approaches to measure the water content of basalts

For the first two aims of this thesis, precise and accurate measurements of the water content of magma are critical. The H_2O contents of the "initial" basaltic magmas can be approached by the direct measurement of melt inclusions captured by phenocrysts of basalts and of the quenched un-degassed glass for some kinds of basalts, or the indirect way recovered from the H_2O content of phenocrysts and the partition coefficients of H_2O between phenocrysts and basaltic melts. The most conventional

method to measure the water contents of magma are quenched un-degassed glass, special for some deep sea basalts, such as MORBs (Michael, 1995; Dixon, 1997), as well as the melt inclusions captured by early crystallized phenocrysts (Dixon and Clague, 2001; Sobolev and Shimizu, 2000). However, due to the restriction of the eruption and the preservation condition for the natural samples, the proper objects are rather limited. Quenched un-degassed glass is more suitable for the deep sea basalts, such as MORBs, seamount basalts which erupt under deep sea, fast cold down under high pressure. Nevertheless, the continental basalts do not only lack the glass, but also generally have undergone serious degassing and water loss, because of low erupting pressure. The water contents measured from inclusions are challenged by the measurement of apparatus and the preservation of water in early phenocrysts. SIMS and FTIR are the most common instruments used to analyze the water content of inclusions. The analysis of FTIR requires large enough size for inclusion bigger than 100μm atleast, if the thickness of double-polished section is considered. The careful blank control, instrumental corrections, proper standards and difficult sample preparation for the analysis of melt inclusion are the nightmare for most laboratories. The most important is that the diffusion of water is too fast between the melt inclusions and the host minerals. It is too hard to preserve its initial water information for the melt inclusions, unless the melt inclusions are big enough and the cooling of the lava is fast enough (Chen et al., 2011; Gaetani et al, 2012), specially for Cenozoic basalts in SE China. Therefore, the direct measurement for quenched un-degassed glass and captured melt inclusion is an impractical analysis plan for our study areas and objects.

Wade et al. (2008) used an Al-IV-dependent partitioning relationship to predict the magmatic water content from direct measurements of H_2O content in clinopyroxene phenocrysts (Fig. 3-1). All the phenocrysts in basalts are NAMs such as cpx, ol, and pl. O'Leary et al. (2010) measured and pooled the $D^{cpx/melt}$ for H_2O values together (Aubaud et al., 2004, 2008; Hauri et al., 2006; Tenner et al., 2009), then offered an equation of $D^{cpx/melt}$ based on the chemical compositions of the cpx phenocrysts, which are suitable for the wide range of the composition of the basaltic melts. The equation provided by O'Leary et al. (2010) based on the chemical compositions of the cpx phenocrysts can be applied on the melts of various Al_2O_3 contents (from 0.2 % to 19 %, i.e. including Al-free to high-Al basaltic melt) at 1.5 GPa pressure and 1275°C temperature, whose error is believed less than 15% (equation 10 in their paper). However, the widely suitable equation of $D^{pl/melt}$ H_2O is still not available. Meanwhile, the water in ol grains

is hard to be preserved, due to the very fast H loss caused by decompression, during the magma ascent (Peslier et al., 2008; Peslier et al., 2015). On the other hand, the uncertainty of applying the integral specific absorption coefficient for cpx (7.09 ppm^{-1} cm^{-2}, Bell et al. 1995) was expected to be <10%, with higher accuracy than that of pl. Due to the relatively high accurate and available $D^{cpx/melt}$, the cpx is one of the best approach to reversely calculate the magmatic water content from the H_2O contents of phenocrysts and the partition coefficients of H_2O between phenocrysts and basaltic melts. Wade et al. (2008) have tested their approach to calculate magmatic water content by the water content in phenocrysts from four arc volcanoes (Galunggung, Irazu, Arenal, and Augustine), compared with the results measured in olivine-hosted melt inclusions (Fig. 3-1). Both of the average and maximum magmatic H_2O contents calculated by the cpx phenocrysts have the error less than 15% of the H_2O contents measured from the melt inclusion for most of the samples.

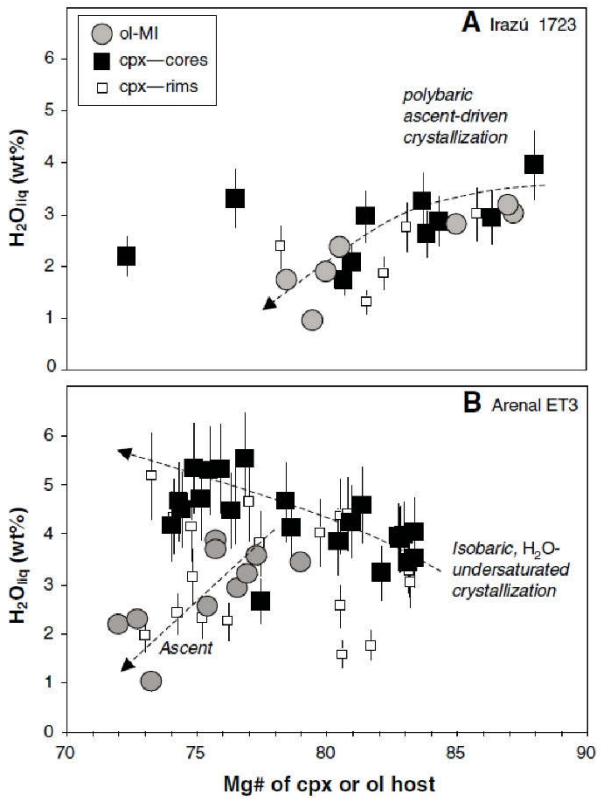

Fig. 3-1 Comparison of cpx and olivine-hosted melt inclusions H_2O and Mg#. Figure 4 of Wade et al. (2008). The error bar is 17%.

3.2.3.1 H_2O contents in cpx phenocrysts measured by FTIR

The H_2O contents (by weight) of cpx phenocrysts were measured on a Nicolet 5700 FTIR spectrometer coupled with a Continuμm microscope at CMME-CAS, at USTC (Fig. 3-2). The shift of the integral areas over absorption bands during analysis monitored by augite megacrysts standard T3 from Cenozoic basaltic volcano, in Jiangsu China is less than 4% (Fig. 3-3). Additional details of the analytical techniques are described in Xia et al. (2013) and Liu et al. (2015). A modified Beer-Lambert law ($c_{H_2O}=A/(I\times t)$) was used to calculate the H_2O content of cpx phenocrysts, where c_{H_2O} is the content of water (H_2O ppm wt.), A is the total integral absorption of -OH bands (cm^{-2}), which is 3 times the integral area of unpolarized absorption (Kovacs et al., 2008; Sambridge et al., 2008), I is the integral specific absorption coefficient (7.09 $ppm^{-1}cm^{-2}$ (Bell et al., 1995)), and *t* is the sample thickness (cm). Analytical uncertainty in the H_2O content of a single cpx phenocryst is less than 50% (Liu et al., 2015; Xia et al., 2013).

Fig. 3-2 Picture of the Nicolet 5700 FTIR spectrometer coupled with a microscope, located at USTC

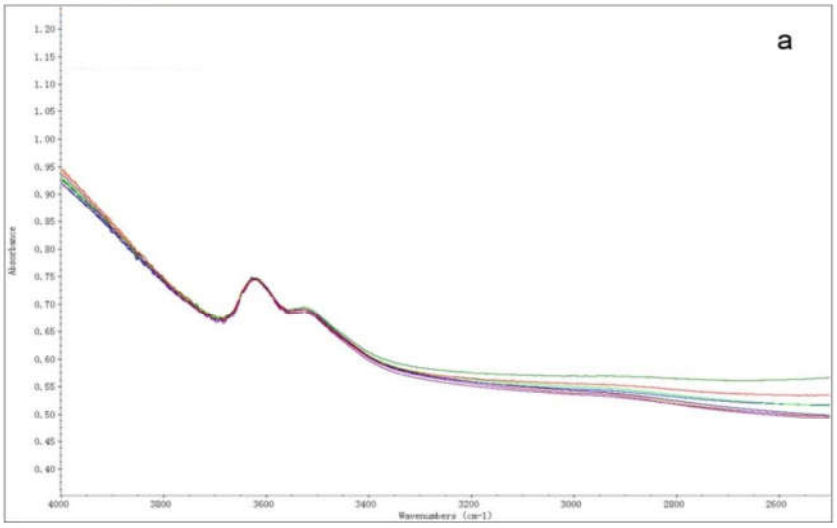

Fig. 3-3 The instrument shift during analysis monitored by augitic megacryst standard T3 from Cenozoic basaltic volcano, in Jiangsu China. The shift of the integral areas over absorption bands of T3 is less than 4%.

3.2.4 Chemical compositions of cpx phenocrysts by EPMA

The major element contents of the cpx phenocrysts were analyzed using a Shimadzu Electron Probe Micro analyzer (EPMA 1600) at CMME-CAS, in USTC, under the following operating conditions: 15 kV accelerating voltage, 20 nA beam current and 1 μm beam diameter. Natural minerals and synthetic oxides were used as standards, and a program based on the ZAF procedure was used for data correction. Analyzed points of the cpx phenocrysts were set within the corresponding FTIR analyzed region. Reproducibility is <1% for elements with concentrations >5% and <3% for elements with concentrations >1%.

The profiles of major element contents of cpx phenocrysts measured after SIMS analysis for Lithium were analyzed using a Cameca SX100 electron microprobe at the Service Commun de Microscopies Electroniques et de Microanalyses X (SCMEM), University of Lorraine (France). The operating conditions were set at an accelerating voltage of 20 kV and a beam current of 20 nA. Alkaline elements were analyzed first to minimize errors due to element migration with counting times of 10 s on peak and 5 s for backgrounds. For other elements, counting times were 20 s on peak and 10 s for backgrounds. Analyzed points of the cpx phenocrysts were set close to the corresponding SIMS analyzed points. Reproducibility is <1% for elements with concentrations >5% and <3% for elements with concentrations >1%.

Table 3-1 The chemical and Lithium isotopic compositions of cpx standards used for SIMS

Standard No.	06JY06CPX[a]	06JY29CPX[a]	06JY31CPX[a]		CLB25CPX	CLB35CPX
SiO_2	52.36	53.58	53.62	SiO_2	52.55	48.09
TiO_2	0.59	0.18	0.29	TiO_2	0.45	1.70
Al_2O_3	0.77	1.18	4.38	Al_2O_3	6.66	8.88
Cr_2O_3	5.09	4.33	1.22	Cr_2O_3	n.d.	n.d.
FeO	3.04	2.44	2.83	Fe_2O_3[b]	3.64	5.57
MnO	0.09	0.08	0.09	MnO	0.10	0.10
MgO	15.31	15.48	16.20	MgO	15.30	13.67
CaO	20.85	20.43	20.51	CaO	19.36	20.52
Na_2O	1.08	1.39	1.17	Na_2O	1.93	1.25
K_2O	0.01	0.01	0.01	K_2O	0.02	0.04
NiO	0.04	0.05	0.05	NiO	n.d.	n.d.
Total	99.23	99.15	100.37	Total	100.01	99.82
Mg#[a]	90.0	91.9	91.1			
				Mg#[c]	89.3	82.9
Si	1.94	1.97	1.93		1.90	1.78
Ti	0.02	0.00	0.01		0.01	0.05
Al	0.03	0.05	0.19		0.28	0.39
Cr	0.15	0.13	0.03		0.00	0.00
Fe	0.09	0.08	0.09		0.10	0.15
Mn	0.00	0.00	0.00		0.00	0.00
Mg	0.85	0.85	0.87		0.83	0.75
Ca	0.83	0.81	0.79		0.75	0.81
Na	0.08	0.10	0.08		0.14	0.09
K	0.00	0.00	0.00		0.00	0.00
Ni	0.00	0.00	0.00		0.00	0.00
Total	3.99	3.99	3.99		4.01	4.03
Li (ppm)	1.10	0.80	1.00		2.55	3.44
δ^7Li (‰)	1.30	-2.60	-2.40		-1.02	-5.68
2σ	0.04	0.53	0.45			

a The mean of their data source. (Su et al., 2015)
b This total ion content are obtained by SARM in CRPG.
c Mg# are re-calculated by the reference materials, which may not as same as the values in their source.

Table 3-2 Replicate analyses for Lithium isotope of the cpx standards.

Analysis Name	^{6}Li	^{7}Li	d ^{7}Li /^{6}Li	Error	SD
NSH9-11@1	3840	48276	46.4	1.0	0.7
NSH9-11@2	3874	48641	45.0	0.9	
NSH9-11@3	3435	43141	46.5	0.8	
NSH9-11@4	3658	45939	45.4	0.8	
NSH9-11@5	3357	42127	45.3	1.0	
NSH9-11@6	3491	43776	44.6	1.0	
NSH9-13@1	3467	43351	41.2	1.1	0.8
NSH9-13@2	2265	28286	41.3	1.5	
NSH9-13@3	2260	28216	41.4	1.5	
NSH9-13@4	2555	31908	43.0	1.1	
NSH9-13@5	2595	32348	40.7	1.3	

3.2.5 In-situ Li and O isotopic analysis of cpx phenocrysts

3.2.5.1 Secondary ion mass spectrometry

The SIMS consists of a primary ion source, a mass spectrometer and a secondary ion detection system (Fig. 3-4), which can quantitatively detect in situ all the elements (especially for light elements, e.g., H, Li, Be, B) reaching detection limits of part per million. The primary ions generally are O^- or Cs^+ ions for geological materials. The O^- source is usually used to generate the positive ions such as Lithium, whereas the Cs^+ source is used to generate the negative ions, such as Oxygen. Primary ions bombard the sample surface with high energy (4 to 20 keV) after focused by a series of electrostatic lenses at proper intensity and beam spot size. The energy of primary ions are transferred to samples. Some atoms obtained energy will break away from sample surface, as secondary ions (Fig. 3-5) and are accelerated by an electric field (Fig. 3-4). The secondary ions are commonly complex, due to uncertainty of the breaking of sample matrix. Then the secondary ions are transferred to mass spectrometry and go through the entrance slit. The SIMS has high resolution mass spectrometer to distinguish different ions and capture out interesting information. The collectors of SIMS usually are Faraday cups and single-ion detectors (electron multiplier), which are used to collect ions with intensities higher and lower than 10^6cps, respectively. Here a noun of 'dead time' is introduced to describe the resetting ability of ion counting systems. The dead time refers to the time after each event during which the system cannot record another event, in the detection systems (SIMS) used to record discrete events, such as electron multiplier. The ion counting systems will lose the counts of secondary ions if two pulses of secondary ions arrive at the detector almost simultaneously before the detector are reset (Deloule et al., 1991). Each element and isotope in different analytical session have its own dead times (Zinner et al., 1986), therefore, "dead time" will be measured at the beginning of every analytical session. The in situ ion microprobe analyses have been performed on Cameca IMS-1270 and IMS-1280 at CRPG-CNRS in Nancy, France (Fig. 3-6).

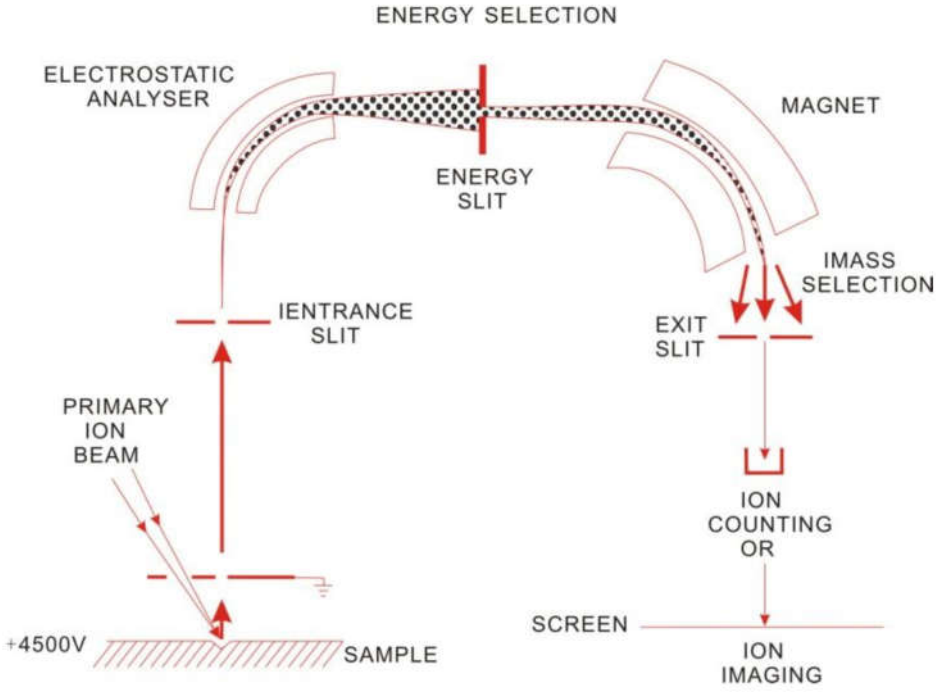

Fig. 3-4 Illustration to represent ion microprobe

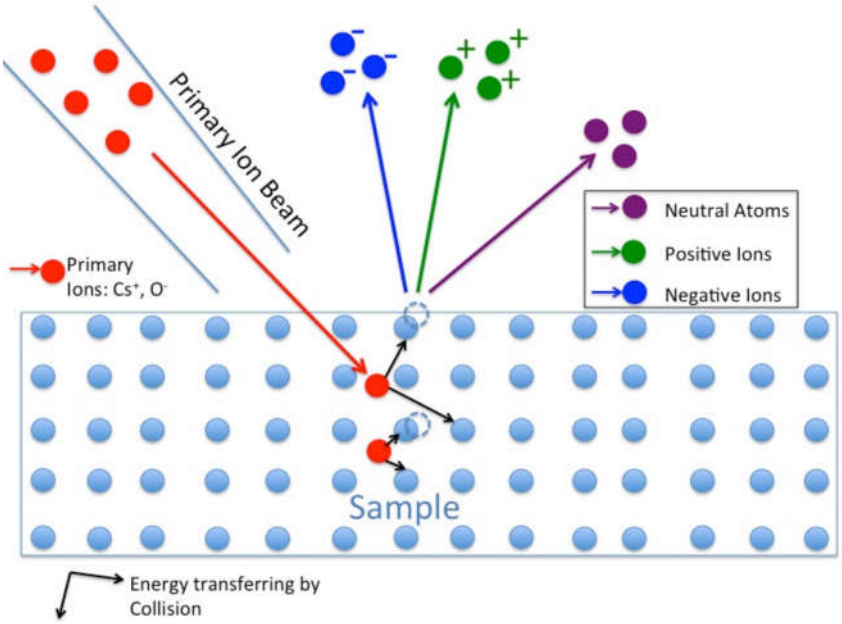

Fig. 3-5 A sketch illustrating the generation of secondary ions

Table 3-3. The chemical composition and $\delta^{18}O$ of cpx standards used for SIMS.

Mineral type	Megacryst	Megacryst	Megacryst	Megacryst	Megacryst	Peridotite	Peridotite	Peridotite		Peridotite	Peridotite
Standard No.	NSH-2	NSH-5	NSH-8	NSH-14	NSH-9	06JY06CPX	06JY29CPX	06JY31CPX		CLB25CPX	CLB35CPX
SiO_2	48.84	50.69	49.42	49.04	50.22	52.36	53.58	53.62	SiO_2	52.55	48.09
TiO_2	1.52	0.82	1.04	1.47	0.89	0.59	0.18	0.29	TiO_2	0.45	1.70
Al_2O_3	9.68	8.20	8.98	9.82	8.50	0.77	1.18	4.38	Al_2O_3	6.66	8.88
Cr_2O_3	0.02	0.00	0.00	0.01	0.00	5.09	4.33	1.22	Cr_2O_3	n.d.	n.d.
FeO	7.84	6.54	6.97	8.02	6.55	3.04	2.44	2.83	Fe_2O_3[b]	3.64	5.57
MnO	0.13	0.08	0.11	0.13	0.18	0.09	0.08	0.09	MnO	0.10	0.10
MgO	11.80	14.99	13.68	11.35	14.74	15.31	15.48	16.20	MgO	15.30	13.67
CaO	17.63	16.87	16.53	17.42	16.43	20.85	20.43	20.51	CaO	19.36	20.52
Na_2O	1.94	0.02	1.81	2.11	1.42	1.08	1.39	1.17	Na_2O	1.93	1.25
K_2O	0.01	1.56	0.02	0.01	n.d.	0.01	0.01	0.01	K_2O	0.02	0.04
NiO	0.00	0.01	0.00	0.00	0.00	0.04	0.05	0.05	NiO	n.d.	n.d.
Total	99.41	99.78	98.56	99.38	98.93	99.23	99.15	100.37	Total	100.01	99.82
Mg#[a]	72.85	80.34	77.77	71.61	80.04	89.98	91.86	91.07	Mg#[a]	89.28	82.94
$\delta^{18}O$ (‰)	5.46	5.88	5.99	5.07	5.33						
2σ	0.07	0.02	0.12	0.15	0.21						
Li (ppm)						1.10	0.80	1.00		2.55	3.44
δ^7Li (‰)						1.30	-2.60	-2.40		-1.02	-5.68
2σ						0.04	0.53	0.45			

a Mg# are re-calculated by the reference materials, which may not as same as the values in their source.
b This total ion content are obtained by SARM in CRPG.

3.2.5.2 In-situ $\delta^{18}O$ analysis

The traditional analytical protocols of Oxygen are usually constrained on the analysis level of bulk rock powder or single mineral grain. The meaning of whole rock $\delta^{18}O$ data has ambiguities. The whole rock $\delta^{18}O$-values have been documented more subtle and resolvable for differences among different types of basaltic lavas and minerals, by later laser-based extraction analysis methods based on small amounts of separated mineral phases (e.g. Eiler et al. 1996, 2000; Dorendorf et al. 2000; Cooper et al. 2004; Bindeman et al. 2004, 2005). The limited spatial resolution of Oxygen traditional analytical protocols constrain the measurement of basalt phenocrysts in situ to study the evolution process of magma in different stages. SIMS analysis show unique superiority of spatial resolution for analysis of isotope and spatial resolution in micro-scale mineral grain samples.

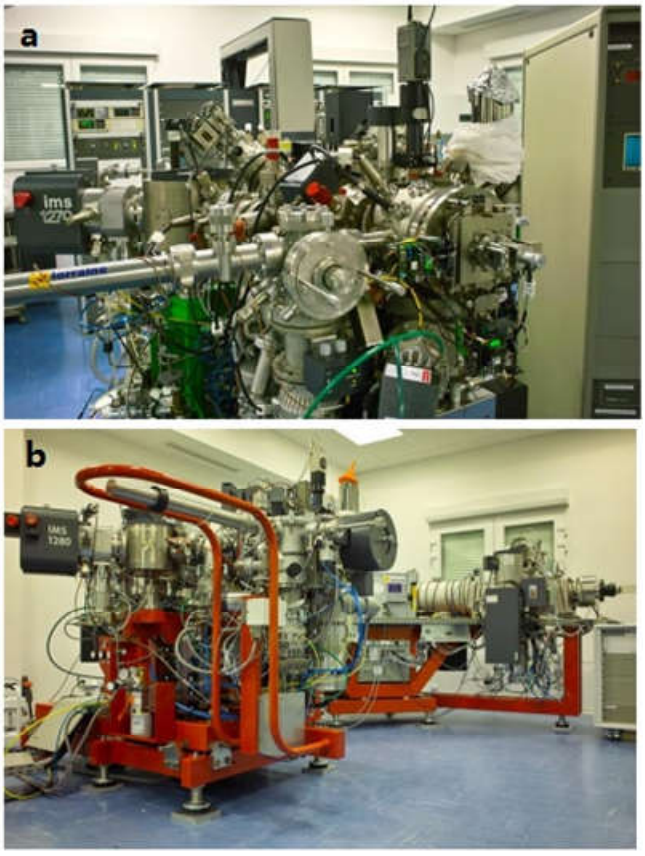

Fig. 3-6 (a) Pictures for the Cameca IMS 1270 and (b) Pictures for the Cameca 1280HR2, located at CRPG, Nancy

To sputter the secondary negative ions ($^{16}O^-$ and $^{18}O^-$), a primary beam of Cs^+ was used at intensities ranging from 8 to 15nA, with a diameter of about 20 μm. An electron flood gun incidence was used to compensate sample charging. The negative secondary ions of $^{18}O^-$ and $^{16}O^-$ counting rates range from 1.2×10^9 to 2×10^9cps and 4×10^6 to 5×10^6 cps, mostly depending on the intensity of the primary beam. The oxygen secondary ions were accelerated through 10 kV and counted by two off-axis Faraday cups, L02 for $^{16}O^-$ and H1 for $^{18}O^-$ in multi-collection mode. The mass resolution was set at 3000 (M/ΔM) to separate isobaric $^{17}OH^-$ or $H_2{}^{16}O^-$ from $^{18}O^-$ and an energy slit were opened at 45 eV without energy offset. To elevate reproducibility, before each analysis of cpx grain, the primary beam and electron beam were tuned carefully, and then the secondary beam were automatically centered again by SIMS, before each measurement. Each analysis session contained a pre-sputtering of 60 s, automated centering and 40 cycles with the counting times of 4.96 s for $^{16}O^-$ and $^{18}O^-$. The internal precision for one spot analysis was usually better than 0.1‰ (2r). Oxygen isotopic composition is expressed as $\delta^{18}O$, relative to Vienna Standard Mean Ocean Water (VSMOW, Gonfiantini (1978)), i.e. $\delta^{18}O = [(^{18}O/^{16}O)_{sample}/(^{18}O/^{16}O)_{V\text{-}SMOW}-1]\times1000$

To calibrate the offset between the true values and the measured values, caused by instrumental mass fractionation (IMF), defined as ΔI_O ($=\delta^{18}O_{SIMS}-\delta^{18}O_{reference}$). ΔI_O consists of matrix effect and the drift of instrument. In chemical analysis, matrix refers to the components of a sample other than the analyte of interest (IUPAC, 1997), which can considerably effect on the conducted analysis and the obtained result quality. Such effects are called matrix effects. The effect which is usually considered correlation to the compositions of cpx, suggested by Gurenko et al. (2001). A series of cpx megacrysts hosted by basanites in Nushan, Eastern China are used, including NSH2, NSH5, NSH8 and NSH14, whose oxygen isotopic ratios were obtained by the laser fluorination method, reported by Xia et al. (2004), listed in Table 3-3, and whose chemical composition is very close to those of the cpx phenocrysts analyzed in this study. The IMF correction of samples analysis is made up by two parts: 1) the matrix effect calculated by the Mg# of unknown sample and the matrix effect line built by cpx standards; 2) the drift of instrument, which is calibrated by the $\delta^{18}O$ difference between cpx standards on the sample holder and the same one on the holder of standards. The $\delta^{18}O$ IMF of the Nushan standards decreases with the Mg# decreasing, and the R^2 usually are better than 0.9 (Fig. 3-7). Meanwhile, to trace a possible instrumental drift during analysis, a reference standard cpx NSH9 or NSH5 was fixed on every section

and was measured repeatedly per 2-4 cpx grain analyses (i.e. 5-15 analyses of points). The raw analytical results of the standard (NSH9 or NSH5) and the Fujian cpx phenocrysts are listed in Table 3-4. The $\delta^{18}O$ IMF of replicate analyses of Nushan standard on several sections are presented in Fig. 3-8, indicating the SIMS drift is limited during every analysis session. The general combined internal precision and external accuracy is better than 0.5‰ (2SD) for each cpx grain.

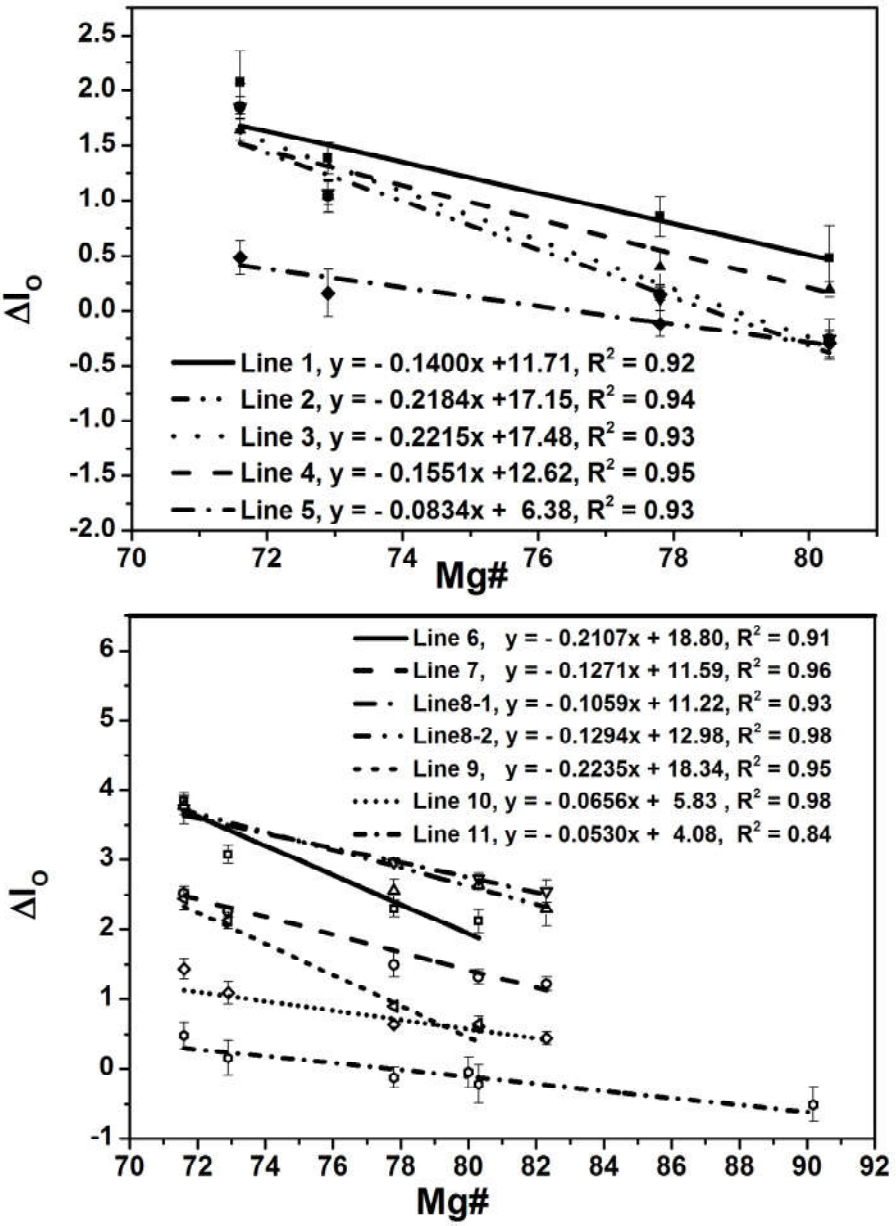

Fig. 3-7 The relation between IMF and the Mg# of cpx standards for Oxygen

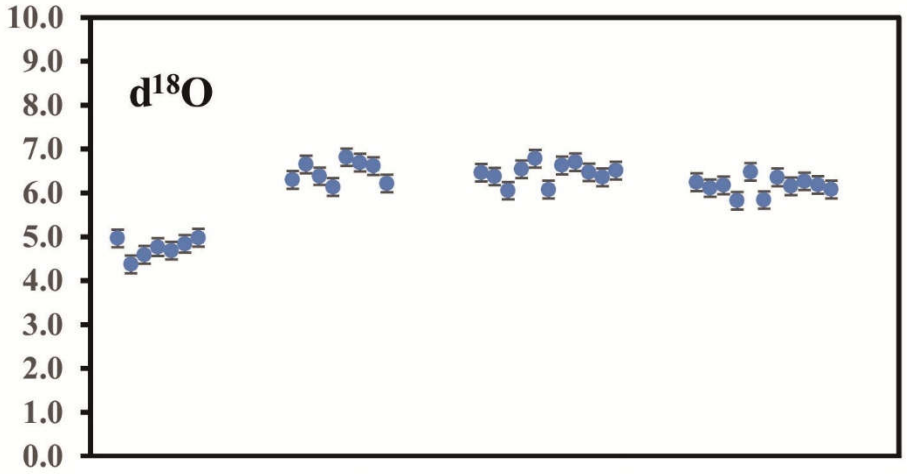

Fig. 3-8 The duplicate analysis of the cpx standards for Oxygen isotope

3.2.5.3 In-situ Li isotope composition

An O^- primary beam was accelerated at 13 kV, with an intensity ranging from 8 to 15 nA, to sputter the secondary positive ions of $^7Li^+$ and $^6Li^+$. The elliptical spot area diameter was approximately 20-30 μm. The secondary ions of Li were accelerated through 10 kV and were counted using an electron multiplier in mono counting mode. The counting rates of $^7Li^+$ and $^6Li^+$ depended on the Li contents of samples and the intensity of the primary beam. The mass resolution was set at 1100 (M/ΔM) to separate the isobaric inference of $^6LiH^+$ on $^7Li^+$. After a pre-sputtering of 120 s, 30 cycles were accumulated with the counting times of 16 s for $^6Li^+$, 4 s for $^7Li^+$ and 4 s for background at the 5.8 relative atomic mass. Li isotopic composition is expressed as δ^7Li, relative to the National Institute of Standards L-SVEC ($^7Li/^6Li$=12.0192, Flesch et al. (1973)), i.e. $\delta^7Li = [(^7Li/^6Li)_{sample}/(^7Li/^6Li)_{L\text{-}SVEC} -1]\times1000$ (‰).

The $^7Li/^6Li$ variations of magmatic phenocrysts are noticed to deduce the cooling history in their parent magmas, and to infer the mantle source processes and the feature of mantle reservoirs. The high spatial resolution of SIMS allows to measure intra-granular profiles of Li concentration and isotope to infer diffusion-process and the variations of surroundings. The SIMS results of unknown samples calibrated by known standards are different from their true values, when the compositions of unknown samples are not close to used standards (Bell et al., 2009; Gurenko et al., 2001). The matrix effects are defined as $\Delta I_{Li} = \delta^7Li_{SIMS} - \delta^7Li_{reference}$ (Decitre et al., 2002). In general,

ΔI_{Li} varies due to change of the instrumental settings or aging of electron multiplier ages between different analytical sessions (Deloule et al., 1992). Decitre et al. (2002) and some other studies considered the matrix effect of Li in SIMS is negligible (Barrat et al., 2005; Beck et al., 2004; Beck et al., 2006), and the IMF of Li in cpx can use the calibration from any kind of reference standard, such as glass. Later studies suggested possible matrix effect in the analysis of Li isotope by SIMS (Kasemann et al., 2005; Herig et al., 2004; Jeffcoate et al., 2007). However, the correlation between the composition of cpx and the matrix effect for analysis by SIMS remain mystery (Decitre et al., 2002; Su et al., 2015). The various matrix effect usually are considered to link to the compositions of samples for Li isotopic system, like that for ol. Bell et al. (2009) and Su et al. (2015) studied the olivine and found that the matrix effect have a relationship to its composition, such as Mg# (Mg# = Mol_{Mg} / (Mol_{Mg} + Mol_{Fe})*100). A series of standard minerals from mantle xenoliths, described in detail by Su et al. (2015) and Xiao et al. (2015), are used to calibrate the offset between the true values and the measured values. The Li concentrations are calculated by comparing the average rates of the ^{7}Li cps (counting per second) of standard, because the sputtered ^{7}Li of specimens can be regarded as being divided by an average ion yield of these standards. The estimated precision of such procedure should be better than 20%. The replicate analyses results for Lithium isotopic data of the standard cpx are listed in Table 3-2 and plotted in Fig. 3-9.

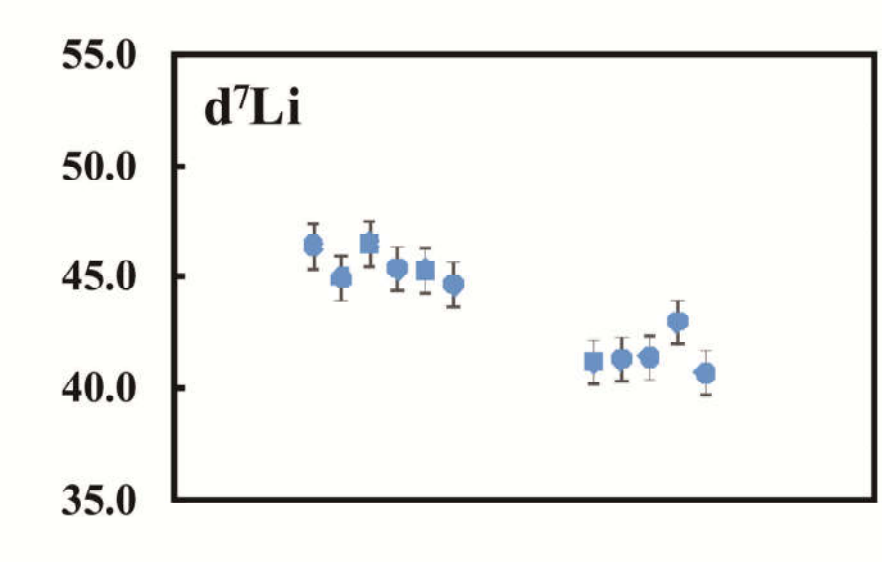

Fig. 3-9 The duplicate analysis of the cpx standards for Lithium isotopic data

The Li concentration and isotopic composition, and major compositions of 06JY06 cpx and 06JY29 cpx follow those in Su et al. (2015), while the Li concentration and isotopic composition, major compositions of CLB-25 cpx and CLB-35 cpx were measured by MC-ICP-MS and SARM/EMP in CRPG, the reference values of standard in detail are presented in Table 3-1. Based on the Li isotope analyses on this series mantle cpx standards, a strong relationship between the composition of cpx and the matrix effect are obtained comparing the results measured by MC-ICP-MS/LA-ICP-MS and SIMS. Our observation prompt that the recognition of the matrix effect of cpx in Li isotopic system in the analysis of SIMS can be calibrated by its composition.

Table 3-4 The raw results and average of SIMS analyses and IMF of Nushan cpx standards for $\delta^{18}O$.

	Analysis Name	d 18O /16O	Error	Mg#	IMF
13/10/2015	NSH14cpx@1	7.1	0.1	71.6	2.0
	NSH14cpx@2	6.8	0.1	71.6	1.8
	NSH14cpx@3	7.6	0.0	71.6	2.6
	NSH14cpx@4	7.3	0.1	71.6	2.2
	NSH14cpx@5	6.9	0.1	71.6	1.8
	NSH8cpx-a@1	6.8	0.1	77.8	0.8
	NSH8cpx-a@2	6.5	0.1	77.8	0.5
	NSH8cpx-a@3	7.1	0.1	77.8	1.1
	NSH8cpx-a@4	6.9	0.1	77.8	0.9
	NSH8cpx-a@5	6.9	0.1	77.8	0.9
	NSH8cpx-a@6	7.0	0.1	77.8	1.1
	NSH8cpx-a@7	6.7	0.1	77.8	0.7
	NSH8cpx-a@8	6.8	0.1	77.8	0.8
	NSH2cpx-a@1	6.9	0.1	72.9	1.5
	NSH2cpx-a@2	6.9	0.1	72.9	1.4
	NSH2cpx-a@3	6.6	0.1	72.9	1.1
	NSH2cpx-a@4	7.0	0.1	72.9	1.5
	NSH5cpx-a@1	6.3	0.1	80.3	0.4
	NSH5cpx-a@2	5.9	0.1	80.3	0.0
	NSH5cpx-a@3	6.7	0.1	80.3	0.8
	NSH5cpx-a@4	6.6	0.1	80.3	0.7
	NSH9CP@1	6.3	0.1	80.0	1.0
	NSH9CP@2	6.6	0.1	80.0	1.3
	NSH9CP@3	6.4	0.1	80.0	1.1
	NSH9CP@4	6.1	0.1	80.0	0.8
	NSH9CP@5	6.8	0.1	80.0	1.5
	NSH9cpx-a@1	6.7	0.1	80.0	1.4
	NSH9cpx-a@2	6.6	0.1	80.0	1.3
	NSH9cpx-a@3	6.2	0.1	80.0	0.9
14/10/2015	NSH14cpx-c@1	7.2	0.1	71.6	2.1
	NSH14cpx-c@2	6.5	0.1	71.6	1.4
	NSH14cpx-c@3	7.1	0.1	71.6	2.0
	NSH5cpx-c@1	6.0	0.1	80.3	0.1
	NSH5cpx-c@2	5.7	0.1	80.3	-0.2
	NSH5cpx-c@3	5.6	0.1	80.3	-0.2
	NSH5cpx-c@4	5.4	0.1	80.3	-0.4
	NSH8cpx-c@1	6.2	0.1	77.8	0.2
	NSH8cpx-c@2	6.2	0.1	77.8	0.2

	NSH8cpx-c@3	6.1	0.1	77.8	0.1
	NSH8cpx-c@4	6.1	0.1	77.8	0.1
	NSH2cpx-c@5	6.7	0.1	72.9	1.2
	NSH2cpx-c@7	6.4	0.1	72.9	0.9
15/10/2015	NSH5cpx-d@5	6.6	0.1	80.3	0.7
	NSH5cpx-d@6	6.4	0.0	80.3	0.5
	NSH5cpx-d@7	6.1	0.1	80.3	0.2
	NSH5cpx-d@8	6.3	0.1	80.3	0.5
	NSH8cpx-d@5	6.3	0.1	77.8	0.3
	NSH8cpx-d@6	6.1	0.1	77.8	0.1
	NSH8cpx-d@7	6.6	0.0	77.8	0.6
	NSH8cpx-d@8	6.3	0.1	77.8	0.3
	NSH2cpx-d@5	6.7	0.1	72.9	1.2
	NSH2cpx-d@6	6.3	0.1	72.9	0.8
	NSH2cpx-d@7	6.5	0.1	72.9	1.1
	NSH2cpx-d@8	6.5	0.1	72.9	1.0
	NSH14cpx-d@5	6.8	0.1	71.6	1.7
	NSH14cpx-d@6	6.6	0.0	71.6	1.5
	NSH14cpx-d@7	6.6	0.1	71.6	1.5
	NSH14cpx-d@8	6.8	0.1	71.6	1.8
	NSH5cpx-d@9	6.1	0.1	80.3	0.3
	NSH5cpx-d@11	6.0	0.1	80.3	0.1
	NSH5cpx-d@12	6.1	0.1	80.3	0.2
	NSH8cpx-d@9	6.4	0.1	77.8	0.5
	NSH8cpx-d@10	6.3	0.0	77.8	0.3
	NSH8cpx-d@11	6.6	0.1	77.8	0.6
	NSH8cpx-d@12	6.5	0.1	77.8	0.5
	NSH5cpx-e@7	5.6	0.1	80.3	-0.3
16/10/2015	NSH5cpx-e@8	5.8	0.1	80.3	-0.1
	NSH5cpx-e@9	5.7	0.1	80.3	-0.2
	NSH5cpx-e@10	5.4	0.1	80.3	-0.4
	NSH14cpx-e@1	7.0	0.1	71.6	1.9
	NSH14cpx-e@2	7.1	0.1	71.6	2.1
	NSH14cpx-e@3	6.9	0.1	71.6	1.8
	NSH14cpx-e@4	6.9	0.1	71.6	1.9
	NSH14cpx-e@5	6.6	0.1	71.6	1.6

	NSH2cpx-e@1	6.7	0.1	72.9	1.3
	NSH2cpx-e@2	6.2	0.1	72.9	0.7
	NSH2cpx-e@5	6.6	0.1	72.9	1.2
	NSH2cpx-e@6	6.4	0.1	72.9	0.9
	NSH2cpx-e@7	6.8	0.1	72.9	1.3
	NSH8cpx-e@1	5.9	0.1	77.8	-0.1
	NSH8cpx-e@5	6.2	0.1	77.8	0.2
	NSH8cpx-e@7	6.4	0.1	77.8	0.4
	NSH8cpx-e@8	6.1	0.1	77.8	0.1
	NSH8cpx-e@9	5.8	0.0	77.8	-0.2
	NSH8cpx-e@11	6.3	0.1	77.8	0.4
	NSH2cpx-e@8	6.7	0.1	72.9	1.2
	NSH2cpx-e@9	6.4	0.1	72.9	0.9
	NSH2cpx-e@10	6.5	0.1	72.9	1.1
17/10/2015	NSH5cpx-f@2	6.2	0.1	80.3	0.4
	NSH5cpx-f@3	6.1	0.1	80.3	0.2
	NSH5cpx-f@5	6.2	0.1	80.3	0.3
	NSH5cpx-f@6	5.8	0.1	80.3	-0.1
	NSH8cpx-f@2	6.6	0.1	77.8	0.6
	NSH8cpx-f@3	6.2	0.1	77.8	0.2
	NSH8cpx-f@5	6.5	0.1	77.8	0.5
	NSH8cpx-f@4	6.0	0.1	77.8	0.1
	NSH8cpx-f@6	6.4	0.1	77.8	0.4
	NSH8cpx-f@7	6.3	0.1	77.8	0.3
	NSH8cpx-f@9	6.4	0.1	77.8	0.4
	NSH8cpx-f@10	6.1	0.1	77.8	0.1
	NSH2cpx-f@1	6.8	0.1	72.9	1.3
	NSH2cpx-f@3	6.9	0.1	72.9	1.5
	NSH2cpx-f@4	6.6	0.1	72.9	1.1
	NSH2cpx-f@5	6.5	0.1	72.9	1.1
	NSH14cpx-f@1	6.2	0.1	71.6	1.2
	NSH14cpx-f@2	6.5	0.1	71.6	1.4
	NSH14cpx-f@3	6.9	0.1	71.6	1.8
	NSH14cpx-f@4	6.5	0.1	71.6	1.4
	NSH5cpx-f@2	6.2	0.1	80.3	0.4
	NSH5cpx-f@3	6.1	0.1	80.3	0.2
	NSH5cpx-f@5	6.2	0.1	80.3	0.3
	NSH5cpx-f@6	5.8	0.1	80.3	-0.1
	NSH5cpx-f@7	6.5	0.1	80.3	0.6

	NSH5cpx-f@8	5.8	0.1	80.3	0.0
	NSH5cpx-f@10	6.4	0.1	80.3	0.5
	NSH5cpx-f@11	6.2	0.1	80.3	0.3
	NSH5cpx-f@12	6.3	0.1	80.3	0.4
	NSH5cpx-f@13	6.2	0.1	80.3	0.3
	NSH5cpx-f@14	6.1	0.1	80.3	0.2
18/10/2015	NSH5cpx-g@1	5.5	0.0	80.3	-0.4
	NSH5cpx-g@2	5.9	0.1	80.3	0.0
	NSH5cpx-g@3	5.7	0.1	80.3	-0.2
	NSH8cpx-g@1	5.7	0.1	77.8	-0.3
	NSH8cpx-g@2	5.2	0.1	0.0	-0.8
	NSH8cpx-g@3	5.2	0.1	0.0	-0.8
	NSH2cpx-g@1	5.9	0.1	72.9	0.4
	NSH2cpx-g@2	5.7	0.1	72.9	0.2
	NSH2cpx-g@3	5.3	0.1	72.9	-0.1
	NSH14cpx-g@1	5.7	0.1	71.6	0.6
	NSH14cpx-g@2	5.6	0.0	71.6	0.5
	NSH14cpx-g@3	5.3	0.1	71.6	0.3
	NSH5cpx-g@4	5.7	0.1	80.3	-0.2
	NSH5cpx-g@5	5.6	0.1	80.3	-0.2
	NSH5cpx-g@6	5.4	0.1	80.3	-0.5
	NSH8cpx-g@4	6.0	0.1	77.8	0.0
	NSH8cpx-g@5	5.9	0.1	77.8	-0.1
	NSH8cpx-g@6	5.7	0.0	77.8	-0.3

			Mean IMF	2SD
10/13/2015	NSH2cpx	72.9	1.4	0.1
	NSH5cpx	80.3	0.5	0.3
	NSH8cpx	77.8	0.9	0.2
	NSH14cpx	71.6	2.1	0.3
10/14/2015	NSH2cpx	72.9	1.0	0.2
	NSH5cpx	80.3	-0.3	0.2
	NSH8cpx	77.8	0.2	0.1
	NSH14cpx	71.6	1.9	0.3
10/15/2015	NSH2cpx	72.9	1.0	0.1
	NSH5cpx	80.3	0.2	0.1
	NSH8cpx	77.8	0.4	0.2
	NSH14cpx	71.6	1.6	0.1
10/16/2015	NSH2cpx	72.9	1.1	0.1
	NSH5cpx	80.3	-0.3	0.1

	NSH8cpx	77.8	0.1	0.1
	NSH14cpx	71.6	1.8	0.1
10/17/2015	NSH2cpx	72.9	1.2	0.2
	NSH5cpx	80.3	0.2	0.2
	NSH8cpx	77.8	0.3	0.2
	NSH14cpx	71.6	1.5	0.2
10/18/2015	NSH2cpx	72.9	0.2	0.2
	NSH5cpx	80.3	-0.3	0.1
	NSH8cpx	77.8	-0.1	0.1
	NSH14cpx	71.6	0.5	0.2
12/07/2015	NSH2cpx	72.9	1.9	0.0
	NSH5cpx	80.3	0.6	0.1
	NSH8cpx	77.8	1.5	0.0
	NSH14cpx	71.6	2.6	0.0
12/08/2015	NSH2cpx	72.9	3.3	0.0
	NSH5cpx	80.3	1.0	0.1
	NSH8cpx	77.8	1.5	0.1
	NSH14cpx	71.6	3.7	0.1
12/09/2015	NSH2cpx	72.9	3.2	0.2
	NSH5cpx	80.3	2.6	0.1
	NSH8cpx	77.8	2.8	0.2
	NSH14cpx	71.6	3.7	0.1
	NSH10cpx	82.3	2.6	0.1
12/10/2015	NSH2cpx	72.9	3.1	0.1
	NSH5cpx	80.3	2.1	0.2
	NSH8cpx	77.8	2.3	0.1
	NSH14cpx	71.6	3.8	0.1
12/11/2015	NSH2cpx	72.9	2.3	0.1
	NSH5cpx	80.3	1.3	0.1
	NSH8cpx	77.8	1.5	0.2
	NSH14cpx	71.6	2.5	0.1
	NSH10cpx	82.3	1.2	0.1
12/12/2015	NSH5cpx	80.3	2.6	0.1
	NSH8cpx	77.8	2.6	0.2
	NSH14cpx	71.6	3.8	0.1
	NSH10cpx	82.3	2.3	0.3
	NSH10cpx	82.3	2.6	0.2
	NSH5cpx	80.3	2.7	0.1
	NSH8cpx	77.8	3.0	0.1
	NSH14cpx	71.6	3.7	0.2

	NSH2cpx	72.9	2.9	0.1
01/05/2016	NSH2cpx	72.9	1.1	0.2
	NSH5cpx	80.3	0.6	0.0
	NSH8cpx	77.8	0.6	0.0
	NSH14cpx	71.6	1.4	0.2
	NSH10cpx	82.3	0.5	0.1
01/06/2016	NSH2cpx	72.9	2.1	0.1
	NSH5cpx	80.3	0.7	0.1
	NSH8cpx	77.8	0.9	0.0
	NSH14cpx	71.6	2.5	0.2
	NSH10cpx	82.3	0.6	0.1
02/05/2016	NSH2cpx	72.9	1.1	0.1
	NSH5cpx	80.3	0.3	0.1
	NSH8cpx	77.8	0.9	0.0
	NSH14cpx	71.6	1.6	0.2
	NSH10cpx	82.3	0.2	0.3

Table 3-5 Replicate analyses results for $\delta^{18}O$ of the cpx standards.

Session No.	Standard No.	Measure $\delta^{18}O$	Error	IMF	SD
1	NSH-cpx-12@1	5.0	0.1	-0.4	0.2
	NSH-cpx-12@2	4.4	0.1	-1.0	
	NSH-cpx-12@3	4.6	0.0	-0.7	
	NSH-cpx-12@4	4.8	0.1	-0.6	
	NSH-cpx-12@5	4.7	0.1	-0.6	
	NSH-cpx-12@6	4.8	0.1	-0.5	
	NSH-cpx-12@7	5.0	0.1	-0.4	
2	NSH-CPX@1	6.3	0.1	1.0	0.2
	NSH-CPX@2	6.6	0.1	1.3	
	NSH-CPX@3	6.4	0.1	1.1	
	NSH-CPX@4	6.1	0.1	0.8	
	NSH-CPX@5	6.8	0.1	1.5	
	NSH-CPX@6	6.7	0.1	1.4	
	NSH-CPX@7	6.6	0.1	1.3	
	NSH-CPX@8	6.2	0.1	0.9	
3	NSH-cpx-b@1	6.5	0.1	1.1	0.2
	NSH-cpx-b@2	6.4	0.1	1.0	
	NSH-cpx-b@3	6.1	0.1	0.7	
	NSH-cpx-b@4	6.5	0.1	1.2	
	NSH-cpx-b@5	6.8	0.1	1.5	
	NSH-cpx-b@6	6.1	0.1	0.7	
	NSH-cpx-b@7	6.6	0.1	1.3	
	NSH-cpx-b@8	6.7	0.1	1.4	
	NSH-cpx-b@9	6.5	0.1	1.1	
	NSH-cpx-b@10	6.4	0.1	1.0	
	NSH-cpx-b@11	6.5	0.1	1.2	
4	NSH-cpx-f@1	6.2	0.1	0.4	0.2
	NSH-cpx-f@2	6.1	0.1	0.2	
	NSH-cpx-f@3	6.2	0.1	0.3	
	NSH-cpx-f@4	5.8	0.1	-0.1	
	NSH-cpx-f@5	6.5	0.1	0.6	
	NSH-cpx-f@6	5.8	0.1	0.0	
	NSH-cpx-f@7	6.4	0.1	0.5	
	NSH-cpx-f@8	6.2	0.1	0.3	
	NSH-cpx-f@9	6.3	0.1	0.4	
	NSH-cpx-f@10	6.2	0.1	0.3	
	NSH-cpx-f@11	6.1	0.1	0.2	

Chapter 4 Calibration of matrix effect in Li isotope analysis of cpx by SIMS

4.1 Calibration of IMF by the composition of cpx

To measure the Li isotopic composition of unknown cpx samples by SIMS, the accurate calibration based on a series of cpx standard with similar composition to the unknown samples of IMF are required. The composition of cpx standards from the peridotites (Table 3-1) are used to calibrate the potential matrix effect for the Li isotope analyzed through SIMS. The Li isotopic data results of the peridotite standards of every analysis point are listed in Table 4-1. The raw Li isotope data are represented as [cps (^{7}Li) /cps (^{6}Li)]$_{SIMS}$. So the Li isotope ratios of [cps (^{7}Li)/cps (^{6}Li)]$_{unknown,\ true}$ are expressed as:

$$\delta^7Li_{\ L\text{-}SVEC} = 1000*\{cps\ (^7Li)/cps\ (^6Li)\ /12.0192–1\}*1000 \quad (4\text{-}1)$$

$$\text{if IMF} = \delta^7Li_{\ SIMS} - \delta^7Li_{\ true}$$

$$= 1000*\{\{[cps\ (^7Li)/cps\ (^6Li)_{\ SIMIS} – cps\ (^7Li)/cps\ (^6Li)_{\ true}]/12.019\text{-}1\} \quad (4\text{-}2)$$

$$\delta^7Li_{\ unknown,\ true} = (\delta^7Li_{\ unknown,\ SIMS} – IMF_{\ unknown}) – (\delta^7Li_{\ Standard,\ SIMS} – IMF_{\ Standard}) + \delta^7Li_{\ Standard,\ true} \quad (4\text{-}3)$$

The $\delta^7Li_{\ unknown,\ SIMS}$ and $\delta^7Li_{\ Standard,\ SIMS}$ are the analysis results measured by SIMS, and the analysis results of standard materials by MC-ICP-MS are represented as the $\delta^7Li_{\ Standard,\ true}$. The matrix effect with variation of cpx major element composition can be observed in our analyses. The raw analysis data of Li isotope measured by SIMS have displayed a clear increase tendency for δ^7Li of IMF with increasing cpx Mg# (Fig. 4-1). The matrix effect (ie. IMF) are plotted as the average difference between the δ^7Li measured by SIMS and the δ^7Li by MC-ICP-MS/LA-ICP-MS vs Mg# in Fig. 4-2. The results of linear fitting show the slopes of IMF for δ^7Li vs. Mg# of cpx phenocrysts increase approximately from 1.0 to 1.2 ‰ per Mg# increase in different session on either IMS 1270 or 1280 (Fig. 2), as described Bell et al. (2009) for olivine (the slop are about 1.3). So:

$$IMF = a*Mg\# + b \quad (4\text{-}4)$$

$$IMF_{\ Standard} - IMF_{\ unknown} = \delta^7Li_{\ Standard,\ SIMS} - \delta^7Li_{\ Standard,\ true} - (\delta^7Li_{\ unknown,\ SIMS} - \delta^7Li_{\ unknown,\ true})$$

$$= a*(Mg\#_{\ standard} – Mg\#_{\ unknown}) \quad (4\text{-}5)$$

$$\delta^7Li_{\ unknown,\ true} = \delta^7Li_{\ unknown,\ SIMS} - IMF_{\ Standard} + a*(Mg\#_{\ standard} – Mg\#_{\ unknown})$$

$$= \delta^7Li_{\ unknown,\ SIMS} - a*Mg\#_{\ unknown} - b \quad (4\text{-}6)$$

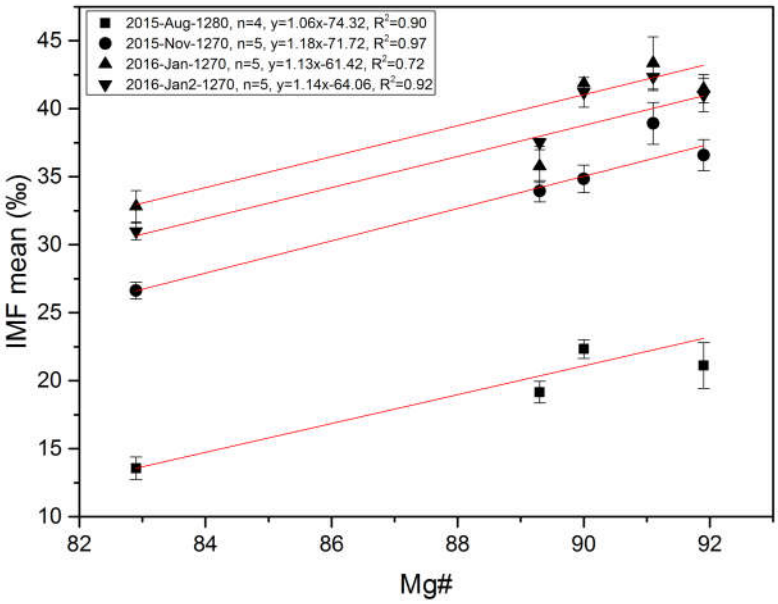

Fig. 4-1 The correlation between the Mg# raw data vs. IMF for Lithium isotope in each session.

Fig. 4-2 The correlation between mean Mg# vs. IMF for Lithium isotope in each session.

Such linear fitting requires the precisely known Li isotopic and chemical

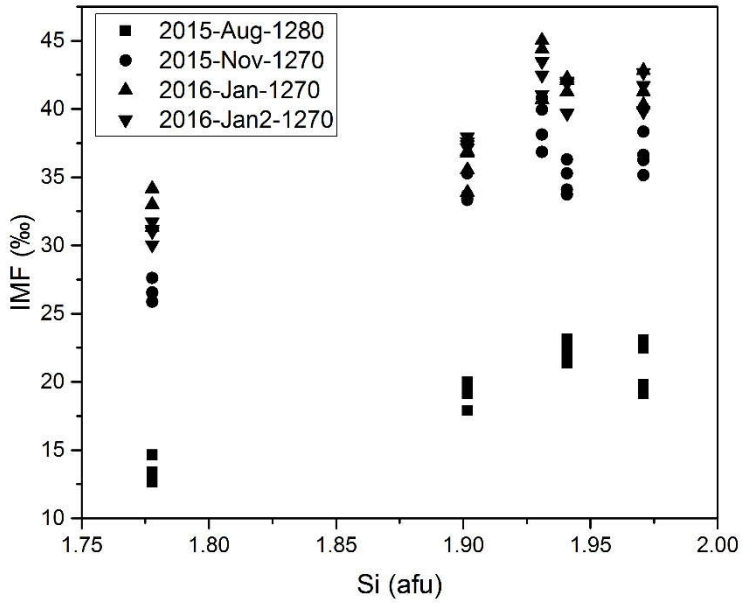

composition of cpx standards before measurement on accurate Li isotope data by SIMS. Relative to olivine, cpx does not show two simple end numbers, but more various composition and more complex crystal structure. Cpx have multiple end numbers, including $MgCaSi_2O_6$, $FeCaSi_2O_6$, $NaAlSi_2O_6$ and so on. Si, Al, Ca, and Ti have relatively high concentration in cpx. Besides Fe-Mg exchange, cpx show more complex isomorphism, such as Si-Al-Ti, Mg-Fe-Cr. So in addition to Mg# and Si, Cr, Ca, Ti, and Al are also plotted in Fig. 4-5 to 4-8 in order to discuss their relationship to IMF. Usually, Si show strong relevance to Mg# (i.e. Fe and Mg content), that the Si usually increase with Mg# decreasing. This relevance also can be observed in the relationship to IMF, the Si (afu) show even stronger correlation with IMF than that of Mg# (Fig. 4-2 and Fig. 4-3). In the plots of Al and Ti vs. IMF in Fig. 4-7 and 4-8, a relatively weaker linear relationship than those of Si and Mg# can be observed. The relevance of Al and Ti to IMF are not stable, with various R^2 in different analysis sessions. In Fig. 4-5 and 4-6, IMF have no relationship with Cr and Ca. Therefore, Cr and Ca contents are not in obvious relevance to the matrix effect of Li isotope analysis by SIMS for cpx. Following the results, the best index to calibrate matrix effect in cpx for Li isotope analysis by SIMS is Si or Mg#.

Fig. 4-3 The correlation between the Si (afu) raw data vs. IMF for Lithium isotope in each session.

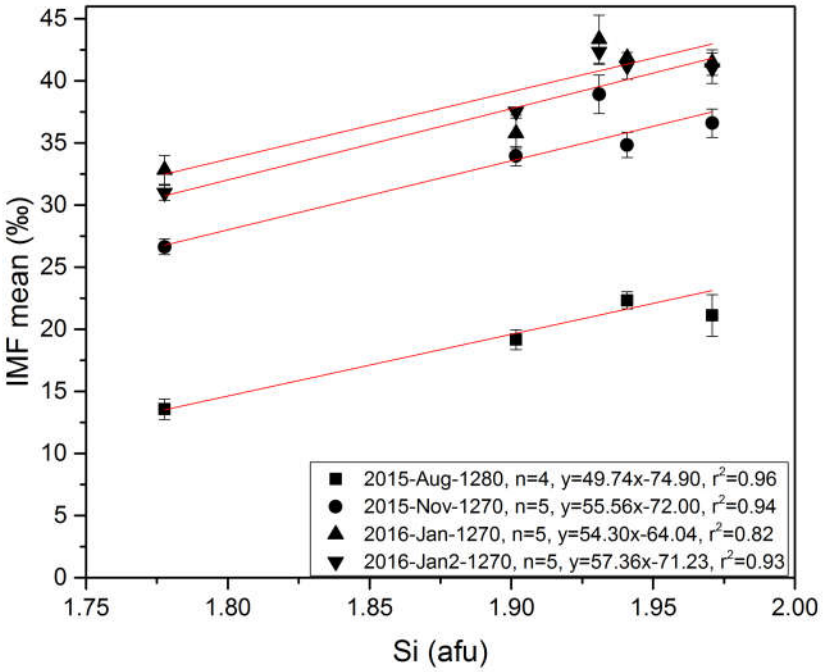

Fig. 4-4 The correlation between mean Si (afu) vs. IMF for Lithium isotope in each session.

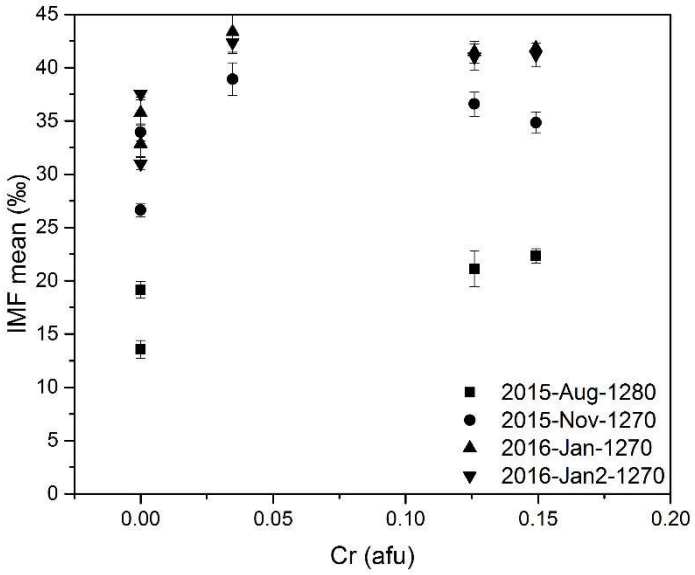

Fig. 4-5 The correlation between mean Cr (afu) vs. IMF for Lithium isotope in each session.

The matrix effect for Li isotope analysis by SIMS for cpx increase up to 1.2‰ per Mg# increasing, or increase up to 5.7‰ per 0.1 afu of Si increasing. It demonstrates that before each analysis by SIMS for Li isotope of cpx unknown samples, the matrix effect relevance to the cpx composition should be evaluated. Despite, Bell et al. (2009) suggested a considerable matrix effect for the Li isotope analysis of olivine, the matrix effect for the Li isotope analysis of cpx have rarely been discussed. Mostly in previous studies (Barrat et al., 2005; Beck et al., 2004; Beck et al., 2006; Jeffcoate et al., 2007; Xiao et al., 2015), even the unknown cpx samples have large chemical composition variation, only one or limited standards are determined to calibrate the matrix effect of analysis by SIMS. Meanwhile, the analysis result of the same cpx standard by SIMS display considerable difference in different sections (Fig. 3-9). In the studies of Bell et al. (2009) opposite trends to the slop of IMF corrected line are displayed, suggesting that either existing slop or intercept is unsuitable to different sections or other kinds of minerals, like Bell et al. (2009) used the IMF corrected line from ol to calibrate the offset of cpx and opx unknown samples. Therefore, a series of cpx standards with known Li isotope and similar chemical composition to unknown cpx samples are needed to determine the Li isotope of unknown cpx with various chemical composition, such as phenocrysts in basaltic rocks or meteor.

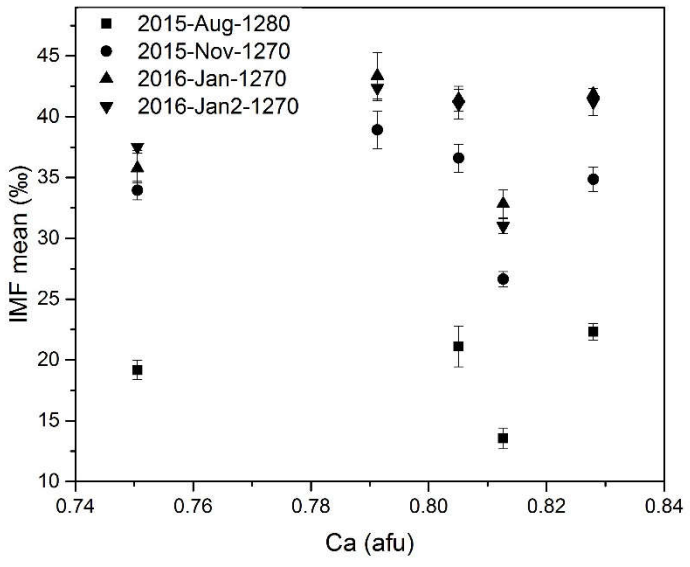

Fig. 4-6 The correlation between mean Ca (afu) vs. IMF for Lithium isotope in each session.

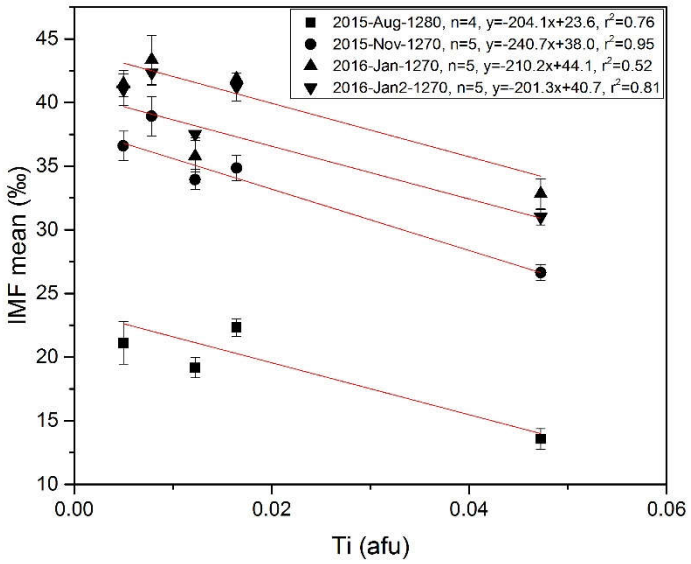

Fig. 4-7 The correlation between mean Ti (afu) vs. IMF for Lithium isotope in each session.

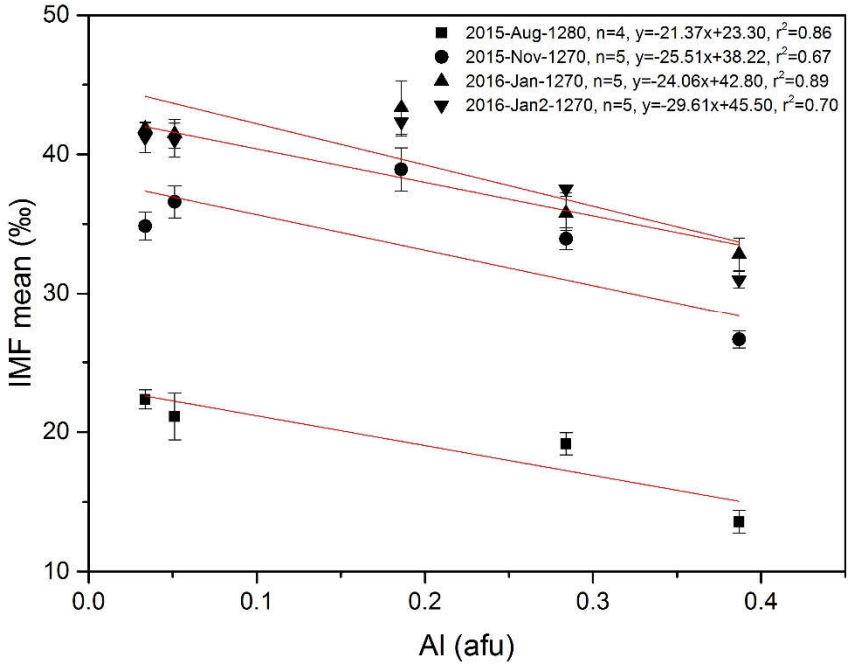

Fig. 4-8 The correlation between mean Al (afu) vs. IMF for Lithium isotope in each session.

4.2 Applications of Li calibration

4.2.1 Li content and isotope results of cpx grains

To facilitate the discussion, the Li isotope result based on calibration of Mg# are mainly discussed in this section. The Li content and isotope of some cpx grains in basaltic rocks from the Fujian region are analyzed by SIMS to test the calibration of cpx, as example. Some cpx grains contain cpx xenocryst core inside the cpx phenocryst rim. The Mg# and Si for the cpx phenocrysts and xenocrysts range from 76 to 91 and from 1.76 to 1.92 (afu) respectively. The known cpx standards have similar relevance between IMF and either Mg# or Si, however, the cpx standards have more similar range of Si to the unknown samples than that of Mg#. Therefore, more cpx phenocrysts fall within the range of Si from 1.78-1.97 (afu) of cpx standards, but not within the range of Mg# from 82.9 to 91.9. The IMF of δ^7Li increase up to 1.2‰ per Mg# increase for known standards, and the 2SD of SIMS and EMP for Li isotope and major elements is about 2‰ and 1% respectively. Therefore, we suggest that the IMF correct line suitable range of Mg# are expanded to compare to that of Si. Four cpx grain profiles of major element compositions and Li isotope in basalts from the Fujian region are measured to discuss the calibration. The details of the profile are listed in Table 4-2. The Li isotope profiles of cpx phenocryst samples were analyzed in the same sessions, according to the IMF line of 2015-Aug-1280 in Fig. 4-2 and 4-4 respectively.

Two kinds of cpx grains are analyzed in this study for the Li isotopic calibration and the Li isotopic change during magma evolution: one kind cpx, type I, has xenocryst core and phenocryst rim. The xenocryst core has relatively high Cr and Mg#, which is the landmark of cpx xenocryst. Another kind of cpx phenocryst, type II, is total phenocryst without xenocryst.

The 5-3-10 and 5-11-7 grains have clinopyroxeney xenocryst core and clinopyroxeney phenocryst rim, as type I cpx phenocrysts. The xenocryst core have Mg# higher than 88, as shown in Fig. 4-9. Based on both of the calibrations, the profiles of 5-3-10 and 5-11-7 show the large difference of Li content and Li isotope between the xenocryst core and the phenocryst rim, as shown in Fig. 4-9. The Li content and Li isotope profile of the grains of 5-3-10 are measured along with the line from one side rim to the core and to another side rim again. The cpx phenocryst rims at both sides have high δ^7Li >10‰ in Mg# calibration and low Li content <8 ppm, but the cpx xenocryst core has low δ^7Li <10‰ in Mg# calibration and high Li content >12ppm

except one point, if following the calibration of Mg#. The core of xenocryst have high Li content but low Li isotopic ratios, especially, in the grain of 5-11-7. The analysis of core xenocryst and rim phenocryst were replicated a few times in the grains 5-11-7, Fig. 4-9. The 5 replicate analyses of cpx xenocryst core and 3 replicate analyses of clinopyroxeney phenocryst rim display relative consistent values respectively.

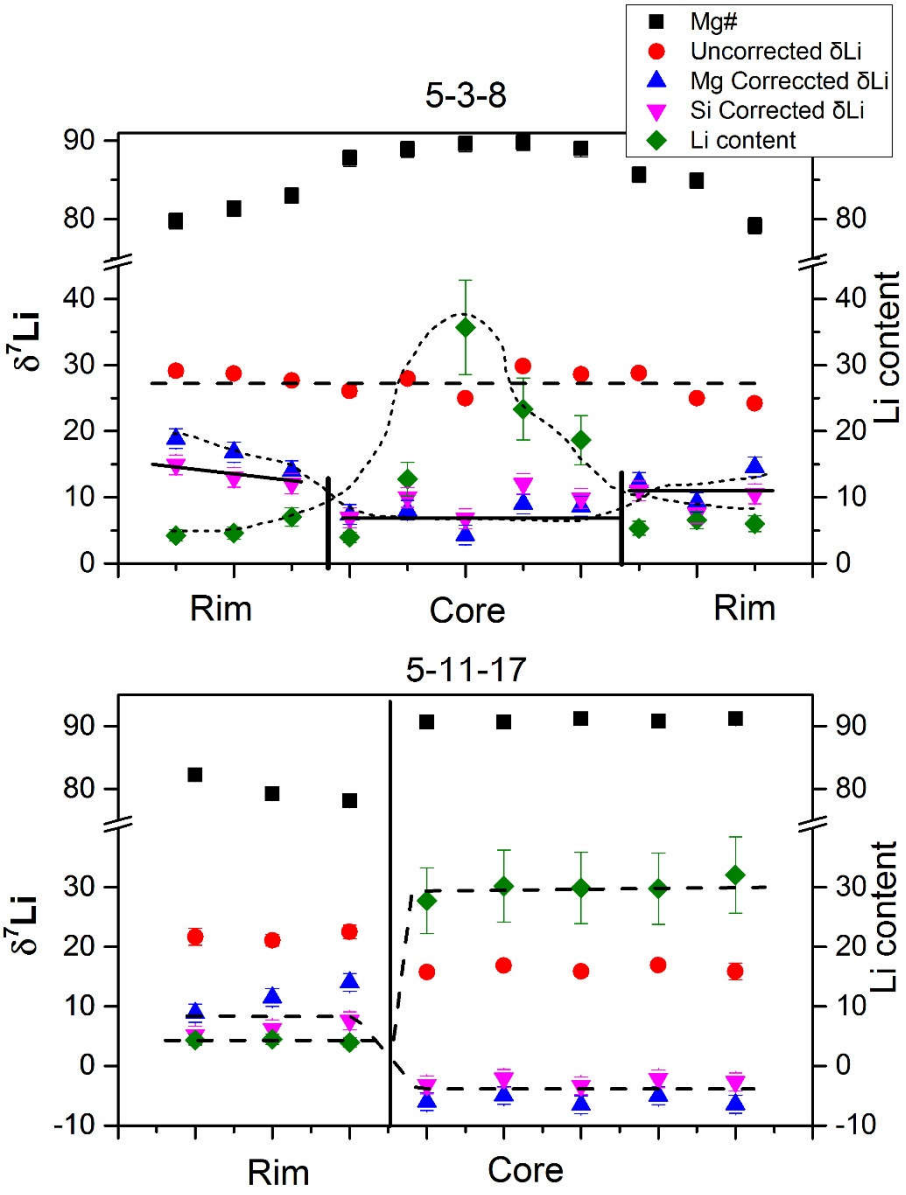

Fig. 4-9 The profile of Mg#, Li content, Li isotope for type I clinopyroxeney phenocryst.

The 5-4-8 and 10-0-17 are entire cpx phenocrysts without xenocryst core, as type II cpx phenocryst. All the analysis points have almost same Mg# except the outermost rim of 10-0-17 (Table 4-2, Fig. 4-10b), and limited variation of Li content respectively (Table 4-2, Fig. 4-10) within the range of error for SIMS analysis method (Chapter 3). However, the δ^7Li 10-0-17 are not totally homogeneous from core to rim. The 5-4-8 show almost same δ^7Li either in the core or rim, as shown in Fig. 4-10 (7-10‰ in Mg# calibration), and share the similar Mg#, Si, and Li content (3-5ppm) from core to rim. The 10-0-17 grain shows more complex δ^7Li profile from core to rim than the 5-4-8 grain: the core of cpx phenocrysts have relative high Mg#, as well as the lower Mg# are observed in mantle and edge of cpx phenocryst grain (Table 4-2, Fig. 4-10b). The center part and the rim of 10-0-17 cpx grain displays high δ^7Li values of 22 to 28 ‰ in Mg# calibration and high Li content of 3-4 ppm, while the mantle of cpx grain have lower δ^7Li values from 13 to 19 ‰ in Mg# calibration, with lower Li content of about 2 ppm (Table 4-2, Fig. 4-10b).

4.2.2 Difference between the calibration of Mg# and Si

The calibration of cpx phenocrysts from Si have relative lower $\delta^7Li_{\text{unknown, corrected}}$ than the calibration of cpx phenocrysts from Mg# (Table 4-2 and Fig. 4-9 and 4-10) for the same grains. The absolute difference between the corrected results of Lithium isotopic data by two calibrations almost agree with those of each other among different analysis points for all the cpx phenocrysts. The difference between the corrected results of xenocryst is larger than those of the phenocryst (Fig. 4-9 and 4-10). The difference between the two kinds of calibrations is because of: 1) the error of the analysis results of major elements composition of cpx measure by EPM, however, unless the error is systematic one, it is hard to explain the different analysis points having such consistent difference of IMF for unknown samples; 2) the co-relationship of Si (afu) vs. Mg# for the composition are different between standards and unknown samples. Mg# about 90 for standards corresponds to 1.95 (afu) of Si, however, for unknown samples the analysis point of 90 Mg# have Si about 1.86 (afu) (Table 4-3). This suggests that the unknown samples have relatively lower Si or higher Al (IV) than the standards. It should be noted that the Si-Al and Mg-Fe is not the same replacing process in pyroxene.

and $Mg^{2+} = Fe^{2+}$ (4-7)

$Mg^{2+} + Si^{4+} = Al^{3+(VI)} + Al^{3+(IV)}$ or $Mg^{2+} + Si^{4+} = Fe^{3+(VI)} + Al^{3+(IV)}$ (4-8)

Unlike olivine, 4-7 is the unique replacement mechanism formula, 4-7 and 4-8

formulas are the two most common replacement mechanism in clinopyroxeney and can take place in clinopyroxeney at the same time. Meanwhile the Fe^{3+} also can enter into the octahedral voids (Morimote, 1988). The 4-7 and 4-8 do not always take place at the same ratio during clinopyroxeney crystallization from magma. It is hard to point out which one among Mg, Fe, Si or other elements or ion results the matrix effect for clinopyroxeney, due to limited number as well as limited composition range of cpx standards. Fortunately, most of unknown clinopyroxeney have similar slop of Si vs. Mg# to that of standard, and the relative change of Li isotopic data between different parts of grains is the key point that we focused on and are interested in (Fig. 4-11). So the calibration of Si and Mg# can calibrate similar Li content and Lithium isotopic information of cpx phenocrysts to recover the diffusion of Li during magma ascent and cooling, if they share similar slop of Si vs. Mg# to the standard, such as the four cpx phenocrysts from Fujian basalts. Although, the core of 5-3-10 and 5-11-7 do not show similar slop of Mg# vs Si to standard or on the same extending line of cpx phenocrysts as shown in Fig. 4-12, they have similar chemical compositions to the know cpx standards. The corrected results by the calibration of Si and Mg# of xenocryst core also have similar variation tendency that the high Li content and depleted δ^7Li are observed from the core to rim of 5-3-10 and 5-11-7, as shown in Fig. 4-9. These corresponding changes of Li content and Lithium isotopic data trends suggest the calibration either of Si or Mg# can be used to distinguish the difference and variation of Li in cpx grains. The difference between the results corrected by the calibration of Si and Mg# may be caused by the difference of composition between standards used to build the correction line and unknown samples. However, the difference between corrected δ^7Li by two kinds of calibrations in single grains are consistent. The consistency suggests the two calibrations can get the same result and conclusion in single grain, but the δ^7Li results corrected by different calibrations among different grains or samples cannot be compared together simply. The calibration of Lithium for ol in Bell et al. (2009) and the calibration of Oxygen for cpx the calculation based on Mg# is used in this work. To simplify discussion, only the calibration of Mg# are used in later chapter.

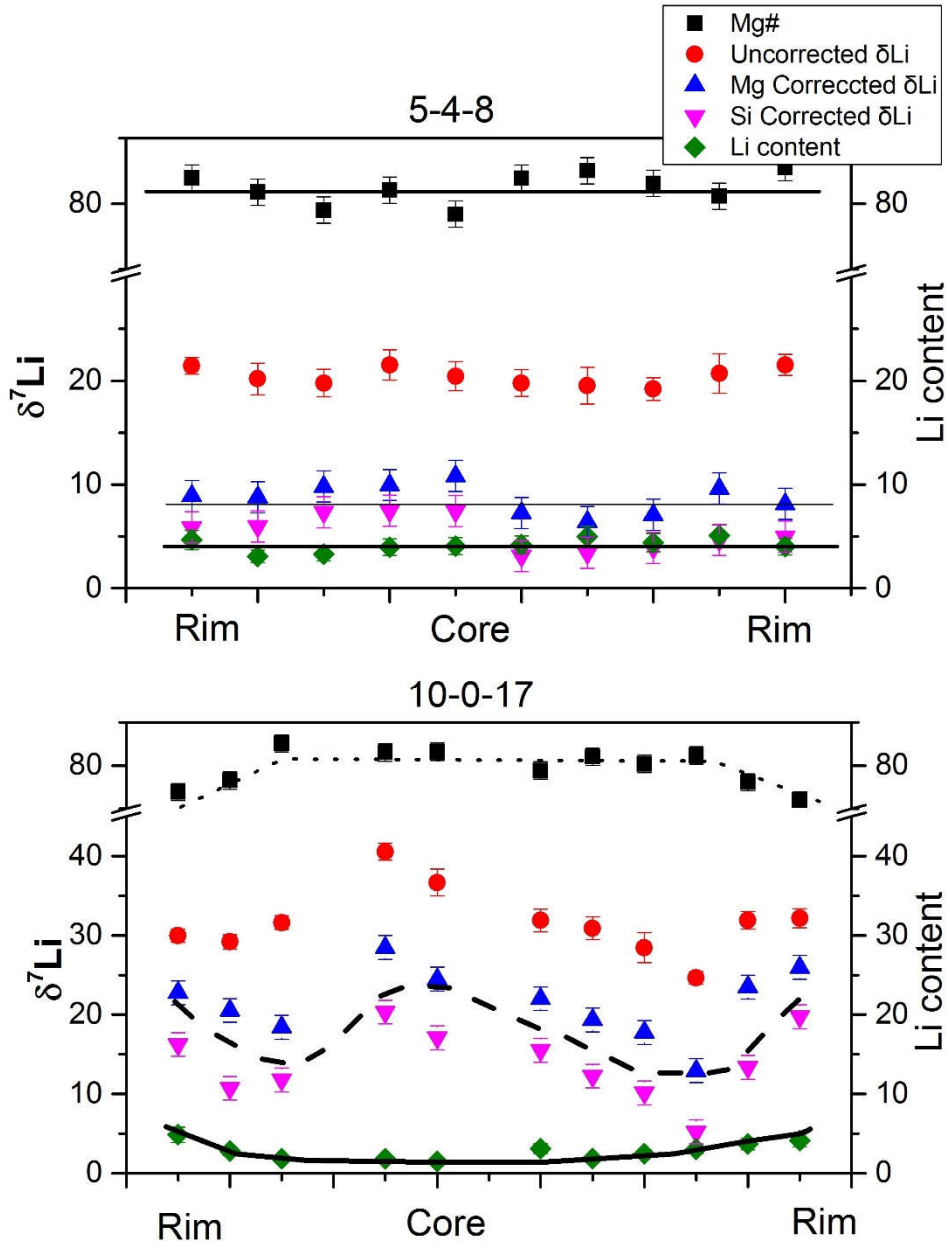

Fig. 4-10 The profile of Mg# Li content and Li isotope for type II clinopyroxeney phenocryst.

4.2.3 Discussion of the variation of Li content and Li isotope

The ^{6}Li diffuses faster than the ^{7}Li during diffusion, the difference of diffusion speed will result in the fraction of ^{6}Li and ^{7}Li. In essence, the physicochemical condition variation result in the fractionation of Li (Richter et al., 2014), such as

temperature ($D_{Li}^{cpx\text{-}melt}$), f_{O_2}, and the variation of ambient Li content and δ^7Li. The different variation of Li content and Li isotope in the cpx grains are considered because of: (1) the evolution of magma, such as ambient temperature decrease, fractional crystallization, and magma mixture; (2) the initial difference between xenocryst and phenocryst; and (3) the later Li diffusion after cpx crystallization from magma.

The calculation of fractional crystallization infer that the Li content does not have large difference when the degrees of fractional crystallization of magma are below 20% (Fig. 4-10), suggesting the high Li content and low δ^7Li inherited from their mantle source, but are not resulted by crystallization. To simplify the calculation, the "Equilibrium Crystallization" and "Fractional Crystallization" models are used for the crystallization of ol, cpx and pl. The calculation results are based on the partition coefficient D between mafic minerals and melts. The $D_{Li}^{cpx/melt}$ =0.2 (Brenan et al.，1998) are assumed during crystallization (Fig. 4-12). The recent experiments conducted at 1.5 GPa and over a broad temperature range of 700 to 1100 °C by Yakob et al. (2012), however, have confirmed a fixed equilibrium partition coefficient of Li between olivine and diopside at 2.0±0.2, independent of temperature. The $D_{Li}^{pl/cpx}$ range from 0.08 to 0.6 when the temperature ranges from 950 to 1200 °C (Coogan et al., 2005). Therefore, the $D_{Li}^{ol/melt}$= 0.4, $D_{Li}^{cpx/melt}$ =0.2, and $D_{Li}^{pl/melt}$ =0.02 are assumed for crystallization calculation. Meanwhile, the crystallization ratios of ol, cpx and pl are assumed for 3:2:1 and 1:1:0 respectively. The D_{rock} is 0.27 and 0.3 respectively. The calculation results are listed in Table 4-3 for F=0.01, 0.02, 0.05, 0.10, 0.15, 0.2 and 0.25, which is the degree of crystallization.

The content of Li and Mg# are calculated below:

$$C_l=C_0/[D*F+(1-F)] \quad (4\text{-}9)$$

$$C_s= D*C_0/[D*F+(1-F)] \quad (4\text{-}10)$$

For "Equilibrium Crystallization" model.

$$C_l=C_o*(1-F)^{D-1} \quad (4\text{-}11)$$

$$C_s= D*C_o*(1-F)^{D-1} \quad (4\text{-}12)$$

For "Fractional Crystallization" model.

The Li content of cpx phenocrysts will increase no more than 20% compared with the initial cpx phenocryst, when the degrees of crystallization of magma are below 0.2 (Table 4-3 and Fig. 4-12). The results suggest the difference of Li content in type I cpx was not caused by the crystallization. The Li would remove from the high content part to the low content part, when Li are re-equilibrated. The Li content in xenocryst core is

higher than that in phenocryst rim disagreeing with later diffusion of Li. Therefore, the large difference of Li content between phenocryst and xenocryst are initial characteristics. The ^{6}Li generally diffuses faster than the ^{7}Li, in melts and minerals (e.g. Richter et al. 2014). If the Li diffuse from the xenocryst core to the phenocryst rim, the ^{6}Li will enter faster into the phenocryst than the ^{7}Li, leaving elevated $\delta^{7}Li$ in the core. The discordant patterns of Li content in type I cpx grains argue against the later diffusion of Li in Fig. 4-10. The homogeneous low $\delta^{7}Li$ in the xenocryst core in 5-11-17 with homogeneous Li content also dissent from the later diffusion of Li. Therefore, the lower $\delta^{7}Li$ and high Li content in the core of type I cpx was not caused by Li diffusion, but the initial characteristic of xenocrysts.

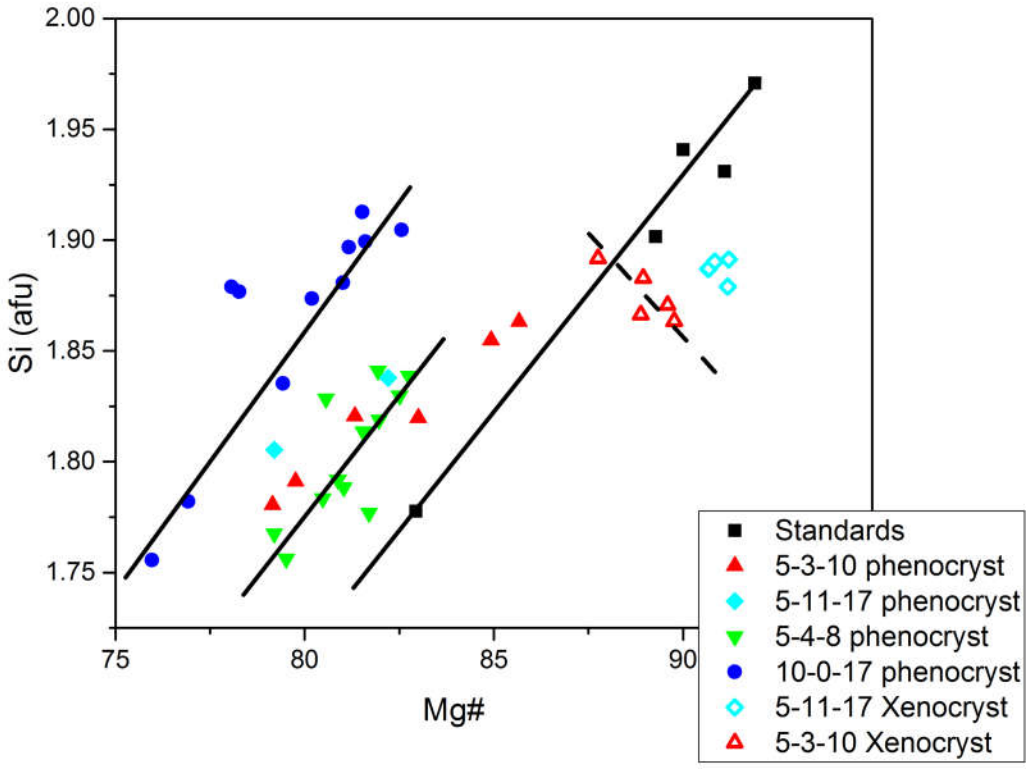

Fig. 4-11 Relationship between Mg# and Si (afu) in clinopyroxeney for stand and unknown samples.

The type II cpx phenocrysts are totally crystallized from the basaltic magma, the Li profiles in cpx phenocrysts are either the magma evolution records or the Li diffusion results. The Mg# zonation are only observed in the outermost in the 10-0-17 grains, as shown in Fig. 4-11. The high fractionation of $\delta^{7}Li$ in the profile in 10-0-17 cpx cannot be the result of the fractional crystallization which is unable to fractionate Li isotopes

more than 1‰ (Tomascak et al., 1999). Meanwhile, the fractionation of Li also appears in the mantle and core of the cpx phenocryst of 10-0-17, where there is no significant difference of Mg#, arguing against magma evolution, including fractional crystallization, magma mixture, and crust assimilation. The "W"-like δ^7Li profile in the 10-0-17 cpx and the high Li content in its rim (Fig. 4-10) is similar to the Li diffusion pattern reported by Beck et al., (2006) and the calculation in Richter et al., (2014). The δ^7Li fractionation is so limited dissent with the result of fractional crystallization (Beck et al., 2004). Richter et al. (2014) have reported two Li content re-equilibrium experimental results: the sample of LiPx16 grain with 755 μm diameter within Li_2SiO_3 as Li diffusion source buffered by Ni-NiO, after 160h and LiPx8 grain with 550 μm diameter within the spodumene as Li diffusion source buffered by Ni-NiO. However, despite the consistency of Li content in the result of Richter et al. (2014), the re-equilibrium require the valley-like.

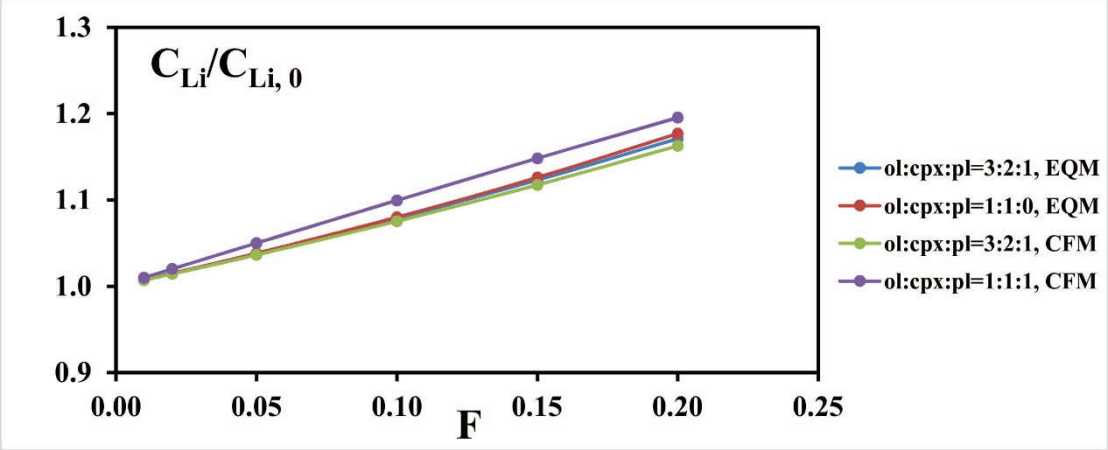

Fig. 4-12 Evolution of Lithium content in melt during the crystallizations of different mineral assemblage.

Therefore, the Li content and δ^7Li profiles together with the major elements profiles of these cpx grains suggest: (1) the xenocryst core of 5-11-7 and 5-3-10 cpx grains have kept their origin features of Li contents and Li isotope, distinct from their phenocryst rims; (2) the Li profiles of the 10-0-17 cpx grains imply the later Li diffusion, rather than magma evolution record; (3) the Li profiles of the 5-4-8 may not be effected by the later Li diffusion.

4.2.4 Conclusion

(1) The composition related matrix effect for the analysis of Lithium isotope by SIMS are confirmed based on the analysis result of the known cpx standards.

(2) The Si and Mg# are the most suitable index to correct the IMF of Li isotope, other than Al, Ti, Ca, or Cr.

(3) The Si and Mg# calibration may result in systematic difference of the corrected Li isotope, due to the compositional difference between cpx standards and unknown samples. This two calibrations can get the same result and conclusion in single grain, but comparison with the corrected results by different calibrations among different grains cannot be used together simply.

(4) The change of Li content and Li isotopic data can be used to distinguish the difference between xenocrysts and phenocrysts, as well as the Li diffusion after cpx crystallization in basalts.

Table 4-1 The raw results of cpx standards for Li isotope analyzed by SIMS.

Time	Standard No.	Account ^{7}Li	cps(7)/nA/content of standard	delta Li by SIMS	error	δ^{7} Li by ICP	Li content by ICP (ppm)	Mg#	IMF	SD
2015 Aug	06JY06-CPX@1	29173	1711	24.4	0.9	1.3	1.1	90.0	23.1	
	06JY06-CPX@2	28431	1657	24.1	1.3	1.3	1.1	90.0	22.8	
	06JY06-CPX@3	28736	1675	23.3	1.3	1.3	1.1	90.0	22.0	
	06JY06-CPX@4	28586	1666	22.7	1.1	1.3	1.1	90.0	21.4	
	Mean							90.0	22.3	0.7
	06JY29-CPX@1	19870	1602	20.5	1.2	-2.6	0.8	91.9	23.1	
	06JY29-CPX@2	15728	1277	19.9	1.9	-2.6	0.8	91.9	22.5	
	06JY29-CPX@3	14768	1191	16.5	1.5	-2.6	0.8	91.9	19.1	
	06JY29-CPX@4	13631	1099	17.2	1.2	-2.6	0.8	91.9	19.8	
	Mean							91.9	21.1	1.7
	CPX25a@1	89491	2221	16.9	0.6	-1.02	2.55	89.3	17.9	
	CPX25a@2	89826	2229	19.0	0.7	-1.02	2.55	89.3	20.0	
	CPX25a@3	90729	2252	18.6	0.6	-1.02	2.55	89.3	19.6	
	CPX25a@4	88353	2193	18.1	0.6	-1.02	2.55	89.3	19.1	
	Mean							89.3	19.2	0.8
	CPX35a@1	88833	1645	7.7	0.6	-5.68	3.44	82.9	13.4	
	CPX35a@2	79318	1469	7.0	0.7	-5.68	3.44	82.9	12.7	
	CPX35a@3	79054	1464	9.0	0.8	-5.68	3.44	82.9	14.6	
	Mean							82.9	13.6	0.8
2016 Jan	06JY06-CPX@1	29781	1793	43.6	1.0	1.3	1.1	90.0	42.3	
	06JY06-CPX@2	29050	1761	43.4	1.2	1.3	1.1	90.0	42.1	
	06JY06-CPX@3	29996	1830	42.6	1.2	1.3	1.1	90.0	41.3	
	Mean							90.0	41.9	0.4
	06JY29-CPX@1	22799	1926	37.7	1.1	-2.6	0.8	91.1	40.3	
	06JY29-CPX@2	22657	1914	38.7	1.3	-2.6	0.8	91.1	41.3	
	06JY29-CPX@3	22756	1922	40.2	1.5	-2.6	0.8	91.1	42.8	
	Mean							91.1	41.5	1.0
	06JY31-CPX@1	20124	1351	42.0	1.1	-2.4	1.0	91.1	44.4	
	06JY31-CPX@2	21397	1436	42.6	1.1	-2.4	1.0	91.1	45.0	
	06JY31-CPX@3	21432	1448	38.3	1.5	-2.4	1.0	91.1	40.7	
	Mean							91.1	43.4	1.9
	CPX25@1	82880	2167	35.9	0.6	-1.02	2.55	89.3	36.9	
	CPX25@2	81364	2127	35.8	0.8	-1.02	2.55	89.3	36.8	
	CPX25@3	82151	2148	34.5	0.6	-1.02	2.55	89.3	35.5	
	CPX25@4	83500	2183	32.9	0.8	-1.02	2.55	89.3	33.9	
	Mean							89.3	35.8	1.2

	CPX35@2	95568	1852	25.7	0.7	-5.68	3.44	82.9	31.3	
	CPX35@3	99836	1948	27.3	0.5	-5.68	3.44	82.9	33.0	
	Mean							82.9	32.8	1.2
2016 Jan-2	06JY06-CPX-A@1	26012	1631	43.3	1.4	1.3	1.1	90.0	42.0	
	06JY06-CPX-A@2	27407	1718	43.2	1.0	1.3	1.1	90.0	41.9	
	06JY06-CPX-A@3	29018	1832	41.0	1.1	1.3	1.1	90.0	39.7	
	Mean							90.0	41.2	1.1
	06JY29-CPX-A@1	21390	1857	37.2	1.3	-2.6	0.8	91.9	39.8	
	06JY29-CPX-A@2	21219	1842	39.1	0.9	-2.6	0.8	91.9	41.7	
	06JY29-CPX-A@3	21188	1839	37.3	0.9	-2.6	0.8	91.9	39.9	
	06JY31-CPX-A@4	22298	1936	40.1	1.5	-2.6	0.8	91.9	42.7	
	Mean							91.9	41.0	1.2
	06JY31-CPX-A@1	18910	1304	38.7	1.2	-2.4	1.0	91.1	41.1	
	06JY31-CPX-A@2	15070	1039	41.1	1.3	-2.4	1.0	91.1	43.5	
	06JY31-CPX-A@3	22298	1548	40.1	1.5	-2.4	1.0	91.1	42.5	
	Mean							91.1	42.3	1.0
	CPX25-B@1	88208	2419	36.4	0.6	-1.02	2.55	89.3	37.4	
	CPX25-B@2	88565	2412	36.1	0.8	-1.02	2.55	89.3	37.2	
	CPX25-B@3	96540	2629	36.9	0.7	-1.02	2.55	89.3	37.9	
	CPX25-A@1	71279	2291	36.6	0.9	-1.02	2.55	89.3	37.6	
	Mean							89.3	37.5	0.3
	CPX35-A@1	67211	1601	24.4	0.9	-5.68	3.44	82.9	30.0	
	CPX35-A@3	91162	1815	26.0	0.5	-5.68	3.44	82.9	31.7	
	CPX35-A@4	86302	1718	25.3	0.8	-5.68	3.44	82.9	31.0	
	Mean							82.9	31.0	0.6
2015-Nov	06JY06Cpx@1	29768	1374	36.6	1.2	1.3	1.1	90.0	35.3	
	06JY06Cpx@2	30172	1385	37.6	1.0	1.3	1.1	90.0	36.3	
	06JY06Cpx@3	29606	1359	35.4	1.2	1.3	1.1	90.0	34.1	
	06JY06Cpx@4	27298	1253	35.0	1.2	1.3	1.1	90.0	33.7	
	Mean							90.0	34.8	1.0
	06JY29Cpx@2	25125	1263	34.0	1.2	-2.6	0.8	91.9	36.6	
	06JY29Cpx@3	24916	1573	32.5	1.3	-2.6	0.8	91.9	35.1	
	06JY29Cpx@4	23633	1500	33.7	1.0	-2.6	0.8	91.9	36.3	
	Mean							91.9	36.6	1.1
	06JY31Cpx@1	23553	1202	38.4	1.3	-2.4	1.0	91.1	40.8	
	06JY31Cpx@2	26110	1325	35.7	1.0	-2.4	1.0	91.1	38.1	
	06JY31Cpx@3	24954	1260	37.6	1.2	-2.4	1.0	91.1	40.0	
	06JY31Cpx@4	26570	1349	34.4	1.0	-2.4	1.0	91.1	36.8	
	Mean							91.1	38.9	1.5

cpx25-b@1	84774	1696	34.3	1.1	-1.02	2.55	89.3	35.3	
cpx25-b@2	79887	1615	32.3	1.0	-1.02	2.55	89.3	33.3	
cpx25-b@3	85392	1744	32.4	0.9	-1.02	2.55	89.3	33.5	
cpx25-b@1	80729	1675	32.7	0.7	-1.02	2.55	89.3	33.7	
Mean							89.3	33.9	0.8
cpx35-b@1	175319	2740	20.9	0.6	-5.68	3.44	82.9	26.5	
cpx35-b@2	152992	2293	20.9	0.7	-5.68	3.44	82.9	26.5	
cpx35-b@3	162122	2429	20.2	0.6	-5.68	3.44	82.9	25.9	
cpx35-b@4	160707	2408	21.9	0.5	-5.68	3.44	82.9	27.6	
Mean							82.9	26.6	0.6

Table 4-2 The raw and corrected Lithium results analyzed by SIMS from Fujian basalts.

Sample No.	Location	Account $^{7}Li/PI$	cps(7)/nA/L $i_{standard}$	$\delta^{7}Li_{SIMS}$	error	Mg#	$Slop_{cor,Mg}$	$intercept_{cor,Mg}$	IMF_{Mg}	$\delta^{7}Li_{cor,Mg}$	Si (afu)	$Slop_{cor,Si}$	$intercept_{cor,Si}$	IMF_{Si}	$\delta^{7}Li_{cor,si}$	Li content	error
5-4-8b@1	MX	5.03E+12	1.64E+12	26.2	1.5	80.9	1.1	-74.3	11.4	14.8	1.8	49.7	-74.9	14.2	12.0	3.1	0.6
5-4-8b@2		5.41E+12		22.8	1.3	79.5	1.1	-74.3	10.0	12.8	1.8	49.7	-74.9	12.4	10.3	3.3	0.7
5-4-8b@3		7.66E+12		21.4	0.8	82.0	1.1	-74.3	12.6	8.9	1.8	49.7	-74.9	15.6	5.9	4.7	0.9
5-4-8b@4		8.19E+12		19.5	1.8	82.5	1.1	-74.3	13.1	6.4	1.8	49.7	-74.9	16.1	3.4	5.0	1.0
5-4-8b@5		7.22E+12		19.2	1.1	81.5	1.1	-74.3	12.1	7.1	1.8	49.7	-74.9	15.3	3.9	4.4	0.9
5-4-8b@6		6.92E+12		19.8	1.3	81.9	1.1	-74.3	12.5	7.2	1.8	49.7	-74.9	16.7	3.1	4.2	0.8
5-4-8b@7		6.51E+12		21.5	1.5	81.0	1.1	-74.3	11.6	10.0	1.8	49.7	-74.9	14.1	7.5	4.0	0.8
5-4-8b@8		6.70E+12		22.4	1.4	79.2	1.1	-74.3	9.6	12.8	1.8	49.7	-74.9	13.0	9.4	4.1	0.8
5-3-10a@06	MX	6.96E+12		29.1	0.7	79.8	1.1	-74.3	10.2	18.9	1.8	49.7	-74.9	14.2	14.9	4.2	0.8
5-3-10a@05		7.58E+12		28.7	0.6	81.3	1.1	-74.3	11.9	16.8	1.8	49.7	-74.9	15.7	13.0	4.6	0.9
5-3-10a@04		1.16E+13		27.7	0.3	83.0	1.1	-74.3	13.7	14.0	1.8	49.7	-74.9	15.6	12.1	7.1	1.4
5-3-10a@03		6.47E+12		26.1	0.8	87.8	1.1	-74.3	18.7	7.4	1.9	49.7	-74.9	19.2	6.9	3.9	0.8
5-3-10a@02		2.10E+13		27.9	0.4	88.9	1.1	-74.3	19.9	8.0	1.9	49.7	-74.9	17.9	10.0	12.8	2.6
5-3-10a@1		5.86E+13		24.9	0.3	89.6	1.1	-74.3	20.6	4.3	1.9	49.7	-74.9	18.2	6.8	35.7	7.1
5-3-10a@07		3.84E+13		29.9	0.3	89.8	1.1	-74.3	20.8	9.0	1.9	49.7	-74.9	17.8	12.1	23.4	4.7
5-3-10a@08		3.07E+13		28.6	0.4	88.9	1.1	-74.3	20.0	8.6	1.9	49.7	-74.9	18.8	9.9	18.7	3.7
5-3-10a@09		8.75E+12		28.8	0.6	85.7	1.1	-74.3	16.5	12.3	1.9	49.7	-74.9	17.8	11.0	5.3	1.1
5-3-10a@10		1.08E+13		24.9	0.5	84.9	1.1	-74.3	15.7	9.2	1.9	49.7	-74.9	17.4	7.6	6.6	1.3
5-3-10a@11		9.85E+12		24.2	0.6	79.2	1.1	-74.3	9.6	14.6	1.8	49.7	-74.9	13.7	10.5	6.0	1.2
5-11-7a@1	MX	7.19E+12		21.7	1.4	82.2	1.1	-74.3	12.8	8.9	1.8	49.7	-74.9	16.5	5.2	4.4	0.9
5-11-7a@2		7.38E+12		21.1	1.0	79.2	1.1	-74.3	9.6	11.5	1.8	49.7	-74.9	14.9	6.2	4.5	0.9
5-11-7a@3		6.47E+12		22.5	1.1	78.1	1.1	-74.3	8.5	14.1	1.8	49.7	-74.9	14.9	7.6	3.9	0.8
5-11-7-2a@1		4.56E+13		15.8	0.8	90.7	1.1	-74.3	21.8	-6.0	1.9	49.7	-74.9	19.0	-3.2	27.8	5.6
5-11-7-2a@2		4.96E+13		16.9	0.8	90.7	1.1	-74.3	21.8	-4.9	1.9	49.7	-74.9	19.0	-2.1	30.2	6.0
5-11-7-2a@3		4.91E+13		15.9	0.8	91.2	1.1	-74.3	22.4	-6.5	1.9	49.7	-74.9	19.2	-3.3	29.9	6.0
5-11-7-2a@4		4.89E+13		17.0	0.8	90.8	1.1	-74.3	22.0	-5.0	1.9	49.7	-74.9	19.1	-2.2	29.8	6.0
5-11-7-2a@5		5.27E+13		15.9	1.4	91.2	1.1	-74.3	22.3	-6.5	1.9	49.7	-74.9	18.6	-2.7	32.1	6.4
10-0-17-0@1	BL	1.40E+05		30.0	0.8	76.9	1.1	-74.3	7.2	22.8	1.8	49.7	-74.9	13.7	16.2	4.9	1.0
10-0-17-0@02		8.11E+04		29.2	0.9	78.3	1.1	-74.3	8.6	20.5	1.9	49.7	-74.9	18.5	10.7	2.8	0.6
10-0-17-0@03		5.26E+04		31.6	0.9	82.6	1.1	-74.3	13.2	18.4	1.9	49.7	-74.9	19.8	11.8	1.8	0.4
10-0-17-0@04		5.17E+04		40.6	1.1	81.5	1.1	-74.3	12.1	28.5	1.9	49.7	-74.9	20.2	20.3	1.8	0.4
10-0-17-0@05		4.31E+04		36.7	1.7	81.6	1.1	-74.3	12.2	24.5	1.9	49.7	-74.9	19.6	17.1	1.5	0.3
10-0-17-0@06		8.70E+04		31.9	1.4	79.4	1.1	-74.3	9.9	22.0	1.8	49.7	-74.9	16.4	15.5	3.1	0.6
10-0-17-0@07		5.16E+04		30.9	1.4	81.0	1.1	-74.3	11.6	19.3	1.9	49.7	-74.9	18.6	12.3	1.9	0.4
10-0-17-0@08		6.27E+04		28.4	1.9	80.2	1.1	-74.3	10.7	17.8	1.9	49.7	-74.9	18.3	10.1	2.4	0.5
10-0-17-0@09		6.90E+04		24.7	0.8	81.2	1.1	-74.3	11.7	12.9	1.9	49.7	-74.9	19.4	5.2	3.0	0.6
10-0-17-0@10		8.01E+04		31.9	1.1	78.1	1.1	-74.3	8.4	23.5	1.9	49.7	-74.9	18.6	13.4	3.7	0.7
10-0-17-0@11		8.62E+04		32.2	1.2	76.0	1.1	-74.3	6.7	26.0	1.8	49.7	-74.9	12.4	19.8	4.1	0.8

Table 4-3 The crystallization calculation of Li content between melt and minerals.

	ol: cpx: pl = 3:2:1					ol: cpx: pl = 1:1:0				
F	D=0.27	C_0=1	C_l/C_0	C_s/C_0	$C_s/C_{s,0}$	D=0.3	C_0=1	C_l/C_0	C_s/C_0	$C_s/C_{s,0}$
0.01	0.27	1.00	1.01	0.20	1.01	0.30	1.00	1.01	0.20	1.01
0.02	0.27	1.00	1.01	0.20	1.01	0.30	1.00	1.01	0.20	1.01
0.05	0.27	1.00	1.04	0.21	1.04	0.30	1.00	1.04	0.21	1.04
0.10	0.27	1.00	1.08	0.22	1.08	0.30	1.00	1.08	0.22	1.08
0.15	0.27	1.00	1.12	0.22	1.12	0.30	1.00	1.12	0.22	1.12
0.20	0.27	1.00	1.17	0.23	1.17	0.30	1.00	1.16	0.23	1.16
0.01	0.27	1.00	1.01	0.20	1.01	0.30	1.00	1.01	0.20	1.01
0.02	0.27	1.00	1.01	0.20	1.01	0.30	1.00	1.02	0.20	1.02
0.05	0.27	1.00	1.04	0.21	1.04	0.30	1.00	1.05	0.21	1.05
0.10	0.27	1.00	1.08	0.22	1.08	0.30	1.00	1.10	0.22	1.10
0.15	0.27	1.00	1.13	0.23	1.13	0.30	1.00	1.15	0.23	1.15
0.20	0.27	1.00	1.18	0.24	1.18	0.30	1.00	1.20	0.24	1.20

Chapter 5 Continuous supply of recycled Pacific oceanic materials in the source of Cenozoic basalts in SE China: the Zhejiang case

5.1 Results

5.1.1 Bulk-rock major and trace elements

Twenty-three samples are plotted on a total alkali versus silica (TAS) diagram (Fig. 5-1). All the samples have low LOI (loss on ignition) < 2.3%, and most have LOI <1.5%. The Zhejiang basalts can be subdivided into two groups with different ages, forming two distinct positive correlations. Group 1: the XL samples, consist of strongly alkaline rocks with older ages (26-24 Ma), have lower SiO_2 (<43%) and higher total alkalis (Na_2O+K_2O, 5.0-7.5%), they lie in the field of basanite. Meanwhile, Group 2: the GP and SC samples are composed of weakly alkaline rocks with younger ages (10-5 Ma), have higher SiO_2 and lower total alkalis and fall in the range from basanite to basalt. Fig. 5-1 shows major oxide contents plotted against MgO as the differentiation index. In the plots of SiO_2, Al_2O_3 and MnO vs. MgO (Fig. 5-2 a-c), a coherent trend is observed from Group 1 through Group 2. In the plots of CaO, TiO_2, Na_2O, $Fe_2O_3^T$, and K_2O vs. MgO (Fig. 5-2 d-h), the Group 2 samples display continuous linear trends marking their cogenetic origin. Meanwhile, the Group 1 basanites do not show a coherent trend with the Group 2 samples, possibly implying a different source composition. In addition to lower SiO_2 and higher total alkali content (Fig. 5-1), the Group 1 basalts have lower Al_2O_3 (<10%) and higher MgO (>12%) content than the Group 2 samples (Fig. 5-2a and 3c).

Chondrite-normalized rare earth element (REE) patterns in the Zhejiang basalts show similar characteristics, with light rare earth element (LREE) enrichment (Fig. 5-3). Group 1 samples have higher concentrations of REEs than Group 2 samples (Fig. 5-3). The $(La/Yb)_N$ ratios (where N represents chondrite-normalized, (Sun and McDonough, 1989)) of the Group 1 samples (31-37) are higher than those of the Group 2 samples (10-16), as are $(Sm/Yb)_N$ and $(La/Sm)_N$. In the Group 2 samples, we observe a slightly positive Eu anomaly (Eu_N/Eu^*=1.04-1.19, $Eu^*=(Eu)_N/((Sm)_N*(Gd)_N)^{1/2}$). The Eu_N/Eu^* values of Group 1 samples range from 1.00 to 1.05 (Fig. 5-3).

Fig. 5-1 TAS plots of the Zhejiang basalts. Classification of rock after Le Bas et al. (1986), and line

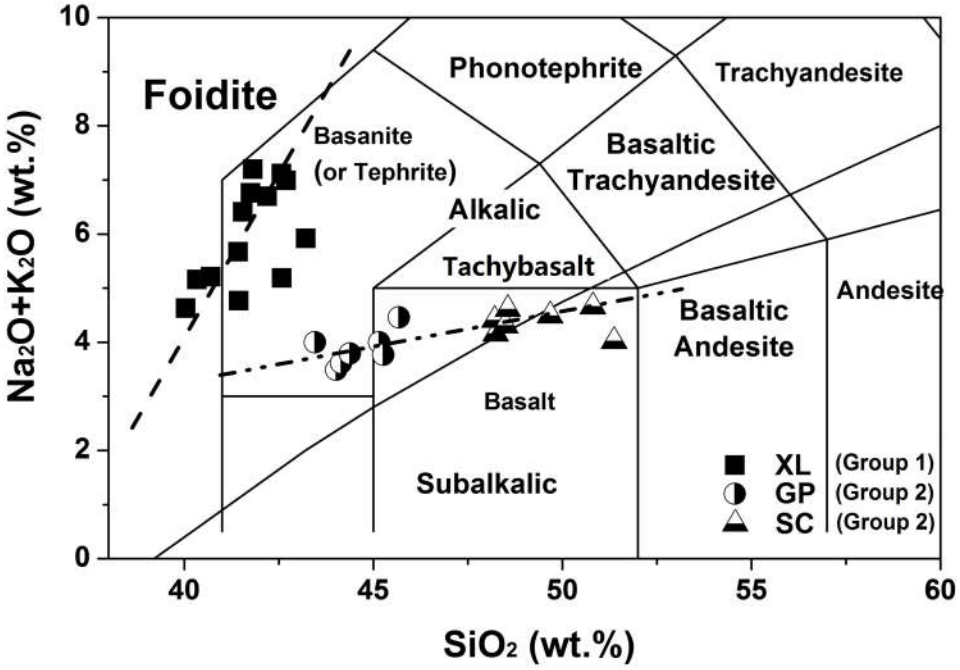

separating the alkali basalts and tholeiites from MacDonald and Katsura (1964).

In the primitive mantle-normalized extended trace element diagrams (Fig. 5-4), all of the samples show OIB-like patterns (i.e., enrichment of large ion lithophile elements and high field strength elements). The Group 1 samples show strongly positive anomalies in Nb and Ta, slightly positive anomalies in Sr and negative anomalies in U, K, Pb, Hf and Ti (Fig. 5-4). Most of the Group 1 samples are characterized by low Ba/Th (67-92) and Rb/Ba ($(Rb/Ba)_n<1$, where n represents primitive mantle normalization (Sun and McDonough, 1989)), high Ce/Pb (28-44) and high Nb/Ta (17.5-20.3) , as shown in Fig. 5-4. The Group 2 samples also exhibit positive anomalies in Nb and Ta and negative anomalies in U and Pb, but do not show pronounced anomalies in K, Ti and Hf. The Group 2 samples show stronger positive Sr and negative U anomalies than the Group 1 samples. The Group 2 samples are also characterized by higher $(Rb/Ba)_n$ (1.13-1.69) ratios and lower Ce/Pb (17-28) ratios than the Group 1 samples (Fig. 5-4). The Nb/Ta (18.3-20.0) ratios of the Group 2 samples share the same range as those of the Group 1 samples. The abundances of incompatible elements are higher in general in the Group 1 samples than those in the Group 2 samples.

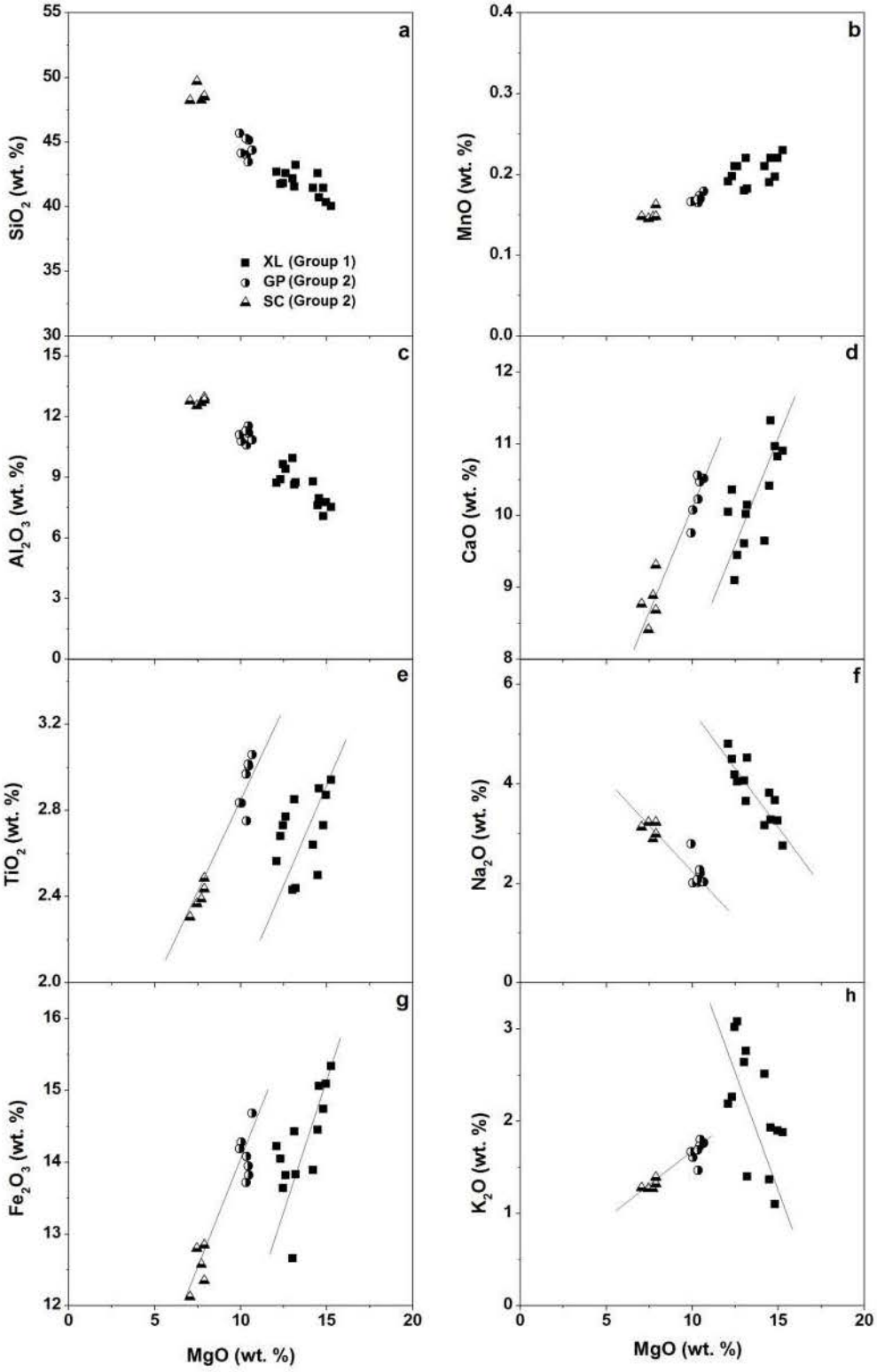

Fig. 5-2 Major element oxides vs. MgO in the Zhejiang basalts.

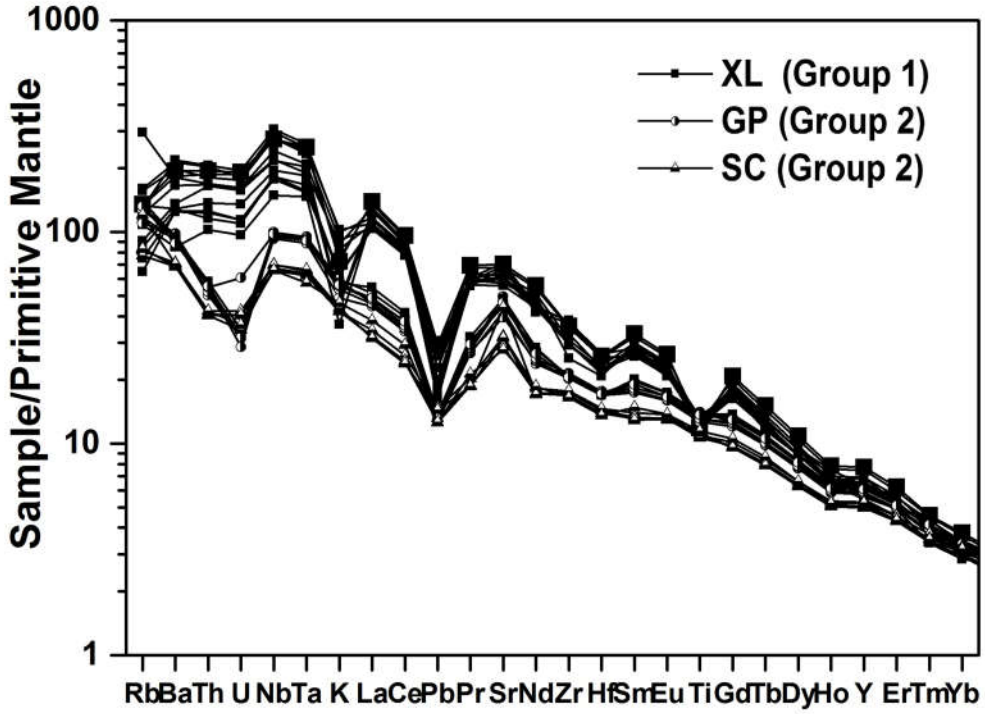

Fig. 5-3 Spider diagram of the Zhejiang basalt samples, normalized primitive mantle values are from Sun and McDonough, (1989).

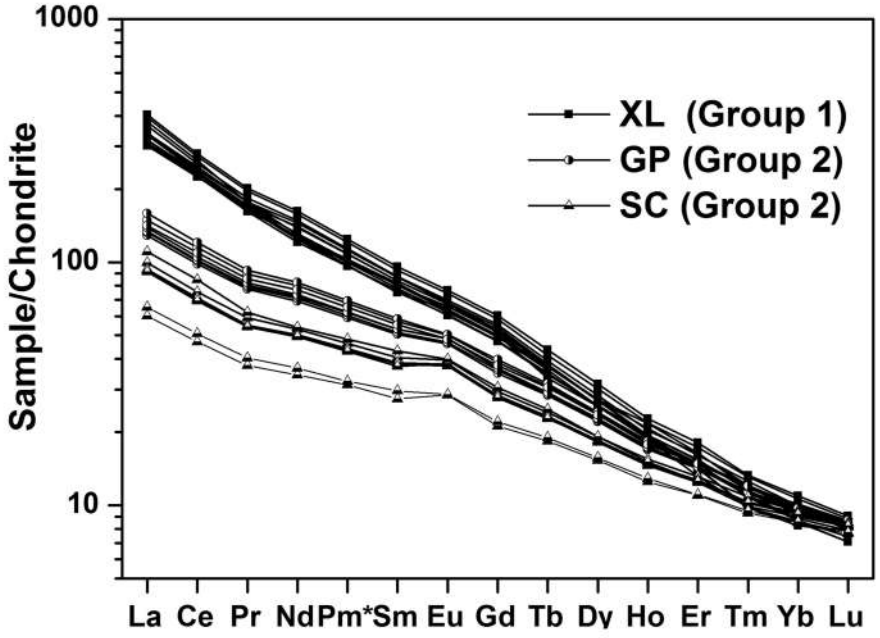

Fig. 5-4 REE of the Zhejiang basalt samples normalized by chondrite values are Sun and McDonough, (1989), whereas $Pm^* = ((Sm)_N * (Nd)_N)^{1/2}$.

5.1.2 Sr-Nd-Pb isotopic compositions

The bulk rock Sr-Nd-Pb isotopic data for the Zhejiang basalts are listed in Table 5-1 and plotted in Fig. 5-5. The Sr-Nd isotopic compositions are determined for both groups of samples and the Pb isotopic compositions only for the Group 2 samples. The Group 1 basanites show a limited range of $^{87}Sr/^{86}Sr$ (0.70366 to 0.70373) and $^{143}Nd/^{144}Nd$ (0.51289 to 0.51290; $\varepsilon Nd_{(t)}$ value approximately +5.0) ratios. Zou et al. (2000) and Ho et al. (2003) previously reported Sr-Nd-Pb isotopic data for XL basanites (Group 1 samples in this study) that were collected at the same locations and have similar geochemical compositions as of our samples. Their $^{87}Sr/^{86}Sr$ (0.70360 to 0.70370) and $^{143}Nd/^{144}Nd$ (0.51286 to 0.51290) ratios are in the same range as in our samples. Their Pb isotopic compositions of $^{206}Pb/^{204}Pb$ (~18.6), $^{207}Pb/^{204}Pb$ (~15.5), and $^{208}Pb/^{204}Pb$ (~38.5) for the basalts are therefore used in this work (Fig. 5-5b). The GP basalts have limited but moderately depleted $^{87}Sr/^{86}Sr$ (0.70326 to 0.70334) and $^{143}Nd/^{144}Nd$ (0.512960 to 0.513048; $\varepsilon Nd_{(t)}$ values of +6.3 to +8.0) ratios compared to those of the XL basanites. The SC alkali olivine basalts have relatively radiogenic $^{87}Sr/^{86}Sr$ ratios (0.70349 to 0.70367) and nonradiogenic $^{143}Nd/^{144}Nd$ ratios (0.51293 to 0.51296 ($\varepsilon Nd_{(t)}$ = +5.7 to 6.3)) compared to those of the GP samples. The plots of $^{87}Sr/^{86}Sr$ vs. $^{143}Nd/^{144}Nd$ ratios show a negative trend from DMM towards the EM components (Fig. 5-5a). The Group 2 samples have $^{206}Pb/^{204}Pb$ ratios of 18.4-18.5, $^{207}Pb/^{204}Pb$ ratios of 15.5-15.6, and $^{208}Pb/^{204}Pb$ ratios of 38.4-38.7. The Sr-Nd-Pb isotopic compositions of the Zhejiang basalts in general are, within the range of previously reported data for Cenozoic basalts from eastern China and within the mixing field of DMM and EMI/II (Chen et al., 2009; Choi et al., 2006; Fan et al., 2014; Guo et al., 2014; Ho et al., 2003; Ho et al., 2013; Huang et al., 2013; Kuang et al., 2012; Kuritani et al., 2011; Li et al., 2014; Sakuyama et al., 2013; Tang et al., 2006; Wang et al., 2012; Wang et al., 2013; Wang et al., 2011; Xu et al., 2005; Xu et al., 2012a; Xu et al., 2012b; Yan and Zhao, 2008; Zeng et al., 2011; Zhang et al., 2002a; Zhang et al., 2009; Zhang et al., 2012; Zhang et al., 2002b; Zhao et al., 2014; Zou and Fan, 2010; Zou et al., 2008; Zou et al., 2003; Zou et al., 2000) , as shown in Fig. 5-5b.

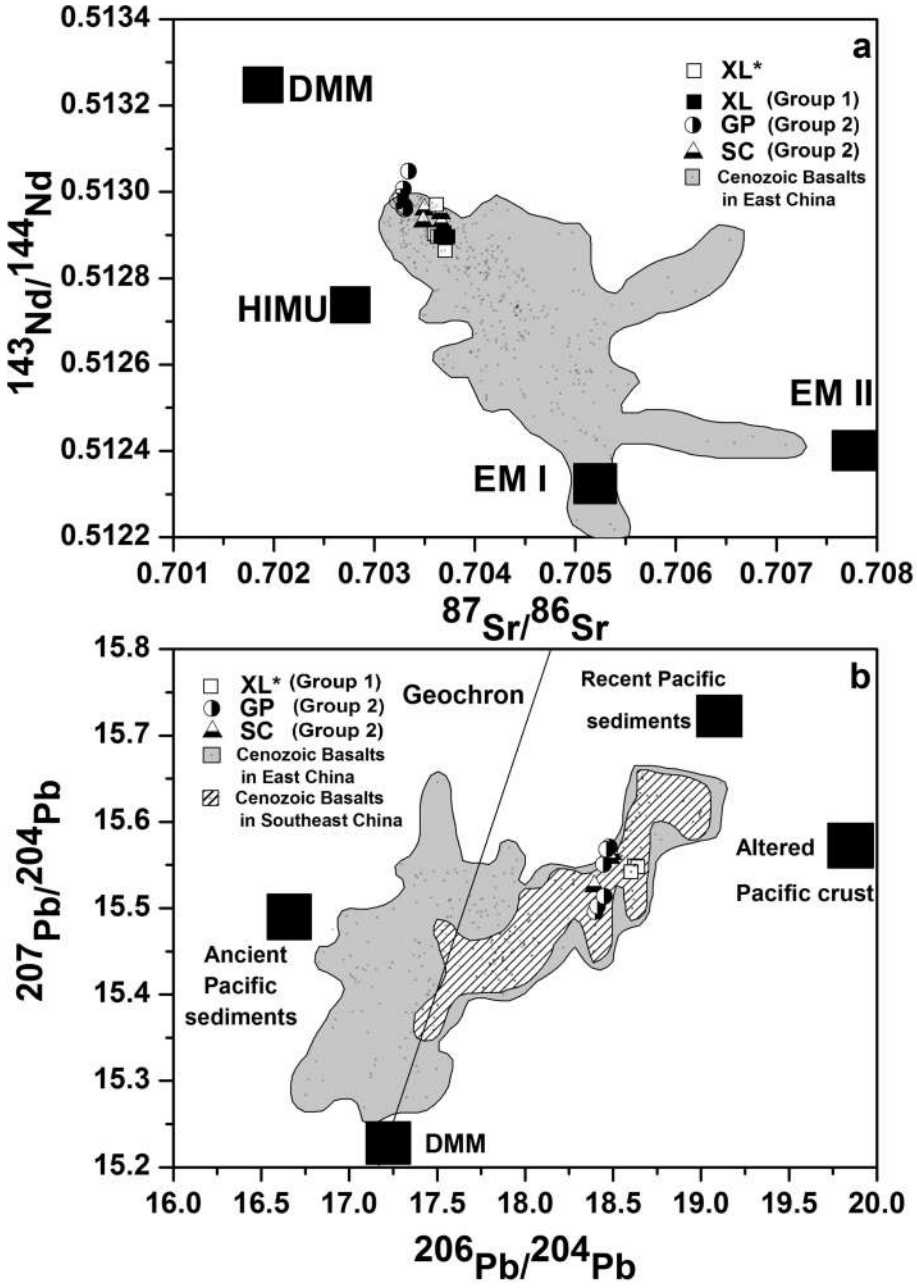

Fig. 5-5 (a) Sr–Nd isotopic compositions for the Zhejiang basalts (XL* from Ho et al. (2003) and Zou et al. (2000)). and (b) Pb isotopic compositions for the Zhejiang basalts (XL* from Ho et al. (2003) and Zou et al. (2000)). Approximate compositions for isotopic mantle end-member components (named DMM, HIMU, EM I, and EM II) obtained from a previous study (Workman and Hart, 2005; Zindler and Hart, 1986) are also shown. Isotopic compositions of Mariana trench sediments (Plank and Langmuir, 1998) and ancient Pacific sediments (1.5 Ga) are assumed to be similar to those of recent sediment components (Rehkämper and Hofmann, 1997). The isotopic compositions of the altered Pacific crust were determined by (Hauff et al., 2003). The isotopic compositions of Cenozoic basalts in East

China (including Southeast China) were obtained from Zou et al. (2000), Zhang et al. (2002a), Zhang et al. (2002b), Zou et al. (2003), Ho et al. (2003), Xu et al. (2005), Choi et al. (2006), Tang et al. (2006), Zou et al. (2008), Yan and Zhao (2008), Chen et al. (2009), Kuritani et al. (2011), Zhang et al. (2009), Zou and Fan (2010), Wang et al. (2011), Wang et al. (2012), Zeng et al. (2011), Xu et al. (2012a), Xu et al. (2012b), Kuang et al. (2012), Wang et al. (2013), Zhang et al. (2012), Ho et al. (2013), Huang et al. (2013), Sakuyama et al. (2013), Fan et al. (2014), Guo et al. (2014), Li et al. (2014) and Zhao et al. (2014).

5.1.3 Water content of cpx phenocrysts and equilibrated melts

The cpx phenocrysts of the Zhejiang basalts are augitic to diopsidic, with Mg# varying from less than 70 to 84. All of the cpx phenocrysts in the Zhejiang basalts exhibit IR absorption spectra in the OH-typical stretching vibration region (3000-3800 cm^{-1}), and the IR bands are centered at 3630 cm^{-1} and 3540 cm^{-1} (Fig. 5-6a), which is consistent with the positions of structural OH bands in cpx from previous studies (Bell et al., 1995; Denis et al., 2013; Ingrin and Skogby, 2000; Kovacs et al., 2012; Li et al., 2008; Peslier et al., 2002; Skogby et al., 1990; Sundvall and Stalder, 2011; Xia et al., 2010; Xia et al., 2013; Xia et al., 2014). The calculated H_2O contents of the cpx phenocrysts for the Group 1 samples range from 13 to 675 ppm, and those for the Group 2 samples range from 0 to 756 ppm (0-264 ppm for the SC samples and 94-756 ppm for the GP samples). The major element contents, absorbance of OH bands, thin section thicknesses, and the calculated H_2O contents of the cpx phenocrysts are listed in the Table 5-3.

The H_2O contents of the equilibrated melts of the cpx phenocrysts can be deduced via the H_2O content of cpx phenocrysts and the partition coefficient ($D^{cpx\text{-}melt}$) for H_2O between cpx phenocrysts and basaltic melts. The latter can be calculated using an equation provided by O'Leary et al. (2010) based on the chemical compositions of the cpx phenocrysts (equation 10 in their paper). The H_2O content of the melts equilibrated with the Zhejiang cpx phenocrysts ranges from 0.2% to 5.5% for Group 1 samples and from 0% to 4.79% for Group 2 samples. The detailed data are listed in Table 5-3.

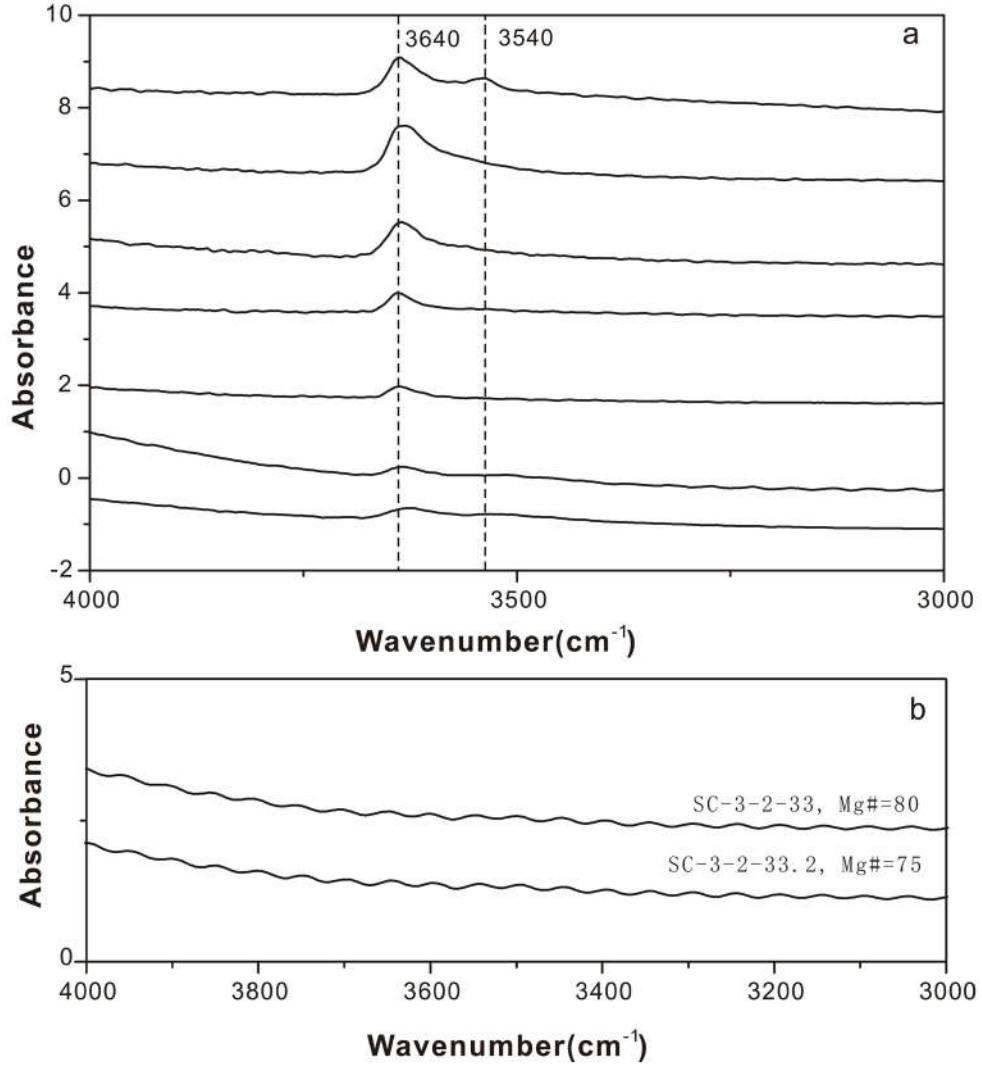

Fig. 5-6 (a) Representative OH IR absorption spectrum of cpx phenocrysts. Dashed lines mark the positions of individual OH bands (normalized to a thickness of 1 cm). (b) The OH IR absorption profile of the "water-loss" phenocrysts of the cpx phenocrysts from SC.

5.2 Discussions

5.2.1 Source or processes?

Prior to eruption, basaltic melts undergo a series of low-pressure magmatic processes, such as crustal contamination and fractional crystallization. These processes could potentially modify the composition of primary basaltic melt. Therefore, we first evaluate the effects of these processes.

5.2.1.1 Crustal contamination

First, the abundance of peridotite xenoliths entrained in most of the Zhejiang basalts required rapid ascent of magma, leaving little time for crustal contamination (O'Reilly and Griffin, 2010). Second, geochemical evidence for negligible crustal contamination in the Zhejiang basalts includes the following: (1) No positive correlation between $^{87}Sr/^{86}Sr$ ratios and 1/Sr concentration (Fig. 5-7a), which is not expected for prominent crustal contamination because the continental crust has a lower Sr concentration and much higher $^{87}Sr/^{86}Sr$ ratios than the Zhejiang basalts (Jahn et al., 1999; Rudnick and Gao, 2003); (2) Strongly negative Pb anomalies observed in all of the Zhejiang basalts (Fig. 5-4), are opposite to the effects of crustal contamination because both the upper and lower crusts contain very high abundances of Pb (Rudnick and Gao, 2003); and (3) No positive correlation between La/Nb and Ba/Nb (Fig. 5-7b), which is contrary to effective crustal contamination because crustal materials are generally characterized by high Ba/Nb and La/Nb ratios (Hofmann et al., 1986; Rudnick and Gao, 2003; Workman and Hart, 2005).

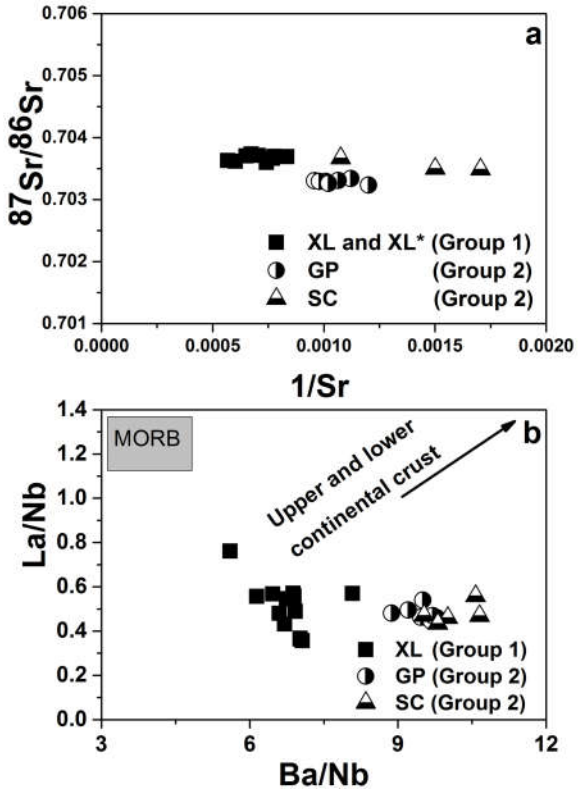

Fig. 5-7 (a) $^{87}Sr/^{86}Sr$ ratios vs. 1/Sr (data for Xilong (XL*) from Ho et al. (2003) and Zou et al. (2000)); (b) La/Nb vs. Ba/Nb (the MORB range was obtained from Rapp et al. (2008)).

5.2.1.2 Fractional crystallization

The correlations between Ni and Cr vs. MgO for the XL and GP samples (Fig. 5-8a and 5-8b) suggest a chemical evolution of their primary magmas controlled by fractional crystallization of minerals, such as olivine and cpx. The SC samples show relatively low Ni (150-170 ppm), Mg# (58 to 60) and MgO content (7-8 wt. %), suggesting that some amount of olivine fractional crystallization might have occurred in this case. If a large amount of fractional crystallization of olivine occurs, the La concentration of the residual magma increases, while the La/Sm ratio remains relatively constant, as we observed in the SC samples. However, this prediction contrasts with the positive correlations between La/Sm and La (Fig. 5-8c) observed in the Group 1 and GP samples, which indicate a low to moderate degree of fractional crystallization of olivine.

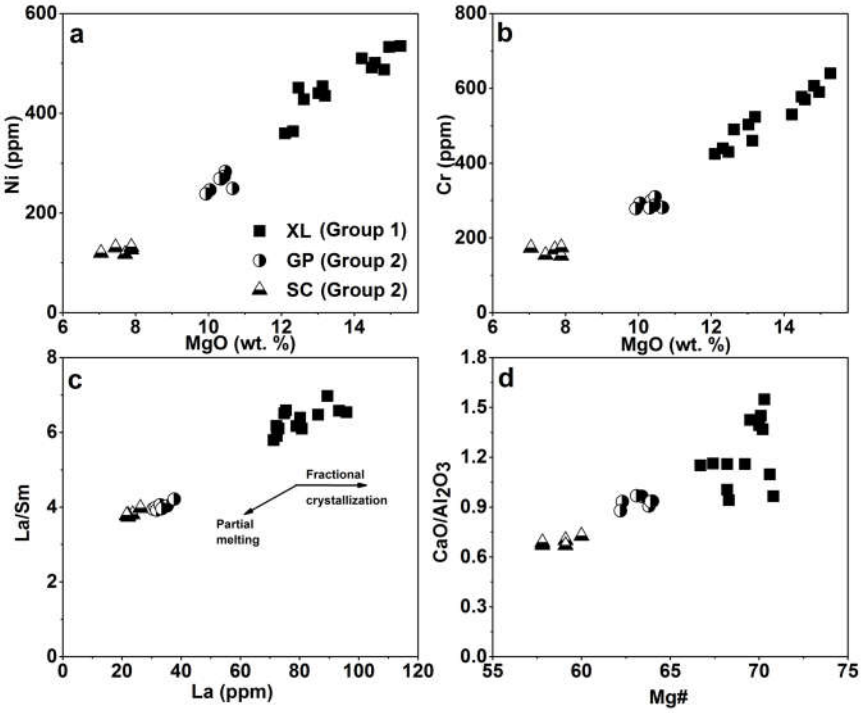

Fig. 5-8 (a) Ni vs. MgO for the Zhejiang samples; (b) Cr vs. MgO for the Zhejiang samples; (c) La/Sm vs. La for the Zhejiang samples; and d) CaO/Al_2O_3 vs. Mg# for the Zhejiang samples.

The high Mg# values of the XL (65-70) and GP (62-64) samples approaching those of primary magmas (Frey et al., 1978), suggest the fractional crystallization of olivine was not very significant, while the Mg# values of the SC samples are the relatively low (58-60). The fractional crystallization of cpx from alkali basaltic magma results in a positive correlation between CaO/Al_2O_3 and Mg# (Spath et al., 2001), which is not

observed in the Zhejiang basalts (Fig. 5-8d). Thus, the fractional crystallization of cpx was limited. Nevertheless, the ratios of incompatible trace elements and Sr–Nd–Pb isotope compositions are not sensitive to olivine fractionation and can thus retain their original features. In addition, positive Ba, Sr and Eu anomalies in all of the Zhejiang basalts (Fig. 5-3 and 5-4) exclude significant fractional crystallization of feldspar.

5.2.2 H_2O content in the initial magmas

To deduce the H_2O content of the "initial" basaltic melts and mantle sources, we need to clarify the following: (1) the evolution of H_2O contents within the ascending magmas, and (2) the H diffusion within the cpx phenocrysts after they crystallized from the magma.

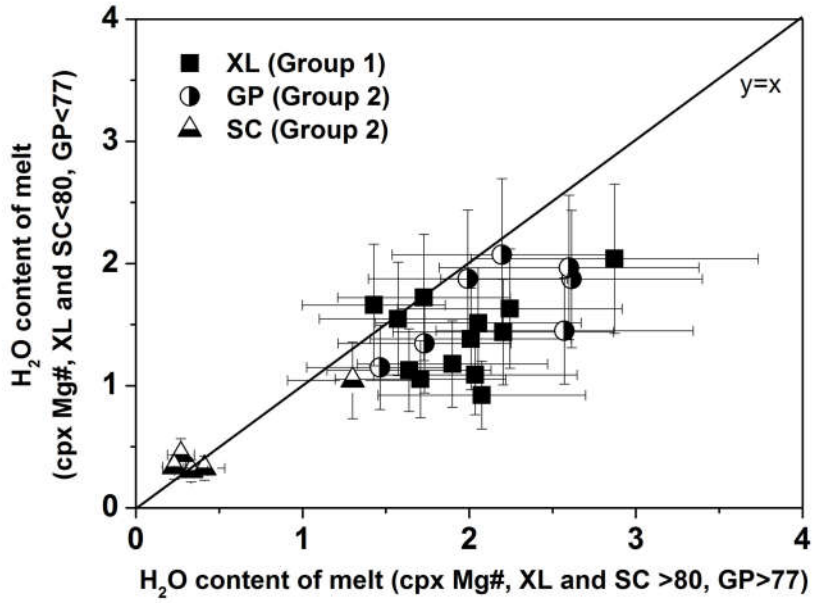

Fig. 5-9 Average H_2O content of the melt calculated from the H_2O content in cpx phenocrysts with the highest Mg# (XL and SC>80, GP >77) vs. the average value of water content estimated from cpx phenocrysts with the lower Mg# (XL and SC<80, GP <77).

Degassing, the fractional crystallization, and assimilation of surrounding rock during magma ascent can change the H_2O content of basaltic melts, which can be reflected in the different H_2O contents of cpx. Fractional crystallization increases the H_2O content of melts because the olivine, cpx, and feldspar are removed, as they have smaller H_2O contents (<1000 ppm). Meanwhile, degassing can intensively reduce the

H_2O content of melts. Because the lower continental crust is usually considered dry (Xia et al., 2006; Yang et al., 2008a), assimilation of a small amount of surrounding rock does not increase the H_2O content of the melt, and may even reduce it. The H_2O content of the Zhejiang basalts estimated from the cpx phenocrysts with high Mg# are mostly higher than the results estimated from those with lower Mg# (Fig. 5-9) in the same sample. This suggests that the parent magma of the lower Mg# cpx had lower H_2O contents than the parent magmas of the higher Mg# cpx for most samples. These observations indicate the following: a) fractional crystallization did not play an important role in the H_2O content variation in different cpx grains, which is consistent with the small numbers of phenocrysts in the basalts studied; b) the melts underwent noticeable degassing during magma ascent, which is reflected in the lower H_2O content of the cpx with lower Mg#; and c) if the melts ascended rapidly, the subsequent degassing had little or no effect on the H_2O content of the early-formed cpx phenocrysts. Because the H_2O content of cpx with low Mg# does not represent the "initial" H_2O content of basalts, we can therefore estimate the "initial" H_2O content from the cpx grains with the highest Mg#. Variations in the resultant "initial" H_2O content between different samples reflect different degrees of partial melting of the same source or heterogeneities in the source materials, rather than the effect of degassing.

Given high diffusion rate of H in cpx ($D=10^{-10}$~$10^{-10.5}$ m^2/s at 900℃ (Hercule and Ingrin, 1999; Ingrin and Blanchard, 2006; Ingrin and Skogby, 2000; Woods et al., 2000)), cpx phenocrysts might suffer diffusive loss of H during the subsequent ascent of the melts. It was noted that some cpx grains from the SC samples (SC-1 to SC-4) are totally "dry", showing no OH-related IR band at either the core or the rim (Fig. 5-6b). In contrast, "dry" cpx phenocrysts are not observed in sample SC-5, which is similar to the GP basalts. Sample SC-5 has the highest inferred initial H_2O content among the SC basalts. Therefore, we suggest the following: (1) some SC cpx phenocrysts might have suffered a loss of H_2O during ascent; therefore the inferred H_2O contents of the corresponding melts are underestimated, and the inferred H_2O contents of these four samples (SC-1 to SC-4) do not represent the "initial" H_2O content of the SC basalts; and (2) SC-5 may have retained the initial value of H_2O, and its H_2O content (1.3%), which is the best value we obtained to represent the "initial" SC basaltic melt.

Thus, to calculate the "initial" H_2O content of the Zhejiang basalts, following rules were adopted: (1) Select cpx grains with high Mg# (>80 for XL and SC, >77 for GP) in each sample, and calculate their $D^{cpx\text{-}melt}$ values of H_2O. (2) Calculate the H_2O content of melts equilibrated with the selected cpx grains and the average H_2O contents for each sample. (3) Finally, omitted the samples whose cpx experienced obvious H diffusion. Based on the above considerations, we suggest that the "initial" H_2O content of the Zhejiang basalts ranged from 1.6 to 2.9 wt. % for the XL samples (Group 1), from 1.5 to 2.6 wt. % for the GP samples (Group 2) and was 1.3 wt. % for the SC samples (Group 2). These values fall within the range of H_2O content expected for back-arc basin basalts (BABBs) and island arc basalts (IABs), as suggested by Dixon et al. (2004), displayed in Fig. 5-10. Note that these values are the minimum values for the H_2O contents in the Zhejiang basalts.

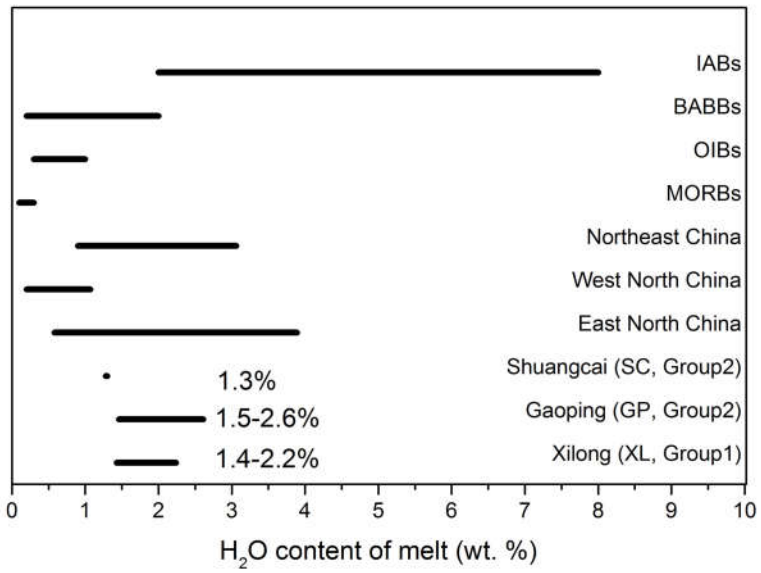

Fig. 5-10 Comparison of the calculated average H_2O content of the Zhejiang "primary" basaltic melts and the ranges of H_2O content for Northeast China, East North China, West North China, OIBs, MORBs, BABBs and IABs (data from Chen et al. (2015); Dixon et al. (2004) and the references therein).

5.2.3 Source lithology

A number of high-pressure melting experiments on peridotites have been conducted during the last 30 years to decipher the genesis of intra-plate alkali basalts

of various compositions (Baker and Stolper, 1994; Falloon and Danyushevsky, 2000; Hirose and Kushiro, 1993; Laporte et al., 2004; Schwab and Johnston, 2001; Walter, 1998; Wasylenki et al., 2003). In the presence of CO_2 and/or H_2O, peridotite melts tend to have less Si and more Fe but are still too low in Ti compared with the Group 1 basalts (Fig. 5-11a-d). However, partial melts in high-pressure melting experiments without CO_2 and/or H_2O for non-peridotites ,such as eclogite, pyroxenite, and hornblendite are too low in alkali content to serve as a single source (Dasgupta et al., 2006; Keshav et al., 2004; Kogiso and Hirschmann, 2001, 2006; Kogiso et al., 2004; Pilet et al., 2008) as shown in Fig. 5-12a. The SiO_2, TiO_2, FeO, and MgO abundances of melts produced from carbonated eclogites are consistent with the Zhejiang samples; however, they are too low in Na and K, and too high in Al (Fig. 11 and 12a). The high alkali content is instead more consistent with a peridotite source (including CO_2-bearing peridotite) (Fig. 5-12a). Therefore, the Zhejiang basalts were likely produced by melting of a mixed source rather than by any single source lithology (Fig. 5-11 a-d).

The presence of non-peridotite sources is also indicated by the Fe/Mn and Nb/Ta ratios. The distribution coefficients of D_{Fe}/D_{Mn} for cpx, opx, and garnet are less than 1, but they are greater than 1 for ol (Le Roux et al., 2011; Pertermann and Hirschmann, 2003a; Walter, 1998). The averages are 1.35, 0.95, 0.65, and 0.69 for ol, opx, cpx, and garnet, respectively. Residual pyroxene in the mantle source thus leads to high Fe/Mn ratios in the basaltic melts. The Fe/Mn ratios are 58-67 (Mn 0.18-0.23%) for Group 1 samples and 67-78 (Mn 0.15-0.18%) for Group 2 samples and plot along the boundary of peridotite- and pyroxenite-derived melts (Fig. 5-11e). Meanwhile, the Nb/Ta ratios range up to 20.7 for Group 1 samples and from 18.2 to 20.0 for Group 2 samples, which are higher than the value of the Primitive Mantle (i.e., PM 17.4, after Sun (1989)). Ti-oxides, such as rutile or ilmenite, are common phases in eclogite or garnet–clinopyroxenite and tend to have higher compatibility for Nb than for Ta (Dasgupta et al., 2004; Kogiso et al., 1997; Pertermann and Hirschmann, 2003a, b; Rapp et al., 1999; Rapp and Watson, 1995; Xiong et al., 2005). The melting of such eclogite or garnet–clinopyroxenite might thus produce the high Nb/Ta ratios observed in the Zhejiang basalts (Klemme et al., 2005). Recycled oceanic basalts transformed into garnet pyroxenites or eclogites are likely the non-peridotite sources of the Zhejiang basalts. In addition, trace elements indicate the presence of CO_2 in the source. The Hf_n/Hf^* values are 0.5-0.7 for Group 1 samples and 0.7-0.9 for Group 2 samples, where $Hf_n/Hf^* = Hf_n/(Nd_n/Sm_n)^{1/2}$ and n represents normalization to the primitive mantle. The deficit of

Hf relative to Nd and Sm could be induced by carbonaceous compositions in the source (Hoernle et al., 2002). The Ti_n/Ti^* values are 0.5-0.7 for Group 1 samples and 0.9-1.0 for Group 2 samples, where $Ti_n/Ti^* = Ti_n/(Gd_n/Eu_n)^{1/2}$. This deficit in Ti is also compatible with the ideas of Hoernle et al. (2002). Note that the high water content of the Zhejiang basalts indicates a hydrated mantle source.

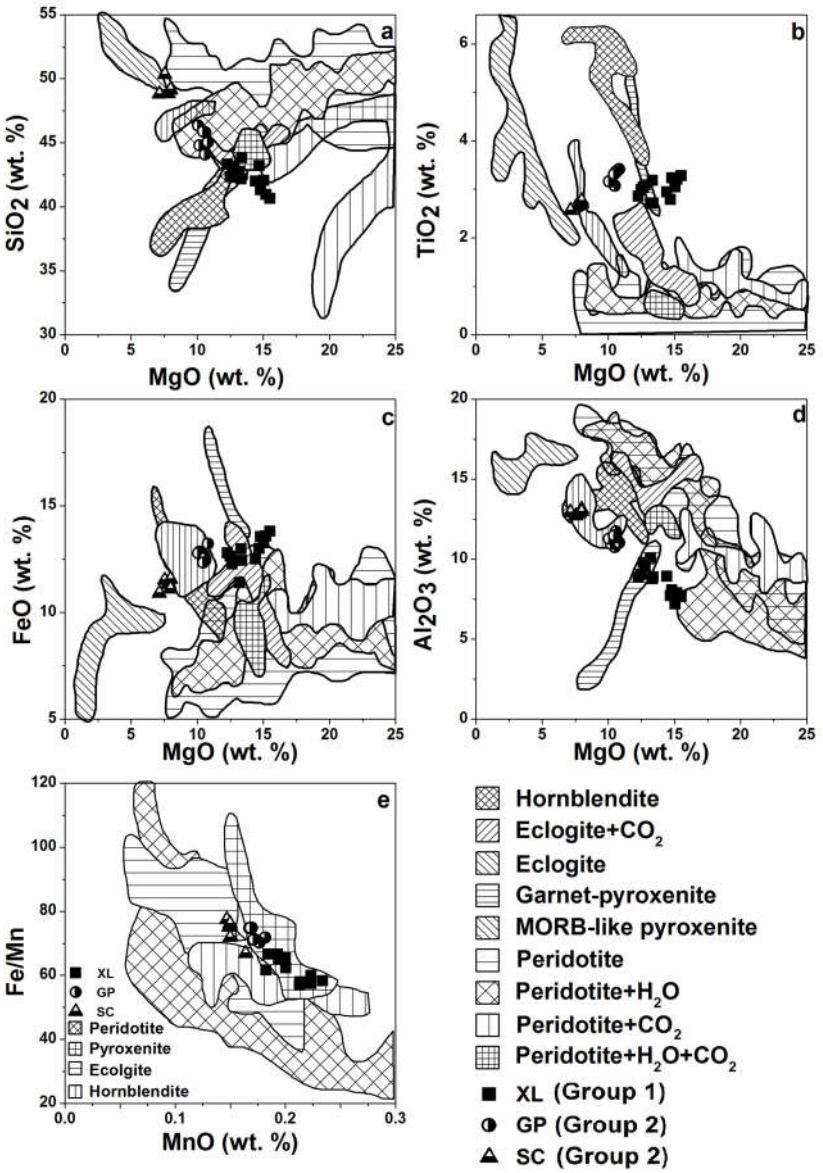

Fig. 5-11 Comparison of Zhejiang basalt samples with high-pressure experimental melts of various starting materials. (a) SiO_2 vs. MgO for the Zhejiang basalt samples; (b) TiO_2 vs. MgO for the Zhejiang basalt samples; (c) $Fe_2O_3^T$ vs. MgO for the Zhejiang basalt samples; (d) CaO

vs. MgO for the Zhejiang basalt samples; (e) Fe/Mn vs. MnO. Data source: Hornblendite (Pilet et al., 2008); Carbonated eclogite (Dasgupta et al., 2006); dry eclogite (Kogiso and Hirschmann, 2006); Garnet-Pyroxenites (Keshav et al., 2004; Kogiso and Hirschmann, 2001; Kogiso et al., 2004); MORB-like Pyroxenites (Pertermann and Hirschmann, 2003b); Peridotite (Baker and Stolper, 1994; Falloon and Danyushevsky, 2000; Hirose and Kushiro, 1993; Laporte et al., 2004; Schwab and Johnston, 2001; Walter, 1998; Wasylenki et al., 2003); Hydrous peridotites (Balta et al., 2011; Falloon and Danyushevsky, 2000; Gaetani and Grove, 1998; Parman and Grove, 2004); Peridotite with CO_2 (Dasgupta et al., 2007); and Hydrous peridotites with CO_2 (Ghosh et al., 2014).

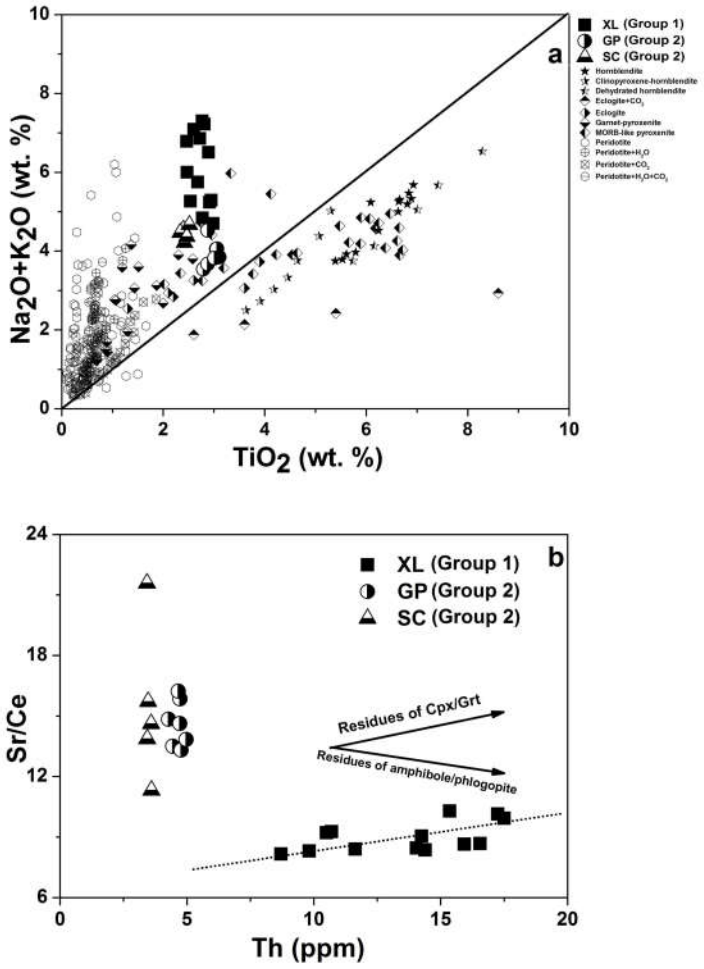

Fig. 5-12 Na_2O+K_2O vs. TiO_2. Data sources are the same as in Fig. 5-11. (b) Sr/Ce vs. Th content, where Cpx indicates clinopyroxene and Grt indicates garnet.

5.2.4 Lithospheric or asthenospheric source?

It has been widely accepted that subducted oceanic material can return to the surface through mantle plumes from a thermal boundary layer or the deep mantle, but there is no evidence for a deep plume-like structure from the lower mantle in the study area in Fig. 2-3 b (Hang and Zhao, 2006; Li and Van der Hilst, 2010; Zhao and Ohtani, 2009; Wei et al., 2012). Therefore, the mantle source of the Zhejiang basalts is either the subcontinental lithospheric mantle or the asthenosphere.

Although Cenozoic basalts from SE China display a DMM-EM II mixing trend in the Sr-Nd-Pb plots (Choi et al., 2006; Zou et al., 2000), contemporaneous lithospheric peridotite xenoliths (including spinel and garnet peridotite) do not show EM II-like characteristics (Fan et al., 2000; Tatsumoto et al., 1992; Xu et al., 2003). The $^{87}Sr/^{86}Sr$ and $^{143}Nd/^{144}Nd$ ratios of the contemporaneous Zhejiang peridotite xenoliths range from 0.70278 to 0.70366 and from 0.51296 to 0.51326 (Fan et al., 2000), respectively. The Zhejiang peridotite xenoliths are more depleted than the Zhejiang Cenozoic basalts. The spinel and garnet peridotites from other sites in SE China, such as Mingxi, are also more depleted than the Zhejiang basalts (Tatsumoto et al., 1992; Xu et al., 2003). Therefore, the radiogenic isotopic data represented by peridotite xenoliths do not support the direct generation of Cenozoic alkali basalts in SE China from the lithospheric mantle.

It can be checked whether the peridotite is "wet" enough to serve solely as the mantle source. To simplify the calculation, the “Continuous Fractional melting” model can be used. The H_2O content of the mantle source for the Zhejiang basalts is calculated based on the initial H_2O content of basaltic magma from cpx and the partition coefficients of H_2O between peridotites and basaltic melts (0.005-0.013 (Hirschmann et al., 2009; O'Leary et al., 2010)). The results are listed in Table 5-2, with F=0.01, 0.02, 0.05, 0.10 and 0.15. When F=0.01 and D=0.005, the H_2O content of the mantle source for Group 1 samples varies from 165 to 332 ppm, and that for Group 2 samples varies from 150 to 300 ppm (excluding dry samples SC-1 to SC-4). It is noteworthy that the H_2O content of the mantle source increases with increasing F value or increasing partition coefficient (Table 5-2). Therefore, all of these results represent the lowest estimations of H_2O content for the source, because we use the lowest partition coefficient. Both the Group 1 and 2 basalts entrained peridotite xenoliths (including spinel and garnet facies). The H_2O contents of the peridotite xenoliths from Southeast China range between 40 and 95 ppm (Yu et al., 2011). Clearly, the lowest estimations

of the H_2O content for the mantle source of the Zhejiang basalts is higher than that of the lithospheric mantle, again contrary to the lithospheric mantle as a direct source for the Zhejiang basalts, if it is represented by peridotite xenoliths.

As noted above, in addition to peridotites, the source of basalts could also be eclogites, pyroxenites or hornblendites (Dasgupta et al., 2006; Keshav et al., 2004; Kogiso and Hirschmann, 2001, 2006; Kogiso et al., 2004; Pilet et al., 2008); regardless of which types of lithologies constitute the source, they should meet the unique trace element characteristics of the melt. Another possible alternative candidate is a lithospheric mantle metasomatized by the infiltration of small amounts of melts/fluids (Pilet et al., 2008 and 2011). The metasomatized lithospheric mantle could contain secondary hydrous minerals (e.g., amphibole or phlogopite) and has been suggested as an OIBs-like basaltic magma source (Class and Goldstein, 1997; Pilet et al., 2011; Pilet et al., 2008; Pilet et al., 2005). Involvement of hydrous minerals in the melting source usually results in the high concentration of incompatible elements (e.g., Rb and Ba), positive Nb (Ta), and possibly Ti anomalies and/or negative U, Th, K, and Pb anomalies in the magmas (Pilet et al., 2011; Pilet et al., 2008). However, the geochemical characteristics of the Zhejiang basalts do not match such features and also differ from the experimental results of hornblendites (Class and Goldstein, 1997; Pilet et al., 2008; Pilet et al., 2005). The difference can be expressed as: (1) Residual K-bearing minerals result in negative K anomalies in basaltic melt as observed in Group 1 samples (Class and Goldstein, 1997), however, Group 2 samples show minor to no negative K anomalies (Fig. 5-4), reflecting a lack of residues of K-bearing minerals in the mantle source of Group 2 basalts; meanwhile, the strongly negative Ti anomalies for Group 1 basalts (Fig. 5-4) are also contrary to the results of the melting experiments of Pilet et al. (2008). (2) The total alkali (K_2O+Na_2O) contents of the Zhejiang basalts are highly variable within a narrow range of TiO_2 content (Fig. 5-12a), which is different from the trend of the hornblendite melting experiments by Pilet et al. (2008); it is also notable that the TiO_2 contents for the Zhejiang basalts are much lower than those of the hornblendite melts. The GP and XL samples contain garnet peridotite xenoliths (Liu et al., 2012; Zhang et al., 2007). The work of Liu et al. (2012) indicates that the equilibrium temperature of the garnet peridotites in Southeast China is higher than 1200℃. Host basalts are produced at greater depths and have higher temperatures, which are too high for hornblendite to be stable. Additionally, phlogopite and amphibole maintain a relatively high compatibility of Sr relative to Ce. Yang et al. (2003)

showed that residual phlogopite or amphibole results in melts that have a negative trend of Sr/Ce vs. Th, which is not the case in our samples (Fig. 5-12b). Instead, a positive trend of Sr/Ce vs. Th is identified in the Group 1 samples. $D^{Sr/Ce}$ for garnet/melt and clinopyroxene/melt are less than 1 (Bennett et al., 2004; Gaetani et al., 2003; Hauri et al., 1994). Therefore, the positive correlation may be caused by residual garnet and/or clinopyroxene in the source. All of these observations indicate that the Zhejiang basalts are not likely to have been produced by residual hornblende and/or phlogopite in the lithospheric mantle. Therefore, the asthenosphere could be a prevalent source for the Zhejiang basalts.

5.2.5 Enriched components in mantle sources

The Zhejiang basalts are characterized by elevated concentrations of incompatible elements and enriched Sr-Nd-Pb isotopic compositions compared with those of MORBs (Figs. 5-4 and Fig. 5-5). These features demand enriched component(s) in the mantle source. Because of the unsuitability of the lithospheric mantle as a source, the enriched components must reside in the asthenosphere. Geophysical imaging has shown that beneath the Zhejiang area, there is seismic evidence for a continuous stagnant subducted slab in the MTZ extending to the Mariana trench (Huang and Zhao, 2006); meanwhile, geochemical studies have suggested that SE China might have undergone lithospheric thinning similar to the NCC during the Mesozoic (Ho et al., 2003; Ma and Wu, 1987; Wu et al., 2003; Xu et al., 2000; Xu et al., 2002). Therefore, the enriched components might be recycled oceanic crust, marine sediments, or oceanic lithospheric mantle (Chen et al., 2015; Kuritani et al., 2011; Liu et al., 2015b; Niu and O'Hara, 2003; Sakuyama et al., 2013; Wang et al., 2011; Xu et al., 2012a; Xu et al., 2012b; Zhang et al., 2009), delaminated continental lithospheric mantle or lower continental crust associated with lithospheric thinning (Chen et al., 2009; Gao et al., 2008; Liu et al., 2008; Zeng et al., 2011). Nevertheless, it should be noted that the Mariana trench lies distant from any major continent, and there is a back-arc basin between the continent and the trench. The Mariana trench is far from any river system, so its sediments show some distinctive geochemistry, such as relatively low radiogenic isotopic ratios, and it contain relatively small amounts of marine sediments (38-221m in thickness, Plank et al. (1998)).

5.2.5.1 Recycled/delaminated lithospheric mantle?

Both subduction processes and lithospheric delamination can carry lithospheric mantle into the asthenosphere, forming distinct sources in the convecting mantle. Niu and O'Hara (2003) and Workman et al. (2004) proposed a model in which the recycled amphibole-bearing metasomatized oceanic lithospheric mantle could be a candidate for the source of OIBs. Amphibole is not stable above 3 GPa (~100 km depth) or 1200℃ (Grove et al., 2006; Niida and Green, 1999), and deep recycling (in the MTZ >450 km) of metasomatized lithospheric veins would cause amphibole breakdown and would not produce an EM-type trace element pattern. Therefore, recycled metasomatized oceanic lithospheric mantle is unlikely to be the source for the Zhejiang basalts.

Indeed, the studies (Gao et al., 2008; Xie et al., 2001) have concluded that Mesozoic alkali basalts from both the NCC and SE China were derived from the lithospheric mantle. Their conclusions were mostly based on the significant negative Nb and Ta anomalies in the extended trace element patterns. Such negative Nb and Ta anomalies are frequently observed in the Mesozoic basalts and are considered as a key characteristic of the continental lithospheric mantle. The Zhejiang Cenozoic basalts, by contrast, do not share similar characteristics, exhibiting instead positive Nb and Ta anomalies (Fig. 5-4). Therefore, the delaminated continental lithospheric mantle is unlikely to be the source of the enriched components of the Zhejiang basalts.

5.2.5.2 Delaminated lower continental crust (LCC)

Delaminated LCC is also a candidate for the enriched source component of the Zhejiang basalts as observed in the Shandong Cenozoic basalts from the NCC (Zheng et al. 2011). However, it is difficult to discriminate delaminated LCC from other enriched components, such as global subducting sediments (GLOSS, Plank and Langmuir (1998)), based only on trace elements and Sr-Nd-Pb isotopes. These different source components (e.g., GLOSS, DMM, MORB, recycled oceanic crust (ROC), and LCC) tend to have distinct H_2O/Ce ratios (Dixon et al., 2004; Dixon et al., 2002; Yang et al., 2008a), and the partition coefficients of H_2O and Ce are similar when partial melting occurs in the mantle (Dixon et al., 2004; Dixon et al., 2002). Therefore, the H_2O/Ce ratio of basalts could represent that of their mantle source, if crustal assimilation and degassing during magma ascent are excluded. In the Section 5.2.2, we estimated the “initial” H_2O content of the Zhejiang basalts. The H_2O/Ce ratios range from 100 to 200 for the Group 1 samples, from 220 to 430 for the GP samples (Group 2), and the ratio for the SC-5 sample (Group 2) is 250. Previous works (Yang et al.,

2008a) reported the H_2O content of the LCC granulite xenoliths in Southeast China ranged from 200 to 375 ppm. The average Ce content of the LCC granulite from the same place is approximately 13 ppm (Dai et al., 2008; Rudnick and Gao, 2003). H_2O/Ce ratios of the LCC in Southeast China can thus be estimated at approximately 15 to 28, which is much lower than those of the Zhejiang basalts. Meanwhile, the H_2O/Ce (67) of the residual Su-Lu eclogites estimated by Liu et al. (2015a) is also much lower than those of the Zhejiang basalts. In addition, the LCC has higher $^{87}Sr/^{86}Sr$, $^{143}Nd/^{144}Nd$, and U/Pb ratios and lower $^{206}Pb/^{204}Pb$ ratios (<18) (Jahn et al., 1999; Rudnick and Gao, 2003). Unlike the basalts in NE China and the NCC, the Zhejiang basalts have relatively high $^{206}Pb/^{204}Pb$ (>18.4) ratios and EM II-like Sr-Nd-Pb isotopic ratios, ruling out the LCC as the source for the Zhejiang basalts.

5.2.5.3 Recycled oceanic materials?

As we have noted above, there is no seismic evidence for a mantle plume beneath SE China, and the basaltic source enrichment likely corresponds to recycled oceanic material in the asthenosphere rather than the lower mantle or subcontinental lithosphere. One possible model is that this enrichment is long-lived and dispersed in the asthenosphere, involving an ancient recycled oceanic slab, delaminated continental lithospheric mantle/lower crust or other source, as in the plum-pudding model (Chung and Sun, 1992), making it impossible to constrain the provenance of these sources. As recycled subducted lithospheric mantle, delaminated continental lithospheric mantle, and the LCC have been ruled out in the previous sections, recycled oceanic materials are the only candidates for the enriched source components of the Zhejiang basalts. Recycled oceanic materials could be derived from ancient or relatively juvenile subduction processes, given the complex subduction history during the geological evolution of South China. However, the moderate depletion in the $^{87}Sr/^{86}Sr$ (low to 0.7032) and $^{143}Nd/^{144}Nd$ (high to 0.51305) ratios and nonradiogenic Pb isotope ($^{206}Pb/^{204}Pb$ low to 18.4) ratios for the Zhejiang basalts argue against enrichment from an old source. Therefore, the recycled oceanic materials require a young origin, which implicates stagnant subducted Pacific oceanic material.

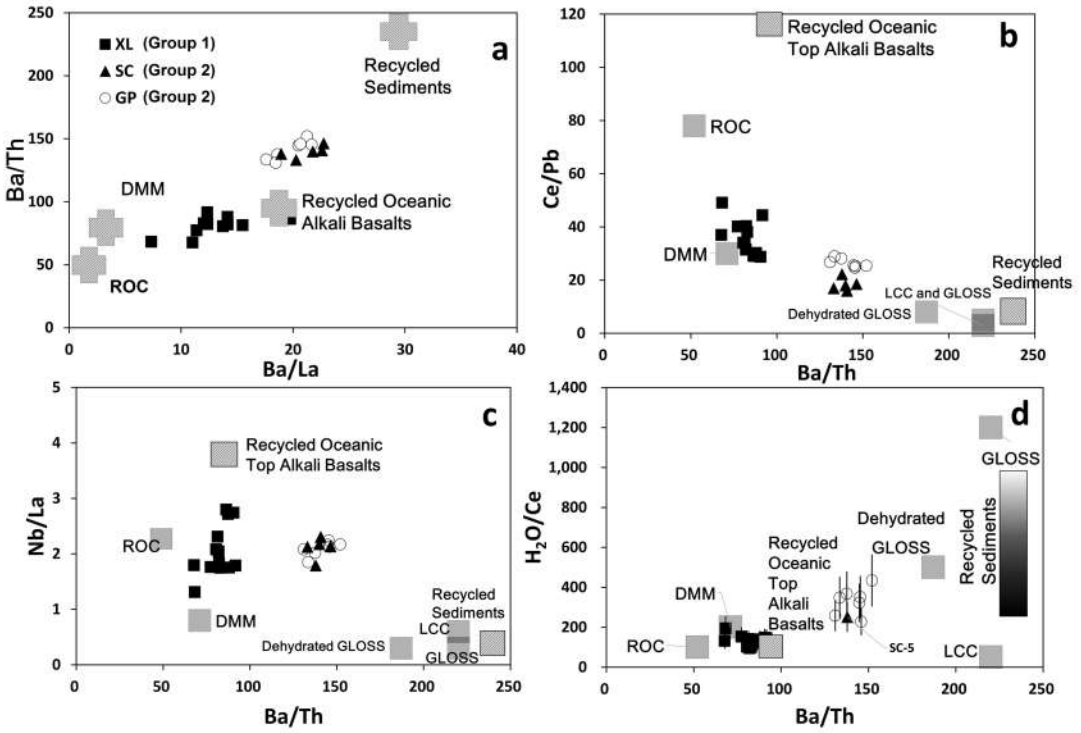

Fig. 5-13 (a) Plots of Ba/Th vs. Ba/La for the Zhejiang basalts. The Ba/Th and Ba/La of DMM, recycled oceanic alkali basalts, and recycled sediments were obtained from Workman and Hart (2005), Kelley et al. (2003), and Plank and Langmuir (1998), respectively, and then calculated and modified by the fluid mobility in Kogiso et al. (1997), Kessel et al. (2005), Aizawa et al. (1999) and Johnson and Plank (1999). (b) Ce/Pb vs. Ba/Th; (c) Nb/La vs. Ba/Th; and (d)H_2O/Ce for the Zhejiang basalts. Gray squares show the possible end members of mantle sources. The ratios of H_2O/Ce for GLOSS (~1280), DMM (~200), ROC (~100), LCC (<50) dehydrated sediments (several hundred) and recycled oceanic top alkali basalts (~100) are from Plank and Langmuir (1998), Shaw et al. (2012), Dixon et al. (2002) and references therein. The ratios of Ba/Th, Ba/La, Ce/Pb and Nb/La of DMM and GLOSS are from Workman and Hart (2005) and Plank and Langmuir (1998). The ratios of Ba/Th, Nb/La and Ce/Pb of ROC and the recycled oceanic alkali basalts are calculated from the concentrations of average MORB and the data of ODPs 801 (Gale et al., 2013; Kelly et al., 2003) and the mobility (Kogiso et al., 1997; Kessel et al., 2005); the ratios of Ba/Th, Nb/La and Ce/Pb of recycled Mariana sediments and dehydrated GLOSS are calculated based on the data from Plank and Langmuir (1998) and the mobility from Aizawa et al. (1999) and Johnson and Plank (1999). The error bar of H_2O/Ce is 30%.

5.2.5.3.1 Recycled oceanic crust in the source of Group 1 basalts

Xu et al. (2012a) and Sakuyama et al. (2013) recognized a recycled oceanic crustal signature in basalts from NE China and the NCC. The Group 1 basalts have high Nb/La (1.8-2.8), Ce/Pb (>30), and $Fe_2O_3^T$ (>12.5%) and low Ba/Th (<90), which are similar to the key features of melts related to recycled oceanic crust (Sakuyama et al., 2013; Xu et al., 2012a). Recycled oceanic crust is composed of upper alkali basalts (sometimes known as seamounts), tholeiitic basalts (i.e. normal oceanic crust, MORBs), and lower gabbro cumulate. Recycled oceanic upper alkali basalts come from the tops of some anomalous oceanic crust segments (Kelley et al. 2003), or from subducted oceanic islands or seamounts (Straub et al. 2015). Meanwhile, recycled oceanic upper alkali basalts are also recognized as an important enrichment source for basalts related to subduction (Staudigel et al. 2010; Straub et al. 2015). These oceanic upper alkali basalts generally have distinctly different enriched isotope and trace element features compared with MORBs (Straub et al. 2015). Therefore, in addition to normal MORBs, the top alkali basalts are also regarded as an important recycled component during plate subduction. Due to the marked mobility of trace elements, the dehydration process, occurring at depths where subduction begins, greatly changes the concentrations (and ratios) of trace elements in the oceanic crust and sediments (Aizawa et al., 1999; Johnson and Plank, 1999; Kessel et al., 2005; Kogiso et al., 1997). La, Ba and Pb are more mobile than Nb, Th and Ce; therefore, the ratios of Nb/La and Ce/Pb are much higher in dehydrated ROC than in fresh oceanic crust, and the Ba/Th ratio is reduced in both dehydrated ROC and sediments (Aizawa et al., 1999; Johnson and Plank, 1999; Kessel et al., 2005; Kogiso et al., 1997). On the basis of mobility (or partition coefficients) from Kogiso et al. (1997) or Kessel et al. (2005) and data for the average MORBs (Gale et al., 2013), the Nb/La, Ce/Pb and Ba/Th ratios of the recycled dehydrated oceanic crust can be changed to 2.0, 74 and 56 from their original values of 0.9, 24 and 71, respectively. Those ratios of recycled common MORBs are still too low to be the precursor source for the XL basalts (Nb/La = 1.8 to 2.8 and Ba/Th = 68 to 90). The Nb/La and Ba/Th ratios of the XL basalts are also higher than those of DMM. The trace element concentrations are more elevated in the upper alkali basalts overlying the tholeiitic basalts in oceanic crust. The ratios of Nb/La, Ce/Pb, and Ba/Th in dehydrated top alkali basalts (TABs) can be changed to 4.0, 120, and 82, from their original values of 1.8, 31, and 156, respectively, if we use the available data for alkali basalts from the ODPs 801, in the Pacific plate (TABs in Kelley et al. (2003)). Meanwhile, the Ba/La

ratio of dehydrated TABs is approximately 26, which is higher than that of ROC and similar to that of the XL basalts (Fig. 5-13 a). All of the Group 1 basalts form an explicit mixing line between the recycled oceanic TABs and DMM in the plots of Ba/La, Ce/Pb, and Nb/La vs. Ba/Th (Fig. 5-13 a-c). Such a mixing line can also be found in the plot of H_2O/Ce vs. Ba/Th (Fig. 5-13d). The dehydrated top oceanic alkali basalts are therefore proposed as the enriched component source in the 26-Myr-old Group 1 samples.

5.2.5.3.2 Recycled sediment signature in the source of Group 2 basalts

Compared with the Group 1 samples, the younger Group 2 basalts have higher SiO_2, H_2O/Ce and Ba/Th ratios and lower Ce/Pb and Nb/La ratios. These features cannot be the result of a simple mixture between the recycled oceanic crust and DMM but require another wetter and more enriched source (Fig. 5-13). Subducted sediments can carry more water into the mantle than subducted oceanic crust (Dixon et al., 2002; Windley et al., 2010). The H_2O/Ce ratios of oceanic sediments can reach up to 1200 (Dixon et al., 2002; Plank and Langmuir, 1998). Depending on the degree of dehydration, the H_2O/Ce ratios of dehydrated GLOSS are thus expected to range from approximately 100 to several hundred, given the ratios of 100 for the recycled crust and 150-200 for the DMM (Dixon et al., 2002; Michael, 1995; Shaw et al., 2012). Other candidates for a wet source include hydrous metasomatic minerals, such as hornblende, within the lithosphere beneath the Zhejiang region or recycled oceanic lithosphere, which was discussed and excluded above. According to the plots of Ba/Th, Ce/Pb and H_2O/Ce vs. Ba/La (Fig. 5-13 a, b and d), the higher Ba/Th and H_2O/Ce and lower Ce/Pb ratios of Group 2 samples require a sediment-like component. Meanwhile, Group 2 also has relatively high Nb/La and high Nb/U; therefore, we suggest that, in addition to a sediment-like component, there should also be a recycled oceanic crust component in the source of Group 2 basalts.

5.2.5.3.3 Modeling source

5.2.5.3.3.1 Start materials and elementary mobility

To better understand the sources of the Group 1 and Group 2 basalts, we use these

starting materials to recover the process of dehydration of the recycled TABs and sediments. The Pacific and Philippine Sea plates are subducting beneath East Asia along the Mariana, Izu-Bonin, Japan, and Ryukyu trenches, but the subduction along the Ryukyu trench stops at approximately 300 km depth (Fukao et al., 1992). Therefore, the recycled subducted materials under SE China can be represented by ODP materials near the Mariana trench.

The trace elements and isotopic compositions of start materials for modeling are Marianas sediments (or global average sea sediments), Pacific Oceanic top alkaline basalts in ODPs 801, and deplete mantle, from Plank and Langmuir (1998), Kelley et al. (2003) and Hauff et al. (2003), and Workman and Hart (2005), respectively, which are listed in Table 5-4. The element mobility of recycled crust is determined from Kogiso et al. (1997), Kessel et al. (2005), Aizawa et al. (1999), and Johnson and Plank (1999), and the dehydration mobility of trace elements in sediments during subduction are from Aizawa et al. (1999) and re-calculated by the data from Johnson and Plank (1999), while Mobility=$(C^s-C^r)/C^r$, (C^s is the start concentration, C^r is the residual concentration). Then, the Mobility values we use are chosen from the calculated results for oceanic materials dehydration. The partition coefficients and the reaction ratio of the modified source follow Salters and Stracke (2004) or Pilet et al. (2011), which are based on the experimental data of Salters and Longhi (1999) and the compilation of Halliday et al. (1995), as well as the GERM partition coefficient database. Then the batch partial melting modeling is used to calculate the trace element composition of melts. The isotopic ratios of recycled materials are different from those of modern oceanic basalts, such as the ODPs 801 we use, due to time-integrated radiogenic ingrowth. Before we calculate the proportion of subducted material, we must estimate the age of the stagnant slab beneath the Zhejiang region. The modern subduction rate at the Mariana trench is 45 mm/a, (Plank and Langmuir, 1998) and the distance in the horizontal direction between the Zhejiang region and the Mariana trench (E117° to E142°) is at least 2400 km, plus the depth of the stagnant slab (approximately 440-660 km, here we use 500 km), which thus moved more than 2900 km (2400 km+500 km) over approximately 65 Myr. If we take the age of the Group 1 basalts (approximately 26 Ma, Ho et al. (2003)), we can assume that these oceanic basalts subducted and dehydrated at least 90 Ma. Considering that the age of the Pacific slab is 157 Ma (Kelley et al., 2003), therefore, we used a slab age of approximately 247 Ma for our recycled oceanic crust component (Kelley et al., 2003). Müller et al. (2008) suggested that the

Pacific plate has been subducting since the Cretaceous, which is consistent with our assumption. The isotopic calculation is based on following assumptions: (1) the recycled TABs and sediments subducted from 90 Ma, and the ages of TABs and sediments were 247 Ma and 90 Ma, respectively; (2) the source of TABs is DMM, and the trace elements and isotopic compositions of DMM are from Workman and Hart (2005); (3) the trace elements of recycled TABs and sediments are the result in Table 5-4; and (4) the isotopic compositions of Sr/Rb, Nd/Sm, U/ Pb (the proportion of ^{87}Rb, ^{147}Sm, ^{235}U, ^{238}U and other radioactive isotopes) are BSE values for DMM. Therefore, the 247 Ma old recycled TABs-like basalts are calculated following the process below:

For recycled TABs:

$$(^{143}Nd/^{144}Nd)_{247Ma\ recycled\ TABs} = (^{143}Nd/^{144}Nd)_{0,247Ma} + (^{147}Sm/^{144}Nd)_{recycled\ TABs} \times (e^{147Sm\lambda\times247Ma} - e^{147Sm\lambda\times157Ma}) + (^{147}Sm/^{144}Nd)_{TABs} \times (e^{147Sm\lambda\times157Ma} - 1) \quad 1\text{-}1$$

$$(^{143}Nd/^{144}Nd)_{0,247Ma} = (^{143}Nd/^{144}Nd)_{0,157Ma} - (^{147}Sm/^{144}Nd)_{DMM} \times (e^{147Sm\lambda\times(247-157)Ma} - 1) \quad 1\text{-}2$$

$$(^{143}Nd/^{144}Nd)_{0,157Ma} = (^{143}Nd/^{144}Nd)_{TABs} - (^{147}Sm/^{144}Nd)_{TABs} \times (e^{147Sm\lambda\times157Ma} - 1) \quad 1\text{-}3$$

For recycled Sediments:

$$(^{143}Nd/^{144}Nd)_{recycled\ Sed} = (^{143}Nd/^{144}Nd)_{0,90Ma} + (^{147}Sm/^{144}Nd)_{recycled\ Sed} \times (e^{147Sm\lambda\times90Ma} - 1) \quad 1\text{-}4$$

$$(^{143}Nd/^{144}Nd)_{0,90Ma} = (^{143}Nd/^{144}Nd)_{Sed} - (^{147}Sm/^{144}Nd)_{Sed} \times (e^{147Sm\lambda\times90Ma} - 1) \quad 1\text{-}5$$

The results are listed in Table 5-4. After taking into account the subduction-dehydration-time accumulation, we estimate that the isotopic ratios of the modified recycled top alkali basalts are 0.512889 for $^{143}Nd/^{144}Nd$, 0.704494 for $^{87}Sr/^{86}Sr$, 21.37 for $^{206}Pb/^{204}Pb$ and 15.65 for $^{207}Pb/^{204}Pb$ (original isotopic and trace element data of TABs are from Kelley et al. (2003) and Hauff et al. (2003), the assumed isotopic data of the DMM source are from Workman and Hart (2005)). To simplify the calculation, we assume that the sediments retained their modern values of trace element concentrations and underwent a dehydration process similar to recycled TABs (ODPs 801). Then, we estimate the 90 Ma-time integrated isotopic compositions of the subducted sediments. Their chemical and isotopic compositions are also listed in Table 5-4. Based on this result, the proportions of recycled TABs (801) are calculated using a mixing equation of the $^{87}Sr/^{86}Sr$ isotopic ratio between the plate and DMM.

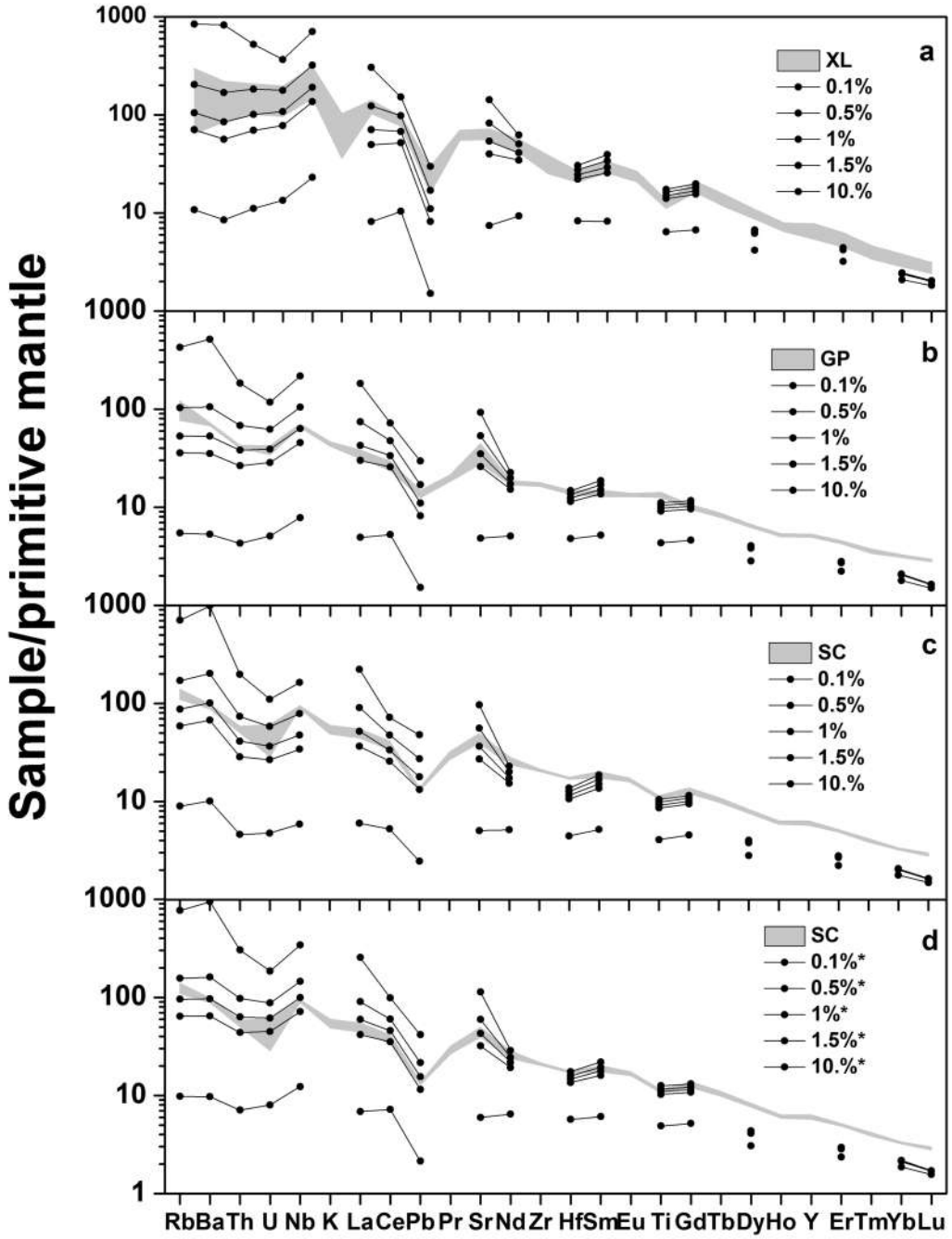

Fig. 5-14 The modeling results of melt mixture sources for XL, GP, SC, and SC*. SC* is modeled by $^{143}Nd/^{144}Nd$=0.512959

As mentioned above in the text, the proportions of recycled TABs and DMM in the Group 1 basalts and recycled TABs and sediments together with DMM in the Group 2 basalts are estimated based on their Sr-Nd isotopic compositions. The concentrations

and the Sr-Nd-Pb isotopic compositions of recycled TABs and sediments are the results from Table 5-4. The concentrations and Sr-Nd-Pb isotopic compositions of DMM are from Workman and Hart (2005) and also listed in Table 5-5. The average $^{87}Sr/^{86}Sr$ ratios of all XL samples are used to calculate the ratios of each recycled material composition. The isotopic compositions of GP-3 and SC-1 are used for GP and SC, respectively. The isotopic compositions of goal mixtures for SC* is 0.703664 for $^{87}Sr/^{86}Sr$ (SC-1), and 0.512959 for $^{143}Nd/^{144}Nd$ (SC-3). The calculated proportions of XL, GP, SC and SC* are listed in Table 5-5. The partition coefficients and the reaction ratios of the modified sources follow Salters and Stracke (2004) or Pilet et al. (2011) (Table 5-5), which are estimated based on the experimental data of Salters and Longhi (1999) and Salters and Longhi (1999), and the compilation of Halliday et al. (1995), as well as the GERM partition coefficient database. The "Batch" melting model are used to calculate the melting compositions. We show the result of melting for XL, when F= 0.1%, 0.5%, 1%, 1.5% and 10% for example, in Table 5-5.

To obtain the average $^{87}Sr/^{86}Sr$ isotopic ratio of the Group 1 basalts, 3.95% recycled TABs (801) and 96.05% DMM are required. We estimate the melt compositions for different degrees of partial melting (0.1-10%) of the mixed source, which are shown in Fig. 5-14a. The modeled melts show similar trace element patterns to the Group 1 basalts. They share most of the features of the trace elements (Fig. 5-14 a), including similar Ce/Pb (49-65 for calculated melts vs. 28-44 for the Group 1 basalts), Nb/La (2.4-2.9 vs. 1.3-2.8) and Ba/Th (62-130 vs. 67-92) ratios. Approximately 0.5-1.0% of melting matches the trace element abundances of the Group 1 basalts well. Our modeled source ($^{143}Nd/^{144}Nd = 0.51293$; $^{206}Pb/^{204}Pb = 19.53$; $^{207}Pb/^{204}Pb = 15.55$), however, has more radiogenic $^{143}Nd/^{144}Nd$ and $^{206}Pb/^{204}Pb$ ratios than the XL basalts (average $^{143}Nd/^{144}Nd = 0.51289$; $^{206}Pb/^{204}Pb = 18.64$; $^{207}Pb/^{204}Pb = 15.55$). Nevertheless, altered oceanic crusts tend to have a wide range of isotopic compositions (e.g., the $^{143}Nd/^{144}Nd$ ratios of the OPDs 801 basalts range down to 0.51236 (Hauff et al., 2003)), and the uncertainties in the ages of recycled oceanic basalts and DMM can also affect their isotopic compositions. Furthermore, the $^{206}Pb/^{204}Pb$ ratio of the recycled oceanic crust depends on the mobility of U, which is controlled by the redox condition of subduction dehydration and the true $^{206}Pb/^{204}Pb$ of DMM. Additionally, Müller et al. (2008) suggested that the early subducted Pacific slab might have been younger than ODPs 801. If this is true, the Sr and Pb isotopic compositions of the source could be less radiogenic. These observations indicate that a recycled oceanic crust component is

needed in the source to produce greatly enriched and OIB-like trace element pattern-like melts with enriched radiogenic Sr-Nd-Pb isotopes (Fig. 5-14a). Meanwhile, even if such recycled oceanic crust components served as the unique enrichment in the source of basaltic melts, the melts could match most of the geochemical features of the Group 1 basalts.

GP-3 and SC-1, which have mid-range values of $^{87}Sr/^{86}Sr$ and $^{143}Nd/^{144}Nd$ for each location, are chosen to calculate the proportion of recycled materials using mixing equations for the $^{87}Sr/^{86}Sr$ and $^{143}Nd/^{144}Nd$ isotopic ratios between the recycled materials and DMM. Approximately 0.3% recycled sediments plus approximately 1% recycled TABs (801) together with 98.7% DMM are required for the GP magmatism, and approximately 1% recycled sediments plus approximately 0.5% recycled TABs (801) together with 98.5% DMM are required for the SC basalts. The melts formed by various degrees of melting of the source materials are shown in Fig. 5-14 b and c. The modeled melts have Ce/Pb ratios of 23.4-33.3 for GP (measured average 26.4) and 14.5-20.5 for SC (measured average 18.3), Ba/Th ratios of 102-231 for GP (measured average 141) and 180-409 for SC (measured average 140), and Nb/La ratios of 1.2-1.7 for GP (measured average 2.1) and 0.8-1.0 for SC (measured average 2.1). Most geochemical features except Nb/La of SC of the mixed melt are similar to those of the Group 2 basalts (Fig. 5-14b, and 14c). Meanwhile, if the $^{143}Nd/^{144}Nd$ of SC-4 (0.512959) is used to estimate the proportion of recycled materials, approximately 0.6% recycled sediments plus approximately 1.8% recycled TABs together with 97.6% DMM are required. Then, the obtained Ce/Pb, Ba/Th, and Nb/La for SC are 23-33, 111-252, and 1.4-1.9 (Fig. 5-14d), respectively, which are close to the observation. Therefore, the model SC melts must fall in between the two described models. The most plausible degrees of melting are 0.6-1.0% and 1.0-1.5% for GP and SC, respectively. The Pb isotopic compositions of the modeled melts are 18.79 for $^{206}Pb/^{204}Pb$ and 15.55 for $^{207}Pb/^{204}Pb$ in GP (the average $^{206}Pb/^{204}Pb$ is 18.44, and the average $^{207}Pb/^{204}Pb$ is 15.53) and 18.78 (or 18.98 if $^{143}Nd/^{144}Nd$ is 0.512959) for $^{206}Pb/^{204}Pb$ and 15.59 (15.58 if $^{143}Nd/^{144}Nd$ is 0.512959) for $^{207}Pb/^{204}Pb$ in SC (the average $^{206}Pb/^{204}Pb$ is 18.46, and the average $^{207}Pb/^{204}Pb$ is 15.55). As we noted above, the Pb isotopic ratios of the modeled melt depend on the mobility of U during the dehydration of recycled oceanic crust. The mobility of U could be higher than the experimental result we use, which would result in a lower Pb isotopic ratio. These calculations successfully demonstrate the possibility of recycled oceanic sediments being one of the enriching components in

the source of the Group 2 basalts. These calculated melts are produced by small degrees of partial melting, and this may explain why the sites and volumes of basalts in Southeast China are so limited.

5.2.6 Links between enriched components and Pacific subduction

The variation in the source of the Zhejiang basalts indicates that the recycled materials in their source changed between 11 and 17 Ma. One of the most plausible interpretations of the change in these two group of basalts is that several new recycled material components were injected into the source of the basalts. On the other hand, intra-plate volcanism in the Zhejiang area, which had started in the Oligocene, continued and became more expansive in the Pliocene (Ho et al., 2003), requiring a continuous material supply. Since 100 Ma, the only plate subducted underneath SE China has been the Pacific Oceanic plate (Fukao et al., 1992; Müller et al., 2008). The presence of a stagnant subducted Pacific slab in the mantle transition zone (MTZ, 440-660 km) beneath eastern China is indicated by seismic images (Huang and Zhao, 2006; Li and van der Hilst, 2010; Wei et al., 2012; Zhao and Ohtani, 2009) (Fig. 2-3b). Therefore, the subducted Pacific slab is the most likely candidate for the recycled materials. Two other clues also point to the recent stagnant subducted Pacific slab. (1) The moderately depleted to slightly enriched Sr-Nd-Pb isotopic compositions require a recent enriched source; the subducted Pacific plate (since 120 Ma, Müller et al. (2008)) is the only young enriched source in South China. Other subductions are older than 200 Ma (Windley et al., 2010), including the Paleo-Asian subduction from before 234 Ma (Chen et al., 2009; Xiao et al., 2003; Xiao et al., 2009) and, the Paleo-Tethyan subduction between North and South China and between South China and Indochina, which occurred either in the Middle or Late Triassic (245 to 210 Ma) (Hacker et al., 2006; Liu et al., 2005), or in the Early Triassic (245 Ma) (Lepvrier et al., 2004). (2) Although the geochemistry of the basalts in East China shows some differences in detail, the rocks share similar trace element features, such as positive anomalies in Nb (Ta) and Sr and negative anomalies in Pb, Ti, Zr, Hf, and Sr-Nd-Pb isotopic compositions (Chen et al., 2015; Kuritani et al., 2011; Li et al., 2015; Liu et al., 2015b; Sakuyama et al., 2013; Wang et al., 2011; Xu et al., 2012a; Xu et al., 2012b; Zhang et al., 2012), implying that Southeast China basalts possibly share a common geodynamic factor with those of North and East China.

As we noted above (Section 5.3.4), the source materials of the Zhejiang basalts

show temporal variation and consist of fusible CO_2-bearing pyroxenite/eclogite veins and wall rock peridotites. The Pacific plate has been subducting with abundant water and other volatiles, such as CO_2 (Dixon et al., 2004; Dixon et al., 2002; Plank and Langmuir, 1998; Shaw et al., 2012) since possibly the Mesozoic (Müller et al., 2008). The presence of CO_2 and H_2O lowers the solidus temperature of peridotites and eclogites/pyroxenites (Dasgupta et al., 2007; Hirose, 1997; Kovacs et al., 2012), which may have triggered the Cenozoic intraplate volcanism in East Asia. Upwelling of this type of mantle started in the Oligocene, which produced the Group 1 (XL) basalts (Fig. 5-15a). With constant subduction of the Pacific plate, the recycled materials were continuously supplied by their source and participated in the melting processes (Fig. 5-15b). The upwelling of the recycled material may have moved eastward due to slab roll back and trench retreat (Fig. 5-15a and b) (Niu, 2013), resulting in a variation in the recycled materials. Most of the volatile components together with some incompatible elements might have been lost during dehydration of the slab approximately at 150 km depth, as shown in Fig. 5-15a (Aizawa et al., 1999; Johnson and Plank, 1999; Kessel et al., 2005; Kogiso et al., 1997). However, considering the scale of the subducted oceanic slab, some water and other volatiles were carried into the deep mantle (the MTZ) by transitioning to high-pressure hydrous phases, such as D and H (Nishi, 2015; Nishi et al., 2014; Ohtani, 2005a, b; Poli and Schmidt, 2002). When these hydrous phases were broken down, they released large amounts of H_2O, which resulted in a reduction of the solidus in the surrounding and overlying mantle (Niu, 2005; Windley et al., 2010) (Fig. 5-15c).

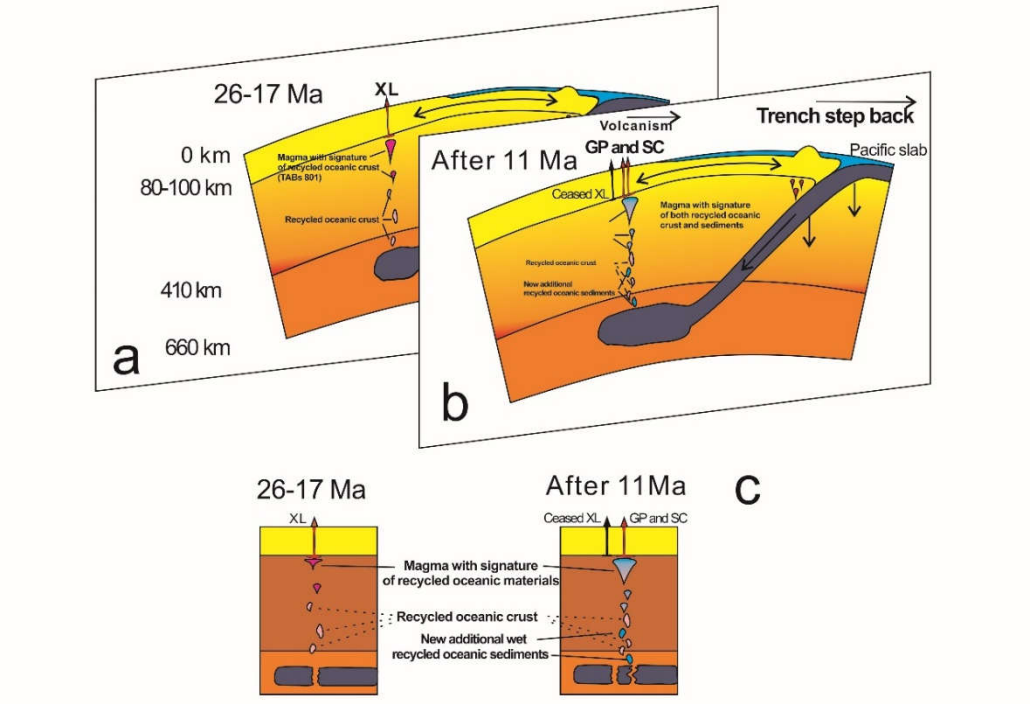

Fig. 5-15 A cartoon to illustrate different subducted oceanic material components in two-stage Zhejiang Cenozoic basalts. (a) Subduction of the Pacific plate beneath Southeast China (Huang and Zhao, 2006) induced upper mantle convection and back-arc extension between 26-17 Ma; (b) Subduction of the Pacific plate beneath Southeast China (Huang and Zhao, 2006) induced upper mantle convection and back-arc extension after 11 Ma. Upwelling mantle flow rolled back and was focused along a fault, a lithospheric weak zone, which consisted of recycled TABs components between 26-17 Ma and contained both recycled TABs and sediment components after 11 Ma, probably derived from stagnant Pacific oceanic slabs in the MTZ. (c) Upwelling mantle flows with a temporal change of components in the source of basalts were caused by a continuous supply of recycled oceanic materials from stagnant Pacific oceanic slabs in the MTZ. Between 26 and 17 Ma, upwelling mantle flows only involved some recycled TABs. The very limited recycled TABs and the surrounding mantle could melt to generate highly alkaline basalts, on account of the relatively low water content in the recycled TABs. After approximately 11 Ma, due to the consumption of recycled TABs and the new supply from the subducted Pacific slab, upwelling mantle flows involved less recycled TABs and included some recycled wet sediments. Wet recycled sediments lowered the solidus of the surrounding mantle and generated both highly alkaline basalts and AOBs, due to the relatively high water content in the recycled sediments. Due to lower components of recycled TABs in their source, these rocks show higher Ba/Th and lower Ce/Pb, Nb/La.

5.3 Conclusions

(1) Two groups of Zhejiang Cenozoic basalts are recognized by their obvious distinctions in major and trace element compositions; furthermore, both the groups erupted during different periods. The samples from Group 1 (older group)are characterized by relatively low Si, Al, and alkali contents, low Ba/Th ratios, and high Ce/Pb and Nb/La ratios. Meanwhile, they exhibit strongly negative K, Ti, Hf, and Pb anomalies in the extended trace element patterns. The Group 2 (younger group) samples have higher Si and Al and less alkali content than the Group 1 samples and exhibit highly positive Sr anomalies without obvious K and Ti anomalies. The two groups are not likely to be genetically linked.

(2) Most of the cpx phenocrysts in the Zhejiang basalts maintain their original H_2O content inherited from the parent magma, despite some basalts possibly experiencing H_2O loss during magma ascent. The "initial" H_2O content of the melts, reversely calculated from the H_2O content of the cpx phenocrysts and the corresponding partition coefficients of H_2O between cpx and basaltic melts, is 1.4 to 2.2 wt. % for the Group 1 samples and 1.3 to 2.6 wt. % for the Group 2 samples. The "initial" H_2O content of the Zhejiang basalts falls within the range of BABBs and IABs, indicating recycled oceanic materials in the mantle source.

(3) The Zhejiang basalts were produced by two components: depleted mantle and enriched recycled materials. The Group 1 samples exhibit higher Nb/La and Ce/Pb ratios than the Group 2 samples, plotting on the mixing curve between DMM and recycled dehydrated oceanic alkali basalts. The Group 2 samples show higher H_2O/Ce and Ba/Th ratios than the Group 1 samples, reflecting enriched sources of recycled dehydrated oceanic sediments together with the oceanic crust. This evidence implies that the stagnant slab of the Pacific plate served as a continuous material source for the Cenozoic basalts in the Zhejiang area.

Table 5-1. The major, trace element compositions, and isotopic ratios of the Zhejiang basalts and the calculated H_2O contents of basaltic melts

Group	Group 1												
Loactaion	Xilong (XL)												
Age [a]	23.7-26.4Ma												
GPS	N 29° 3'46.00"		E 118°58'52.40"										
Analysis No.	XL-1	XL-2	XL-3	XL-4	XL-5	XL-6	XL-7	XL-8	XL-9	XL-10	XL-11	XL-12	XL-13
Rock type	Basanite	Basanite	Basanite	Basanite	Basanite	Basanite	Basanite	Basanite	Basanite	Basanite	Basanite	Basanite	Basanite
SiO_2	41.76	42.58	41.44	43.22	42.70	40.70	40.04	42.57	41.81	40.34	41.55	42.19	41.43
TiO_2	2.68	2.50	2.73	2.44	2.56	2.90	2.94	2.77	2.73	2.87	2.85	2.43	2.64
Al_2O_3	8.91	7.61	7.08	8.76	8.73	7.95	7.52	9.41	9.66	7.77	8.65	9.96	8.80
Fe_2O_3	14.05	14.45	14.74	13.83	14.22	15.06	15.34	13.82	13.64	15.09	14.43	12.66	13.89
MnO	0.20	0.19	0.20	0.18	0.19	0.22	0.23	0.21	0.21	0.22	0.22	0.18	0.21
MgO	12.32	14.48	14.82	13.20	12.10	14.57	15.27	12.62	12.47	14.96	13.13	13.02	14.21
CaO	10.36	10.41	10.96	10.15	10.05	11.32	10.90	9.45	9.10	10.82	10.02	9.61	9.65
Na_2O	4.50	3.82	3.67	4.52	4.80	3.28	2.75	4.04	4.18	3.26	3.65	4.06	3.16
K_2O	2.27	1.37	1.10	1.40	2.19	1.93	1.88	3.08	3.02	1.90	2.76	2.64	2.51
P_2O_5	1.23	1.08	1.18	1.11	1.19	1.18	1.14	1.01	1.06	1.16	1.01	1.17	1.02
LOI	0.81	1.20	1.10	1.53	0.70	0.29	1.21	0.93	1.07	0.78	0.66	0.53	1.99
Total	99.07	99.69	99.02	100.34	99.44	99.40	99.22	99.91	98.95	99.17	98.93	98.45	99.51
Mg#[b]	67.4	70.2	70.3	69.2	66.7	69.5	70.1	68.2	68.3	70.0	68.2	70.8	70.6
Ba	1282	900	594	952	1357	870	900	1490	1530	880	1390	1266	1160
Be	3.4	2.6	2.3	3.0	3.3	1.8	2.0	2.7	2.9	2.0	2.6	3.1	2.6
Ce	166	144	147	156	171	141	142	143	151	137	138	161	143
Co	62	69	71	64	61	68	74	57	59	70	61	62	64
Cr	440	577	606	524	424	570	640	490	430	590	460	503	530
Cs	1.8	1.8	2.6	2.6	1.6	1.2	0.8	1.4	1.6	1.1	1.3	2.3	1.1
Cu	54	51	53	52	54	61	50	45	64	56	54	48	42
Dy	7.7	6.9	6.9	7.2	8.0	6.5	6.5	6.9	6.9	6.5	6.6	6.8	6.5
Er	2.9	2.6	2.5	2.7	3.0	2.4	2.3	2.7	2.7	2.2	2.3	2.5	2.4
Eu	4.3	3.9	4.0	4.0	4.4	3.8	3.6	3.7	3.7	3.7	3.5	3.9	3.5
Ga	21	19	19	20	22	20	21	22	24	19	22	21	21
Gd	12	11	11	11	12	11	10	10	10	10	10	11	10
Ge	1.4	1.5	1.5	1.4	1.4	0.2	0.2	0.2	0.2	0.2	0.2	1.4	0.2
Hf	7.9	6.9	6.4	7.2	8.0	6.8	7.0	7.9	8.2	6.6	7.8	6.6	7.0
Ho	1.2	1.1	1.1	1.2	1.3	1.1	1.1	1.2	1.2	1.1	1.1	1.1	1.1
La	93	79	81	86	96	72	73	75	80	71	72	89	75
Li	22	21	26	14	20	14	15	19	20	15	16	21	17
Lu	0.22	0.21	0.19	0.21	0.23	0.18	0.20	0.22	0.22	0.18	0.20	0.22	0.20
Nb	194	139	106	155	196	127	131	211	218	131	198	157	173
Nd	74	65	68	69	76	61	59	59	60	59	56	65	58
Ni	364	492	488	435	360	501	535	428	451	533	454	440	510
Pb	4.89	3.58	2.99	4.21	5.44	3.70	3.20	4.90	5.20	3.40	4.80	5.32	4.20
Pr	19	16	17	17	19	16	16	16	17	16	15	17	16
Rb	84	84	69	58	86	48	54	102	83	41	99	187	77
Sc	16	18	19	17	16	17	19	14	14	16	15	16	15
Sm	14	13	13	13	15	12	12	11	13	12	12	13	12
Sr	1439	1209	1200	1316	1486	1300	1180	1450	1500	1270	1420	1343	1290
Ta	10.1	7.6	6.0	8.3	10.3	6.3	6.4	10.3	10.7	6.8	9.6	7.8	8.6
Tb	1.55	1.40	1.42	1.47	1.63	1.35	1.35	1.39	1.40	1.25	1.29	1.41	1.31
Th	16	12	9	14	17	11	10	17	18	11	15	14	14
Tm	0.33	0.29	0.27	0.31	0.34	0.25	0.25	0.32	0.30	0.25	0.29	0.30	0.28
U	3.9	2.8	2.0	3.3	4.0	2.4	2.3	3.8	4.1	2.4	3.7	3.4	3.4
V	174	181	194	180	171	182	180	160	161	173	174	159	157
Y	34	30	29	31	35	25	26	27	29	25	27	31	27
Yb	1.8	1.6	1.5	1.7	1.9	1.5	1.4	1.7	1.7	1.5	1.7	1.7	1.5
Zn	160	151	151	148	159	172	172	171	169	174	181	140	162
Zr	397	326	284	346	401	331	329	429	421	334	416	332	370
H_2O[c] (wt%)	1.7	2.2	2.9	2.1	1.6	1.4	2.1	1.7	1.9	1.6	2.0	2.2	2.0
H_2O[d] (wt%)	1.3	1.7	2.7	1.7	1.4	1.1	1.9	1.7	1.7	1.4	1.8	2.0	1.6
$^{87}Sr/^{86}Sr$			0.703692		0.703734	0.703664					0.703713		0.703697
2σ			5		9	5					1		4
$^{143}Nd/^{144}Nd$			0.512905		0.512896	0.512896					0.512894		0.512896
2σ			13		16	13					14		14
$^{206}Pb/^{204}Pb$													
$^{207}Pb/^{204}Pb$													
$^{208}Pb/^{204}Pb$													

a The data of age are from the Ho et al. (2003) and Zou et al. (2000)

b $Mg\#=Mg^{2+}/(Mg^{2+}+\Sigma Fe^{2+})$, values were calculated assuming $Fe^{2+}/\Sigma Fe = 0.85$.

c The average of H_2O content calculated from cpx phenocrysts with Mg# >80 (Mg# >77 for GP samples).

d The average of H_2O content calculated from cpx phenocrysts with Mg# >75.

e AOB: Alkali olivine basalt.

f The water content of SC are the original calculated results from data, and only the water content SC-5 is used to stand for their "initial" water content.

Group	Group 2							Group 2				
Loactaion	Gaoping (GP, Xinchang)							Shuangcai (SC, Xinchang)				
Age	4.7-5.3Ma							8.4-9.3Ma				
GPS	N 29° 3'46.00"		E 118°58'52.40"					N 29°20'9.40"		E 120°51'15.10"		
Analysis No.	GP-1	GP-2	GP-3	GP-4	GP-5	GP-6	GP-7	SC-1	SC-2	SC-3	SC-4	SC-5
Rock type	Basanite	Basanite	Basanite	AOB[e]	AOB[e]	Basanite	AOB[e]	AOB[e]	AOB[e]	AOB[e]	AOB[e]	AOB[e]
SiO_2	44.02	44.15	44.39	45.68	45.16	43.46	45.27	49.68	48.24	48.21	48.49	48.56
TiO_2	2.75	2.83	3.06	2.84	3.01	3.02	2.97	2.37	2.39	2.30	2.43	2.48
Al_2O_3	10.61	10.80	10.87	11.11	11.21	11.55	11.31	12.54	12.69	12.77	12.96	12.82
Fe_2O_3	14.08	14.28	14.69	14.19	13.82	13.95	13.72	12.80	12.58	12.12	12.85	12.35
MnO	0.17	0.17	0.18	0.17	0.17	0.17	0.17	0.15	0.15	0.15	0.15	0.16
MgO	10.35	10.04	10.67	9.93	10.46	10.43	10.31	7.45	7.71	7.05	7.88	7.88
CaO	10.23	10.08	10.52	9.76	10.49	10.47	10.56	8.41	8.89	8.77	8.68	9.31
Na_2O	2.02	2.01	2.03	2.79	2.20	2.27	2.08	3.22	2.89	3.13	2.99	3.22
K_2O	1.47	1.61	1.77	1.67	1.80	1.73	1.69	1.27	1.27	1.28	1.32	1.39
P_2O_5	0.48	0.49	0.52	0.51	0.57	0.62	0.55	0.38	0.38	0.37	0.38	0.51
LOI	2.16	1.88	1.42	1.53	0.93	0.97	1.14	1.80	2.33	2.19	2.03	1.32
Total	98.34	98.34	100.09	100.17	99.81	98.64	99.76	100.06	99.52	98.34	100.16	100.00
Mg#[a]	63.4	62.3	63.1	62.2	64.0	63.8	63.9	57.8	59.1	57.8	59.1	60.0
Ba	649	643	687	680	656	663	618	478	501	481	488	496
Be	1.7	1.7	1.7	1.8	1.9	1.9	1.8	1.4	1.3	1.4	1.3	1.5
Ce	60	62	62	64	71	74	67	46	43	44	42	52
Co	61	60	62	60	66	65	65	50	46	47	48	51
Cr	300	293	281	278	310	287	280	154	169	173	152	174
Cs	0.6	0.6	0.5	0.5	0.6	0.5	0.6	0.5	0.4	0.2	0.4	0.2
Cu	85	78	68	78	78	79	91	61	61	58	58	65
Dy	5.6	5.7	5.7	5.8	6.1	6.1	6.0	4.9	4.6	4.7	4.7	4.9
Er	2.3	2.3	2.4	2.4	2.5	2.5	2.5	2.2	2.1	2.1	2.1	2.1
Eu	2.7	2.7	2.8	2.8	2.9	2.9	2.8	2.3	2.2	2.2	2.2	2.3
Ga	21	22	20	22	22	22	21	22	21	22	22	22
Gd	7	7	8	8	8	8	8	6	6	6	6	6
Ge	1.5	1.4	1.5	1.4	1.6	1.5	1.6	1.4	1.4	1.4	1.4	1.5
Hf	5.2	5.3	5.5	5.4	5.3	5.2	5.3	4.5	4.3	4.4	4.5	4.2
Ho	1.0	1.0	1.0	1.0	1.0	1.0	1.0	0.9	0.8	0.8	0.8	0.9
La	31	31	32	33	35	38	33	24	22	22	22	26
Li	10	11	9	9	9	10	9	7	7	6	6	6
Lu	0.21	0.21	0.21	0.21	0.22	0.22	0.22	0.22	0.21	0.21	0.21	0.21
Nb	66	68	71	70	71	70	70	50	47	48	50	47
Nd	32	33	34	34	37	39	36	25	23	23	23	25
Ni	268	246	249	238	283	273	269	131	117	120	127	132
Pb	2.36	2.41	2.53	2.54	2.51	2.55	2.50	2.73	2.32	2.43	2.66	2.34
Pr	7	8	8	8	8	9	8	6	5	5	5	6
Rb	71	74	80	70	84	89	84	53	52	49	53	76
Sc	22	22	22	21	22	22	23	21	21	22	21	22
Sm	8	8	8	8	9	9	8	6	6	6	6	7
Sr	892	833	991	1044	939	1021	979	676	929	606	666	587
Ta	3.6	3.7	3.9	3.8	3.8	3.7	3.7	2.7	2.6	2.6	2.7	2.4
Tb	1.06	1.07	1.09	1.09	1.16	1.19	1.14	0.90	0.86	0.87	0.85	0.93
Th	4	4	5	5	5	5	5	4	3	3	3	4
Tm	0.29	0.29	0.29	0.29	0.30	0.31	0.31	0.28	0.25	0.26	0.26	0.26
U	0.7	0.7	0.7	1.3	0.7	0.7	0.6	0.9	0.8	0.7	0.9	0.8
V	231	224	224	220	228	223	232	178	195	197	191	193
Y	26	26	27	27	28	29	28	24	23	23	23	24
Yb	1.6	1.6	1.6	1.6	1.6	1.7	1.7	1.6	1.5	1.6	1.6	1.6
Zn	140	140	146	140	151	151	148	127	120	122	123	124
Zr	227	231	241	238	234	231	230	198	189	194	198	184
H_2O[b] (wt%)	2.6	2.0	2.2	1.5	2.6	2.6	1.7	0.3[f]	0.3[f]	0.2[f]	0.4[f]	1.3[f]
H_2O[c] (wt%)	2.4	2.1	2.5	1.3	2.3	1.6	1.7	0.3[f]	0.4[f]	0.3[f]	0.3[f]	1.1[f]
$^{87}Sr/^{86}Sr$	0.703340	0.703233	0.703292	0.703303	0.703307	0.703290	0.703262	0.703664	0.703667		0.703499	0.703486
2σ	7	11	14	9	10	11	8	6	12		9	11
$^{143}Nd/^{144}Nd$	0.513048	0.512978	0.513007	0.512968	0.512960	0.512964	0.512988	0.512950	0.512928		0.512959	0.512931
2σ	5	8	8	7	8	9	6	14	10		8	7
$^{206}Pb/^{204}Pb$	18.398	18.413		18.451	18.447	18.479	18.465		18.495		18.485	18.394
$^{207}Pb/^{204}Pb$	15.496	15.502		15.514	15.551	15.571	15.568		15.562		15.558	15.525
$^{208}Pb/^{204}Pb$	38.453	38.451		38.463	38.546	38.599	38.573		38.675		38.646	38.467

Table 5-2. The calculated H_2O contents of mantle source for Zhejiang basalts.

	D-H_2O in source =0.005					D-H_2O in source =0.013				
F(%)	1.00	2.00	5.00	10.00	15.00	1.00	2.00	5.00	10.00	15.00
XL-1	197	348	854	1707	2561	317	433	870	1708	2561
XL-2	254	449	1102	2203	3305	409	559	1123	2204	3305
Xl-3	332	585	1436	2872	4308	533	728	1464	2873	4308
XL-4	237	418	1027	2054	3081	381	521	1047	2055	3081
XL-5	189	334	820	1639	2458	304	416	836	1639	2458
XL-6	165	291	714	1428	2142	265	362	728	1428	2142
XL-7	240	422	1038	2075	3113	385	526	1058	2076	3113
XL-8	200	352	864	1728	2592	321	438	881	1729	2592
XL-9	219	387	950	1899	2849	353	482	968	1900	2849
XL-10	182	320	786	1573	2359	292	399	802	1573	2359
XL-11	235	414	1018	2036	3054	378	516	1038	2037	3054
XL-12	259	457	1122	2243	3365	417	569	1144	2244	3365
XL-13	232	409	1005	2010	3015	373	510	1025	2011	3015
GP-1	302	532	1307	2614	3921	486	663	1333	2615	3921
GP-2	230	405	996	1991	2987	370	505	1015	1992	2987
GP-3	253	447	1098	2195	3293	408	557	1119	2196	3293
GP-4	169	298	732	1464	2197	272	371	747	1465	2197
GP-5	300	529	1299	2599	3898	483	659	1325	2600	3898
GP-6	297	523	1286	2571	3857	478	652	1311	2572	3857
GP-7	200	353	866	1732	2598	322	439	883	1733	2598
SC-1	38	67	166	332	497	62	84	169	332	497
SC-2	46	81	200	400	600	74	101	204	400	600
SC-3	39	69	170	340	510	63	86	173	340	510
SC-4	47	83	205	410	615	76	104	209	410	615
SC-5	150	265	650	1300	1950	241	330	663	1300	1950

Table 5-3 EPMA and FTIR data for the CPX phenocrysts of the Zhejiang basalts.

Sample No.	XL-1							
Section No.	1			2			8	
Point No.	1	2	3	1	2	3	1	2
SiO_2	49.87	51.47	48.01	50.45	53.90	51.03	47.95	49.29
TiO_2	1.24	1.19	2.51	1.05	0.06	1.61	2.65	2.27
Al_2O3	5.91	3.26	4.45	7.55	3.23	1.99	4.77	3.71
Cr_2O3	0.56	0.82	0.03	0.00	1.40	0.01	0.11	0.00
FeO	5.51	5.54	7.10	6.45	3.05	5.86	6.76	6.63
MnO	0.10	0.09	0.11	0.10	0.11	0.11	0.09	0.06
MgO	12.36	13.93	12.90	14.42	18.36	14.05	12.73	12.94
CaO	22.34	23.33	23.92	17.23	20.05	23.84	23.69	24.07
Na_2O	1.24	0.53	0.48	1.66	0.43	0.69	0.47	0.51
K_2O	0.01	0.00	0.00	0.02	0.02	0.01	0.01	0.01
NiO	0.01	0.00	0.01	0.05	0.06	0.02	0.01	0.03
Total	99.14	100.15	99.51	98.97	100.66	99.21	99.22	99.50
Si	1.86	1.90	1.81	1.86	1.93	1.91	1.81	1.85
Ti	0.03	0.03	0.07	0.03	0.00	0.05	0.08	0.06
Al	0.26	0.14	0.20	0.33	0.14	0.09	0.21	0.16
Cr	0.02	0.02	0.00	0.00	0.04	0.00	0.00	0.00
Fe	0.17	0.17	0.22	0.20	0.09	0.18	0.21	0.21
Mn	0.00	0.00	0.00	0.00	0.00	0.00	0.00	0.00
Mg	0.69	0.77	0.73	0.79	0.98	0.78	0.72	0.72
Ca	0.89	0.92	0.97	0.68	0.77	0.96	0.96	0.97
Na	0.09	0.04	0.04	0.12	0.03	0.05	0.03	0.04
K	0.00	0.00	0.00	0.00	0.00	0.00	0.00	0.00
Ni	0.00	0.00	0.00	0.00	0.00	0.00	0.00	0.00
Total	4.01	4.00	4.04	4.01	3.99	4.02	4.02	4.02
Mg#	79.99	81.75	76.43	79.94	91.48	81.03	77.05	77.67
$D^{(cpx\text{-}melt)}_{H_2O}$	0.0154	0.0113	0.0195	0.0191	0.0107	0.0102	0.0199	0.0149
Absorbance of cpx (cm^{-1})	3.30	3.69	4.95	3.10	3.50	4.30	2.90	2.30
Thickness of cpx (0.001mm)	96	110	75	105	103	100	54	59
Absorbance normalized to 1 cm (cm^{-1})	344	335	660	295	340	430	537	390
H_2O-cpx (ppm)	145	142	279	125	144	182	227	165
H_2O-melt (wt%)	0.95	1.25	1.43	0.65	1.35	1.78	1.14	1.10

Sample No. Section No. Point No.	3	4	5	6	7	8	9	10
SiO_2	44.67	51.85	46.44	47.42	52.47	46.16	46.05	47.13
TiO_2	4.06	1.78	3.03	2.35	0.78	3.23	2.90	2.99
Al_2O3	7.43	2.11	6.44	5.54	2.01	6.07	5.95	6.21
Cr_2O3	0.03	0.01	0.09	0.17	0.24	0.03	0.04	0.00
FeO	7.71	6.06	7.29	6.88	5.20	7.70	7.61	6.87
MnO	0.02	0.09	0.05	0.07	0.09	0.05	0.05	0.07
MgO	11.18	14.07	11.88	12.27	14.91	11.72	12.16	11.81
CaO	23.41	23.89	23.85	23.58	23.72	23.51	23.65	23.60
Na_2O	0.67	0.65	0.56	0.65	0.58	0.60	0.53	0.63
K_2O	0.07	0.01	0.01	0.00	0.03	0.00	0.01	0.00
NiO	0.03	0.09	0.02	0.02	0.00	0.06	0.06	0.02
Total	99.28	100.62	99.65	98.93	100.04	99.13	99.01	99.32
Si	1.70	1.91	1.75	1.80	1.94	1.76	1.75	1.78
Ti	0.12	0.05	0.09	0.07	0.02	0.09	0.08	0.08
Al	0.33	0.09	0.29	0.25	0.09	0.27	0.27	0.28
Cr	0.00	0.00	0.00	0.00	0.01	0.00	0.00	0.00
Fe	0.25	0.19	0.23	0.22	0.16	0.24	0.24	0.22
Mn	0.00	0.00	0.00	0.00	0.00	0.00	0.00	0.00
Mg	0.63	0.77	0.67	0.69	0.82	0.66	0.69	0.66
Ca	0.96	0.94	0.96	0.96	0.94	0.96	0.97	0.95
Na	0.05	0.05	0.04	0.05	0.04	0.04	0.04	0.05
K	0.00	0.00	0.00	0.00	0.00	0.00	0.00	0.00
Ni	0.00	0.00	0.00	0.00	0.00	0.00	0.00	0.00
Total	4.04	4.01	4.04	4.03	4.02	4.04	4.05	4.02
Mg#	72.12	80.54	74.41	76.07	83.64	73.06	74.03	75.39
$D^{(cpx\text{-}melt)}_{H_2O}$	0.0403	0.0102	0.0283	0.0216	0.0089	0.0280	0.0281	0.0245
Absorbance of cpx (cm^{-1})	3.20	2.50	3.50	1.95	3.30	2.61	3.10	2.30
Thickness of cpx (0.001mm)	55	61	61	59	60	52	52	46
Absorbance normalized to 1 cm (cm^{-1})	582	410	574	331	550	502	596	500
H_2O-cpx (ppm)	246	173	243	140	233	212	252	212
H_2O-melt (wt%)	0.61	1.70	0.86	0.65	2.62	0.76	0.90	0.86

Sample No. Section No. Point No.	11	12	13	14	14.2	14.3	15	16
SiO_2	51.92	48.73	47.67	48.00	51.45	49.10	47.67	47.27
TiO_2	1.46	2.45	2.66	2.67	1.72	1.85	2.37	2.95
Al_2O3	1.44	3.95	5.35	4.52	2.13	4.40	5.55	5.04
Cr_2O3	0.04	0.04	0.00	0.05	0.04	0.13	0.09	0.07
FeO	5.73	7.12	7.32	7.28	5.92	6.69	6.84	7.60
MnO	0.10	0.07	0.10	0.08	0.09	0.09	0.06	0.05
MgO	14.18	13.00	12.50	12.48	14.11	13.14	12.74	12.27
CaO	23.99	24.08	23.99	23.69	23.50	23.65	23.59	23.73
Na_2O	0.56	0.48	0.50	0.52	0.64	0.48	0.43	0.48
K_2O	0.01	0.00	0.01	0.00	0.03	0.00	0.01	0.00
NiO	0.00	0.00	0.01	0.02	0.00	0.03	0.04	0.03
Total	99.43	99.93	100.10	99.29	99.61	99.55	99.39	99.49
Si	1.94	1.83	1.79	1.81	1.92	1.84	1.80	1.79
Ti	0.04	0.07	0.08	0.08	0.05	0.05	0.07	0.08
Al	0.06	0.17	0.24	0.20	0.09	0.19	0.25	0.22
Cr	0.00	0.00	0.00	0.00	0.00	0.00	0.00	0.00
Fe	0.18	0.22	0.23	0.23	0.18	0.21	0.22	0.24
Mn	0.00	0.00	0.00	0.00	0.00	0.00	0.00	0.00
Mg	0.79	0.73	0.70	0.70	0.78	0.73	0.72	0.69
Ca	0.96	0.97	0.96	0.96	0.94	0.95	0.95	0.96
Na	0.04	0.04	0.04	0.04	0.05	0.04	0.03	0.04
K	0.00	0.00	0.00	0.00	0.00	0.00	0.00	0.00
Ni	0.00	0.00	0.00	0.00	0.00	0.00	0.00	0.00
Total	4.01	4.03	4.04	4.03	4.01	4.03	4.03	4.03
Mg#	81.51	76.49	75.27	75.34	80.96	77.78	76.87	74.22
$D^{(cpx\text{-}melt)}_{H_2O}$	0.0087	0.0173	0.0225	0.0192	0.0102	0.0163	0.0219	0.0226
Absorbance of cpx (cm^{-1})	1.70	3.40	3.80	2.97	1.50	3.30	1.80	2.90
Thickness of cpx (0.001mm)	51	52	54	49	49	49	47	44
Absorbance normalized to 1 cm (cm^{-1})	333	654	704	606	306	673	383	659
H_2O-cpx (ppm)	141	277	298	256	130	285	162	279
H_2O-melt (wt%)	1.62	1.60	1.33	1.34	1.27	1.75	0.74	1.23

Sample No.	XL-2							
Section No.	1							
Point No.	1	2	3	4	6	7	8	9
SiO_2	49.50	48.72	47.39	47.20	49.54	47.92	46.13	48.47
TiO_2	1.87	2.30	2.80	2.67	1.84	2.43	3.08	2.30
Al_2O3	3.80	4.06	4.99	5.77	3.55	5.42	6.49	4.49
Cr_2O3	0.11	0.02	0.02	0.05	0.23	0.13	0.14	0.00
FeO	6.68	6.51	6.57	7.17	5.76	6.59	6.94	6.84
MnO	0.08	0.07	0.05	0.08	0.04	0.02	0.05	0.09
MgO	13.40	13.33	12.66	12.41	13.63	12.76	11.98	12.85
CaO	23.75	23.67	23.77	23.54	23.68	23.77	23.54	23.91
Na_2O	0.40	0.50	0.45	0.52	0.48	0.46	0.55	0.49
K_2O	0.00	0.01	0.02	0.00	0.01	0.00	0.00	0.00
NiO	0.01	0.05	0.00	0.00	0.03	0.00	0.04	0.02
Total	99.60	99.24	98.72	99.42	98.79	99.50	98.92	99.47
Si	1.85	1.83	1.80	1.78	1.86	1.80	1.75	1.82
Ti	0.05	0.07	0.08	0.08	0.05	0.07	0.09	0.07
Al	0.17	0.18	0.22	0.26	0.16	0.24	0.29	0.20
Cr	0.00	0.00	0.00	0.00	0.01	0.00	0.00	0.00
Fe	0.21	0.20	0.21	0.23	0.18	0.21	0.22	0.22
Mn	0.00	0.00	0.00	0.00	0.00	0.00	0.00	0.00
Mg	0.75	0.75	0.72	0.70	0.76	0.71	0.68	0.72
Ca	0.95	0.95	0.97	0.95	0.95	0.96	0.96	0.96
Na	0.03	0.04	0.03	0.04	0.03	0.03	0.04	0.04
K	0.00	0.00	0.00	0.00	0.00	0.00	0.00	0.00
Ni	0.00	0.00	0.00	0.00	0.00	0.00	0.00	0.00
Total	4.02	4.03	4.03	4.03	4.02	4.03	4.03	4.03
Mg#	78.15	78.50	77.45	75.52	80.83	77.53	75.48	76.99
$D^{(cpx\text{-}melt)}_{H_2O}$	0.0148	0.0169	0.0212	0.0240	0.0139	0.0211	0.0289	0.0179
Absorbance of cpx (cm^{-1})	6.70	5.60	8.00	4.00	7.00	11.00	13.00	4.50
Thickness of cpx (0.001mm)	92	92	106	104	112	106	114	114
Absorbance normalized to 1 cm (cm^{-1})	728	609	755	385	625	1038	1140	395
H_2O-cpx (ppm)	308	258	319	163	264	439	483	167
H_2O-melt (wt%)	2.08	1.52	1.50	0.68	1.90	2.08	1.67	0.93

Sample No. Section No. Point No.	10	11	12	13	14	15	16	17
SiO_2	48.92	47.83	50.18	48.52	47.70	48.62	49.55	51.93
TiO_2	1.97	2.43	1.82	2.18	2.65	2.36	1.37	0.92
Al_2O3	3.83	4.35	2.71	3.87	4.66	3.96	4.65	2.86
Cr_2O3	0.09	0.00	0.02	0.00	0.01	0.08	0.92	0.62
FeO	6.74	6.89	5.95	6.70	7.09	6.66	5.55	4.97
MnO	0.08	0.08	0.13	0.05	0.07	0.10	0.10	0.08
MgO	13.25	12.92	13.45	13.18	12.48	13.16	13.21	14.00
CaO	23.58	23.65	24.10	23.66	23.62	23.87	22.83	22.74
Na_2O	0.49	0.50	0.61	0.52	0.57	0.36	0.64	0.77
K_2O	0.01	0.01	0.01	0.01	0.02	0.00	0.02	0.00
NiO	0.02	0.05	0.01	0.00	0.01	0.02	0.06	0.09
Total	98.97	98.69	98.98	98.70	98.87	99.19	98.90	98.97
Si	1.85	1.82	1.89	1.84	1.81	1.83	1.86	1.93
Ti	0.06	0.07	0.05	0.06	0.08	0.07	0.04	0.03
Al	0.17	0.19	0.12	0.17	0.21	0.18	0.21	0.13
Cr	0.00	0.00	0.00	0.00	0.00	0.00	0.03	0.02
Fe	0.21	0.22	0.19	0.21	0.23	0.21	0.17	0.15
Mn	0.00	0.00	0.00	0.00	0.00	0.00	0.00	0.00
Mg	0.75	0.73	0.75	0.74	0.71	0.74	0.74	0.78
Ca	0.95	0.96	0.97	0.96	0.96	0.96	0.92	0.91
Na	0.04	0.04	0.04	0.04	0.04	0.03	0.05	0.06
K	0.00	0.00	0.00	0.00	0.00	0.00	0.00	0.00
Ni	0.00	0.00	0.00	0.00	0.00	0.00	0.00	0.00
Total	4.03	4.03	4.02	4.03	4.03	4.02	4.01	4.00
Mg#	77.81	76.98	80.13	77.81	75.83	77.90	80.93	83.39
$D^{(cpx\text{-}melt)}_{H_2O}$	0.0156	0.0188	0.0118	0.0164	0.0197	0.0168	0.0151	0.0095
Absorbance of cpx (cm^{-1})	4.60	10.00	11.00	3.80	4.60	6.80	3.70	5.40
Thickness of cpx (0.001mm)	114	114	114	115	115	121	117	116
Absorbance normalized to 1 cm (cm^{-1})	404	877	965	330	400	562	316	466
H_2O-cpx (ppm)	171	371	408	140	169	238	134	197
H_2O-melt (wt%)	1.09	1.97	3.47	0.85	0.86	1.41	0.89	2.08

Sample No. Section No. Point No.	18	19	20	21	23	24	25	26
SiO_2	49.11	46.09	49.32	47.79	48.30	51.00	48.75	47.03
TiO_2	2.34	3.20	2.15	1.51	2.29	1.49	2.14	2.58
Al_2O3	4.09	6.50	4.27	8.06	4.45	3.06	4.02	5.46
Cr_2O3	0.01	0.01	0.06	0.14	0.07	0.44	0.07	0.00
FeO	6.70	7.33	6.55	7.47	7.05	5.69	6.43	7.43
MnO	0.07	0.04	0.05	0.14	0.09	0.11	0.04	0.07
MgO	13.13	11.78	13.07	11.54	12.97	13.87	13.26	12.19
CaO	23.76	23.60	23.69	21.61	23.70	23.39	23.76	23.79
Na_2O	0.47	0.57	0.44	0.87	0.44	0.66	0.47	0.44
K_2O	0.00	0.00	0.01	0.01	0.01	0.00	0.00	0.01
NiO	0.00	0.01	0.00	0.00	0.06	0.02	0.04	0.03
Total	99.66	99.13	99.61	99.13	99.42	99.72	98.97	99.02
Si	1.84	1.75	1.85	1.79	1.82	1.90	1.84	1.79
Ti	0.07	0.09	0.06	0.04	0.06	0.04	0.06	0.07
Al	0.18	0.29	0.19	0.36	0.20	0.13	0.18	0.24
Cr	0.00	0.00	0.00	0.00	0.00	0.01	0.00	0.00
Fe	0.21	0.23	0.21	0.23	0.22	0.18	0.20	0.24
Mn	0.00	0.00	0.00	0.00	0.00	0.00	0.00	0.00
Mg	0.73	0.67	0.73	0.65	0.73	0.77	0.75	0.69
Ca	0.95	0.96	0.95	0.87	0.96	0.93	0.96	0.97
Na	0.03	0.04	0.03	0.06	0.03	0.05	0.03	0.03
K	0.00	0.00	0.00	0.00	0.00	0.00	0.00	0.00
Ni	0.00	0.00	0.00	0.00	0.00	0.00	0.00	0.00
Total	4.02	4.03	4.01	4.01	4.03	4.01	4.03	4.03
Mg#	77.75	74.13	78.04	73.37	76.63	81.29	78.62	74.53
$D^{(cpx\text{-}melt)}_{H_2O}$	0.0163	0.0292	0.0158	0.0240	0.0185	0.0116	0.0163	0.0228
Absorbance of cpx (cm^{-1})	9.60	7.30	4.90	4.90	4.30	5.00	4.90	5.60
Thickness of cpx (0.001mm)	117	116	120	125	105	105	101	94
Absorbance normalized to 1 cm (cm^{-1})	821	629	408	392	410	476	485	596
H_2O-cpx (ppm)	347	266	173	166	173	201	205	252
H_2O-melt (wt%)	2.13	0.91	1.09	0.69	0.94	1.73	1.26	1.10

Sample No.							
Section No.			2				
Point No.	27	28	1.2	2	3	4	5
SiO_2	49.00	50.12	49.51	52.40	46.87	50.38	52.99
TiO_2	2.23	1.52	2.26	0.55	2.70	2.18	0.71
Al_2O3	3.48	3.35	3.52	7.18	6.16	3.01	2.35
Cr_2O3	0.02	0.18	0.00	0.75	0.21	0.05	1.13
FeO	6.23	5.27	6.30	3.21	6.41	5.95	4.20
MnO	0.07	0.05	0.12	0.08	0.06	0.06	0.11
MgO	13.17	13.98	13.38	14.41	12.24	13.60	14.80
CaO	23.96	23.85	24.09	19.25	23.44	23.43	22.49
Na_2O	0.54	0.48	0.48	1.87	0.62	0.65	0.69
K_2O	0.03	0.00	0.01	0.01	0.00	0.00	0.01
NiO	0.00	0.03	0.03	0.05	0.03	0.00	0.04
Total	98.72	98.81	99.70	99.75	98.72	99.31	99.52
Si	1.85	1.88	1.85	1.89	1.78	1.88	1.95
Ti	0.06	0.04	0.06	0.01	0.08	0.06	0.02
Al	0.15	0.15	0.16	0.31	0.27	0.13	0.10
Cr	0.00	0.01	0.00	0.02	0.01	0.00	0.03
Fe	0.20	0.17	0.20	0.10	0.20	0.19	0.13
Mn	0.00	0.00	0.00	0.00	0.00	0.00	0.00
Mg	0.74	0.78	0.75	0.78	0.69	0.76	0.81
Ca	0.97	0.96	0.97	0.75	0.95	0.94	0.89
Na	0.04	0.03	0.04	0.13	0.05	0.05	0.05
K	0.00	0.00	0.00	0.00	0.00	0.00	0.00
Ni	0.00	0.00	0.00	0.00	0.00	0.00	0.00
Total	4.03	4.02	4.02	3.99	4.03	4.01	3.99
Mg#	79.04	82.55	79.12	88.90	77.29	80.29	86.26
$D^{(cpx\text{-}melt)}_{H_2O}$	0.0147	0.0126	0.0148	0.0141	0.0248	0.0125	0.0085
Absorbance of cpx (cm^{-1})	4.70	9.00	14.00	5.60	11.00	8.20	5.20
Thickness of cpx (0.001mm)	94	100	107	110	111	120	122
Absorbance normalized to 1 cm (cm^{-1})	500	900	1308	509	991	683	426
H_2O-cpx (ppm)	212	381	554	215	419	289	180
H_2O-melt (wt%)	1.44	3.03	3.75	1.53	1.69	2.32	2.11

Sample No.	XL-3							
Section No.	8							
Point No.	1	1.2	2	3	3.2	3.3	4	5
SiO_2	48.04	51.07	48.35	46.36	47.76	51.53	50.58	51.56
TiO_2	2.35	1.63	2.36	3.56	2.66	1.84	1.67	1.71
Al_2O3	4.62	2.35	4.07	5.82	4.38	2.18	3.01	2.58
Cr_2O3	0.01	0.03	0.02	0.03	0.03	0.00	0.03	0.00
FeO	7.17	5.95	6.70	7.56	7.39	5.99	6.00	5.86
MnO	0.06	0.14	0.10	0.09	0.09	0.08	0.06	0.03
MgO	12.56	13.41	12.98	11.72	12.65	14.19	13.75	13.84
CaO	23.98	24.05	24.09	23.67	23.81	23.68	23.55	23.83
Na_2O	0.40	0.50	0.56	0.58	0.50	0.75	0.61	0.55
K_2O	0.01	0.03	0.01	0.00	0.01	0.02	0.04	0.01
NiO	0.00	0.00	0.00	0.00	0.07	0.00	0.08	0.05
Total	99.20	99.17	99.23	99.38	99.34	100.25	99.37	100.02
Si	1.82	1.91	1.83	1.76	1.81	1.91	1.89	1.91
Ti	0.07	0.05	0.07	0.10	0.08	0.05	0.05	0.05
Al	0.21	0.10	0.18	0.26	0.20	0.10	0.13	0.11
Cr	0.00	0.00	0.00	0.00	0.00	0.00	0.00	0.00
Fe	0.23	0.19	0.21	0.24	0.23	0.19	0.19	0.18
Mn	0.00	0.00	0.00	0.00	0.00	0.00	0.00	0.00
Mg	0.71	0.75	0.73	0.66	0.71	0.78	0.77	0.76
Ca	0.97	0.97	0.97	0.96	0.97	0.94	0.94	0.95
Na	0.03	0.04	0.04	0.04	0.04	0.05	0.04	0.04
K	0.00	0.00	0.00	0.00	0.00	0.00	0.00	0.00
Ni	0.00	0.00	0.00	0.00	0.00	0.00	0.00	0.00
Total	4.03	4.01	4.04	4.03	4.04	4.02	4.02	4.01
Mg#	75.74	80.08	77.54	73.43	75.33	80.87	80.34	80.81
$D^{(cpx\text{-}melt)}_{H_2O}$	0.0187	0.0100	0.0175	0.0276	0.0199	0.0106	0.0119	0.0104
Absorbance of cpx (cm^{-1})	3.80	3.80	2.80	6.30	8.00	5.20	4.70	2.60
Thickness of cpx (0.001mm)	60	60	60	60	60	60	66	61
Absorbance normalized to 1 cm (cm^{-1})	633	633	467	1050	1333	867	712	426
H_2O-cpx (ppm)	268	268	197	444	564	367	301	180
H_2O-melt (wt%)	1.44	2.67	1.13	1.61	2.84	3.45	2.54	1.73

Sample No.								
Section No.								
Point No.	5.2	5.3	6	7	8	9	10	10.2
SiO_2	50.26	51.91	44.66	50.36	51.79	51.31	50.58	51.95
TiO_2	1.43	1.55	3.89	1.62	1.82	1.66	1.97	1.75
Al_2O3	5.21	1.96	7.08	3.29	1.93	2.22	2.85	1.87
Cr_2O3	1.72	0.00	0.01	0.00	0.01	0.00	0.00	0.03
FeO	4.75	5.69	7.87	5.50	5.88	5.65	6.59	6.02
MnO	0.10	0.09	0.05	0.05	0.07	0.11	0.10	0.09
MgO	12.55	14.08	10.81	13.84	13.51	14.07	13.50	14.11
CaO	22.33	24.03	23.84	24.09	23.83	23.90	23.72	23.97
Na_2O	1.11	0.55	0.60	0.52	0.56	0.52	0.55	0.52
K_2O	0.02	0.01	0.04	0.01	0.02	0.00	0.00	0.00
NiO	0.09	0.04	0.00	0.07	0.04	0.03	0.03	0.04
Total	99.56	99.91	98.85	99.36	99.44	99.47	99.88	100.34
Si	1.86	1.93	1.71	1.88	1.93	1.91	1.89	1.92
Ti	0.04	0.04	0.11	0.05	0.05	0.05	0.06	0.05
Al	0.23	0.09	0.32	0.14	0.08	0.10	0.13	0.08
Cr	0.05	0.00	0.00	0.00	0.00	0.00	0.00	0.00
Fe	0.15	0.18	0.25	0.17	0.18	0.18	0.21	0.19
Mn	0.00	0.00	0.00	0.00	0.00	0.00	0.00	0.00
Mg	0.69	0.78	0.62	0.77	0.75	0.78	0.75	0.78
Ca	0.89	0.95	0.98	0.96	0.95	0.95	0.95	0.95
Na	0.08	0.04	0.04	0.04	0.04	0.04	0.04	0.04
K	0.00	0.00	0.00	0.00	0.00	0.00	0.00	0.00
Ni	0.00	0.00	0.00	0.00	0.00	0.00	0.00	0.00
Total	4.00	4.01	4.04	4.02	4.00	4.01	4.02	4.01
Mg#	82.48	81.52	71.00	81.77	80.38	81.60	78.50	80.70
$D^{(cpx\text{-}melt)}_{H_2O}$	0.0149	0.0094	0.0369	0.0124	0.0091	0.0102	0.0121	0.0097
Absorbance of cpx (cm^{-1})	4.00	2.00	4.50	5.80	2.80	4.90	2.70	6.80
Thickness of cpx (0.001mm)	61	61	61	65	65	64	64	64
Absorbance normalized to 1 cm (cm^{-1})	656	328	738	892	431	766	422	1063
H_2O-cpx (ppm)	277	139	312	378	182	324	179	450
H_2O-melt (wt%)	1.86	1.48	0.85	3.05	2.00	3.18	1.47	4.66

Sample No. Section No. Point No.	11	12	13	13.2	14	15	16	16.2
SiO_2	46.75	51.46	52.51	52.67	51.38	47.74	48.85	51.23
TiO_2	3.31	1.26	1.52	1.54	1.75	2.60	1.74	1.77
Al_2O3	6.12	3.44	1.92	1.75	2.16	4.82	5.06	2.42
Cr_2O3	0.01	0.86	0.03	0.00	0.02	0.00	0.88	0.03
FeO	7.58	5.49	5.74	6.00	5.81	7.10	5.71	6.14
MnO	0.07	0.02	0.05	0.11	0.08	0.09	0.09	0.10
MgO	11.72	14.03	14.19	14.41	13.92	12.63	13.08	13.80
CaO	23.64	23.20	23.69	23.65	23.71	23.81	23.15	23.76
Na_2O	0.44	0.62	0.61	0.61	0.58	0.45	0.40	0.53
K_2O	0.01	0.00	0.01	0.00	0.01	0.01	0.00	0.02
NiO	0.00	0.09	0.02	0.07	0.03	0.00	0.02	0.03
Total	99.65	100.46	100.29	100.83	99.43	99.24	98.99	99.81
Si	1.76	1.89	1.94	1.93	1.92	1.80	1.83	1.91
Ti	0.09	0.03	0.04	0.04	0.05	0.07	0.05	0.05
Al	0.27	0.15	0.08	0.08	0.09	0.21	0.22	0.11
Cr	0.00	0.02	0.00	0.00	0.00	0.00	0.03	0.00
Fe	0.24	0.17	0.18	0.18	0.18	0.22	0.18	0.19
Mn	0.00	0.00	0.00	0.00	0.00	0.00	0.00	0.00
Mg	0.66	0.77	0.78	0.79	0.77	0.71	0.73	0.77
Ca	0.96	0.92	0.94	0.93	0.95	0.96	0.93	0.95
Na	0.03	0.04	0.04	0.04	0.04	0.03	0.03	0.04
K	0.00	0.00	0.00	0.00	0.00	0.00	0.00	0.00
Ni	0.00	0.00	0.00	0.00	0.00	0.00	0.00	0.00
Total	4.02	4.01	4.00	4.01	4.01	4.03	4.01	4.01
Mg#	73.38	82.00	81.51	81.07	81.01	76.02	80.33	80.03
$D^{(cpx\text{-}melt)}_{H_2O}$	0.0266	0.0119	0.0089	0.0090	0.0100	0.0203	0.0175	0.0107
Absorbance of cpx (cm^{-1})	4.90	5.30	2.90	2.70	5.50	4.50	2.50	6.40
Thickness of cpx (0.001mm)	64	79	69	69	66	62	60	60
Absorbance normalized to 1 cm (cm^{-1})	766	671	420	391	500	290	483	1067
H_2O-cpx (ppm)	324	284	178	166	212	123	205	451
H_2O-melt (wt%)	1.22	2.39	1.99	1.83	2.11	0.60	1.17	4.23

Sample No. Section No. Point No.	17	18	18.2	19	20	21	22	23
SiO_2	48.23	51.48	50.20	51.06	50.09	49.41	51.52	51.01
TiO_2	2.67	1.64	2.05	1.35	1.61	1.99	1.69	1.73
Al_2O3	4.51	2.04	2.78	2.05	2.43	3.79	2.15	2.38
Cr_2O3	0.02	0.04	0.07	0.01	0.02	0.18	0.02	0.02
FeO	6.94	5.87	6.32	5.76	6.30	6.40	6.03	5.93
MnO	0.07	0.12	0.08	0.13	0.08	0.08	0.09	0.06
MgO	12.66	13.47	13.55	14.00	13.73	12.82	14.02	13.81
CaO	23.71	23.90	23.74	23.89	23.72	23.93	23.88	23.93
Na_2O	0.49	0.61	0.54	0.56	0.59	0.48	0.52	0.41
K_2O	0.00	0.01	0.00	0.03	0.00	0.00	0.02	0.00
NiO	0.01	0.00	0.02	0.00	0.03	0.05	0.00	0.03
Total	99.32	99.17	99.35	98.83	98.59	99.12	99.92	99.32
Si	1.82	1.93	1.88	1.92	1.89	1.86	1.91	1.91
Ti	0.08	0.05	0.06	0.04	0.05	0.06	0.05	0.05
Al	0.20	0.09	0.12	0.09	0.11	0.17	0.09	0.10
Cr	0.00	0.00	0.00	0.00	0.00	0.01	0.00	0.00
Fe	0.22	0.18	0.20	0.18	0.20	0.20	0.19	0.19
Mn	0.00	0.00	0.00	0.00	0.00	0.00	0.00	0.00
Mg	0.71	0.75	0.76	0.78	0.77	0.72	0.78	0.77
Ca	0.96	0.96	0.95	0.96	0.96	0.97	0.95	0.96
Na	0.04	0.04	0.04	0.04	0.04	0.03	0.04	0.03
K	0.00	0.00	0.00	0.00	0.00	0.00	0.00	0.00
Ni	0.00	0.00	0.00	0.00	0.00	0.00	0.00	0.00
Total	4.02	4.00	4.02	4.02	4.03	4.01	4.01	4.01
Mg#	76.48	80.35	79.26	81.23	79.53	78.13	80.56	80.59
$D^{(cpx\text{-}melt)}_{H_2O}$	0.0187	0.0093	0.0124	0.0098	0.0115	0.0142	0.0101	0.0106
Absorbance of cpx (cm^{-1})	5.30	4.50	2.30	7.80	6.30	11.00	5.80	3.00
Thickness of cpx (0.001mm)	60	40	40	61	53	69	69	57
Absorbance normalized to 1 cm (cm^{-1})	883	1125	575	1279	1189	1594	841	526
H_2O-cpx (ppm)	374	476	243	541	503	675	356	223
H_2O-melt (wt%)	2.00	5.12	1.96	5.54	4.39	4.76	3.51	2.11

Sample No.		XL-4					
Section No.		1					
Point No.	24	1	2	3	4	5	6
SiO_2	50.32	47.90	49.94	49.04	49.75	51.52	51.06
TiO_2	2.13	2.88	2.18	2.51	2.24	1.48	2.01
Al_2O3	3.49	4.40	3.66	4.26	3.87	2.38	3.23
Cr_2O3	0.03	0.03	0.00	0.00	0.06	0.00	0.06
FeO	6.49	6.69	6.15	6.68	6.68	5.81	6.14
MnO	0.10	0.04	0.10	0.07	0.09	0.05	0.10
MgO	13.19	12.97	13.53	12.54	13.00	14.00	13.46
CaO	23.79	24.28	24.28	24.08	23.98	24.22	24.01
Na_2O	0.54	0.54	0.48	0.51	0.39	0.59	0.62
K_2O	0.00	0.00	0.00	0.01	0.01	0.02	0.01
NiO	0.06	0.03	0.03	0.02	0.00	0.05	0.04
Total	100.15	99.77	100.36	99.70	100.07	100.12	100.74
Si	1.87	1.80	1.86	1.84	1.86	1.91	1.88
Ti	0.06	0.08	0.06	0.07	0.06	0.04	0.06
Al	0.15	0.20	0.16	0.19	0.17	0.10	0.14
Cr	0.00	0.00	0.00	0.00	0.00	0.00	0.00
Fe	0.20	0.21	0.19	0.21	0.21	0.18	0.19
Mn	0.00	0.00	0.00	0.00	0.00	0.00	0.00
Mg	0.73	0.73	0.75	0.70	0.72	0.77	0.74
Ca	0.95	0.98	0.97	0.97	0.96	0.96	0.95
Na	0.04	0.04	0.03	0.04	0.03	0.04	0.04
K	0.00	0.00	0.00	0.00	0.00	0.00	0.00
Ni	0.00	0.00	0.00	0.00	0.00	0.00	0.00
Total	4.01	4.04	4.02	4.02	4.01	4.02	4.01
Mg#	78.37	77.57	79.69	76.98	77.65	81.12	79.63
$D^{(cpx\text{-}melt)}_{H_2O}$	0.0134	0.0204	0.0146	0.0163	0.0148	0.0103	0.0123
Absorbance of cpx (cm^{-1})	3.20	7.80	4.10	4.40	9.00	7.20	8.00
Thickness of cpx (0.001mm)	49	100	111	102	102	114	113
Absorbance normalized to 1 cm (cm^{-1})	653	780	369	431	882	632	708
H_2O-cpx (ppm)	276	330	156	183	373	267	300
H_2O-melt (wt%)	2.07	1.62	1.07	1.12	2.53	2.61	2.44

Sample No.								
Section No.						2		
Point No.	7	8	9	10	11	1	2	3
SiO_2	49.15	45.37	48.93	49.72	51.35	49.07	48.14	46.03
TiO_2	1.90	3.52	2.48	1.37	1.46	2.20	2.39	3.27
Al_2O3	3.84	7.37	3.56	4.63	2.74	3.77	4.40	6.95
Cr_2O3	0.08	0.11	0.00	0.85	0.00	0.05	0.05	0.07
FeO	5.94	7.36	6.66	6.19	5.71	6.04	6.91	7.26
MnO	0.10	0.03	0.11	0.06	0.14	0.00	0.07	0.09
MgO	13.44	11.60	13.09	12.73	14.04	13.51	12.89	11.84
CaO	23.97	23.30	24.06	22.27	24.02	23.82	23.74	24.00
Na_2O	0.49	0.56	0.37	1.00	0.63	0.39	0.20	0.50
K_2O	0.00	0.02	0.00	0.00	0.01	0.00	0.00	0.00
NiO	0.03	0.00	0.02	0.02	0.03	0.07	0.02	0.06
Total	98.94	99.23	99.27	98.83	100.12	98.92	98.81	100.08
Si	1.85	1.72	1.84	1.87	1.90	1.85	1.82	1.73
Ti	0.05	0.10	0.07	0.04	0.04	0.06	0.07	0.09
Al	0.17	0.33	0.16	0.21	0.12	0.17	0.20	0.31
Cr	0.00	0.00	0.00	0.03	0.00	0.00	0.00	0.00
Fe	0.19	0.23	0.21	0.19	0.18	0.19	0.22	0.23
Mn	0.00	0.00	0.00	0.00	0.00	0.00	0.00	0.00
Mg	0.75	0.66	0.74	0.71	0.78	0.76	0.73	0.66
Ca	0.97	0.95	0.97	0.90	0.95	0.96	0.96	0.97
Na	0.04	0.04	0.03	0.07	0.04	0.03	0.01	0.04
K	0.00	0.00	0.00	0.00	0.00	0.00	0.00	0.00
Ni	0.00	0.00	0.00	0.00	0.00	0.00	0.00	0.00
Total	4.03	4.03	4.02	4.01	4.02	4.02	4.02	4.04
Mg#	80.13	73.77	77.80	78.58	81.43	79.94	76.88	74.41
$D^{(cpx\text{-}melt)}_{H_2O}$	0.0150	0.0357	0.0156	0.0145	0.0109	0.0154	0.0180	0.0324
Absorbance of cpx (cm^{-1})	6.00	8.40	6.40	7.90	5.90	4.60	4.70	5.70
Thickness of cpx (0.001mm)	86	94	93	109	109	103	99	106
Absorbance normalized to 1 cm (cm^{-1})	698	894	688	725	541	447	475	538
H_2O-cpx (ppm)	295	378	291	307	229	189	201	228
H_2O-melt (wt%)	1.97	1.06	1.86	2.12	2.10	1.23	1.11	0.70

Sample No. Section No. Point No.	4	5	6	7	8	9	10	11
SiO_2	47.61	47.87	47.87	49.03	49.28	51.17	48.61	50.38
TiO_2	2.51	2.56	2.56	2.11	2.12	1.88	2.31	1.79
Al_2O3	4.89	4.50	4.50	4.71	4.05	2.56	4.50	2.71
Cr_2O3	0.00	0.01	0.01	0.20	0.00	0.04	0.02	0.01
FeO	7.51	6.99	6.99	6.31	6.39	6.02	6.67	6.61
MnO	0.06	0.06	0.06	0.09	0.10	0.06	0.10	0.07
MgO	12.60	12.61	12.61	13.19	13.27	13.78	12.81	13.53
CaO	23.64	23.63	23.63	23.73	23.58	23.60	23.96	23.99
Na_2O	0.40	0.51	0.51	0.52	0.47	0.64	0.55	0.59
K_2O	0.00	0.02	0.02	0.00	0.00	0.01	0.01	0.01
NiO	0.06	0.07	0.07	0.07	0.00	0.02	0.04	0.03
Total	99.28	98.84	98.84	99.96	99.26	99.76	99.57	99.70
Si	1.80	1.82	1.82	1.83	1.85	1.90	1.83	1.89
Ti	0.07	0.07	0.07	0.06	0.06	0.05	0.07	0.05
Al	0.22	0.20	0.20	0.21	0.18	0.11	0.20	0.12
Cr	0.00	0.00	0.00	0.01	0.00	0.00	0.00	0.00
Fe	0.24	0.22	0.22	0.20	0.20	0.19	0.21	0.21
Mn	0.00	0.00	0.00	0.00	0.00	0.00	0.00	0.00
Mg	0.71	0.71	0.71	0.73	0.74	0.76	0.72	0.76
Ca	0.96	0.96	0.96	0.95	0.95	0.94	0.96	0.96
Na	0.03	0.04	0.04	0.04	0.03	0.05	0.04	0.04
K	0.00	0.00	0.00	0.00	0.00	0.00	0.00	0.00
Ni	0.00	0.00	0.00	0.00	0.00	0.00	0.00	0.00
Total	4.03	4.03	4.03	4.02	4.02	4.01	4.03	4.03
Mg#	74.95	76.29	76.29	78.83	78.72	80.32	77.40	78.49
$D^{(cpx\text{-}melt)}_{H_2O}$	0.0208	0.0189	0.0189	0.0176	0.0154	0.0109	0.0176	0.0120
Absorbance of cpx (cm^{-1})	8.00	8.90	5.50	8.20	3.90	4.00	3.60	7.30
Thickness of cpx (0.001mm)	97	109	109	116	112	116	111	111
Absorbance normalized to 1 cm (cm^{-1})	825	817	505	707	348	345	324	658
H_2O-cpx (ppm)	349	345	214	299	147	146	137	278
H_2O-melt (wt%)	1.68	1.82	1.13	1.70	0.96	1.33	0.78	2.31

Sample No.						XL-5	
Section No.						7	
Point No.	13	14	15	16	17	1	2
SiO_2	47.86	51.38	52.58	48.52	48.10	48.90	50.02
TiO_2	2.63	1.58	1.29	2.42	2.43	2.36	1.89
Al_2O3	4.73	2.01	1.34	4.16	4.20	4.11	3.75
Cr_2O3	0.02	0.04	0.04	0.08	0.04	0.02	0.18
FeO	6.98	6.06	5.70	6.38	7.12	6.58	6.05
MnO	0.06	0.10	0.05	0.07	0.11	0.05	0.09
MgO	12.69	14.30	14.38	13.29	12.89	12.55	13.74
CaO	23.90	23.61	23.66	23.63	23.85	23.97	23.88
Na_2O	0.48	0.64	0.76	0.44	0.47	0.41	0.54
K_2O	0.00	0.03	0.00	0.01	0.00	0.00	0.00
NiO	0.00	0.01	0.00	0.00	0.03	0.01	0.00
Total	99.35	99.77	99.81	98.99	99.24	98.97	100.12
Si	1.81	1.91	1.95	1.83	1.82	1.85	1.86
Ti	0.07	0.04	0.04	0.07	0.07	0.07	0.05
Al	0.21	0.09	0.06	0.18	0.19	0.18	0.16
Cr	0.00	0.00	0.00	0.00	0.00	0.00	0.01
Fe	0.22	0.19	0.18	0.20	0.23	0.21	0.19
Mn	0.00	0.00	0.00	0.00	0.00	0.00	0.00
Mg	0.71	0.79	0.79	0.75	0.73	0.71	0.76
Ca	0.97	0.94	0.94	0.95	0.97	0.97	0.95
Na	0.04	0.05	0.05	0.03	0.03	0.03	0.04
K	0.00	0.00	0.00	0.00	0.00	0.00	0.00
Ni	0.00	0.00	0.00	0.00	0.00	0.00	0.00
Total	4.03	4.02	4.01	4.02	4.03	4.01	4.02
Mg#	76.42	80.78	81.80	78.79	76.35	77.28	80.19
$D^{(cpx\text{-}melt)}_{H_2O}$	0.0200	0.0103	0.0082	0.0174	0.0184	0.0155	0.0145
Absorbance of cpx (cm^{-1})	4.20	2.90	6.50	7.00	7.80	2.90	3.40
Thickness of cpx (0.001mm)	107	108	105	96	92	58	61
Absorbance normalized to 1 cm (cm^{-1})	393	269	619	729	848	500	557
H_2O-cpx (ppm)	166	114	262	309	359	212	236
H_2O-melt (wt%)	0.83	1.10	3.21	1.77	1.95	1.36	1.63

Sample No. Section No. Point No.	3	4	5	6	7	8	9	10
SiO_2	52.71	51.76	50.81	45.04	50.01	45.23	49.01	49.27
TiO_2	1.30	1.46	1.15	4.17	1.83	3.38	2.15	2.36
Al_2O3	1.50	1.54	3.54	7.11	3.56	6.87	3.97	4.09
Cr_2O3	0.01	0.13	0.68	0.07	0.05	0.25	0.06	0.01
FeO	5.35	5.88	5.74	8.08	6.23	7.57	6.52	6.73
MnO	0.09	0.12	0.07	0.11	0.07	0.08	0.08	0.09
MgO	14.63	14.22	13.81	11.19	13.41	11.31	13.38	13.20
CaO	23.86	23.36	22.87	23.70	24.16	23.77	23.84	23.78
Na_2O	0.53	0.66	0.68	0.53	0.47	0.62	0.43	0.56
K_2O	0.02	0.00	0.01	0.00	0.03	0.00	0.01	0.00
NiO	0.05	0.00	0.10	0.05	0.07	0.00	0.02	0.00
Total	100.04	99.13	99.47	100.05	99.89	99.09	99.46	100.10
Si	1.95	1.94	1.89	1.71	1.87	1.73	1.84	1.84
Ti	0.04	0.04	0.03	0.12	0.05	0.10	0.06	0.07
Al	0.07	0.07	0.16	0.32	0.16	0.31	0.18	0.18
Cr	0.00	0.00	0.02	0.00	0.00	0.01	0.00	0.00
Fe	0.17	0.18	0.18	0.26	0.19	0.24	0.20	0.21
Mn	0.00	0.00	0.00	0.00	0.00	0.00	0.00	0.00
Mg	0.81	0.79	0.77	0.63	0.75	0.64	0.75	0.73
Ca	0.94	0.94	0.91	0.96	0.97	0.97	0.96	0.95
Na	0.04	0.05	0.05	0.04	0.03	0.05	0.03	0.04
K	0.00	0.00	0.00	0.00	0.00	0.00	0.00	0.00
Ni	0.00	0.00	0.00	0.00	0.00	0.00	0.00	0.00
Total	4.00	4.01	4.01	4.04	4.02	4.04	4.03	4.02
Mg#	82.97	81.18	81.09	71.16	79.32	72.69	78.55	77.76
$D^{(cpx\text{-}melt)}_{H_2O}$	0.0083	0.0090	0.0121	0.0390	0.0136	0.0339	0.0162	0.0165
Absorbance of cpx (cm^{-1})	1.40	2.96	3.70	7.00	3.12	1.40	3.30	3.90
Thickness of cpx (0.001mm)	64	64	61	64	69	68	69	67
Absorbance normalized to 1 cm (cm^{-1})	219	463	607	1094	452	206	478	582
H_2O-cpx (ppm)	93	196	257	463	191	87	202	246
H_2O-melt (wt%)	1.12	2.19	2.12	1.19	1.40	0.26	1.25	1.49

Sample No. Section No. Point No.	11	12	13	14	15	16	17	18
SiO_2	49.00	49.19	49.38	48.89	51.47	48.69	47.84	48.21
TiO_2	1.67	1.77	1.94	2.00	1.74	2.50	2.66	2.36
Al_2O3	5.53	4.01	4.50	4.08	2.07	4.33	4.43	4.46
Cr_2O3	0.79	0.03	0.30	0.08	0.02	0.00	0.04	0.08
FeO	5.79	6.99	5.98	6.39	6.15	6.84	7.03	6.88
MnO	0.08	0.09	0.10	0.06	0.04	0.05	0.05	0.10
MgO	13.25	13.00	13.49	13.20	13.95	12.78	12.76	12.91
CaO	23.11	23.92	23.32	23.76	23.71	24.10	24.22	24.18
Na_2O	0.78	0.50	0.57	0.59	0.64	0.58	0.47	0.52
K_2O	0.00	0.00	0.01	0.00	0.00	0.00	0.00	0.01
NiO	0.06	0.00	0.07	0.02	0.03	0.00	0.00	0.05
Total	100.05	99.48	99.65	99.08	99.82	99.86	99.51	99.77
Si	1.82	1.85	1.84	1.84	1.92	1.83	1.81	1.81
Ti	0.05	0.05	0.05	0.06	0.05	0.07	0.08	0.07
Al	0.24	0.18	0.20	0.18	0.09	0.19	0.20	0.20
Cr	0.02	0.00	0.01	0.00	0.00	0.00	0.00	0.00
Fe	0.18	0.22	0.19	0.20	0.19	0.21	0.22	0.22
Mn	0.00	0.00	0.00	0.00	0.00	0.00	0.00	0.00
Mg	0.73	0.73	0.75	0.74	0.77	0.71	0.72	0.72
Ca	0.92	0.96	0.93	0.96	0.95	0.97	0.98	0.97
Na	0.06	0.04	0.04	0.04	0.05	0.04	0.03	0.04
K	0.00	0.00	0.00	0.00	0.00	0.00	0.00	0.00
Ni	0.00	0.00	0.00	0.00	0.00	0.00	0.00	0.00
Total	4.03	4.03	4.02	4.03	4.01	4.03	4.04	4.04
Mg#	80.32	76.81	80.08	78.64	80.17	76.90	76.39	76.99
$D^{(cpx\text{-}melt)}_{H_2O}$	0.0191	0.0152	0.0164	0.0160	0.0101	0.0176	0.0198	0.0190
Absorbance of cpx (cm^{-1})	2.20	3.60	2.80	3.16	3.34	2.80	2.96	3.46
Thickness of cpx (0.001mm)	62	65	65	65	67	61	60	52
Absorbance normalized to 1 cm (cm^{-1})	355	554	431	486	499	459	493	665
H_2O-cpx (ppm)	150	234	182	206	211	194	209	282
H_2O-melt (wt%)	0.79	1.54	1.11	1.29	2.09	1.10	1.05	1.48

Sample No. Section No. Point No.	20	21	21.2	22	22.2	23	24	25
SiO_2	46.65	47.62	40.67	46.99	50.09	52.64	51.99	47.05
TiO_2	2.90	2.59	2.16	2.92	1.82	1.47	1.30	2.79
Al_2O3	6.15	4.78	4.07	5.79	3.59	1.68	1.55	6.00
Cr_2O3	0.12	0.01	0.02	0.01	0.04	0.00	0.02	0.20
FeO	6.99	7.07	4.29	6.53	5.72	5.90	5.90	6.20
MnO	0.07	0.04	0.06	0.07	0.07	0.14	0.08	0.05
MgO	11.96	12.47	11.68	12.43	13.54	14.17	14.31	12.14
CaO	23.87	24.11	18.73	24.23	24.25	23.91	24.11	23.76
Na_2O	0.54	0.54	0.58	0.48	0.42	0.61	0.59	0.61
K_2O	0.00	0.01	0.01	0.01	0.05	0.01	0.00	0.00
NiO	0.04	0.00	0.04	0.02	0.04	0.00	0.04	0.01
Total	99.27	99.24	82.29	99.46	99.63	100.53	99.88	98.80
Si	1.77	1.80	1.83	1.77	1.87	1.94	1.93	1.78
Ti	0.08	0.07	0.07	0.08	0.05	0.04	0.04	0.08
Al	0.27	0.21	0.22	0.26	0.16	0.07	0.07	0.27
Cr	0.00	0.00	0.00	0.00	0.00	0.00	0.00	0.01
Fe	0.22	0.22	0.16	0.21	0.18	0.18	0.18	0.20
Mn	0.00	0.00	0.00	0.00	0.00	0.00	0.00	0.00
Mg	0.67	0.70	0.78	0.70	0.75	0.78	0.79	0.69
Ca	0.97	0.98	0.90	0.98	0.97	0.94	0.96	0.96
Na	0.04	0.04	0.05	0.04	0.03	0.04	0.04	0.04
K	0.00	0.00	0.00	0.00	0.00	0.00	0.00	0.00
Ni	0.00	0.00	0.00	0.00	0.00	0.00	0.00	0.00
Total	4.03	4.04	4.02	4.03	4.02	4.01	4.02	4.03
Mg#	75.32	75.87	82.94	77.23	80.84	81.06	81.22	77.75
$D^{(cpx\text{-}melt)}_{H_2O}$	0.0261	0.0203	0.0186	0.0248	0.0133	0.0086	0.0089	0.0238
Absorbance of cpx (cm^{-1})	5.07	1.60	2.40	2.20	2.10	2.55	2.00	1.89
Thickness of cpx (0.001mm)	59	52	52	46	46	46	53	45
Absorbance normalized to 1 cm (cm^{-1})	859	308	462	478	457	554	377	420
H_2O-cpx (ppm)	364	130	195	202	193	235	160	178
H_2O-melt (wt%)	1.39	0.64	1.05	0.82	1.45	2.71	1.79	0.75

Sample No.		XL-6					
Section No.		1					
Point No.	25.2	1	2	3	4	5	6
SiO_2	48.54	54.00	53.43	54.29	54.23	54.47	54.04
TiO_2	2.27	0.43	0.86	0.49	0.34	0.29	0.75
Al_2O3	4.19	0.27	0.67	0.36	0.29	0.26	0.34
Cr_2O3	0.02	0.00	0.01	0.04	0.04	0.02	0.01
FeO	6.67	7.09	6.70	6.05	6.95	6.85	7.06
MnO	0.02	0.12	0.13	0.12	0.11	0.10	0.14
MgO	13.12	14.26	14.26	15.09	14.18	14.44	14.13
CaO	23.99	23.22	23.23	23.46	23.05	23.15	22.73
Na_2O	0.53	0.72	0.68	0.61	0.72	0.66	0.79
K_2O	0.00	0.00	0.00	0.01	0.01	0.01	0.00
NiO	0.00	0.02	0.03	0.07	0.00	0.04	0.07
Total	99.34	100.13	99.99	100.59	99.92	100.27	100.06
Si	1.83	2.00	1.98	1.99	2.01	2.01	2.00
Ti	0.06	0.01	0.02	0.01	0.01	0.01	0.02
Al	0.19	0.01	0.03	0.02	0.01	0.01	0.01
Cr	0.00	0.00	0.00	0.00	0.00	0.00	0.00
Fe	0.21	0.22	0.21	0.19	0.22	0.21	0.22
Mn	0.00	0.00	0.00	0.00	0.00	0.00	0.00
Mg	0.74	0.79	0.79	0.83	0.78	0.79	0.78
Ca	0.97	0.92	0.92	0.92	0.91	0.91	0.90
Na	0.04	0.05	0.05	0.04	0.05	0.05	0.06
K	0.00	0.00	0.00	0.00	0.00	0.00	0.00
Ni	0.00	0.00	0.00	0.00	0.00	0.00	0.00
Total	4.03	4.01	4.01	4.01	4.00	4.00	4.00
Mg#	77.82	78.19	79.14	81.65	78.43	78.98	78.10
$D^{(cpx\text{-}melt)}_{H_2O}$	0.0174	0.0060	0.0068	0.0062	0.0057	0.0057	0.0061
Absorbance of cpx (cm^{-1})	1.89	1.28	2.34	2.53	0.52	0.32	0.40
Thickness of cpx (0.001mm)	45	101	101	101	104	104	104
Absorbance normalized to 1 cm (cm^{-1})	420	127	232	250	50	31	39
H_2O-cpx (ppm)	178	54	98	106	21	13	16
H_2O-melt (wt%)	1.02	0.90	1.45	1.70	0.37	0.23	0.27

Sample No. Section No. Point No.	7	8	9	10	11	12	13	14
SiO_2	54.34	54.15	53.90	53.64	53.74	52.99	53.30	53.15
TiO_2	0.70	1.04	0.59	1.09	0.58	1.45	0.97	0.96
Al_2O3	0.30	0.51	0.34	0.70	0.28	0.81	0.49	0.45
Cr_2O3	0.05	0.00	0.01	0.01	0.00	0.02	0.03	0.03
FeO	6.79	7.04	6.29	6.59	6.38	7.36	7.17	6.84
MnO	0.13	0.10	0.11	0.12	0.12	0.10	0.10	0.07
MgO	14.40	14.07	14.64	13.56	14.57	13.92	13.98	14.30
CaO	22.98	22.45	23.00	23.03	23.23	22.49	22.28	22.73
Na_2O	0.68	0.80	0.69	0.66	0.60	0.85	0.87	0.76
K_2O	0.00	0.01	0.00	0.00	0.00	0.02	0.01	0.00
NiO	0.00	0.02	0.00	0.05	0.05	0.03	0.04	0.01
Total	100.37	100.18	99.56	99.46	99.55	100.03	99.24	99.30
Si	2.00	2.00	2.00	1.99	2.00	1.97	1.99	1.98
Ti	0.02	0.03	0.02	0.03	0.02	0.04	0.03	0.03
Al	0.01	0.02	0.01	0.03	0.01	0.04	0.02	0.02
Cr	0.00	0.00	0.00	0.00	0.00	0.00	0.00	0.00
Fe	0.21	0.22	0.19	0.20	0.20	0.23	0.22	0.21
Mn	0.00	0.00	0.00	0.00	0.00	0.00	0.00	0.00
Mg	0.79	0.77	0.81	0.75	0.81	0.77	0.78	0.80
Ca	0.91	0.89	0.91	0.92	0.92	0.89	0.89	0.91
Na	0.05	0.06	0.05	0.05	0.04	0.06	0.06	0.05
K	0.00	0.00	0.00	0.00	0.00	0.00	0.00	0.00
Ni	0.00	0.00	0.00	0.00	0.00	0.00	0.00	0.00
Total	4.00	3.99	4.00	3.98	4.00	4.00	4.00	4.01
Mg#	79.08	78.09	80.59	78.59	80.29	77.13	77.67	78.84
$D^{(cpx\text{-}melt)}_{H_2O}$	0.0060	0.0062	0.0060	0.0062	0.0061	0.0075	0.0065	0.0067
Absorbance of cpx (cm^{-1})	1.15	1.68	0.71	1.12	1.20	0.39	0.69	0.44
Thickness of cpx (0.001mm)	104	104	104	104	100	96	96	96
Absorbance normalized to 1 cm (cm^{-1})	111	162	68	108	120	41	72	46
H_2O-cpx (ppm)	47	68	29	46	51	17	30	19
H_2O-melt (wt%)	0.78	1.10	0.48	0.73	0.83	0.23	0.47	0.29

Sample No. Section No. Point No.	16	17	18	18.2	19	19.2	20	21
SiO_2	53.06	52.62	53.39	52.18	52.29	52.77	52.14	50.63
TiO_2	1.19	1.37	0.97	1.45	1.32	1.09	1.64	2.03
Al_2O3	0.91	1.02	0.79	1.10	1.23	0.89	1.38	1.66
Cr_2O3	0.01	0.03	0.00	0.04	0.05	0.00	0.01	0.00
FeO	6.57	7.28	6.25	7.24	6.55	6.24	6.76	7.13
MnO	0.13	0.11	0.10	0.12	0.12	0.11	0.09	0.10
MgO	14.45	13.90	13.89	13.38	13.76	14.21	13.91	13.47
CaO	22.99	22.63	23.37	22.62	23.22	23.08	22.90	22.84
Na_2O	0.63	0.86	0.64	0.77	0.69	0.76	0.79	0.81
K_2O	0.00	0.01	0.00	0.01	0.00	0.01	0.00	0.00
NiO	0.03	0.02	0.00	0.06	0.00	0.02	0.00	0.05
Total	99.96	99.84	99.41	98.96	99.22	99.18	99.62	98.73
Si	1.97	1.96	1.99	1.96	1.96	1.97	1.94	1.91
Ti	0.03	0.04	0.03	0.04	0.04	0.03	0.05	0.06
Al	0.04	0.04	0.03	0.05	0.05	0.04	0.06	0.07
Cr	0.00	0.00	0.00	0.00	0.00	0.00	0.00	0.00
Fe	0.20	0.23	0.19	0.23	0.20	0.19	0.21	0.23
Mn	0.00	0.00	0.00	0.00	0.00	0.00	0.00	0.00
Mg	0.80	0.77	0.77	0.75	0.77	0.79	0.77	0.76
Ca	0.91	0.90	0.93	0.91	0.93	0.92	0.91	0.93
Na	0.05	0.06	0.05	0.06	0.05	0.06	0.06	0.06
K	0.00	0.00	0.00	0.00	0.00	0.00	0.00	0.00
Ni	0.00	0.00	0.00	0.00	0.00	0.00	0.00	0.00
Total	4.00	4.01	3.99	4.00	4.00	4.01	4.01	4.02
Mg#	79.69	77.31	79.85	76.71	78.94	80.24	78.58	77.12
$D^{(cpx\text{-}melt)}_{H_2O}$	0.0075	0.0079	0.0065	0.0078	0.0079	0.0073	0.0087	0.0104
Absorbance of cpx (cm^{-1})	1.38	2.43	1.89	2.19	3.06	1.39	2.28	3.64
Thickness of cpx (0.001mm)	100	100	100	100	100	100	100	80
Absorbance normalized to 1 cm (cm^{-1})	138	243	189	219	306	139	228	455
H_2O-cpx (ppm)	58	103	80	93	129	59	96	193
H_2O-melt (wt%)	0.78	1.30	1.23	1.19	1.64	0.81	1.11	1.86

Sample No. Section No. Point No.	22	23	24	25	26	27	28	29
SiO_2	48.07	49.36	49.61	46.11	51.16	48.37	51.61	49.43
TiO_2	3.98	3.40	3.41	3.64	1.35	2.37	1.87	2.19
Al_2O3	3.55	2.37	3.03	6.25	2.86	4.45	2.09	3.69
Cr_2O3	0.00	0.00	0.00	0.01	0.19	0.14	0.03	0.01
FeO	8.16	8.79	8.03	7.25	5.61	8.11	6.49	6.68
MnO	0.13	0.15	0.11	0.08	0.03	0.05	0.11	0.09
MgO	12.27	12.14	12.26	11.87	14.44	12.75	13.75	12.91
CaO	21.75	21.42	21.67	23.36	23.80	21.75	22.83	23.50
Na_2O	1.14	1.30	1.15	0.51	0.45	0.42	0.84	0.55
K_2O	0.00	0.00	0.00	0.02	0.00	0.52	0.00	0.00
NiO	0.00	0.03	0.01	0.10	0.02	0.00	0.05	0.00
Total	99.06	98.96	99.27	99.19	99.90	98.93	99.67	99.06
Si	1.83	1.88	1.87	1.75	1.90	1.83	1.92	1.86
Ti	0.11	0.10	0.10	0.10	0.04	0.07	0.05	0.06
Al	0.16	0.11	0.13	0.28	0.13	0.20	0.09	0.16
Cr	0.00	0.00	0.00	0.00	0.01	0.00	0.00	0.00
Fe	0.26	0.28	0.25	0.23	0.17	0.26	0.20	0.21
Mn	0.00	0.00	0.00	0.00	0.00	0.00	0.00	0.00
Mg	0.69	0.69	0.69	0.67	0.80	0.72	0.76	0.72
Ca	0.88	0.87	0.88	0.95	0.95	0.88	0.91	0.95
Na	0.08	0.10	0.08	0.04	0.03	0.03	0.06	0.04
K	0.00	0.00	0.00	0.00	0.00	0.02	0.00	0.00
Ni	0.00	0.00	0.00	0.00	0.00	0.00	0.00	0.00
Total	4.02	4.02	4.01	4.03	4.02	4.02	4.01	4.01
Mg#	72.84	71.13	73.13	74.49	82.11	73.70	79.06	77.51
$D^{(cpx\text{-}melt)}_{H_2O}$	0.0193	0.0140	0.0145	0.0297	0.0114	0.0182	0.0100	0.0143
Absorbance of cpx (cm^{-1})	2.75	2.59	4.89	7.00	2.90	5.89	1.48	3.21
Thickness of cpx (0.001mm)	80	80	80	111	106	101	75	60
Absorbance normalized to 1 cm (cm^{-1})	344	324	611	631	274	583	197	535
H_2O-cpx (ppm)	145	137	259	267	116	247	83	226
H_2O-melt (wt%)	0.75	0.98	1.79	0.90	1.02	1.36	0.84	1.59

Sample No.								
Section No.	2							
Point No.	1	2	3	4	5	6	7	8
SiO_2	51.81	43.44	51.86	38.73	51.44	50.19	52.90	50.88
TiO_2	1.58	4.79	1.61	0.83	1.66	2.21	1.39	1.66
Al_2O3	1.97	7.32	1.73	1.21	2.02	2.84	1.36	2.69
Cr_2O3	0.05	0.02	0.00	0.03	0.06	0.04	0.00	0.03
FeO	5.50	7.88	5.81	2.27	5.93	6.64	5.61	6.17
MnO	0.07	0.09	0.08	0.01	0.07	0.09	0.09	0.10
MgO	14.49	11.18	14.37	12.45	14.03	13.83	14.28	14.05
CaO	23.55	23.57	23.60	14.42	23.46	23.41	23.43	23.35
Na_2O	0.56	0.66	0.58	0.55	0.59	0.62	0.62	0.60
K_2O	0.00	0.00	0.01	0.00	0.00	0.04	0.00	0.02
NiO	0.04	0.08	0.00	0.00	0.01	0.00	0.00	0.08
Total	99.61	99.03	99.64	70.49	99.27	99.90	99.68	99.63
Si	1.92	1.67	1.93	1.98	1.92	1.87	1.96	1.90
Ti	0.04	0.14	0.04	0.03	0.05	0.06	0.04	0.05
Al	0.09	0.33	0.08	0.07	0.09	0.12	0.06	0.12
Cr	0.00	0.00	0.00	0.00	0.00	0.00	0.00	0.00
Fe	0.17	0.25	0.18	0.10	0.19	0.21	0.17	0.19
Mn	0.00	0.00	0.00	0.00	0.00	0.00	0.00	0.00
Mg	0.80	0.64	0.80	0.95	0.78	0.77	0.79	0.78
Ca	0.94	0.97	0.94	0.79	0.94	0.94	0.93	0.93
Na	0.04	0.05	0.04	0.05	0.04	0.04	0.04	0.04
K	0.00	0.00	0.00	0.00	0.00	0.00	0.00	0.00
Ni	0.00	0.00	0.00	0.00	0.00	0.00	0.00	0.00
Total	4.01	4.05	4.01	3.98	4.01	4.02	4.00	4.02
Mg#	82.44	71.67	81.51	90.74	80.84	78.79	81.95	80.24
$D^{(cpx\text{-}melt)}_{H_2O}$	0.0097	0.0495	0.0093	0.0077	0.0098	0.0133	0.0077	0.0115
Absorbance of cpx (cm^{-1})	2.44	4.80	3.30	4.40	4.70	4.10	2.90	4.18
Thickness of cpx (0.001mm)	85	85	97	106	107	106	104	96
Absorbance normalized to 1 cm (cm^{-1})	287	565	340	415	439	387	279	435
H_2O-cpx (ppm)	121	239	144	176	186	164	118	184
H_2O-melt (wt%)	1.26	0.48	1.54	2.28	1.90	1.23	1.52	1.60

Sample No.							
Section No.				3			
Point No.	9	10	11	1	2	3	4
SiO_2	52.33	46.56	51.74	52.70	52.02	52.68	50.49
TiO_2	1.63	3.11	1.50	0.98	1.62	1.35	2.03
Al_2O3	1.89	6.14	1.84	1.75	2.23	1.58	2.68
Cr_2O3	0.03	0.15	0.00	0.05	0.05	0.05	0.00
FeO	5.80	6.91	5.78	5.85	5.67	5.62	6.06
MnO	0.08	0.04	0.06	0.06	0.06	0.07	0.08
MgO	14.48	12.48	14.22	14.55	14.18	14.33	13.90
CaO	23.59	23.11	23.65	23.68	23.70	23.87	23.64
Na_2O	0.57	0.62	0.58	0.52	0.58	0.55	0.57
K_2O	0.01	0.00	0.00	0.01	0.00	0.00	0.00
NiO	0.00	0.05	0.01	0.00	0.00	0.02	0.04
Total	100.41	99.17	99.36	100.13	100.12	100.12	99.49
Si	1.93	1.76	1.93	1.95	1.92	1.95	1.89
Ti	0.05	0.09	0.04	0.03	0.05	0.04	0.06
Al	0.08	0.27	0.08	0.08	0.10	0.07	0.12
Cr	0.00	0.00	0.00	0.00	0.00	0.00	0.00
Fe	0.18	0.22	0.18	0.18	0.18	0.17	0.19
Mn	0.00	0.00	0.00	0.00	0.00	0.00	0.00
Mg	0.80	0.70	0.79	0.80	0.78	0.79	0.77
Ca	0.93	0.94	0.94	0.94	0.94	0.94	0.95
Na	0.04	0.05	0.04	0.04	0.04	0.04	0.04
K	0.00	0.00	0.00	0.00	0.00	0.00	0.00
Ni	0.00	0.00	0.00	0.00	0.00	0.00	0.00
Total	4.01	4.03	4.01	4.01	4.00	4.00	4.02
Mg#	81.64	76.29	81.45	81.61	81.70	81.96	80.36
$D^{(cpx\text{-}melt)}_{H_2O}$	0.0094	0.0278	0.0093	0.0084	0.0097	0.0083	0.0121
Absorbance of cpx (cm^{-1})	2.78	5.10	3.20	3.60	4.20	3.60	4.90
Thickness of cpx (0.001mm)	96	93	93	96	93	101	104
Absorbance normalized to 1 cm (cm^{-1})	290	548	344	375	452	356	471
H_2O-cpx (ppm)	123	232	146	159	191	151	199
H_2O-melt (wt%)	1.30	0.84	1.57	1.89	1.96	1.81	1.64

Sample No.	XL-7							
Section No.	2							
Point No.	1	2	3	4	5	6	7	8
SiO_2	51.12	48.82	46.60	47.80	48.95	49.90	48.51	48.34
TiO_2	1.40	2.47	3.31	3.18	2.40	2.14	2.35	2.50
Al_2O3	2.36	4.03	5.84	4.47	3.75	3.39	3.79	4.37
Cr_2O3	0.01	0.00	0.02	0.01	0.01	0.05	0.00	0.05
FeO	5.67	6.13	7.09	7.24	6.01	5.73	6.35	6.12
MnO	0.10	0.10	0.09	0.03	0.11	0.06	0.05	0.13
MgO	14.16	13.27	12.07	12.71	13.23	13.71	13.23	13.14
CaO	23.49	23.57	23.13	23.36	23.70	23.51	23.65	23.31
Na_2O	0.60	0.54	0.52	0.42	0.55	0.55	0.45	0.56
K_2O	0.00	0.01	0.01	0.00	0.01	0.00	0.00	0.00
NiO	0.03	0.05	0.05	0.02	0.00	0.00	0.00	0.04
Total	98.93	98.99	98.72	99.24	98.72	99.04	98.35	98.56
Si	1.91	1.84	1.77	1.81	1.85	1.87	1.84	1.83
Ti	0.04	0.07	0.09	0.09	0.07	0.06	0.07	0.07
Al	0.10	0.18	0.26	0.20	0.17	0.15	0.17	0.20
Cr	0.00	0.00	0.00	0.00	0.00	0.00	0.00	0.00
Fe	0.18	0.19	0.23	0.23	0.19	0.18	0.20	0.19
Mn	0.00	0.00	0.00	0.00	0.00	0.00	0.00	0.00
Mg	0.79	0.75	0.68	0.72	0.74	0.77	0.75	0.74
Ca	0.94	0.95	0.94	0.95	0.96	0.94	0.96	0.94
Na	0.04	0.04	0.04	0.03	0.04	0.04	0.03	0.04
K	0.00	0.00	0.00	0.00	0.00	0.00	0.00	0.00
Ni	0.00	0.00	0.00	0.00	0.00	0.00	0.00	0.00
Total	4.02	4.02	4.02	4.02	4.02	4.01	4.02	4.02
Mg#	81.66	79.44	75.21	75.78	79.71	81.00	78.79	79.29
$D^{(cpx\text{-}melt)}_{H_2O}$	0.0102	0.0165	0.0258	0.0205	0.0154	0.0135	0.0161	0.0177
Absorbance of cpx (cm^{-1})	5.80	8.60	8.10	7.70	8.20	7.80	7.60	5.50
Thickness of cpx (0.001mm)	93	102	86	96	103	111	111	115
Absorbance normalized to 1 cm (cm^{-1})	624	843	942	802	796	703	685	478
H_2O-cpx (ppm)	264	357	399	339	337	297	290	202
H_2O-melt (wt%)	2.59	2.16	1.54	1.66	2.18	2.20	1.80	1.14

Sample No. Section No. Point No.	9	10	11	12	13	14	15	16
SiO_2	48.61	49.54	49.23	49.31	50.72	47.66	50.45	49.15
TiO_2	2.19	2.21	2.21	2.10	1.86	2.64	1.78	2.24
Al_2O3	3.99	4.39	4.03	3.27	3.15	5.60	2.49	3.88
Cr_2O3	0.54	0.04	0.02	0.01	0.02	0.17	0.06	0.08
FeO	6.20	6.20	6.28	6.19	5.98	6.31	5.59	5.86
MnO	0.07	0.10	0.08	0.02	0.06	0.11	0.05	0.09
MgO	13.20	13.31	13.47	13.63	13.78	12.76	14.04	13.49
CaO	23.27	23.86	23.32	23.59	23.35	22.94	23.67	23.38
Na_2O	0.51	0.45	0.54	0.45	0.52	0.66	0.51	0.60
K_2O	0.08	0.01	0.00	0.01	0.02	0.00	0.00	0.01
NiO	0.04	0.00	0.03	0.02	0.00	0.01	0.08	0.01
Total	98.69	100.12	99.20	98.59	99.46	98.85	98.71	98.78
Si	1.84	1.84	1.85	1.86	1.89	1.80	1.90	1.85
Ti	0.06	0.06	0.06	0.06	0.05	0.07	0.05	0.06
Al	0.18	0.19	0.18	0.15	0.14	0.25	0.11	0.17
Cr	0.02	0.00	0.00	0.00	0.00	0.00	0.00	0.00
Fe	0.20	0.19	0.20	0.20	0.19	0.20	0.18	0.18
Mn	0.00	0.00	0.00	0.00	0.00	0.00	0.00	0.00
Mg	0.74	0.74	0.75	0.77	0.77	0.72	0.79	0.76
Ca	0.94	0.95	0.94	0.95	0.93	0.93	0.95	0.94
Na	0.04	0.03	0.04	0.03	0.04	0.05	0.04	0.04
K	0.00	0.00	0.00	0.00	0.00	0.00	0.00	0.00
Ni	0.00	0.00	0.00	0.00	0.00	0.00	0.00	0.00
Total	4.02	4.02	4.02	4.02	4.01	4.02	4.02	4.02
Mg#	79.16	79.28	79.27	79.71	80.42	78.30	81.74	80.41
$D^{(cpx\text{-}melt)}_{H_2O}$	0.0167	0.0161	0.0158	0.0141	0.0120	0.0220	0.0113	0.0154
Absorbance of cpx (cm^{-1})	7.60	10.40	6.70	9.26	6.30	7.40	5.90	7.70
Thickness of cpx (0.001mm)	115	112	112	112	112	120	120	120
Absorbance normalized to 1 cm (cm^{-1})	661	929	598	827	563	617	492	642
H_2O-cpx (ppm)	280	393	253	350	238	261	208	272
H_2O-melt (wt%)	1.68	2.43	1.60	2.49	1.98	1.19	1.84	1.76

Sample No. Section No. Point No.	17	18	18.2	19	20	21	22	22.1
SiO_2	49.20	49.63	49.95	47.09	48.55	51.19	49.55	49.13
TiO_2	2.06	2.21	2.07	2.99	1.98	1.71	1.90	1.99
Al_2O3	3.88	4.08	3.53	5.43	4.49	2.61	3.74	4.43
Cr_2O3	0.00	0.04	0.04	0.02	0.07	0.00	0.04	0.50
FeO	6.44	6.47	5.93	6.57	6.34	5.36	6.09	5.38
MnO	0.08	0.06	0.11	0.05	0.06	0.11	0.08	0.07
MgO	13.40	13.07	13.48	12.72	13.18	14.14	13.80	14.09
CaO	23.49	23.58	23.29	23.46	23.22	23.44	23.36	23.11
Na_2O	0.56	0.45	0.60	0.57	0.66	0.50	0.30	0.59
K_2O	0.00	0.00	0.01	0.00	0.00	0.00	0.00	0.00
NiO	0.03	0.03	0.02	0.02	0.03	0.01	0.02	0.04
Total	99.15	99.64	99.02	98.92	98.57	99.06	98.88	99.32
Si	1.85	1.86	1.87	1.78	1.84	1.91	1.86	1.84
Ti	0.06	0.06	0.06	0.08	0.06	0.05	0.05	0.06
Al	0.17	0.18	0.16	0.24	0.20	0.11	0.17	0.19
Cr	0.00	0.00	0.00	0.00	0.00	0.00	0.00	0.01
Fe	0.20	0.20	0.19	0.21	0.20	0.17	0.19	0.17
Mn	0.00	0.00	0.00	0.00	0.00	0.00	0.00	0.00
Mg	0.75	0.73	0.75	0.72	0.74	0.79	0.77	0.78
Ca	0.95	0.94	0.94	0.95	0.94	0.94	0.94	0.93
Na	0.04	0.03	0.04	0.04	0.05	0.04	0.02	0.04
K	0.00	0.00	0.00	0.00	0.00	0.00	0.00	0.00
Ni	0.00	0.00	0.00	0.00	0.00	0.00	0.00	0.00
Total	4.03	4.01	4.01	4.03	4.03	4.00	4.01	4.03
Mg#	78.76	78.28	80.22	77.54	78.75	82.48	80.16	82.36
$D^{(cpx\text{-}melt)}_{H_2O}$	0.0154	0.0150	0.0134	0.0238	0.0169	0.0106	0.0144	0.0173
Absorbance of cpx (cm^{-1})	6.40	7.60	6.90	6.10	6.50	5.90	8.40	9.09
Thickness of cpx (0.001mm)	101	101	101	101	108	116	116	116
Absorbance normalized to 1 cm (cm^{-1})	634	752	683	604	602	509	724	784
H_2O-cpx (ppm)	268	318	289	256	255	215	306	332
H_2O-melt (wt%)	1.74	2.13	2.15	1.07	1.50	2.04	2.13	1.92

Sample No.					XL-8		
Section No.					1		
Point No.	23	24	25	26	1	2	3
SiO_2	50.18	48.70	48.67	50.34	52.25	51.90	51.55
TiO_2	1.97	2.33	2.34	1.91	1.43	1.56	1.62
Al_2O3	3.29	4.28	4.17	2.97	1.87	1.79	2.04
Cr_2O3	0.11	0.05	0.00	0.00	0.04	0.02	0.01
FeO	5.73	6.19	6.72	5.54	5.63	5.78	5.64
MnO	0.06	0.09	0.04	0.07	0.04	0.10	0.08
MgO	13.60	13.19	13.14	13.70	14.18	14.50	14.20
CaO	23.63	23.32	23.73	23.77	23.16	23.82	23.67
Na_2O	0.54	0.55	0.48	0.53	0.56	0.50	0.55
K_2O	0.01	0.01	0.01	0.00	0.00	0.01	0.00
NiO	0.06	0.00	0.01	0.06	0.00	0.01	0.00
Total	99.18	98.71	99.30	98.87	99.16	99.98	99.37
Si	1.88	1.84	1.83	1.89	1.94	1.92	1.92
Ti	0.06	0.07	0.07	0.05	0.04	0.04	0.05
Al	0.15	0.19	0.19	0.13	0.08	0.08	0.09
Cr	0.00	0.00	0.00	0.00	0.00	0.00	0.00
Fe	0.18	0.20	0.21	0.17	0.18	0.18	0.18
Mn	0.00	0.00	0.00	0.00	0.00	0.00	0.00
Mg	0.76	0.74	0.74	0.77	0.79	0.80	0.79
Ca	0.95	0.94	0.96	0.96	0.92	0.95	0.95
Na	0.04	0.04	0.03	0.04	0.04	0.04	0.04
K	0.00	0.00	0.00	0.00	0.00	0.00	0.00
Ni	0.00	0.00	0.00	0.00	0.00	0.00	0.00
Total	4.01	4.02	4.03	4.01	3.99	4.01	4.01
Mg#	80.89	79.17	77.72	81.53	81.79	81.73	81.77
$D^{(cpx\text{-}melt)}_{H_2O}$	0.0128	0.0167	0.0171	0.0119	0.0086	0.0096	0.0097
Absorbance of cpx (cm^{-1})	5.30	8.10	5.50	7.70	2.00	2.20	3.80
Thickness of cpx (0.001mm)	116	116	116	101	96	94	93
Absorbance normalized to 1 cm (cm^{-1})	457	698	474	762	208	234	409
H_2O-cpx (ppm)	193	295	201	323	88	99	173
H_2O-melt (wt%)	1.51	1.77	1.17	2.71	1.03	1.04	1.78

Sample No.								
Section No.								2
Point No.	4	5	6	7	8	9	11	1
SiO_2	46.06	51.89	52.28	51.02	52.37	52.42	50.32	50.66
TiO_2	3.36	1.51	1.15	1.98	1.34	1.45	2.03	2.62
Al_2O3	6.16	2.24	1.99	2.63	1.38	1.56	2.82	2.56
Cr_2O3	0.08	0.03	0.02	0.00	0.02	0.03	0.04	0.01
FeO	7.40	5.66	5.75	5.99	5.73	5.61	1.73	7.08
MnO	0.02	0.08	0.09	0.10	0.10	0.06	0.11	0.09
MgO	12.02	14.10	14.47	13.61	14.74	14.07	13.51	12.95
CaO	23.50	23.80	23.70	23.48	23.59	23.59	23.76	22.55
Na_2O	0.52	0.59	0.56	0.57	0.61	0.59	0.00	1.01
K_2O	0.00	0.00	0.01	0.01	0.00	0.00	0.00	0.00
NiO	0.04	0.02	0.03	0.05	0.04	0.00	0.00	0.02
Total	99.15	99.92	100.03	99.43	99.90	99.39	94.31	99.53
Si	1.75	1.92	1.93	1.90	1.94	1.95	1.94	1.90
Ti	0.10	0.04	0.03	0.06	0.04	0.04	0.06	0.07
Al	0.28	0.10	0.09	0.12	0.06	0.07	0.13	0.11
Cr	0.00	0.00	0.00	0.00	0.00	0.00	0.00	0.00
Fe	0.24	0.18	0.18	0.19	0.18	0.17	0.06	0.22
Mn	0.00	0.00	0.00	0.00	0.00	0.00	0.00	0.00
Mg	0.68	0.78	0.80	0.76	0.81	0.78	0.78	0.72
Ca	0.96	0.94	0.94	0.94	0.94	0.94	0.98	0.90
Na	0.04	0.04	0.04	0.04	0.04	0.04	0.00	0.07
K	0.00	0.00	0.00	0.00	0.00	0.00	0.00	0.00
Ni	0.00	0.00	0.00	0.00	0.00	0.00	0.00	0.00
Total	4.04	4.01	4.01	4.00	4.01	4.00	3.94	4.01
Mg#	74.33	81.62	81.78	80.19	82.11	81.72	93.28	76.53
$D^{(cpx\text{-}melt)}_{H_2O}$	0.0294	0.0096	0.0090	0.0110	0.0087	0.0082	0.0085	0.0119
Absorbance of cpx (cm^{-1})	4.50	4.10	3.50	4.80	2.80	2.60	3.40	4.20
Thickness of cpx (0.001mm)	93	104	98	112	93	93	93	88
Absorbance normalized to 1 cm (cm^{-1})	484	394	357	429	301	280	366	477
H_2O-cpx (ppm)	205	167	151	181	127	118	155	202
H_2O-melt (wt%)	0.70	1.73	1.67	1.66	1.47	1.45	1.83	1.70

Sample No. Section No. Point No.	2	3	4	5	6	7	7.2	8
SiO_2	48.66	52.30	52.45	51.56	50.49	51.44	52.51	52.29
TiO_2	3.80	1.72	1.34	1.84	1.45	1.69	1.27	1.54
Al_2O3	3.41	1.15	1.93	2.33	8.18	2.17	1.19	1.98
Cr_2O3	0.00	0.02	0.01	0.03	0.04	0.01	0.05	0.00
FeO	8.60	7.67	5.89	5.79	8.30	5.93	5.32	5.83
MnO	0.10	0.15	0.08	0.07	0.12	0.08	0.09	0.06
MgO	11.62	13.05	14.24	13.97	11.03	13.86	14.38	14.06
CaO	21.60	22.22	23.58	23.54	17.89	23.26	23.56	23.64
Na_2O	1.28	0.96	0.47	0.61	2.57	0.62	0.56	0.60
K_2O	0.00	0.00	0.01	0.00	0.00	0.01	0.00	0.00
NiO	0.00	0.01	0.07	0.00	0.03	0.03	0.00	0.05
Total	99.07	99.25	100.05	99.74	100.10	99.11	98.93	100.03
Si	1.85	1.96	1.94	1.91	1.86	1.92	1.96	1.93
Ti	0.11	0.05	0.04	0.05	0.04	0.05	0.04	0.04
Al	0.15	0.05	0.08	0.10	0.35	0.10	0.05	0.09
Cr	0.00	0.00	0.00	0.00	0.00	0.00	0.00	0.00
Fe	0.27	0.24	0.18	0.18	0.26	0.19	0.17	0.18
Mn	0.00	0.00	0.00	0.00	0.00	0.00	0.00	0.00
Mg	0.66	0.73	0.78	0.77	0.61	0.77	0.80	0.78
Ca	0.88	0.89	0.93	0.94	0.71	0.93	0.94	0.94
Na	0.09	0.07	0.03	0.04	0.18	0.05	0.04	0.04
K	0.00	0.00	0.00	0.00	0.00	0.00	0.00	0.00
Ni	0.00	0.00	0.00	0.00	0.00	0.00	0.00	0.00
Total	4.01	4.00	4.00	4.00	4.01	4.00	4.00	4.00
Mg#	70.67	75.21	81.16	81.15	70.33	80.66	82.82	81.14
$D^{(cpx\text{-}melt)}_{H_2O}$	0.0168	0.0079	0.0088	0.0103	0.0183	0.0098	0.0076	0.0090
Absorbance of cpx (cm^{-1})	3.90	2.00	4.40	3.10	3.60	2.77	5.00	4.60
Thickness of cpx (0.001mm)	88	88	88	92	92	108	108	102
Absorbance normalized to 1 cm (cm^{-1})	443	227	500	337	391	256	463	451
H_2O-cpx (ppm)	188	96	212	143	166	109	196	191
H_2O-melt (wt%)	1.12	1.22	2.41	1.39	0.90	1.11	2.56	2.11

Sample No.							XL-9
Section No.							1
Point No.	9	10	11	12	13	14	1
SiO_2	48.50	53.86	51.51	51.29	50.87	50.34	49.50
TiO_2	2.16	1.02	0.99	1.73	1.85	1.38	2.04
Al_2O3	4.33	0.72	2.95	2.43	2.56	3.80	3.63
Cr_2O3	0.12	0.04	0.71	0.00	0.04	0.51	0.09
FeO	6.65	6.14	5.03	5.89	5.98	5.48	6.87
MnO	0.09	0.13	0.08	0.08	0.10	0.09	0.11
MgO	13.06	14.10	14.66	13.80	13.96	13.48	13.26
CaO	23.71	22.92	23.41	23.47	23.35	23.38	23.81
Na_2O	0.48	0.85	0.57	0.58	0.59	0.73	0.49
K_2O	0.00	0.01	0.00	0.01	0.00	0.05	0.00
NiO	0.06	0.04	0.02	0.05	0.08	0.04	0.02
Total	99.15	99.83	99.92	99.32	99.39	99.28	99.81
Si	1.83	1.99	1.90	1.91	1.90	1.88	1.85
Ti	0.06	0.03	0.03	0.05	0.05	0.04	0.06
Al	0.19	0.03	0.13	0.11	0.11	0.17	0.16
Cr	0.00	0.00	0.02	0.00	0.00	0.02	0.00
Fe	0.21	0.19	0.16	0.18	0.19	0.17	0.22
Mn	0.00	0.00	0.00	0.00	0.00	0.00	0.00
Mg	0.73	0.78	0.81	0.77	0.78	0.75	0.74
Ca	0.96	0.91	0.93	0.94	0.93	0.94	0.96
Na	0.03	0.06	0.04	0.04	0.04	0.05	0.04
K	0.00	0.00	0.00	0.00	0.00	0.00	0.00
Ni	0.00	0.00	0.00	0.00	0.00	0.00	0.00
Total	4.03	3.99	4.01	4.01	4.01	4.02	4.02
Mg#	77.77	80.36	83.87	80.68	80.62	81.45	77.47
$D^{(cpx\text{-}melt)}_{H_2O}$	0.0174	0.0064	0.0111	0.0103	0.0113	0.0128	0.0149
Absorbance of cpx (cm^{-1})	6.70	3.90	6.20	5.10	4.40	5.20	4.90
Thickness of cpx (0.001mm)	114	109	113	105	103	105	77
Absorbance normalized to 1 cm (cm^{-1})	588	358	549	486	427	495	636
H_2O-cpx (ppm)	249	151	232	206	181	210	269
H_2O-melt (wt%)	1.43	2.37	2.09	2.00	1.60	1.63	1.81

Sample No.								
Section No.								
Point No.	2	3	4	5	6	7	8	8.2
SiO_2	51.76	50.77	51.52	51.76	48.53	51.02	51.51	50.45
TiO_2	1.65	1.15	1.73	1.62	2.24	0.75	1.71	2.05
Al_2O3	2.52	3.17	2.64	2.36	4.14	4.19	2.50	3.31
Cr_2O3	0.05	0.53	0.03	0.03	0.05	0.86	0.04	0.11
FeO	5.70	5.33	6.13	5.59	6.94	5.88	5.72	5.91
MnO	0.11	0.03	0.06	0.10	0.08	0.05	0.11	0.10
MgO	13.91	14.25	13.03	14.02	13.10	13.81	14.01	13.43
CaO	24.07	23.79	24.05	23.92	23.70	22.14	24.01	23.69
Na_2O	0.50	0.44	0.53	0.56	0.54	0.96	0.56	0.61
K_2O	0.00	0.02	0.00	0.03	0.00	0.01	0.00	0.00
NiO	0.00	0.00	0.01	0.06	0.05	0.01	0.00	0.05
Total	100.25	99.49	99.74	100.05	99.36	99.67	100.16	99.72
Si	1.91	1.89	1.92	1.92	1.83	1.89	1.91	1.88
Ti	0.05	0.03	0.05	0.05	0.06	0.02	0.05	0.06
Al	0.11	0.14	0.12	0.10	0.18	0.18	0.11	0.15
Cr	0.00	0.02	0.00	0.00	0.00	0.03	0.00	0.00
Fe	0.18	0.17	0.19	0.17	0.22	0.18	0.18	0.18
Mn	0.00	0.00	0.00	0.00	0.00	0.00	0.00	0.00
Mg	0.77	0.79	0.72	0.77	0.74	0.76	0.77	0.75
Ca	0.95	0.95	0.96	0.95	0.96	0.88	0.95	0.95
Na	0.04	0.03	0.04	0.04	0.04	0.07	0.04	0.04
K	0.00	0.00	0.00	0.00	0.00	0.00	0.00	0.00
Ni	0.00	0.00	0.00	0.00	0.00	0.00	0.00	0.00
Total	4.00	4.02	4.00	4.01	4.03	4.02	4.01	4.01
Mg#	81.30	82.67	79.14	81.72	77.09	80.71	81.37	80.20
$D^{(cpx\text{-}melt)}_{H_2O}$	0.0102	0.0118	0.0098	0.0100	0.0174	0.0126	0.0106	0.0127
Absorbance of cpx (cm^{-1})	4.00	4.20	4.50	6.20	5.30	6.00	4.90	4.20
Thickness of cpx (0.001mm)	83	83	88	96	90	90	96	96
Absorbance normalized to 1 cm (cm^{-1})	482	506	511	646	589	667	510	438
H_2O-cpx (ppm)	204	214	216	273	249	282	216	185
H_2O-melt (wt%)	2.00	1.81	2.20	2.73	1.43	2.25	2.04	1.46

Sample No.								
Section No.							2	
Point No.	9	10	11	12	13	14	1	2
SiO_2	51.66	48.36	49.44	47.92	49.09	50.95	46.56	51.30
TiO_2	1.73	2.70	2.26	2.66	2.44	1.78	2.71	1.86
Al_2O3	2.38	4.57	3.96	4.55	3.99	2.51	5.93	2.70
Cr_2O3	0.06	0.02	0.09	0.01	0.05	0.03	0.06	0.01
FeO	5.88	6.68	6.55	7.44	7.02	6.40	7.11	6.12
MnO	0.05	0.06	0.07	0.08	0.07	0.10	0.09	0.12
MgO	13.24	12.81	13.41	12.71	13.06	13.73	12.42	13.50
CaO	23.75	24.07	23.73	24.24	23.94	23.80	23.73	23.72
Na_2O	0.53	0.44	0.50	0.45	0.50	0.53	0.49	0.64
K_2O	0.01	0.02	0.00	0.01	0.00	0.00	0.00	0.02
NiO	0.06	0.00	0.00	0.00	0.02	0.03	0.00	0.04
Total	99.36	99.73	99.99	100.07	100.20	99.85	99.12	100.04
Si	1.93	1.82	1.84	1.80	1.83	1.90	1.77	1.90
Ti	0.05	0.08	0.06	0.08	0.07	0.05	0.08	0.05
Al	0.10	0.20	0.17	0.20	0.18	0.11	0.27	0.12
Cr	0.00	0.00	0.00	0.00	0.00	0.00	0.00	0.00
Fe	0.18	0.21	0.20	0.23	0.22	0.20	0.23	0.19
Mn	0.00	0.00	0.00	0.00	0.00	0.00	0.00	0.00
Mg	0.74	0.72	0.75	0.71	0.73	0.76	0.70	0.75
Ca	0.95	0.97	0.95	0.98	0.96	0.95	0.96	0.94
Na	0.04	0.03	0.04	0.03	0.04	0.04	0.04	0.05
K	0.00	0.00	0.00	0.00	0.00	0.00	0.00	0.00
Ni	0.00	0.00	0.00	0.00	0.00	0.00	0.00	0.00
Total	3.99	4.02	4.02	4.04	4.03	4.01	4.04	4.01
Mg#	80.05	77.37	78.49	75.27	76.83	79.27	75.70	79.72
$D^{(cpx\text{-}melt)}_{H_2O}$	0.0094	0.0189	0.0159	0.0204	0.0168	0.0112	0.0262	0.0109
Absorbance of cpx (cm^{-1})	5.10	6.60	5.50	8.00	2.50	4.70	6.40	7.20
Thickness of cpx (0.001mm)	97	100	100	91	91	78	118	119
Absorbance normalized to 1 cm (cm^{-1})	526	660	550	879	275	603	542	605
H_2O-cpx (ppm)	222	279	233	372	116	255	229	256
H_2O-melt (wt%)	2.37	1.48	1.46	1.82	0.69	2.28	0.88	2.36

Sample No.								
Section No.								
Point No.	3	4	5	6	7	8	9	10
SiO_2	51.94	51.77	52.13	50.07	50.49	50.91	49.89	48.63
TiO_2	1.67	1.68	1.64	1.95	1.74	2.08	2.35	2.46
Al_2O3	2.42	2.19	2.28	3.16	2.66	2.79	3.82	4.21
Cr_2O3	0.02	0.00	0.09	0.01	0.03	0.05	0.01	0.00
FeO	5.33	5.66	5.67	6.13	5.75	5.73	6.11	6.75
MnO	0.05	0.07	0.08	0.07	0.07	0.06	0.08	0.08
MgO	14.16	13.88	14.16	13.60	14.08	13.81	13.27	12.91
CaO	24.02	23.88	24.03	23.86	23.95	23.85	23.83	23.97
Na_2O	0.59	0.56	0.55	0.58	0.57	0.55	0.50	0.52
K_2O	0.00	0.02	0.01	0.00	0.00	0.00	0.00	0.00
NiO	0.06	0.01	0.00	0.02	0.01	0.01	0.00	0.03
Total	100.26	99.71	100.66	99.44	99.34	99.85	99.86	99.56
Si	1.92	1.92	1.92	1.87	1.89	1.89	1.86	1.83
Ti	0.05	0.05	0.05	0.05	0.05	0.06	0.07	0.07
Al	0.11	0.10	0.10	0.14	0.12	0.12	0.17	0.19
Cr	0.00	0.00	0.00	0.00	0.00	0.00	0.00	0.00
Fe	0.16	0.18	0.17	0.19	0.18	0.18	0.19	0.21
Mn	0.00	0.00	0.00	0.00	0.00	0.00	0.00	0.00
Mg	0.78	0.77	0.78	0.76	0.79	0.77	0.74	0.72
Ca	0.95	0.95	0.95	0.96	0.96	0.95	0.95	0.97
Na	0.04	0.04	0.04	0.04	0.04	0.04	0.04	0.04
K	0.00	0.00	0.00	0.00	0.00	0.00	0.00	0.00
Ni	0.00	0.00	0.00	0.00	0.00	0.00	0.00	0.00
Total	4.01	4.00	4.01	4.02	4.02	4.01	4.01	4.03
Mg#	82.57	81.38	81.65	79.82	81.37	81.13	79.46	77.32
$D^{(cpx\text{-}melt)}_{H_2O}$	0.0100	0.0096	0.0099	0.0130	0.0118	0.0117	0.0145	0.0174
Absorbance of cpx (cm^{-1})	5.00	4.50	4.40	3.70	5.60	4.80	4.60	8.20
Thickness of cpx (0.001mm)	119	119	112	115	123	124	125	125
Absorbance normalized to 1 cm (cm^{-1})	420	378	393	322	455	387	368	656
H_2O-cpx (ppm)	178	160	166	136	193	164	156	278
H_2O-melt (wt%)	1.77	1.67	1.67	1.05	1.63	1.40	1.07	1.59

Sample No.	XL-10							
Section No.	1							
Point No.	1	2	3	4	5	6	6.2	7
SiO_2	52.18	53.08	51.99	49.47	47.91	47.64	48.84	50.88
TiO_2	1.38	1.47	1.92	2.38	2.60	2.90	2.45	1.59
Al_2O3	1.52	1.83	2.39	4.06	4.46	4.65	4.03	3.42
Cr_2O3	0.01	0.03	0.03	0.00	0.02	0.10	0.02	0.05
FeO	5.46	5.50	5.92	6.73	6.73	6.91	6.77	6.05
MnO	0.06	0.09	0.12	0.07	0.07	0.11	0.11	0.05
MgO	14.38	14.58	14.07	13.10	13.16	13.05	13.42	14.03
CaO	23.32	23.64	23.63	23.73	24.00	23.87	23.83	23.58
Na_2O	0.68	0.55	0.65	0.50	0.47	0.57	0.46	0.54
K_2O	0.00	0.00	0.02	0.01	0.01	0.00	0.00	0.01
NiO	0.01	0.04	0.00	0.05	0.08	0.04	0.01	0.03
Total	99.00	100.82	100.73	100.10	99.52	99.82	99.91	100.21
Si	1.95	1.94	1.91	1.85	1.81	1.79	1.83	1.88
Ti	0.04	0.04	0.05	0.07	0.07	0.08	0.07	0.04
Al	0.07	0.08	0.10	0.18	0.20	0.21	0.18	0.15
Cr	0.00	0.00	0.00	0.00	0.00	0.00	0.00	0.00
Fe	0.17	0.17	0.18	0.21	0.21	0.22	0.21	0.19
Mn	0.00	0.00	0.00	0.00	0.00	0.00	0.00	0.00
Mg	0.80	0.80	0.77	0.73	0.74	0.73	0.75	0.77
Ca	0.93	0.93	0.93	0.95	0.97	0.96	0.96	0.94
Na	0.05	0.04	0.05	0.04	0.03	0.04	0.03	0.04
K	0.00	0.00	0.00	0.00	0.00	0.00	0.00	0.00
Ni	0.00	0.00	0.00	0.00	0.00	0.00	0.00	0.00
Total	4.01	4.00	4.01	4.02	4.04	4.04	4.03	4.02
Mg#	82.45	82.53	80.90	77.62	77.70	77.10	77.95	80.51
$D^{(cpx\text{-}melt)}_{H_2O}$	0.0084	0.0086	0.0104	0.0159	0.0201	0.0220	0.0175	0.0125
Absorbance of cpx (cm^{-1})	1.10	1.50	2.70	2.40	2.80	3.70	3.60	3.10
Thickness of cpx (0.001mm)	55	55	62	69	71	65	65	65
Absorbance normalized to 1 cm (cm^{-1})	200	273	435	348	394	569	554	477
H_2O-cpx (ppm)	85	115	184	147	167	241	234	202
H_2O-melt (wt%)	1.01	1.34	1.77	0.93	0.83	1.09	1.34	1.61

Sample No.								
Section No.								
Point No.	8	9	10	11	12	13	14	15
SiO_2	48.68	46.78	49.85	49.32	50.30	48.11	51.47	47.84
TiO_2	2.71	3.21	2.03	2.26	1.73	2.56	1.62	1.88
Al_2O3	4.21	6.08	3.75	4.15	3.98	5.48	1.95	3.73
Cr_2O3	0.03	0.02	0.11	0.01	0.10	0.27	0.04	0.01
FeO	7.08	7.36	6.15	6.79	6.30	6.59	5.97	6.49
MnO	0.05	0.06	0.07	0.09	0.06	0.10	0.10	0.10
MgO	13.23	12.23	13.77	12.97	13.71	12.70	14.32	11.95
CaO	23.91	23.53	23.94	23.60	23.90	23.87	23.77	27.48
Na_2O	0.35	0.50	0.39	0.60	0.38	0.62	0.69	0.50
K_2O	0.01	0.01	0.00	0.00	0.02	0.01	0.01	0.02
NiO	0.05	0.00	0.04	0.02	0.00	0.00	0.00	0.02
Total	100.31	99.77	100.09	99.81	100.47	100.31	99.93	100.01
Si	1.82	1.76	1.85	1.85	1.86	1.80	1.91	1.81
Ti	0.08	0.09	0.06	0.06	0.05	0.07	0.05	0.05
Al	0.19	0.27	0.16	0.18	0.17	0.24	0.09	0.17
Cr	0.00	0.00	0.00	0.00	0.00	0.01	0.00	0.00
Fe	0.22	0.23	0.19	0.21	0.19	0.21	0.19	0.21
Mn	0.00	0.00	0.00	0.00	0.00	0.00	0.00	0.00
Mg	0.74	0.69	0.76	0.72	0.76	0.71	0.79	0.67
Ca	0.96	0.95	0.95	0.95	0.95	0.95	0.95	1.12
Na	0.03	0.04	0.03	0.04	0.03	0.04	0.05	0.04
K	0.00	0.00	0.00	0.00	0.00	0.00	0.00	0.00
Ni	0.00	0.00	0.00	0.00	0.00	0.00	0.00	0.00
Total	4.02	4.03	4.02	4.02	4.02	4.03	4.02	4.07
Mg#	76.91	74.78	79.96	77.31	79.51	77.46	81.04	76.66
$D^{(cpx\text{-}melt)}_{H_2O}$	0.0187	0.0273	0.0149	0.0159	0.0143	0.0218	0.0102	0.0166
Absorbance of cpx (cm^{-1})	3.20	3.70	2.60	3.10	2.90	4.10	2.10	4.00
Thickness of cpx (0.001mm)	69	66	71	70	70	69	71	64
Absorbance normalized to 1 cm (cm^{-1})	464	561	366	443	414	594	296	625
H_2O-cpx (ppm)	196	237	155	187	175	251	125	264
H_2O-melt (wt%)	1.05	0.87	1.04	1.18	1.23	1.15	1.22	1.59

Sample No. Section No. Point No.	16	16.2	17	18	19	20	21	22
SiO_2	48.81	48.64	51.42	48.87	48.39	46.15	52.22	47.65
TiO_2	2.49	2.73	1.39	2.74	2.45	1.63	1.90	2.55
Al_2O3	4.38	4.65	2.82	4.25	4.53	9.24	2.38	5.81
Cr_2O3	0.03	0.00	0.06	0.01	0.04	3.96	0.00	0.26
FeO	6.57	7.05	5.12	6.40	6.60	5.22	5.68	6.62
MnO	0.09	0.06	0.09	0.07	0.08	0.11	0.07	0.08
MgO	13.34	12.82	14.38	12.83	12.93	9.97	13.30	12.61
CaO	23.70	23.55	23.20	23.62	23.83	19.11	23.72	23.46
Na_2O	0.47	0.49	0.60	0.59	0.45	3.58	0.62	0.61
K_2O	0.00	0.01	0.00	0.01	0.00	1.04	0.00	0.00
NiO	0.03	0.01	0.00	0.01	0.02	0.00	0.02	0.00
Total	99.92	100.00	99.06	99.41	99.31	100.01	99.91	99.66
Si	1.83	1.82	1.91	1.83	1.82	1.73	1.93	1.79
Ti	0.07	0.08	0.04	0.08	0.07	0.05	0.05	0.07
Al	0.19	0.20	0.12	0.19	0.20	0.41	0.10	0.26
Cr	0.00	0.00	0.00	0.00	0.00	0.12	0.00	0.01
Fe	0.21	0.22	0.16	0.20	0.21	0.16	0.18	0.21
Mn	0.00	0.00	0.00	0.00	0.00	0.00	0.00	0.00
Mg	0.74	0.72	0.80	0.72	0.73	0.56	0.73	0.71
Ca	0.95	0.94	0.93	0.95	0.96	0.77	0.94	0.94
Na	0.03	0.04	0.04	0.04	0.03	0.26	0.04	0.04
K	0.00	0.00	0.00	0.00	0.00	0.05	0.00	0.00
Ni	0.00	0.00	0.00	0.00	0.00	0.00	0.00	0.00
Total	4.03	4.02	4.01	4.02	4.02	4.11	3.99	4.03
Mg#	78.36	76.43	83.35	78.13	77.74	77.31	80.67	77.25
$D^{(cpx\text{-}melt)}_{H_2O}$	0.0181	0.0188	0.0104	0.0170	0.0182	0.0392	0.0091	0.0231
Absorbance of cpx (cm^{-1})	2.20	2.10	2.10	3.00	2.40	3.00	2.40	2.20
Thickness of cpx (0.001mm)	65	53	53	59	59	58	64	64
Absorbance normalized to 1 cm (cm^{-1})	338	396	396	508	407	517	375	344
H_2O-cpx (ppm)	143	168	168	215	172	219	159	145
H_2O-melt (wt%)	0.79	0.89	1.61	1.27	0.94	0.56	1.74	0.63

Sample No.								
Section No.		2						
Point No.	22.1	1	2	3	4	5	6	7
SiO_2	51.13	49.42	52.34	51.68	52.13	51.59	50.15	49.96
TiO_2	1.70	2.62	1.41	1.42	1.39	1.83	0.97	1.89
Al_2O3	2.29	4.27	1.73	1.91	1.68	2.32	5.26	3.48
Cr_2O3	0.03	0.00	0.03	0.01	0.00	0.01	0.81	0.00
FeO	5.83	6.85	5.63	5.84	6.10	5.99	5.09	6.01
MnO	0.12	0.10	0.10	0.10	0.13	0.13	0.08	0.10
MgO	14.33	13.20	14.16	14.31	14.07	13.85	14.17	13.65
CaO	23.57	23.87	23.60	23.49	23.93	23.83	22.69	24.34
Na_2O	0.68	0.35	0.61	0.58	0.61	0.61	0.89	0.46
K_2O	0.01	0.01	0.00	0.00	0.02	0.00	0.00	0.00
NiO	0.05	0.00	0.02	0.00	0.07	0.00	0.02	0.04
Total	99.75	100.70	99.61	99.32	100.13	100.15	100.13	99.92
Si	1.90	1.83	1.94	1.93	1.93	1.91	1.85	1.86
Ti	0.05	0.07	0.04	0.04	0.04	0.05	0.03	0.05
Al	0.10	0.19	0.08	0.08	0.07	0.10	0.23	0.15
Cr	0.00	0.00	0.00	0.00	0.00	0.00	0.02	0.00
Fe	0.18	0.21	0.17	0.18	0.19	0.19	0.16	0.19
Mn	0.00	0.00	0.00	0.00	0.00	0.00	0.00	0.00
Mg	0.80	0.73	0.78	0.80	0.78	0.76	0.78	0.76
Ca	0.94	0.95	0.94	0.94	0.95	0.95	0.90	0.97
Na	0.05	0.03	0.04	0.04	0.04	0.04	0.06	0.03
K	0.00	0.00	0.00	0.00	0.00	0.00	0.00	0.00
Ni	0.00	0.00	0.00	0.00	0.00	0.00	0.00	0.00
Total	4.02	4.01	4.00	4.01	4.01	4.01	4.03	4.02
Mg#	81.41	77.45	81.77	81.38	80.43	80.48	83.23	80.20
$D^{(cpx\text{-}melt)}_{H_2O}$	0.0110	0.0172	0.0085	0.0094	0.0090	0.0103	0.0162	0.0138
Absorbance of cpx (cm^{-1})	1.80	1.90	1.92	2.40	2.60	2.20	3.70	2.50
Thickness of cpx (0.001mm)	64	59	56	45	66	69	70	68
Absorbance normalized to 1 cm (cm^{-1})	281	322	343	533	394	319	529	368
H_2O-cpx (ppm)	119	136	145	226	167	135	224	156
H_2O-melt (wt%)	1.08	0.79	1.70	2.40	1.86	1.30	1.38	1.12

Sample No. Section No. Point No.	8	9	10	11	11.2	12	13	14
SiO_2	52.30	45.45	47.80	50.15	49.83	50.59	51.70	52.28
TiO_2	1.36	3.56	2.52	1.50	1.73	1.69	1.44	1.49
Al_2O3	1.73	7.46	4.06	1.96	2.31	2.16	1.65	1.60
Cr_2O3	0.01	0.01	0.00	0.00	0.01	0.01	0.06	0.04
FeO	5.45	7.17	6.79	5.79	5.17	5.24	6.51	5.20
MnO	0.10	0.07	0.06	0.12	0.05	0.09	0.08	0.11
MgO	14.40	11.46	12.92	13.72	13.36	13.53	13.46	14.47
CaO	23.59	24.35	25.35	22.21	22.25	22.67	23.43	23.39
Na_2O	0.58	0.60	0.51	0.58	0.64	0.58	0.65	0.57
K_2O	0.01	0.01	0.02	0.01	0.00	0.02	0.03	0.01
NiO	0.00	0.00	0.01	0.02	0.03	0.01	0.00	0.00
Total	99.53	100.14	100.03	96.06	95.39	96.60	99.00	99.17
Si	1.94	1.71	1.80	1.93	1.93	1.93	1.94	1.94
Ti	0.04	0.10	0.07	0.04	0.05	0.05	0.04	0.04
Al	0.08	0.33	0.18	0.09	0.11	0.10	0.07	0.07
Cr	0.00	0.00	0.00	0.00	0.00	0.00	0.00	0.00
Fe	0.17	0.23	0.21	0.19	0.17	0.17	0.20	0.16
Mn	0.00	0.00	0.00	0.00	0.00	0.00	0.00	0.00
Mg	0.80	0.64	0.73	0.79	0.77	0.77	0.75	0.80
Ca	0.94	0.98	1.02	0.92	0.92	0.93	0.94	0.93
Na	0.04	0.04	0.04	0.04	0.05	0.04	0.05	0.04
K	0.00	0.00	0.00	0.00	0.00	0.00	0.00	0.00
Ni	0.00	0.00	0.00	0.00	0.00	0.00	0.00	0.00
Total	4.00	4.04	4.06	4.00	3.99	3.99	4.01	4.00
Mg#	82.49	74.03	77.23	80.86	82.15	82.17	78.68	83.22
$D^{(cpx\text{-}melt)}_{H_2O}$	0.0086	0.0364	0.0196	0.0094	0.0096	0.0092	0.0086	0.0085
Absorbance of cpx (cm^{-1})	2.50	2.30	3.00	1.60	1.90	1.90	4.00	2.10
Thickness of cpx (0.001mm)	64	70	67	58	58	58	65	65
Absorbance normalized to 1 cm (cm^{-1})	391	329	448	276	328	328	615	323
H_2O-cpx (ppm)	165	139	189	117	139	139	260	137
H_2O-melt (wt%)	1.92	0.38	0.97	1.25	1.45	1.51	3.02	1.62

Sample No.					XL-11		
Section No.					2		
Point No.	15	16	17	18	1	2	3
SiO_2	51.92	50.31	48.80	51.99	52.53	51.91	49.85
TiO_2	1.40	1.62	2.43	1.47	1.20	1.42	1.72
Al_2O3	1.61	3.45	4.38	1.98	1.34	1.88	3.51
Cr_2O3	0.07	0.02	0.06	0.00	0.00	0.03	0.02
FeO	5.74	5.80	6.95	5.70	5.57	6.20	6.88
MnO	0.08	0.06	0.07	0.08	0.10	0.13	0.06
MgO	14.27	13.84	12.86	14.24	14.51	14.21	13.20
CaO	23.63	23.48	23.83	24.01	24.04	24.09	24.22
Na_2O	0.51	0.55	0.53	0.61	0.69	0.50	0.48
K_2O	0.02	0.01	0.00	0.04	0.01	0.01	0.01
NiO	0.00	0.00	0.02	0.00	0.00	0.02	0.00
Total	99.25	99.15	99.95	100.11	99.99	100.38	99.94
Si	1.94	1.88	1.83	1.92	1.95	1.92	1.86
Ti	0.04	0.05	0.07	0.04	0.03	0.04	0.05
Al	0.07	0.15	0.19	0.09	0.06	0.08	0.15
Cr	0.00	0.00	0.00	0.00	0.00	0.00	0.00
Fe	0.18	0.18	0.22	0.18	0.17	0.19	0.22
Mn	0.00	0.00	0.00	0.00	0.00	0.00	0.00
Mg	0.79	0.77	0.72	0.79	0.80	0.78	0.74
Ca	0.94	0.94	0.96	0.95	0.95	0.96	0.97
Na	0.04	0.04	0.04	0.04	0.05	0.04	0.03
K	0.00	0.00	0.00	0.00	0.00	0.00	0.00
Ni	0.00	0.00	0.00	0.00	0.00	0.00	0.00
Total	4.01	4.02	4.03	4.01	4.02	4.02	4.03
Mg#	81.59	80.98	76.75	81.66	82.27	80.35	77.39
$D^{(cpx\text{-}melt)}_{H_2O}$	0.0088	0.0126	0.0177	0.0095	0.0083	0.0096	0.0137
Absorbance of cpx (cm^{-1})	2.10	4.60	4.10	3.20	1.72	3.40	3.80
Thickness of cpx (0.001mm)	72	69	69	69	57	56	60
Absorbance normalized to 1 cm (cm^{-1})	292	667	594	464	302	607	633
H_2O-cpx (ppm)	123	282	251	196	128	257	268
H_2O-melt (wt%)	1.40	2.24	1.42	2.08	1.55	2.67	1.95

Sample No. Section No. Point No.	4	5	6	7	7.2	8	9	10
SiO_2	49.60	48.03	51.14	51.37	49.57	52.27	51.64	52.24
TiO_2	2.18	2.45	1.96	1.56	1.68	1.45	1.60	1.34
Al_2O3	3.93	4.59	2.80	2.26	4.67	2.11	2.29	1.63
Cr_2O3	0.05	0.00	0.03	0.02	0.56	0.04	0.06	0.00
FeO	6.91	7.32	6.02	5.82	5.70	5.60	5.67	6.34
MnO	0.06	0.11	0.06	0.10	0.09	0.06	0.08	0.06
MgO	13.19	12.80	13.85	14.40	13.23	14.17	14.32	14.05
CaO	24.21	24.05	23.82	24.12	23.82	23.92	24.27	24.10
Na_2O	0.43	0.35	0.63	0.52	0.63	0.73	0.54	0.45
K_2O	0.01	0.01	0.02	0.02	0.00	0.01	0.00	0.01
NiO	0.00	0.02	0.03	0.00	0.04	0.05	0.01	0.00
Total	100.57	99.72	100.37	100.17	99.98	100.42	100.48	100.22
Si	1.84	1.81	1.89	1.90	1.84	1.93	1.91	1.94
Ti	0.06	0.07	0.05	0.04	0.05	0.04	0.04	0.04
Al	0.17	0.20	0.12	0.10	0.20	0.09	0.10	0.07
Cr	0.00	0.00	0.00	0.00	0.02	0.00	0.00	0.00
Fe	0.21	0.23	0.19	0.18	0.18	0.17	0.18	0.20
Mn	0.00	0.00	0.00	0.00	0.00	0.00	0.00	0.00
Mg	0.73	0.72	0.76	0.80	0.73	0.78	0.79	0.78
Ca	0.96	0.97	0.94	0.96	0.95	0.94	0.96	0.96
Na	0.03	0.03	0.05	0.04	0.05	0.05	0.04	0.03
K	0.00	0.00	0.00	0.00	0.00	0.00	0.00	0.00
Ni	0.00	0.00	0.00	0.00	0.00	0.00	0.00	0.00
Total	4.02	4.03	4.01	4.02	4.02	4.01	4.02	4.01
Mg#	77.28	75.72	80.40	81.53	80.53	81.85	81.83	79.80
$D^{(cpx\text{-}melt)}_{H_2O}$	0.0157	0.0196	0.0117	0.0107	0.0160	0.0094	0.0105	0.0088
Absorbance of cpx (cm^{-1})	2.90	3.20	1.70	3.30	5.30	2.60	3.60	3.00
Thickness of cpx (0.001mm)	60	57	60	67	67	63	63	58
Absorbance normalized to 1 cm (cm^{-1})	483	561	283	493	791	413	571	517
H_2O-cpx (ppm)	205	238	120	208	335	175	242	219
H_2O-melt (wt%)	1.30	1.21	1.02	1.94	2.09	1.86	2.30	2.50

Sample No.								
Section No.								
Point No.	11	12	13	14	15	16	17	18
SiO_2	49.91	49.88	48.15	49.65	48.83	46.43	49.51	49.25
TiO_2	2.22	2.08	2.65	2.04	2.41	2.75	2.32	1.86
Al_2O3	4.00	3.59	4.28	3.87	4.66	6.32	4.17	3.72
Cr_2O3	0.09	0.00	0.05	0.05	0.17	0.09	0.18	0.13
FeO	6.45	6.22	6.96	6.15	6.50	7.25	6.23	6.63
MnO	0.09	0.08	0.12	0.07	0.05	0.04	0.03	0.03
MgO	13.23	13.42	13.01	13.50	12.79	11.15	13.09	13.58
CaO	23.78	24.46	24.10	23.52	24.00	23.83	24.05	23.99
Na_2O	0.54	0.45	0.47	0.47	0.40	0.52	0.60	0.51
K_2O	0.00	0.00	0.00	0.02	0.00	0.00	0.00	0.00
NiO	0.06	0.00	0.00	0.01	0.05	0.02	0.05	0.05
Total	100.36	100.18	99.78	99.34	99.85	98.37	100.23	99.74
Si	1.85	1.86	1.81	1.86	1.83	1.77	1.84	1.85
Ti	0.06	0.06	0.07	0.06	0.07	0.08	0.06	0.05
Al	0.18	0.16	0.19	0.17	0.21	0.28	0.18	0.16
Cr	0.00	0.00	0.00	0.00	0.00	0.00	0.01	0.00
Fe	0.20	0.19	0.22	0.19	0.20	0.23	0.19	0.21
Mn	0.00	0.00	0.00	0.00	0.00	0.00	0.00	0.00
Mg	0.73	0.74	0.73	0.75	0.71	0.64	0.73	0.76
Ca	0.95	0.98	0.97	0.94	0.96	0.98	0.96	0.96
Na	0.04	0.03	0.03	0.03	0.03	0.04	0.04	0.04
K	0.00	0.00	0.00	0.00	0.00	0.00	0.00	0.00
Ni	0.00	0.00	0.00	0.00	0.00	0.00	0.00	0.00
Total	4.02	4.02	4.04	4.02	4.01	4.02	4.02	4.04
Mg#	78.52	79.36	76.93	79.64	77.82	73.29	78.94	78.49
$D^{(cpx\text{-}melt)}_{H_2O}$	0.0151	0.0143	0.0194	0.0146	0.0177	0.0245	0.0160	0.0156
Absorbance of cpx (cm^{-1})	4.20	4.80	5.60	2.60	5.30	4.00	4.20	5.90
Thickness of cpx (0.001mm)	58	63	73	75	75	79	73	67
Absorbance normalized to 1 cm (cm^{-1})	724	762	767	347	707	506	575	881
H_2O-cpx (ppm)	306	322	325	147	299	214	243	373
H_2O-melt (wt%)	2.03	2.25	1.68	1.00	1.69	0.87	1.52	2.39

Sample No.							
Section No.							
Point No.	19	20	21	22	27	28	29
SiO_2	49.71	51.88	46.17	48.76	50.36	51.13	47.92
TiO_2	2.11	1.67	3.40	2.27	2.04	1.86	2.60
Al_2O3	4.05	2.25	6.74	4.35	3.09	2.96	4.48
Cr_2O3	0.13	0.01	0.16	0.14	0.02	0.00	0.00
FeO	5.70	5.78	7.21	6.54	6.00	5.96	6.91
MnO	0.04	0.08	0.10	0.04	0.10	0.12	0.09
MgO	13.24	14.18	12.16	13.13	13.59	13.99	12.76
CaO	23.94	24.13	23.95	23.80	23.70	23.87	24.05
Na_2O	0.59	0.51	0.58	0.42	0.60	0.58	0.44
K_2O	0.00	0.02	0.01	0.00	0.01	0.01	0.00
NiO	0.00	0.00	0.00	0.04	0.00	0.03	0.04
Total	99.52	100.49	100.48	99.50	99.50	100.51	99.28
Si	1.86	1.91	1.73	1.83	1.88	1.89	1.81
Ti	0.06	0.05	0.10	0.06	0.06	0.05	0.07
Al	0.18	0.10	0.30	0.19	0.14	0.13	0.20
Cr	0.00	0.00	0.00	0.00	0.00	0.00	0.00
Fe	0.18	0.18	0.23	0.21	0.19	0.18	0.22
Mn	0.00	0.00	0.00	0.00	0.00	0.00	0.00
Mg	0.74	0.78	0.68	0.73	0.76	0.77	0.72
Ca	0.96	0.95	0.96	0.96	0.95	0.94	0.97
Na	0.04	0.04	0.04	0.03	0.04	0.04	0.03
K	0.00	0.00	0.00	0.00	0.00	0.00	0.00
Ni	0.00	0.00	0.00	0.00	0.00	0.00	0.00
Total	4.01	4.01	4.04	4.02	4.02	4.02	4.03
Mg#	80.55	81.40	75.04	78.15	80.17	80.73	76.70
$D^{(cpx\text{-}melt)}_{H_2O}$	0.0147	0.0101	0.0329	0.0173	0.0126	0.0120	0.0193
Absorbance of cpx (cm^{-1})	4.30	5.00	7.30	4.60	4.10	4.40	4.00
Thickness of cpx (0.001mm)	75	75	75	72	65	65	71
Absorbance normalized to 1 cm (cm^{-1})	573	667	973	639	631	677	563
H_2O-cpx (ppm)	243	282	412	270	267	286	238
H_2O-melt (wt%)	1.66	2.79	1.25	1.56	2.12	2.39	1.23

Sample No.	XL-12							
Section No.	1							
Point No.	1	2	3	4	5.1	5.2	5.3	5.4
SiO_2	47.73	51.39	50.42	50.70	51.51	49.61	48.52	50.81
TiO_2	2.60	1.70	1.92	2.07	1.75	2.31	2.28	1.70
Al_2O3	5.90	2.44	2.76	3.29	2.11	4.13	4.12	2.91
Cr_2O3	0.18	0.04	0.04	0.05	0.03	0.03	0.08	0.02
FeO	6.74	5.78	5.62	5.86	5.49	6.14	6.33	5.63
MnO	0.03	0.06	0.11	0.05	0.08	0.07	0.07	0.10
MgO	12.37	14.34	13.96	13.63	14.28	12.78	13.37	13.95
CaO	23.28	23.35	22.97	22.84	23.58	23.37	23.67	23.43
Na_2O	0.59	0.72	0.68	0.64	0.66	0.60	0.44	0.63
K_2O	0.01	0.03	0.01	0.02	0.01	0.00	0.00	0.00
NiO	0.00	0.01	0.04	0.07	0.06	0.03	0.00	0.00
Total	99.42	99.85	98.52	99.20	99.55	99.07	98.89	99.17
Si	1.79	1.91	1.90	1.89	1.92	1.86	1.83	1.90
Ti	0.07	0.05	0.05	0.06	0.05	0.07	0.06	0.05
Al	0.26	0.11	0.12	0.14	0.09	0.18	0.18	0.13
Cr	0.01	0.00	0.00	0.00	0.00	0.00	0.00	0.00
Fe	0.21	0.18	0.18	0.18	0.17	0.19	0.20	0.18
Mn	0.00	0.00	0.00	0.00	0.00	0.00	0.00	0.00
Mg	0.69	0.79	0.78	0.76	0.79	0.71	0.75	0.78
Ca	0.94	0.93	0.93	0.91	0.94	0.94	0.96	0.94
Na	0.04	0.05	0.05	0.05	0.05	0.04	0.03	0.05
K	0.00	0.00	0.00	0.00	0.00	0.00	0.00	0.00
Ni	0.00	0.00	0.00	0.00	0.00	0.00	0.00	0.00
Total	4.02	4.02	4.01	4.00	4.01	4.00	4.03	4.01
Mg#	76.59	81.56	81.57	80.58	82.27	78.76	79.00	81.54
$D^{(cpx\text{-}melt)}_{H_2O}$	0.0224	0.0108	0.0117	0.0122	0.0101	0.0144	0.0172	0.0114
Absorbance of cpx (cm^{-1})	2.28	3.11	3.14	3.00	3.20	4.00	4.20	4.40
Thickness of cpx (0.001mm)	46	44	46	50	50	50	50	50
Absorbance normalized to 1 cm (cm^{-1})	496	707	683	600	640	800	840	880
H_2O-cpx (ppm)	210	299	289	254	271	339	355	372
H_2O-melt (wt%)	0.94	2.76	2.47	2.09	2.68	2.35	2.07	3.26

Sample No. Section No. Point No.	6	7	7.2	8	9	10	11	12
SiO_2	51.18	51.67	51.29	51.43	51.13	47.34	52.00	50.09
TiO_2	1.88	1.70	1.68	1.71	1.79	3.03	1.72	2.34
Al_2O3	2.10	2.48	2.56	2.52	2.67	6.43	2.54	3.20
Cr_2O3	0.00	0.00	0.03	0.03	0.03	0.00	0.04	0.03
FeO	6.07	5.59	5.74	5.71	5.41	7.24	5.38	6.52
MnO	0.04	0.06	0.06	0.03	0.05	0.06	0.08	0.08
MgO	14.13	14.16	14.10	14.31	14.23	11.90	14.09	13.29
CaO	23.31	23.58	23.74	23.72	23.03	23.45	23.91	22.73
Na_2O	0.59	0.60	0.58	0.53	0.61	0.60	0.61	0.84
K_2O	0.00	0.00	0.00	0.02	0.01	0.01	0.01	0.07
NiO	0.00	0.03	0.01	0.06	0.07	0.00	0.01	0.00
Total	99.29	99.86	99.80	100.07	99.02	100.04	100.38	99.18
Si	1.91	1.91	1.90	1.90	1.91	1.77	1.92	1.88
Ti	0.05	0.05	0.05	0.05	0.05	0.09	0.05	0.07
Al	0.09	0.11	0.11	0.11	0.12	0.28	0.11	0.14
Cr	0.00	0.00	0.00	0.00	0.00	0.00	0.00	0.00
Fe	0.19	0.17	0.18	0.18	0.17	0.23	0.17	0.20
Mn	0.00	0.00	0.00	0.00	0.00	0.00	0.00	0.00
Mg	0.79	0.78	0.78	0.79	0.79	0.66	0.77	0.74
Ca	0.93	0.94	0.94	0.94	0.92	0.94	0.94	0.91
Na	0.04	0.04	0.04	0.04	0.04	0.04	0.04	0.06
K	0.00	0.00	0.00	0.00	0.00	0.00	0.00	0.00
Ni	0.00	0.00	0.00	0.00	0.00	0.00	0.00	0.00
Total	4.01	4.01	4.01	4.01	4.00	4.02	4.00	4.02
Mg#	80.58	81.88	81.43	81.71	82.42	74.57	82.38	78.42
$D^{(cpx\text{-}melt)}_{H_2O}$	0.0105	0.0103	0.0108	0.0109	0.0109	0.0255	0.0101	0.0132
Absorbance of cpx (cm^{-1})	2.12	2.88	3.15	2.14	3.85	3.50	4.20	3.20
Thickness of cpx (0.001mm)	56	55	55	58	57	57	54	57
Absorbance normalized to 1 cm (cm^{-1})	379	524	573	369	675	614	778	561
H_2O-cpx (ppm)	160	222	242	156	286	260	329	238
H_2O-melt (wt%)	1.53	2.15	2.24	1.43	2.63	1.02	3.25	1.80

Sample No. Section No. Point No.	13	14	15	16	17	18	19	19.2
SiO_2	47.99	48.10	51.91	49.10	47.95	46.53	50.74	48.07
TiO_2	2.44	2.70	1.64	2.03	2.76	3.25	1.65	2.76
Al_2O3	5.20	4.78	2.46	4.10	4.30	6.21	2.46	4.73
Cr_2O3	0.07	0.00	0.00	0.20	0.00	0.03	0.01	0.00
FeO	6.78	7.12	5.34	6.14	6.49	7.20	5.45	6.52
MnO	0.10	0.08	0.07	0.11	0.07	0.08	0.02	0.10
MgO	12.49	12.55	13.93	13.62	13.11	11.96	14.08	12.90
CaO	23.51	23.33	23.45	23.35	23.57	23.61	23.48	23.53
Na_2O	0.44	0.48	0.59	0.32	0.45	0.50	0.57	0.47
K_2O	0.00	0.00	0.00	0.00	0.00	0.00	0.01	0.01
NiO	0.00	0.00	0.07	0.06	0.00	0.03	0.03	0.04
Total	99.04	99.13	99.46	99.01	98.71	99.40	98.50	99.11
Si	1.81	1.82	1.93	1.85	1.82	1.76	1.91	1.81
Ti	0.07	0.08	0.05	0.06	0.08	0.09	0.05	0.08
Al	0.23	0.21	0.11	0.18	0.19	0.28	0.11	0.21
Cr	0.00	0.00	0.00	0.01	0.00	0.00	0.00	0.00
Fe	0.21	0.22	0.17	0.19	0.21	0.23	0.17	0.21
Mn	0.00	0.00	0.00	0.00	0.00	0.00	0.00	0.00
Mg	0.70	0.71	0.77	0.76	0.74	0.67	0.79	0.73
Ca	0.95	0.94	0.93	0.94	0.96	0.96	0.95	0.95
Na	0.03	0.04	0.04	0.02	0.03	0.04	0.04	0.03
K	0.00	0.00	0.00	0.00	0.00	0.00	0.00	0.00
Ni	0.00	0.00	0.00	0.00	0.00	0.00	0.00	0.00
Total	4.02	4.02	3.99	4.02	4.03	4.03	4.01	4.02
Mg#	76.66	75.86	82.29	79.82	78.28	74.76	82.16	77.92
$D^{(cpx\text{-}melt)}_{H_2O}$	0.0197	0.0193	0.0095	0.0160	0.0190	0.0275	0.0107	0.0196
Absorbance of cpx (cm^{-1})	5.80	4.14	2.40	4.30	4.80	5.00	2.20	2.86
Thickness of cpx (0.001mm)	61	61	56	61	65	65	56	56
Absorbance normalized to 1 cm (cm^{-1})	951	679	429	705	738	770	393	511
H_2O-cpx (ppm)	402	287	181	298	312	326	166	216
H_2O-melt (wt%)	2.04	1.49	1.91	1.87	1.65	1.18	1.56	1.10

Sample No. Section No. Point No.	20	21	22	23	24	25	26	27
SiO_2	48.45	50.62	51.54	51.26	51.05	45.96	49.06	51.09
TiO_2	2.28	2.25	1.63	1.53	1.90	3.23	2.09	1.92
Al_2O3	4.02	3.07	2.16	2.04	2.41	6.41	3.40	2.81
Cr_2O3	0.02	0.03	0.05	0.01	0.05	0.09	0.09	0.08
FeO	6.76	6.01	5.51	6.04	5.82	7.26	6.28	5.63
MnO	0.05	0.08	0.10	0.12	0.07	0.05	0.10	0.12
MgO	13.06	13.65	14.28	14.04	14.17	11.91	13.58	13.58
CaO	23.87	23.31	23.75	24.10	23.61	23.26	23.53	23.42
Na_2O	0.44	0.62	0.57	0.59	0.45	0.49	0.56	0.63
K_2O	0.02	0.03	0.00	0.01	0.01	0.00	0.00	0.00
NiO	0.00	0.04	0.02	0.03	0.00	0.04	0.01	0.05
Total	98.96	99.71	99.61	99.77	99.51	98.69	98.70	99.33
Si	1.83	1.88	1.92	1.91	1.90	1.75	1.85	1.90
Ti	0.06	0.06	0.05	0.04	0.05	0.09	0.06	0.05
Al	0.18	0.13	0.09	0.09	0.11	0.29	0.15	0.12
Cr	0.00	0.00	0.00	0.00	0.00	0.00	0.00	0.00
Fe	0.21	0.19	0.17	0.19	0.18	0.23	0.20	0.18
Mn	0.00	0.00	0.00	0.00	0.00	0.00	0.00	0.00
Mg	0.74	0.76	0.79	0.78	0.79	0.68	0.77	0.75
Ca	0.97	0.93	0.95	0.96	0.94	0.95	0.95	0.94
Na	0.03	0.05	0.04	0.04	0.03	0.04	0.04	0.05
K	0.00	0.00	0.00	0.00	0.00	0.00	0.00	0.00
Ni	0.00	0.00	0.00	0.00	0.00	0.00	0.00	0.00
Total	4.03	4.01	4.01	4.02	4.01	4.03	4.03	4.00
Mg#	77.50	80.20	82.22	80.56	81.27	74.51	79.41	81.12
$D^{(cpx\text{-}melt)}_{H_2O}$	0.0169	0.0125	0.0101	0.0102	0.0110	0.0293	0.0149	0.0109
Absorbance of cpx (cm^{-1})	4.60	3.50	3.50	4.00	3.18	3.80	4.70	3.80
Thickness of cpx (0.001mm)	65	69	64	64	64	63	68	68
Absorbance normalized to 1 cm (cm^{-1})	708	507	547	625	497	603	691	559
H_2O-cpx (ppm)	299	215	231	264	210	255	292	236
H_2O-melt (wt%)	1.77	1.71	2.30	2.59	1.90	0.87	1.96	2.16

Sample No. Section No. Point No.	28	28.2	29	30	31	33	33.2	34
SiO_2	47.68	50.38	48.55	50.72	49.08	51.39	47.46	48.25
TiO_2	2.38	1.10	2.26	1.65	2.68	1.82	2.81	2.67
Al_2O3	4.95	5.29	4.03	2.77	4.62	2.57	6.10	5.32
Cr_2O3	0.09	0.86	0.18	0.02	0.02	0.01	0.13	0.33
FeO	6.65	5.04	6.19	6.02	7.00	5.73	6.87	6.36
MnO	0.08	0.06	0.04	0.10	0.05	0.06	0.09	0.09
MgO	12.97	13.96	13.53	14.08	12.99	14.13	12.45	12.90
CaO	23.36	22.52	23.41	23.75	23.69	23.49	23.66	23.46
Na_2O	0.59	1.01	0.50	0.47	0.34	0.60	0.58	0.46
K_2O	0.00	0.01	0.00	0.00	0.00	0.00	0.01	0.01
NiO	0.01	0.06	0.02	0.00	0.03	0.00	0.00	0.02
Total	98.75	100.28	98.70	99.58	100.49	99.81	100.15	99.87
Si	1.81	1.85	1.83	1.89	1.83	1.91	1.78	1.80
Ti	0.07	0.03	0.06	0.05	0.07	0.05	0.08	0.08
Al	0.22	0.23	0.18	0.12	0.20	0.11	0.27	0.23
Cr	0.00	0.02	0.01	0.00	0.00	0.00	0.00	0.01
Fe	0.21	0.16	0.20	0.19	0.22	0.18	0.21	0.20
Mn	0.00	0.00	0.00	0.00	0.00	0.00	0.00	0.00
Mg	0.73	0.77	0.76	0.78	0.72	0.78	0.69	0.72
Ca	0.95	0.89	0.95	0.95	0.94	0.93	0.95	0.94
Na	0.04	0.07	0.04	0.03	0.02	0.04	0.04	0.03
K	0.00	0.00	0.00	0.00	0.00	0.00	0.00	0.00
Ni	0.00	0.00	0.00	0.00	0.00	0.00	0.00	0.00
Total	4.04	4.02	4.03	4.02	4.01	4.01	4.03	4.02
Mg#	77.66	83.17	79.58	80.65	76.79	81.47	76.36	78.34
$D^{(cpx\text{-}melt)}_{H_2O}$	0.0204	0.0159	0.0171	0.0117	0.0182	0.0108	0.0250	0.0211
Absorbance of cpx (cm^{-1})	4.25	3.70	3.40	4.40	4.85	3.55	2.85	3.04
Thickness of cpx (0.001mm)	65	65	52	57	58	55	55	51
Absorbance normalized to 1 cm (cm^{-1})	654	569	654	772	836	645	518	596
H_2O-cpx (ppm)	277	241	277	327	354	273	219	252
H_2O-melt (wt%)	1.35	1.51	1.62	2.79	1.94	2.52	0.88	1.20

Sample No.						XL-13	
Section No.						2	
Point No.	35	36	37	38	38.2	1	2
SiO_2	49.67	50.95	50.82	51.61	48.79	50.46	47.64
TiO_2	1.82	1.29	1.90	1.75	2.43	1.69	2.39
Al_2O3	3.73	4.77	2.93	2.71	3.85	3.23	4.72
Cr_2O3	0.11	0.81	0.02	0.03	0.00	0.04	0.02
FeO	5.88	5.01	5.95	5.71	6.54	6.12	7.17
MnO	0.09	0.10	0.13	0.10	0.06	0.09	0.05
MgO	13.80	14.05	13.83	14.08	13.47	13.83	12.54
CaO	23.17	22.35	23.47	23.63	23.68	24.28	23.76
Na_2O	0.53	0.80	0.59	0.57	0.50	0.53	0.43
K_2O	0.00	0.00	0.01	0.00	0.02	0.00	0.00
NiO	0.02	0.06	0.00	0.05	0.00	0.01	0.00
Total	98.82	100.19	99.64	100.23	99.34	100.28	98.72
Si	1.87	1.87	1.89	1.91	1.84	1.87	1.81
Ti	0.05	0.04	0.05	0.05	0.07	0.05	0.07
Al	0.17	0.21	0.13	0.12	0.17	0.14	0.21
Cr	0.00	0.02	0.00	0.00	0.00	0.00	0.00
Fe	0.18	0.15	0.19	0.18	0.21	0.19	0.23
Mn	0.00	0.00	0.00	0.00	0.00	0.00	0.00
Mg	0.77	0.77	0.77	0.78	0.76	0.77	0.71
Ca	0.93	0.88	0.94	0.94	0.95	0.97	0.97
Na	0.04	0.06	0.04	0.04	0.04	0.04	0.03
K	0.00	0.00	0.00	0.00	0.00	0.00	0.00
Ni	0.00	0.00	0.00	0.00	0.00	0.00	0.00
Total	4.02	4.00	4.01	4.01	4.03	4.03	4.03
Mg#	80.71	83.32	80.56	81.47	78.61	80.10	75.72
$D^{(cpx\text{-}melt)}_{H_2O}$	0.0141	0.0142	0.0118	0.0108	0.0169	0.0129	0.0195
Absorbance of cpx (cm^{-1})	5.66	3.97	4.55	2.80	3.25	3.70	2.10
Thickness of cpx (0.001mm)	61	64	71	64	64	50	49
Absorbance normalized to 1 cm (cm^{-1})	928	620	641	438	508	740	429
H_2O-cpx (ppm)	393	262	271	185	215	313	181
H_2O-melt (wt%)	2.78	1.85	2.29	1.71	1.27	2.42	0.93

Sample No.								
Section No.								
Point No.	2.1	3	4	5	6	6.2	7	8
SiO_2	47.13	49.74	51.36	48.78	47.59	50.82	48.32	49.72
TiO_2	2.46	1.93	1.79	2.42	2.59	1.73	2.32	2.04
Al_2O3	5.44	3.69	2.37	4.00	5.40	2.57	4.12	3.25
Cr_2O3	0.05	0.16	0.00	0.00	0.18	0.00	0.04	0.03
FeO	7.04	6.21	5.65	6.63	6.29	5.80	6.92	6.21
MnO	0.09	0.00	0.09	0.10	0.12	0.05	0.11	0.10
MgO	12.33	13.47	13.17	12.48	12.61	14.00	12.97	13.63
CaO	23.83	23.92	23.93	24.00	23.71	23.98	23.72	23.75
Na_2O	0.50	0.43	0.52	0.50	0.53	0.56	0.41	0.64
K_2O	0.00	0.01	0.02	0.01	0.00	0.00	0.00	0.00
NiO	0.02	0.02	0.03	0.00	0.00	0.00	0.02	0.00
Total	98.89	99.57	98.92	98.91	99.02	99.51	98.93	99.36
Si	1.79	1.86	1.92	1.84	1.80	1.90	1.83	1.87
Ti	0.07	0.05	0.05	0.07	0.07	0.05	0.07	0.06
Al	0.24	0.16	0.10	0.18	0.24	0.11	0.18	0.14
Cr	0.00	0.00	0.00	0.00	0.01	0.00	0.00	0.00
Fe	0.22	0.19	0.18	0.21	0.20	0.18	0.22	0.19
Mn	0.00	0.00	0.00	0.00	0.00	0.00	0.00	0.00
Mg	0.70	0.75	0.74	0.70	0.71	0.78	0.73	0.76
Ca	0.97	0.96	0.96	0.97	0.96	0.96	0.96	0.95
Na	0.04	0.03	0.04	0.04	0.04	0.04	0.03	0.05
K	0.00	0.00	0.00	0.00	0.00	0.00	0.00	0.00
Ni	0.00	0.00	0.00	0.00	0.00	0.00	0.00	0.00
Total	4.04	4.02	3.99	4.02	4.03	4.02	4.03	4.03
Mg#	75.75	79.45	80.61	77.04	78.14	81.15	76.97	79.66
$D^{(cpx\text{-}melt)}_{H_2O}$	0.0223	0.0143	0.0094	0.0156	0.0215	0.0113	0.0174	0.0139
Absorbance of cpx (cm^{-1})	2.40	4.00	3.10	3.20	4.30	3.50	2.40	3.80
Thickness of cpx (0.001mm)	49	38	49	53	55	55	46	54
Absorbance normalized to 1 cm (cm^{-1})	490	1053	633	604	782	636	522	704
H_2O-cpx (ppm)	207	445	268	255	331	269	221	298
H_2O-melt (wt%)	0.93	3.13	2.84	1.64	1.54	2.39	1.27	2.15

Sample No. Section No. Point No.	8.2	9	10	11	11.2	12	12.2	13
SiO_2	50.12	47.13	47.95	52.24	50.18	51.30	48.01	48.85
TiO_2	2.11	2.93	2.65	1.40	2.20	1.66	2.58	2.26
Al_2O3	2.99	4.92	4.74	1.15	3.27	2.51	4.39	4.32
Cr_2O3	0.07	0.04	0.05	0.01	0.07	0.01	0.05	0.02
FeO	5.88	7.20	6.83	6.65	6.24	5.60	6.57	6.80
MnO	0.08	0.09	0.06	0.12	0.00	0.10	0.06	0.10
MgO	13.67	12.63	12.72	13.95	13.38	13.97	12.86	13.18
CaO	23.71	23.73	24.02	22.73	23.74	24.06	23.75	23.92
Na_2O	0.61	0.51	0.52	0.93	0.62	0.55	0.46	0.51
K_2O	0.02	0.00	0.00	0.02	0.01	0.00	0.00	0.00
NiO	0.00	0.02	0.06	0.00	0.00	0.00	0.07	0.00
Total	99.25	99.19	99.60	99.19	99.71	99.74	98.82	99.95
Si	1.88	1.79	1.81	1.95	1.87	1.91	1.82	1.83
Ti	0.06	0.08	0.08	0.04	0.06	0.05	0.07	0.06
Al	0.13	0.22	0.21	0.05	0.14	0.11	0.20	0.19
Cr	0.00	0.00	0.00	0.00	0.00	0.00	0.00	0.00
Fe	0.18	0.23	0.22	0.21	0.19	0.17	0.21	0.21
Mn	0.00	0.00	0.00	0.00	0.00	0.00	0.00	0.00
Mg	0.76	0.71	0.71	0.78	0.74	0.77	0.73	0.74
Ca	0.95	0.96	0.97	0.91	0.95	0.96	0.96	0.96
Na	0.04	0.04	0.04	0.07	0.04	0.04	0.03	0.04
K	0.00	0.00	0.00	0.00	0.00	0.00	0.00	0.00
Ni	0.00	0.00	0.00	0.00	0.00	0.00	0.00	0.00
Total	4.02	4.04	4.03	4.01	4.01	4.01	4.03	4.03
Mg#	80.56	75.78	76.86	78.89	79.28	81.64	77.73	77.57
$D^{(cpx\text{-}melt)}_{H_2O}$	0.0128	0.0229	0.0201	0.0081	0.0132	0.0106	0.0186	0.0175
Absorbance of cpx (cm^{-1})	3.30	2.90	3.80	2.60	3.90	1.60	2.60	1.90
Thickness of cpx (0.001mm)	54	55	59	60	60	49	49	49
Absorbance normalized to 1 cm (cm^{-1})	611	527	644	433	650	327	531	388
H_2O-cpx (ppm)	259	223	273	183	275	138	225	164
H_2O-melt (wt%)	2.02	0.97	1.35	2.27	2.08	1.31	1.21	0.94

Sample No. Section No. Point No.	14	14.2	15	16	17	18	19	20
SiO_2	49.22	50.23	48.03	49.77	51.33	52.01	48.92	46.62
TiO_2	2.06	1.76	2.51	1.98	1.64	1.51	2.36	3.16
Al_2O3	3.62	2.75	5.75	3.96	2.46	2.15	4.07	6.60
Cr_2O3	0.03	0.02	0.22	0.12	0.02	0.03	0.02	0.02
FeO	6.54	5.84	6.50	6.23	5.84	5.96	6.73	6.76
MnO	0.05	0.07	0.06	0.04	0.06	0.06	0.09	0.06
MgO	13.44	13.99	12.64	13.42	13.15	14.36	13.08	12.09
CaO	24.08	23.74	23.88	23.63	24.07	24.11	23.98	23.57
Na_2O	0.38	0.63	0.50	0.51	0.48	0.58	0.43	0.58
K_2O	0.00	0.00	0.00	0.01	0.00	0.00	0.00	0.00
NiO	0.00	0.02	0.03	0.00	0.00	0.07	0.01	0.01
Total	99.40	99.04	100.11	99.67	99.06	100.83	99.70	99.46
Si	1.85	1.89	1.79	1.86	1.92	1.91	1.84	1.76
Ti	0.06	0.05	0.07	0.06	0.05	0.04	0.07	0.09
Al	0.16	0.12	0.25	0.17	0.11	0.09	0.18	0.29
Cr	0.00	0.00	0.01	0.00	0.00	0.00	0.00	0.00
Fe	0.21	0.18	0.20	0.19	0.18	0.18	0.21	0.21
Mn	0.00	0.00	0.00	0.00	0.00	0.00	0.00	0.00
Mg	0.75	0.78	0.70	0.75	0.73	0.79	0.73	0.68
Ca	0.97	0.95	0.96	0.95	0.97	0.95	0.96	0.95
Na	0.03	0.05	0.04	0.04	0.03	0.04	0.03	0.04
K	0.00	0.00	0.00	0.00	0.00	0.00	0.00	0.00
Ni	0.00	0.00	0.00	0.00	0.00	0.00	0.00	0.00
Total	4.03	4.03	4.02	4.02	4.00	4.02	4.02	4.03
Mg#	78.55	81.04	77.62	79.35	80.05	81.12	77.62	76.14
$D^{(cpx\text{-}melt)}_{H_2O}$	0.0151	0.0122	0.0221	0.0147	0.0095	0.0101	0.0167	0.0281
Absorbance of cpx (cm^{-1})	3.30	3.30	2.82	3.20	2.50	3.70	3.07	3.70
Thickness of cpx (0.001mm)	60	60	61	60	61	61	61	61
Absorbance normalized to 1 cm (cm^{-1})	550	550	462	533	410	607	503	607
H_2O-cpx (ppm)	233	233	196	226	173	257	213	257
H_2O-melt (wt%)	1.54	1.91	0.89	1.54	1.82	2.54	1.28	0.91

Sample No. Section No. Point No.	21	22	23	24	25	26	27	27.2
SiO_2	50.04	51.73	48.04	48.73	51.18	51.41	50.17	51.66
TiO_2	1.61	1.61	2.76	2.57	1.95	1.70	1.99	1.69
Al_2O3	4.61	2.48	4.61	4.45	2.96	2.47	3.10	2.55
Cr_2O3	0.71	0.02	0.01	0.00	0.03	0.04	0.05	0.00
FeO	5.46	5.57	6.45	6.74	5.82	5.75	5.86	5.72
MnO	0.08	0.07	0.08	0.08	0.09	0.08	0.07	0.06
MgO	13.55	14.13	12.95	12.96	13.85	14.20	13.15	13.58
CaO	23.86	24.15	24.01	24.14	24.03	24.06	23.83	23.84
Na_2O	0.52	0.48	0.62	0.54	0.59	0.59	0.64	0.62
K_2O	0.01	0.02	0.01	0.01	0.01	0.01	0.00	0.00
NiO	0.01	0.02	0.00	0.05	0.00	0.00	0.04	0.00
Total	100.45	100.28	99.53	100.26	100.52	100.31	98.89	99.72
Si	1.85	1.91	1.81	1.82	1.89	1.90	1.89	1.92
Ti	0.04	0.04	0.08	0.07	0.05	0.05	0.06	0.05
Al	0.20	0.11	0.20	0.20	0.13	0.11	0.14	0.11
Cr	0.02	0.00	0.00	0.00	0.00	0.00	0.00	0.00
Fe	0.17	0.17	0.20	0.21	0.18	0.18	0.18	0.18
Mn	0.00	0.00	0.00	0.00	0.00	0.00	0.00	0.00
Mg	0.75	0.78	0.73	0.72	0.76	0.78	0.74	0.75
Ca	0.94	0.96	0.97	0.97	0.95	0.95	0.96	0.95
Na	0.04	0.03	0.05	0.04	0.04	0.04	0.05	0.04
K	0.00	0.00	0.00	0.00	0.00	0.00	0.00	0.00
Ni	0.00	0.00	0.00	0.00	0.00	0.00	0.00	0.00
Total	4.01	4.01	4.03	4.03	4.01	4.02	4.01	4.00
Mg#	81.56	81.90	78.17	77.42	80.92	81.49	79.99	80.88
$D^{(cpx\text{-}melt)}_{H_2O}$	0.0156	0.0103	0.0199	0.0184	0.0118	0.0109	0.0120	0.0099
Absorbance of cpx (cm^{-1})	3.60	2.10	2.90	3.20	3.50	2.40	2.20	2.70
Thickness of cpx (0.001mm)	53	61	53	63	61	60	50	50
Absorbance normalized to 1 cm (cm^{-1})	679	344	547	508	574	400	440	540
H_2O-cpx (ppm)	287	146	232	215	243	169	186	228
H_2O-melt (wt%)	1.84	1.41	1.16	1.17	2.05	1.55	1.55	2.31

Sample No.								
Section No.								
Point No.	28	29	30	31	32	33	34	35
SiO_2	51.19	48.99	48.74	49.13	49.01	48.79	50.25	48.56
TiO_2	1.70	2.41	2.69	2.12	2.44	2.46	2.13	2.52
Al_2O3	2.53	3.84	4.24	4.93	4.04	3.87	3.16	5.20
Cr_2O3	0.01	0.02	0.01	0.26	0.00	0.00	0.00	0.10
FeO	5.75	6.74	6.35	6.13	6.78	6.38	6.09	6.92
MnO	0.09	0.08	0.08	0.03	0.10	0.08	0.07	0.13
MgO	14.08	13.15	13.01	13.08	13.14	13.25	13.63	12.61
CaO	24.20	23.88	24.11	24.05	23.94	24.37	23.76	23.84
Na_2O	0.59	0.48	0.45	0.49	0.54	0.39	0.63	0.52
K_2O	0.01	0.01	0.01	0.00	0.01	0.00	0.00	0.01
NiO	0.00	0.01	0.00	0.04	0.01	0.01	0.06	0.00
Total	100.15	99.61	99.69	100.27	100.01	99.60	99.78	100.40
Si	1.90	1.84	1.83	1.83	1.83	1.83	1.87	1.81
Ti	0.05	0.07	0.08	0.06	0.07	0.07	0.06	0.07
Al	0.11	0.17	0.19	0.22	0.18	0.17	0.14	0.23
Cr	0.00	0.00	0.00	0.01	0.00	0.00	0.00	0.00
Fe	0.18	0.21	0.20	0.19	0.21	0.20	0.19	0.22
Mn	0.00	0.00	0.00	0.00	0.00	0.00	0.00	0.00
Mg	0.78	0.74	0.73	0.72	0.73	0.74	0.76	0.70
Ca	0.96	0.96	0.97	0.96	0.96	0.98	0.95	0.95
Na	0.04	0.04	0.03	0.04	0.04	0.03	0.05	0.04
K	0.00	0.00	0.00	0.00	0.00	0.00	0.00	0.00
Ni	0.00	0.00	0.00	0.00	0.00	0.00	0.00	0.00
Total	4.02	4.02	4.02	4.02	4.03	4.03	4.02	4.02
Mg#	81.36	77.67	78.52	79.17	77.56	78.74	79.97	76.47
$D^{(cpx\text{-}melt)}_{H_2O}$	0.0111	0.0163	0.0175	0.0178	0.0169	0.0167	0.0132	0.0199
Absorbance of cpx (cm^{-1})	2.40	1.80	2.70	2.20	1.90	2.20	2.20	1.90
Thickness of cpx (0.001mm)	53	50	44	41	44	47	50	44
Absorbance normalized to 1 cm (cm^{-1})	453	360	614	537	432	468	440	432
H_2O-cpx (ppm)	192	152	260	227	183	198	186	183
H_2O-melt (wt%)	1.73	0.93	1.48	1.28	1.08	1.18	1.41	0.92

Sample No.	GP-1							
Section No.	1							
Point No.	1	2	3	4	5	6	7	8
SiO_2	46.48	47.71	47.52	46.13	46.55	46.51	46.49	49.65
TiO_2	3.04	2.53	2.73	3.10	3.09	2.83	3.06	1.71
Al_2O3	6.45	5.25	5.97	6.18	6.14	5.96	6.15	3.77
Cr_2O3	0.26	0.04	0.01	0.16	0.07	0.07	0.10	0.02
FeO	7.78	7.51	7.84	7.99	7.87	7.47	7.61	7.39
MnO	0.05	0.12	0.09	0.09	0.10	0.05	0.08	0.13
MgO	11.96	12.35	12.20	12.15	12.23	12.11	11.79	12.39
CaO	21.96	22.41	22.48	22.37	22.37	22.12	22.58	22.56
Na_2O	0.32	0.39	0.50	0.50	0.48	0.46	0.49	0.58
K_2O	0.01	0.01	0.01	0.00	0.00	0.00	0.00	0.01
NiO	0.03	0.02	0.09	0.01	0.00	0.03	0.00	0.03
Total	98.35	98.34	99.43	98.68	98.90	97.61	98.35	98.23
Si	1.77	1.81	1.79	1.76	1.77	1.78	1.77	1.88
Ti	0.09	0.07	0.08	0.09	0.09	0.08	0.09	0.05
Al	0.29	0.24	0.27	0.28	0.27	0.27	0.28	0.17
Cr	0.01	0.00	0.00	0.00	0.00	0.00	0.00	0.00
Fe	0.25	0.24	0.25	0.25	0.25	0.24	0.24	0.23
Mn	0.00	0.00	0.00	0.00	0.00	0.00	0.00	0.00
Mg	0.68	0.70	0.69	0.69	0.69	0.69	0.67	0.70
Ca	0.90	0.91	0.91	0.91	0.91	0.91	0.92	0.92
Na	0.02	0.03	0.04	0.04	0.04	0.03	0.04	0.04
K	0.00	0.00	0.00	0.00	0.00	0.00	0.00	0.00
Ni	0.00	0.00	0.00	0.00	0.00	0.00	0.00	0.00
Total	4.01	4.01	4.02	4.03	4.02	4.02	4.02	4.00
Mg#	73.27	74.56	73.50	73.07	73.47	74.30	73.41	74.93
$D^{(cpx\text{-}melt)}_{H_2O}$	0.0271	0.0201	0.0235	0.0288	0.0274	0.0246	0.0259	0.0127
Absorbance of cpx (cm^{-1})	3.40	9.40	10.60	10.00	6.20	13.00	13.00	13.00
Thickness of cpx (0.001mm)	73	78	92	73	73	73	114	123
Absorbance normalized to 1 cm (cm^{-1})	466	1205	1152	1370	849	1781	1140	1057
H_2O-cpx (ppm)	197	510	488	580	359	754	483	447
H_2O-melt (wt%)	0.73	2.54	2.08	2.01	1.31	3.07	1.86	3.53

Sample No. Section No. Point No.	9	10	11	11.2	12	13	14	15
SiO_2	45.39	47.85	46.85	44.07	48.37	48.41	47.54	46.65
TiO_2	3.14	2.76	3.15	4.42	2.32	2.70	2.20	2.71
Al_2O3	6.76	5.22	5.82	7.72	4.36	4.90	5.01	6.25
Cr_2O3	0.00	0.03	0.15	0.07	0.02	0.06	0.37	0.02
FeO	9.08	8.01	7.06	8.06	7.41	7.68	6.33	7.63
MnO	0.11	0.11	0.08	0.09	0.08	0.10	0.05	0.06
MgO	11.16	12.22	12.26	10.97	12.43	11.96	13.44	12.10
CaO	21.79	22.34	22.82	22.58	22.53	22.20	22.61	22.23
Na_2O	0.58	0.45	0.46	0.41	0.57	0.66	0.48	0.47
K_2O	0.00	0.00	0.00	0.00	0.00	0.00	0.00	0.00
NiO	0.01	0.04	0.07	0.06	0.00	0.03	0.06	0.02
Total	98.04	99.03	98.73	98.46	98.08	98.69	98.08	98.13
Si	1.75	1.81	1.78	1.69	1.84	1.83	1.81	1.78
Ti	0.09	0.08	0.09	0.13	0.07	0.08	0.06	0.08
Al	0.31	0.23	0.26	0.35	0.20	0.22	0.22	0.28
Cr	0.00	0.00	0.00	0.00	0.00	0.00	0.01	0.00
Fe	0.29	0.25	0.22	0.26	0.24	0.24	0.20	0.24
Mn	0.00	0.00	0.00	0.00	0.00	0.00	0.00	0.00
Mg	0.64	0.69	0.69	0.63	0.71	0.68	0.76	0.69
Ca	0.90	0.91	0.93	0.93	0.92	0.90	0.92	0.91
Na	0.04	0.03	0.03	0.03	0.04	0.05	0.04	0.03
K	0.00	0.00	0.00	0.00	0.00	0.00	0.00	0.00
Ni	0.00	0.00	0.00	0.00	0.00	0.00	0.00	0.00
Total	4.03	4.01	4.02	4.02	4.01	4.00	4.03	4.02
Mg#	68.65	73.12	75.59	70.82	74.96	73.53	79.10	73.86
$D^{(cpx\text{-}melt)}_{H_2O}$	0.0312	0.0207	0.0251	0.0440	0.0165	0.0179	0.0208	0.0252
Absorbance of cpx (cm^{-1})	8.70	12.00	17.00	13.00	8.70	8.00	13.00	8.80
Thickness of cpx (0.001mm)	122	117	125	125	119	104	119	118
Absorbance normalized to 1 cm (cm^{-1})	713	1026	1360	1040	731	769	1092	746
H_2O-cpx (ppm)	302	434	575	440	309	325	462	316
H_2O-melt (wt%)	0.97	2.10	2.29	1.00	1.87	1.81	2.22	1.25

Sample No.								
Section No.								
Point No.	15.2	16	17	18	18.1	19	20	21
SiO_2	49.62	49.11	49.72	48.80	48.89	46.32	46.51	46.19
TiO_2	1.99	2.19	2.02	1.77	2.30	3.50	3.10	2.94
Al_2O3	3.62	3.94	3.89	4.75	4.23	6.64	6.35	6.34
Cr_2O3	0.08	0.07	0.16	0.10	0.01	0.04	0.02	0.11
FeO	7.40	7.94	6.75	6.35	7.70	7.22	7.63	7.48
MnO	0.11	0.13	0.09	0.08	0.12	0.12	0.09	0.04
MgO	13.12	12.87	13.66	13.86	12.71	11.83	11.97	12.08
CaO	22.59	22.22	22.60	22.01	22.24	22.80	22.33	22.61
Na_2O	0.28	0.31	0.34	0.50	0.42	0.51	0.48	0.47
K_2O	0.00	0.00	0.00	0.00	0.00	0.00	0.01	0.00
NiO	0.02	0.01	0.01	0.00	0.04	0.01	0.04	0.04
Total	98.83	98.78	99.24	98.22	98.66	98.96	98.51	98.29
Si	1.87	1.86	1.86	1.84	1.85	1.75	1.77	1.76
Ti	0.06	0.06	0.06	0.05	0.07	0.10	0.09	0.08
Al	0.16	0.18	0.17	0.21	0.19	0.30	0.28	0.29
Cr	0.00	0.00	0.00	0.00	0.00	0.00	0.00	0.00
Fe	0.23	0.25	0.21	0.20	0.24	0.23	0.24	0.24
Mn	0.00	0.00	0.00	0.00	0.00	0.00	0.00	0.00
Mg	0.74	0.73	0.76	0.78	0.72	0.67	0.68	0.69
Ca	0.91	0.90	0.91	0.89	0.90	0.93	0.91	0.92
Na	0.02	0.02	0.02	0.04	0.03	0.04	0.04	0.03
K	0.00	0.00	0.00	0.00	0.00	0.00	0.00	0.00
Ni	0.00	0.00	0.00	0.00	0.00	0.00	0.00	0.00
Total	4.00	4.00	4.00	4.02	4.00	4.02	4.02	4.02
Mg#	75.97	74.30	78.30	79.56	74.64	74.52	73.67	74.23
$D^{(cpx\text{-}melt)}_{H_2O}$	0.0138	0.0153	0.0148	0.0171	0.0160	0.0292	0.0269	0.0276
Absorbance of cpx (cm^{-1})	13.00	5.90	10.00	5.50	4.80	10.70	8.60	11.00
Thickness of cpx (0.001mm)	118	67	85	85	85	98	109	109
Absorbance normalized to 1 cm (cm^{-1})	1102	881	1176	647	565	1092	789	1009
H_2O-cpx (ppm)	466	373	498	274	239	462	334	427
H_2O-melt (wt%)	3.37	2.43	3.36	1.60	1.49	1.58	1.24	1.55

Sample No.								
Section No.	2							
Point No.	1	2	3	5	6	6.2	7	8
SiO_2	50.69	48.20	45.10	48.48	48.93	47.81	48.06	49.05
TiO_2	1.66	2.64	3.63	2.35	2.36	2.51	2.56	2.01
Al_2O3	3.11	5.08	7.32	4.95	4.26	5.71	5.05	4.09
Cr_2O3	0.17	0.02	0.00	0.06	0.11	0.29	0.04	0.06
FeO	7.00	7.24	8.16	7.15	7.42	7.46	7.29	7.53
MnO	0.10	0.13	0.06	0.13	0.12	0.11	0.11	0.08
MgO	13.57	12.36	11.13	12.67	12.73	12.61	12.46	13.11
CaO	22.36	22.34	22.26	22.36	21.92	21.94	22.43	22.00
Na_2O	0.30	0.46	0.53	0.47	0.32	0.44	0.41	0.32
K_2O	0.01	0.00	0.01	0.01	0.00	0.01	0.00	0.02
NiO	0.00	0.05	0.02	0.05	0.03	0.01	0.03	0.01
Total	98.98	98.51	98.22	98.69	98.20	98.89	98.46	98.26
Si	1.90	1.83	1.73	1.83	1.86	1.81	1.82	1.86
Ti	0.05	0.08	0.10	0.07	0.07	0.07	0.07	0.06
Al	0.14	0.23	0.33	0.22	0.19	0.25	0.23	0.18
Cr	0.01	0.00	0.00	0.00	0.00	0.01	0.00	0.00
Fe	0.22	0.23	0.26	0.23	0.24	0.24	0.23	0.24
Mn	0.00	0.00	0.00	0.00	0.00	0.00	0.00	0.00
Mg	0.76	0.70	0.64	0.71	0.72	0.71	0.70	0.74
Ca	0.90	0.91	0.91	0.91	0.89	0.89	0.91	0.89
Na	0.02	0.03	0.04	0.03	0.02	0.03	0.03	0.02
K	0.00	0.00	0.00	0.00	0.00	0.00	0.00	0.00
Ni	0.00	0.00	0.00	0.00	0.00	0.00	0.00	0.00
Total	3.99	4.00	4.02	4.01	3.99	4.01	4.01	4.00
Mg#	77.56	75.27	70.87	75.98	75.37	75.09	75.29	75.64
$D^{(cpx\text{-}melt)}_{H_2O}$	0.0116	0.0187	0.0348	0.0180	0.0157	0.0219	0.0190	0.0152
Absorbance of cpx (cm^{-1})	7.00	8.10	9.00	7.00	7.01	8.60	9.00	8.00
Thickness of cpx (0.001mm)	72	92	92	83	84	84	84	85
Absorbance normalized to 1 cm (cm^{-1})	972	880	978	843	835	1024	1071	941
H_2O-cpx (ppm)	411	373	414	357	353	433	453	398
H_2O-melt (wt%)	3.54	1.99	1.19	1.98	2.25	1.98	2.38	2.62

Sample No.					GP-2		
Section No.					1		
Point No.	9	10	10.2	11	1	2	3
SiO_2	48.62	49.71	49.81	46.25	49.35	50.05	48.30
TiO_2	2.51	1.86	1.89	2.97	2.04	1.75	2.49
Al_2O3	4.99	3.51	3.58	6.67	4.27	3.76	5.01
Cr_2O3	0.04	0.12	0.07	0.08	0.07	0.31	0.01
FeO	7.15	7.11	7.56	8.18	7.80	6.71	8.27
MnO	0.12	0.11	0.12	0.07	0.11	0.08	0.09
MgO	12.49	13.39	13.42	11.71	13.07	13.89	12.74
CaO	22.49	22.49	22.46	22.10	22.80	22.93	22.17
Na_2O	0.43	0.28	0.35	0.44	0.38	0.31	0.50
K_2O	0.00	0.01	0.00	0.00	0.01	0.01	0.00
NiO	0.01	0.02	0.01	0.02	0.00	0.00	0.02
Total	98.85	98.61	99.27	98.49	99.89	99.80	99.60
Si	1.83	1.88	1.87	1.76	1.85	1.87	1.82
Ti	0.07	0.05	0.05	0.09	0.06	0.05	0.07
Al	0.22	0.16	0.16	0.30	0.19	0.17	0.22
Cr	0.00	0.00	0.00	0.00	0.00	0.01	0.00
Fe	0.23	0.22	0.24	0.26	0.24	0.21	0.26
Mn	0.00	0.00	0.00	0.00	0.00	0.00	0.00
Mg	0.70	0.75	0.75	0.67	0.73	0.77	0.71
Ca	0.91	0.91	0.90	0.90	0.91	0.92	0.89
Na	0.03	0.02	0.03	0.03	0.03	0.02	0.04
K	0.00	0.00	0.00	0.00	0.00	0.00	0.00
Ni	0.00	0.00	0.00	0.00	0.00	0.00	0.00
Total	4.00	4.00	4.01	4.02	4.01	4.01	4.02
Mg#	75.70	77.05	76.00	71.84	74.91	78.68	73.31
$D^{(cpx\text{-}melt)}_{H_2O}$	0.0178	0.0135	0.0140	0.0282	0.0162	0.0144	0.0201
Absorbance of cpx (cm^{-1})	12.00	8.40	8.10	5.40	6.50	6.30	11.00
Thickness of cpx (0.001mm)	110	112	112	112	113	92	96
Absorbance normalized to 1 cm (cm^{-1})	1091	750	723	482	575	685	1146
H_2O-cpx (ppm)	462	317	306	204	243	290	485
H_2O-melt (wt%)	2.59	2.35	2.18	0.72	1.50	2.01	2.41

Sample No.								
Section No.								
Point No.	3.1	3.2	4	5	6	6.2	7	8
SiO_2	50.14	48.87	48.99	47.55	49.37	49.75	50.34	49.94
TiO_2	2.33	2.35	2.45	3.21	2.53	2.42	2.24	1.73
Al_2O3	4.03	4.70	4.49	5.12	3.95	3.85	3.85	3.92
Cr_2O3	0.00	0.03	0.01	0.37	0.00	0.03	0.05	0.00
FeO	7.31	7.87	7.86	8.50	7.37	7.65	7.78	7.83
MnO	0.10	0.10	0.11	0.07	0.10	0.10	0.09	0.09
MgO	13.14	12.81	11.93	12.54	13.29	13.29	12.95	13.08
CaO	22.77	22.66	22.78	21.22	22.95	22.88	22.92	22.90
Na_2O	0.42	0.46	0.45	0.36	0.33	0.38	0.45	0.53
K_2O	0.01	0.00	0.03	0.00	0.00	0.00	0.00	0.01
NiO	0.04	0.06	0.02	0.00	0.01	0.03	0.01	0.05
Total	100.30	99.89	99.11	98.94	99.89	100.38	100.67	100.07
Si	1.86	1.83	1.85	1.80	1.85	1.85	1.87	1.87
Ti	0.07	0.07	0.07	0.09	0.07	0.07	0.06	0.05
Al	0.18	0.21	0.20	0.23	0.17	0.17	0.17	0.17
Cr	0.00	0.00	0.00	0.01	0.00	0.00	0.00	0.00
Fe	0.23	0.25	0.25	0.27	0.23	0.24	0.24	0.24
Mn	0.00	0.00	0.00	0.00	0.00	0.00	0.00	0.00
Mg	0.73	0.72	0.67	0.71	0.74	0.74	0.72	0.73
Ca	0.91	0.91	0.92	0.86	0.92	0.91	0.91	0.92
Na	0.03	0.03	0.03	0.03	0.02	0.03	0.03	0.04
K	0.00	0.00	0.00	0.00	0.00	0.00	0.00	0.00
Ni	0.00	0.00	0.00	0.00	0.00	0.00	0.00	0.00
Total	4.00	4.02	4.00	4.00	4.01	4.01	4.00	4.02
Mg#	76.21	74.36	73.02	72.47	76.27	75.58	74.78	74.86
$D^{(cpx\text{-}melt)}_{H_2O}$	0.0148	0.0181	0.0159	0.0230	0.0163	0.0158	0.0143	0.0144
Absorbance of cpx (cm^{-1})	6.10	8.80	7.10	6.00	9.60	10.50	8.20	8.20
Thickness of cpx (0.001mm)	96	96	102	102	108	108	91	102
Absorbance normalized to 1 cm (cm^{-1})	635	917	696	588	889	972	901	804
H_2O-cpx (ppm)	269	388	295	249	376	411	381	340
H_2O-melt (wt%)	1.81	2.14	1.86	1.08	2.31	2.61	2.66	2.37

Sample No. Section No. Point No.	9	10	11	12	13	14	15	16
SiO_2	49.69	48.19	49.57	44.88	47.34	47.27	49.46	49.46
TiO_2	2.35	2.79	1.90	4.33	2.77	2.86	2.05	2.05
Al_2O3	4.59	6.11	4.04	7.81	5.87	6.04	4.09	4.09
Cr_2O3	0.09	0.25	0.15	0.02	0.05	0.04	0.11	0.11
FeO	7.09	7.78	7.00	8.25	7.83	7.43	7.32	7.32
MnO	0.10	0.06	0.06	0.12	0.05	0.11	0.27	0.27
MgO	13.32	12.45	13.67	10.91	11.93	11.62	12.80	12.80
CaO	22.84	22.63	22.96	22.56	22.67	22.56	22.39	22.39
Na_2O	0.41	0.42	0.39	0.51	0.51	0.51	0.39	0.39
K_2O	0.00	0.02	0.00	0.00	0.01	0.02	0.01	0.01
NiO	0.02	0.01	0.04	0.08	0.01	0.05	0.34	0.34
Total	100.49	100.71	99.78	99.46	99.03	98.51	99.23	99.23
Si	1.84	1.79	1.85	1.70	1.79	1.80	1.86	1.86
Ti	0.07	0.08	0.05	0.12	0.08	0.08	0.06	0.06
Al	0.20	0.27	0.18	0.35	0.26	0.27	0.18	0.18
Cr	0.00	0.01	0.00	0.00	0.00	0.00	0.00	0.00
Fe	0.22	0.24	0.22	0.26	0.25	0.24	0.23	0.23
Mn	0.00	0.00	0.00	0.00	0.00	0.00	0.01	0.01
Mg	0.74	0.69	0.76	0.62	0.67	0.66	0.72	0.72
Ca	0.91	0.90	0.92	0.92	0.92	0.92	0.90	0.90
Na	0.03	0.03	0.03	0.04	0.04	0.04	0.03	0.03
K	0.00	0.00	0.00	0.00	0.00	0.00	0.00	0.00
Ni	0.00	0.00	0.00	0.00	0.00	0.00	0.01	0.01
Total	4.01	4.01	4.02	4.02	4.02	4.01	4.00	4.00
Mg#	77.02	74.05	77.69	70.22	73.09	73.60	75.72	75.72
$D^{(cpx\text{-}melt)}_{H_2O}$	0.0169	0.0237	0.0157	0.0412	0.0230	0.0225	0.0150	0.0150
Absorbance of cpx (cm^{-1})	7.90	9.30	6.40	8.40	6.70	7.80	11.40	8.40
Thickness of cpx (0.001mm)	91	91	91	84	86	86	87	87
Absorbance normalized to 1 cm (cm^{-1})	868	1022	703	1000	779	907	1310	966
H_2O-cpx (ppm)	367	432	298	423	330	384	554	409
H_2O-melt (wt%)	2.17	1.82	1.90	1.03	1.43	1.70	3.70	2.73

Sample No. Section No. Point No.	24	25	25.1	26	27	28	29	30
SiO_2	47.54	51.05	50.32	47.18	46.22	47.33	49.62	47.78
TiO_2	2.59	1.63	1.51	3.31	3.14	2.90	1.90	2.81
Al_2O3	5.95	3.33	3.36	5.79	6.73	6.27	3.64	6.12
Cr_2O3	0.04	0.20	0.30	0.00	0.12	0.43	0.11	0.23
FeO	7.95	7.18	6.99	8.07	8.12	7.20	7.74	7.80
MnO	0.11	0.09	0.10	0.06	0.09	0.07	0.09	0.05
MgO	12.44	13.93	14.05	12.23	12.03	12.20	13.34	11.39
CaO	22.76	22.67	22.48	22.71	22.74	22.65	22.72	22.60
Na_2O	0.47	0.35	0.33	0.40	0.43	0.43	0.42	0.47
K_2O	0.01	0.00	0.00	0.00	0.00	0.00	0.02	0.00
NiO	0.02	0.01	0.06	0.02	0.06	0.01	0.00	0.04
Total	99.86	100.44	99.50	99.77	99.66	99.48	99.60	99.28
Si	1.79	1.89	1.88	1.78	1.75	1.78	1.86	1.80
Ti	0.07	0.05	0.04	0.09	0.09	0.08	0.05	0.08
Al	0.26	0.15	0.15	0.26	0.30	0.28	0.16	0.27
Cr	0.00	0.01	0.01	0.00	0.00	0.01	0.00	0.01
Fe	0.25	0.22	0.22	0.25	0.26	0.23	0.24	0.25
Mn	0.00	0.00	0.00	0.00	0.00	0.00	0.00	0.00
Mg	0.70	0.77	0.78	0.69	0.68	0.68	0.75	0.64
Ca	0.92	0.90	0.90	0.92	0.92	0.91	0.91	0.91
Na	0.03	0.02	0.02	0.03	0.03	0.03	0.03	0.03
K	0.00	0.00	0.00	0.00	0.00	0.00	0.00	0.00
Ni	0.00	0.00	0.00	0.00	0.00	0.00	0.00	0.00
Total	4.03	4.00	4.01	4.02	4.03	4.01	4.02	4.00
Mg#	73.62	77.57	78.18	72.98	72.55	75.12	75.45	72.24
$D^{(cpx\text{-}melt)}_{H_2O}$	0.0241	0.0126	0.0132	0.0256	0.0311	0.0252	0.0147	0.0218
Absorbance of cpx (cm^{-1})	8.80	3.60	7.00	14.00	7.70	6.80	5.30	3.90
Thickness of cpx (0.001mm)	94	111	111	107	103	103	97	79
Absorbance normalized to 1 cm (cm^{-1})	936	324	631	1308	748	660	546	494
H_2O-cpx (ppm)	396	137	267	554	316	279	231	209
H_2O-melt (wt%)	1.65	1.09	2.02	2.16	1.02	1.11	1.57	0.96

Sample No.	GP-3							
Section No.	1							
Point No.	1	1.2	2	2.2	3	4	5	6
SiO_2	47.11	47.73	46.52	48.11	49.27	48.43	48.01	48.17
TiO_2	2.49	2.64	3.11	2.42	2.01	2.50	2.53	2.74
Al_2O3	5.85	5.15	6.70	4.13	3.70	5.47	5.49	5.93
Cr_2O3	0.07	0.11	0.08	0.16	0.15	0.04	0.00	0.04
FeO	7.74	7.62	8.27	7.89	6.99	7.99	7.64	7.61
MnO	0.09	0.10	0.08	0.11	0.10	0.10	0.09	0.11
MgO	12.50	12.93	11.80	13.42	13.74	12.77	12.87	12.35
CaO	22.34	22.61	22.52	22.15	22.54	22.42	22.65	22.44
Na_2O	0.40	0.47	0.46	0.38	0.33	0.59	0.43	0.45
K_2O	0.01	0.01	0.00	0.00	0.01	0.01	0.01	0.00
NiO	0.02	0.00	0.05	0.03	0.02	0.10	0.05	0.08
Total	98.62	99.36	99.58	98.79	98.85	100.40	99.77	99.92
Si	1.79	1.80	1.76	1.83	1.86	1.81	1.80	1.80
Ti	0.07	0.07	0.09	0.07	0.06	0.07	0.07	0.08
Al	0.26	0.23	0.30	0.18	0.16	0.24	0.24	0.26
Cr	0.00	0.00	0.00	0.00	0.00	0.00	0.00	0.00
Fe	0.25	0.24	0.26	0.25	0.22	0.25	0.24	0.24
Mn	0.00	0.00	0.00	0.00	0.00	0.00	0.00	0.00
Mg	0.71	0.73	0.66	0.76	0.77	0.71	0.72	0.69
Ca	0.91	0.91	0.91	0.90	0.91	0.90	0.91	0.90
Na	0.03	0.03	0.03	0.03	0.02	0.04	0.03	0.03
K	0.00	0.00	0.00	0.00	0.00	0.00	0.00	0.00
Ni	0.00	0.00	0.00	0.00	0.00	0.00	0.00	0.00
Total	4.02	4.03	4.02	4.02	4.01	4.02	4.02	4.01
Mg#	74.22	75.15	71.80	75.21	77.80	74.03	75.02	74.32
$D^{(cpx\text{-}melt)}_{H_2O}$	0.0237	0.0220	0.0292	0.0190	0.0153	0.0214	0.0219	0.0221
Absorbance of cpx (cm^{-1})	6.00	5.60	9.80	6.30	6.14	10.00	10.00	9.50
Thickness of cpx (0.001mm)	61	61	64	64	61	82	82	90
Absorbance normalized to 1 cm (cm^{-1})	984	918	1531	984	1007	1220	1220	1056
H_2O-cpx (ppm)	416	388	648	417	426	516	516	447
H_2O-melt (wt%)	1.76	1.76	2.22	2.19	2.79	2.41	2.35	2.02

Sample No. Section No. Point No.	6.2	6.3	7	8	9	10	11	11.1
SiO_2	49.54	47.49	49.60	47.86	48.57	47.11	47.12	48.11
TiO_2	2.37	2.77	2.06	2.50	2.44	2.49	2.71	2.52
Al_2O3	4.43	5.82	3.82	4.68	4.23	5.85	6.05	5.41
Cr_2O3	0.03	0.04	0.07	0.02	0.01	0.07	0.08	0.01
FeO	7.82	8.15	8.16	8.20	7.57	7.74	7.69	7.48
MnO	0.10	0.09	0.13	0.12	0.08	0.09	0.10	0.09
MgO	12.77	12.35	13.48	12.83	12.99	12.50	12.25	12.67
CaO	22.38	22.72	22.47	22.48	22.71	22.34	22.78	22.60
Na_2O	0.52	0.51	0.38	0.44	0.32	0.40	0.41	0.41
K_2O	0.00	0.02	0.01	0.00	0.00	0.01	0.00	0.00
NiO	0.07	0.01	0.00	0.00	0.02	0.02	0.02	0.02
Total	100.04	99.97	100.18	99.12	98.92	98.62	99.21	99.33
Si	1.85	1.78	1.85	1.81	1.84	1.79	1.78	1.81
Ti	0.07	0.08	0.06	0.07	0.07	0.07	0.08	0.07
Al	0.19	0.26	0.17	0.21	0.19	0.26	0.27	0.24
Cr	0.00	0.00	0.00	0.00	0.00	0.00	0.00	0.00
Fe	0.24	0.26	0.25	0.26	0.24	0.25	0.24	0.24
Mn	0.00	0.00	0.00	0.00	0.00	0.00	0.00	0.00
Mg	0.71	0.69	0.75	0.72	0.73	0.71	0.69	0.71
Ca	0.90	0.91	0.90	0.91	0.92	0.91	0.92	0.91
Na	0.04	0.04	0.03	0.03	0.02	0.03	0.03	0.03
K	0.00	0.00	0.00	0.00	0.00	0.00	0.00	0.00
Ni	0.00	0.00	0.00	0.00	0.00	0.00	0.00	0.00
Total	4.01	4.03	4.02	4.03	4.01	4.02	4.02	4.01
Mg#	74.43	72.97	74.65	73.61	75.36	74.22	73.96	75.12
$D^{(cpx\text{-}melt)}_{H_2O}$	0.0163	0.0243	0.0159	0.0203	0.0173	0.0237	0.0247	0.0206
Absorbance of cpx (cm^{-1})	6.25	7.90	4.05	3.20	10.00	11.00	2.70	2.15
Thickness of cpx (0.001mm)	90	90	60	78	102	102	90	90
Absorbance normalized to 1 cm (cm^{-1})	694	878	675	410	980	1078	300	239
H_2O-cpx (ppm)	294	371	286	174	415	456	127	101
H_2O-melt (wt%)	1.81	1.53	1.80	0.86	2.39	1.93	0.51	0.49

Sample No. Section No. Point No.	11.2	12	13	14	15	16	17	18
SiO_2	45.15	47.46	49.59	49.36	48.34	47.99	49.55	50.27
TiO_2	3.53	3.02	2.22	2.33	2.25	2.70	1.59	1.93
Al_2O3	7.23	5.88	3.71	4.25	4.92	5.58	3.41	3.60
Cr_2O3	0.04	0.05	0.06	0.05	0.05	0.05	0.11	0.13
FeO	8.30	7.56	7.59	7.66	7.34	7.85	7.07	7.85
MnO	0.08	0.07	0.08	0.04	0.11	0.08	0.04	0.11
MgO	11.42	12.14	13.52	13.20	12.78	12.44	13.90	13.37
CaO	22.60	22.64	22.31	22.88	22.74	22.61	22.98	22.38
Na_2O	0.55	0.52	0.43	0.36	0.45	0.49	0.37	0.35
K_2O	0.00	0.00	0.00	0.01	0.02	0.00	0.00	0.00
NiO	0.00	0.04	0.03	0.02	0.01	0.00	0.05	0.00
Total	98.90	99.36	99.53	100.15	99.01	99.79	99.07	99.98
Si	1.72	1.79	1.86	1.84	1.83	1.80	1.87	1.88
Ti	0.10	0.09	0.06	0.07	0.06	0.08	0.05	0.05
Al	0.33	0.26	0.16	0.19	0.22	0.25	0.15	0.16
Cr	0.00	0.00	0.00	0.00	0.00	0.00	0.00	0.00
Fe	0.26	0.24	0.24	0.24	0.23	0.25	0.22	0.24
Mn	0.00	0.00	0.00	0.00	0.00	0.00	0.00	0.00
Mg	0.65	0.68	0.76	0.73	0.72	0.70	0.78	0.74
Ca	0.92	0.91	0.90	0.91	0.92	0.91	0.93	0.89
Na	0.04	0.04	0.03	0.03	0.03	0.04	0.03	0.03
K	0.00	0.00	0.00	0.00	0.00	0.00	0.00	0.00
Ni	0.00	0.00	0.00	0.00	0.00	0.00	0.00	0.00
Total	4.03	4.01	4.01	4.01	4.02	4.02	4.03	4.00
Mg#	71.05	74.13	76.06	75.44	75.65	73.86	77.80	75.22
$D^{(cpx\text{-}melt)}_{H_2O}$	0.0360	0.0237	0.0153	0.0168	0.0186	0.0220	0.0142	0.0138
Absorbance of cpx (cm^{-1})	2.40	9.60	3.80	10.00	8.70	3.70	3.70	7.80
Thickness of cpx (0.001mm)	90	96	105	83	83	64	69	64
Absorbance normalized to 1 cm (cm^{-1})	267	1000	362	1205	1048	578	536	1219
H_2O-cpx (ppm)	113	423	153	510	444	245	227	516
H_2O-melt (wt%)	0.31	1.79	1.00	3.04	2.38	1.11	1.60	3.73

Sample No.								
Section No.								
Point No.	19	20	22	23	24	25	26	27
SiO_2	49.27	48.43	47.55	49.06	48.94	45.26	50.02	49.23
TiO_2	2.04	2.66	2.41	2.47	2.35	3.54	1.79	2.27
Al_2O3	4.50	5.73	5.49	4.83	4.63	7.16	3.67	4.34
Cr_2O3	0.08	0.26	0.08	0.02	0.03	0.12	0.12	0.05
FeO	7.69	7.70	7.75	7.50	7.44	8.43	7.61	7.90
MnO	0.09	0.05	0.11	0.07	0.10	0.08	0.09	0.06
MgO	12.98	12.31	12.52	12.58	12.77	11.56	13.57	12.89
CaO	22.74	22.22	22.59	22.64	22.59	22.26	22.36	22.31
Na_2O	0.40	0.37	0.46	0.53	0.47	0.51	0.36	0.52
K_2O	0.00	0.00	0.00	0.01	0.01	0.01	0.00	0.00
NiO	0.00	0.02	0.06	0.05	0.01	0.00	0.05	0.04
Total	99.78	99.75	99.02	99.76	99.34	98.92	99.64	99.59
Si	1.84	1.81	1.80	1.84	1.84	1.73	1.87	1.85
Ti	0.06	0.07	0.07	0.07	0.07	0.10	0.05	0.06
Al	0.20	0.25	0.25	0.21	0.21	0.32	0.16	0.19
Cr	0.00	0.01	0.00	0.00	0.00	0.00	0.00	0.00
Fe	0.24	0.24	0.25	0.23	0.23	0.27	0.24	0.25
Mn	0.00	0.00	0.00	0.00	0.00	0.00	0.00	0.00
Mg	0.72	0.69	0.71	0.70	0.72	0.66	0.76	0.72
Ca	0.91	0.89	0.92	0.91	0.91	0.91	0.90	0.90
Na	0.03	0.03	0.03	0.04	0.03	0.04	0.03	0.04
K	0.00	0.00	0.00	0.00	0.00	0.00	0.00	0.00
Ni	0.00	0.00	0.00	0.00	0.00	0.00	0.00	0.00
Total	4.01	4.00	4.02	4.01	4.01	4.03	4.01	4.01
Mg#	75.06	74.05	74.21	74.94	75.36	70.98	76.07	74.42
$D^{(cpx\text{-}melt)}_{H_2O}$	0.0165	0.0208	0.0219	0.0175	0.0172	0.0359	0.0141	0.0165
Absorbance of cpx (cm^{-1})	10.60	8.50	7.50	3.30	4.40	5.00	5.50	2.80
Thickness of cpx (0.001mm)	64	64	42	42	42	42	42	42
Absorbance normalized to 1 cm (cm^{-1})	1656	1328	1786	786	1048	1190	1310	667
H_2O-cpx (ppm)	701	562	756	332	443	504	554	282
H_2O-melt (wt%)	4.24	2.70	3.45	1.90	2.58	1.40	3.93	1.71

Sample No.		GP-4						
Section No.		1						
Point No.	28	1	2	3	4	5	6	7
SiO_2	49.90	49.32	50.37	46.36	48.71	49.88	47.82	49.44
TiO_2	1.80	2.31	1.92	3.53	2.74	2.12	2.50	2.29
Al_2O3	3.35	3.79	3.33	6.78	5.36	3.90	5.81	4.60
Cr_2O3	0.03	0.01	0.10	0.04	0.08	0.10	0.00	0.01
FeO	7.43	7.69	7.24	8.19	7.05	7.78	7.22	7.07
MnO	0.08	0.11	0.07	0.08	0.07	0.04	0.08	0.11
MgO	13.84	12.99	13.59	11.64	12.64	12.43	12.46	12.73
CaO	22.87	22.46	22.71	22.49	22.64	22.64	22.67	22.84
Na_2O	0.39	0.47	0.38	0.46	0.44	0.39	0.50	0.49
K_2O	0.00	0.00	0.01	0.00	0.01	0.00	0.09	0.01
NiO	0.00	0.00	0.00	0.00	0.00	0.00	0.00	0.01
Total	99.68	99.15	99.71	99.57	99.74	99.29	99.15	99.60
Si	1.87	1.86	1.88	1.75	1.82	1.87	1.80	1.85
Ti	0.05	0.07	0.05	0.10	0.08	0.06	0.07	0.06
Al	0.15	0.17	0.15	0.30	0.24	0.17	0.26	0.20
Cr	0.00	0.00	0.00	0.00	0.00	0.00	0.00	0.00
Fe	0.23	0.24	0.23	0.26	0.22	0.24	0.23	0.22
Mn	0.00	0.00	0.00	0.00	0.00	0.00	0.00	0.00
Mg	0.77	0.73	0.76	0.66	0.70	0.70	0.70	0.71
Ca	0.92	0.91	0.91	0.91	0.91	0.91	0.92	0.92
Na	0.03	0.03	0.03	0.03	0.03	0.03	0.04	0.04
K	0.00	0.00	0.00	0.00	0.00	0.00	0.00	0.00
Ni	0.00	0.00	0.00	0.00	0.00	0.00	0.00	0.00
Total	4.02	4.01	4.00	4.01	4.00	3.99	4.02	4.00
Mg#	76.85	75.06	77.01	71.69	76.17	74.01	75.48	76.25
$D^{(cpx\text{-}melt)}_{H_2O}$	0.0141	0.0152	0.0131	0.0305	0.0195	0.0137	0.0217	0.0160
Absorbance of cpx (cm^{-1})	5.00	6.90	5.70	9.90	8.20	6.97	7.30	5.00
Thickness of cpx (0.001mm)	51	98	100	114	114	115	118	117
Absorbance normalized to 1 cm (cm^{-1})	980	704	570	868	719	606	619	427
H_2O-cpx (ppm)	415	298	241	367	304	256	262	181
H_2O-melt (wt%)	2.94	1.96	1.84	1.21	1.56	1.88	1.21	1.13

Sample No. Section No. Point No.	8	9	9.2	10	11	12	13	14
SiO_2	47.93	47.09	47.45	49.53	46.81	50.02	50.27	48.57
TiO_2	2.47	3.07	2.74	2.04	3.15	1.84	1.63	2.45
Al_2O3	5.15	6.27	5.81	4.12	6.47	3.57	3.75	5.24
Cr_2O3	0.06	0.02	0.06	0.11	0.06	0.06	0.12	0.05
FeO	7.76	7.49	7.77	7.34	7.51	7.10	7.52	7.27
MnO	0.12	0.04	0.12	0.07	0.09	0.05	0.03	0.06
MgO	12.79	12.14	12.33	13.20	12.06	13.51	13.64	12.57
CaO	22.36	22.97	22.60	22.55	22.75	22.55	22.22	22.80
Na_2O	0.40	0.33	0.46	0.41	0.41	0.39	0.38	0.45
K_2O	0.00	0.00	0.00	0.01	0.01	0.00	0.01	0.00
NiO	0.00	0.05	0.02	0.00	0.02	0.00	0.00	0.02
Total	99.04	99.47	99.36	99.38	99.33	99.08	99.58	99.48
Si	1.81	1.77	1.79	1.86	1.77	1.88	1.88	1.82
Ti	0.07	0.09	0.08	0.06	0.09	0.05	0.05	0.07
Al	0.23	0.28	0.26	0.18	0.29	0.16	0.17	0.23
Cr	0.00	0.00	0.00	0.00	0.00	0.00	0.00	0.00
Fe	0.25	0.24	0.25	0.23	0.24	0.22	0.23	0.23
Mn	0.00	0.00	0.00	0.00	0.00	0.00	0.00	0.00
Mg	0.72	0.68	0.69	0.74	0.68	0.76	0.76	0.70
Ca	0.91	0.93	0.91	0.91	0.92	0.91	0.89	0.92
Na	0.03	0.02	0.03	0.03	0.03	0.03	0.03	0.03
K	0.00	0.00	0.00	0.00	0.00	0.00	0.00	0.00
Ni	0.00	0.00	0.00	0.00	0.00	0.00	0.00	0.00
Total	4.02	4.01	4.02	4.01	4.01	4.00	4.01	4.01
Mg#	74.62	74.29	73.90	76.23	74.12	77.22	76.39	75.50
$D^{(cpx\text{-}melt)}_{H_2O}$	0.0206	0.0258	0.0235	0.0153	0.0272	0.0134	0.0136	0.0190
Absorbance of cpx (cm^{-1})	5.46	5.20	4.70	5.61	3.88	3.45	3.50	3.20
Thickness of cpx (0.001mm)	118	88	88	88	86	86	85	97
Absorbance normalized to 1 cm (cm^{-1})	463	591	534	638	451	401	412	330
H_2O-cpx (ppm)	196	250	226	270	191	170	174	140
H_2O-melt (wt%)	0.95	0.97	0.96	1.76	0.70	1.27	1.28	0.73

Sample No.								
Section No.		2						
Point No.	15	1	2	3	4	5	6	7
SiO_2	49.79	48.74	49.12	49.49	48.26	47.75	46.99	47.62
TiO_2	2.14	1.34	2.40	2.14	2.70	2.89	2.90	2.90
Al_2O3	4.23	5.68	4.48	3.76	5.49	6.21	6.39	6.42
Cr_2O3	0.06	0.00	0.01	0.02	0.06	0.03	0.14	0.04
FeO	7.09	8.05	7.21	7.59	7.36	7.48	7.86	7.52
MnO	0.13	0.11	0.12	0.09	0.08	0.09	0.14	0.08
MgO	13.33	13.28	12.54	12.97	12.61	11.91	11.83	12.21
CaO	22.57	21.64	22.67	22.53	22.72	22.64	22.38	22.67
Na_2O	0.44	0.57	0.54	0.40	0.48	0.46	0.46	0.47
K_2O	0.01	0.01	0.01	0.00	0.00	0.00	0.01	0.00
NiO	0.07	0.01	0.01	0.06	0.00	0.06	0.07	0.03
Total	99.87	99.44	99.11	99.04	99.76	99.52	99.16	99.96
Si	1.86	1.83	1.85	1.87	1.81	1.79	1.78	1.78
Ti	0.06	0.04	0.07	0.06	0.08	0.08	0.08	0.08
Al	0.19	0.25	0.20	0.17	0.24	0.27	0.28	0.28
Cr	0.00	0.00	0.00	0.00	0.00	0.00	0.00	0.00
Fe	0.22	0.25	0.23	0.24	0.23	0.24	0.25	0.24
Mn	0.00	0.00	0.00	0.00	0.00	0.00	0.00	0.00
Mg	0.74	0.74	0.70	0.73	0.70	0.67	0.67	0.68
Ca	0.90	0.87	0.91	0.91	0.91	0.91	0.91	0.91
Na	0.03	0.04	0.04	0.03	0.03	0.03	0.03	0.03
K	0.00	0.00	0.00	0.00	0.00	0.00	0.00	0.00
Ni	0.00	0.00	0.00	0.00	0.00	0.00	0.00	0.00
Total	4.01	4.03	4.00	4.00	4.01	4.00	4.01	4.01
Mg#	77.02	74.62	75.60	75.28	75.32	73.95	72.85	74.32
$D^{(cpx\text{-}melt)}_{H_2O}$	0.0155	0.0191	0.0161	0.0145	0.0210	0.0230	0.0257	0.0249
Absorbance of cpx (cm^{-1})	5.48	6.40	5.70	4.80	8.00	7.70	8.02	8.40
Thickness of cpx (0.001mm)	116	94	98	93	121	116	116	124
Absorbance normalized to 1 cm (cm^{-1})	472	681	582	516	661	664	691	677
H_2O-cpx (ppm)	200	288	246	218	280	281	293	287
H_2O-melt (wt%)	1.29	1.51	1.53	1.50	1.33	1.22	1.14	1.15

Sample No. Section No. Point No.	9	10	11	12	12.1	12.2	13	13.2
SiO_2	48.81	48.98	47.49	46.83	48.26	50.26	47.85	46.88
TiO_2	2.28	2.49	3.11	3.23	2.84	1.35	2.58	3.13
Al_2O3	4.48	5.02	5.29	6.57	5.63	4.96	5.44	6.63
Cr_2O3	0.00	0.02	0.01	0.04	0.06	0.00	0.07	0.06
FeO	7.45	7.43	7.33	7.63	7.11	8.89	7.13	7.54
MnO	0.02	0.09	0.08	0.08	0.14	0.09	0.12	0.12
MgO	12.77	12.67	12.45	12.04	12.47	13.20	12.59	12.03
CaO	22.81	22.85	22.86	22.69	22.73	20.28	22.83	22.80
Na_2O	0.40	0.40	0.44	0.50	0.40	0.69	0.50	0.52
K_2O	0.00	0.00	0.00	0.01	0.00	0.00	0.00	0.00
NiO	0.03	0.03	0.00	0.00	0.00	0.03	0.04	0.03
Total	99.04	99.97	99.07	99.61	99.65	99.75	99.15	99.74
Si	1.84	1.83	1.80	1.76	1.81	1.87	1.80	1.76
Ti	0.06	0.07	0.09	0.09	0.08	0.04	0.07	0.09
Al	0.20	0.22	0.24	0.29	0.25	0.22	0.24	0.29
Cr	0.00	0.00	0.00	0.00	0.00	0.00	0.00	0.00
Fe	0.24	0.23	0.23	0.24	0.22	0.28	0.22	0.24
Mn	0.00	0.00	0.00	0.00	0.00	0.00	0.00	0.00
Mg	0.72	0.71	0.70	0.68	0.70	0.73	0.71	0.67
Ca	0.92	0.91	0.93	0.92	0.91	0.81	0.92	0.92
Na	0.03	0.03	0.03	0.04	0.03	0.05	0.04	0.04
K	0.00	0.00	0.00	0.00	0.00	0.00	0.00	0.00
Ni	0.00	0.00	0.00	0.00	0.00	0.00	0.00	0.00
Total	4.01	4.00	4.01	4.02	4.00	4.00	4.02	4.02
Mg#	75.33	75.26	75.18	73.78	75.78	72.58	75.88	74.00
$D^{(cpx\text{-}melt)}_{H_2O}$	0.0168	0.0182	0.0225	0.0280	0.0211	0.0151	0.0212	0.0280
Absorbance of cpx (cm^{-1})	6.30	5.81	7.80	2.20	2.45	2.70	6.60	3.10
Thickness of cpx (0.001mm)	123	117	119	99	99	99	106	106
Absorbance normalized to 1 cm (cm^{-1})	512	497	655	222	247	273	623	292
H_2O-cpx (ppm)	217	210	277	94	105	115	263	124
H_2O-melt (wt%)	1.29	1.15	1.24	0.34	0.50	0.76	1.24	0.44

Sample No.		GP-5						
Section No.		2						
Point No.	14	1	2	3	4	4.2	5	6
SiO_2	46.76	49.67	48.94	49.11	47.34	46.23	51.43	35.73
TiO_2	3.03	2.05	2.26	2.50	2.80	3.43	1.45	1.39
Al_2O3	6.45	4.02	4.09	4.56	5.80	6.97	2.83	4.48
Cr_2O3	0.04	0.16	0.03	0.00	0.02	0.07	0.49	0.04
FeO	7.50	7.28	7.20	7.44	7.83	8.17	6.33	3.03
MnO	0.09	0.15	0.07	0.04	0.07	0.05	0.11	0.01
MgO	11.97	13.06	12.95	12.97	12.36	11.66	14.78	10.27
CaO	22.68	22.60	22.58	23.10	22.46	22.60	22.80	14.08
Na_2O	0.47	0.48	0.53	0.36	0.39	0.51	0.32	0.45
K_2O	0.00	0.02	0.00	0.00	0.00	0.00	0.02	0.00
NiO	0.04	0.04	0.01	0.01	0.00	0.02	0.03	0.02
Total	99.04	99.52	98.65	100.07	99.06	99.71	100.58	69.50
Si	1.77	1.86	1.85	1.83	1.79	1.74	1.90	1.87
Ti	0.09	0.06	0.06	0.07	0.08	0.10	0.04	0.05
Al	0.29	0.18	0.18	0.20	0.26	0.31	0.12	0.28
Cr	0.00	0.00	0.00	0.00	0.00	0.00	0.01	0.00
Fe	0.24	0.23	0.23	0.23	0.25	0.26	0.20	0.13
Mn	0.00	0.00	0.00	0.00	0.00	0.00	0.00	0.00
Mg	0.68	0.73	0.73	0.72	0.70	0.66	0.81	0.80
Ca	0.92	0.91	0.91	0.92	0.91	0.91	0.90	0.79
Na	0.03	0.03	0.04	0.03	0.03	0.04	0.02	0.05
K	0.00	0.00	0.00	0.00	0.00	0.00	0.00	0.00
Ni	0.00	0.00	0.00	0.00	0.00	0.00	0.00	0.00
Total	4.02	4.01	4.01	4.01	4.01	4.02	4.01	3.96
Mg#	73.99	76.19	76.22	75.66	73.78	71.79	80.64	85.81
$D^{(cpx\text{-}melt)}_{H_2O}$	0.0266	0.0149	0.0158	0.0176	0.0235	0.0316	0.0120	0.0163
Absorbance of cpx (cm^{-1})	5.60	6.60	7.50	4.60	6.20	6.00	7.30	7.50
Thickness of cpx (0.001mm)	126	78	74	70	70	70	74	79
Absorbance normalized to 1 cm (cm^{-1})	444	846	1014	657	886	857	986	949
H_2O-cpx (ppm)	188	358	429	278	375	363	417	402
H_2O-melt (wt%)	0.71	2.40	2.71	1.58	1.59	1.15	3.47	2.46

Sample No. Section No. Point No.	7	8	9	10	11	12	13	14
SiO_2	49.66	48.82	50.19	49.61	50.40	50.27	46.65	48.40
TiO_2	2.19	2.32	1.78	2.01	1.66	1.62	3.29	2.23
Al_2O3	4.68	4.77	3.25	4.22	3.27	3.27	6.61	5.05
Cr_2O3	0.11	0.10	0.28	0.06	0.03	0.20	0.09	0.48
FeO	7.37	7.04	6.56	7.53	7.20	7.16	7.88	6.62
MnO	0.07	0.06	0.04	0.08	0.07	0.09	0.11	0.06
MgO	13.12	13.04	14.09	13.20	14.07	14.18	11.87	13.08
CaO	22.92	22.97	23.12	22.85	22.54	22.39	22.76	22.79
Na_2O	0.42	0.48	0.31	0.43	0.24	0.34	0.48	0.39
K_2O	0.01	0.00	0.01	0.02	0.00	0.00	0.01	0.00
NiO	0.08	0.01	0.00	0.02	0.00	0.01	0.04	0.00
Total	100.64	99.60	99.62	100.03	99.48	99.53	99.79	99.10
Si	1.84	1.83	1.87	1.85	1.88	1.88	1.76	1.82
Ti	0.06	0.07	0.05	0.06	0.05	0.05	0.09	0.06
Al	0.20	0.21	0.14	0.19	0.14	0.14	0.29	0.22
Cr	0.00	0.00	0.01	0.00	0.00	0.01	0.00	0.01
Fe	0.23	0.22	0.20	0.23	0.23	0.22	0.25	0.21
Mn	0.00	0.00	0.00	0.00	0.00	0.00	0.00	0.00
Mg	0.73	0.73	0.78	0.73	0.78	0.79	0.67	0.73
Ca	0.91	0.92	0.92	0.91	0.90	0.90	0.92	0.92
Na	0.03	0.04	0.02	0.03	0.02	0.02	0.03	0.03
K	0.00	0.00	0.00	0.00	0.00	0.00	0.00	0.00
Ni	0.00	0.00	0.00	0.00	0.00	0.00	0.00	0.00
Total	4.01	4.02	4.01	4.01	4.01	4.01	4.02	4.01
Mg#	76.04	76.76	79.31	75.77	77.69	77.93	72.87	77.89
$D^{(cpx\text{-}melt)}_{H_2O}$	0.0170	0.0181	0.0135	0.0158	0.0130	0.0134	0.0291	0.0192
Absorbance of cpx (cm^{-1})	4.70	5.80	5.70	7.10	7.40	7.00	6.40	5.60
Thickness of cpx (0.001mm)	69	70	82	71	79	84	67	82
Absorbance normalized to 1 cm (cm^{-1})	681	829	695	1000	937	833	955	683
H_2O-cpx (ppm)	288	351	294	423	396	353	404	289
H_2O-melt (wt%)	1.70	1.94	2.17	2.69	3.06	2.63	1.39	1.50

Sample No. Section No. Point No.	15	15.2	15.3	17	18	19	20	21
SiO_2	46.12	47.93	48.77	48.51	47.90	48.71	49.77	49.74
TiO_2	3.51	2.74	2.42	2.76	2.43	2.30	2.40	2.00
Al_2O3	6.56	5.53	4.93	5.25	5.44	4.79	3.95	3.73
Cr_2O3	0.13	0.01	0.02	0.02	0.09	0.02	0.06	0.07
FeO	7.65	7.86	7.30	7.43	8.18	7.46	7.09	7.32
MnO	0.03	0.08	0.11	0.10	0.10	0.13	0.08	0.07
MgO	11.97	11.96	12.58	12.40	12.81	12.26	13.51	13.65
CaO	22.48	22.85	22.55	22.84	22.18	22.69	23.20	23.14
Na_2O	0.43	0.54	0.38	0.42	0.36	0.46	0.38	0.38
K_2O	0.00	0.02	0.00	0.00	0.00	0.01	0.00	0.00
NiO	0.00	0.01	0.00	0.05	0.02	0.00	0.00	0.04
Total	98.88	99.53	99.07	99.78	99.49	98.83	100.42	100.13
Si	1.75	1.81	1.84	1.82	1.80	1.84	1.85	1.86
Ti	0.10	0.08	0.07	0.08	0.07	0.07	0.07	0.06
Al	0.29	0.25	0.22	0.23	0.24	0.21	0.17	0.16
Cr	0.00	0.00	0.00	0.00	0.00	0.00	0.00	0.00
Fe	0.24	0.25	0.23	0.23	0.26	0.24	0.22	0.23
Mn	0.00	0.00	0.00	0.00	0.00	0.00	0.00	0.00
Mg	0.68	0.67	0.71	0.69	0.72	0.69	0.75	0.76
Ca	0.91	0.92	0.91	0.92	0.89	0.92	0.92	0.92
Na	0.03	0.04	0.03	0.03	0.03	0.03	0.03	0.03
K	0.00	0.00	0.00	0.00	0.00	0.00	0.00	0.00
Ni	0.00	0.00	0.00	0.00	0.00	0.00	0.00	0.00
Total	4.02	4.01	4.00	4.00	4.02	4.00	4.01	4.02
Mg#	73.61	73.07	75.44	74.83	73.62	74.55	77.26	76.88
$D^{(cpx\text{-}melt)}_{H_2O}$	0.0303	0.0211	0.0176	0.0197	0.0219	0.0168	0.0159	0.0153
Absorbance of cpx (cm^{-1})	10.00	9.60	11.00	12.00	7.79	9.00	12.00	9.80
Thickness of cpx (0.001mm)	92	92	92	85	87	82	91	87
Absorbance normalized to 1 cm (cm^{-1})	1087	1043	1196	1412	895	1098	1319	1126
H_2O-cpx (ppm)	460	442	506	597	379	464	558	477
H_2O-melt (wt%)	1.52	2.09	2.88	3.04	1.73	2.76	3.50	3.12

Sample No. Section No. Point No.	22	23	23.2	23.3	24	24.2	25	26
SiO_2	47.38	47.38	47.37	49.49	49.29	47.77	47.21	48.80
TiO_2	2.92	2.81	2.69	2.31	2.51	2.85	2.98	2.35
Al_2O3	6.12	5.96	5.75	4.71	5.18	5.97	5.60	4.32
Cr_2O3	0.41	0.02	0.07	0.06	0.09	0.04	0.05	0.02
FeO	7.21	7.57	7.72	7.10	7.37	7.46	7.98	8.01
MnO	0.05	0.08	0.05	0.07	0.12	0.10	0.10	0.10
MgO	12.21	12.32	12.40	12.89	12.69	12.19	12.43	13.07
CaO	22.87	22.57	22.52	22.93	22.74	22.51	23.02	22.90
Na_2O	0.43	0.45	0.44	0.48	0.53	0.49	0.43	0.39
K_2O	0.00	0.00	0.00	0.00	0.01	0.01	0.01	0.00
NiO	0.00	0.00	0.00	0.03	0.04	0.01	0.00	0.03
Total	99.60	99.15	99.01	100.05	100.57	99.40	99.80	99.98
Si	1.78	1.79	1.79	1.84	1.83	1.80	1.78	1.83
Ti	0.08	0.08	0.08	0.06	0.07	0.08	0.08	0.07
Al	0.27	0.26	0.26	0.21	0.23	0.26	0.25	0.19
Cr	0.01	0.00	0.00	0.00	0.00	0.00	0.00	0.00
Fe	0.23	0.24	0.24	0.22	0.23	0.23	0.25	0.25
Mn	0.00	0.00	0.00	0.00	0.00	0.00	0.00	0.00
Mg	0.68	0.69	0.70	0.72	0.70	0.68	0.70	0.73
Ca	0.92	0.91	0.91	0.91	0.90	0.91	0.93	0.92
Na	0.03	0.03	0.03	0.03	0.04	0.04	0.03	0.03
K	0.00	0.00	0.00	0.00	0.00	0.00	0.00	0.00
Ni	0.00	0.00	0.00	0.00	0.00	0.00	0.00	0.00
Total	4.01	4.02	4.02	4.01	4.01	4.01	4.03	4.02
Mg#	75.12	74.37	74.11	76.40	75.42	74.43	73.52	74.42
$D^{(cpx\text{-}melt)}_{H_2O}$	0.0248	0.0237	0.0232	0.0166	0.0185	0.0227	0.0249	0.0180
Absorbance of cpx (cm^{-1})	6.90	9.80	11.00	9.70	5.70	6.70	7.30	10.50
Thickness of cpx (0.001mm)	83	92	92	92	91	91	81	91
Absorbance normalized to 1 cm (cm^{-1})	831	1065	1196	1054	626	736	901	1154
H_2O-cpx (ppm)	352	451	506	446	265	312	381	488
H_2O-melt (wt%)	1.42	1.90	2.18	2.68	1.43	1.37	1.53	2.71

Sample No.								
Section No.								
Point No.	27	28	28.2	29	29.2	30	30.2	30.3
SiO_2	48.87	50.23	50.70	46.85	46.37	49.04	48.11	47.64
TiO_2	1.77	1.84	1.61	2.89	3.06	2.64	2.28	2.80
Al_2O3	4.98	3.63	3.47	6.45	6.50	4.91	5.76	5.94
Cr_2O3	0.02	0.23	0.25	0.00	0.15	0.01	0.13	0.01
FeO	7.27	6.66	6.40	7.17	7.50	7.55	7.38	7.63
MnO	0.09	0.06	0.07	0.10	0.05	0.16	0.10	0.04
MgO	13.22	13.85	14.16	12.15	12.09	12.72	12.40	12.27
CaO	22.28	23.01	22.91	22.95	22.95	22.97	23.01	22.92
Na_2O	0.49	0.35	0.25	0.49	0.43	0.52	0.48	0.45
K_2O	0.00	0.00	0.00	0.00	0.00	0.01	0.00	0.00
NiO	0.02	0.06	0.01	0.02	0.02	0.00	0.07	0.00
Total	99.00	99.90	99.82	99.06	99.11	100.52	99.72	99.69
Si	1.84	1.87	1.88	1.77	1.76	1.82	1.81	1.79
Ti	0.05	0.05	0.04	0.08	0.09	0.07	0.06	0.08
Al	0.22	0.16	0.15	0.29	0.29	0.22	0.25	0.26
Cr	0.00	0.01	0.01	0.00	0.00	0.00	0.00	0.00
Fe	0.23	0.21	0.20	0.23	0.24	0.23	0.23	0.24
Mn	0.00	0.00	0.00	0.00	0.00	0.00	0.00	0.00
Mg	0.74	0.77	0.78	0.68	0.68	0.71	0.69	0.69
Ca	0.90	0.92	0.91	0.93	0.93	0.92	0.93	0.92
Na	0.04	0.03	0.02	0.04	0.03	0.04	0.03	0.03
K	0.00	0.00	0.00	0.00	0.00	0.00	0.00	0.00
Ni	0.00	0.00	0.00	0.00	0.00	0.00	0.00	0.00
Total	4.02	4.01	4.00	4.02	4.02	4.01	4.02	4.02
Mg#	76.43	78.75	79.77	75.12	74.20	75.01	74.98	74.13
$D^{(cpx\text{-}melt)}_{H_2O}$	0.0174	0.0140	0.0129	0.0262	0.0287	0.0188	0.0211	0.0233
Absorbance of cpx (cm^{-1})	6.00	8.00	5.40	7.60	8.30	6.90	7.40	8.20
Thickness of cpx (0.001mm)	96	88	88	83	83	76	76	76
Absorbance normalized to 1 cm (cm^{-1})	625	909	614	916	1000	908	974	1079
H_2O-cpx (ppm)	264	385	260	387	423	384	412	457
H_2O-melt (wt%)	1.52	2.75	2.01	1.48	1.48	2.05	1.95	1.96

Sample No. Section No. Point No.	30.4	31.1	31.2	31.4	32	33	34	35
SiO_2	48.55	46.92	47.03	46.33	49.10	49.41	50.90	50.77
TiO_2	2.64	3.17	2.85	3.58	2.41	2.24	1.75	1.79
Al_2O3	5.43	5.85	6.12	6.89	4.61	3.89	3.43	3.37
Cr_2O3	0.04	0.01	0.05	0.04	0.03	0.08	0.05	0.29
FeO	7.49	7.49	7.53	7.78	7.51	7.91	6.89	6.55
MnO	0.12	0.10	0.07	0.06	0.07	0.10	0.15	0.11
MgO	12.50	12.24	12.32	11.65	12.36	12.96	13.85	13.87
CaO	22.92	22.95	22.90	22.79	22.77	22.25	23.13	23.10
Na_2O	0.43	0.42	0.50	0.51	0.51	0.44	0.40	0.30
K_2O	0.00	0.01	0.00	0.01	0.00	0.00	0.00	0.00
NiO	0.03	0.00	0.00	0.02	0.00	0.09	0.02	0.01
Total	100.15	99.15	99.38	99.66	99.36	99.36	100.57	100.17
Si	1.81	1.78	1.78	1.75	1.85	1.86	1.88	1.88
Ti	0.07	0.09	0.08	0.10	0.07	0.06	0.05	0.05
Al	0.24	0.26	0.27	0.31	0.20	0.17	0.15	0.15
Cr	0.00	0.00	0.00	0.00	0.00	0.00	0.00	0.01
Fe	0.23	0.24	0.24	0.25	0.24	0.25	0.21	0.20
Mn	0.00	0.00	0.00	0.00	0.00	0.00	0.00	0.00
Mg	0.70	0.69	0.69	0.65	0.69	0.73	0.76	0.77
Ca	0.92	0.93	0.93	0.92	0.92	0.90	0.92	0.92
Na	0.03	0.03	0.04	0.04	0.04	0.03	0.03	0.02
K	0.00	0.00	0.00	0.00	0.00	0.00	0.00	0.00
Ni	0.00	0.00	0.00	0.00	0.00	0.00	0.00	0.00
Total	4.01	4.02	4.03	4.02	4.00	4.01	4.01	4.00
Mg#	74.86	74.44	74.48	72.75	74.59	74.49	78.18	79.06
$D^{(cpx\text{-}melt)}_{H_2O}$	0.0203	0.0254	0.0256	0.0310	0.0164	0.0153	0.0129	0.0129
Absorbance of cpx (cm^{-1})	7.90	5.90	5.70	4.20	9.40	5.50	7.50	5.50
Thickness of cpx (0.001mm)	76	73	73	73	81	87	87	87
Absorbance normalized to 1 cm (cm^{-1})	1039	808	781	575	1160	632	862	632
H_2O-cpx (ppm)	440	342	330	243	491	267	365	267
H_2O-melt (wt%)	2.17	1.35	1.29	0.79	3.00	1.75	2.82	2.08

Sample No.			GP-6					
Section No.			2					
Point No.	36	37	1	2.2	2.3	3	5	6
SiO_2	48.69	49.45	48.43	47.06	47.09	48.33	48.54	48.70
TiO_2	2.47	2.27	2.48	2.83	3.12	2.42	1.58	2.37
Al_2O3	5.15	4.52	5.50	6.07	6.46	5.29	4.35	4.27
Cr_2O3	0.04	0.05	0.06	0.09	0.06	0.09	0.04	0.06
FeO	7.39	7.38	6.90	7.79	7.60	7.28	7.93	7.15
MnO	0.08	0.08	0.08	0.10	0.04	0.09	0.12	0.04
MgO	12.77	13.26	12.58	12.11	11.32	12.69	12.71	13.00
CaO	22.92	22.97	22.92	22.82	22.91	22.88	20.80	23.03
Na_2O	0.45	0.45	0.45	0.44	0.45	0.46	0.45	0.40
K_2O	0.00	0.02	0.00	0.01	0.00	0.00	0.04	0.00
NiO	0.06	0.08	0.01	0.02	0.01	0.04	0.06	0.06
Total	100.00	100.52	99.40	99.33	99.06	99.58	96.64	99.07
Si	1.82	1.84	1.82	1.78	1.78	1.81	1.87	1.84
Ti	0.07	0.06	0.07	0.08	0.09	0.07	0.05	0.07
Al	0.23	0.20	0.24	0.27	0.29	0.23	0.20	0.19
Cr	0.00	0.00	0.00	0.00	0.00	0.00	0.00	0.00
Fe	0.23	0.23	0.22	0.25	0.24	0.23	0.26	0.23
Mn	0.00	0.00	0.00	0.00	0.00	0.00	0.00	0.00
Mg	0.71	0.73	0.70	0.68	0.64	0.71	0.73	0.73
Ca	0.92	0.91	0.92	0.92	0.93	0.92	0.86	0.93
Na	0.03	0.03	0.03	0.03	0.03	0.03	0.03	0.03
K	0.00	0.00	0.00	0.00	0.00	0.00	0.00	0.00
Ni	0.00	0.00	0.00	0.00	0.00	0.00	0.00	0.00
Total	4.01	4.02	4.01	4.02	4.00	4.02	4.00	4.02
Mg#	75.50	76.20	76.49	73.50	72.63	75.65	74.08	76.44
$D^{(cpx\text{-}melt)}_{H_2O}$	0.0193	0.0173	0.0197	0.0251	0.0246	0.0200	0.0147	0.0171
Absorbance of cpx (cm^{-1})	6.20	11.00	4.99	5.41	5.30	7.00	8.50	5.20
Thickness of cpx (0.001mm)	90	90	89	79	79	99	90	95
Absorbance normalized to 1 cm (cm^{-1})	689	1222	561	685	671	707	944	547
H_2O-cpx (ppm)	291	517	237	290	284	299	400	232
H_2O-melt (wt%)	1.51	2.99	1.21	1.15	1.16	1.50	2.72	1.36

Sample No.								
Section No.								
Point No.	6.2	7	8	8.2	9	10	10.1	11
SiO_2	50.31	49.38	48.81	47.39	48.65	47.32	47.61	49.38
TiO_2	1.62	1.98	2.47	2.96	2.20	2.78	2.52	2.15
Al_2O3	3.96	4.19	5.50	6.34	4.60	5.72	5.52	3.90
Cr_2O3	0.37	0.02	0.03	0.05	0.02	0.13	0.05	0.14
FeO	6.99	7.26	7.38	7.39	7.59	7.50	7.25	7.58
MnO	0.13	0.09	0.08	0.05	0.09	0.07	0.04	0.06
MgO	13.99	13.03	12.63	11.93	12.88	12.25	12.66	13.24
CaO	22.66	22.92	22.85	22.98	22.70	22.95	22.98	22.78
Na_2O	0.35	0.41	0.49	0.46	0.37	0.37	0.38	0.40
K_2O	0.01	0.00	0.00	0.00	0.00	0.00	0.00	0.01
NiO	0.00	0.03	0.05	0.01	0.04	0.08	0.00	0.02
Total	100.38	99.31	100.30	99.54	99.15	99.18	99.01	99.65
Si	1.86	1.86	1.82	1.78	1.83	1.79	1.80	1.85
Ti	0.05	0.06	0.07	0.08	0.06	0.08	0.07	0.06
Al	0.17	0.19	0.24	0.28	0.20	0.25	0.25	0.17
Cr	0.01	0.00	0.00	0.00	0.00	0.00	0.00	0.00
Fe	0.22	0.23	0.23	0.23	0.24	0.24	0.23	0.24
Mn	0.00	0.00	0.00	0.00	0.00	0.00	0.00	0.00
Mg	0.77	0.73	0.70	0.67	0.72	0.69	0.71	0.74
Ca	0.90	0.92	0.91	0.93	0.92	0.93	0.93	0.92
Na	0.03	0.03	0.04	0.03	0.03	0.03	0.03	0.03
K	0.00	0.00	0.00	0.00	0.00	0.00	0.00	0.00
Ni	0.00	0.00	0.00	0.00	0.00	0.00	0.00	0.00
Total	4.01	4.01	4.01	4.01	4.01	4.02	4.02	4.01
Mg#	78.10	76.18	75.33	74.23	75.17	74.44	75.68	75.68
$D^{(cpx\text{-}melt)}_{H_2O}$	0.0147	0.0153	0.0198	0.0245	0.0176	0.0233	0.0218	0.0157
Absorbance of cpx (cm^{-1})	7.60	8.20	5.50	5.70	5.70	6.40	6.80	5.80
Thickness of cpx (0.001mm)	95	92	92	92	95	94	94	91
Absorbance normalized to 1 cm (cm^{-1})	800	891	598	620	600	681	723	637
H_2O-cpx (ppm)	339	377	253	262	254	288	306	270
H_2O-melt (wt%)	2.30	2.47	1.28	1.07	1.45	1.24	1.40	1.72

Sample No. Section No. Point No.	12	13	14	15	15.2	16	17	17.2
SiO_2	48.76	51.43	48.72	48.13	45.79	49.70	48.53	47.46
TiO_2	2.26	1.57	2.61	2.71	3.77	1.78	2.73	3.05
Al_2O3	4.89	3.32	5.39	4.51	6.59	4.21	5.24	5.97
Cr_2O3	0.01	0.34	0.04	0.00	0.00	0.07	0.02	0.02
FeO	7.65	7.00	7.20	7.11	7.57	2.03	7.09	7.50
MnO	0.11	0.06	0.05	0.11	0.07	0.08	0.07	0.04
MgO	12.23	14.22	12.77	13.13	11.65	13.37	12.40	11.96
CaO	22.78	22.47	22.89	22.96	22.78	22.23	22.96	22.79
Na_2O	0.44	0.29	0.47	0.33	0.44	0.00	0.45	0.51
K_2O	0.00	0.00	0.00	0.02	0.00	0.00	0.01	0.00
NiO	0.09	0.02	0.05	0.03	0.00	0.10	0.03	0.00
Total	99.23	100.71	100.18	99.03	98.65	93.55	99.53	99.30
Si	1.84	1.89	1.82	1.82	1.74	1.92	1.82	1.79
Ti	0.06	0.04	0.07	0.08	0.11	0.05	0.08	0.09
Al	0.22	0.14	0.24	0.20	0.30	0.19	0.23	0.27
Cr	0.00	0.01	0.00	0.00	0.00	0.00	0.00	0.00
Fe	0.24	0.22	0.22	0.22	0.24	0.07	0.22	0.24
Mn	0.00	0.00	0.00	0.00	0.00	0.00	0.00	0.00
Mg	0.69	0.78	0.71	0.74	0.66	0.77	0.69	0.67
Ca	0.92	0.89	0.91	0.93	0.93	0.92	0.92	0.92
Na	0.03	0.02	0.03	0.02	0.03	0.00	0.03	0.04
K	0.00	0.00	0.00	0.00	0.00	0.00	0.00	0.00
Ni	0.00	0.00	0.00	0.00	0.00	0.00	0.00	0.00
Total	4.01	4.00	4.01	4.02	4.02	3.93	4.00	4.01
Mg#	74.04	78.36	75.96	76.70	73.30	92.16	75.73	73.99
$D^{(cpx\text{-}melt)}_{H_2O}$	0.0172	0.0123	0.0200	0.0194	0.0311	0.0099	0.0192	0.0235
Absorbance of cpx (cm^{-1})	5.60	6.50	8.20	9.40	10.90	10.80	9.10	7.40
Thickness of cpx (0.001mm)	96	87	102	102	102	96	101	101
Absorbance normalized to 1 cm (cm^{-1})	583	747	804	922	1069	1125	901	733
H_2O-cpx (ppm)	247	316	340	390	452	476	381	310
H_2O-melt (wt%)	1.44	2.56	1.70	2.01	1.45	4.79	1.99	1.32

Sample No. Section No. Point No.	18	19	20	21	21.2	22	23	24
SiO_2	50.78	48.21	49.54	48.22	47.37	52.60	50.10	49.20
TiO_2	1.74	2.67	2.25	2.51	2.73	1.19	1.76	2.25
Al_2O3	3.34	5.37	3.96	5.32	5.86	2.37	3.65	4.62
Cr_2O3	0.26	0.04	0.00	0.01	0.05	0.54	0.08	0.00
FeO	7.05	7.33	7.67	7.31	7.42	5.99	7.52	7.11
MnO	0.06	0.09	0.14	0.07	0.09	0.08	0.08	0.07
MgO	13.16	12.62	12.91	12.67	12.53	15.18	13.68	12.88
CaO	22.51	22.79	22.67	22.87	22.96	22.67	22.59	22.97
Na_2O	0.36	0.50	0.41	0.43	0.39	0.28	0.34	0.51
K_2O	0.01	0.00	0.00	0.00	0.00	0.00	0.01	0.03
NiO	0.00	0.06	0.00	0.04	0.01	0.00	0.00	0.00
Total	99.26	99.68	99.55	99.44	99.41	100.90	99.79	99.64
Si	1.90	1.81	1.86	1.81	1.79	1.92	1.87	1.84
Ti	0.05	0.08	0.06	0.07	0.08	0.03	0.05	0.06
Al	0.15	0.24	0.18	0.24	0.26	0.10	0.16	0.20
Cr	0.01	0.00	0.00	0.00	0.00	0.02	0.00	0.00
Fe	0.22	0.23	0.24	0.23	0.23	0.18	0.23	0.22
Mn	0.00	0.00	0.00	0.00	0.00	0.00	0.00	0.00
Mg	0.73	0.71	0.72	0.71	0.70	0.83	0.76	0.72
Ca	0.90	0.92	0.91	0.92	0.93	0.89	0.90	0.92
Na	0.03	0.04	0.03	0.03	0.03	0.02	0.02	0.04
K	0.00	0.00	0.00	0.00	0.00	0.00	0.00	0.00
Ni	0.00	0.00	0.00	0.00	0.00	0.00	0.00	0.00
Total	3.99	4.01	4.01	4.01	4.02	4.00	4.01	4.01
Mg#	76.89	75.44	75.01	75.56	75.07	81.89	76.44	76.36
$D^{(cpx\text{-}melt)}_{H_2O}$	0.0117	0.0208	0.0151	0.0202	0.0240	0.0101	0.0140	0.0167
Absorbance of cpx (cm^{-1})	5.30	7.50	6.20	6.20	6.60	6.70	3.00	5.90
Thickness of cpx (0.001mm)	102	92	90	82	82	98	93	97
Absorbance normalized to 1 cm (cm^{-1})	520	815	689	756	805	684	323	608
H_2O-cpx (ppm)	220	345	291	320	341	289	136	257
H_2O-melt (wt%)	1.88	1.66	1.93	1.58	1.42	2.85	0.97	1.54

Sample No.								
Section No.								
Point No.	25	26	27	28	29	30	31	32
SiO_2	47.95	47.94	49.61	47.28	49.12	47.45	48.35	48.86
TiO_2	2.62	2.52	2.19	2.74	2.10	2.73	2.43	2.34
Al_2O3	5.59	5.70	3.76	6.54	4.40	5.68	5.31	5.15
Cr_2O3	0.06	0.05	0.04	0.10	0.16	0.04	0.04	0.05
FeO	7.36	7.45	6.91	7.67	7.32	7.24	7.24	7.13
MnO	0.09	0.06	0.10	0.10	0.10	0.08	0.07	0.04
MgO	12.73	12.58	13.44	12.08	13.23	12.61	12.69	12.80
CaO	22.85	22.80	23.04	22.93	23.02	22.84	23.05	22.81
Na_2O	0.49	0.47	0.42	0.44	0.40	0.48	0.46	0.46
K_2O	0.00	0.01	0.01	0.00	0.00	0.00	0.00	0.00
NiO	0.00	0.00	0.04	0.01	0.04	0.05	0.00	0.01
Total	99.74	99.56	99.56	99.88	99.88	99.18	99.64	99.65
Si	1.80	1.80	1.86	1.77	1.84	1.79	1.81	1.83
Ti	0.07	0.07	0.06	0.08	0.06	0.08	0.07	0.07
Al	0.25	0.25	0.17	0.29	0.19	0.25	0.23	0.23
Cr	0.00	0.00	0.00	0.00	0.00	0.00	0.00	0.00
Fe	0.23	0.23	0.22	0.24	0.23	0.23	0.23	0.22
Mn	0.00	0.00	0.00	0.00	0.00	0.00	0.00	0.00
Mg	0.71	0.70	0.75	0.68	0.74	0.71	0.71	0.71
Ca	0.92	0.92	0.92	0.92	0.92	0.92	0.93	0.91
Na	0.04	0.03	0.03	0.03	0.03	0.04	0.03	0.03
K	0.00	0.00	0.00	0.00	0.00	0.00	0.00	0.00
Ni	0.00	0.00	0.00	0.00	0.00	0.00	0.00	0.00
Total	4.02	4.02	4.01	4.02	4.02	4.02	4.02	4.01
Mg#	75.50	75.08	77.62	73.76	76.32	75.64	75.75	76.20
$D^{(cpx\text{-}melt)}_{H_2O}$	0.0222	0.0218	0.0150	0.0258	0.0171	0.0232	0.0199	0.0184
Absorbance of cpx (cm^{-1})	4.80	6.90	9.30	7.50	7.50	3.69	6.30	5.00
Thickness of cpx (0.001mm)	95	102	102	99	99	89	97	91
Absorbance normalized to 1 cm (cm^{-1})	505	676	912	758	758	415	649	549
H_2O-cpx (ppm)	214	286	386	321	321	176	275	232
H_2O-melt (wt%)	0.96	1.31	2.57	1.24	1.87	0.76	1.38	1.26

Sample No.				GP-7				
Section No.				1				
Point No.	33	34	34.2	1	2	3	4	5
SiO_2	46.95	47.74	46.92	49.66	47.95	46.90	49.41	47.32
TiO_2	2.89	2.55	3.07	1.69	2.49	3.18	2.34	2.75
Al_2O3	6.80	5.92	6.58	3.55	5.75	6.54	4.04	5.93
Cr_2O3	0.03	0.17	0.01	0.37	0.09	0.05	0.00	0.03
FeO	7.88	7.26	7.45	7.17	7.60	7.73	6.80	7.89
MnO	0.10	0.08	0.08	0.09	0.08	0.08	0.06	0.08
MgO	11.84	12.40	11.61	13.98	12.43	11.85	13.49	12.22
CaO	22.81	23.14	22.92	22.44	22.53	22.74	23.07	22.66
Na_2O	0.49	0.40	0.50	0.40	0.32	0.46	0.35	0.47
K_2O	0.01	0.01	0.00	0.00	0.01	0.01	0.00	0.00
NiO	0.03	0.03	0.00	0.03	0.01	0.00	0.00	0.05
Total	99.82	99.68	99.15	99.38	99.24	99.55	99.57	99.38
Si	1.77	1.79	1.77	1.86	1.81	1.77	1.85	1.79
Ti	0.08	0.07	0.09	0.05	0.07	0.09	0.07	0.08
Al	0.30	0.26	0.29	0.16	0.26	0.29	0.18	0.26
Cr	0.00	0.01	0.00	0.01	0.00	0.00	0.00	0.00
Fe	0.25	0.23	0.24	0.22	0.24	0.24	0.21	0.25
Mn	0.00	0.00	0.00	0.00	0.00	0.00	0.00	0.00
Mg	0.66	0.69	0.65	0.78	0.70	0.67	0.75	0.69
Ca	0.92	0.93	0.93	0.90	0.91	0.92	0.92	0.92
Na	0.04	0.03	0.04	0.03	0.02	0.03	0.03	0.03
K	0.00	0.00	0.00	0.00	0.00	0.00	0.00	0.00
Ni	0.00	0.00	0.00	0.00	0.00	0.00	0.00	0.00
Total	4.02	4.02	4.01	4.02	4.01	4.01	4.01	4.02
Mg#	72.80	75.28	73.53	77.66	74.47	73.20	77.96	73.40
$D^{(cpx\text{-}melt)}_{H_2O}$	0.0275	0.0228	0.0259	0.0148	0.0213	0.0272	0.0159	0.0240
Absorbance of cpx (cm^{-1})	5.11	4.59	5.40	3.46	2.50	4.80	5.90	5.12
Thickness of cpx (0.001mm)	91	91	91	69	86	82	85	85
Absorbance normalized to 1 cm (cm^{-1})	562	504	593	501	291	585	694	602
H_2O-cpx (ppm)	238	213	251	212	123	248	294	255
H_2O-melt (wt%)	0.86	0.94	0.97	1.43	0.58	0.91	1.84	1.06

Sample No. Section No. Point No.	6	7	8	8.2	9	10	11	12
SiO_2	49.54	50.50	49.82	49.94	48.71	50.21	51.44	47.92
TiO_2	2.02	2.00	2.05	2.24	2.45	1.88	1.66	2.56
Al_2O3	3.76	4.13	3.98	4.65	5.09	3.63	3.35	5.91
Cr_2O3	0.15	0.08	0.00	0.08	0.02	0.11	0.18	0.28
FeO	7.61	7.24	7.44	7.68	7.53	7.22	7.38	7.72
MnO	0.09	0.09	0.10	0.08	0.08	0.07	0.12	0.10
MgO	13.25	13.20	13.23	13.14	12.64	13.84	14.02	12.45
CaO	22.49	22.72	22.51	22.45	22.78	22.68	22.07	22.54
Na_2O	0.42	0.38	0.44	0.47	0.48	0.35	0.36	0.50
K_2O	0.01	0.01	0.01	0.00	0.01	0.00	0.01	0.00
NiO	0.06	0.07	0.00	0.02	0.00	0.04	0.00	0.06
Total	99.38	100.41	99.58	100.75	99.79	100.01	100.57	100.02
Si	1.86	1.87	1.86	1.85	1.82	1.87	1.90	1.79
Ti	0.06	0.06	0.06	0.06	0.07	0.05	0.05	0.07
Al	0.17	0.18	0.18	0.20	0.22	0.16	0.15	0.26
Cr	0.00	0.00	0.00	0.00	0.00	0.00	0.01	0.01
Fe	0.24	0.22	0.23	0.24	0.24	0.22	0.23	0.24
Mn	0.00	0.00	0.00	0.00	0.00	0.00	0.00	0.00
Mg	0.74	0.73	0.74	0.72	0.71	0.77	0.77	0.69
Ca	0.91	0.90	0.90	0.89	0.91	0.90	0.87	0.90
Na	0.03	0.03	0.03	0.03	0.03	0.02	0.03	0.04
K	0.00	0.00	0.00	0.00	0.00	0.00	0.00	0.00
Ni	0.00	0.00	0.00	0.00	0.00	0.00	0.00	0.00
Total	4.01	4.00	4.01	4.00	4.01	4.01	3.99	4.02
Mg#	75.64	76.47	76.01	75.31	74.94	77.37	77.21	74.20
$D^{(cpx\text{-}melt)}_{H_2O}$	0.0149	0.0141	0.0147	0.0166	0.0188	0.0142	0.0122	0.0231
Absorbance of cpx (cm^{-1})	6.90	6.80	5.20	4.88	4.60	4.11	6.90	6.80
Thickness of cpx (0.001mm)	90	80	86	86	92	84	94	96
Absorbance normalized to 1 cm (cm^{-1})	767	850	605	567	500	489	734	708
H_2O-cpx (ppm)	324	360	256	240	212	207	311	300
H_2O-melt (wt%)	2.18	2.55	1.74	1.45	1.12	1.46	2.54	1.30

Sample No.								
Section No.								
Point No.	13	13.2	13.3	14	15	16	17	18
SiO_2	49.81	49.74	47.52	48.17	50.10	45.75	47.54	48.56
TiO_2	2.15	2.40	2.95	2.43	1.69	3.83	2.83	2.50
Al_2O3	4.16	4.35	5.93	5.72	3.43	7.39	5.75	4.91
Cr_2O3	0.02	0.04	0.06	0.14	0.13	0.04	0.06	0.02
FeO	7.24	7.55	7.75	7.67	7.19	8.05	7.87	7.36
MnO	0.08	0.03	0.09	0.10	0.13	0.07	0.12	0.11
MgO	13.04	13.00	12.28	12.58	13.72	11.30	12.03	12.65
CaO	22.70	22.88	22.88	22.42	22.86	22.74	22.50	22.71
Na_2O	0.51	0.50	0.49	0.45	0.35	0.56	0.52	0.44
K_2O	0.00	0.02	0.02	0.01	0.00	0.00	0.00	0.00
NiO	0.02	0.04	0.03	0.02	0.02	0.02	0.06	0.00
Total	99.74	100.56	99.98	99.70	99.64	99.76	99.28	99.25
Si	1.86	1.85	1.78	1.81	1.87	1.73	1.80	1.83
Ti	0.06	0.07	0.08	0.07	0.05	0.11	0.08	0.07
Al	0.18	0.19	0.26	0.25	0.15	0.33	0.26	0.22
Cr	0.00	0.00	0.00	0.00	0.00	0.00	0.00	0.00
Fe	0.23	0.23	0.24	0.24	0.23	0.25	0.25	0.23
Mn	0.00	0.00	0.00	0.00	0.00	0.00	0.00	0.00
Mg	0.73	0.72	0.69	0.70	0.77	0.64	0.68	0.71
Ca	0.91	0.91	0.92	0.90	0.92	0.92	0.91	0.92
Na	0.04	0.04	0.04	0.03	0.03	0.04	0.04	0.03
K	0.00	0.00	0.00	0.00	0.00	0.00	0.00	0.00
Ni	0.00	0.00	0.00	0.00	0.00	0.00	0.00	0.00
Total	4.01	4.01	4.02	4.01	4.01	4.02	4.01	4.01
Mg#	76.27	75.44	73.86	74.51	77.27	71.46	73.15	75.39
$D^{(cpx\text{-}melt)}_{H_2O}$	0.0150	0.0163	0.0245	0.0214	0.0136	0.0352	0.0228	0.0184
Absorbance of cpx (cm^{-1})	7.80	5.85	6.69	3.59	5.63	7.10	4.80	4.30
Thickness of cpx (0.001mm)	95	95	95	98	87	92	88	84
Absorbance normalized to 1 cm (cm^{-1})	821	616	704	366	647	772	545	512
H_2O-cpx (ppm)	347	261	298	155	274	327	231	217
H_2O-melt (wt%)	2.32	1.60	1.22	0.72	2.02	0.93	1.01	1.18

Sample No. Section No. Point No.	18.2	18.3	19	20	21	22	23	24
SiO_2	48.19	48.51	48.94	49.40	51.07	49.87	50.07	50.78
TiO_2	2.50	2.37	2.33	1.98	1.49	2.01	1.22	2.03
Al_2O3	5.22	5.31	4.80	4.44	3.19	3.83	4.25	3.50
Cr_2O3	0.06	0.08	0.00	0.08	0.16	0.10	0.04	0.21
FeO	7.44	7.41	7.43	7.48	6.84	7.02	7.74	6.54
MnO	0.08	0.11	0.09	0.09	0.11	0.09	0.10	0.10
MgO	12.58	12.75	12.98	12.55	14.16	13.30	13.54	13.92
CaO	22.72	22.96	22.63	22.75	22.73	22.40	21.86	23.22
Na_2O	0.51	0.45	0.47	0.41	0.33	0.47	0.37	0.36
K_2O	0.00	0.01	0.01	0.00	0.00	0.00	0.00	0.00
NiO	0.04	0.06	0.01	0.03	0.01	0.02	0.00	0.06
Total	99.34	100.01	99.68	99.22	100.07	99.12	99.18	100.72
Si	1.81	1.81	1.83	1.86	1.89	1.87	1.88	1.87
Ti	0.07	0.07	0.07	0.06	0.04	0.06	0.03	0.06
Al	0.23	0.23	0.21	0.20	0.14	0.17	0.19	0.15
Cr	0.00	0.00	0.00	0.00	0.00	0.00	0.00	0.01
Fe	0.23	0.23	0.23	0.24	0.21	0.22	0.24	0.20
Mn	0.00	0.00	0.00	0.00	0.00	0.00	0.00	0.00
Mg	0.71	0.71	0.72	0.70	0.78	0.74	0.76	0.77
Ca	0.92	0.92	0.91	0.92	0.90	0.90	0.88	0.92
Na	0.04	0.03	0.03	0.03	0.02	0.03	0.03	0.03
K	0.00	0.00	0.00	0.00	0.00	0.00	0.00	0.00
Ni	0.00	0.00	0.00	0.00	0.00	0.00	0.00	0.00
Total	4.02	4.02	4.01	4.00	4.00	4.00	4.01	4.00
Mg#	75.10	75.40	75.71	74.96	78.67	77.15	75.72	79.14
$D^{(cpx\text{-}melt)}_{H_2O}$	0.0200	0.0200	0.0179	0.0151	0.0121	0.0141	0.0139	0.0136
Absorbance of cpx (cm^{-1})	4.60	4.80	4.22	5.60	3.52	3.75	4.11	3.24
Thickness of cpx (0.001mm)	84	84	77	84	82	78	74	67
Absorbance normalized to 1 cm (cm^{-1})	548	571	548	667	429	481	555	484
H_2O-cpx (ppm)	232	242	232	282	182	203	235	205
H_2O-melt (wt%)	1.16	1.21	1.29	1.86	1.50	1.45	1.69	1.50

Sample No. Section No. Point No.	25	26	27	28	29	29.2	30	31
SiO_2	50.40	49.03	46.76	48.08	48.27	49.89	47.23	47.39
TiO_2	1.74	2.48	3.24	2.89	2.61	2.17	2.99	2.84
Al_2O3	3.34	5.00	6.46	5.89	5.21	3.94	5.84	5.54
Cr_2O3	0.25	0.04	0.03	0.09	0.04	0.00	0.14	0.13
FeO	7.19	7.05	7.63	7.68	7.21	7.03	8.12	8.80
MnO	0.06	0.09	0.14	0.07	0.09	0.00	0.11	0.13
MgO	13.72	12.85	11.77	12.15	12.85	12.98	11.65	11.75
CaO	22.17	22.84	22.78	22.84	22.81	22.98	22.63	22.40
Na_2O	0.47	0.46	0.48	0.45	0.39	0.47	0.48	0.62
K_2O	0.03	0.03	0.00	0.01	0.01	0.02	0.00	0.00
NiO	0.03	0.00	0.05	0.03	0.02	0.00	0.00	0.04
Total	99.40	99.88	99.34	100.17	99.51	99.47	99.19	99.63
Si	1.89	1.83	1.77	1.80	1.81	1.87	1.79	1.79
Ti	0.05	0.07	0.09	0.08	0.07	0.06	0.09	0.08
Al	0.15	0.22	0.29	0.26	0.23	0.17	0.26	0.25
Cr	0.01	0.00	0.00	0.00	0.00	0.00	0.00	0.00
Fe	0.22	0.22	0.24	0.24	0.23	0.22	0.26	0.28
Mn	0.00	0.00	0.00	0.00	0.00	0.00	0.00	0.00
Mg	0.77	0.71	0.66	0.68	0.72	0.72	0.66	0.66
Ca	0.89	0.91	0.92	0.91	0.92	0.92	0.92	0.91
Na	0.03	0.03	0.03	0.03	0.03	0.03	0.04	0.05
K	0.00	0.00	0.00	0.00	0.00	0.00	0.00	0.00
Ni	0.00	0.00	0.00	0.00	0.00	0.00	0.00	0.00
Total	4.01	4.01	4.01	4.01	4.01	4.00	4.01	4.02
Mg#	77.29	76.46	73.34	73.83	76.06	76.70	71.88	70.42
$D^{(cpx\text{-}melt)}_{H_2O}$	0.0130	0.0181	0.0272	0.0225	0.0203	0.0142	0.0236	0.0233
Absorbance of cpx (cm^{-1})	4.27	5.28	3.88	4.00	4.47	3.48	3.67	3.08
Thickness of cpx (0.001mm)	75	75	66	74	77	77	64	53
Absorbance normalized to 1 cm (cm^{-1})	569	704	588	541	581	452	573	581
H_2O-cpx (ppm)	241	298	249	229	246	191	243	246
H_2O-melt (wt%)	1.85	1.64	0.91	1.02	1.21	1.35	1.03	1.06

Sample No.		
Section No.		
Point No.	31.2	32
SiO_2	49.41	48.32
TiO_2	2.29	2.90
Al_2O3	4.49	5.43
Cr_2O3	0.14	0.05
FeO	7.55	7.86
MnO	0.07	0.09
MgO	12.89	12.11
CaO	22.15	22.63
Na_2O	0.54	0.55
K_2O	0.02	0.01
NiO	0.01	0.04
Total	99.56	99.98
Si	1.85	1.81
Ti	0.06	0.08
Al	0.20	0.24
Cr	0.00	0.00
Fe	0.24	0.25
Mn	0.00	0.00
Mg	0.72	0.68
Ca	0.89	0.91
Na	0.04	0.04
K	0.00	0.00
Ni	0.00	0.00
Total	4.00	4.01
Mg#	75.26	73.32
$D^{(cpx\text{-}melt)}_{H_2O}$	0.0163	0.0208
Absorbance of cpx (cm^{-1})	4.19	2.46
Thickness of cpx (0.001mm)	53	49
Absorbance normalized to 1 cm (cm^{-1})	791	502
H_2O-cpx (ppm)	335	212
H_2O-melt (wt%)	2.05	1.02

Sample No.	SC-1							
Section No.	1							
Point No.	1	2	2.1	3	4	5	5.2	6
SiO_2	52.03	52.01	51.41	48.92	51.73	48.13	51.61	50.21
TiO_2	0.91	0.93	1.09	1.74	1.01	1.96	1.14	1.31
Al_2O3	3.03	2.76	2.99	5.18	3.09	5.57	2.96	5.56
Cr_2O3	0.08	0.17	0.08	0.18	0.02	0.10	0.24	0.07
FeO	7.36	6.52	6.70	7.71	7.81	7.79	6.34	8.71
MnO	0.12	0.13	0.14	0.13	0.14	0.11	0.05	0.12
MgO	15.15	15.43	14.85	13.27	14.55	13.12	14.75	14.92
CaO	20.51	21.60	21.27	21.68	20.59	21.92	21.76	18.21
Na_2O	0.41	0.38	0.39	0.50	0.35	0.49	0.40	0.59
K_2O	0.04	0.00	0.00	0.00	0.00	0.00	0.00	0.00
NiO	0.01	0.03	0.02	0.00	0.03	0.00	0.00	0.03
Total	99.65	99.95	98.94	99.31	99.32	99.19	99.26	99.74
Si	1.93	1.92	1.92	1.84	1.93	1.81	1.92	1.86
Ti	0.03	0.03	0.03	0.05	0.03	0.06	0.03	0.04
Al	0.13	0.12	0.13	0.23	0.14	0.25	0.13	0.24
Cr	0.00	0.01	0.00	0.01	0.00	0.00	0.01	0.00
Fe	0.23	0.20	0.21	0.24	0.24	0.25	0.20	0.27
Mn	0.00	0.00	0.00	0.00	0.00	0.00	0.00	0.00
Mg	0.84	0.85	0.83	0.74	0.81	0.74	0.82	0.82
Ca	0.81	0.85	0.85	0.87	0.82	0.88	0.87	0.72
Na	0.03	0.03	0.03	0.04	0.03	0.04	0.03	0.04
K	0.00	0.00	0.00	0.00	0.00	0.00	0.00	0.00
Ni	0.00	0.00	0.00	0.00	0.00	0.00	0.00	0.00
Total	4.00	4.01	4.00	4.02	3.99	4.02	4.00	4.00
Mg#	78.59	80.83	79.82	75.42	76.85	75.02	80.57	75.33
$D^{(cpx\text{-}melt)}_{H_2O}$	0.0108	0.0108	0.0110	0.0182	0.0107	0.0209	0.0108	0.0182
Absorbance of cpx (cm^{-1})	0.90	0.36	1.20	0.91	0.69	1.57	0.82	0.69
Thickness of cpx (0.001mm)	87	85	85	90	90	102	102	108
Absorbance normalized to 1 cm (cm^{-1})	103	42	141	101	77	154	80	64
H_2O-cpx (ppm)	44	18	60	43	32	65	34	27
H_2O-melt (wt%)	0.41	0.17	0.55	0.23	0.30	0.31	0.32	0.15

Sample No. Section No. Point No.	6.2	7	8	9	10	11	12	12.1
SiO_2	51.12	48.76	51.22	50.52	51.46	50.56	50.59	51.33
TiO_2	1.36	1.74	1.23	1.53	1.18	1.45	1.44	1.11
Al_2O3	3.60	5.45	3.40	5.17	2.95	3.20	3.48	3.13
Cr_2O3	0.02	0.08	0.24	0.37	0.15	0.00	0.00	0.11
FeO	7.89	8.06	6.68	6.74	6.71	8.10	7.71	7.63
MnO	0.10	0.12	0.16	0.07	0.11	0.13	0.12	0.13
MgO	14.00	13.65	14.37	14.08	14.84	13.78	13.64	14.71
CaO	21.36	21.07	22.60	21.46	21.71	21.33	21.78	20.70
Na_2O	0.41	0.54	0.37	0.50	0.34	0.31	0.41	0.44
K_2O	0.00	0.00	0.01	0.00	0.00	0.00	0.00	0.00
NiO	0.01	0.04	0.03	0.00	0.06	0.07	0.00	0.00
Total	99.88	99.51	100.30	100.44	99.50	98.93	99.17	99.29
Si	1.90	1.83	1.89	1.86	1.91	1.90	1.90	1.91
Ti	0.04	0.05	0.03	0.04	0.03	0.04	0.04	0.03
Al	0.16	0.24	0.15	0.22	0.13	0.14	0.15	0.14
Cr	0.00	0.00	0.01	0.01	0.00	0.00	0.00	0.00
Fe	0.24	0.25	0.21	0.21	0.21	0.25	0.24	0.24
Mn	0.00	0.00	0.01	0.00	0.00	0.00	0.00	0.00
Mg	0.78	0.76	0.79	0.77	0.82	0.77	0.76	0.82
Ca	0.85	0.85	0.89	0.85	0.86	0.86	0.87	0.83
Na	0.03	0.04	0.03	0.04	0.02	0.02	0.03	0.03
K	0.00	0.00	0.00	0.00	0.00	0.00	0.00	0.00
Ni	0.00	0.00	0.00	0.00	0.00	0.00	0.00	0.00
Total	4.00	4.02	4.01	4.00	4.00	4.00	4.00	4.00
Mg#	76.00	75.11	79.31	78.83	79.77	75.21	75.92	77.45
$D^{(cpx\text{-}melt)}_{H_2O}$	0.0124	0.0199	0.0122	0.0161	0.0112	0.0121	0.0123	0.0116
Absorbance of cpx (cm^{-1})	1.12	0.46	0.47	1.31	1.77	0.34	0.50	0.41
Thickness of cpx (0.001mm)	108	997	96	88	88	96	87	87
Absorbance normalized to 1 cm (cm^{-1})	104	5	49	149	201	35	57	47
H_2O-cpx (ppm)	44	2	21	63	85	15	24	20
H_2O-melt (wt%)	0.35	0.01	0.17	0.39	0.76	0.12	0.20	0.17

Sample No.								
Section No.								
Point No.	12.2	12.3	13	13.2	14	14.1	14.2	15
SiO_2	50.20	51.74	51.87	50.97	48.79	51.24	48.71	51.03
TiO_2	1.48	1.12	0.92	1.11	1.99	0.70	1.59	1.55
Al_2O3	4.01	3.01	2.96	3.33	5.95	4.56	5.67	4.97
Cr_2O3	0.04	0.14	0.10	0.06	0.13	0.20	0.10	0.31
FeO	7.73	6.54	6.59	7.11	7.93	7.44	7.99	6.79
MnO	0.15	0.08	0.10	0.13	0.08	0.13	0.10	0.10
MgO	13.45	15.23	14.83	14.49	12.79	15.36	13.19	14.27
CaO	21.78	21.67	21.40	21.41	21.19	18.96	21.02	21.51
Na_2O	0.42	0.40	0.34	0.43	0.48	0.64	0.55	0.55
K_2O	0.01	0.00	0.00	0.01	0.01	0.00	0.00	0.00
NiO	0.01	0.00	0.03	0.02	0.02	0.04	0.03	0.09
Total	99.29	99.93	99.14	99.07	99.34	99.26	98.95	101.17
Si	1.88	1.91	1.93	1.90	1.83	1.90	1.83	1.86
Ti	0.04	0.03	0.03	0.03	0.06	0.02	0.04	0.04
Al	0.18	0.13	0.13	0.15	0.26	0.20	0.25	0.21
Cr	0.00	0.00	0.00	0.00	0.00	0.01	0.00	0.01
Fe	0.24	0.20	0.20	0.22	0.25	0.23	0.25	0.21
Mn	0.00	0.00	0.00	0.00	0.00	0.00	0.00	0.00
Mg	0.75	0.84	0.82	0.81	0.71	0.85	0.74	0.78
Ca	0.87	0.86	0.85	0.86	0.85	0.75	0.85	0.84
Na	0.03	0.03	0.02	0.03	0.03	0.05	0.04	0.04
K	0.00	0.00	0.00	0.00	0.00	0.00	0.00	0.00
Ni	0.00	0.00	0.00	0.00	0.00	0.00	0.00	0.00
Total	4.00	4.01	3.99	4.01	4.00	4.00	4.02	4.00
Mg#	75.63	80.59	80.05	78.43	74.19	78.63	74.65	78.94
$D^{(cpx\text{-}melt)}_{H_2O}$	0.0136	0.0114	0.0102	0.0119	0.0196	0.0138	0.0190	0.0156
Absorbance of cpx (cm^{-1})	0.92	0.95	0.50	0.44	2.30	2.70	2.50	1.70
Thickness of cpx (0.001mm)	87	87	108	108	111	111	111	99
Absorbance normalized to 1 cm (cm^{-1})	106	109	46	41	207	243	225	172
H_2O-cpx (ppm)	45	46	20	17	88	103	95	73
H_2O-melt (wt%)	0.33	0.41	0.19	0.15	0.45	0.75	0.50	0.47

Sample No. Section No. Point No.	16	17	18	18.2	19	20	21	22
SiO_2	49.81	51.39	50.62	49.44	48.08	49.01	51.72	51.11
TiO_2	1.36	0.72	1.13	1.73	1.92	1.33	1.15	1.39
Al_2O3	5.54	4.33	4.79	4.97	5.65	6.22	3.57	4.37
Cr_2O3	0.12	0.25	0.13	0.13	0.01	0.07	0.03	0.12
FeO	8.08	7.81	8.07	7.33	8.10	8.41	7.64	7.47
MnO	0.09	0.08	0.15	0.13	0.08	0.11	0.12	0.12
MgO	14.06	16.22	15.39	13.17	12.64	13.70	14.06	14.57
CaO	19.98	17.64	18.17	21.98	21.93	20.28	21.27	21.03
Na_2O	0.54	0.59	0.63	0.43	0.57	0.57	0.43	0.37
K_2O	0.00	0.00	0.00	0.00	0.00	0.01	0.00	0.00
NiO	0.04	0.04	0.06	0.04	0.03	0.00	0.03	0.05
Total	99.62	99.08	99.15	99.34	99.02	99.71	100.01	100.60
Si	1.85	1.90	1.88	1.85	1.82	1.83	1.91	1.88
Ti	0.04	0.02	0.03	0.05	0.05	0.04	0.03	0.04
Al	0.24	0.19	0.21	0.22	0.25	0.27	0.16	0.19
Cr	0.00	0.01	0.00	0.00	0.00	0.00	0.00	0.00
Fe	0.25	0.24	0.25	0.23	0.26	0.26	0.24	0.23
Mn	0.00	0.00	0.00	0.00	0.00	0.00	0.00	0.00
Mg	0.78	0.90	0.85	0.73	0.71	0.76	0.78	0.80
Ca	0.80	0.70	0.72	0.88	0.89	0.81	0.84	0.83
Na	0.04	0.04	0.05	0.03	0.04	0.04	0.03	0.03
K	0.00	0.00	0.00	0.00	0.00	0.00	0.00	0.00
Ni	0.00	0.00	0.00	0.00	0.00	0.00	0.00	0.00
Total	4.01	4.00	4.00	4.00	4.02	4.02	3.99	4.00
Mg#	75.62	78.75	77.28	76.22	73.57	74.38	76.65	77.66
$D^{(cpx\text{-}melt)}_{H_2O}$	0.0177	0.0141	0.0158	0.0164	0.0203	0.0205	0.0113	0.0143
Absorbance of cpx (cm^{-1})	1.20	1.70	1.58	0.88	0.52	0.89	0.70	0.83
Thickness of cpx (0.001mm)	101	98	111	111	116	119	127	128
Absorbance normalized to 1 cm (cm^{-1})	119	173	142	79	45	75	55	65
H_2O-cpx (ppm)	50	73	60	34	19	32	23	27
H_2O-melt (wt%)	0.28	0.52	0.38	0.20	0.09	0.15	0.21	0.19

Sample No. Section No. Point No.	23	24	25	26	27	28	29	30
SiO_2	52.23	51.33	52.46	52.03	48.97	51.27	49.56	51.91
TiO_2	1.09	1.10	0.85	0.99	1.61	1.29	1.69	1.16
Al_2O3	3.01	3.03	2.90	2.73	5.96	3.28	4.73	3.07
Cr_2O3	0.13	0.18	0.11	0.16	0.09	0.04	0.09	0.11
FeO	7.10	6.59	7.16	6.66	8.17	7.76	7.51	7.47
MnO	0.17	0.07	0.15	0.13	0.08	0.09	0.12	0.10
MgO	15.02	14.58	15.14	14.98	13.38	14.16	13.63	14.76
CaO	21.91	21.85	20.67	21.69	20.92	21.71	21.94	21.59
Na_2O	0.30	0.41	0.44	0.38	0.57	0.34	0.45	0.37
K_2O	0.00	0.00	0.00	0.00	0.00	0.00	0.01	0.00
NiO	0.00	0.03	0.00	0.00	0.02	0.08	0.00	0.02
Total	100.96	99.16	99.88	99.75	99.76	100.02	99.72	100.56
Si	1.91	1.91	1.93	1.92	1.83	1.90	1.85	1.91
Ti	0.03	0.03	0.02	0.03	0.05	0.04	0.05	0.03
Al	0.13	0.13	0.13	0.12	0.26	0.14	0.21	0.13
Cr	0.00	0.01	0.00	0.00	0.00	0.00	0.00	0.00
Fe	0.22	0.21	0.22	0.21	0.25	0.24	0.23	0.23
Mn	0.01	0.00	0.00	0.00	0.00	0.00	0.00	0.00
Mg	0.82	0.81	0.83	0.83	0.74	0.78	0.76	0.81
Ca	0.86	0.87	0.82	0.86	0.84	0.86	0.88	0.85
Na	0.02	0.03	0.03	0.03	0.04	0.02	0.03	0.03
K	0.00	0.00	0.00	0.00	0.00	0.00	0.00	0.00
Ni	0.00	0.00	0.00	0.00	0.00	0.00	0.00	0.00
Total	4.00	4.00	3.99	4.00	4.02	4.00	4.01	4.00
Mg#	79.04	79.78	79.04	80.04	74.49	76.48	76.40	77.89
$D^{(cpx\text{-}melt)}_{H_2O}$	0.0112	0.0110	0.0101	0.0104	0.0200	0.0119	0.0166	0.0114
Absorbance of cpx (cm^{-1})	0.82	0.84	2.15	2.33	1.80	1.24	1.30	0.54
Thickness of cpx (0.001mm)	128	131	132	130	128	121	124	129
Absorbance normalized to 1 cm (cm^{-1})	64	64	163	179	141	102	105	42
H_2O-cpx (ppm)	27	27	69	76	60	43	44	18
H_2O-melt (wt%)	0.24	0.25	0.68	0.73	0.30	0.37	0.27	0.16

Sample No.							
Section No.							
Point No.	31	32	33	34	35	36	37
SiO_2	49.67	52.20	51.02	48.52	49.17	52.07	51.46
TiO_2	1.76	1.12	1.30	1.76	1.85	0.93	1.29
Al_2O3	4.87	2.95	4.86	6.09	5.40	3.48	3.92
Cr_2O3	0.15	0.11	0.16	0.05	0.12	0.08	0.39
FeO	7.80	6.82	7.04	8.04	7.90	7.62	6.51
MnO	0.08	0.06	0.08	0.09	0.10	0.13	0.10
MgO	12.76	15.34	14.41	13.20	12.85	15.50	14.17
CaO	21.98	21.69	21.06	20.75	22.33	19.84	21.91
Na_2O	0.40	0.37	0.54	0.60	0.45	0.48	0.42
K_2O	0.00	0.00	0.00	0.00	0.00	0.00	0.00
NiO	0.00	0.00	0.01	0.06	0.07	0.00	0.11
Total	99.46	100.67	100.46	99.16	100.24	100.13	100.27
Si	1.86	1.91	1.87	1.82	1.83	1.92	1.90
Ti	0.05	0.03	0.04	0.05	0.05	0.03	0.04
Al	0.21	0.13	0.21	0.27	0.24	0.15	0.17
Cr	0.00	0.00	0.00	0.00	0.00	0.00	0.01
Fe	0.24	0.21	0.22	0.25	0.25	0.23	0.20
Mn	0.00	0.00	0.00	0.00	0.00	0.00	0.00
Mg	0.71	0.84	0.79	0.74	0.71	0.85	0.78
Ca	0.88	0.85	0.83	0.83	0.89	0.78	0.86
Na	0.03	0.03	0.04	0.04	0.03	0.03	0.03
K	0.00	0.00	0.00	0.00	0.00	0.00	0.00
Ni	0.00	0.00	0.00	0.00	0.00	0.00	0.00
Total	4.00	4.00	4.00	4.02	4.01	4.00	3.99
Mg#	74.48	80.03	78.50	74.54	74.36	78.39	79.52
$D^{(cpx\text{-}melt)}_{H_2O}$	0.0155	0.0112	0.0148	0.0208	0.0184	0.0119	0.0124
Absorbance of cpx (cm^{-1})	1.87	0.60	0.96	1.40	1.07	0.94	0.97
Thickness of cpx (0.001mm)	127	127	124	100	99	126	126
Absorbance normalized to 1 cm (cm^{-1})	147	47	77	140	108	75	77
H_2O-cpx (ppm)	62	20	33	59	46	32	33
H_2O-melt (wt%)	0.40	0.18	0.22	0.28	0.25	0.27	0.26

Sample No.	SC-2							
Section No.								
Point No.	1	2	3	4	5	6	7	8
SiO_2	52.57	51.90	48.64	52.08	51.94	51.75	51.53	49.94
TiO_2	0.76	1.12	1.76	0.99	0.94	0.98	1.06	1.35
Al_2O3	2.72	2.81	5.10	2.69	2.74	3.02	2.83	4.08
Cr_2O3	0.19	0.22	0.12	0.13	0.21	0.12	0.04	0.33
FeO	6.99	6.46	7.52	6.49	6.53	6.72	6.64	6.52
MnO	0.16	0.09	0.08	0.07	0.08	0.09	0.15	0.13
MgO	15.56	15.01	13.41	14.96	15.28	15.09	15.33	13.96
CaO	20.60	21.71	21.92	21.70	21.68	21.68	21.03	22.18
Na_2O	0.41	0.31	0.44	0.46	0.29	0.43	0.34	0.44
K_2O	0.00	0.00	0.01	0.00	0.00	0.00	0.01	0.02
NiO	0.10	0.05	0.08	0.00	0.03	0.05	0.05	0.07
Total	100.06	99.69	99.07	99.58	99.72	99.93	99.01	99.03
Si	1.93	1.92	1.83	1.93	1.92	1.91	1.92	1.87
Ti	0.02	0.03	0.05	0.03	0.03	0.03	0.03	0.04
Al	0.12	0.12	0.23	0.12	0.12	0.13	0.12	0.18
Cr	0.01	0.01	0.00	0.00	0.01	0.00	0.00	0.01
Fe	0.21	0.20	0.24	0.20	0.20	0.21	0.21	0.20
Mn	0.01	0.00	0.00	0.00	0.00	0.00	0.00	0.00
Mg	0.85	0.83	0.75	0.83	0.84	0.83	0.85	0.78
Ca	0.81	0.86	0.88	0.86	0.86	0.86	0.84	0.89
Na	0.03	0.02	0.03	0.03	0.02	0.03	0.02	0.03
K	0.00	0.00	0.00	0.00	0.00	0.00	0.00	0.00
Ni	0.00	0.00	0.00	0.00	0.00	0.00	0.00	0.00
Total	4.00	4.00	4.02	4.00	4.00	4.01	4.00	4.01
Mg#	79.88	80.57	76.06	80.44	80.66	80.00	80.44	79.23
$D^{(cpx\text{-}melt)}_{H_2O}$	0.0102	0.0107	0.0186	0.0101	0.0106	0.0112	0.0110	0.0142
Absorbance of cpx (cm^{-1})	1.41	0.47	1.28	0.82	0.85	1.02	0.45	1.73
Thickness of cpx (0.001mm)	85	64	64	92	96	96	96	95
Absorbance normalized to 1 cm (cm^{-1})	166	73	200	90	89	107	47	182
H_2O-cpx (ppm)	70	31	84	38	38	45	20	77
H_2O-melt (wt%)	0.69	0.29	0.45	0.38	0.35	0.40	0.18	0.54

Sample No. Section No. Point No.	9	10	11	12	13	14	15	16
SiO_2	51.66	50.57	50.92	51.36	48.92	51.10	52.16	51.90
TiO_2	0.76	1.29	1.28	0.99	1.79	1.16	0.93	0.81
Al_2O3	4.52	3.65	3.47	3.32	5.72	2.99	3.36	4.18
Cr_2O3	0.20	0.08	0.08	0.04	0.09	0.07	0.06	0.19
FeO	7.59	8.15	8.28	7.82	7.75	7.30	8.50	7.93
MnO	0.13	0.12	0.13	0.19	0.11	0.12	0.07	0.15
MgO	16.45	14.14	14.26	15.34	13.09	14.56	15.47	15.48
CaO	17.27	21.34	20.60	19.88	21.28	21.49	19.52	18.70
Na_2O	0.59	0.43	0.41	0.47	0.55	0.42	0.48	0.57
K_2O	0.00	0.01	0.00	0.00	0.00	0.00	0.00	0.00
NiO	0.01	0.07	0.03	0.02	0.10	0.07	0.02	0.10
Total	99.16	99.84	99.45	99.44	99.38	99.27	100.57	100.01
Si	1.90	1.89	1.90	1.91	1.83	1.91	1.92	1.91
Ti	0.02	0.04	0.04	0.03	0.05	0.03	0.03	0.02
Al	0.20	0.16	0.15	0.15	0.25	0.13	0.15	0.18
Cr	0.01	0.00	0.00	0.00	0.00	0.00	0.00	0.01
Fe	0.23	0.25	0.26	0.24	0.24	0.23	0.26	0.24
Mn	0.00	0.00	0.00	0.01	0.00	0.00	0.00	0.00
Mg	0.90	0.79	0.79	0.85	0.73	0.81	0.85	0.85
Ca	0.68	0.85	0.82	0.79	0.85	0.86	0.77	0.74
Na	0.04	0.03	0.03	0.03	0.04	0.03	0.03	0.04
K	0.00	0.00	0.00	0.00	0.00	0.00	0.00	0.00
Ni	0.00	0.00	0.00	0.00	0.00	0.00	0.00	0.00
Total	3.99	4.01	4.00	4.01	4.01	4.01	4.00	4.00
Mg#	79.45	75.58	75.43	77.76	75.07	78.06	76.43	77.69
$D^{(cpx\text{-}melt)}_{H_2O}$	0.0141	0.0135	0.0126	0.0123	0.0191	0.0116	0.0120	0.0130
Absorbance of cpx (cm^{-1})	2.39	1.33	0.80	0.67	1.60	1.01	0.48	0.57
Thickness of cpx (0.001mm)	94	67	92	78	78	92	92	94
Absorbance normalized to 1 cm (cm^{-1})	255	119	72	205	205	110	52	61
H_2O-cpx (ppm)	108	50	31	87	87	46	22	26
H_2O-melt (wt%)	0.76	0.37	0.24	0.70	0.45	0.40	0.18	0.20

Sample No.								
Section No.								
Point No.	17	18	19	20	21	21.2	22	23
SiO_2	51.62	51.44	52.53	49.54	51.88	50.74	51.41	49.67
TiO_2	0.97	1.25	1.10	1.72	1.20	1.30	1.03	1.82
Al_2O3	3.32	2.93	3.14	4.66	2.85	3.38	3.26	5.39
Cr_2O3	0.07	0.14	0.10	0.16	0.11	0.10	0.19	0.15
FeO	7.69	7.10	7.20	7.72	7.12	7.70	6.82	7.58
MnO	0.16	0.17	0.12	0.11	0.16	0.14	0.12	0.08
MgO	14.14	14.83	14.71	13.40	15.10	14.21	14.89	13.53
CaO	20.62	21.70	21.74	21.96	21.58	21.41	21.69	21.72
Na_2O	0.43	0.42	0.36	0.36	0.41	0.43	0.39	0.52
K_2O	0.00	0.00	0.00	0.00	0.00	0.00	0.00	0.00
NiO	0.02	0.01	0.00	0.00	0.00	0.00	0.00	0.01
Total	99.04	99.99	100.99	99.62	100.41	99.42	99.80	100.48
Si	1.93	1.91	1.92	1.85	1.91	1.90	1.90	1.84
Ti	0.03	0.03	0.03	0.05	0.03	0.04	0.03	0.05
Al	0.15	0.13	0.14	0.21	0.12	0.15	0.14	0.24
Cr	0.00	0.00	0.00	0.00	0.00	0.00	0.01	0.00
Fe	0.24	0.22	0.22	0.24	0.22	0.24	0.21	0.23
Mn	0.00	0.01	0.00	0.00	0.00	0.00	0.00	0.00
Mg	0.79	0.82	0.80	0.75	0.83	0.79	0.82	0.75
Ca	0.82	0.86	0.85	0.88	0.85	0.86	0.86	0.86
Na	0.03	0.03	0.03	0.03	0.03	0.03	0.03	0.04
K	0.00	0.00	0.00	0.00	0.00	0.00	0.00	0.00
Ni	0.00	0.00	0.00	0.00	0.00	0.00	0.00	0.00
Total	3.99	4.01	3.99	4.01	4.01	4.01	4.01	4.01
Mg#	76.62	78.84	78.46	75.57	79.08	76.69	79.57	76.10
$D^{(cpx\text{-}melt)}_{H_2O}$	0.0106	0.0117	0.0107	0.0163	0.0114	0.0126	0.0118	0.0182
Absorbance of cpx (cm^{-1})	1.62	1.16	1.53	0.93	0.53	1.09	1.60	1.86
Thickness of cpx (0.001mm)	78	73	80	84	92	92	92	92
Absorbance normalized to 1 cm (cm^{-1})	208	159	191	111	58	119	173	202
H_2O-cpx (ppm)	88	67	81	47	24	50	73	86
H_2O-melt (wt%)	0.83	0.57	0.76	0.29	0.22	0.40	0.62	0.47

Sample No. Section No. Point No.	24	25	26	27	28	29	30	30.2
SiO_2	51.85	52.31	51.70	51.67	50.80	50.46	51.43	51.48
TiO_2	1.00	0.92	1.07	0.75	1.32	1.44	1.03	1.07
Al_2O3	2.84	2.80	2.94	3.40	3.45	4.76	2.57	2.62
Cr_2O3	0.10	0.16	0.15	0.14	0.15	0.14	0.19	0.18
FeO	6.68	6.61	6.51	7.52	7.37	7.08	6.50	6.55
MnO	0.12	0.09	0.10	0.12	0.12	0.06	0.14	0.09
MgO	14.47	15.43	14.94	13.96	14.37	13.55	15.26	15.10
CaO	21.45	21.32	21.57	21.29	22.27	21.59	21.94	22.00
Na_2O	0.38	0.38	0.41	0.38	0.38	0.53	0.36	0.31
K_2O	0.01	0.01	0.00	0.00	0.01	0.00	0.00	0.01
NiO	0.03	0.03	0.04	0.01	0.05	0.02	0.07	0.00
Total	98.92	100.05	99.43	99.23	100.29	99.64	99.47	99.41
Si	1.93	1.93	1.92	1.93	1.88	1.87	1.91	1.91
Ti	0.03	0.03	0.03	0.02	0.04	0.04	0.03	0.03
Al	0.12	0.12	0.13	0.15	0.15	0.21	0.11	0.11
Cr	0.00	0.00	0.00	0.00	0.00	0.00	0.01	0.01
Fe	0.21	0.20	0.20	0.23	0.23	0.22	0.20	0.20
Mn	0.00	0.00	0.00	0.00	0.00	0.00	0.00	0.00
Mg	0.80	0.85	0.83	0.78	0.79	0.75	0.85	0.84
Ca	0.86	0.84	0.86	0.85	0.88	0.86	0.87	0.88
Na	0.03	0.03	0.03	0.03	0.03	0.04	0.03	0.02
K	0.00	0.00	0.00	0.00	0.00	0.00	0.00	0.00
Ni	0.00	0.00	0.00	0.00	0.00	0.00	0.00	0.00
Total	3.99	4.00	4.00	3.99	4.02	4.00	4.01	4.01
Mg#	79.42	80.62	80.35	76.80	77.65	77.33	80.71	80.42
$D^{(cpx\text{-}melt)}_{H_2O}$	0.0099	0.0105	0.0108	0.0104	0.0132	0.0143	0.0111	0.0109
Absorbance of cpx (cm^{-1})	0.69	0.53	0.36	0.63	0.48	1.22	0.33	0.36
Thickness of cpx (0.001mm)	90	90	90	96	96	76	99	99
Absorbance normalized to 1 cm (cm^{-1})	77	59	40	65	50	161	34	36
H_2O-cpx (ppm)	33	25	17	28	21	68	14	15
H_2O-melt (wt%)	0.33	0.24	0.16	0.26	0.16	0.48	0.13	0.14

Sample No.								
Section No.								
Point No.	36	37	38	39	40	41	42	43
SiO_2	52.17	49.95	50.07	49.39	52.38	50.21	47.56	51.88
TiO_2	0.74	1.34	1.42	1.61	0.82	1.48	2.33	0.81
Al_2O3	3.73	4.06	4.94	4.81	2.82	3.32	6.30	4.33
Cr_2O3	0.38	0.65	0.36	0.21	0.19	0.06	0.00	0.20
FeO	7.18	6.71	6.71	7.06	6.74	7.26	8.57	7.24
MnO	0.10	0.07	0.11	0.05	0.09	0.14	0.14	0.13
MgO	16.60	14.00	13.97	13.75	15.65	14.08	12.20	15.96
CaO	18.88	22.33	21.10	22.20	20.73	22.29	21.71	19.04
Na_2O	0.49	0.42	0.54	0.43	0.44	0.37	0.55	0.60
K_2O	0.00	0.00	0.00	0.01	0.01	0.01	0.00	0.00
NiO	0.06	0.02	0.02	0.06	0.06	0.00	0.01	0.03
Total	100.34	99.57	99.24	99.57	99.91	99.22	99.36	100.20
Si	1.91	1.86	1.86	1.84	1.93	1.88	1.79	1.90
Ti	0.02	0.04	0.04	0.05	0.02	0.04	0.07	0.02
Al	0.16	0.18	0.22	0.21	0.12	0.15	0.28	0.19
Cr	0.01	0.02	0.01	0.01	0.01	0.00	0.00	0.01
Fe	0.22	0.21	0.21	0.22	0.21	0.23	0.27	0.22
Mn	0.00	0.00	0.00	0.00	0.00	0.00	0.00	0.00
Mg	0.90	0.78	0.78	0.77	0.86	0.79	0.69	0.87
Ca	0.74	0.89	0.84	0.89	0.82	0.90	0.88	0.75
Na	0.03	0.03	0.04	0.03	0.03	0.03	0.04	0.04
K	0.00	0.00	0.00	0.00	0.00	0.00	0.00	0.00
Ni	0.00	0.00	0.00	0.00	0.00	0.00	0.00	0.00
Total	4.00	4.01	4.00	4.02	4.00	4.01	4.02	4.00
Mg#	80.47	78.82	78.77	77.63	80.54	77.57	71.73	79.71
$D^{(cpx\text{-}melt)}_{H_2O}$	0.0130	0.0148	0.0156	0.0169	0.0105	0.0131	0.0237	0.0136
Absorbance of cpx (cm^{-1})	0.85	0.57	2.31	1.24	0.96	0.92	1.33	1.76
Thickness of cpx (0.001mm)	79	98	98	99	101	99	95	88
Absorbance normalized to 1 cm (cm^{-1})	108	58	236	125	95	92	140	200
H_2O-cpx (ppm)	46	25	100	53	40	39	59	84
H_2O-melt (wt%)	0.35	0.17	0.64	0.31	0.38	0.30	0.25	0.62

Sample No.						SC-3		
Section No.						2		
Point No.	44	45	45.2	46	47	1	1.2	2
SiO_2	51.94	50.99	49.59	50.37	50.98	50.46	50.43	51.47
TiO_2	1.11	1.02	1.45	1.62	1.36	1.20	1.23	1.18
Al_2O3	3.02	4.66	5.61	4.89	3.43	3.71	3.61	3.40
Cr_2O3	0.15	0.14	0.07	0.22	0.02	0.11	0.08	0.11
FeO	6.78	7.99	8.07	6.80	7.82	7.71	8.12	7.66
MnO	0.13	0.12	0.13	0.11	0.13	0.12	0.06	0.12
MgO	14.86	15.83	13.84	13.34	14.11	14.52	14.47	14.84
CaO	22.17	18.47	19.98	21.13	21.21	21.00	20.79	20.22
Na_2O	0.39	0.62	0.62	0.60	0.42	0.43	0.46	0.40
K_2O	0.00	0.00	0.00	0.00	0.02	0.00	0.00	0.00
NiO	0.09	0.04	0.00	0.01	0.00	0.02	0.08	0.07
Total	100.63	99.87	99.37	99.10	99.50	99.29	99.34	99.47
Si	1.91	1.88	1.85	1.88	1.90	1.89	1.89	1.91
Ti	0.03	0.03	0.04	0.05	0.04	0.03	0.03	0.03
Al	0.13	0.20	0.25	0.21	0.15	0.16	0.16	0.15
Cr	0.00	0.00	0.00	0.01	0.00	0.00	0.00	0.00
Fe	0.21	0.25	0.25	0.21	0.24	0.24	0.25	0.24
Mn	0.00	0.00	0.00	0.00	0.00	0.00	0.00	0.00
Mg	0.81	0.87	0.77	0.74	0.78	0.81	0.81	0.82
Ca	0.87	0.73	0.80	0.84	0.85	0.84	0.83	0.80
Na	0.03	0.04	0.04	0.04	0.03	0.03	0.03	0.03
K	0.00	0.00	0.00	0.00	0.00	0.00	0.00	0.00
Ni	0.00	0.00	0.00	0.00	0.00	0.00	0.00	0.00
Total	4.01	4.01	4.01	3.99	4.00	4.01	4.01	3.99
Mg#	79.63	77.93	75.36	77.76	76.28	77.06	76.05	77.54
$D^{(cpx\text{-}melt)}_{H_2O}$	0.0113	0.0158	0.0179	0.0143	0.0122	0.0136	0.0136	0.0119
Absorbance of cpx (cm^{-1})	0.72	0.93	1.33	1.73	0.28	1.16	1.01	1.16
Thickness of cpx (0.001mm)	79	87	87	81	93	72	72	72
Absorbance normalized to 1 cm (cm^{-1})	91	107	153	213	30	160	140	160
H_2O-cpx (ppm)	38	45	65	90	13	68	59	68
H_2O-melt (wt%)	0.34	0.29	0.36	0.63	0.10	0.50	0.43	0.57

Sample No.								
Section No.								
Point No.	2.2	3	4	4.2	5	5.1	5.2	5.3
SiO_2	51.30	48.28	51.49	48.40	51.81	48.57	50.64	48.49
TiO_2	0.99	2.01	0.98	1.98	1.14	1.68	1.54	2.16
Al_2O3	4.69	5.69	4.39	5.54	3.15	5.93	4.45	5.99
Cr_2O3	0.16	0.04	0.26	0.10	0.11	0.10	0.26	0.08
FeO	7.92	8.66	7.85	8.48	7.06	7.89	7.05	8.07
MnO	0.17	0.12	0.14	0.11	0.12	0.07	0.14	0.16
MgO	15.75	13.04	15.81	13.12	14.83	13.41	14.05	13.10
CaO	17.74	20.88	18.57	21.39	21.94	21.63	21.94	21.61
Na_2O	0.62	0.55	0.62	0.50	0.43	0.56	0.44	0.56
K_2O	0.00	0.01	0.00	0.00	0.01	0.00	0.00	0.00
NiO	0.01	0.04	0.02	0.04	0.03	0.00	0.00	0.05
Total	99.36	99.31	100.12	99.65	100.62	99.82	100.50	100.27
Si	1.89	1.82	1.89	1.82	1.91	1.81	1.87	1.81
Ti	0.03	0.06	0.03	0.06	0.03	0.05	0.04	0.06
Al	0.20	0.25	0.19	0.24	0.14	0.26	0.19	0.26
Cr	0.00	0.00	0.01	0.00	0.00	0.00	0.01	0.00
Fe	0.24	0.27	0.24	0.27	0.22	0.25	0.22	0.25
Mn	0.01	0.00	0.00	0.00	0.00	0.00	0.00	0.00
Mg	0.87	0.73	0.87	0.73	0.81	0.75	0.77	0.73
Ca	0.70	0.84	0.73	0.86	0.86	0.87	0.87	0.86
Na	0.04	0.04	0.04	0.04	0.03	0.04	0.03	0.04
K	0.00	0.00	0.00	0.00	0.00	0.00	0.00	0.00
Ni	0.00	0.00	0.00	0.00	0.00	0.00	0.00	0.00
Total	4.00	4.02	4.00	4.02	4.01	4.03	4.00	4.02
Mg#	78.01	72.87	78.21	73.40	78.92	75.19	78.05	74.32
$D^{(cpx\text{-}melt)}_{H_2O}$	0.0147	0.0212	0.0146	0.0209	0.0116	0.0211	0.0149	0.0223
Absorbance of cpx (cm^{-1})	2.52	1.65	0.51	0.63	0.89	0.66	0.90	0.74
Thickness of cpx (0.001mm)	72	79	87	87	87	87	87	87
Absorbance normalized to 1 cm (cm^{-1})	350	209	59	72	102	76	103	84
H_2O-cpx (ppm)	148	88	25	31	43	32	44	36
H_2O-melt (wt%)	1.01	0.42	0.17	0.15	0.37	0.15	0.29	0.16

Sample No.								
Section No.								
Point No.	5.4	6	6.1	7	8	9	9.1	10
SiO_2	48.95	51.45	49.24	51.57	51.43	51.95	51.42	51.79
TiO_2	1.91	0.97	1.78	1.14	1.15	1.05	1.24	1.08
Al_2O3	4.90	3.99	5.49	2.92	3.47	3.36	3.34	3.34
Cr_2O3	0.02	0.02	0.13	0.05	0.11	0.08	0.07	0.05
FeO	8.69	8.30	7.46	6.97	7.49	7.41	7.70	7.67
MnO	0.11	0.11	0.10	0.09	0.09	0.08	0.14	0.14
MgO	13.05	14.35	13.44	14.90	14.85	15.07	14.59	14.94
CaO	21.34	19.85	21.53	21.65	21.44	20.85	20.97	20.40
Na_2O	0.53	0.62	0.54	0.39	0.41	0.45	0.34	0.43
K_2O	0.01	0.07	0.00	0.00	0.00	0.02	0.00	0.00
NiO	0.00	0.06	0.02	0.01	0.00	0.00	0.03	0.00
Total	99.51	99.79	99.75	99.68	100.44	100.30	99.84	99.84
Si	1.84	1.91	1.84	1.91	1.90	1.91	1.91	1.92
Ti	0.05	0.03	0.05	0.03	0.03	0.03	0.03	0.03
Al	0.22	0.17	0.24	0.13	0.15	0.15	0.15	0.15
Cr	0.00	0.00	0.00	0.00	0.00	0.00	0.00	0.00
Fe	0.27	0.26	0.23	0.22	0.23	0.23	0.24	0.24
Mn	0.00	0.00	0.00	0.00	0.00	0.00	0.00	0.00
Mg	0.73	0.79	0.75	0.82	0.82	0.83	0.81	0.82
Ca	0.86	0.79	0.86	0.86	0.85	0.82	0.83	0.81
Na	0.04	0.04	0.04	0.03	0.03	0.03	0.02	0.03
K	0.00	0.00	0.00	0.00	0.00	0.00	0.00	0.00
Ni	0.00	0.00	0.00	0.00	0.00	0.00	0.00	0.00
Total	4.02	4.00	4.01	4.01	4.01	4.00	4.00	4.00
Mg#	72.81	75.50	76.26	79.22	77.95	78.38	77.17	77.65
$D^{(cpx\text{-}melt)}_{H_2O}$	0.0180	0.0124	0.0185	0.0112	0.0126	0.0117	0.0120	0.0116
Absorbance of cpx (cm^{-1})	0.87	1.56	1.86	1.19	0.96	0.84	0.75	1.16
Thickness of cpx (0.001mm)	87	87	87	85	94	96	96	113
Absorbance normalized to 1 cm (cm^{-1})	100	179	214	140	102	87	78	103
H_2O-cpx (ppm)	42	76	90	59	43	37	33	43
H_2O-melt (wt%)	0.23	0.61	0.49	0.53	0.34	0.32	0.28	0.37

Sample No.								
Section No.								
Point No.	11	12	13	13.1	13.2	13.3	14	14.2
SiO_2	50.84	51.83	51.96	52.08	52.18	52.29	50.08	50.27
TiO_2	1.43	0.73	1.24	0.96	0.78	0.89	1.49	1.50
Al_2O3	3.62	4.48	2.86	2.61	3.11	3.48	4.76	4.23
Cr_2O3	0.04	0.22	0.10	0.19	0.11	0.08	0.27	0.44
FeO	7.49	7.73	6.99	6.70	7.12	7.78	6.91	6.67
MnO	0.06	0.17	0.09	0.09	0.10	0.16	0.10	0.10
MgO	14.21	16.50	15.01	15.04	15.20	15.32	14.33	13.92
CaO	21.66	17.20	21.73	21.70	21.08	19.88	21.18	22.20
Na_2O	0.43	0.64	0.36	0.37	0.42	0.56	0.57	0.43
K_2O	0.00	0.02	0.00	0.00	0.00	0.00	0.00	0.00
NiO	0.03	0.00	0.05	0.01	0.00	0.01	0.00	0.07
Total	99.82	99.53	100.38	99.75	100.12	100.45	99.67	99.81
Si	1.89	1.91	1.91	1.93	1.92	1.92	1.86	1.87
Ti	0.04	0.02	0.03	0.03	0.02	0.02	0.04	0.04
Al	0.16	0.19	0.12	0.11	0.14	0.15	0.21	0.19
Cr	0.00	0.01	0.00	0.01	0.00	0.00	0.01	0.01
Fe	0.23	0.24	0.22	0.21	0.22	0.24	0.21	0.21
Mn	0.00	0.01	0.00	0.00	0.00	0.01	0.00	0.00
Mg	0.79	0.90	0.82	0.83	0.83	0.84	0.79	0.77
Ca	0.86	0.68	0.86	0.86	0.83	0.78	0.84	0.88
Na	0.03	0.05	0.03	0.03	0.03	0.04	0.04	0.03
K	0.00	0.00	0.00	0.00	0.00	0.00	0.00	0.00
Ni	0.00	0.00	0.00	0.00	0.00	0.00	0.00	0.00
Total	4.01	4.00	4.00	4.00	4.00	4.00	4.01	4.01
Mg#	77.18	79.19	79.29	80.02	79.19	77.84	78.71	78.81
$D^{(cpx\text{-}melt)}_{H_2O}$	0.0130	0.0141	0.0112	0.0102	0.0108	0.0116	0.0161	0.0146
Absorbance of cpx (cm^{-1})	1.29	1.65	0.46	1.04	0.23	1.16	1.59	1.16
Thickness of cpx (0.001mm)	103	106	111	111	111	111	115	115
Absorbance normalized to 1 cm (cm^{-1})	125	156	41	93	20	105	138	100
H_2O-cpx (ppm)	53	66	18	39	9	44	59	42
H_2O-melt (wt%)	0.41	0.47	0.16	0.39	0.08	0.38	0.36	0.29

Sample No. Section No. Point No.	14.3	14.4	15	15.2	15.3	16	16.2	17
SiO_2	52.01	50.21	51.00	48.60	50.54	47.77	49.13	50.01
TiO_2	0.97	1.32	1.33	1.97	1.49	2.27	2.12	1.31
Al_2O3	2.76	4.13	3.78	5.42	3.98	5.90	5.01	4.71
Cr_2O3	0.02	0.28	0.12	0.00	0.00	0.08	0.03	0.21
FeO	7.77	6.34	7.48	8.39	7.91	8.29	8.20	6.96
MnO	0.17	0.10	0.15	0.13	0.16	0.13	0.11	0.10
MgO	15.43	14.48	14.41	12.64	13.88	12.74	12.96	14.23
CaO	20.64	21.82	21.24	21.91	21.62	21.89	21.75	21.22
Na_2O	0.32	0.45	0.42	0.53	0.46	0.43	0.49	0.58
K_2O	0.00	0.00	0.00	0.00	0.02	0.00	0.01	0.00
NiO	0.00	0.05	0.02	0.06	0.00	0.01	0.00	0.00
Total	100.08	99.18	99.93	99.65	100.05	99.52	99.81	99.34
Si	1.92	1.87	1.89	1.83	1.88	1.80	1.84	1.86
Ti	0.03	0.04	0.04	0.06	0.04	0.06	0.06	0.04
Al	0.12	0.18	0.17	0.24	0.17	0.26	0.22	0.21
Cr	0.00	0.01	0.00	0.00	0.00	0.00	0.00	0.01
Fe	0.24	0.20	0.23	0.26	0.25	0.26	0.26	0.22
Mn	0.01	0.00	0.00	0.00	0.00	0.00	0.00	0.00
Mg	0.85	0.81	0.80	0.71	0.77	0.72	0.72	0.79
Ca	0.82	0.87	0.84	0.88	0.86	0.88	0.87	0.85
Na	0.02	0.03	0.03	0.04	0.03	0.03	0.04	0.04
K	0.00	0.00	0.00	0.00	0.00	0.00	0.00	0.00
Ni	0.00	0.00	0.00	0.00	0.00	0.00	0.00	0.00
Total	4.00	4.01	4.00	4.02	4.01	4.02	4.01	4.01
Mg#	77.96	80.28	77.45	72.86	75.78	73.26	73.80	78.48
$D^{(cpx\text{-}melt)}_{H_2O}$	0.0111	0.0143	0.0131	0.0193	0.0139	0.0231	0.0180	0.0156
Absorbance of cpx (cm^{-1})	0.75	1.05	1.01	1.53	1.11	1.05	0.96	1.85
Thickness of cpx (0.001mm)	115	115	103	103	103	103	103	116
Absorbance normalized to 1 cm (cm^{-1})	65	91	98	149	108	102	93	159
H_2O-cpx (ppm)	28	39	41	63	46	43	39	67
H_2O-melt (wt%)	0.25	0.27	0.31	0.32	0.33	0.19	0.22	0.43

Sample No.								
Section No.								
Point No.	17.2	18	19.1	19.2	20	20.1	20.2	21
SiO_2	51.81	49.08	51.00	50.15	50.77	50.47	51.19	50.56
TiO_2	0.84	1.54	0.99	1.45	1.09	1.37	1.14	0.90
Al_2O3	3.13	4.94	4.33	4.16	3.31	3.92	3.34	4.95
Cr_2O3	0.11	0.19	0.22	0.38	0.08	0.04	0.10	0.12
FeO	6.83	7.69	7.60	7.40	8.21	7.68	7.15	7.73
MnO	0.14	0.10	0.13	0.11	0.13	0.19	0.11	0.15
MgO	15.19	13.41	15.80	14.36	14.25	14.07	14.41	15.30
CaO	21.17	21.59	18.88	21.11	20.72	21.45	21.55	18.88
Na_2O	0.38	0.42	0.57	0.42	0.41	0.45	0.42	0.59
K_2O	0.00	0.00	0.01	0.00	0.00	0.00	0.01	0.01
NiO	0.01	0.02	0.04	0.02	0.02	0.03	0.00	0.04
Total	99.62	98.97	99.56	99.55	99.00	99.67	99.41	99.22
Si	1.92	1.85	1.89	1.87	1.90	1.88	1.91	1.88
Ti	0.02	0.04	0.03	0.04	0.03	0.04	0.03	0.03
Al	0.14	0.22	0.19	0.18	0.15	0.17	0.15	0.22
Cr	0.00	0.01	0.01	0.01	0.00	0.00	0.00	0.00
Fe	0.21	0.24	0.23	0.23	0.26	0.24	0.22	0.24
Mn	0.00	0.00	0.00	0.00	0.00	0.01	0.00	0.00
Mg	0.84	0.75	0.87	0.80	0.80	0.78	0.80	0.85
Ca	0.84	0.87	0.75	0.84	0.83	0.86	0.86	0.75
Na	0.03	0.03	0.04	0.03	0.03	0.03	0.03	0.04
K	0.00	0.00	0.00	0.00	0.00	0.00	0.00	0.00
Ni	0.00	0.00	0.00	0.00	0.00	0.00	0.00	0.00
Total	4.00	4.01	4.01	4.01	4.01	4.01	4.00	4.01
Mg#	79.85	75.67	78.77	77.57	75.58	76.55	78.23	77.91
$D^{(cpx\text{-}melt)}_{H_2O}$	0.0111	0.0171	0.0149	0.0151	0.0122	0.0138	0.0117	0.0157
Absorbance of cpx (cm^{-1})	1.40	1.43	0.65	0.42	0.56	1.37	0.56	1.91
Thickness of cpx (0.001mm)	116	116	116	116	104	104	104	100
Absorbance normalized to 1 cm (cm^{-1})	120	123	56	36	53	131	53	191
H_2O-cpx (ppm)	51	52	24	15	23	56	23	81
H_2O-melt (wt%)	0.46	0.30	0.16	0.10	0.19	0.40	0.19	0.51

Sample No. Section No. Point No.	22	23	23.2	24	24.1	24.2	25	26
SiO_2	51.41	50.04	50.69	51.49	50.27	49.78	50.46	49.16
TiO_2	1.09	1.47	1.35	0.77	1.46	1.44	1.25	1.74
Al_2O3	3.19	4.11	3.59	4.63	4.61	5.56	4.12	5.20
Cr_2O3	0.15	0.30	0.00	0.17	0.20	0.08	0.24	0.12
FeO	7.22	6.76	7.77	7.55	7.47	8.01	6.66	7.75
MnO	0.16	0.07	0.16	0.08	0.12	0.13	0.08	0.09
MgO	15.07	13.99	14.19	15.66	13.94	14.09	14.35	13.39
CaO	21.25	22.39	21.06	18.62	21.64	20.18	22.13	21.55
Na_2O	0.40	0.39	0.43	0.50	0.37	0.59	0.46	0.49
K_2O	0.00	0.00	0.00	0.00	0.01	0.00	0.00	0.00
NiO	0.00	0.00	0.04	0.09	0.04	0.03	0.05	0.03
Total	99.93	99.52	99.27	99.55	100.12	99.89	99.78	99.52
Si	1.90	1.87	1.89	1.90	1.86	1.85	1.87	1.84
Ti	0.03	0.04	0.04	0.02	0.04	0.04	0.03	0.05
Al	0.14	0.18	0.16	0.20	0.20	0.24	0.18	0.23
Cr	0.00	0.01	0.00	0.00	0.01	0.00	0.01	0.00
Fe	0.22	0.21	0.24	0.23	0.23	0.25	0.21	0.24
Mn	0.00	0.00	0.01	0.00	0.00	0.00	0.00	0.00
Mg	0.83	0.78	0.79	0.86	0.77	0.78	0.79	0.75
Ca	0.84	0.89	0.84	0.74	0.86	0.80	0.88	0.86
Na	0.03	0.03	0.03	0.04	0.03	0.04	0.03	0.04
K	0.00	0.00	0.00	0.00	0.00	0.00	0.00	0.00
Ni	0.00	0.00	0.00	0.00	0.00	0.00	0.00	0.00
Total	4.01	4.01	4.00	4.00	4.01	4.01	4.01	4.01
Mg#	78.83	78.67	76.51	78.72	76.90	75.81	79.35	75.50
$D^{(cpx\text{-}melt)}_{H_2O}$	0.0121	0.0146	0.0128	0.0139	0.0154	0.0181	0.0141	0.0180
Absorbance of cpx (cm^{-1})	0.56	1.71	0.99	1.76	0.96	1.61	0.87	0.98
Thickness of cpx (0.001mm)	104	100	100	102	102	102	104	102
Absorbance normalized to 1 cm (cm^{-1})	53	171	99	172	94	157	84	96
H_2O-cpx (ppm)	23	72	42	73	40	67	35	40
H_2O-melt (wt%)	0.19	0.50	0.33	0.52	0.26	0.37	0.25	0.22

Sample No. Section No. Point No.	26.2	27	27.2	28.2	29	30	31	32
SiO_2	51.53	52.26	51.66	51.36	51.84	50.77	49.63	50.65
TiO_2	0.94	0.87	1.01	1.05	0.83	0.65	1.52	1.32
Al_2O3	4.60	2.80	3.19	2.89	3.07	4.96	4.72	3.43
Cr_2O3	0.17	0.14	0.06	0.09	0.07	0.13	0.19	0.05
FeO	7.22	6.75	7.10	7.01	8.17	7.96	7.49	8.62
MnO	0.07	0.10	0.13	0.13	0.12	0.13	0.08	0.09
MgO	15.96	15.62	14.62	15.11	15.91	15.41	13.64	14.56
CaO	18.12	20.50	21.79	21.21	18.95	18.45	21.69	20.85
Na_2O	0.58	0.44	0.38	0.40	0.45	0.65	0.42	0.42
K_2O	0.01	0.01	0.01	0.00	0.01	0.00	0.01	0.00
NiO	0.07	0.08	0.00	0.08	0.00	0.00	0.00	0.04
Total	99.26	99.58	99.94	99.34	99.42	99.11	99.39	100.02
Si	1.90	1.93	1.91	1.91	1.92	1.89	1.86	1.89
Ti	0.03	0.02	0.03	0.03	0.02	0.02	0.04	0.04
Al	0.20	0.12	0.14	0.13	0.13	0.22	0.21	0.15
Cr	0.00	0.00	0.00	0.00	0.00	0.00	0.01	0.00
Fe	0.22	0.21	0.22	0.22	0.25	0.25	0.23	0.27
Mn	0.00	0.00	0.00	0.00	0.00	0.00	0.00	0.00
Mg	0.88	0.86	0.81	0.84	0.88	0.85	0.76	0.81
Ca	0.72	0.81	0.86	0.85	0.75	0.73	0.87	0.83
Na	0.04	0.03	0.03	0.03	0.03	0.05	0.03	0.03
K	0.00	0.00	0.00	0.00	0.00	0.00	0.00	0.00
Ni	0.00	0.00	0.00	0.00	0.00	0.00	0.00	0.00
Total	3.99	4.00	4.00	4.01	4.00	4.01	4.01	4.02
Mg#	79.77	80.50	78.59	79.35	77.63	77.53	76.44	75.06
$D^{(cpx\text{-}melt)}_{H_2O}$	0.0140	0.0105	0.0112	0.0114	0.0117	0.0152	0.0160	0.0137
Absorbance of cpx (cm^{-1})	0.98	0.50	0.83	0.78	0.93	1.25	1.58	0.81
Thickness of cpx (0.001mm)	102	95	95	95	95	84	101	101
Absorbance normalized to 1 cm (cm^{-1})	96	52	87	82	98	148	156	80
H_2O-cpx (ppm)	40	22	37	35	41	63	66	34
H_2O-melt (wt%)	0.29	0.21	0.33	0.30	0.35	0.41	0.41	0.25

Sample No.				SC-4			
Section No.				1			
Point No.	33	33.2	34	1	1.2	2	3
SiO_2	52.19	48.26	49.86	49.75	49.40	51.56	52.20
TiO_2	0.72	1.55	1.70	1.45	1.83	1.10	0.83
Al_2O3	2.92	5.57	4.49	4.34	4.81	3.18	2.82
Cr_2O3	0.17	0.20	0.21	0.12	0.11	0.18	0.14
FeO	6.88	7.86	7.04	7.28	7.88	6.68	7.46
MnO	0.09	0.10	0.14	0.04	0.11	0.11	0.13
MgO	15.50	13.43	13.82	14.14	13.32	15.07	16.23
CaO	20.50	21.51	21.55	21.58	21.53	21.78	19.43
Na_2O	0.43	0.48	0.43	0.49	0.39	0.32	0.42
K_2O	0.00	0.02	0.01	0.00	0.00	0.00	0.01
NiO	0.00	0.07	0.03	0.10	0.01	0.05	0.00
Total	99.40	99.05	99.26	99.29	99.40	100.04	99.67
Si	1.93	1.82	1.86	1.86	1.85	1.90	1.93
Ti	0.02	0.04	0.05	0.04	0.05	0.03	0.02
Al	0.13	0.25	0.20	0.19	0.21	0.14	0.12
Cr	0.01	0.01	0.01	0.00	0.00	0.01	0.00
Fe	0.21	0.25	0.22	0.23	0.25	0.21	0.23
Mn	0.00	0.00	0.00	0.00	0.00	0.00	0.00
Mg	0.86	0.75	0.77	0.79	0.74	0.83	0.89
Ca	0.81	0.87	0.86	0.86	0.86	0.86	0.77
Na	0.03	0.04	0.03	0.04	0.03	0.02	0.03
K	0.00	0.00	0.00	0.00	0.00	0.00	0.00
Ni	0.00	0.00	0.00	0.00	0.00	0.00	0.00
Total	4.00	4.03	4.00	4.02	4.00	4.00	4.00
Mg#	80.08	75.29	77.77	77.60	75.08	80.09	79.51
$D^{(cpx\text{-}melt)}_{H_2O}$	0.0104	0.0204	0.0154	0.0156	0.0167	0.0118	0.0112
Absorbance of cpx (cm^{-1})	0.00	0.00	1.26	0.72	0.95	0.73	1.09
Thickness of cpx (0.001mm)	59	59	71	98	98	102	102
Absorbance normalized to 1 cm (cm^{-1})	0	0	177	73	97	72	107
H_2O-cpx (ppm)	5	0	75	31	41	30	45
H_2O-melt (wt%)	0.00	0.00	0.49	0.20	0.25	0.26	0.40

Sample No.								
Section No.								
Point No.	4	5	6	6.2	7	8	8.2	9.1
SiO_2	50.21	50.69	51.81	49.68	50.93	51.45	49.88	48.41
TiO_2	1.30	1.29	1.03	1.69	1.28	1.19	1.42	1.86
Al_2O3	4.39	4.13	2.96	5.00	3.78	3.36	4.54	5.45
Cr_2O3	0.07	0.17	0.12	0.15	0.18	0.09	0.36	0.00
FeO	7.36	7.43	6.36	7.17	8.09	7.51	6.54	8.36
MnO	0.11	0.09	0.07	0.05	0.13	0.12	0.09	0.16
MgO	14.09	14.43	14.91	13.65	14.31	14.75	14.26	12.69
CaO	21.41	21.07	21.58	21.96	20.80	21.43	22.04	21.58
Na_2O	0.44	0.39	0.39	0.47	0.42	0.38	0.41	0.59
K_2O	0.00	0.00	0.00	0.00	0.00	0.01	0.00	0.00
NiO	0.01	0.04	0.01	0.01	0.00	0.04	0.02	0.00
Total	99.39	99.72	99.26	99.82	99.93	100.33	99.55	99.08
Si	1.87	1.88	1.92	1.85	1.89	1.90	1.86	1.83
Ti	0.04	0.04	0.03	0.05	0.04	0.03	0.04	0.05
Al	0.19	0.18	0.13	0.22	0.17	0.15	0.20	0.24
Cr	0.00	0.00	0.00	0.00	0.01	0.00	0.01	0.00
Fe	0.23	0.23	0.20	0.22	0.25	0.23	0.20	0.26
Mn	0.00	0.00	0.00	0.00	0.00	0.00	0.00	0.00
Mg	0.78	0.80	0.82	0.76	0.79	0.81	0.79	0.71
Ca	0.86	0.84	0.86	0.88	0.83	0.85	0.88	0.87
Na	0.03	0.03	0.03	0.03	0.03	0.03	0.03	0.04
K	0.00	0.00	0.00	0.00	0.00	0.00	0.00	0.00
Ni	0.00	0.00	0.00	0.00	0.00	0.00	0.00	0.00
Total	4.01	4.00	4.00	4.01	4.00	4.01	4.01	4.02
Mg#	77.34	77.58	80.69	77.24	75.93	77.77	79.54	73.02
$D^{(cpx\text{-}melt)}_{H_2O}$	0.0146	0.0140	0.0105	0.0168	0.0133	0.0123	0.0158	0.0193
Absorbance of cpx (cm^{-1})	0.75	1.50	1.17	1.80	1.47	1.48	1.74	1.15
Thickness of cpx (0.001mm)	102	111	117	117	117	126	126	127
Absorbance normalized to 1 cm (cm^{-1})	74	135	100	154	126	117	138	91
H_2O-cpx (ppm)	31	57	42	65	53	50	58	38
H_2O-melt (wt%)	0.21	0.41	0.40	0.39	0.40	0.40	0.37	0.20

Sample No. Section No. Point No.	9.2	9.3	10	11	12	12.1	13	14
SiO_2	50.39	47.69	49.93	51.78	48.85	51.75	48.96	50.59
TiO_2	1.50	2.19	1.40	1.14	1.83	0.90	1.78	1.14
Al_2O3	4.29	6.09	5.11	2.99	4.96	2.63	5.01	3.91
Cr_2O3	0.04	0.07	0.29	0.40	0.21	0.16	0.15	0.08
FeO	7.55	8.72	6.90	7.24	7.38	6.62	7.59	7.48
MnO	0.09	0.11	0.13	0.13	0.11	0.10	0.10	0.07
MgO	13.73	12.66	14.08	14.90	13.51	15.49	13.52	14.41
CaO	21.43	21.30	20.94	21.32	21.90	21.17	21.79	21.52
Na_2O	0.44	0.52	0.58	0.38	0.51	0.39	0.42	0.48
K_2O	0.00	0.00	0.00	0.00	0.00	0.00	0.00	0.00
NiO	0.03	0.00	0.00	0.00	0.02	0.00	0.06	0.00
Total	99.48	99.35	99.35	100.27	99.29	99.22	99.38	99.68
Si	1.88	1.80	1.86	1.91	1.83	1.92	1.84	1.88
Ti	0.04	0.06	0.04	0.03	0.05	0.03	0.05	0.03
Al	0.19	0.27	0.22	0.13	0.22	0.12	0.22	0.17
Cr	0.00	0.00	0.01	0.01	0.01	0.00	0.00	0.00
Fe	0.24	0.27	0.21	0.22	0.23	0.21	0.24	0.23
Mn	0.00	0.00	0.00	0.00	0.00	0.00	0.00	0.00
Mg	0.76	0.71	0.78	0.82	0.76	0.86	0.76	0.80
Ca	0.86	0.86	0.83	0.84	0.88	0.84	0.88	0.86
Na	0.03	0.04	0.04	0.03	0.04	0.03	0.03	0.03
K	0.00	0.00	0.00	0.00	0.00	0.00	0.00	0.00
Ni	0.00	0.00	0.00	0.00	0.00	0.00	0.00	0.00
Total	4.00	4.02	4.01	4.00	4.02	4.01	4.02	4.02
Mg#	76.42	72.13	78.43	78.58	76.55	80.67	76.06	77.43
$D^{(cpx\text{-}melt)}_{H_2O}$	0.0140	0.0235	0.0163	0.0116	0.0184	0.0106	0.0182	0.0136
Absorbance of cpx (cm^{-1})	0.74	1.56	1.18	0.68	1.50	0.95	0.29	0.65
Thickness of cpx (0.001mm)	127	127	123	123	122	122	118	102
Absorbance normalized to 1 cm (cm^{-1})	58	123	96	55	123	78	25	64
H_2O-cpx (ppm)	25	52	41	23	52	33	10	27
H_2O-melt (wt%)	0.18	0.22	0.25	0.20	0.28	0.31	0.06	0.20

Sample No.								
Section No.								
Point No.	15	16	17	18	18.2	18.3	18.4	18.5
SiO_2	52.03	51.78	51.54	51.19	48.87	50.72	51.61	48.62
TiO_2	0.81	0.78	0.98	1.24	1.94	1.12	1.04	2.11
Al_2O3	2.80	4.18	3.07	3.45	5.66	3.29	3.01	5.56
Cr_2O3	0.20	0.48	0.10	0.05	0.03	0.03	0.09	0.09
FeO	6.88	7.31	7.14	6.92	7.92	7.83	6.94	7.93
MnO	0.16	0.18	0.10	0.11	0.09	0.09	0.10	0.10
MgO	16.06	17.25	15.01	14.54	12.95	14.42	14.91	12.98
CaO	19.96	17.36	20.71	21.83	21.93	21.13	22.01	21.22
Na_2O	0.32	0.48	0.40	0.41	0.49	0.35	0.40	0.43
K_2O	0.00	0.00	0.01	0.00	0.00	0.01	0.00	0.00
NiO	0.00	0.03	0.10	0.00	0.01	0.01	0.05	0.02
Total	99.22	99.84	99.14	99.75	99.89	98.99	100.15	99.06
Si	1.93	1.90	1.92	1.90	1.83	1.90	1.91	1.83
Ti	0.02	0.02	0.03	0.03	0.05	0.03	0.03	0.06
Al	0.12	0.18	0.13	0.15	0.25	0.15	0.13	0.25
Cr	0.01	0.01	0.00	0.00	0.00	0.00	0.00	0.00
Fe	0.21	0.22	0.22	0.21	0.25	0.25	0.21	0.25
Mn	0.00	0.01	0.00	0.00	0.00	0.00	0.00	0.00
Mg	0.89	0.94	0.83	0.80	0.72	0.81	0.82	0.73
Ca	0.79	0.68	0.83	0.87	0.88	0.85	0.87	0.85
Na	0.02	0.03	0.03	0.03	0.04	0.03	0.03	0.03
K	0.00	0.00	0.00	0.00	0.00	0.00	0.00	0.00
Ni	0.00	0.00	0.00	0.00	0.00	0.00	0.00	0.00
Total	4.00	4.00	4.00	4.01	4.01	4.01	4.01	4.00
Mg#	80.63	80.79	78.95	78.93	74.44	76.66	79.30	74.49
$D^{(cpx\text{-}melt)}_{H_2O}$	0.0109	0.0148	0.0111	0.0121	0.0194	0.0122	0.0114	0.0195
Absorbance of cpx (cm^{-1})	1.91	1.95	1.37	1.76	2.47	1.01	1.10	1.40
Thickness of cpx (0.001mm)	134	118	137	136	136	136	136	136
Absorbance normalized to 1 cm (cm^{-1})	143	165	100	129	182	74	81	103
H_2O-cpx (ppm)	60	70	42	55	77	31	34	44
H_2O-melt (wt%)	0.55	0.47	0.38	0.45	0.40	0.26	0.30	0.22

Sample No. Section No. Point No.	19	19.2	20	21	21.2	22	22.1	23
SiO_2	51.37	50.24	49.38	50.99	49.12	49.13	50.77	51.55
TiO_2	1.36	1.33	1.75	0.88	1.65	1.76	1.38	1.18
Al_2O3	3.45	4.13	5.38	3.35	5.01	5.90	3.44	3.07
Cr_2O3	0.19	0.34	0.16	0.08	0.08	0.07	0.09	0.16
FeO	6.77	6.56	7.65	7.24	7.72	8.01	7.40	6.94
MnO	0.11	0.06	0.08	0.12	0.10	0.09	0.17	0.12
MgO	14.53	13.67	13.42	14.70	13.63	13.44	14.60	14.30
CaO	22.14	22.43	21.67	21.59	21.52	20.13	21.78	22.22
Na_2O	0.45	0.40	0.52	0.39	0.49	0.61	0.39	0.28
K_2O	0.00	0.00	0.00	0.00	0.00	0.01	0.00	0.00
NiO	0.04	0.00	0.02	0.07	0.03	0.00	0.03	0.03
Total	100.40	99.16	100.03	99.40	99.36	99.14	100.07	99.85
Si	1.89	1.88	1.84	1.90	1.84	1.84	1.88	1.91
Ti	0.04	0.04	0.05	0.02	0.05	0.05	0.04	0.03
Al	0.15	0.18	0.24	0.15	0.22	0.26	0.15	0.13
Cr	0.01	0.01	0.00	0.00	0.00	0.00	0.00	0.00
Fe	0.21	0.20	0.24	0.23	0.24	0.25	0.23	0.22
Mn	0.00	0.00	0.00	0.00	0.00	0.00	0.01	0.00
Mg	0.80	0.76	0.74	0.82	0.76	0.75	0.81	0.79
Ca	0.87	0.90	0.86	0.86	0.86	0.81	0.87	0.88
Na	0.03	0.03	0.04	0.03	0.04	0.04	0.03	0.02
K	0.00	0.00	0.00	0.00	0.00	0.00	0.00	0.00
Ni	0.00	0.00	0.00	0.00	0.00	0.00	0.00	0.00
Total	4.01	4.00	4.01	4.01	4.02	4.00	4.01	4.00
Mg#	79.27	78.80	75.77	78.35	75.88	74.95	77.87	78.59
$D^{(cpx\text{-}melt)}_{H_2O}$	0.0124	0.0135	0.0183	0.0121	0.0178	0.0192	0.0134	0.0110
Absorbance of cpx (cm^{-1})	1.97	0.51	1.89	1.07	1.20	2.47	0.20	1.13
Thickness of cpx (0.001mm)	120	120	119	118	118	125	125	133
Absorbance normalized to 1 cm (cm^{-1})	164	43	159	91	102	198	16	85
H_2O-cpx (ppm)	69	18	67	38	43	84	7	36
H_2O-melt (wt%)	0.56	0.13	0.37	0.32	0.24	0.44	0.05	0.33

Sample No.								
Section No.								
Point No.	24.1	24.2	24.3	24.4	24.5	25	25.2	26
SiO_2	51.41	51.46	51.60	51.95	52.03	52.09	51.37	51.13
TiO_2	0.99	1.19	1.08	0.61	0.97	0.89	1.07	1.10
Al_2O3	3.84	3.12	2.49	2.83	2.90	2.74	3.06	4.69
Cr_2O3	0.04	0.06	0.09	0.22	0.13	0.18	0.10	0.32
FeO	8.27	7.34	6.71	6.63	7.21	6.74	6.66	7.17
MnO	0.12	0.13	0.04	0.13	0.13	0.08	0.11	0.13
MgO	14.64	14.77	15.14	16.22	15.33	15.48	14.84	14.69
CaO	19.93	21.30	21.99	20.19	21.05	20.85	21.73	20.38
Na_2O	0.42	0.42	0.41	0.35	0.34	0.29	0.42	0.44
K_2O	0.00	0.01	0.00	0.01	0.01	0.00	0.00	0.00
NiO	0.05	0.00	0.00	0.00	0.05	0.03	0.02	0.01
Total	99.71	99.80	99.55	99.13	100.14	99.38	99.38	100.04
Si	1.91	1.91	1.92	1.93	1.92	1.93	1.91	1.88
Ti	0.03	0.03	0.03	0.02	0.03	0.02	0.03	0.03
Al	0.17	0.14	0.11	0.12	0.13	0.12	0.13	0.20
Cr	0.00	0.00	0.00	0.01	0.00	0.01	0.00	0.01
Fe	0.26	0.23	0.21	0.21	0.22	0.21	0.21	0.22
Mn	0.00	0.00	0.00	0.00	0.00	0.00	0.00	0.00
Mg	0.81	0.82	0.84	0.90	0.84	0.85	0.82	0.81
Ca	0.79	0.85	0.88	0.80	0.83	0.83	0.87	0.80
Na	0.03	0.03	0.03	0.03	0.02	0.02	0.03	0.03
K	0.00	0.00	0.00	0.00	0.00	0.00	0.00	0.00
Ni	0.00	0.00	0.00	0.00	0.00	0.00	0.00	0.00
Total	4.00	4.00	4.01	4.01	4.00	3.99	4.01	4.00
Mg#	75.94	78.20	80.10	81.36	79.13	80.37	79.90	78.51
$D^{(cpx\text{-}melt)}_{H_2O}$	0.0125	0.0117	0.0107	0.0109	0.0111	0.0104	0.0113	0.0143
Absorbance of cpx (cm^{-1})	2.42	1.57	1.56	1.66	1.40	1.70	1.81	2.49
Thickness of cpx (0.001mm)	134	134	134	134	134	134	134	134
Absorbance normalized to 1 cm (cm^{-1})	181	117	116	124	104	127	135	186
H_2O-cpx (ppm)	76	50	49	52	44	54	57	79
H_2O-melt (wt%)	0.61	0.42	0.46	0.48	0.40	0.52	0.51	0.55

Sample No. Section No. Point No.	26.2	27	28	29	30	30.2	31	31.2
SiO_2	50.21	49.20	50.21	48.04	47.64	52.30	49.52	50.10
TiO_2	1.41	1.70	1.24	2.27	2.01	0.74	1.39	1.30
Al_2O3	4.56	5.15	3.85	5.85	6.14	4.20	5.52	5.04
Cr_2O3	0.20	0.18	0.01	0.09	0.01	0.19	0.12	0.14
FeO	6.78	7.14	7.84	8.14	8.34	8.18	8.22	7.85
MnO	0.10	0.08	0.11	0.08	0.10	0.13	0.11	0.11
MgO	13.77	13.86	14.14	12.87	12.70	16.77	13.88	14.34
CaO	22.02	21.57	21.28	21.86	21.44	17.10	19.65	19.69
Na_2O	0.43	0.51	0.42	0.43	0.54	0.55	0.55	0.59
K_2O	0.01	0.00	0.00	0.01	0.00	0.01	0.00	0.00
NiO	0.05	0.00	0.00	0.06	0.00	0.01	0.05	0.09
Total	99.52	99.38	99.09	99.68	98.92	100.17	99.00	99.24
Si	1.87	1.84	1.88	1.80	1.80	1.91	1.85	1.87
Ti	0.04	0.05	0.03	0.06	0.06	0.02	0.04	0.04
Al	0.20	0.23	0.17	0.26	0.27	0.18	0.24	0.22
Cr	0.01	0.01	0.00	0.00	0.00	0.01	0.00	0.00
Fe	0.21	0.22	0.25	0.26	0.26	0.25	0.26	0.24
Mn	0.00	0.00	0.00	0.00	0.00	0.00	0.00	0.00
Mg	0.76	0.77	0.79	0.72	0.72	0.91	0.77	0.80
Ca	0.88	0.86	0.85	0.88	0.87	0.67	0.79	0.79
Na	0.03	0.04	0.03	0.03	0.04	0.04	0.04	0.04
K	0.00	0.00	0.00	0.00	0.00	0.00	0.00	0.00
Ni	0.00	0.00	0.00	0.00	0.00	0.00	0.00	0.00
Total	4.00	4.02	4.01	4.02	4.02	3.99	4.00	4.01
Mg#	78.35	77.59	76.28	73.81	73.08	78.52	75.06	76.52
$D^{(cpx\text{-}melt)}_{H_2O}$	0.0146	0.0181	0.0137	0.0224	0.0228	0.0136	0.0177	0.0162
Absorbance of cpx (cm^{-1})	2.34	1.22	2.35	2.20	1.01	1.26	1.73	2.36
Thickness of cpx (0.001mm)	134	134	132	137	142	142	139	139
Absorbance normalized to 1 cm (cm^{-1})	175	91	178	161	71	89	124	170
H_2O-cpx (ppm)	74	39	75	68	30	38	53	72
H_2O-melt (wt%)	0.51	0.21	0.55	0.30	0.13	0.28	0.30	0.44

Sample No. Section No. Point No.	32	33	34	34.2	35	35.2	36	37
SiO_2	50.46	49.41	51.37	50.86	50.96	51.69	52.04	51.20
TiO_2	1.56	1.58	1.20	1.17	1.08	0.73	1.12	1.09
Al_2O3	4.41	4.68	3.06	3.39	3.10	3.56	3.20	3.59
Cr_2O3	0.33	0.24	0.06	0.12	0.13	0.13	0.11	0.05
FeO	6.46	6.81	6.98	7.08	6.97	7.84	7.10	8.20
MnO	0.10	0.10	0.13	0.12	0.09	0.13	0.08	0.16
MgO	14.06	13.84	14.57	14.76	14.92	16.24	14.44	15.03
CaO	22.08	22.28	21.46	21.45	21.59	18.32	21.56	19.92
Na_2O	0.46	0.32	0.40	0.41	0.41	0.48	0.36	0.44
K_2O	0.00	0.00	0.00	0.01	0.00	0.00	0.00	0.00
NiO	0.04	0.04	0.00	0.07	0.02	0.01	0.06	0.03
Total	99.97	99.29	99.22	99.43	99.26	99.13	100.07	99.69
Si	1.87	1.85	1.91	1.89	1.90	1.92	1.92	1.90
Ti	0.04	0.04	0.03	0.03	0.03	0.02	0.03	0.03
Al	0.19	0.21	0.13	0.15	0.14	0.16	0.14	0.16
Cr	0.01	0.01	0.00	0.00	0.00	0.00	0.00	0.00
Fe	0.20	0.21	0.22	0.22	0.22	0.24	0.22	0.25
Mn	0.00	0.00	0.00	0.00	0.00	0.00	0.00	0.00
Mg	0.78	0.77	0.81	0.82	0.83	0.90	0.79	0.83
Ca	0.88	0.89	0.86	0.86	0.86	0.73	0.85	0.79
Na	0.03	0.02	0.03	0.03	0.03	0.03	0.03	0.03
K	0.00	0.00	0.00	0.00	0.00	0.00	0.00	0.00
Ni	0.00	0.00	0.00	0.00	0.00	0.00	0.00	0.00
Total	4.00	4.01	4.00	4.01	4.01	4.00	3.99	4.01
Mg#	79.51	78.37	78.83	78.80	79.23	78.70	78.40	76.56
$D^{(cpx\text{-}melt)}_{H_2O}$	0.0147	0.0164	0.0112	0.0126	0.0121	0.0125	0.0107	0.0129
Absorbance of cpx (cm^{-1})	0.91	1.03	0.72	1.47	0.91	1.07	0.95	0.57
Thickness of cpx (0.001mm)	132	134	75	75	125	125	101	98
Absorbance normalized to 1 cm (cm^{-1})	69	77	96	196	73	86	94	58
H_2O-cpx (ppm)	29	33	41	83	31	36	40	25
H_2O-melt (wt%)	0.20	0.20	0.36	0.66	0.26	0.29	0.37	0.19

Sample No. Section No. Point No.	38	39	40	41	41.2	42	42.2	43
SiO_2	51.50	51.03	51.21	51.68	51.69	51.54	52.29	51.84
TiO_2	1.23	1.21	1.18	0.88	1.01	1.00	0.71	1.24
Al_2O3	3.24	3.98	3.73	2.61	2.67	3.25	3.75	3.34
Cr_2O3	0.07	0.23	0.20	0.20	0.11	0.07	0.17	0.00
FeO	7.79	6.89	7.00	6.67	6.64	7.59	7.16	6.83
MnO	0.18	0.10	0.08	0.13	0.10	0.09	0.14	0.12
MgO	14.90	14.49	14.41	15.23	14.72	14.71	16.82	14.58
CaO	20.95	21.70	21.76	21.26	22.28	20.86	18.23	21.69
Na_2O	0.35	0.44	0.45	0.39	0.35	0.45	0.56	0.37
K_2O	0.00	0.00	0.02	0.00	0.00	0.00	0.00	0.00
NiO	0.00	0.00	0.04	0.07	0.00	0.02	0.06	0.00
Total	100.22	100.08	100.05	99.10	99.57	99.57	99.87	100.01
Si	1.90	1.89	1.89	1.92	1.92	1.91	1.92	1.91
Ti	0.03	0.03	0.03	0.02	0.03	0.03	0.02	0.03
Al	0.14	0.17	0.16	0.11	0.12	0.14	0.16	0.15
Cr	0.00	0.01	0.01	0.01	0.00	0.00	0.00	0.00
Fe	0.24	0.21	0.22	0.21	0.21	0.24	0.22	0.21
Mn	0.01	0.00	0.00	0.00	0.00	0.00	0.00	0.00
Mg	0.82	0.80	0.79	0.85	0.82	0.81	0.92	0.80
Ca	0.83	0.86	0.86	0.85	0.89	0.83	0.72	0.86
Na	0.03	0.03	0.03	0.03	0.03	0.03	0.04	0.03
K	0.00	0.00	0.00	0.00	0.00	0.00	0.00	0.00
Ni	0.00	0.00	0.00	0.00	0.00	0.00	0.00	0.00
Total	4.00	4.01	4.01	4.00	4.00	4.00	4.00	3.99
Mg#	77.32	78.94	78.59	80.27	79.81	77.56	80.74	79.18
$D^{(cpx\text{-}melt)}_{H_2O}$	0.0123	0.0133	0.0126	0.0105	0.0104	0.0114	0.0127	0.0112
Absorbance of cpx (cm^{-1})	1.37	0.33	0.70	0.97	1.47	0.99	1.61	1.19
Thickness of cpx (0.001mm)	110	111	132	128	128	122	122	131
Absorbance normalized to 1 cm (cm^{-1})	125	30	53	76	115	81	132	91
H_2O-cpx (ppm)	53	13	22	32	49	34	56	38
H_2O-melt (wt%)	0.43	0.09	0.18	0.31	0.47	0.30	0.44	0.34

Sample No. Section No. Point No.	44	45	45.2	46	47	47.2	48	49
SiO_2	51.77	49.80	52.91	50.69	50.01	50.94	51.57	51.51
TiO_2	1.19	1.58	0.60	1.21	1.59	0.93	1.15	0.86
Al_2O3	3.10	4.90	2.59	3.48	4.94	3.36	2.94	3.65
Cr_2O3	0.11	0.16	0.13	0.03	0.13	0.07	0.11	0.01
FeO	6.82	7.67	7.49	7.70	7.71	8.15	7.04	8.11
MnO	0.14	0.10	0.12	0.09	0.07	0.13	0.12	0.15
MgO	14.84	13.77	16.94	14.45	13.81	15.53	15.01	14.72
CaO	22.23	21.42	18.54	21.33	21.88	19.40	21.51	20.59
Na_2O	0.38	0.44	0.38	0.43	0.48	0.51	0.39	0.53
K_2O	0.00	0.00	0.01	0.00	0.00	0.00	0.00	0.00
NiO	0.00	0.04	0.06	0.04	0.00	0.05	0.02	0.00
Total	100.57	99.88	99.77	99.45	100.60	99.06	99.85	100.13
Si	1.90	1.85	1.94	1.89	1.85	1.90	1.91	1.91
Ti	0.03	0.04	0.02	0.03	0.04	0.03	0.03	0.02
Al	0.13	0.21	0.11	0.15	0.22	0.15	0.13	0.16
Cr	0.00	0.00	0.00	0.00	0.00	0.00	0.00	0.00
Fe	0.21	0.24	0.23	0.24	0.24	0.25	0.22	0.25
Mn	0.00	0.00	0.00	0.00	0.00	0.00	0.00	0.00
Mg	0.81	0.76	0.93	0.80	0.76	0.86	0.83	0.81
Ca	0.88	0.85	0.73	0.85	0.87	0.78	0.85	0.82
Na	0.03	0.03	0.03	0.03	0.03	0.04	0.03	0.04
K	0.00	0.00	0.00	0.00	0.00	0.00	0.00	0.00
Ni	0.00	0.00	0.00	0.00	0.00	0.00	0.00	0.00
Total	4.01	4.01	4.00	4.01	4.01	4.02	4.01	4.01
Mg#	79.52	76.19	80.13	76.99	76.15	77.25	79.17	76.39
$D^{(cpx\text{-}melt)}_{H_2O}$	0.0116	0.0166	0.0105	0.0129	0.0168	0.0131	0.0115	0.0123
Absorbance of cpx (cm^{-1})	1.35	1.74	1.00	1.69	1.47	1.94	0.98	1.10
Thickness of cpx (0.001mm)	131	129	129	129	130	130	135	126
Absorbance normalized to 1 cm (cm^{-1})	103	135	78	131	113	149	73	87
H_2O-cpx (ppm)	44	57	33	55	48	63	31	37
H_2O-melt (wt%)	0.38	0.34	0.31	0.43	0.28	0.48	0.27	0.30

Sample No.	SC-5							
Section No.	1							
Point No.	1	2	4	4.1	4.2	4.3	5	6
SiO_2	51.84	52.32	52.07	51.32	47.86	48.81	49.12	51.86
TiO_2	0.90	1.04	1.09	1.11	2.08	1.79	1.83	1.05
Al_2O3	2.80	2.73	2.86	3.20	5.71	5.44	4.92	2.88
Cr_2O3	0.21	0.06	0.13	0.07	0.00	0.06	0.11	0.11
FeO	6.83	7.49	6.97	7.41	8.64	8.96	8.13	7.57
MnO	0.13	0.14	0.08	0.11	0.12	0.14	0.14	0.14
MgO	15.53	14.98	15.27	14.58	12.74	12.73	13.69	15.05
CaO	20.44	20.83	21.68	21.29	21.60	21.14	21.29	20.68
Na_2O	0.39	0.42	0.36	0.42	0.54	0.49	0.49	0.45
K_2O	0.00	0.00	0.00	0.02	0.00	0.00	0.00	0.00
NiO	0.02	0.00	0.05	0.04	0.00	0.01	0.02	0.01
Total	99.08	100.01	100.55	99.57	99.29	99.56	99.74	99.79
Si	1.93	1.93	1.91	1.91	1.81	1.83	1.84	1.92
Ti	0.03	0.03	0.03	0.03	0.06	0.05	0.05	0.03
Al	0.12	0.12	0.12	0.14	0.25	0.24	0.22	0.13
Cr	0.01	0.00	0.00	0.00	0.00	0.00	0.00	0.00
Fe	0.21	0.23	0.21	0.23	0.27	0.28	0.25	0.23
Mn	0.00	0.00	0.00	0.00	0.00	0.00	0.00	0.00
Mg	0.86	0.82	0.84	0.81	0.72	0.71	0.76	0.83
Ca	0.81	0.82	0.85	0.85	0.87	0.85	0.85	0.82
Na	0.03	0.03	0.03	0.03	0.04	0.04	0.04	0.03
K	0.00	0.00	0.00	0.00	0.00	0.00	0.00	0.00
Ni	0.00	0.00	0.00	0.00	0.00	0.00	0.00	0.00
Total	4.00	3.99	4.01	4.00	4.03	4.01	4.02	4.00
Mg#	80.21	78.10	79.61	77.81	72.46	71.69	75.00	78.00
$D^{(cpx\text{-}melt)}_{H_2O}$	0.0107	0.0103	0.0112	0.0116	0.0220	0.0189	0.0184	0.0110
Absorbance of cpx (cm^{-1})	2.92	3.20	1.71	2.02	2.73	1.83	2.80	2.70
Thickness of cpx (0.001mm)	57	58	59	59	59	59	59	59
Absorbance normalized to 1 cm (cm^{-1})	512	552	290	342	463	310	475	458
H_2O-cpx (ppm)	217	233	123	145	196	131	201	194
H_2O-melt (wt%)	2.02	2.27	1.09	1.25	0.89	0.70	1.09	1.75

Sample No. Section No. Point No.	7	8	8.2	8.3	9	9.2	10	11
SiO_2	50.84	46.90	49.87	49.93	50.29	50.10	48.27	50.21
TiO_2	1.39	2.51	1.45	1.75	1.40	1.44	2.05	1.45
Al_2O3	3.57	6.71	4.72	4.65	4.23	5.10	5.84	4.25
Cr_2O3	0.00	0.08	0.17	0.21	0.34	0.15	0.05	0.28
FeO	8.78	8.73	7.26	7.91	6.74	8.51	9.35	7.05
MnO	0.13	0.12	0.07	0.11	0.01	0.11	0.13	0.05
MgO	14.13	12.38	13.73	13.76	13.82	13.49	12.56	13.79
CaO	21.22	21.23	21.70	21.50	22.28	20.88	20.39	22.00
Na_2O	0.46	0.52	0.48	0.45	0.42	0.50	0.54	0.45
K_2O	0.01	0.00	0.00	0.00	0.00	0.00	0.00	0.00
NiO	0.00	0.00	0.00	0.00	0.00	0.01	0.03	0.00
Total	100.52	99.17	99.45	100.27	99.53	100.29	99.19	99.53
Si	1.89	1.77	1.86	1.85	1.87	1.86	1.82	1.87
Ti	0.04	0.07	0.04	0.05	0.04	0.04	0.06	0.04
Al	0.16	0.30	0.21	0.20	0.19	0.22	0.26	0.19
Cr	0.00	0.00	0.00	0.01	0.01	0.00	0.00	0.01
Fe	0.27	0.28	0.23	0.25	0.21	0.26	0.29	0.22
Mn	0.00	0.00	0.00	0.00	0.00	0.00	0.00	0.00
Mg	0.78	0.70	0.76	0.76	0.77	0.75	0.71	0.77
Ca	0.84	0.86	0.87	0.85	0.89	0.83	0.82	0.88
Na	0.03	0.04	0.04	0.03	0.03	0.04	0.04	0.03
K	0.00	0.00	0.00	0.00	0.00	0.00	0.00	0.00
Ni	0.00	0.00	0.00	0.00	0.00	0.00	0.00	0.00
Total	4.01	4.02	4.01	4.01	4.01	4.01	4.01	4.01
Mg#	74.15	71.67	77.12	75.63	78.51	73.86	70.55	77.72
$D^{(cpx\text{-}melt)}_{H_2O}$	0.0136	0.0276	0.0155	0.0166	0.0141	0.0164	0.0210	0.0143
Absorbance of cpx (cm^{-1})	1.16	2.80	2.07	1.88	1.05	2.25	3.50	1.27
Thickness of cpx (0.001mm)	59	68	68	68	68	68	56	55
Absorbance normalized to 1 cm (cm^{-1})	197	412	304	276	154	331	625	231
H_2O-cpx (ppm)	83	174	129	117	65	140	264	98
H_2O-melt (wt%)	0.61	0.63	0.83	0.71	0.46	0.85	1.26	0.68

Sample No. Section No. Point No.	12	13	14	15	15.2	16	17	17.2
SiO_2	51.54	50.50	51.12	50.52	50.65	49.80	48.60	51.17
TiO_2	0.69	1.38	1.11	1.06	1.26	1.51	1.91	0.93
Al_2O3	2.71	4.03	3.49	3.40	3.43	4.73	5.39	3.24
Cr_2O3	0.16	0.10	0.12	0.10	0.04	0.23	0.17	0.05
FeO	6.60	7.76	7.85	7.64	8.30	7.83	7.90	8.42
MnO	0.08	0.06	0.14	0.10	0.13	0.13	0.14	0.11
MgO	15.16	14.25	14.55	14.58	14.19	13.60	13.36	15.34
CaO	21.86	21.64	20.94	20.92	20.89	21.20	21.40	19.37
Na_2O	0.36	0.44	0.41	0.46	0.39	0.44	0.47	0.46
K_2O	0.00	0.00	0.00	0.00	0.00	0.00	0.00	0.00
NiO	0.00	0.00	0.02	0.02	0.01	0.02	0.01	0.00
Total	99.17	100.15	99.74	98.80	99.27	99.50	99.34	99.09
Si	1.92	1.87	1.90	1.90	1.90	1.86	1.82	1.91
Ti	0.02	0.04	0.03	0.03	0.04	0.04	0.05	0.03
Al	0.12	0.18	0.15	0.15	0.15	0.21	0.24	0.14
Cr	0.00	0.00	0.00	0.00	0.00	0.01	0.01	0.00
Fe	0.21	0.24	0.24	0.24	0.26	0.24	0.25	0.26
Mn	0.00	0.00	0.00	0.00	0.00	0.00	0.00	0.00
Mg	0.84	0.79	0.81	0.82	0.79	0.76	0.75	0.85
Ca	0.87	0.86	0.83	0.84	0.84	0.85	0.86	0.77
Na	0.03	0.03	0.03	0.03	0.03	0.03	0.03	0.03
K	0.00	0.00	0.00	0.00	0.00	0.00	0.00	0.00
Ni	0.00	0.00	0.00	0.00	0.00	0.00	0.00	0.00
Total	4.01	4.01	4.01	4.01	4.01	4.01	4.02	4.01
Mg#	80.37	76.60	76.78	77.28	75.29	75.58	75.10	76.46
$D^{(cpx\text{-}melt)}_{H_2O}$	0.0105	0.0144	0.0125	0.0127	0.0127	0.0159	0.0198	0.0124
Absorbance of cpx (cm^{-1})	1.42	1.85	2.80	2.04	2.04	2.54	2.08	2.35
Thickness of cpx (0.001mm)	55	60	67	66	66	66	52	52
Absorbance normalized to 1 cm (cm^{-1})	258	308	418	309	309	385	400	452
H_2O-cpx (ppm)	109	130	177	131	131	163	169	191
H_2O-melt (wt%)	1.04	0.91	1.42	1.03	1.03	1.02	0.85	1.54

Sample No. Section No. Point No.	18	19	20	21	22	23	24	25
SiO_2	50.71	51.47	50.59	50.76	50.80	51.73	48.41	49.94
TiO_2	1.33	1.17	1.39	1.27	1.18	0.73	1.99	1.47
Al_2O3	4.15	3.09	3.83	3.66	3.30	4.24	5.17	4.34
Cr_2O3	0.21	0.12	0.01	0.19	0.04	0.27	0.09	0.19
FeO	6.79	7.26	8.01	6.90	8.36	7.22	8.24	7.30
MnO	0.05	0.16	0.13	0.07	0.10	0.11	0.08	0.05
MgO	14.07	14.88	14.11	14.29	14.27	16.98	13.24	13.78
CaO	22.32	20.77	21.62	21.88	20.56	17.62	22.00	21.84
Na_2O	0.43	0.39	0.44	0.39	0.41	0.56	0.39	0.39
K_2O	0.00	0.01	0.02	0.00	0.00	0.00	0.00	0.00
NiO	0.04	0.08	0.00	0.03	0.00	0.03	0.03	0.03
Total	100.09	99.40	100.13	99.43	99.02	99.48	99.63	99.33
Si	1.88	1.91	1.88	1.89	1.90	1.90	1.82	1.87
Ti	0.04	0.03	0.04	0.04	0.03	0.02	0.06	0.04
Al	0.18	0.14	0.17	0.16	0.15	0.18	0.23	0.19
Cr	0.01	0.00	0.00	0.01	0.00	0.01	0.00	0.01
Fe	0.21	0.23	0.25	0.21	0.26	0.22	0.26	0.23
Mn	0.00	0.00	0.00	0.00	0.00	0.00	0.00	0.00
Mg	0.78	0.82	0.78	0.79	0.80	0.93	0.74	0.77
Ca	0.89	0.83	0.86	0.87	0.83	0.69	0.89	0.87
Na	0.03	0.03	0.03	0.03	0.03	0.04	0.03	0.03
K	0.00	0.00	0.00	0.00	0.00	0.00	0.00	0.00
Ni	0.00	0.00	0.00	0.00	0.00	0.00	0.00	0.00
Total	4.01	4.00	4.01	4.00	4.00	4.00	4.02	4.01
Mg#	78.69	78.52	75.85	78.68	75.27	80.76	74.13	77.09
$D^{(cpx\text{-}melt)}_{H_2O}$	0.0137	0.0115	0.0139	0.0128	0.0122	0.0142	0.0201	0.0148
Absorbance of cpx (cm^{-1})	1.85	1.44	1.99	1.25	1.33	3.22	1.95	2.60
Thickness of cpx (0.001mm)	53	60	60	52	52	54	56	56
Absorbance normalized to 1 cm (cm^{-1})	349	240	332	240	256	596	348	464
H_2O-cpx (ppm)	148	102	140	102	108	252	147	196
H_2O-melt (wt%)	1.08	0.88	1.01	0.80	0.89	1.77	0.73	1.33

Sample No. Section No. Point No.	26	27	27.2	28	29	30	30.2
SiO_2	52.04	51.64	48.90	50.81	51.18	50.58	51.18
TiO_2	0.89	0.91	1.62	1.07	1.51	1.42	1.32
Al_2O3	3.01	2.76	4.67	3.19	3.83	4.83	3.38
Cr_2O3	0.11	0.16	0.24	0.13	0.00	0.00	0.05
FeO	7.79	6.98	7.36	7.61	8.07	7.18	7.73
MnO	0.10	0.09	0.06	0.12	0.13	0.13	0.13
MgO	14.96	15.34	13.87	14.74	13.91	13.86	14.48
CaO	20.81	21.18	22.06	21.46	21.55	21.61	21.17
Na_2O	0.36	0.32	0.47	0.45	0.37	0.47	0.42
K_2O	0.00	0.00	0.00	0.01	0.00	0.00	0.01
NiO	0.05	0.01	0.04	0.04	0.00	0.06	0.00
Total	100.11	99.38	99.30	99.63	100.54	100.14	99.86
Si	1.92	1.92	1.84	1.89	1.89	1.87	1.90
Ti	0.02	0.03	0.05	0.03	0.04	0.04	0.04
Al	0.13	0.12	0.21	0.14	0.17	0.21	0.15
Cr	0.00	0.00	0.01	0.00	0.00	0.00	0.00
Fe	0.24	0.22	0.23	0.24	0.25	0.22	0.24
Mn	0.00	0.00	0.00	0.00	0.00	0.00	0.00
Mg	0.82	0.85	0.78	0.82	0.77	0.76	0.80
Ca	0.82	0.84	0.89	0.86	0.85	0.86	0.84
Na	0.03	0.02	0.03	0.03	0.03	0.03	0.03
K	0.00	0.00	0.00	0.00	0.00	0.00	0.00
Ni	0.00	0.00	0.00	0.00	0.00	0.00	0.00
Total	4.00	4.00	4.03	4.02	4.00	4.00	4.00
Mg#	77.40	79.66	77.05	77.54	75.45	77.48	76.97
$D^{(cpx\text{-}melt)}_{H_2O}$	0.0109	0.0110	0.0179	0.0126	0.0130	0.0148	0.0124
Absorbance of cpx (cm^{-1})	1.50	2.26	2.44	1.18	1.84	2.21	1.85
Thickness of cpx (0.001mm)	64	66	66	66	65	56	56
Absorbance normalized to 1 cm (cm^{-1})	234	342	370	179	283	395	330
H_2O-cpx (ppm)	99	145	156	76	120	167	140
H_2O-melt (wt%)	0.91	1.32	0.87	0.60	0.92	1.13	1.13

Sample No. Section No. Point No.	31	32	33	34	35	36	37
SiO_2	50.56	50.27	50.41	50.24	49.50	51.80	52.03
TiO_2	1.42	1.46	1.34	1.36	1.78	0.96	0.95
Al_2O3	3.41	4.00	3.92	4.55	4.95	2.82	2.95
Cr_2O3	0.00	0.21	0.03	0.20	0.09	0.17	0.12
FeO	8.21	7.09	8.29	7.72	7.56	6.49	7.16
MnO	0.10	0.05	0.12	0.09	0.09	0.11	0.13
MgO	14.20	14.34	13.87	13.90	13.48	14.94	15.07
CaO	21.58	21.94	21.63	20.96	22.05	22.17	21.63
Na_2O	0.42	0.43	0.41	0.45	0.41	0.36	0.35
K_2O	0.00	0.00	0.00	0.02	0.00	0.00	0.00
NiO	0.03	0.07	0.04	0.06	0.01	0.05	0.05
Total	99.93	99.84	100.06	99.54	99.92	99.87	100.44
Si	1.88	1.87	1.88	1.87	1.84	1.92	1.92
Ti	0.04	0.04	0.04	0.04	0.05	0.03	0.03
Al	0.15	0.18	0.17	0.20	0.22	0.12	0.13
Cr	0.00	0.01	0.00	0.01	0.00	0.01	0.00
Fe	0.26	0.22	0.26	0.24	0.24	0.20	0.22
Mn	0.00	0.00	0.00	0.00	0.00	0.00	0.00
Mg	0.79	0.79	0.77	0.77	0.75	0.82	0.83
Ca	0.86	0.87	0.86	0.84	0.88	0.88	0.85
Na	0.03	0.03	0.03	0.03	0.03	0.03	0.02
K	0.00	0.00	0.00	0.00	0.00	0.00	0.00
Ni	0.00	0.00	0.00	0.00	0.00	0.00	0.00
Total	4.02	4.01	4.01	4.00	4.01	4.01	4.00
Mg#	75.51	78.28	74.90	76.24	76.08	80.42	78.97
$D^{(cpx\text{-}melt)}_{H_2O}$	0.0134	0.0146	0.0141	0.0149	0.0171	0.0107	0.0110
Absorbance of cpx (cm^{-1})	1.95	2.69	1.86	2.32	3.40	0.89	1.69
Thickness of cpx (0.001mm)	52	62	66	66	65	60	45
Absorbance normalized to 1 cm (cm^{-1})	375	434	282	352	523	148	376
H_2O-cpx (ppm)	159	184	119	149	221	63	159
H_2O-melt (wt%)	1.18	1.25	0.85	1.00	1.29	0.59	1.44

Sample No. Section No. Point No.	38	38.2	39	40	41	42	43	44
SiO_2	51.11	52.06	50.46	51.40	49.92	51.96	51.82	52.37
TiO_2	1.11	0.76	1.32	1.02	1.17	1.18	1.05	0.86
Al_2O3	3.42	4.18	4.10	3.51	4.43	3.00	3.05	2.79
Cr_2O3	0.08	0.30	0.37	0.09	0.32	0.20	0.12	0.11
FeO	7.84	7.81	6.46	8.54	6.51	6.88	6.84	7.11
MnO	0.12	0.09	0.12	0.12	0.09	0.11	0.12	0.14
MgO	14.64	16.95	14.44	15.14	14.77	15.24	14.80	15.71
CaO	21.11	17.84	22.21	19.46	21.00	21.28	22.00	20.11
Na_2O	0.39	0.56	0.39	0.45	0.52	0.40	0.39	0.39
K_2O	0.00	0.00	0.00	0.00	0.00	0.00	0.00	0.00
NiO	0.03	0.08	0.05	0.00	0.00	0.00	0.07	0.06
Total	99.86	100.62	99.92	99.73	98.75	100.25	100.24	99.65
Si	1.90	1.90	1.87	1.91	1.87	1.91	1.91	1.93
Ti	0.03	0.02	0.04	0.03	0.03	0.03	0.03	0.02
Al	0.15	0.18	0.18	0.15	0.20	0.13	0.13	0.12
Cr	0.00	0.01	0.01	0.00	0.01	0.01	0.00	0.00
Fe	0.24	0.24	0.20	0.26	0.20	0.21	0.21	0.22
Mn	0.00	0.00	0.00	0.00	0.00	0.00	0.00	0.00
Mg	0.81	0.92	0.80	0.84	0.82	0.84	0.81	0.86
Ca	0.84	0.70	0.88	0.77	0.84	0.84	0.87	0.80
Na	0.03	0.04	0.03	0.03	0.04	0.03	0.03	0.03
K	0.00	0.00	0.00	0.00	0.00	0.00	0.00	0.00
Ni	0.00	0.00	0.00	0.00	0.00	0.00	0.00	0.00
Total	4.01	4.01	4.01	4.00	4.02	4.00	4.00	3.99
Mg#	76.90	79.46	79.94	75.96	80.17	79.79	79.42	79.75
$D^{(cpx\text{-}melt)}_{H_2O}$	0.0125	0.0145	0.0144	0.0127	0.0153	0.0114	0.0111	0.0105
Absorbance of cpx (cm^{-1})	1.01	1.27	2.55	0.12	2.00	2.82	2.39	1.98
Thickness of cpx (0.001mm)	46	46	48	43	51	57	55	59
Absorbance normalized to 1 cm (cm^{-1})	220	276	531	28	392	495	435	336
H_2O-cpx (ppm)	93	117	225	12	166	209	184	142
H_2O-melt (wt%)	0.74	0.80	1.56	0.09	1.09	1.83	1.65	1.36

Sample No.	
Section No.	
Point No.	45
SiO_2	49.21
TiO_2	1.80
Al_2O3	5.28
Cr_2O3	0.14
FeO	7.22
MnO	0.12
MgO	13.50
CaO	21.28
Na_2O	0.50
K_2O	0.00
NiO	0.04
Total	99.09
Si	1.84
Ti	0.05
Al	0.23
Cr	0.00
Fe	0.23
Mn	0.00
Mg	0.75
Ca	0.85
Na	0.04
K	0.00
Ni	0.00
Total	4.01
Mg#	76.93
$D^{(cpx\text{-}melt)}_{H_2O}$	0.0177
Absorbance of cpx (cm^{-1})	1.73
Thickness of cpx (0.001mm)	61
Absorbance normalized to 1 cm (cm^{-1})	284
H_2O-cpx (ppm)	120
H_2O-melt (wt%)	0.68

Table 5-4. Source materials calculation for the Zhejiang basalts

	Start Materials			Mobility				Using Values	
	Sed	TABs	DMM	Sed[a]	Sed[b]	TABs[c]	TABs[d]	Sed	TABs
Temperature (℃)				900	900	900	800		
Pressure (GPa)				5.5	4.0	5.5	4		
Trace Elements		(ppm)							
Sc	6.94	15.9			4.5	0.3	0.33	6.63	15.85
V	90	150			23.2	2.6		69.09	146.10
Cr	164.5	76.4				3.2			73.96
Co	21.6	24.5			18.9	-1.7		17.53	
Ni	99.5	61				2.5			59.48
Cu	68.4	41.5		4		50.4		65.66	20.58
Zn	64.2	69.9				0.9			69.27
Rb	57	43.5	0.05	18	27.9	63	92	46.74	16.10
Cs	1.32	0.716		30	32.7	50.8	98	0.92	0.35
Sr	327	324	7.664	9.2	31.9	40.8	30.1	259.82	226.53
Ba	776	383	0.563	12	29.0	52.5	76	616.78	136.26
Y	25.9	27.2	3.328		6.6	-0.5	0.21	24.20	27.14
Zr	86	221	5.082		8.3		1.01	78.89	218.76
Hf	1.9	4.73	0.157		11.5		1.42	1.68	4.66
Nb	11.04	40.3	0.1485	4	9.3	3.6	7.9	10.60	38.85
Ta	0.758	2.42	0.0096		5.1	-0.4	2.35	0.72	2.36
La	20.78	22.2	0.192	7.5	3.1	56.1	19.3	19.22	9.75
Ce	31.54	51.9	0.55	7.3	10.1	50.7	11.1	29.24	35.87
Pr		6.81	0.107			42.4			3.92
Nd	21.03	27	0.581	8.3	7.0	30.7	3.20	19.55	22.42
Sm	4.62	5.87	0.239	5.2	3.9	13.6	1.45	4.44	5.43
Eu	1.15	1.92	0.096		-0.1	8.3	1.07		1.83
Gd	4.2	5.95	0.358		6.9	5	0.67	3.91	5.78
Tb		0.944	0.07			1.4			0.93
Dy	3.81	5.17	0.505		5.5	3.6	0.23	3.60	5.07
Ho		0.959	0.115			2.8			0.93
Er	2.12	2.55	0.348		3.5	0.6	0.11	2.04	2.54
Yb	1.86	2.21	0.365	0	28.1	1.4	0.09	1.34	2.19
Lu	0.268	0.337	0.058		1.1	-0.4	0.12	0.27	0.34
Pb	6	1.74	0.018	51	48.8	84.6	81	2.94	0.30
Th	2.62	2.44	0.0079	14	18.5	37.7	9.1	2.25	2.22
U	0.58	0.922	0.0032	12	26.4	29.1	18.8	0.43	0.65
Age (Ma)		157							
$^{87}Sr/^{86}Sr$	0.706170	0.704259	0.702190						
$^{143}Nd/^{144}Nd$	0.512520	0.512941	0.513130						
$^{206}Pb/^{204}Pb$	18.917	19.363	18.275						
$^{207}Pb/^{204}Pb$	15.646	15.553	15.486						
$^{208}Pb/^{204}Pb$	38.918	38.622							

Table 5-5. Modeling Source calculation for the Zhejiang basalts.

	DMM	RTABs	RSed		XL	GP	SC	SC*
				DMM	96.05%	98.70%	98.58%	97.61%
				R TABs	3.95%	1.02%	0.47%	1.77%
				R Sed		0.29%	0.95%	0.62%
Trace Elements	(ppm)							
Rb	0.05	16.10	46.74		0.68	0.35	0.57	0.62
Ba	0.56	136.26	616.78		5.92	3.71	7.08	6.79
Th	0.01	2.22	2.25		0.10	0.04	0.04	0.06
U	0.00	0.65	0.43		0.03	0.01	0.01	0.02
Nb	0.15	38.85	10.60		1.68	0.57	0.43	0.90
K			994					
La	0.19	9.75	19.22		0.57	0.34	0.42	0.48
Ce	0.55	35.87	29.24		1.95	0.99	0.99	1.35
Pb	0.02	0.30	2.94		0.03	0.03	0.05	0.04
Pr	0.11	3.92			0.26	0.15	0.12	0.17
Sr	7.66	226.53	259.82		16.31	10.61	11.10	13.10
Nd	0.58	22.42	19.55		1.44	0.86	0.86	1.09
Zr	5.08	218.76	78.89		13.53	7.47	6.79	9.32
Hf	0.16	4.66	1.68		0.34	0.21	0.19	0.25
Sm	0.24	5.43	4.44		0.44	0.30	0.30	0.36
Eu	0.10	1.83			0.16	0.11	0.10	0.13
Ti	716	13860	3993		1236	859.34	809.28	969.25
Gd	0.36	5.78	3.91		0.57	0.42	0.42	0.48
Tb	0.07	0.93			0.10	0.08	0.07	0.08
Dy	0.51	5.07	3.60		0.69	0.56	0.56	0.61
Ho	0.12	0.93			0.15	0.12	0.12	0.13
Y	3.33	27.14	24.20		4.27	3.63	3.64	3.88
Er	0.35	2.54	2.04		0.43	0.38	0.37	0.40
Tm								
Yb	0.37	2.19	1.34		0.44	0.39	0.38	0.40
Lu	0.06	0.34	0.27		0.07	0.06	0.06	0.06
$^{87}Sr/^{86}Sr$	0.70260	0.70449	0.70619					
$^{143}Nd/^{144}Nd$	0.51310	0.51289	0.51252					
$^{206}Pb/^{204}Pb$	18.27	21.38	18.97					
$^{207}Pb/^{204}Pb$	15.49	15.65	15.65					
$^{87}Sr/^{86}Sr$					0.70364	0.70326	0.70358	0.70362
$^{143}Nd/^{144}Nd$					0.51293	0.51301	0.51295	0.51296
$^{206}Pb/^{204}Pb$					19.53	18.79	18.78	18.98
$^{207}Pb/^{204}Pb$					15.55	15.55	15.59	15.58

Table 5-5 (continued)

	Partition coefficient				XL Melting Degree				
	ol	opx	cpx	grt					
Mineral modes	0.73	0.15	0.06	0.06	0.10%	0.50%	1.00%	1.50%	10.00%
Melt reaction	-0.0005	0.0049	-0.0131	-0.0013					
Rb	3E-4	2E-4	4E-4	2E-4	534.35	129.57	66.55	44.78	6.82
Ba	5E-6	6E-6	4E-4	7E-5	5766.62	1178.51	590.87	394.27	59.23
Th	5E-5	2E-3	5.7E-3	9E-3	44.51	15.52	8.55	5.90	0.94
U	3.8E-4	2E-3	1.1E-2	2.8E-2	7.69	3.73	2.27	1.63	0.28
Nb	5E-4	4E-3	1E-2	1.5E-2	503.59	229.13	136.28	96.98	16.43
K	2E-5	1E-4	1E-3	1.3E-2					
La	5E-4	4E-3	1.5E-2	7E-4	208.82	84.74	48.63	34.10	5.61
Ce	5E-4	4E-3	8.6E-2	2.1E-2	268.91	173.55	120.25	92.00	18.42
Pb	3E-3	9E-3	9E-3	5E-3	5.49	3.13	2.04	1.51	0.28
Pr									
Sr	4E-5	7E-4	9.1E-2	7E-4	2997.41	1730.87	1132.64	841.72	156.85
Nd	4.2E-4	1.2E-2	1.9E-1	8.7E-2	84.12	68.43	55.50	46.67	12.60
Zr									
Hf	1.1E-3	2.4E-2	1.4E-1	4E-1	9.43	8.51	7.58	6.83	2.56
Sm	1.1E-3	2E-2	1.5E-1	2.3E-1	17.45	15.13	12.97	11.35	3.64
Eu									
Ti	1.5E-2	8.6E-2	3.8E-1	2E-1	22559.63	21101.53	19524.15	18166.20	8323.97
Gd	1.1E-3	6.5E-2	1.6E-1	5E-1	11.79	10.93	10.02	9.25	4.01
Tb									
Dy	2.7E-3	6.5E-2	1.7E-1	2E+00	4.96	4.84	4.69	4.56	3.06
Ho									
Y									
Er	1.3E-2	6.5E-2	1.8E-1	3	2.12	2.09	2.05	2.01	1.53
Tm									
Yb	2E-2	8E-2	2.5E-1	5.5	1.21	1.20	1.19	1.18	1.03
Lu	2E-2	1.2E-1	2.8E-1	7	0.15	0.15	0.15	0.15	0.13

Table 5-5 continuted

Mineral modes Melt reaction	Partition coefficient Melting Degree					XL Melting Degree				
	0.10%	0.50%	1.00%	1.50%	10.00%	0.10%	0.50%	1.00%	1.50%	10.00%	0.10%
Rb	271.38	65.71	33.74	22.70	3.46	446.78	108.18	55.55	37.37	5.69	488.02
Ba	3600.62	736.78	369.46	246.54	37.04	6879.24	1407.66	705.87	471.04	70.77	6593.80
Th	15.57	5.79	3.24	2.25	0.36	16.80	6.24	3.50	2.43	0.39	25.79
U	2.48	1.31	0.82	0.60	0.11	2.31	1.22	0.77	0.56	0.10	3.90
Nb	154.86	74.45	45.15	32.40	5.58	116.40	55.96	33.94	24.35	4.20	243.20
K											
La	125.75	51.09	29.32	20.56	3.38	153.14	62.21	35.71	25.04	4.12	175.35
Ce	127.95	84.58	59.40	45.78	9.34	127.74	84.43	59.30	45.70	9.33	174.65
Pb	5.47	3.13	2.04	1.51	0.28	8.83	5.06	3.30	2.45	0.45	7.69
Pr											
Sr	1943.91	1123.96	735.94	547.07	102.01	2033.00	1175.48	769.67	572.15	106.69	2400.11
Nd	30.63	26.89	23.33	20.60	6.90	30.88	27.11	23.52	20.77	6.95	38.77
Zr											
Hf	4.55	4.20	3.83	3.52	1.48	4.24	3.91	3.56	3.27	1.38	5.41
Sm	8.30	7.51	6.71	6.06	2.30	8.29	7.50	6.70	6.06	2.30	9.75
Eu											
Ti	14468.91	13606.12	12662.29	11840.92	5631.14	13626.04	12813.51	11924.66	11151.13	5303.10	16319.44
Gd	6.94	6.54	6.10	5.71	2.75	6.85	6.45	6.01	5.63	2.71	7.81
Tb											
Dy	2.98	2.93	2.87	2.81	2.09	2.95	2.90	2.84	2.79	2.07	3.22
Ho											
Y											
Er	1.34	1.33	1.31	1.30	1.07	1.34	1.33	1.31	1.29	1.07	1.42
Tm											
Yb	1.03	1.02	1.01	1.00	0.88	1.02	1.01	1.00	0.99	0.87	1.07
Lu	0.12	0.12	0.12	0.12	0.11	0.12	0.12	0.12	0.12	0.11	0.13

Chapter 6 Geochemical heterogeneity in the source of Cenozoic basaltic rocks in the Fujian region

6.1 Results

6.1.1 Bulk-rock major and trace elements

The Fujian samples are plotted within a total alkali versus silica (TAS) diagram (Fig. 6-1), which all have low LOI less than 1.5 wt. % and mostly less than 1 wt. %, except the SH basalts (2.1-3%). The Fujian samples show a continuous trend in TAS diagram through basanites to trachybasalts. The MX basalts have low SiO_2 (<40 wt. %) and Al_2O_3 (<10.5 wt. %), high MgO (>12 wt. %), Fe_2O_3 (>13 wt. %), Mg# (>67), and TiO_2 (>2.8 wt. %). Meanwhile, the BL and NTS samples have lower MgO (<11 wt. %), Fe_2O_3 (<12 wt. %), Mg# (<67), and TiO_2 (<2.4 wt. %), higher Al_2O_3 (>11 wt. %). The SH basalts share the features of MgO, Fe_2O_3, and Al_2O_3 with BL and NTS, but have more TiO_2. In the plots of MgO vs. SiO_2, TiO_2, MnO, Na_2O, Fe_2O_3, and Al_2O_3 (Fig. 6-2) all the Fujian basalts show almost coherent trend, while the BL samples are missed in the plots of MgO vs. TiO_2 (Fig. 6-2e). The NTS samples are not in the plots of MgO vs. CaO and K_2O coherent trend of other samples as shown in Fig. 6-2g and h, and the internal variation of the BL samples in the plots of MgO vs. K_2O (Fig. 6-2h) have coherent trend with the NTS samples. Some MX samples with high MgO contents deviate far away from the main trend in the plots of MgO vs. MnO, Na_2O, Fe_2O_3, CaO, and K_2O in the plots of Fig. 6-2 c, d, f, g and h. All the detailed major elements results are listed in Table 6-1.

In the primitive mantle-normalized extended trace element patterns (Fig. 6-3a), all of the samples display OIBs-like patterns. All the Fujian samples have positive Nb (Ta) anomalies and negative Th and U anomalies. The Fujian samples except the NTS samples also share the negative Zr, Hf, and Ti anomalies. These geochemical characteristics have shared some similar points with those Cenozoic basalts in the Zhejiang region (Li et al., 2015 and Chapter 5). The NTS and BL samples also do not have the positive K anomalies, unlike the MX and SH samples. The NTS have the unique strong positive Zr, Hf, Ti, and Y anomalies, without the negative Pb anomalies, different from other Fujian samples. Most of the Fujian samples are characterized by high Ba/Th (100-160), Ce/Pb (>30), and high Nb/Ta (>17) in Fig. 6-3b, except the NTS

samples. Some SH samples have $(Rb/Ba)_n$ <1(n represents primitive mantle normalization(Sun and McDonough, 1989)), meanwhile, other Fujian samples have $(Rb/Ba)_n$ >1.

Fig. 2-1 TAS plots of the Fujian basalts. Classification of rock after Le Bas et al. (1986), and line

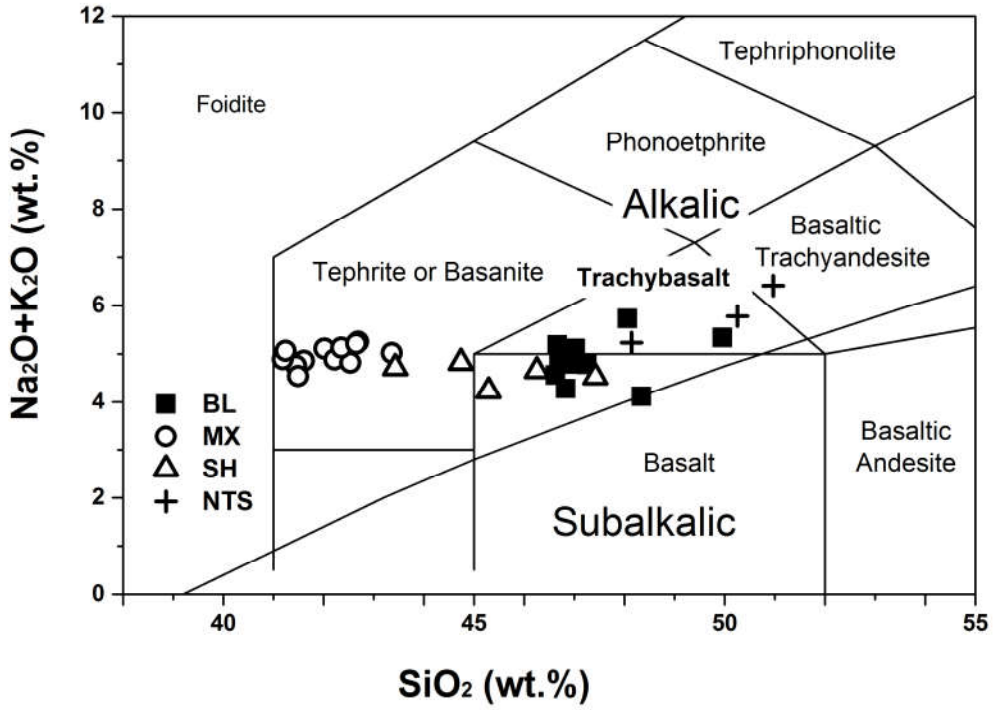

separating the alkali basalts and tholeiites from MacDonald and Katsura (1964).

Chondrite-normalized rare earth element (REE) patterns of the Fujian basalts show similar characteristics, with light rare earth element (LREE) enrichment and heavy rare earth elements (HREE) depletion (Fig. 6-3b), except the NTS samples. The REEs concentration of the Fujian samples decrease in order from MX, SH, BL to NTS (Fig. 6-3b). The $(La/Yb)_N$ (N represents chondrite-normalized, (Sun and McDonough, 1989)) of the Fujian samples approximately range from 17.3 to 24.1, from 22.7 to 25.6, from 27.2 to 39.0, and 56.9 to 97.0 for the BL, SH, MX, and NTS samples, respectively. Meanwhile, the NTS have the most depleted HREE contents and complex HREE pattern (Fig. 6-3b). The slightly positive Eu anomaly ($Eu_N/Eu^* = Eu_N/(Sm_N * Gd_N)^{1/2}$) are commonly observed for the Fujian samples.

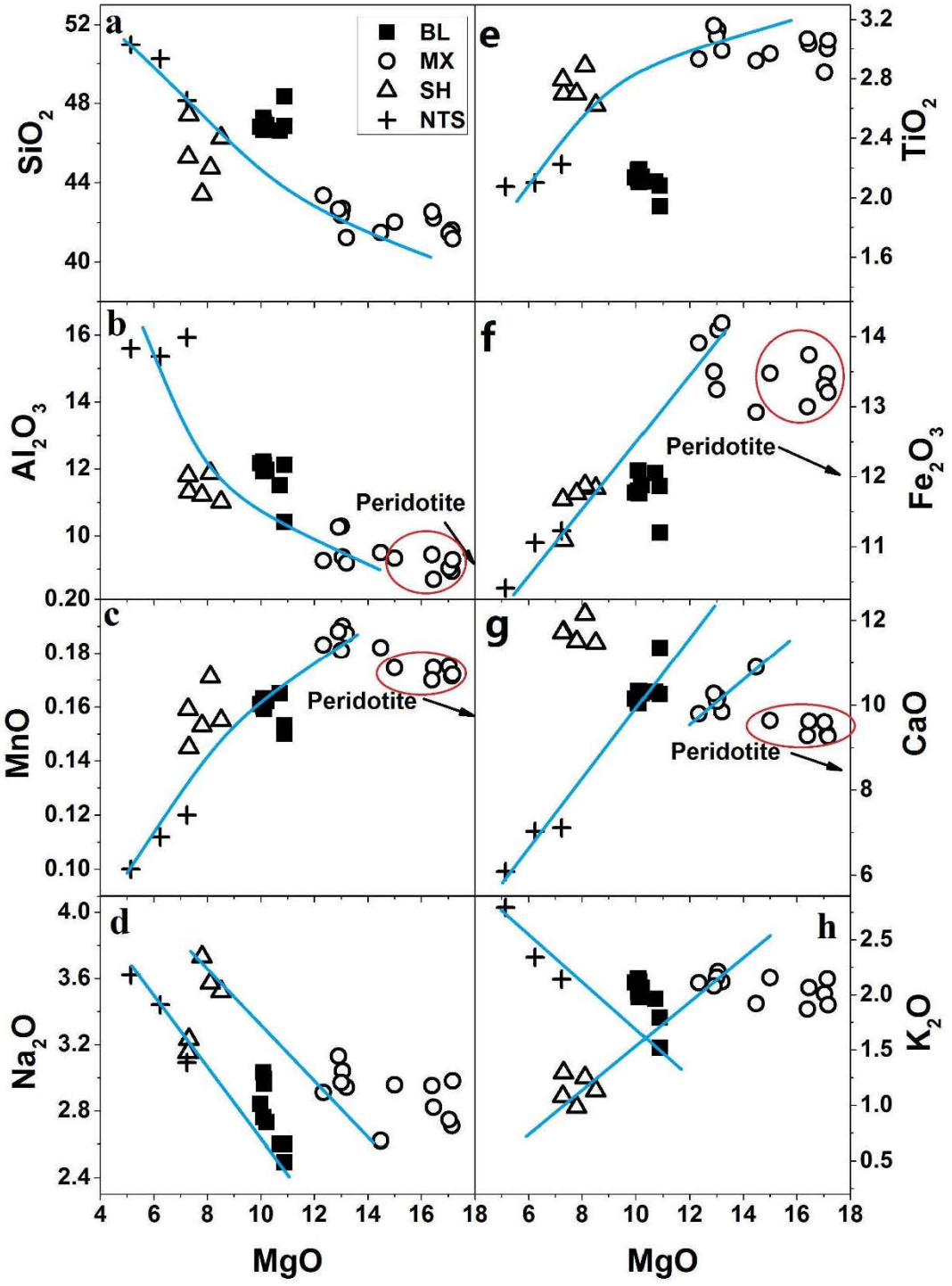

Fig. 6-2 Major element oxides vs. MgO in the Fujian basalts.

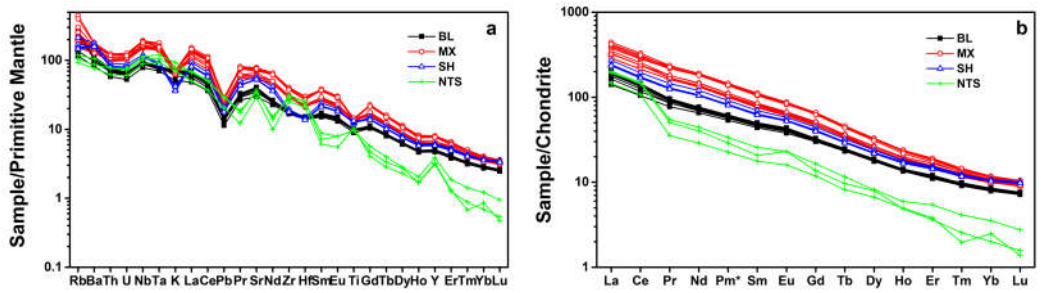

Fig. 6-3 Trace element abundances normalized by primitive mantle values and REE normalized by chondrite values in whole rocks of the Fujian basalts (Sun and McDonough, 1989) , whereas Pm*=((Sm)N *(Nd)N)1/2).

6.1.2 Sr-Nd-Pb isotopic compositions

Bulk rock Sr-Nd-Pb isotopic compositions of the Fujian samples are listed in Table 6-1 and plotted in Fig. 6-4. The MX basanites have homogeneous $^{87}Sr/^{86}Sr$ ratios from 0.703596 to 0.703676, $^{143}Nd/^{144}Nd$ ratios from 0.512849 to 0.512909 ($\varepsilon_{Nd(t)}$ values range from 4.1 to 5.3), $^{206}Pb/^{204}Pb$ ratios from 18.243 to 18.308, $^{207}Pb/^{204}Pb$ ratios from 15.503 to 15.591, and $^{208}Pb/^{204}Pb$ ratios of 38.320 to 38.620. Zou et al. (2000) has reported some Sr-Nd-Pb isotopic data for the MX basalts from 0.703601 to 0.703745, from 0.512903 to 0.512921, from 18.273 to 18.281, from 15.527 to 15.540, and from 38.211 to 38.274 for $^{87}Sr/^{86}Sr$, $^{143}Nd/^{144}Nd$, $^{206}Pb/^{204}Pb$, $^{207}Pb/^{204}Pb$, and $^{208}Pb/^{204}Pb$, respectively. These radiogenic isotope composition share similar range to our results. The SH samples have more radiogenic ratios of $^{87}Sr/^{86}Sr$ (0.704029-0.704243) and less radiogenic ratios of $^{143}Nd/^{144}Nd$ (0.512862-0.512892) than those of the MX samples. The ratios of $^{206}Pb/^{204}Pb$, $^{207}Pb/^{204}Pb$, and $^{208}Pb/^{204}Pb$ of the SH samples are 18.301-18.377, 15.487-15.570 and 38.328-38.606, respectively. The BL diabases have the ratios of $^{87}Sr/^{86}Sr$, $^{143}Nd/^{144}Nd$, $^{206}Pb/^{204}Pb$, $^{207}Pb/^{204}Pb$, and $^{208}Pb/^{204}Pb$ from 0.703847 to 0.704027, from 0.512794 to 0.512818, from 18.652 to 18.670, from 15.525 to 15.533 and from 38.862 to 38.872, respectively. The NTS samples have the most radiogenic ratios of $^{206}Pb/^{204}Pb$, $^{207}Pb/^{204}Pb$, and $^{208}Pb/^{204}Pb$ in all the Fujian basalts, which are from 18.915 to 18.941, from 15.581 to 15.594 and from 39.279 to 39.345, respectively. The Sr-Nd isotopic ratio of the NTS samples are from 0.703999 to 0.704049 and from 0.512778 to 0.512840, respectively. The Fujian samples share almost similar radiogenic Sr-Nd isotopic composition, consistent with the previous studies (Zou et al., 2000; Ho

et al., 2003). The plots of $^{87}Sr/^{86}Sr$ vs. $^{143}Nd/^{144}Nd$ ratios of the Fujian samples display a mixing trend together from DMM with EM components (Fig. 6-4a and b) and within the range of previously reported data for the Cenozoic basalts from eastern China (Chen et al., 2009; Choi et al., 2006; Fan et al., 2014; Guo et al., 2014; Ho et al., 2003; Ho et al., 2013; Huang et al., 2013; Kuang et al., 2012; Kuritani et al., 2011; Li et al., 2014; Sakuyama et al., 2013; Tang et al., 2006; Wang et al., 2012; Wang et al., 2013; Wang et al., 2011; Xu et al., 2005; Xu et al., 2012a; Xu et al., 2012b; Yan and Zhao, 2008; Zeng et al., 2011; Zhang et al., 2002a; Zhang et al., 2009; Zhang et al., 2012; Zhang et al., 2002b; Zhao et al., 2014; Zou and Fan, 2010; Zou et al., 2008; Zou et al., 2003; Zou et al., 2000). However, weak positive trends for the MX samples and other samples together are observed in the plots of Fig. 6-4b respectively. All the plots of $^{207}Pb/^{204}Pb$ vs. $^{206}Pb/^{204}Pb$ in Fig. 6-4c fall within the data region of SE China (reference are as same as Fig. 6-4a), located the right part to the Meteorite isochron.

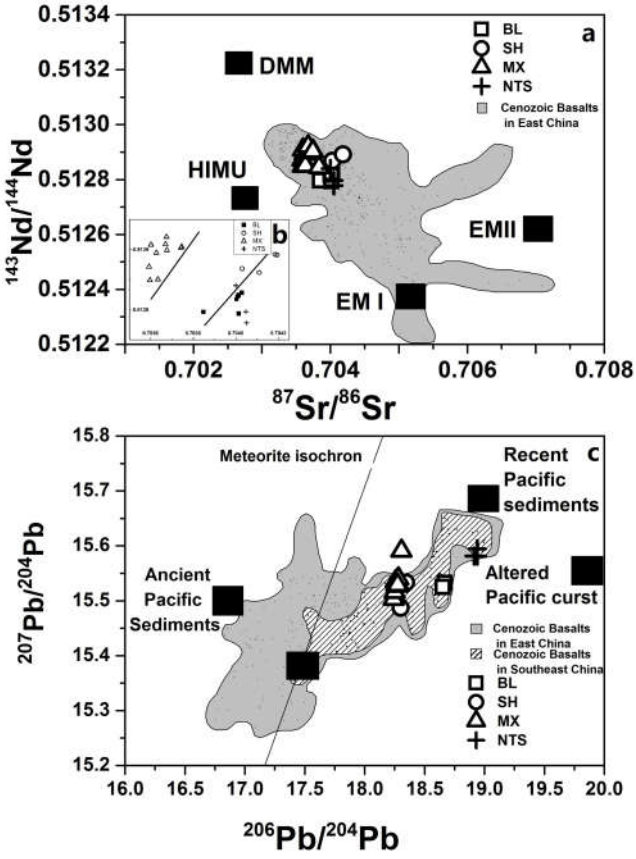

Fig. 6-4 (a) Sr–Nd isotopic compositions for the Fujian basalts; (b) Pb isotopic compositions for the Fujian basalts. The data source of Cenozoic basalts are the same as in Fig. 5-5.

6.1.3 Chemical and isotopic composition of cpx phenocrysts

6.1.3.1 Major elements of cpx phenocrysts

The cpx phenocrysts in the Fujian samples range from the augitic to the diopsidic, with Mg# varying from less than 70 to higher than 84, which are 68-84, 67-83 and 65-83, in SH, MX and BL, respectively. Most of the SH cpx phenocrysts have homogenous composition from core and rim, and the difference of Mg# in the same cpx phenocryst usually are less than 3 (Table 3). Some MX cpx phenocrysts have the xenocryst core inside the phenocryst rim. The MX cpx phenocrysts mostly are homogenous, while very few zonation are observed in a few MX cpx phenocrysts basalts showing relative high difference of Mg# between core and rim, which can be as high as 7, despite the xenocryst core. The BL cpx phenocrysts usually have growth zoning and show a relatively high difference between core and rim, ranging from 2 to 7, mostly about 5. The cpx phenocrysts show relatively low Cr_2O_3 and lower Mg#, in common, which are distinct from those of the cpx xenocrysts. The detailed cpx phenocryst major element compositions are listed in Table 6-2.

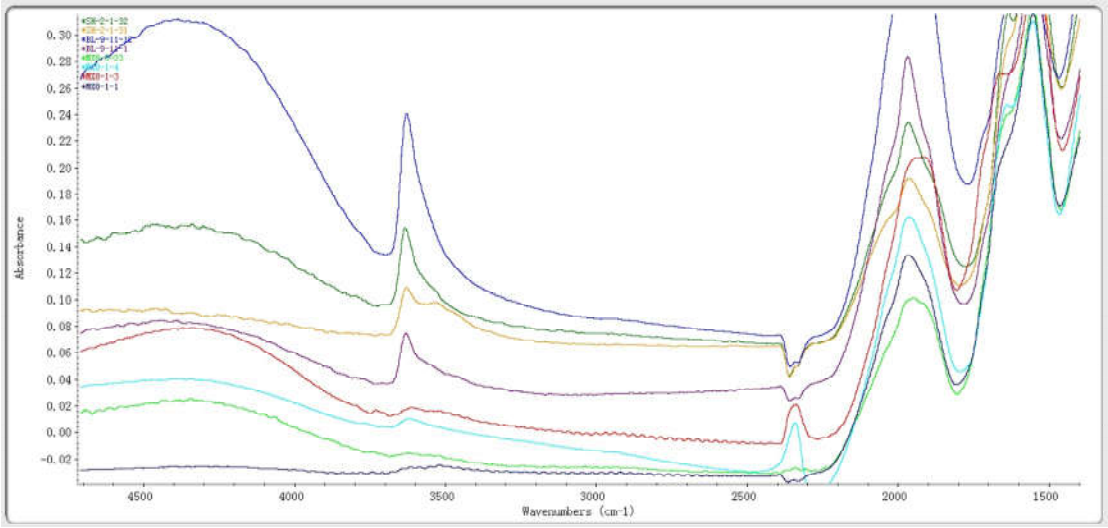

Fig. 6-5 (a) Representative OH IR absorption spectrum of the Fujian cpx phenocrysts.

6.1.3.2 Water content of cpx phenocrysts and equilibrated melts

The cpx phenocrysts of the Fujian samples have OH-typical IR absorption spectra in its stretching vibration region (3000-3800 cm^{-1}), and their IR bands are centered at 3630 cm^{-1} and 3540 cm^{-1} (Fig. 6-5), which consist with typical structural OH bands of cpx in previous studies (Bell et al., 1995; Denis et al., 2013; Ingrin and Skogby, 2000; Kovacs et al., 2012; Li et al., 2008; Peslier et al., 2002; Skogby et al., 1990; Sundvall and Stalder, 2011; Xia et al., 2010; Xia et al., 2013; Xia et al., 2014). The H_2O contents of the cpx phenocrysts for the MX samples range from 20 to 174 ppm, those of the SH samples range from 410 to 1079 ppm, and those of the BL samples range from 101 to 462 ppm. The detailed major element contents, absorbance of OH bands, section thicknesses, and the calculated H_2O content of the cpx phenocrysts are listed in Table 6-2. Some xenocrysts in the MX basalts have more enriched water contents (from 128 to 221 ppm) than those of the cpx phenocrysts, their IR absorption spectra are shown in Fig. 6-6, which fall within the range of cpx water content from the MX xenoliths (from 118 to 488 ppm) reported by Yu et al. (2011).

The partition coefficient ($D^{cpx\text{-}melt}$) of H_2O between cpx phenocryst and basaltic melt can be calculated using the equation provided by O'Leary (2010) O'Leary et al. (2010) which depend on cpx phenocryst chemistry. Therefore, the H_2O content of a corresponding equilibrated melts for each cpx phenocryst can be deduced from its H_2O content and its corresponding partition coefficient ($D^{cpx\text{-}melt}$) of H_2O between cpx phenocryst and basaltic melt. The preliminary results of the H_2O content of corresponding equilibrated basaltic melts range from less than 0.1% upto 1.2% for the MX samples, from 2.4% to 5.5% for the SH samples and from 1.7% to 4.0% for the BL samples. The detailed calculated data of water content for cpx grains and corresponding equilibrated basaltic melts are presented in Table 6-2.

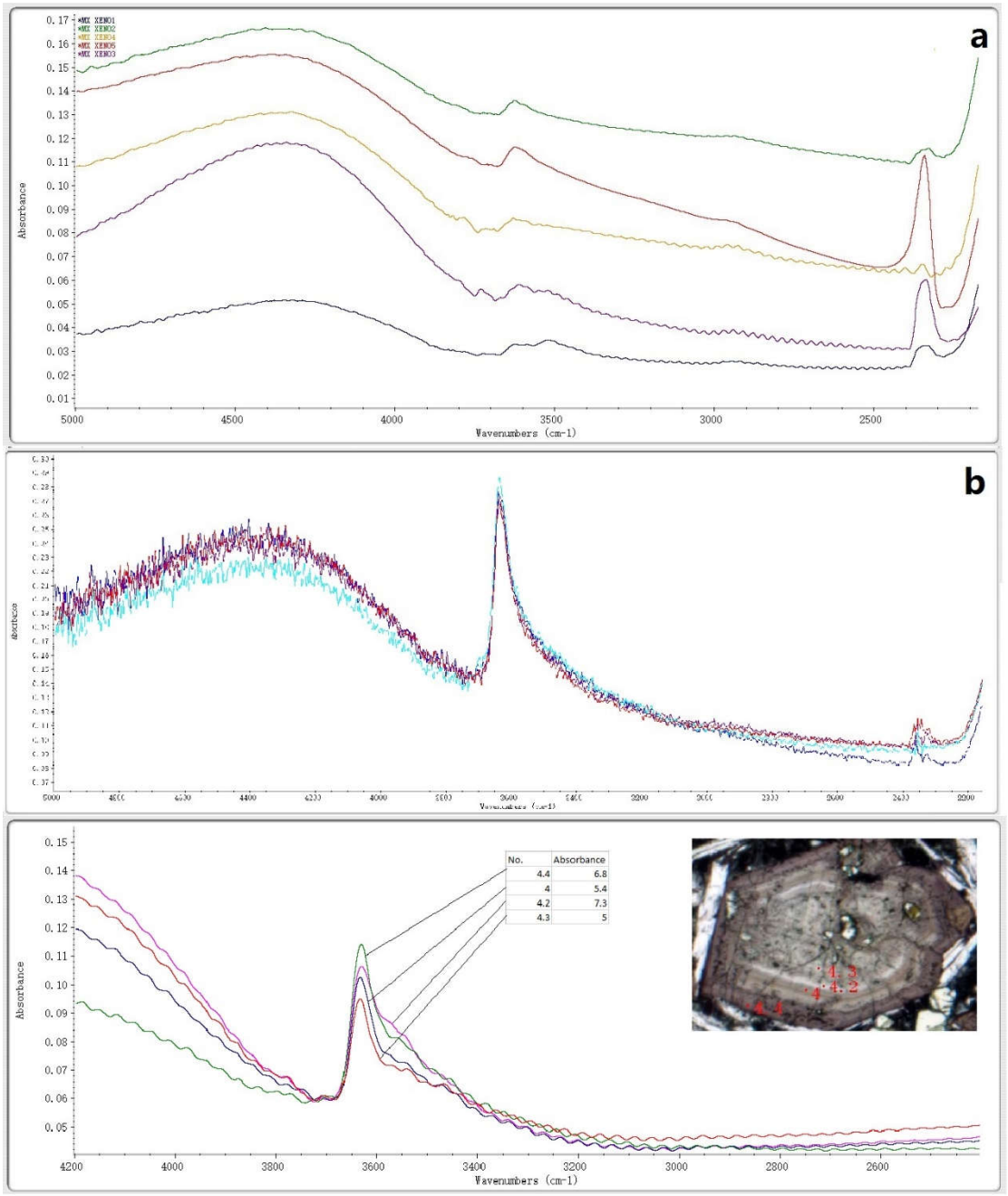

Fig. 6-6 (a) Representative OH IR absorption spectrum of the MX cpx xenocrysts; (b) the profiles of OH IR absorption spectrum of the SH cpx phenocrysts; and (c) the profiles of OH IR absorption spectrum of the BL cpx phenocrysts.

6.1.3.3 Li and O isotopic compositions of cpx phenocrysts

The Li and O isotope of cpx phenocrysts are analyzed for the MX, SH, and BL samples. All the analytical sessions of both Li and O isotope for the cpx standards display associated chemical composition matrix effect (Fig. 6-7).

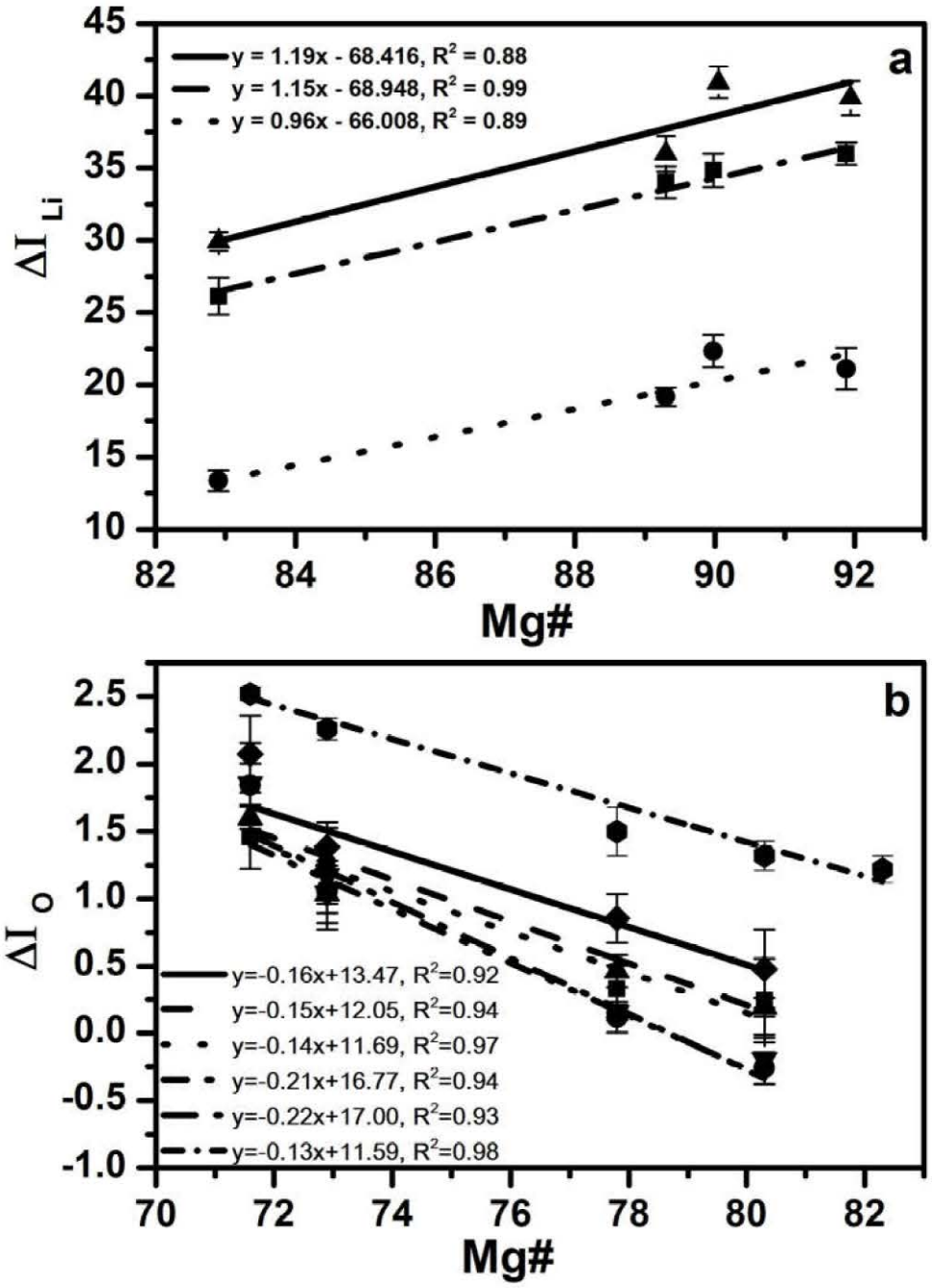

Fig. 6-7 (a) Plots of matrix effect vs. composition of standard for Lithium and (b) Plots of matrix effect vs. composition of standard for Lithium Oxygen.

6.1.3.3.1 Li content and Li isotopic compositions

The matrix effect in the Li analysis through SMIS with various cpx element composition can be observed in our analysis (Fig. 6-7). The slopes of δ^7Li IMF to Mg# for cpx phenocrysts are approximately from 1.0 to 1.2 in different session either on IMS 1270 or IMS 1280 (Fig. 6-7), as described by Bell et al. (2009) for olivine (the slop of Mg# vs. IMF for ol is about 1.3). All the number of the measured samples are listed and presented in the Table 6-3. The variation of IMF with cpx chemical composition is discussed in detail in the Chapter 4. The most suitable range of Mg# and Si for the unknown samples is from 80 to 94 and from 1.78 to 1.94, respectively. The Li content calculation also follow the methods described in Chapter 4, and are listed and presented in the Table 6-3 and Fig. 6-8, despite the range of Mg#. The results of corrected δ^7Li are presented in Table 6-3 and Fig. 6-8. When the δ^7Li of cpx phenocryst are compared among different grains they will be limited within the range of Mg# from 78 to 92. As we discussed in Chapter 4, when δ^7Li profile in single grain is discussed, the extend range of Mg# are used to correct the IMF.

The corrected δ^7Li values of the MX cpx phenocrysts range from +5 to +25‰, mostly falling within the range from +10 to +25 ‰ and Li content of the MX cpx phenocrysts have almost from 2 to 6 ppm (Fig. 6-8a). However, the cpx xenocrysts in MX have much lower δ^7Li ranging from -6 ‰ to +10 ‰ (mostly from -6 to -2‰), with higher Li content of more than 20 ppm (Fig. 6-8c). The intra-grain Li content profiles of the cpx xenocrysts and phenocrysts are almost homogeneous for each grain, respectively (Fig. 6-8b). Limited various δ^7Li are observed in some cpx phenocrysts, in Fig. 6-8b. When the xenocrysts are excluded, the Mg# of cpx phenocrysts do not display linear relationship with corrected δ^7Li values or Li content (Fig. 6-8c), both the lowest δ^7Li and the highest δ^7Li cpx phenocrysts are observed with Mg# around 80.

The Li contents of cpx phenocrysts in SH range from 1.3 to 18.5 ppm and the δ^7Li values range from -10 to +35‰ (Fig. 6-8d). In the plots of δ^7Li values vs. Li contents, most of the cpx phenocrysts fall below the line of y=-0.5x+20, suggesting the cpx phenocrysts with low Li contents usually have high δ^7Li while the cpx phenocryst with high Li content have low δ^7L. The detailed intra-grain profiles of these cpx phenocrysts are more complex and can be divided into two kinds of profiles (Fig. 6-8e): a) some cpx phenocrysts have high δ^7Li and high Li content in the core but lower δ^7Li and low Li content than those at the rim; b) some cpx phenocryst grains have the opposite of above trend. However, the homogeneous Li content and δ^7Li are rarely found in cpx

phenocrysts. The Li contents and δ^7Li do not show correlation with Mg # (Fig. 6-8f). The Li contents can increase from less than 5ppm up to more than 15ppm in single grains.

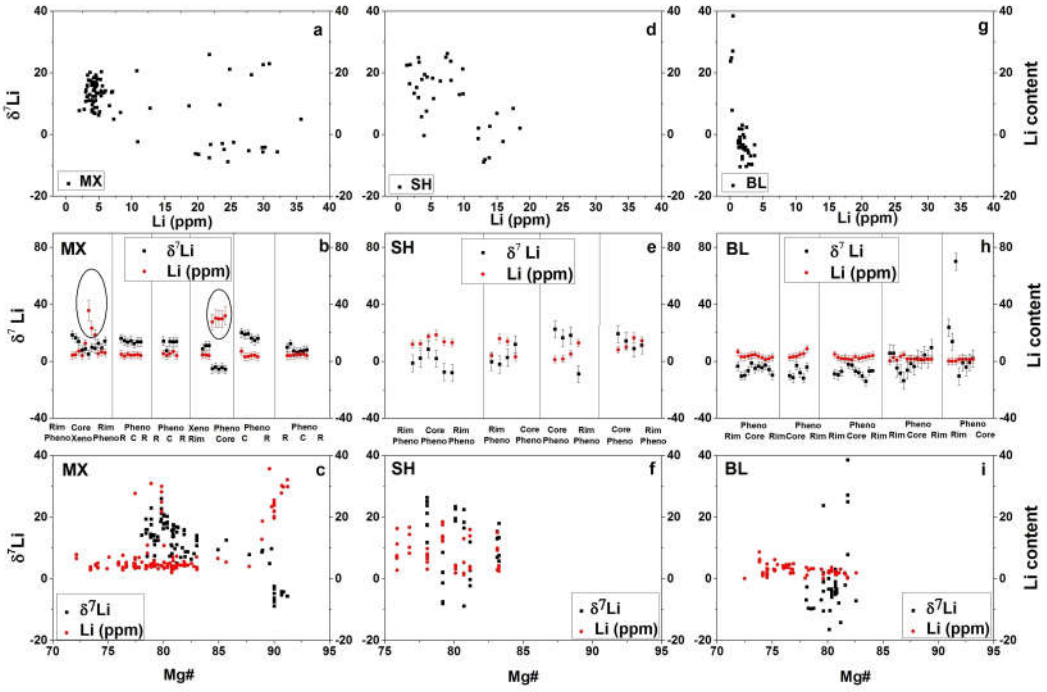

Fig. 6-8 (a) Plots of Lithium isotopic data vs Lithium content for cpx phenocryst and xenocrysts of the MX basalts; (b) Profiles of cpx phenocryst intra-grain δ7Li and Li content of the MX basalts; (c) Plots of δ7Li and Li vs. Mg# of the MX basalts; (d) Plots of Lithium isotopic data vs Lithium content for cpx phenocryst and xenocrysts of the SH basalts; (e) Profiles of cpx phenocryst intra-grain δ7Li and Li content of the SH basalts; (f) Plots of δ7Li and Li vs. Mg# of the SH basalts; (g) Plots of Lithium isotopic data vs Lithium content for cpx phenocryst and xenocrysts of the BL basalts; (h) Profiles of cpx phenocryst intra-grain δ7Li and Li content of the BL basalts; and (i) Plots of δ7Li and Li vs. Mg# of the BL basalts.

The BL samples have some very large cpx phenocryst grains of up to 0.8 cm size, which allow more point analyses on them. The SIMS results show that the Li content of cpx phenocrysts in BL range from 0.1 to 9 ppm and the δ^7Li range from -16 to 38‰ (Fig. 6-8g), meanwhile, the most highest δ^7Li value appear at the grains with the lowest Li content. Some cpx phenocryst with growth zone usually have lower Mg# at the outermost rim and higher Mg# at the core and the mantle of cpx grains. The cpx

phenocrysts in BL have two kinds of Li content and δ^7Li values profiles: a) the rim has higher Li content and the core has lower Li content, with unclear δ^7Li profiles; b) the cpx phenocrysts have homogeneous Li content but low δ^7Li valley at the core (Fig. 6-8h); (c) the cpx phenocrysts have homogeneous Li content but high δ^7Li peak at the core. Unlike the MX and SH cpx phenocrysts, BL cpx phenocrysts have larger range of δ^7Li but limited range of the Li contents with the highest Mg# (Fig. 6-8f).

6.1.3.3.2 O isotopic compositions

Beside very few parts, the chemical compositions of the Fujian cpx phenocrysts fall within the range of chemical composition of standards (Table 3-3). The δ^{18}O IMF of the Nushan standards decrease with the decreasing Mg# (Fig. 6-7), and the R^2 usually are better than 0.9. The drift of SIMS are monitored by the standard grains fixed on the analysis sections. The raw analytical results of the standard (NSH9 or NSH5) and Fujian cpx phenocrysts are listed in Table 6-4.

The δ^{18}O values with their Ca/Al, Si/^{IV}Al, and Mg# values are plotted in Fig 6-9 a, b, and c. The features observed in Fig 6-9a, b, and c are: (1) the δ^{18}O values of the MX and BL cpx phenocrysts range from +4.3‰ to +8.2‰ and from +4.3‰ to +8.2‰, respectively, which straddle the typical normal mantle value of 5.7±0.2‰ (Eiler 2001; Mattey et al., 1994), and the SH cpx phenocrysts range from +5.4‰ to +8.2‰, most of the Fujian cpx phenocrysts have higher δ^{18}O than the normal mantle value; (2) the highest δ^{18}O values appear despite the Mg# of cpx phenocrysts in BL and SH basalts, but a weak positive relationship between the δ^{18}O and the Mg# are observed in MX basalts, (3) the highest δ^{18}O values appear in the cpx phenocryst with intermediate Ca/Al or Si/Al.

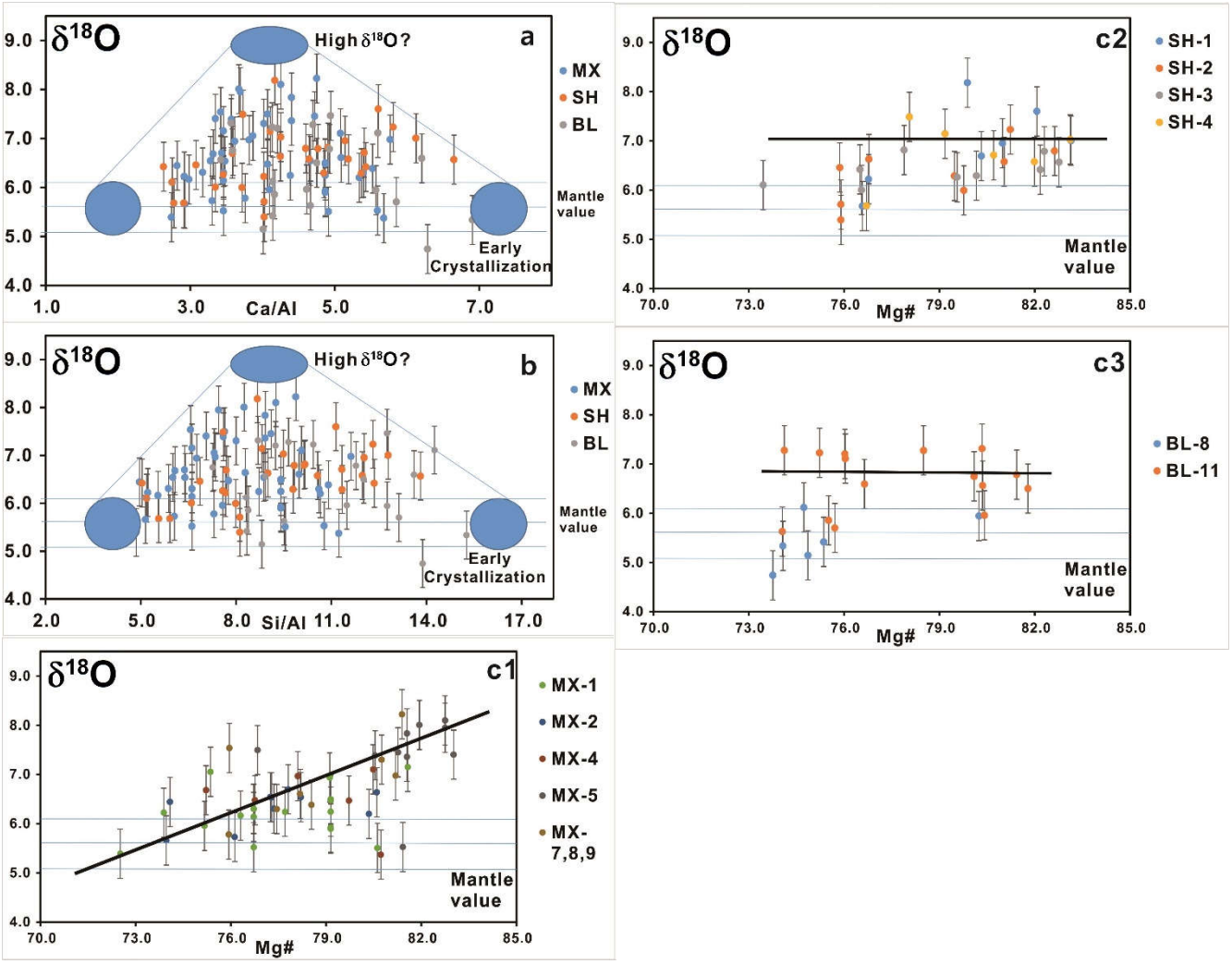

Fig. 6-9 (a) the plots of the $\delta^{18}O$ values vs. Ca/Al (afu ratios) for the Fujian basalts samples; (b) the plots of the $\delta^{18}O$ values vs. Si/^{IV}Al (afu ratios) for the Fujian basalts samples; and (c) the plots of the $\delta^{18}O$ values vs. Mg# for the Fujian basalts samples.

6.2 Discussions

6.2.1 Crustal/peridotite assimilation and fractional crystallization

The assimilation of continental crusts or co-existing plutonic ultramafic xenoliths/xenocrysts and the fractional crystallization are potential influence factors for the chemical compositions of our samples. Because (1) some Fujian basalts have considerable xenocrysts and peridotite xenoliths, which may be reacted with and assimilated by magma or mixed into bulk rock powders by mistakes; (2) the BL

diabases are intrusive body leaving long residence time for cooling and crystallization; (3) the SH basalts contain limited peridotite xenocrysts and the NTS samples are tholeiites, both of them may have a low ascent speed and leave long residence time before eruption (O'Reilly and Griffin, 2010). Abundant peridotite xenoliths were entrained by the MX samples implying that the MX samples ascend rapidly leaving little time for continental crustal contamination (O'Reilly and Griffin, 2010). Therefore, the assimilation of the co-existing plutonic ultramafic xenoliths/xenocrysts is needed to focus on for the MX samples, while the assimilation of continental crusts is needed to focus on for other Fujian samples. Assimilation of continental crustal and fractional crystallization will result in the composition variation of the basaltic melts. Pb and U are relatively enriched in crust (Jahn et al., 1999; Rudnick and Gao, 2003), but Nb are relatively depleted, so if the continental crust sneaked into the basaltic melts, the low ratios of Nb/U and Ce/Pb will be observed in the plots in Fig. 6-10a. However, most of the Fujian samples have OIBs-like high Ce/Pb (>25), and high Nb/U ratios (>50), as shown in Fig. 6-10a, consistent with the values for the global primary OIBs and MORBs (Ce/Pb=25±5, Nb/U=40±7, Hoffmann et al., 1986), despite the low Ce/Pb (19.7-21.1) in the NTS samples. Meanwhile, the plots for 1/Sr vs $^{87}Sr/^{86}Sr$ in Fig. 6-10b do not show negative trend which is also arguing against the assimilation of continental crust.

The fractional crystallization/ assimilation of olivine xenocryst will cause a positive trend in the plots of Ni vs. MgO, due to Ni are enriched in peridotites, as well as MgO, but not so enriched in cpx and opx. A positive Ni-MgO correlation is observed in the MX and NTS samples (Fig. 6-11a), but not in other Fujian samples, suggesting the fractional crystallization/assimilation of olivine is limited in the SH and BL samples, while the MX samples whose Ni content are higher than 500ppm might involve some olivine xenocryst and the NTS samples have undergone fractional crystallization of ol. Meanwhile, Cr are enriched in peridotites, but CaO are lower than those in basaltic rocks, because of low Cr and CaO content in opx and ol. The assimilation of cpx will result in a negative trend in the plots of Cr vs. CaO, as the six samples of the MX basalts shown in the plots of Fig. 6-11b, which also have the highest Ni and MgO content, in Fig. 6-11a. The influence of peridotite assimilation for these six MX samples are also suspected from the plots of major elements vs. MgO in Fig. 6-2c, f, and g. The assimilation of xenocrysts or mixture of xenocrysts into bulk rock powder should have limited influence on other MX samples. Although the major element compositions of these six MX samples are influenced by broken peridotite xenocrysts, the ratios of trace

elements, and radiogenic isotopes such as Ce/Pb, Nb/La, and Ba/Th are hard to be changed by xenocrysts, because of the high concentration of these incompatible trace elements in basaltic magma. The high $Fe_2O_3^T$ should also be an original feature, due to relatively low Fe in the peridotite xenocrysts. Although, the BL and NTS samples contain a few peridotite xenoliths, the bulk rock composition of BL and NTS can represent their original geochemical characteristics, because the peridotite xenoliths in the BL and NTS basalts are unbroken and only the xenolith-free fragments are chosen for later crushing during bulk rock powder preparation, demonstrated by the plots Fig. 6-2 and 6-11.

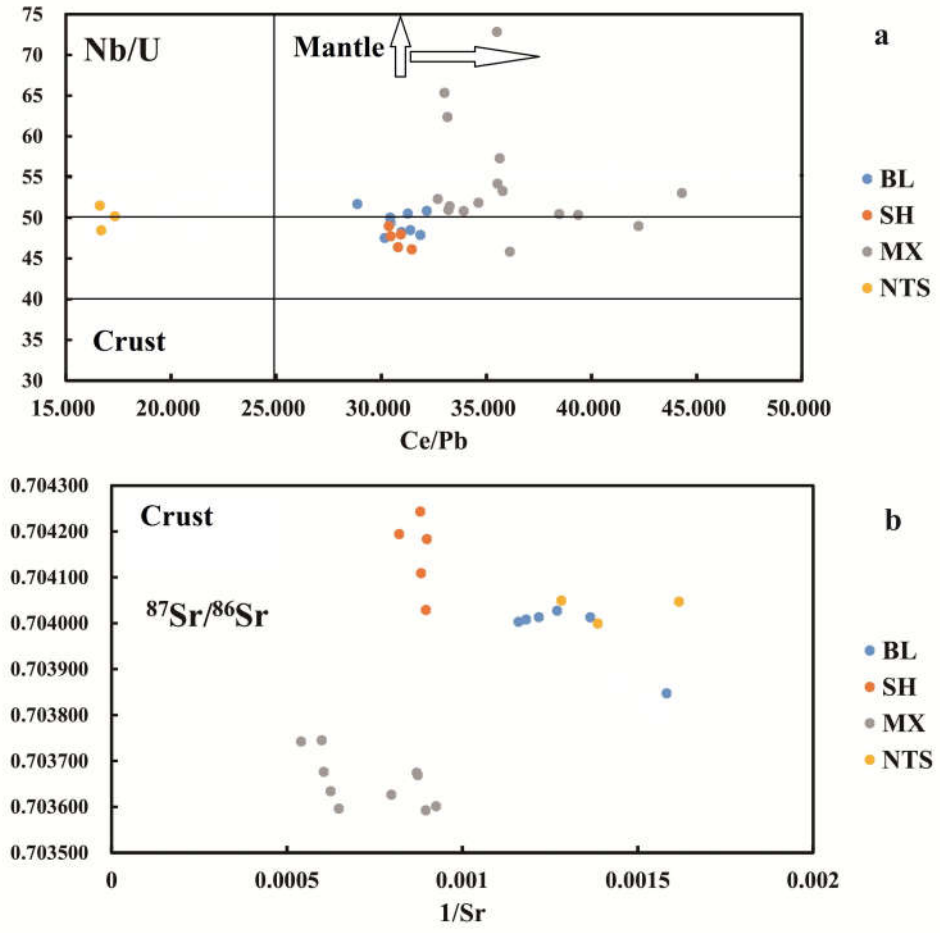

Fig. 6-10 (a) Ce/Pb vs. Nb/U for the Fujian basalts samples (the MORB range was obtained from Rapp et al. (2008)); and (b) $^{87}Sr/^{86}Sr$ ratios vs. 1/Sr for the Fujian basalts samples.

The BL and SH samples have almost same Ni concentration, suggest limited ol fractional crystallization or assimilation (Fig. 6-11a). Due to high contents of CaO in cpx, fractional crystallization of cpx from a basaltic magma results in decreasing

CaO/Al_2O_3 with Mg# decrease (Spath et al., 2001). In the plot of CaO/Al_2O_3 vs. Mg# (Fig. 6-11c), such a clear trend are found in the BL diabases, and the weaker trend in the NTS, MX and SH is noticed. It suggests the fractional crystallization of cpx is limited in SH and NTS samples and certain proportion of cpx fractional crystallization occurred in BL diabases. Because of potential xenocryst assimilation in some MX samples, it is hard to make sure that such disorder CaO/Al_2O_3 vs. Mg# in the MX samples is caused by either the xenocryst assimilation together with fractional crystallization of cpx or no fractional crystallization of cpx. The Cr in cpx phenocrysts ranging from 0 to 0.6% with an average of about 0.15% (1500 ppm) is higher than the Cr content in basaltic rocks, and the CaO is about 20%. When the basaltic rocks have undergone significant fractional crystallization of cpx, they will exhibit a positive trend in the plot of Cr vs. CaO. All the MX samples have high CaO content, suggesting the cpx fractional crystallization is insignificant. In addition, positive Ba and Eu anomalies of all the Fujian basalts (Fig. 6-3) exclude a significant fractional crystallization of pl. In no case, the ratios of incompatible trace elements and Sr-Nd-Pb isotope are not sensitive to fractional crystallization of ol even cpx and the assimilation of peridotite, due to the relative low trace elements contents in conglomerates and peridotites to basaltic magma.

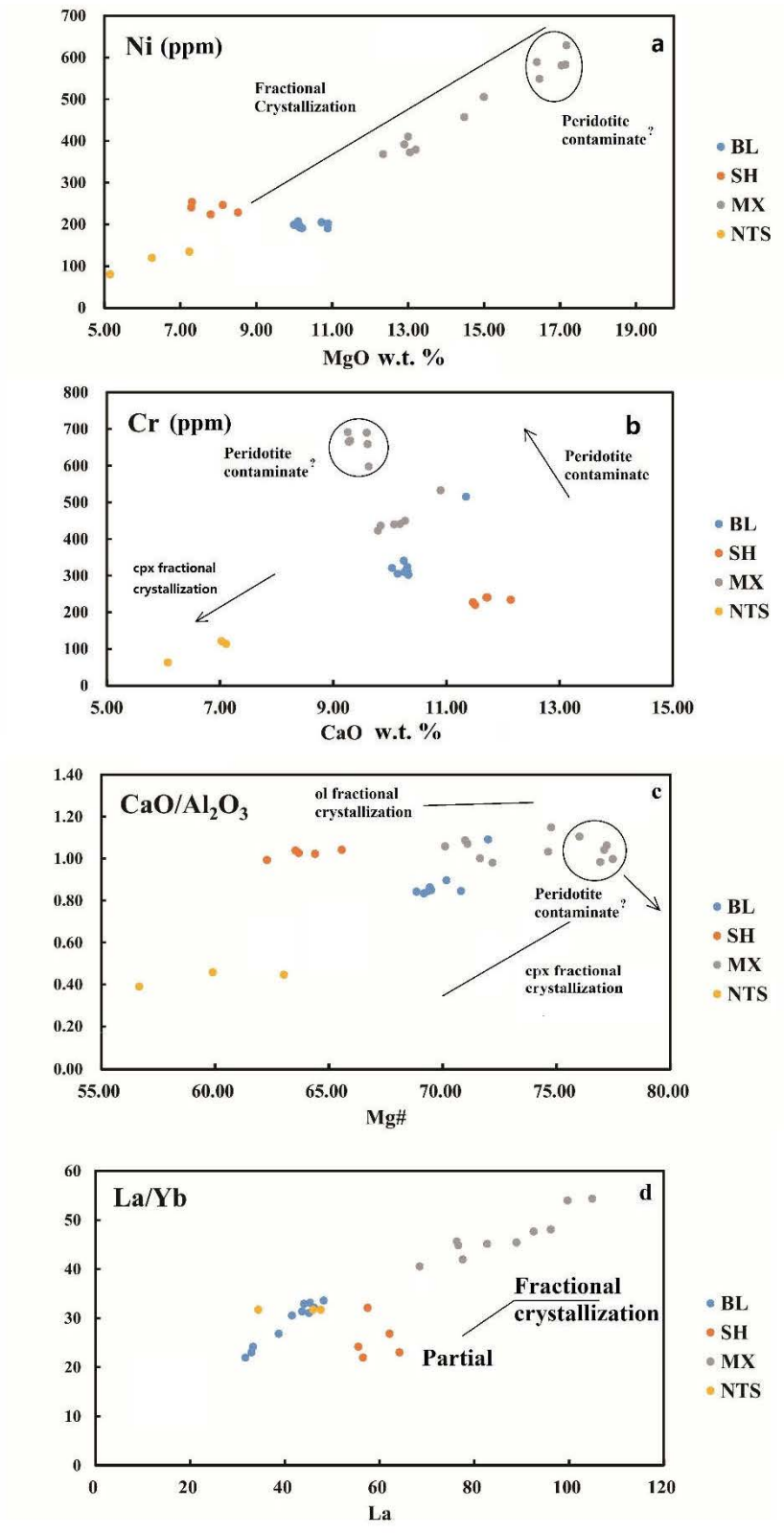

Fig. 6-11 (a) Ni vs. MgO for the Fujian basalts samples; (b) Cr vs.CaO for the Fujian basalts samples; (c) CaO/Al_2O_3 vs. Mg# for the Fujian basalts samples; and (d) La/Sm vs. La for the Fujian basalts samples.

6.2.2 Variation of δ^7Li and Li content

The entire δ^7Li and Li content variation of the Fujian basalts have been described in section 6.1.3. The variation of δ^7Li and Li content in cpx phenocryst are either the record of the magma evolution or the result of Li diffusion. Relative to the SH and BL cpx phenocrysts, the MX cpx phenocrysts that do not have xenocryst core have limited variation of δ^7Li and Li content. The SH and BL cpx phenocryst have more complex δ^7Li and Li content zonation. This zonation is an inherent feature of pristine phenocryst material and is not the result from an alteration effect from Li isotope fractionation during secondary alteration (Pistiner and Henderson, 2003). The obvious complication to the zonation lies in the profiles observed in the cpx phenocrysts from the Fujian basalts (Fig. 6-8). The variability of Li isotope and Li content in the cpx phenocrysts must arise from changing physicochemical conditions during crystal growth or subsequent diffusion of Li in solid-state after magma eruption or invasion (Rudnick et al., 2007). The high diffusivity of Li ensure rapid isotopic equilibration at magmatic temperatures, equilibrium may be disturbed by continued diffusive movement of Li during cooling, at temperatures well below the point at which most cations are effectively immobile. The ^{6}Li diffuses faster than the ^{7}Li, the difference of diffusion speed will result in the fractionation of ^{6}Li and ^{7}Li. The variation of temperature ($D_{Li}^{cpx\text{-}melt}$), f_{O_2}, the Li content, and δ^7Li in melts can result in the fractionation of Li (Richter et al., 2014). The Li diffuses fast in melts and minerals (Richter et al., 2003), especially for cpx, with several orders of magnitude faster than other common metal cations in melts at magma temperature (Coogan et al., 2005; Van Orman et al., 2001; Giletti and Shanahan, 1997). The 1 mm wide zone of Li in cpx can disappear in thousands of years when temperature is 900 to 1000 ºC, corresponding to a Li diffusion coefficient from 10^{-13} to 10^{-12} m^2s^{-1} (Rudnick et al., 2007). Any isotopic disequilibrium of Li can be generated in short before the magma cooling below Li isotope exchange closure temperature (700 ºC, Coogan et al., 2005).

All the xenocryst cores in the MX samples have relatively higher Li content than the cpx phenocrysts (Fig. 3-10 and Fig. 6-8c). The Li content is only about 8 ppm in the host magma of the 5-3-10 and 5-11-7 grains, disagreeing with the very high Li content signature in the xenocryst cores are caused by the later host magma Li entering. The heterogeneity of Li content suggests the information of Li contents in xenocrysts were preserved after entrained within the basalts magma and were not eliminated by later Li exchange. The cpx xenocryst cores also have lower δ^7Li than coexisting cpx

phenocrysts (Fig. 3-10 and Fig 6-8c). If the xenocrysts and phenocrysts stay long enough time after leaving from mantle source, then any Li isotopic heterogeneity in the mantle will be erased in a relatively short time (Parkinson et al., 2007; Halama et al., 2008; Gallagher and Elliott, 2009). The isochronous preserved information of δ^7Li and Li content for the xenocrysts also disagree with "totally rebalance" of cpx phenocrysts, but escaping co-existing xenocrysts.

The Li content of the MX bulk rock range from 7.7 to 11.0 ppm by ICP-MS, while the cpx phenocryst Li content mostly range from 2.0 to 7.0 ppm. The $*D_{Li}^{cpx\text{-}melt}$ (about 0.5) calculated from the cpx phenocrysts and the melts is higher than the $D_{Li}^{cpx\text{-}melt}$ (0.2) reported by Brenan et al. (1998). When the Li content are compared among different samples, the larger range of the Li contents are observed in Fig. 6-8c (from 3 to 40ppm, mostly from 3 to 7 ppm), beyond the variation of Li equilibrium between the melts and cpx phenocrysts (Beck et al., 2004 and 2006; Jeffcoate et al., 2007; Rudnick et al., 2007). The cpx grain 5-3-9 has very high Li content (up to 30 ppm) but low Mg# (79). This grain cannot be crystallized from the MX magma directly, but may be the crystal from other magma or surrounding rocks. The Li content have limited intra-granular variation for most MX cpx phenocrysts, as shown in Fig. 6-8b. However, the wide range of δ^7Li can be observed in Fig. 6-8c, although the Li content variation is limited, suggesting either the Li content or δ^7Li is non-equilibrium. This non-equilibrium may be explained by (1) the mixture of magma from different source; (2) the later diffusion of Li; (3) the record of magma evolution, such as fractional crystallization. As mentioned above, the fractionation of Li during fractional crystallization is less than 1‰, suggesting the expulsion of (3). The very limited various δ^7Li values observed in 5-4-8 grain (Fig. 4-11a) together with its almost homogeneous Li content and Mg# suggest it have insignificant effect of Li diffusion. Although, some cpx grains have a little heavy δ^7Li in the rims of phenocrysts, the cores of the cpx phenocrysts have almost homogeneous δ^7Li and Li content, suggesting only limited Li diffusion were occurred in the rim of cpx phenocryst, not effecting the phenocryst cores. Therefore, (1) the MX cpx phenocrysts have not undergone obvious Li diffusion after the crystallization, and (2) some cpx phenocrysts may not share the same source as other cpx phenocrysts.

The cpx phenocryst in the SH basalts display a relatively large variation of Li content and δ^7Li. The cores of phenocrysts usually have low Li content and heavy δ^7Li, but the rims of phenocrysts have high Li content and light δ^7Li, suggesting faster diffusion of ^{6}Li relative to ^{7}Li into a crystal (Fig. 6-8f). Only one grain have inconsistent

trend of Li content and δ^7Li (Fig. 6-8f). Meanwhile, the Li content is weak correlated with δ^7Li (Fig. 6-8e). The difference between SH and MX can be caused by three possibilities: (1) the SH basaltic magma is heterogeneous. The heterogeneity can be leaded by complex magma mixing from different sources before eruption. Then the heterogeneous Li information were preserved from the rebalance. The isochronous variation of Li content and δ^7Li record the variation of composition of magma; (2) the cpx phenocrysts have undergone several metasomatic events after crystallization like the lithospheric mantle peridotites (Rudnick et al., 2007; Xiao et al., 2015); (3) the later diffusion of Li. The second situation is less impossible due to several different compositions of fluids or new melting are required to react with cpx phenocrysts in such a short time, before magma cooling. Therefore, the heterogeneity should be inherited from the magma or its source, or the result of Li diffusion. The isochronous Li content and δ^7Li variation of cpx phenocrysts in SH basalts is the result of obvious Li diffusion. The cpx phenocryst with heavy δ^7Li core also have higher Li content than other cpx phenocrysts, suggesting it was crystallized from different parent magma and magma mixture occurred.

The BL basalts have homogeneous Li content but relatively heterogeneous δ^7Li despite Mg# variation of cpx phenocrysts (Fig. 6-8i). The largest δ^7Li intra-granular variation (bigger than 80‰) are observed in the BL cpx phenocrysts. Such large intra-granular variation of δ^7Li is not caused by IMF correction or magma process, but can only be the results by either Li diffusion or magma mixing. Accordingly, the great heterogeneous δ^7Li within grains and increased Li contents at the mineral rims, unambiguously point to a Li addition from later melts/fluids. The homogeneous Li contents but the large heterogeneous δ^7Li within grains imply the Li diffusion process after re-equilibrium of Li. Otherwise, any later isotopic disequilibrium of δ^7Li will be erased after re-equilibrium of Li content. The larger fraction of ^{7}Li observed in the BL cpx phenocrysts require a distinct Li source from the BL samples (Richter et al., 2014), implying the high Li melts/fluids permeated with very short stay, if relative low Li content of bulk rocks are considered. Due to the long residence in deep crust the BL samples had enough time to experience such complex process.

Therefore, (1) the cpx phenocrysts do not have large diffusion with the host magma after their formation in the MX samples; but (2) the SH samples may have undergone the Li diffusion; (3) the Li content and δ^7Li of the BL cpx phenocrysts have undergone

re-equilibrium and later Li diffusion after crystallization.

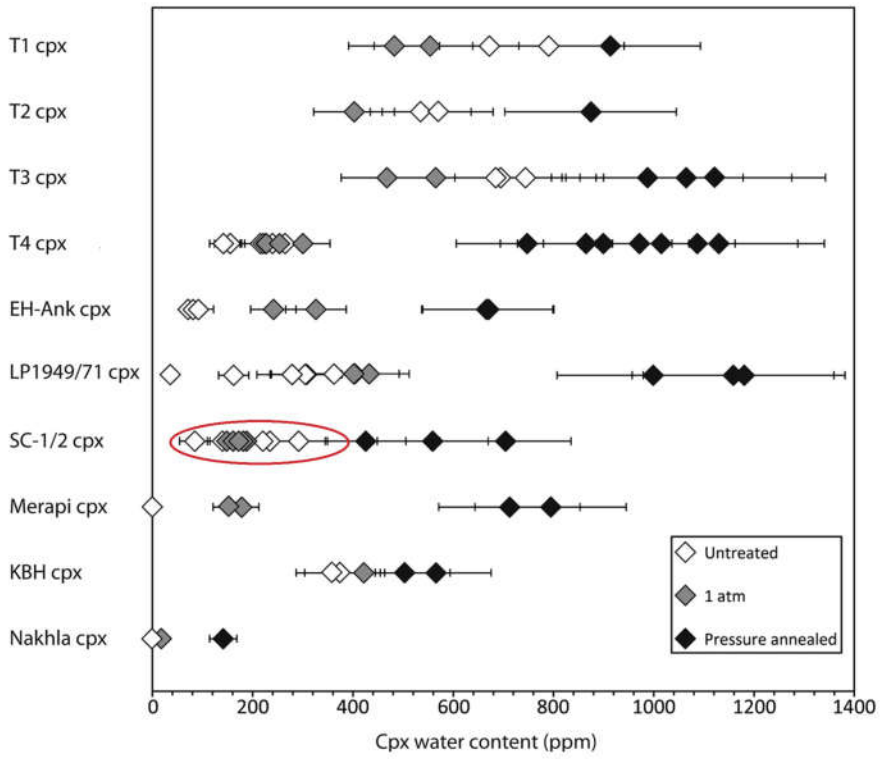

Sample	Pressure (kbar)	Time (h)	Water content (ppm weight H_2O)
SC-1(1)	2	0, 72	110, 425
SC-2 (1)	2	0, 72	193, 704
SC-2 (2)	0.5	0, 72	202, 559

Notes: For time intervals the value 0 refers to the starting value of the crystal prior to annealing. Estimated uncertainty for water contents is ±20%.

Fig. 6-12 Distribution of measured water contents for clinopyroxene crystals from this study before and after thermal annealing at 1 atm and under pressure modified from Fig. 3 and Table 4 in Weis et al. (2016). Error bars represent the 20% uncertainty in the FTIR analysis.

6.2.3 H_2O content of initial magma

Water is one of the most important factors influencing the melting process in the mantle (Dixon et al., 2004; Hirth and Kohlstedt, 1996; Karato, 2010). The primary information of water in basalts are recovered based on the water content of cpx phenocryst and the corresponding partition coefficient of H_2O between the cpx phenocryst and basaltic melts. Prior to declare the H_2O content of the "initial" basaltic melts, it is important to understand: (1) the evolution history of magma H_2O after they left melting source and during ascent to surface of earth, and (2) the H diffusion of cpx phenocrysts after they crystallized from magma, as suggested in Chapter 5. Meanwhile, the Li isotope are also used to trace the later diffusion of cpx phenocrysts.

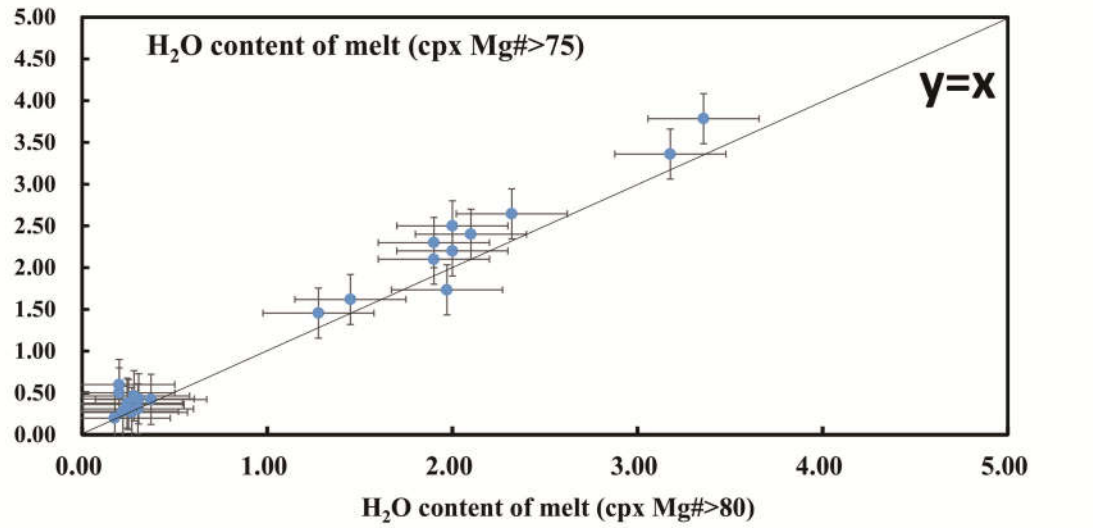

Fig. 6-13 Average H_2O content of the melts calculated from cpx phenocrysts with Mg# higher than 80 vs. the average water contents estimated from cpx phenocrysts with Mg# higher than 75.

The evolution process of magma H_2O and their geochemical composition in different stages can be recorded by cpx xenocrysts whose composition depend on their parent magma when they are crystallized. The H_2O content of basaltic melts can be changed by degassing, fractional crystallization, and assimilation of surrounding rocks/xenoliths during magma ascent. Fractional crystallization usually increase the H_2O content of melts, due to the low H_2O (<<1000 ppm, 0.1%) in those removed crystals i.e., olivine and cpx, if the magma are not so "dry". On the other hand, low degree fractional crystallization will not change the H_2O content of melts remarkably (Chen et al., 2015). The lower continental crust and peridotites are usually considered dry (Hao et al., 2014; Xia et al., 2006; Yang et al., 2008b; Yu et al., 2011), so the

assimilation of a few surrounding rocks or peridotite xenoliths does not increase the H_2O content of melts, or even reduce it.

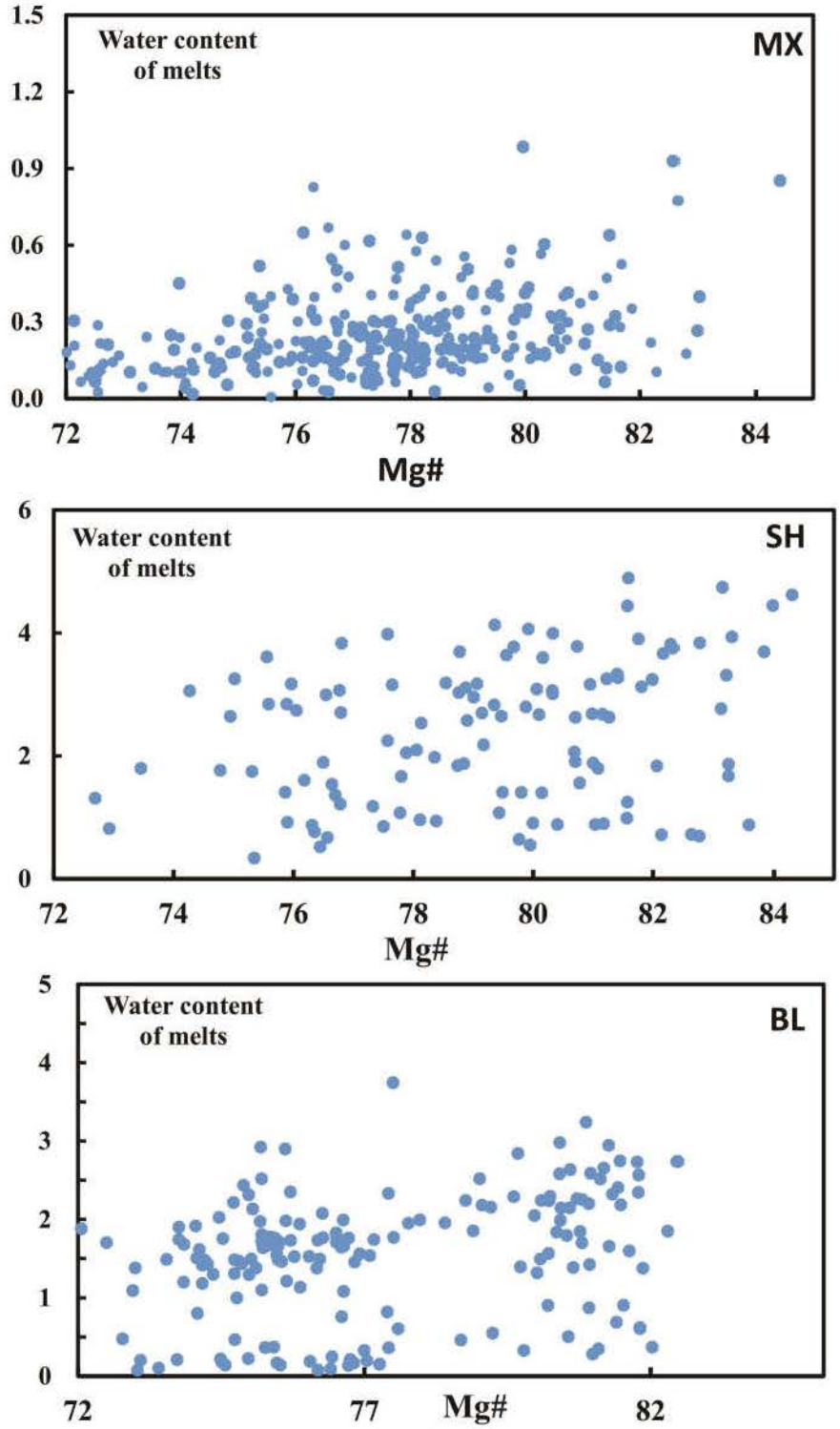

Fig. 6-14 (a)The plots of Mg# vs. the water content of corresponding melts for the MX basalts; (b) The plots of Mg# vs. the water content of corresponding melts for the SH basalts; and (c) The plots of Mg# vs. the water content of corresponding melts for the BL samples.

Nevertheless, due to a rapid pressure decrease, the degassing process will intensively reduce the H_2O content of the melts. The degassing usually takes place at the later stage of the magma eruption, which is corresponding to an evolved magma composition, i.e. low MgO of phenocryst. So, it can usually be observed that the parent melts corresponding to the cpx phenocrysts with low MgO or Mg# have lower water than those with higher MgO. This concludes that the parent melts of the cpx with higher MgO/Mg# are wetter than those with lower MgO/Mg#. So those cpx with lower MgO/Mg# cannot offer the "true" information of the "initial" melts. All trace elements and radiogenic isotopes are measured as bulk rock features. These features almost remain unchanged, if the erupted magma are considered as a nearly closed system in the Fujian region. So, when the H_2O content of the magma are compared to other geochemical data, the "initial" H_2O content are required. The "initial" H_2O content of magma can only be estimated from those cpx with the highest Mg#/MgO. It is suggested to use those cpx phenocryst with Mg#>80 to stand the most early magma. The water contents of the Fujian basalts estimated from the cpx phenocryst with Mg#>80 (if there are too rare cpx with Mg#>80, the cpx with Mg#>75 are used to satisfy statistical requirement) are 1.7-2.5%, 1.5-3.8%, 0.3-0.5%, for the BL, SH, and MX samples, respectively.

The second question is whether the cpx phenocryst can survive from later evolution and preserve its information of water. Due to a fast diffusion rate of H in cpx phenocryst measured by experiments ($D=10^{-10}\sim10^{-10.5}$ m^2 /s at 900℃, Hercule and Ingrin, 1999; Ingrin and Blanchard, 2006; Ingrin and Skogby, 2000; Woods et al., 2000), the cpx phenocryst may suffer H-loss during magma ascent. The redox reaction:

$$OH^- + Fe^{2+} \leftrightarrow O^{2-} + Fe^{3+} + 1/2\ H_2 \qquad (6\text{-}1)$$

is another possible ways for H loss (Weis et al., 2016). Weis et al. (2015) and Weis et al. (2016) have proved the cpx phenocrysts from Canary basalt have undergone significant H-loss, they suggest such H-loss mostly is related to an oxidation-driving and occurred during a long stage at shallow depth. Meanwhile, Weis et al. (2016) suggested the cpx crystals may undergo pressure-related and oxidation-related dehydration during the eruption as the SC basalts were observed in Chapter 5. Therefore, the water content of erupted clinopyroxene phenocrysts cannot be taken as the proxy to recover magmatic or mantle water contents directly, due to the fast dehydration, even the magma ascent rapid, only degas at minimal degree, and erupt subsequently more violently, that lead to quick quenching of the erupted crystals (Weis et al., 2016). The

dehydrated SC cpx phenocryst are rehydrated from 425 to 559 ppm by Weis et al. (2016) , as shown in Fig. 6-12. Actually, the dehydration for most of the SC samples have been demonstrated in Chapter 5, and the result of their recovered water content is consistent with the estimated water content for the Group 2 basalts (in Chapter 5). On the other hand, the water content after annealing rehydration failed to distinguish the ability to store water and the real water contents, as usual debate for the water content of Ringwood in deep mantle. Meanwhile, the estimated water content result falls in the range of the lowest limit of the water content for the basaltic magma.

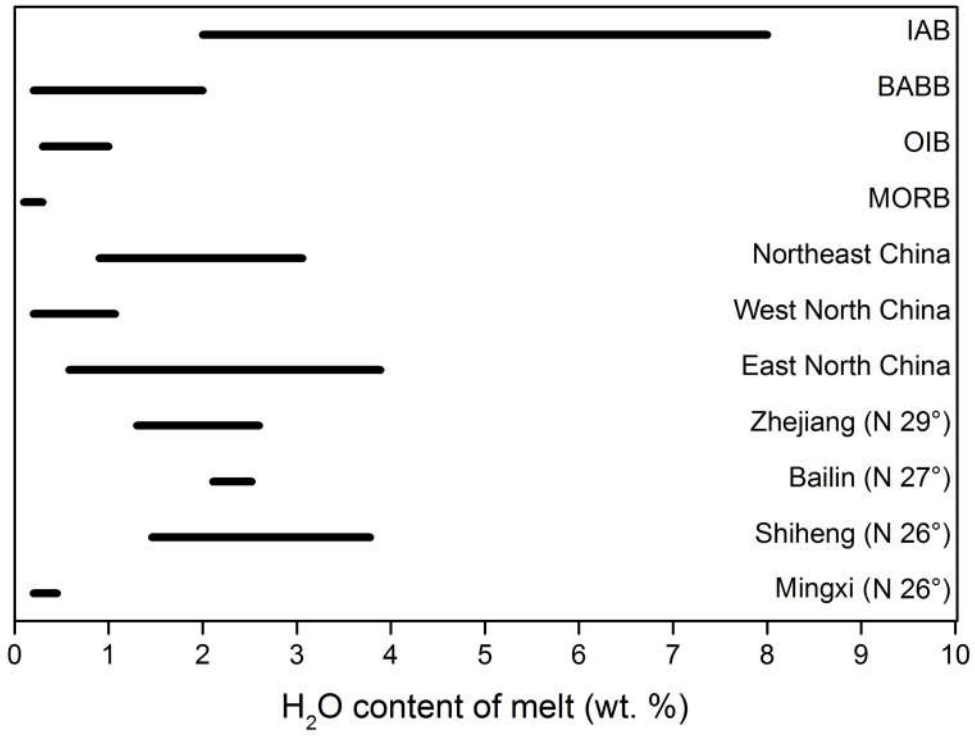

Fig. 6-15 Comparison of the calculated average H_2O content of the Fujian "primary" basaltic melts and the ranges of H_2O content for the Zhejiang "primary" basaltic melts, Northeast China, East North China, West North China, OIBs, MORBs, BABBs and IABs (data from Chen et al. (2015); Dixon et al. (2004) and the references therein).

There are two clues to trace the H loss or diffusion. As well as, the Li also has a fast diffusion under 900 to 1000 ºC, corresponding to the Li diffusion coefficient from 10^{-13} to 10^{-12} m^2 /s (Rudnick et al., 2007), which can index to the H diffusion in cpx phenocryst, indirectly. The Li isotopic data suggest limited diffusion of Li occurred in

MX, but significantly in SH and BL. The water contents of the cpx phenocrysts in the MX basalts are relatively low, suggesting H loss at first glance. It can be inferred whether the relative low water content is the natural feature of these cpx phenocrysts or a result of diffusion-driving H-loss, from following: (1) a large number of peridotite xenoliths and xenocrysts carried by the MX basalts, suggest a high eruption speed and leave short time to shallow process; (2) cpx xenocrysts show a relative high water content as similar as the peridotite xenoliths (Yu et al., 2011), if H-loss is the dominant cause for the low water content of cpx phenocrysts in the MX basalts, these concomitant cpx xenocrysts cannot survive from the same process; (3) the H-loss should be in disorder and unselective. However, a strong positive relationship between the water content of corresponding melts and cpx Mg# (Fig. 6-13), as well as, the cpx phenocryst with high Mg# have the higher water content of corresponding melts (Fig. 6-14a) excluding a later disorder diffusion of H. (4) The limited Li diffusion indirectly exclude a synchronous H diffusion; (5) the clear negative correlation of H_2O/Ce with Ba/Th and Ce/Pb in Fig. 6-12.

The cpx phenocrysts in SH and BL contain relatively high water content, implying their H-diffusion were insignificant or re-equilibrated. The SH basalts have the similar pattern of cpx phenocryst Mg# and the water content of corresponding melts (Fig. 6-14b) to MX disagreeing disorder H diffusion. Although the SH cpx phenocrysts also display Li diffusion, its -OH profile of SH-1-13 (Fig. 6-6b) cpx grain has limited variation arguing against the H re-equilibrium. Meanwhile, the SH basalts also contain some peridotite xenolith/xenocrysts, suggesting a rapid eruption and leaving short time to shallow process. However, although the BL diabases carried numbers of peridotite xenoliths, the Mg# of cpx phenocrysts related to corresponding melts water content is very weak (Fig. 6-14c). The -OH profile of BL-6-4 cpx grain also proves the large H variation (Fig. 6-6c), implying H re-equilibrium of the BL cpx phenocrysts. Therefore, the result of magma water content estimated from the cpx phenocrysts are suggested to stand for the “initial” system water content for the MX basalts, but not sure for the BL sample. The SH basalts may keep their original water content, at least the value of “initial” magma water is the low limit of the magma water. The true water content of the BL diabases may be concealed under the re-equilibrium of H_2O if estimated from cpx phenocrysts.

The “initial” water contents of the SH and MX basalts are 1.5-3.8% and 0.3-0.5% respectively (Fig. 6-15). The water content of the SH basalts fall within the range of

BABBs and IABs, however, those of the MX basalts fall with the range of OIBs and MORBs (Dixon et al., 2004).

6.2.4 Origin of the oxygen isotopic anomaly

6.2.4.1 Origin of high $\delta^{18}O$ value and its large variation

The fractionation of $\delta^{18}O$ between cpx phenocrysts and basaltic melt is about -0.1 to -0.3 ‰, if are calculated from the difference between $\Delta^{18}O_{cpx\text{-}ol}$ of 0.4‰ and $\Delta^{18}O_{melt\text{-}ol}$ of 0.4 to 0.5‰ (Eiler, 2001), or follow $\Delta_{cpx\text{-}melt}$= -0.3 (Kyser et al., 1981; Harris et al., 2005), therefore, the measured $\delta^{18}O$ of cpx phenocrysts can be looked approximately as those of corresponding basaltic magma. The cpx phenocrysts in the Fujian basaltic rocks have much higher and wider $\delta^{18}O$ ranges (Fig. 6-9) than those of typical MORBs (5.7±0.2‰, Mattey et al., 1994; Eiler et al., 1997, for $\delta^{18}O_{cpx}$ range from +5.6±0.5‰, if $\Delta_{cpx\text{-}melt}$=-0.1) (Fig. 6-9), as well as higher than cpx $\delta^{18}O$ from different kinds of OIBs lavas (+5.0 to 5.5%, +5.5 to 5.7% and +5.8 to +6.5%, for HIMU, EMII and EM II type OIBs, respectively Eiler et al. (1997); Widom and Farquhar, (2003), for $\delta^{18}O_{cpx}$ from +4.9 to 5.4%, +5.4 to 5.6% and +5.7 to +6.4%, respectively). Auer et al. (2009) have reported Kamchatka cpx phenocrysts from Klyuchevskoy volcano displaying a similar $\delta^{18}O$ range to our samples from +5.5 to +8.0‰, which are re-calculated by its ol phenocryst $\delta^{18}O$ (+5.1 to +7.6%) and $\Delta^{18}O_{cpx\text{-}ol}$ (0.4%).

Magmatic processes, secondary alteration, crustal contamination, and so on will change the original Oxygen isotopic composition of magma. The variation of the $\delta^{18}O$ of the magma caused by high temperature magma process should be less than the level of 0.1‰ (e.g. Eiler 2001; Zhao and Zheng, 2003), by large numbers of natural observation and theoretical consideration. The effect at high temperature in closed system, such as partial melting, fractional crystallization, degassing excluding AFC processes, is not very large for Oxygen isotope (Eiler, 2001). The accuracy of SIMS analysis for Oxygen isotope is about 0.5‰, (Section 6.1.3.3), covering the variation of the $\delta^{18}O$ of the magma caused by high temperature magma process. Meanwhile, the Fujian samples have relative high bulk MgO contents except NTS, higher than 8 wt. %, (Kuang et al., 2012; Yang and Li, 2008; Zhang et al., 2000) arguing against $\delta^{18}O$ effected by complex magmatic processes. However, the AFC processes and later water-rock will prominently alter the primary Oxygen isotopic composition. The crustal contamination or assimilation will not serve as a significant factor for the Fujian basalts

as we mentioned in section 6.2.1, such as the bulk rock Ce/Pb and Nb/U ratios of most the Fujian basalts are higher than 28 except NTS and higher than 46, respectively. Secondary alteration after eruption also does not seem a suitable explanation. Variable high $\delta^{18}O$ values cannot be the result of altered hydrous minerals in cpx excluded by no hydrous mineral peak in the FTIR analysis and during the sample preparation. Secondly, the oxygen diffusion rate in cpx at low temperature is too low, to result such significant $\delta^{18}O$ increase for the young Fujian basalts (D_0 is about 10^5 m^2s^{-1}, 10^{15} magnitude slower than those at 1000℃ (Farver and Giletti, 1989)). At the same time, the high $\delta^{18}O$ values are not correlated with the LOI (loss on ignition) values of the bulk rocks. The SH have the highest LOI, but share the similar range of $\delta^{18}O$ values as the MX and BL samples.

Overall, the dominantly high $\delta^{18}O$ values are considered as the original signature of the parent magmas, i.e. the characteristics of the mantle sources, especially for the cpx with higher Mg#. The heterogeneous $\delta^{18}O$ of intra-granular and intergranular variations from single basalt sample can be up to 2‰, in the Taihang and Shandong Cenozoic basalts (Liu et al., 2015a and 2015b), the Canary Island basalts (Gurenko et al. 2011), the Borgarhraun basalt (Winpenny and Maclennan, 2014), and the Chifeng basalts (Wang et al., 2015). These heterogeneous $\delta^{18}O$ are explained as complex magma system from heterogeneous mantle source region (Gurenko et al. 2011; Winpenny and Maclennan, 2014).

6.2.4.2 Magma mixture

The positive correlation between $\delta^{18}O$ and Mg# of the cpx phenocrysts in MX samples can be explained as five possibilities: (1) the systematic deviation caused by the correction of IMF; (2) meteoric water interaction with the magma at high temperature during crystallization of mafic minerals; (3) AFC process of the lower continental crust; (4) the composition or geochemical variation in the closed magma system; (5) magma mixing.

From the above possibilities, the (3) and (4) can be excluded at earliest based on the discussion in section 6.2.5.1. The (1) is excluded because of following: All the Fujian samples $\delta^{18}O$ are measured in disorder, and the MX samples were analyzed in different sessions. On the one hand, the IMF in different sessions is different, but the MX samples share the similar positive trend. On the other hand, the plots of the BL and SH samples do not display such a trend. If the $\delta^{18}O$ decrease with Mg# decreasing were

caused by (2), it means the meteoric water probably penetrated into the lower continental crust, but it is too hard to penetrate for so large meteoric water. In addition, it is too difficult for the meteoric water to keep their low $\delta^{18}O$ after penetration the thick crust without interaction with surrounding lower continental crusts, which have high $\delta^{18}O$. On the other hand the later water addition should also be recorded by the cpx, inconsistent of the lower water content in the cpx phenocrysts with low Mg#. The complex magma mixture and crystallization with variable $\delta^{18}O$ values in plumbing system are considered to explain the various measured $\delta^{18}O$ values, where distinct magma percolated along their separate channels (Sobolev and Shimizu, 1993; Kelemen et al., 1997; Spiegelman and Kelemen, 2003; Gurenko et al., 2011; Ruprecht and Plank, 2013). Then the cpx phenocrysts with heterogeneous $\delta^{18}O$ were entrained by subsequent magmas and erupted on the surface of earth. The highest $\delta^{18}O$ values are observed in the intermediate Ca/Al and Si/^{IV}Al ratios of the MX, BL, and SH cpx phenocrysts in Fig 6-9a and b, also suggesting that the mixture between complex magma occurred.

6.2.5 Mantle heterogeneity and recycled component

6.2.5.1 $\delta^{18}O$ heterogeneity

The high $\delta^{18}O$ anomalies of the cpx phenocrysts in all the Fujian basalts (Fig. 6-9) are inherited from their parental magmas and mantle sources, indicating recycled components in their source. The recycled oceanic/continental crust or crustal derived sediments usually have higher $\delta^{18}O$ values than normal mantle. The high $\delta^{18}O$ anomalies are considered by such recycled components involved in the mantle sources of the Fujian basalts (Eiler et al., 1997; Eiler 2001). The continental crust and sediments, subducted slab related fluids and melts, oceanic crust experienced water-rock interaction at low-T (<350°C), and marine sediments are expected to be the possible candidates being responsible for the high $\delta^{18}O$ anomalies (Eiler 2001; Auer et al., 2008; Martin et al., 2011; Muehlenbachs 1986; Taylor and Sheppard, 1986). As discussed in Chapter 5, the high Nb/La, Nb/U and Ce/Pb ratios in the Fujian basalts (Fig. 6-16a) stifle possibility of the dominant proportion of continent-related components, including continental crust and sediments, as well as fluids from subducted slab, corresponding to high values of Pb and low values of Nb in continental crust (Tatsumi et al., 1986; Rudnick and Gao 2003; Grove et al., 2002). Therefore, the high $\delta^{18}O$ values of cpx

phenocrysts indicate the involvement of recycled oceanic crust components exclusively in the mantle source of Fujian Cenozoic basalts. Although the low-temperature water-rock altered oceanic rocks were involved in the source of Fujian basalts, the higher Ba/Th and high Ba/U may also suggest another enrichment source. The enrichments are considered to involve dehydrated marine sediments, mantle source carbonate or recycled calc-silicate, appearing as relevant as limestone interaction and likely form a continuum in the subvolcanic environment (e.g., Gaeta et al., 2009; Deegan et al., 2010). The $\delta^{18}O$ of carbonates usually are up to 30‰, clearly higher than that of the normal mantle.

6.2.5.2 Constraints for the enrichment origin

The high Nd and Ta content of the Fujian basalts require an asthenospheric mantle source, not the lithospheric mantle, as the Cenozoic basalts in Zhejiang and in the NCC (e.g. Liu et al., 2015a and b). The plots of $^{143}Nd/^{144}Nd$ vs. Ce/Pb (Fig. 6-16a) form a positive trend suggesting a mixture depleted source end member with high Ce/Pb with enriched source end member with low Ce/Pb. The depleted but high Ce/Pb mantle source of Fujian Cenozoic basalts suggests the depleted mantle member pointing to young recycled oceanic crust (Xu et al., 2012) and the ambient mantle source for the Cenozoic basalts. On the one side, the La and Nb in peridotite and pyroxenite-melt systems display opposing partitioning behavior: the Nb and La share the really similar partition coefficient in the peridotite-melt system, however, the Nb have lower compatibility in the pyroxenite-melt systems. The Nb/La ratio is a potentially suitable tracer to distinct pyroxenite and peridotite source signature (Stracke and Bourdon, 2009). All the Fujian lavas have high Nb/La (Fig. 6-16b), indicating melting of a pyroxenite source (Stracke and Bourdon 2009), pointing to the asthenosphere and the recycled oceanic crust. On the contrary, the Ce and Pb share the really similar partition coefficient in the pyroxenite system, however, the Pb have lower compatibility than Ce in the pyroxenite-melt systems. The Ce/Pb are considered to be the corresponding indexes as Nb/La (Stracke and Bourdon 2009). The negative of Nb/La vs. Ce/Pb together of the BL and SH samples are observed in Fig. 6-16b, whereas the MX samples show very weak correlation between Nb/La and Ce/Pb. The correlation between Nb/La vs. Ce/Pb can be caused by either different partial melting degree for source mantle rocks or the different proportion of pyroxenite in the mantle. The crucial factor to respond to the correlation between Nb/La vs. Ce/Pb of the BL and SH samples, should

be the different proportion of pyroxenite in the mantle, which is illustrated by a rough positive correlation of Sr_n/Sr^* vs. Eu_N/Eu^* in Fig. 6-16c ($Sr^*=(Ce_n*Nd_n)^{1/2}$, n means primitive-mantle normalized, meanwhile, $Eu^*=(Sm_N/Nd_N)^{1/2}$, N means chondrite normalized) in the SH basalts and the BL diabases. The Sr have different partitioning behavior with Sr* ($D_{Sr^*} = (D_{Ce}/D_{Nd})^{1/2}$, Stracke and Bourdon 2009) in peridotite and pyroxenite-melt systems, the Sr_n/Sr^* will increase when the proportion of pyroxenite increases in the melting source. The Eu does not have big fractionation than other REEs during the magma process in the mantle, without addition or loss of large numbers of fsp in system. Meanwhile, the variations of the partition coefficients between Eu_N and Eu* ($D_{Eu*} = (D_{Sm}/D_{Nd})^{1/2}$) are also not sensitive to the change of the proportion of pyroxenite in the melting source (Stracke and Bourdon 2009). If the crucial factor to respond to the correlation between Nb/La vs. Ce/Pb is the result of partial melting, variation of Sr_n/Sr^* should be observed with narrow range of Eu_N/Eu^*. Therefore, the anomalies of Eu should be inherited from their source of basalts, when the fractionation or assimilation of fsp during magma ascent are excluded. The Sr_n/Sr^* increase with increasing Al_2O_3 imply the assimilation of plagioclase for the gabbros of lower oceanic crust for the BL and SH samples (Fig. 6-16d). The BL and SH samples may share similar source in the mantle. Due to the re-equilibrated the water content of the BL sample are considered not to represent the origin information of the mantle source. The high H_2O/Ce of the SH imply a wet mantle source (Fig. 6-17a and b), pointing to the recycled oceanic sediments. The common relative high Sr_n/Sr^*, Eu/Eu*, $^{143}Nd/^{144}Nd$ and Pb radiogenic ratios for the BL and SH samples are considered as the result of the low-temperature water-rock altered oceanic upper crust and fsp-enriched lower crust together with the oceanic sediments.

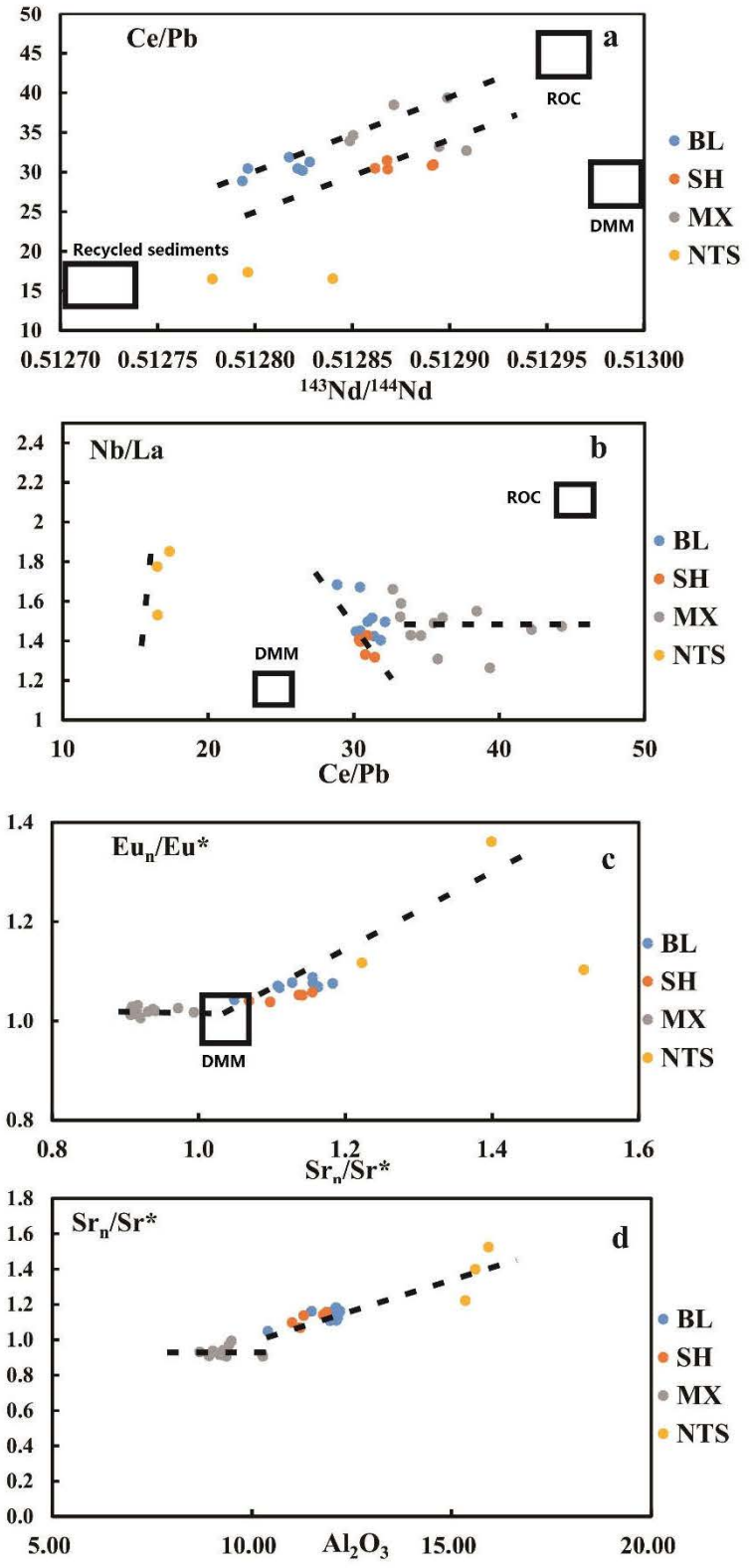

Fig. 6-16 (a) Plots of $^{143}Nd/^{144}Nd$ vs. Ce/Pb for the Fujian basalts; (b) Plots of Nb/La vs. Ce/Pb for the Fujian basalts; (c) Plots of Eu_N/Eu^* vs. Sr_n/Sr^* for the Fujian basalts; and (d) Plots of Sr_n/Sr^* vs. Al_2O_3 for the Fujian basalts.

The MX basalts display weak correlation in the plots of Nb/La vs. Ce/Pb and Sr_n/Sr^* vs Eu_N/Eu^* (Fig. 6-16b and c). These trends declare against the simple increasing proportion of pyroxenite or different partial melting degree in the mantle source. The appearance of simultaneously depleted Sr isotopic ratios and lower Nb/La suggest the source for the MX samples are different than the SH and BL samples. It consists with the positive relationship between Zr/Hf vs $^{87}Sr/^{86}Sr$ (Fig. 6-18). The partition coefficients of Zr and Hf are almost same in both peridotite and pyroxenite-melt systems (Stracke and Bourdon 2009), keeping its original ratio from mantle melting and magma evolution. The $^{87}Sr/^{86}Sr$ ratio also can stay from melting or magma process. The positive relationship of between Zr/Hf vs $^{87}Sr/^{86}Sr$ (Fig. 6-18) are believed the results of mixture between normal silicate magma with carbonated peridotite/pyroxenite or carbonatite (Dasgupta et al., 2007; Bizimis et al., 2003), suggesting an enriched-carbon component in the mantle source. The MX basalts have almost uniform Eu_N/Eu^*, with Sr_n/Sr^* variation. The low $Sr_n/Sr^* <1$ and very weak Eu_N/Eu^* disagree with the dominant role of fsp component in its mantle source, against oceanic gabbro in the mantle source. The horizontal variation of Sr_n/Sr^* and Al_2O_3 also reject the high proportion of gabbro component in the mantle source by Fig. 6-16d. The inconsistency in the MX basalts are also observed in the H_2O/Ce and water content. The H_2O/Ce and water content are believed to be able to distinct the different origins of enrichment in the mantle source of basalts (Liu et al., 2015a and b; Xia et al., 2013). However, despite the high Ba/Th in the MX samples, the MX basalts are almost dry relative to other intra-plate Cenozoic basalts in East China (Fig. 6-15a). The relative low water content are also observed in Shandong and SC (Liu et al., 2015 and Chapter 5), which has been proven to be the results of H loss in later magma process. When the H loss during later magma process are regarded as uselessness for the MX basalts, the low water contents are regarded as the natural feature of its source. The relative low water content is hard to answer whether the sediments exist or not. The low water content and high Ce/Pb, intermediate Ba/Th as well as high $\delta^{18}O$ and $^{143}Nd/^{144}Nd$ all call up a recycled low temperature water-rock reaction altered oceanic crust in the mantle source of the Fujian basalts, without gabbro components from recycled low oceanic crust. The MX samples share more common characteristics with the XL basalt in Zhejiang. The lower water content in MX may suggest the deeper dehydration of enriched recycled oceanic crust component than the XL basalts.

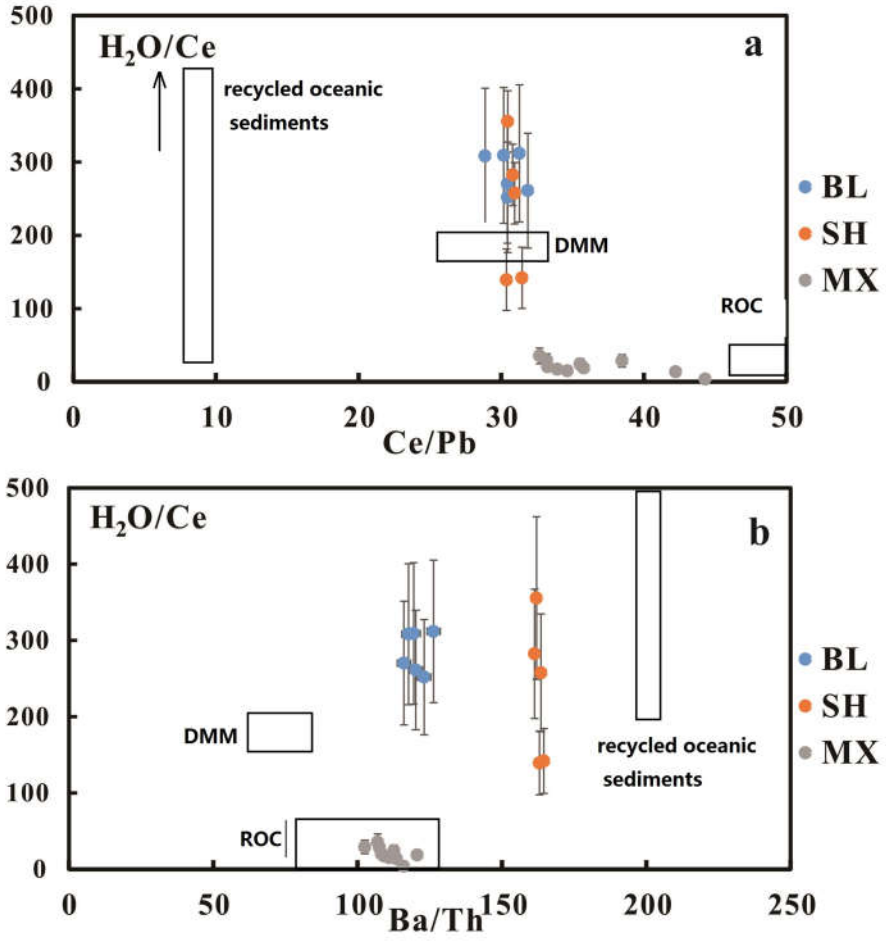

Fig. 6-17 (a) Plots of Ce/Pb vs. H_2O/Ce for the Fujian basalts. (b) Plots of Ba/Th vs. H_2O/Ce for the Zhejiang basalts. The error bar of H_2O/Ce is 30%. The source data are the same as in Fig. 5-13.

The NTS basalts show different evolution path which is the other than that of the Fujian basalts (Fig. 6-2). Despite its relative high SiO_2 and low MgO, the NTS basalts also survived from the contamination of continent crust and secondary alteration. The NTS samples consist of tracybasalts and basaltic trachy-andesite in Fig. 6-1. The NTS samples have the HIMU-like pattern with high content of HFSEs, high Nb (Ta) and Zr (Hf). The NTS samples have the highest Pb radiogenic isotopic ratio in all the Cenozoic basalts in East China. Enriched Pb isotope signatures with time-integrated high Th/U and $^{235}U/Pb$, in the mantle source, suggesting recycled oceanic crust components. The high HFSEs are caught by the Ti-enrich minerals, implying the involvement of the deep partial melting relicts of oceanic crust, i.e. eclogite. The eclogite contain large number of Ti-enrich minerals, such as rutile, consisting of the strong positive Ti anomaly (Fig.

6-2). The high Eu_N/Eu^* and Sr_n/Sr^* (Fig. 6-16d), high Zr, Hf, and Ti all suggest original fsp-rutile-zircon-sphene-like component melting. These component in Fig. 6-16b and c suggest that the NTS samples share the similar source lithology to other Fujian basalts, but the unlike source trace elements compositions in the source. The NTS melts generated are dominantly from the earlier melting residue of lower oceanic crust and some recycled sediments, accounting for their relatively high Eu/Eu^*, Sr_n/Sr^* and more enrichment radiogenic isotopic data.

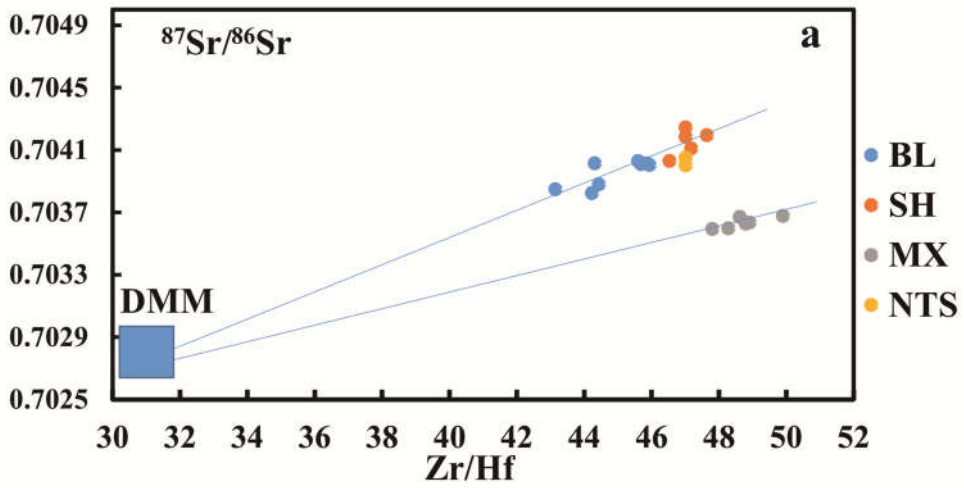

Fig. 6-18 Plots of Zr/Hf vs. $^{143}Nd/^{144}Nd$ for the Fujian basalts.

6.2.6 Implications for the mantle source

Two candidates are considered to reserve the enrichments: one is the metasomatic lithosphere/asthenosphere by upwelling melts generated from disappeared recycled oceanic slabs, another is the odd "pudding"-like fragments distributed in upper mantle separated from disappeared recycled oceanic slabs. The metasomatic lithosphere were involved to explain the genesis of some Cenozoic basalts in the NCC and in the Guangdong region (Xu et al. 2012b; Huang et al., 2013). Due to the large number of high $\delta^{18}O$ cpx phenocrysts, it is too hard to image the large-scale lithospheric rock replacement by limited recycled melts, otherwise the high $\delta^{18}O$ anomalies usually are buffered by large volume of ambient lithosphere rocks. The pudding-like fragments distributed in upper mantle from disappeared recycled oceanic slabs are more like to serve as the enrichment source. In fact, it is hard to identify exactly from which subducted slab the enrichment was divided. Because of the moderate radiogenic Sr-Nd-

Pb ratios, the most recent Pacific slab is the most-likely candidate. The involvement of oceanic crust components is also indirectly supported by the relationships among the basalts and the stagnant slab in close region, such as Zhejiang. Several studies have linked the stagnant slab from the Pacific plate from multiple independent lines of evidence (e.g. Sakuyama et al., 2013; Xu et al., 2012a; Liu et al., 2015a and b; Liu et al., 2016). Despite the dubious existence of stagnant slab by many seismic topography studies, the similar geochemical and geological history imply a relevant geodynamics process. Because of the obscure existence of subducted slab, these recycled oceanic material component are most likely the residue of the previous subducted slab distributed in the upper mantle, after stagnant slab sunk to the lower mantle.

6.3 Conclusions

(1) The Li content and the Lithium isotopic results demonstrate all the cpx phenocrysts from the Fujian basaltic rocks have undergone varying degrees Li diffusion. The Li diffusion in the MX basalts is limited, however, the SH basalts and the BL diabases have undergone relatively significant Li diffusion.

(2) The "initial" water contents of the MX and SH basalts are 0.3-0.5% and 1.5-3.8%, respectively. However, the BL diabases display re-equilibrated content of 2.1-2.5% for diabases. The diffusion of Li can help to identify whether the cpx phenocrysts preserve the information of Li from latter diffusion or not indirectly.

(3) The cpx phenocrysts in the Fujian basaltic rocks have higher $\delta^{18}O$ values than o those of normal mantle cpx. These $\delta^{18}O$ values are inherited from their source, implying recycled materials were involved in the mantle source of the Fujian basaltic rocks.

(4) The SH basalts and BL diabases involved both the upper and lower recycled oceanic crust components together with the recycled marine sediment components in their source, the MX basalts most likely involved the upper oceanic crust components together with the sediment components, at last, the NTS melts generation dominantly involved the re-melting of lower oceanic crust and recycled sediments residual components. The pronounced recycled oceanic materials are most likely the residue of the previous subducted slab distributed in the upper mantle.

Table 6-1 Major and trace element compositions and isotopic ratios of the Fujian basalts and the calculated H_2O content of the basaltic melts.

Location	Bailin								
GPS	N 27°9'38.4 E 120°10'4.44"								
Age	Pleistocene								
Rock type	Diabase	Diabase	Diabase	Diabase	Diabase	Diabase	Diabase	Diabase	Diabase
Sample No.	BL-3	BL-4	BL-5	BL-6	BL-7	BL-8	BL-9	BL-10	BL-11
SiO_2	46.66	48.34	46.83	47.25	46.62	47.02	46.82	46.70	46.90
TiO_2	2.18	1.94	2.08	2.13	2.11	2.19	2.14	2.10	2.14
Al_2O_3	11.92	10.40	12.12	12.21	11.50	11.96	12.16	12.11	11.96
Fe_2O_3	12.08	11.20	11.86	11.80	12.05	11.79	11.77	11.76	11.87
MnO	0.2	0.2	0.2	0.2	0.2	0.2	0.2	0.2	0.2
MgO	10.10	10.89	10.88	10.11	10.72	10.13	9.99	10.13	10.21
CaO	10.04	11.35	10.25	10.33	10.31	10.32	10.14	10.29	10.26
Na_2O	3.03	2.60	2.49	2.76	2.60	2.99	2.84	2.96	2.73
K_2O	2.15	1.52	1.79	2.02	1.96	2.12	2.11	1.98	2.06
P_2O_5	0.56	0.39	0.47	0.59	0.54	0.58	0.60	0.57	0.57
LOI（%）	0.07	0.40	0.72	0.43	0.32	0.40	0.37	0.16	0.41
Total	98.95	99.18	99.64	99.78	98.89	99.66	99.10	98.92	99.27
Mg# [a]	0.69	0.72	0.71	0.69	0.70	0.69	0.69	0.69	0.69
Ti	13066	11621	12460	12736	12616	13120	12796	12598	12832
K	17893	12650	14897	16811	16312	17643	17560	16478	17144
Li	8.2	5.8	6.2	7.3	7.1	7.2	7.4	7.2	6.9
Be	1.6	1.1	1.3	1.4	1.3	1.5	1.5	1.4	1.4
Sc	28.22	35.49	29.48	27.56	28.29	28.15	27.55	27.40	27.48
V	215	237	214	202	204	207	205	202	201
Cr	321	515	341	302	324	310	305	315	309
Co	62.3	56.5	57.5	58.0	59.7	57.0	60.0	58.5	57.8
Ni	207	202	190	196	205	193	199	197	191
Cu	66.6	50.0	54.1	60.3	58.1	62.1	62.6	59.6	55.6
Zn	118	99	107	109	108	109	112	108	107
Ga	19.5	16.9	18.2	19.3	18.5	19.2	19.8	19.0	18.8
Ge	1.6	1.5	1.5	1.5	1.5	1.5	1.5	1.5	1.5
Rb	169	74	86	153	148	155	153	142	147
Sr	857	632	732	846	787	811	862	838	821
Y	22.8	21.9	22.0	22.2	21.4	22.6	23.0	21.9	22.0
Zr	212	186	208	203	195	209	208	196	200
Nb	69.1	55.7	65.2	65.8	62.9	67.5	67.6	62.7	63.2
Cs	1.1	0.8	1.0	1.3	1.2	1.4	1.2	1.1	1.1
Ba	806	572	678	765	728	775	783	739	733
La	46.2	33.3	38.7	45.3	41.5	45.1	48.2	44.1	43.7
Ce	84.7	64.0	71.4	83.4	77.0	83.3	88.1	81.0	80.9
Pr	8.9	7.3	8.1	8.7	8.1	8.7	9.1	8.5	8.5
Nd	35.1	30.6	32.9	34.2	32.2	34.7	35.8	33.5	33.6
Sm	7.6	6.7	7.0	7.4	7.1	7.4	7.7	7.2	7.2
Eu	2.5	2.2	2.3	2.4	2.3	2.5	2.5	2.4	2.4
Gd	6.6	6.2	6.2	6.5	6.2	6.6	6.8	6.3	6.5
Tb	0.9	0.9	0.9	0.9	0.9	0.9	0.9	0.9	0.9
Dy	4.7	4.6	4.6	4.6	4.5	4.7	4.8	4.6	4.6
Ho	0.8	0.8	0.8	0.8	0.8	0.8	0.8	0.8	0.8
Er	1.9	2.0	1.9	1.9	1.8	2.0	2.0	1.9	1.9
Tm	0.3	0.2	0.2	0.2	0.2	0.2	0.2	0.2	0.2
Yb	1.4	1.4	1.4	1.4	1.4	1.5	1.4	1.3	1.4
Lu	0.2	0.2	0.2	0.2	0.2	0.2	0.2	0.2	0.2
Hf	4.6	4.3	4.7	4.4	4.3	4.6	4.5	4.3	4.4
Ta	3.3	2.9	3.4	3.2	3.1	3.3	3.3	3.0	3.1
Pb	2.6	2.1	2.5	2.7	2.5	2.7	2.8	2.6	2.7
Th	5.9	4.9	5.8	6.2	5.8	6.4	6.5	5.9	6.1
U	1.4	1.1	1.3	1.3	1.2	1.4	1.4	1.3	1.3
H_2O [b] (wt. %)		1.97	2.00	1.90	2.10		1.90		2.00
H_2O [c] (wt. %)		1.73	2.20	2.10	2.40		2.30		2.50
Recommend H_2O (wt. %)									
$^{87}Sr/^{86}Sr$		0.703847	0.704013	0.704008	0.704027		0.704003		0.704013
2σ		11	12	5	4		4		
$^{143}Nd/^{144}Nd$		0.512796	0.512794	0.512822	0.512828		0.512818		0.512824
2σ		10	9	12	15		16		18
$^{206}Pb/^{204}Pb$		18.670	18.652						
$^{207}Pb/^{204}Pb$		15.533	15.525						
$^{208}Pb/^{204}Pb$		38.872	38.862						

a Mg#=$Mg^{2+}/(Mg^{2+}+\Sigma Fe^{2+})$, values were calculated assuming $Fe^{2+}/\Sigma Fe = 0.85$.

b The average of H_2O content calculated from cpx phenocrysts with Mg# >80 (Mg# >77 for GP samples).

c The average of H_2O content calculated from cpx phenocrysts with Mg# >75.

d AOB: Alkali olivine basalt.

Mingxi											
N 26°25'22.71"			E 117°7'7.09"				N 26°24'21.25"			E 117°7'6.08"	
1.2-2.2Ma							1.2-2.2Ma				
Basanite	Basanite	Basanite	Basanite	Basanite	Basanite	Basanite	Basanite	Basanite	Basanite	Basanite	Basanite
MX-1	MX-2	MX-3	MX-4	MX-5	MX-6	MX-7	MX-8	MX-9	MX-10	MX-11	MX-12
42.02	41.61	41.45	42.22	41.18	42.53	41.49	42.69	43.36	41.24	42.35	42.65
2.97	3.00	2.84	3.03	3.06	3.07	2.92	3.13	2.93	2.99	3.09	3.16
9.33	8.93	9.03	8.70	9.28	9.43	9.49	9.37	9.25	9.19	10.28	10.26
13.48	13.47	13.30	13.74	13.20	13.00	12.92	14.10	13.91	14.19	13.24	13.50
0.2	0.2	0.2	0.2	0.2	0.2	0.2	0.2	0.2	0.2	0.2	0.2
15.00	17.15	17.04	16.46	17.17	16.39	14.48	13.05	12.34	13.20	13.00	12.90
9.63	9.31	9.60	9.61	9.26	9.28	10.90	10.18	9.79	9.84	10.08	10.27
2.96	2.71	2.75	2.82	2.98	2.95	2.62	3.04	2.91	2.94	2.97	3.13
2.16	2.15	2.01	2.07	1.91	1.87	1.92	2.21	2.11	2.12	2.16	2.08
1.05	0.92	0.92	0.91	1.00	0.95	1.08	1.16	1.13	1.12	1.29	1.29
0.44	(0.02)	0.17	0.01	(0.05)	0.09	1.50	0.48	1.18	0.75	0.40	0.46
99.18	99.38	99.27	99.73	99.16	99.73	99.50	99.58	99.09	99.56	99.04	99.89
0.75	0.77	0.77	0.76	0.77	0.77	0.75	0.71	0.70	0.71	0.72	0.72
17783	17980	17036	18181	18340	18394	17495	18775	17567	17915	18496	18939
17935	17851	16728	17186	15896	15563	15979	18392	17560	17643	17976	17311
8.6	7.7	8.2	9.1	9.1	9.4	8.2	10.2	10.0	9.9	10.9	11.0
2.3	2.0	2.1	2.1	2.2	2.3	2.0	2.4	2.5	2.6	2.6	2.5
22.62	21.96	23.60	22.04	21.65	23.55	22.16	21.04	20.71	21.06	21.12	20.46
223	223	217	216	215	217	219	217	214	219	211	206
597	668	689	691	665	533	659	440	423	436	439	449
69.9	74.9	73.3	76.2	74.1	67.6	71.9	64.2	63.9	65.3	66.7	63.7
505	583	581	629	589	457	548	372	368	379	410	391
55.2	50.4	57.1	51.7	52.5	57.3	48.1	44.5	46.6	46.4	49.3	47.7
131	127	125	129	129	130	129	158	156	161	158	154
18.7	17.7	17.4	18.7	18.6	18.7	17.7	21.5	21.5	22.1	22.7	21.6
1.5	1.5	1.5	1.5	1.5	1.5	1.5	1.6	1.6	1.6	1.6	1.6
119	102	97	161	192	122	97	116	137	127	284	254
1253	1116	1145	1238	1264	1389	1142	1489	1542	1599	1651	1588
30.3	28.0	28.5	28.9	28.8	30.6	27.9	34.8	35.2	36.5	36.4	35.1
345	318	323	324	325	338	325	443	439	454	428	419
118	106	114	112	116	122	108	132	132	137	133	130
1.0	0.9	0.9	1.0	1.1	1.1	0.9	0.9	1.2	1.0	1.7	1.7
950	892	915	1017	1110	1066	892	1123	1130	1169	1257	1211
77.5	68.5	68.6	76.6	76.3	82.7	68.2	88.9	92.5	96.1	105	99.7
146	131	131	146	146	156	131	173	178	185	202	192
17.1	15.4	15.4	16.1	15.9	17.1	15.4	20.7	21.3	22.1	22.4	21.4
68.6	62.0	61.5	64.1	62.7	67.7	62.1	84.2	86.1	88.9	88.8	84.3
12.8	11.6	11.5	12.4	12.2	13.0	11.7	15.9	16.1	16.7	17.1	16.4
3.8	3.6	3.5	3.7	3.7	3.9	3.6	4.8	4.8	5.0	5.1	4.9
10.5	9.6	9.6	10.2	9.8	10.6	9.7	13.0	13.2	13.6	13.5	12.8
1.4	1.3	1.2	1.3	1.3	1.3	1.3	1.7	1.7	1.7	1.7	1.6
6.7	6.2	6.2	6.4	6.2	6.7	6.3	8.1	8.1	8.4	8.2	7.8
1.1	1.0	1.0	1.0	1.0	1.1	1.0	1.3	1.3	1.3	1.3	1.2
2.7	2.5	2.6	2.5	2.4	2.6	2.5	3.1	3.1	3.2	3.0	2.9
0.3	0.3	0.3	0.3	0.3	0.3	0.3	0.4	0.4	0.4	0.3	0.3
1.8	1.7	1.8	1.7	1.7	1.8	1.7	2.0	1.9	2.0	1.9	1.8
0.3	0.2	0.2	0.2	0.2	0.2	0.2	0.3	0.3	0.3	0.2	0.2
7.1	6.6	6.6	6.7	6.4	6.7	6.9	9.2	9.1	9.3	8.6	8.3
6.3	5.7	6.0	5.7	5.7	5.9	5.9	7.1	7.1	7.3	6.6	6.4
4.4	3.4	4.0	3.5	4.0	3.5	3.9	4.9	5.3	5.3	5.1	5.4
9.3	8.3	8.5	9.0	10.5	9.2	8.2	10.0	10.4	10.5	10.6	10.0
2.3	2.1	2.2	2.3	2.5	2.3	2.1	2.4	2.6	2.6	2.6	2.4
0.31	0.24	0.28	0.18		0.45	0.27	0.37	0.30	0.22		0.25
0.43	0.38	0.46	0.20			0.27	0.42	0.31	0.28		0.36
0.43	0.38	0.46	0.20		0.45	0.27	0.42	0.31	0.28		0.36
0.703626 9	0.703592 11	0.703669 8						0.703596 12	0.703634 11	0.703676 9	
0.512895 6	0.512871 9	0.512999 9						0.512849 8	0.512851 12	0.512899 21	
18.264	18.260	18.308						18.243	18.252		
15.530	15.536	15.591						15.503	15.516		
38.449	38.443	38.620						38.322	38.368		

Shiheng					Nuitoushan					
N 26°20'37"	E 117°16'12.2"				N 24°13'12.6(	118° 2'26.80"				
2.95 Ma										
AOB[d]	AOB[d]	AOB[d]	AOB[d]	AOB[d]	Transitional basalt	Transitional basalt	Transitional basalt	Transitional basalt	Transitional basalt	Transitional basalt
SH-1	SH-2	SH-3	SH-4	SH-5	NTS-1	NTS-2	NTS-3	NTS-4	NTS-5	NTS-6
46.25	47.42	45.29	44.74	43.43	52.48	50.45	50.10	48.14	50.25	50.97
2.62	2.70	2.79	2.89	2.70	2.03	1.44	1.46	2.22	2.10	2.07
11.01	11.30	11.79	11.87	11.21	14.68	15.30	15.01	15.93	15.35	15.6
11.83	11.09	11.67	11.87	11.76	10.51	11.63	11.88	11.23	11.06	10.41
0.2	0.1	0.2	0.2	0.2	0.1	0.1	0.2	0.1	0.1	0.1
8.52	7.31	7.29	8.12	7.80	6.57	7.12	7.65	7.24	6.25	5.15
11.47	11.73	11.71	12.14	11.51	7.67	9.64	9.35	7.11	7.03	6.08
3.52	3.23	3.15	3.57	3.73	3.19	2.97	3.00	3.09	3.44	3.62
1.13	1.29	1.08	1.25	0.98	1.46	0.49	0.37	2.14	2.34	2.79
1.13	0.96	1.00	1.11	1.10	0.31	0.16	0.18	0.34	0.49	0.46
2.14	2.45	2.91	3.05	3.49	(0.38)	0.16	0.64	1.75	1.22	2.22
99.78	99.62	98.84	100.77	97.86	99.33	99.50	99.66	99.33	99.66	99.50
0.66	0.64	0.62	0.64	0.64	0.62	0.62	0.63	0.63	0.60	0.57
15697	16170	16722	17297	16164	13324	12592	12425	13324	12592	12425
9404	10736	8988	10403	8156	17810	19474	23219	17810	19474	23219
8.3	7.0	7.0	6.9	7.3	3.7	3.4	3.9	7.3	6.9	6.6
1.5	1.3	1.4	1.4	1.5	1.1	0.5	0.5	1.8	1.9	2.2
24.95	26.17	25.65	25.39	24.59	16.90	19.80	19.40	17.90	15.90	13.30
208	227	219	220	216	150	155	147	173	168	143
227	241	240	234	220	205	191	206	114	121	63
60.6	61.2	61.5	62.0	57.0	39.4	43.7	45.8	46.6	44.3	38.1
228	253	240	246	224	151	134	179	135	120	80
77.8	87.3	85.4	84.3	82.3	57.3	78.5	70.8	45.0	40.5	33.7
116	113	115	113	112	117	107	103	149	152	158
19.2	19.4	19.4	19.1	18.9	21.8	19.5	19.1	24.2	24.8	25.1
1.5	1.5	1.5	1.5	1.4	0.2	0.2	0.2	0.1	0.1	0.1
136	108	97	93	100	23	11	7	59	66	75
1219	1115	1133	1112	1135	460	303	295	618	721	780
28.2	26.8	27.3	26.3	27.3	15.1	13.5	13.6	14.7	17.7	14.3
217	202	202	199	205	223	98	98	284	316	349
85.4	79.4	80.2	79.2	81.8	29.3	15.0	14.9	63.7	72.9	81.6
1.4	1.5	1.2	0.9	0.9	0.3	0.1	0.1	0.4	0.5	0.4
1241	1109	1135	1103	1062	269	136	124	539	607	745
64.2	56.5	57.5	55.5	62.1	19.1	10.5	10.6	34.4	47.6	46.0
119	105	106	103	114	40	21	22	66	91	89
13.8	12.1	12.2	11.9	13.1	5.1	2.6	2.7	3.4	5.2	4.8
56.0	49.7	49.9	48.7	53.4	20.6	11.1	10.8	13.5	20.7	18.8
10.7	9.7	9.6	9.4	10.3	4.4	2.7	2.5	2.7	3.9	3.2
3.4	3.1	3.1	3.0	3.2	1.9	1.1	1.2	0.9	1.3	1.3
9.1	8.4	8.5	8.2	8.7	4.6	3.2	3.2	2.4	3.4	2.8
1.2	1.1	1.1	1.1	1.1	0.7	0.5	0.5	0.3	0.4	0.4
6.0	5.6	5.7	5.5	5.9	3.4	2.7	2.8	1.7	2.1	2.0
1.0	1.0	1.0	0.9	1.0	0.6	0.5	0.5	0.3	0.3	0.3
2.6	2.4	2.5	2.4	2.5	1.6	1.4	1.4	0.6	0.9	0.6
0.3	0.3	0.3	0.3	0.3	0.2	0.2	0.2	0.1	0.1	0.1
1.8	1.8	1.8	1.8	1.8	1.1	1.0	1.0	0.4	0.6	0.3
0.3	0.3	0.3	0.2	0.2	0.2	0.2	0.2	0.0	0.1	0.0
4.6	4.3	4.3	4.2	4.4	5.4	2.5	2.6	6.4	7.3	7.9
3.8	3.6	3.6	3.6	3.6	1.7	0.9	0.8	3.8	4.4	4.9
3.9	3.4	3.5	3.3	3.6	1.9	1.0	1.1	3.8	5.5	5.4
7.7	6.8	7.0	6.7	7.4	2.4	1.4	1.3	5.3	6.5	6.6
1.8	1.6	1.7	1.7	1.8	0.6	0.3	0.3	1.3	1.5	1.6
3.18	1.28	3.36	2.32	1.45						
3.36	1.46	3.78	2.64	1.62						
3.36	1.46	3.78	2.64	1.62						
#######	#######	#######	#######	#######				0.703596	0.703634	0.703676
13	9	12	13	14				12	11	9
#######	#######	#######	#######	#######				0.512849	0.512851	0.512899
7	11	8	12	8				8	12	21
18.371	18.345	18.377	18.301	18.340				18.243	18.252	
15.543	15.533	15.570	15.487	15.536				15.503	15.516	
38.519	38.480	38.606	38.328	38.499				38.322	38.368	

Table 6-2 EPMA and FTIR data for the CPX phenocrysts of the Fujian basalts.

Sample No.	MX-1							
Section No.	6							
Point No.	1	4	5	6	7	8	9	10
SiO_2	50.55	48.73	47.07	48.86	46.71	47.13	46.65	46.23
TiO_2	1.88	2.20	3.02	2.03	2.86	2.83	3.11	3.06
Al_2O3	3.53	4.33	5.09	4.75	5.39	6.10	5.35	6.48
Cr_2O3	0.19	0.18	0.00	0.00	0.13	0.23	0.00	0.28
FeO	5.80	5.89	7.24	6.91	6.76	6.63	6.75	6.39
MnO	0.05	0.07	0.07	0.08	0.02	0.05	0.08	0.06
MgO	14.31	13.74	12.51	13.52	12.91	12.67	12.76	12.49
CaO	23.43	23.40	23.37	22.93	23.23	23.35	23.38	23.37
Na_2O	0.38	0.37	0.36	0.62	0.69	0.49	0.45	0.54
K_2O	0.01	0.00	0.01	0.01	0.05	0.00	0.00	0.00
NiO	0.00	0.00	0.06	0.02	0.00	0.00	0.02	0.03
Total	100.12	98.91	98.80	99.73	98.73	99.46	98.55	98.94
Si	1.87	1.83	1.79	1.83	1.77	1.77	1.78	1.75
Ti	0.05	0.06	0.09	0.06	0.08	0.08	0.09	0.09
Al	0.15	0.19	0.23	0.21	0.24	0.27	0.24	0.29
Cr	0.01	0.01	0.00	0.00	0.00	0.01	0.00	0.01
Fe	0.18	0.19	0.23	0.22	0.21	0.21	0.21	0.20
Mn	0.00	0.00	0.00	0.00	0.00	0.00	0.00	0.00
Mg	0.79	0.77	0.71	0.75	0.73	0.71	0.72	0.71
Ca	0.93	0.94	0.95	0.92	0.95	0.94	0.95	0.95
Na	0.03	0.03	0.03	0.04	0.05	0.04	0.03	0.04
K	0.00	0.00	0.00	0.00	0.00	0.00	0.00	0.00
Ni	0.00	0.00	0.00	0.00	0.00	0.00	0.00	0.00
Total	4.01	4.02	4.02	4.03	4.05	4.03	4.03	4.03
Mg#	81.47	80.62	75.50	77.71	77.29	77.33	77.12	77.70
$D^{(cpx\text{-}melt)}_{H2O}$	0.0137	0.0173	0.0229	0.0183	0.0251	0.0256	0.0249	0.0294
Absorbance of cpx (cm^{-1})	1.3	1.1	0.8	0.8	2.6	0.8	1.1	0.7
Thickness of cpx (0.001mm)	63	83	77	73	71	72	77	76
Absorbance normalized to 1 cm (cm^{-1})	206	133	104	110	366	117	143	92
H_2O-cpx (ppm)	87	56	44	46	155	49	60	39
H_2O-melt (wt%)	0.64	0.32	0.19	0.25	0.62	0.19	0.24	0.13

Sample No.								
Section No.								
Point No.	11	12	13	14	14.2	15	16	17
SiO_2	48.70	46.41	44.14	48.50	47.08	46.85	48.01	47.45
TiO_2	2.38	3.34	4.04	2.34	2.41	3.24	2.75	3.00
Al_2O3	4.77	5.20	7.72	4.37	6.66	5.48	4.79	5.27
Cr_2O3	0.14	0.01	0.00	0.02	0.74	0.03	0.02	0.05
FeO	6.53	7.43	7.70	6.34	6.01	7.30	6.96	7.09
MnO	0.06	0.08	0.10	0.09	0.05	0.08	0.10	0.08
MgO	13.41	12.62	11.39	13.50	12.57	12.53	12.61	12.77
CaO	23.32	23.42	23.26	23.41	22.43	23.04	23.71	23.25
Na_2O	0.48	0.50	0.42	0.41	0.65	0.41	0.33	0.39
K_2O	0.01	0.01	0.04	0.01	0.00	0.02	0.00	0.00
NiO	0.08	0.02	0.00	0.04	0.01	0.03	0.00	0.00
Total	99.86	99.04	98.80	99.01	98.61	98.99	99.28	99.34
Si	1.82	1.77	1.69	1.83	1.78	1.78	1.81	1.79
Ti	0.07	0.10	0.12	0.07	0.07	0.09	0.08	0.09
Al	0.21	0.23	0.35	0.19	0.30	0.24	0.21	0.23
Cr	0.00	0.00	0.00	0.00	0.02	0.00	0.00	0.00
Fe	0.20	0.24	0.25	0.20	0.19	0.23	0.22	0.22
Mn	0.00	0.00	0.00	0.00	0.00	0.00	0.00	0.00
Mg	0.75	0.72	0.65	0.76	0.71	0.71	0.71	0.72
Ca	0.93	0.95	0.95	0.94	0.91	0.94	0.96	0.94
Na	0.03	0.04	0.03	0.03	0.05	0.03	0.02	0.03
K	0.00	0.00	0.00	0.00	0.00	0.00	0.00	0.00
Ni	0.00	0.00	0.00	0.00	0.00	0.00	0.00	0.00
Total	4.02	4.04	4.04	4.02	4.02	4.02	4.02	4.02
Mg#	78.54	75.17	72.51	79.15	78.84	75.38	76.36	76.24
$D^{(cpx\text{-}melt)}_{H2O}$	0.0191	0.0265	0.0438	0.0180	0.0257	0.0252	0.0197	0.0230
Absorbance of cpx (cm^{-1})	0.6	1.1	0.6	0.8	1.0	1.1	1.2	0.8
Thickness of cpx (0.001mm)	73	75	75	86	86	89	84	73
Absorbance normalized to 1 cm (cm^{-1})	86	149	81	87	110	124	143	110
H_2O-cpx (ppm)	37	63	34	37	47	52	60	46
H_2O-melt (wt%)	0.19	0.24	0.08	0.21	0.18	0.21	0.31	0.20

Sample No.								
Section No.								
Point No.	18	19	20	21	22	23	24	25
SiO_2	49.15	44.76	51.88	46.89	45.82	46.92	46.89	47.56
TiO_2	2.40	3.55	1.65	2.65	3.45	3.11	2.77	2.82
Al_2O3	4.05	7.27	2.19	6.21	7.02	5.44	5.88	4.47
Cr_2O3	0.05	0.02	0.08	0.17	0.16	0.02	0.32	0.03
FeO	6.31	7.48	6.55	6.55	6.75	7.33	6.12	6.87
MnO	0.05	0.09	0.11	0.10	0.04	0.07	0.10	0.07
MgO	13.65	11.86	13.69	12.78	12.19	12.57	13.00	13.01
CaO	23.61	23.35	22.16	22.85	23.02	23.15	23.41	23.49
Na_2O	0.38	0.54	0.86	0.56	0.48	0.38	0.52	0.26
K_2O	0.00	0.02	0.04	0.02	0.00	0.00	0.00	0.00
NiO	0.00	0.03	0.07	0.00	0.01	0.00	0.04	0.00
Total	99.66	98.95	99.28	98.77	98.93	98.98	99.04	98.58
Si	1.84	1.71	1.94	1.77	1.74	1.78	1.77	1.81
Ti	0.07	0.10	0.05	0.08	0.10	0.09	0.08	0.08
Al	0.18	0.33	0.10	0.28	0.31	0.24	0.26	0.20
Cr	0.00	0.00	0.00	0.00	0.00	0.00	0.01	0.00
Fe	0.20	0.24	0.20	0.21	0.21	0.23	0.19	0.22
Mn	0.00	0.00	0.00	0.00	0.00	0.00	0.00	0.00
Mg	0.76	0.67	0.76	0.72	0.69	0.71	0.73	0.74
Ca	0.95	0.95	0.89	0.93	0.93	0.94	0.95	0.96
Na	0.03	0.04	0.06	0.04	0.04	0.03	0.04	0.02
K	0.00	0.00	0.00	0.00	0.00	0.00	0.00	0.00
Ni	0.00	0.00	0.00	0.00	0.00	0.00	0.00	0.00
Total	4.02	4.05	4.00	4.03	4.03	4.02	4.03	4.02
Mg#	79.41	73.89	78.84	77.66	76.30	75.36	79.12	77.15
$D^{(cpx\text{-}melt)}_{H2O}$	0.0167	0.0388	0.0094	0.0258	0.0328	0.0246	0.0259	0.0202
Absorbance of cpx (cm^{-1})	1.3	1.5	0.6	1.4	0.9	1.4	1.2	1.2
Thickness of cpx (0.001mm)	81	88	82	76	83	67	83	91
Absorbance normalized to 1 cm (cm^{-1})	163	174	76	184	113	209	145	132
H_2O-cpx (ppm)	69	74	32	78	48	88	61	56
H_2O-melt (wt%)	0.41	0.19	0.34	0.30	0.15	0.36	0.24	0.28

Sample No.						MX-2	
Section No.						6	
Point No.	26	27	28	29	29.2	1	2
SiO_2	48.08	48.52	49.52	47.03	49.09	46.89	48.35
TiO_2	2.66	2.49	2.01	3.01	2.28	2.99	2.69
Al_2O3	5.01	4.69	3.68	6.03	4.14	5.41	4.98
Cr_2O3	0.07	0.08	0.04	0.02	0.05	0.34	0.01
FeO	6.53	6.52	5.58	6.87	6.07	6.64	6.64
MnO	0.08	0.05	0.07	0.05	0.06	0.09	0.03
MgO	13.14	13.51	13.87	12.70	13.62	12.76	13.26
CaO	23.79	23.32	23.45	22.96	23.49	23.14	23.30
Na_2O	0.36	0.40	0.44	0.52	0.41	0.73	0.40
K_2O	0.01	0.01	0.01	0.01	0.00	0.02	0.00
NiO	0.00	0.09	0.02	0.00	0.03	0.00	0.03
Total	99.72	99.66	98.69	99.20	99.23	99.01	99.67
Si	1.80	1.82	1.86	1.77	1.84	1.78	1.81
Ti	0.08	0.07	0.06	0.09	0.06	0.09	0.08
Al	0.22	0.21	0.16	0.27	0.18	0.24	0.22
Cr	0.00	0.00	0.00	0.00	0.00	0.01	0.00
Fe	0.20	0.20	0.18	0.22	0.19	0.21	0.21
Mn	0.00	0.00	0.00	0.00	0.00	0.00	0.00
Mg	0.73	0.75	0.78	0.71	0.76	0.72	0.74
Ca	0.96	0.94	0.94	0.93	0.94	0.94	0.93
Na	0.03	0.03	0.03	0.04	0.03	0.05	0.03
K	0.00	0.00	0.00	0.00	0.00	0.00	0.00
Ni	0.00	0.00	0.00	0.00	0.00	0.00	0.00
Total	4.02	4.02	4.02	4.03	4.02	4.04	4.02
Mg#	78.21	78.71	81.57	76.72	80.00	77.39	78.08
$D^{(cpx\text{-}melt)}_{H2O}$	0.0209	0.0194	0.0143	0.0258	0.0164	0.0251	0.0202
Absorbance of cpx (cm^{-1})	2.6	0.7	1.0	2.3	1.2	1.0	0.5
Thickness of cpx (0.001mm)	84	80	92	75	75	69	69
Absorbance normalized to 1 cm (cm^{-1})	310	88	109	307	160	145	75
H_2O-cpx (ppm)	131	37	46	130	68	61	32
H_2O-melt (wt%)	0.63	0.19	0.32	0.50	0.41	0.24	0.16

Sample No. Section No. Point No.	3	4	5	6	7	8	9	10
SiO_2	49.99	46.11	46.40	46.64	44.52	46.93	43.97	48.01
TiO_2	2.23	3.07	3.18	3.38	4.04	3.08	4.47	2.62
Al_2O3	3.91	6.51	6.16	5.72	7.62	6.24	7.86	5.01
Cr_2O3	0.13	0.18	0.20	0.05	0.03	0.28	0.06	0.09
FeO	5.61	6.25	6.57	7.00	7.23	6.44	7.57	6.42
MnO	0.07	0.00	0.07	0.05	0.09	0.06	0.04	0.06
MgO	14.02	12.58	12.53	12.60	11.59	12.67	11.54	12.57
CaO	23.43	23.49	23.56	23.49	23.60	23.59	23.33	23.38
Na_2O	0.38	0.46	0.48	0.40	0.50	0.44	0.54	0.39
K_2O	0.00	0.01	0.01	0.02	0.02	0.01	0.01	0.00
NiO	0.00	0.01	0.00	0.04	0.00	0.04	0.06	0.00
Total	99.77	98.65	99.13	99.39	99.24	99.77	99.44	98.54
Si	1.86	1.75	1.76	1.76	1.69	1.76	1.67	1.82
Ti	0.06	0.09	0.09	0.10	0.12	0.09	0.13	0.07
Al	0.17	0.29	0.27	0.25	0.34	0.28	0.35	0.22
Cr	0.00	0.01	0.01	0.00	0.00	0.01	0.00	0.00
Fe	0.17	0.20	0.21	0.22	0.23	0.20	0.24	0.20
Mn	0.00	0.00	0.00	0.00	0.00	0.00	0.00	0.00
Mg	0.78	0.71	0.71	0.71	0.66	0.71	0.65	0.71
Ca	0.93	0.95	0.95	0.95	0.96	0.95	0.95	0.95
Na	0.03	0.03	0.03	0.03	0.04	0.03	0.04	0.03
K	0.00	0.00	0.00	0.00	0.00	0.00	0.00	0.00
Ni	0.00	0.00	0.00	0.00	0.00	0.00	0.00	0.00
Total	4.01	4.03	4.03	4.03	4.04	4.03	4.04	4.01
Mg#	81.67	78.21	77.28	76.24	74.08	77.81	73.12	77.72
$D^{(cpx\text{-}melt)}_{H2O}$	0.0150	0.0294	0.0284	0.0272	0.0422	0.0275	0.0488	0.0191
Absorbance of cpx (cm^{-1})	0.3	0.7	0.4	0.6	0.3	1.1	1.0	0.5
Thickness of cpx (0.001mm)	69	59	59	44	68	68	81	70
Absorbance normalized to 1 cm (cm^{-1})	43	125	71	141	43	162	119	71
H_2O-cpx (ppm)	18	53	30	60	18	68	50	30
H_2O-melt (wt%)	0.12	0.18	0.11	0.22	0.04	0.25	0.10	0.16

Sample No. Section No. Point No.	11	12	13	14	14.2	15	16	17
SiO_2	48.72	51.95	41.67	50.02	47.64	55.21	45.04	47.23
TiO_2	2.36	1.15	5.71	2.07	2.65	0.18	3.83	3.11
Al_2O3	5.58	3.63	9.28	3.98	5.15	1.75	7.35	6.13
Cr_2O3	0.40	0.63	0.00	0.09	0.13	1.66	0.06	0.03
FeO	6.18	4.87	8.02	6.04	6.54	4.52	6.85	6.84
MnO	0.05	0.06	0.08	0.04	0.11	0.12	0.05	0.04
MgO	13.03	14.80	10.27	13.85	13.06	17.69	11.68	12.62
CaO	22.94	23.16	23.09	23.39	23.49	18.17	23.72	23.55
Na_2O	0.58	0.52	0.62	0.42	0.43	0.95	0.47	0.44
K_2O	0.00	0.00	0.02	0.01	0.01	0.38	0.00	0.05
NiO	0.05	0.03	0.08	0.06	0.00	0.04	0.04	0.00
Total	99.89	100.78	98.83	99.97	99.20	100.67	99.08	100.03
Si	1.81	1.90	1.60	1.86	1.80	1.99	1.71	1.77
Ti	0.07	0.03	0.17	0.06	0.08	0.00	0.11	0.09
Al	0.24	0.16	0.42	0.17	0.23	0.07	0.33	0.27
Cr	0.01	0.02	0.00	0.00	0.00	0.05	0.00	0.00
Fe	0.19	0.15	0.26	0.19	0.21	0.14	0.22	0.21
Mn	0.00	0.00	0.00	0.00	0.00	0.00	0.00	0.00
Mg	0.72	0.81	0.59	0.77	0.73	0.95	0.66	0.70
Ca	0.91	0.91	0.95	0.93	0.95	0.70	0.97	0.94
Na	0.04	0.04	0.05	0.03	0.03	0.07	0.03	0.03
K	0.00	0.00	0.00	0.00	0.00	0.02	0.00	0.00
Ni	0.00	0.00	0.00	0.00	0.00	0.00	0.00	0.00
Total	4.01	4.00	4.04	4.01	4.03	3.99	4.03	4.03
Mg#	79.00	84.42	69.54	80.35	78.07	87.47	75.26	76.68
$D^{(cpx\text{-}melt)}_{H2O}$	0.0201	0.0118	0.0756	0.0149	0.0218	0.0081	0.0375	0.0263
Absorbance of cpx (cm^{-1})	1.7	2.0	1.4	0.4	0.7	0.6	0.9	0.5
Thickness of cpx (0.001mm)	70	84	73	70	70	70	85	70
Absorbance normalized to 1 cm (cm^{-1})	240	238	192	61	106	87	105	66
H_2O-cpx (ppm)	102	101	81	26	45	37	44	28
H_2O-melt (wt%)	0.51	0.85	0.11	0.17	0.20	0.46	0.12	0.11

Sample No.								
Section No.								7
Point No.	18	20	21	22	23	24	25	1
SiO_2	47.74	44.68	46.81	45.48	48.55	46.71	45.01	48.51
TiO_2	2.92	3.96	2.87	3.78	2.69	3.38	3.83	2.37
Al_2O3	5.76	7.42	6.30	7.13	4.46	6.79	7.25	5.66
Cr_2O3	0.01	0.04	0.22	0.04	0.04	0.10	0.09	0.38
FeO	6.94	7.24	6.85	7.40	6.81	7.16	7.08	6.34
MnO	0.06	0.08	0.00	0.00	0.01	0.01	0.00	0.02
MgO	12.79	11.30	12.40	11.95	13.37	12.29	12.03	12.99
CaO	23.66	23.54	23.49	23.50	23.55	23.56	23.04	23.44
Na_2O	0.47	0.45	0.47	0.56	0.41	0.49	0.47	0.54
K_2O	0.01	0.02	0.00	0.01	0.01	0.00	0.00	0.01
NiO	0.02	0.03	0.00	0.00	0.01	0.01	0.00	0.02
Total	100.37	98.75	99.41	99.84	99.91	100.50	98.79	100.28
Si	1.78	1.71	1.76	1.72	1.82	1.74	1.71	1.80
Ti	0.08	0.11	0.08	0.11	0.08	0.09	0.11	0.07
Al	0.25	0.33	0.28	0.32	0.20	0.30	0.33	0.25
Cr	0.00	0.00	0.01	0.00	0.00	0.00	0.00	0.01
Fe	0.22	0.23	0.22	0.23	0.21	0.22	0.23	0.20
Mn	0.00	0.00	0.00	0.00	0.00	0.00	0.00	0.00
Mg	0.71	0.64	0.70	0.67	0.75	0.68	0.68	0.72
Ca	0.95	0.96	0.95	0.95	0.94	0.94	0.94	0.93
Na	0.03	0.03	0.03	0.04	0.03	0.04	0.03	0.04
K	0.00	0.00	0.00	0.00	0.00	0.00	0.00	0.00
Ni	0.00	0.00	0.00	0.00	0.00	0.00	0.00	0.00
Total	4.03	4.03	4.03	4.04	4.02	4.03	4.03	4.02
Mg#	76.66	73.56	76.36	74.21	77.79	75.39	75.19	78.51
$D^{(cpx\text{-}melt)}_{H2O}$	0.0242	0.0387	0.0270	0.0368	0.0192	0.0308	0.0381	0.0212
Absorbance of cpx (cm^{-1})	0.7	0.9	0.9	0.1	2.1	1.4	1.3	1.5
Thickness of cpx (0.001mm)	84	84	89	89	90	90	90	95
Absorbance normalized to 1 cm (cm^{-1})	80	107	101	15	233	156	144	158
H_2O-cpx (ppm)	34	45	43	6	99	66	61	67
H_2O-melt (wt%)	0.14	0.12	0.16	0.02	0.51	0.21	0.16	0.32

Sample No. Section No. Point No.	2	3	4	5	6	7	8	8.2
SiO_2	46.29	49.07	48.39	49.04	47.39	47.06	44.70	46.15
TiO_2	3.10	2.08	2.60	2.60	2.95	2.71	3.63	3.40
Al_2O3	6.69	5.02	4.63	4.29	6.36	6.08	7.37	6.46
Cr_2O3	0.24	0.55	0.00	0.00	0.28	0.07	0.08	0.14
FeO	6.60	5.85	6.92	6.59	6.50	6.33	7.45	6.65
MnO	0.03	0.01	0.03	0.00	0.09	0.03	0.05	0.06
MgO	12.65	13.62	13.17	13.54	12.76	12.61	11.87	11.88
CaO	23.33	23.47	23.73	23.45	23.53	23.62	23.72	23.48
Na_2O	0.57	0.46	0.44	0.34	0.49	0.44	0.52	0.42
K_2O	0.03	0.00	0.00	0.00	0.00	0.00	0.00	0.00
NiO	0.03	0.01	0.03	0.00	0.09	0.03	0.05	0.06
Total	99.56	100.14	99.93	99.85	100.42	99.01	99.41	98.70
Si	1.74	1.82	1.81	1.83	1.77	1.78	1.70	1.75
Ti	0.09	0.06	0.07	0.07	0.08	0.08	0.10	0.10
Al	0.30	0.22	0.20	0.19	0.28	0.27	0.33	0.29
Cr	0.01	0.02	0.00	0.00	0.01	0.00	0.00	0.00
Fe	0.21	0.18	0.22	0.21	0.20	0.20	0.24	0.21
Mn	0.00	0.00	0.00	0.00	0.00	0.00	0.00	0.00
Mg	0.71	0.75	0.74	0.75	0.71	0.71	0.67	0.67
Ca	0.94	0.93	0.95	0.94	0.94	0.96	0.97	0.96
Na	0.04	0.03	0.03	0.02	0.04	0.03	0.04	0.03
K	0.00	0.00	0.00	0.00	0.00	0.00	0.00	0.00
Ni	0.00	0.00	0.00	0.00	0.00	0.00	0.00	0.00
Total	4.04	4.02	4.03	4.01	4.03	4.03	4.05	4.02
Mg#	77.36	80.60	77.25	78.55	77.77	78.02	73.97	76.12
$D^{(cpx\text{-}melt)}_{H2O}$	0.0311	0.0188	0.0196	0.0177	0.0268	0.0246	0.0405	0.0287
Absorbance of cpx (cm^{-1})	1.7	1.2	0.7	1.2	0.9	1.2	0.9	1.0
Thickness of cpx (0.001mm)	99	99	99	94	97	94	92	92
Absorbance normalized to 1 cm (cm^{-1})	172	121	71	128	95	128	98	109
H_2O-cpx (ppm)	73	51	30	54	40	54	41	46
H_2O-melt (wt%)	0.23	0.27	0.15	0.30	0.15	0.22	0.10	0.16

Sample No.			MX-3				
Section No.			6				
Point No.	9	10	1	2	2.2	3	4
SiO_2	49.06	45.50	47.55	48.08	47.64	47.64	48.69
TiO_2	2.53	3.43	2.78	2.27	2.29	2.29	2.11
Al_2O3	4.36	7.27	4.98	5.40	5.75	5.75	5.53
Cr_2O3	0.07	0.04	0.14	0.43	0.56	0.56	0.47
FeO	6.54	7.36	6.52	5.69	5.91	5.91	5.85
MnO	0.00	0.00	0.02	0.04	0.01	0.01	0.00
MgO	13.18	12.07	13.01	12.82	13.17	13.17	13.41
CaO	23.56	23.30	23.21	23.64	23.47	23.47	23.83
Na_2O	0.37	0.47	0.45	0.42	0.52	0.52	0.39
K_2O	0.00	0.01	0.01	0.01	0.02	0.02	0.01
NiO	0.00	0.00	0.02	0.04	0.01	0.01	0.00
Total	99.68	99.44	98.66	98.84	99.34	99.34	100.29
Si	1.83	1.72	1.80	1.81	1.79	1.79	1.81
Ti	0.07	0.10	0.08	0.06	0.06	0.06	0.06
Al	0.19	0.32	0.22	0.24	0.25	0.25	0.24
Cr	0.00	0.00	0.00	0.01	0.02	0.02	0.01
Fe	0.20	0.23	0.21	0.18	0.19	0.19	0.18
Mn	0.00	0.00	0.00	0.00	0.00	0.00	0.00
Mg	0.73	0.68	0.73	0.72	0.74	0.74	0.74
Ca	0.94	0.94	0.94	0.95	0.94	0.94	0.95
Na	0.03	0.03	0.03	0.03	0.04	0.04	0.03
K	0.00	0.00	0.00	0.00	0.00	0.00	0.00
Ni	0.00	0.00	0.00	0.00	0.00	0.00	0.00
Total	4.01	4.04	4.02	4.01	4.03	4.03	4.02
Mg#	78.23	74.51	78.06	80.06	79.90	79.90	80.34
$D^{(cpx\text{-}melt)}_{H2O}$	0.0172	0.0359	0.0213	0.0198	0.0231	0.0231	0.0205
Absorbance of cpx (cm^{-1})	0.7	1.3	0.7	1.5	1.4	0.2	2.1
Thickness of cpx (0.001mm)	87	96	58	74	74	72	72
Absorbance normalized to 1 cm (cm^{-1})	80	135	126	203	189	28	292
H_2O-cpx (ppm)	34	57	53	86	80	12	123
H_2O-melt (wt%)	0.20	0.16	0.25	0.43	0.35	0.05	0.60

Sample No. Section No. Point No.	5	6	7	8	9	10	11	12
SiO_2	51.05	45.97	43.87	50.01	43.81	46.48	49.84	47.14
TiO_2	1.25	3.06	4.54	1.90	4.27	3.31	2.11	2.75
Al_2O3	4.00	7.20	8.46	3.87	8.79	7.29	4.60	6.77
Cr_2O3	0.59	0.13	0.11	0.19	0.25	0.11	0.03	0.34
FeO	5.79	6.98	7.61	5.64	7.53	7.10	6.39	6.30
MnO	0.01	0.05	0.02	0.19	0.02	0.00	0.00	0.00
MgO	15.39	11.83	11.05	13.56	11.18	12.15	13.56	12.56
CaO	21.63	23.90	23.52	23.97	23.61	23.12	23.23	23.72
Na_2O	0.61	0.42	0.43	0.32	0.44	0.50	0.40	0.40
K_2O	0.01	0.00	0.00	0.00	0.01	0.01	0.00	0.00
NiO	0.01	0.05	0.02	0.19	0.02	0.00	0.00	0.00
Total	100.35	99.57	99.62	99.83	99.93	100.06	100.16	99.98
Si	1.87	1.73	1.66	1.86	1.66	1.74	1.85	1.76
Ti	0.03	0.09	0.13	0.05	0.12	0.09	0.06	0.08
Al	0.17	0.32	0.38	0.17	0.39	0.32	0.20	0.30
Cr	0.02	0.00	0.00	0.01	0.01	0.00	0.00	0.01
Fe	0.18	0.22	0.24	0.18	0.24	0.22	0.20	0.20
Mn	0.00	0.00	0.00	0.00	0.00	0.00	0.00	0.00
Mg	0.84	0.67	0.62	0.75	0.63	0.68	0.75	0.70
Ca	0.85	0.97	0.96	0.96	0.96	0.93	0.92	0.95
Na	0.04	0.03	0.03	0.02	0.03	0.04	0.03	0.03
K	0.00	0.00	0.00	0.00	0.00	0.00	0.00	0.00
Ni	0.00	0.00	0.00	0.01	0.00	0.00	0.00	0.00
Total	4.02	4.03	4.03	4.01	4.04	4.02	4.01	4.02
Mg#	82.58	75.15	72.14	81.09	72.59	75.30	79.09	78.04
$D^{(cpx\text{-}melt)}_{H2O}$	0.0145	0.0320	0.0513	0.0141	0.0536	0.0323	0.0161	0.0275
Absorbance of cpx (cm^{-1})	2.0	1.5	2.5	0.7	1.2	1.2	1.4	1.1
Thickness of cpx (0.001mm)	63	68	68	78	84	90	90	87
Absorbance normalized to 1 cm (cm^{-1})	317	221	368	90	143	133	156	129
H_2O-cpx (ppm)	134	93	156	38	60	56	66	54
H_2O-melt (wt%)	0.93	0.29	0.30	0.27	0.11	0.17	0.41	0.20

Sample No.								
Section No.							7	
Point No.	12.2	13	14	15	16	17	1	2
SiO_2	46.68	46.70	49.91	46.21	47.42	48.63	45.26	47.11
TiO_2	2.93	2.94	2.04	3.16	2.53	2.25	3.72	3.00
Al_2O3	6.64	6.18	3.48	5.96	5.15	4.83	7.40	6.41
Cr_2O3	0.48	0.32	0.24	0.10	0.12	0.20	0.00	0.18
FeO	6.76	6.05	5.21	6.96	6.74	5.97	7.13	6.61
MnO	0.01	0.04	0.01	0.01	0.02	0.03	0.00	0.02
MgO	12.31	12.34	14.24	12.57	12.91	13.40	11.29	12.58
CaO	23.25	23.57	23.69	23.58	23.72	23.72	23.56	23.81
Na_2O	0.53	0.44	0.35	0.39	0.33	0.33	0.42	0.44
K_2O	0.00	0.00	0.00	0.00	0.00	0.00	0.00	0.00
NiO	0.01	0.04	0.01	0.01	0.02	0.03	0.00	0.02
Total	99.61	98.61	99.15	98.95	98.96	99.39	98.78	100.18
Si	1.76	1.77	1.86	1.75	1.79	1.82	1.72	1.76
Ti	0.08	0.08	0.06	0.09	0.07	0.06	0.11	0.08
Al	0.29	0.28	0.15	0.27	0.23	0.21	0.33	0.28
Cr	0.01	0.01	0.01	0.00	0.00	0.01	0.00	0.01
Fe	0.21	0.19	0.16	0.22	0.21	0.19	0.23	0.21
Mn	0.00	0.00	0.00	0.00	0.00	0.00	0.00	0.00
Mg	0.69	0.70	0.79	0.71	0.73	0.75	0.64	0.70
Ca	0.94	0.96	0.95	0.96	0.96	0.95	0.96	0.95
Na	0.04	0.03	0.03	0.03	0.02	0.02	0.03	0.03
K	0.00	0.00	0.00	0.00	0.00	0.00	0.00	0.00
Ni	0.00	0.00	0.00	0.00	0.00	0.00	0.00	0.00
Total	4.03	4.02	4.01	4.04	4.03	4.02	4.02	4.03
Mg#	76.44	78.43	82.98	76.31	77.36	80.00	73.83	77.23
$D^{(cpx\text{-}melt)}_{H2O}$	0.0288	0.0258	0.0141	0.0285	0.0218	0.0184	0.0349	0.0275
Absorbance of cpx (cm^{-1})	1.2	0.1	0.8	0.4	1.2	1.2	1.6	0.5
Thickness of cpx (0.001mm)	87	86	85	85	77	82	80	96
Absorbance normalized to 1 cm (cm^{-1})	138	16	88	47	156	146	205	52
H_2O-cpx (ppm)	58	7	37	20	66	62	87	22
H_2O-melt (wt%)	0.20	0.03	0.26	0.07	0.30	0.34	0.25	0.08

Sample No.							
Section No.							
Point No.	3	4	5	5.2	6	7	8
SiO_2	46.20	47.52	43.87	50.95	46.08	47.59	48.93
TiO_2	2.12	1.86	3.99	0.70	3.60	2.68	2.03
Al_2O3	6.66	4.82	8.46	4.95	7.06	5.65	4.98
Cr_2O3	0.33	0.03	0.10	0.18	0.29	0.19	0.52
FeO	6.07	6.64	6.87	8.11	6.85	6.34	5.53
MnO	0.01	0.06	0.00	0.00	0.00	0.02	0.00
MgO	12.40	12.28	11.45	12.14	11.98	13.10	13.63
CaO	21.89	21.53	23.71	22.28	23.50	23.77	23.42
Na_2O	0.62	1.01	0.47	0.73	0.58	0.39	0.54
K_2O	0.00	0.01	0.01	0.01	0.00	0.01	0.00
NiO	0.01	0.06	0.00	0.00	0.00	0.02	0.00
Total	96.32	95.82	98.94	100.04	99.94	99.76	99.58
Si	1.78	1.85	1.67	1.89	1.73	1.78	1.82
Ti	0.06	0.05	0.11	0.02	0.10	0.08	0.06
Al	0.30	0.22	0.38	0.22	0.31	0.25	0.22
Cr	0.01	0.00	0.00	0.01	0.01	0.01	0.02
Fe	0.20	0.22	0.22	0.25	0.21	0.20	0.17
Mn	0.00	0.00	0.00	0.00	0.00	0.00	0.00
Mg	0.71	0.71	0.65	0.67	0.67	0.73	0.76
Ca	0.91	0.90	0.97	0.89	0.95	0.95	0.94
Na	0.05	0.08	0.03	0.05	0.04	0.03	0.04
K	0.00	0.00	0.00	0.00	0.00	0.00	0.00
Ni	0.00	0.00	0.00	0.00	0.00	0.00	0.00
Total	4.02	4.03	4.04	4.00	4.03	4.03	4.02
Mg#	78.47	76.73	74.81	72.73	75.72	78.67	81.47
$D^{(cpx\text{-}melt)}_{H2O}$	0.0248	0.0167	0.0485	0.0124	0.0337	0.0237	0.0184
Absorbance of cpx (cm^{-1})	1.5	1.1	0.6	0.6	1.1	1.2	1.1
Thickness of cpx (0.001mm)	97	97	101	101	101	92	88
Absorbance normalized to 1 cm (cm^{-1})	155	113	61	61	113	126	125
H_2O-cpx (ppm)	65	48	26	26	48	53	53
H_2O-melt (wt%)	0.26	0.29	0.05	0.21	0.14	0.22	0.29

Sample No.	MX-5							
Section No.	3							
Point No.	1	2	4	6	7	8	9	10.2
SiO_2	48.86	48.43	48.63	49.09	47.65	47.50	49.87	47.77
TiO_2	2.13	2.86	2.86	2.00	2.98	2.40	1.91	2.57
Al_2O3	4.89	4.48	4.80	4.99	5.29	5.95	6.03	5.99
Cr_2O3	0.28	0.01	0.00	0.26	0.09	0.49	0.38	0.36
FeO	5.93	6.30	6.77	5.69	6.99	5.74	6.02	6.16
MnO	0.02	0.08	0.07	0.05	0.05	0.04	0.07	0.07
MgO	13.48	13.35	13.28	13.51	13.01	13.16	13.35	12.41
CaO	23.17	23.32	23.58	23.13	23.68	23.69	21.96	23.19
Na_2O	0.54	0.43	0.35	0.57	0.34	0.50	0.80	0.68
K_2O	0.00	0.01	0.00	0.00	0.00	0.00	0.04	0.02
NiO	0.06	0.08	0.02	0.04	0.02	0.05	0.04	0.04
Total	99.37	99.35	100.35	99.31	100.10	99.52	100.47	99.27
Si	1.83	1.82	1.81	1.83	1.78	1.78	1.83	1.79
Ti	0.06	0.08	0.08	0.06	0.08	0.07	0.05	0.07
Al	0.22	0.20	0.21	0.22	0.23	0.26	0.26	0.27
Cr	0.01	0.00	0.00	0.01	0.00	0.01	0.01	0.01
Fe	0.19	0.20	0.21	0.18	0.22	0.18	0.19	0.19
Mn	0.00	0.00	0.00	0.00	0.00	0.00	0.00	0.00
Mg	0.75	0.75	0.74	0.75	0.73	0.74	0.73	0.69
Ca	0.93	0.94	0.94	0.93	0.95	0.95	0.87	0.93
Na	0.04	0.03	0.03	0.04	0.02	0.04	0.06	0.05
K	0.00	0.00	0.00	0.00	0.00	0.00	0.00	0.00
Ni	0.00	0.00	0.00	0.00	0.00	0.00	0.00	0.00
Total	4.02	4.02	4.02	4.02	4.03	4.03	4.01	4.02
Mg#	80.20	79.07	77.77	80.88	76.84	80.34	79.81	78.21
$D^{(cpx\text{-}melt)}_{H2O}$	0.0181	0.0191	0.0201	0.0175	0.0236	0.0241	0.0185	0.0224
Absorbance of cpx (cm^{-1})	0.6	0.6	0.8	0.4	0.9	1.0	1.7	1.1
Thickness of cpx (0.001mm)	80	77	80	77	102	102	123	124
Absorbance normalized to 1 cm (cm^{-1})	74	75	98	47	90	96	135	89
H_2O-cpx (ppm)	31	32	41	20	38	41	57	38
H_2O-melt (wt%)	0.17	0.17	0.21	0.11	0.16	0.17	0.31	0.17

Sample No.								
Section No.								
Point No.	10.3	10.4	11	13	17.2	18	19	20
SiO_2	45.62	45.75	49.62	46.76	48.28	48.41	45.72	48.17
TiO_2	3.74	3.68	1.42	3.63	2.67	2.69	3.65	2.44
Al_2O3	7.18	6.79	5.96	5.60	5.34	4.43	7.45	5.62
Cr_2O3	0.07	0.00	1.07	0.05	0.09	0.04	0.00	0.26
FeO	6.95	7.25	4.92	7.18	6.82	6.90	7.02	6.16
MnO	0.06	0.10	0.05	0.10	0.06	0.05	0.06	0.05
MgO	11.49	11.93	13.49	12.05	13.05	13.41	11.99	12.80
CaO	23.28	23.42	21.95	23.72	23.75	23.38	23.59	23.32
Na_2O	0.65	0.57	0.99	0.44	0.53	0.42	0.51	0.46
K_2O	0.01	0.02	0.01	0.00	0.00	0.00	0.00	0.00
NiO	0.02	0.05	0.03	0.02	0.01	0.04	0.06	0.04
Total	99.09	99.56	99.50	99.54	100.60	99.76	100.03	99.31
Si	1.73	1.73	1.84	1.77	1.80	1.82	1.72	1.81
Ti	0.11	0.10	0.04	0.10	0.07	0.08	0.10	0.07
Al	0.32	0.30	0.26	0.25	0.23	0.20	0.33	0.25
Cr	0.00	0.00	0.03	0.00	0.00	0.00	0.00	0.01
Fe	0.22	0.23	0.15	0.23	0.21	0.22	0.22	0.19
Mn	0.00	0.00	0.00	0.00	0.00	0.00	0.00	0.00
Mg	0.65	0.67	0.74	0.68	0.72	0.75	0.67	0.72
Ca	0.95	0.95	0.87	0.96	0.95	0.94	0.95	0.94
Na	0.05	0.04	0.07	0.03	0.04	0.03	0.04	0.03
K	0.00	0.00	0.00	0.00	0.00	0.00	0.00	0.00
Ni	0.00	0.00	0.00	0.00	0.00	0.00	0.00	0.00
Total	4.03	4.04	4.01	4.02	4.03	4.03	4.03	4.01
Mg#	74.68	74.59	83.02	74.95	77.33	77.61	75.28	78.73
$D^{(cpx\text{-}melt)}_{H2O}$	0.0337	0.0336	0.0179	0.0262	0.0219	0.0195	0.0363	0.0207
Absorbance of cpx (cm^{-1})	1.4	1.0	2.1	1.3	1.4	1.5	1.2	0.7
Thickness of cpx (0.001mm)	124	124	124	115	120	106	115	111
Absorbance normalized to 1 cm (cm^{-1})	109	82	169	113	116	138	105	59
H_2O-cpx (ppm)	46	35	71	48	49	58	45	25
H_2O-melt (wt%)	0.14	0.10	0.40	0.18	0.22	0.30	0.12	0.12

Sample No.	MX-5							
Section No.	4							
Point No.	22	22.1	2	3	4	5	6	7
SiO_2	47.34	47.45	43.74	47.28	47.95	45.33	49.95	47.68
TiO_2	2.70	2.44	4.00	2.88	2.84	3.62	1.94	2.76
Al_2O3	6.12	6.06	8.04	5.03	4.78	6.61	4.06	5.32
Cr_2O3	0.02	0.30	0.01	0.22	0.00	0.00	0.12	0.06
FeO	6.94	6.47	7.60	6.91	6.61	7.46	5.85	6.82
MnO	0.05	0.04	0.01	0.08	0.06	0.06	0.07	0.07
MgO	12.70	12.65	11.24	12.81	13.29	12.04	13.75	12.98
CaO	23.55	23.32	22.94	23.43	23.77	23.11	23.84	23.41
Na_2O	0.52	0.58	0.49	0.41	0.36	0.42	0.48	0.48
K_2O	0.00	0.00	0.01	0.01	0.00	0.01	0.00	0.01
NiO	0.03	0.00	0.00	0.00	0.01	0.07	0.07	0.00
Total	99.96	99.30	98.07	99.05	99.67	98.73	100.13	99.58
Si	1.77	1.79	1.68	1.79	1.80	1.73	1.85	1.79
Ti	0.08	0.07	0.12	0.08	0.08	0.10	0.05	0.08
Al	0.27	0.27	0.36	0.22	0.21	0.30	0.18	0.24
Cr	0.00	0.01	0.00	0.01	0.00	0.00	0.00	0.00
Fe	0.22	0.20	0.24	0.22	0.21	0.24	0.18	0.21
Mn	0.00	0.00	0.00	0.00	0.00	0.00	0.00	0.00
Mg	0.71	0.71	0.64	0.72	0.74	0.68	0.76	0.73
Ca	0.95	0.94	0.95	0.95	0.96	0.94	0.95	0.94
Na	0.04	0.04	0.04	0.03	0.03	0.03	0.03	0.03
K	0.00	0.00	0.00	0.00	0.00	0.00	0.00	0.00
Ni	0.00	0.00	0.00	0.00	0.00	0.00	0.00	0.00
Total	4.03	4.03	4.04	4.03	4.03	4.03	4.02	4.03
Mg#	76.53	77.71	72.51	76.77	78.19	74.22	80.75	77.24
$D^{(cpx\text{-}melt)}_{H2O}$	0.0253	0.0237	0.0455	0.0227	0.0212	0.0338	0.0150	0.0226
Absorbance of cpx (cm^{-1})	1.0	0.6	0.7	0.4	0.4	0.7	0.9	0.2
Thickness of cpx (0.001mm)	108	108	92	84	82	81	62	62
Absorbance normalized to 1 cm (cm^{-1})	95	56	71	50	54	90	147	32
H_2O-cpx (ppm)	40	24	30	21	23	38	62	14
H_2O-melt (wt%)	0.16	0.10	0.07	0.09	0.11	0.11	0.41	0.06

Sample No.								
Section No.								
Point No.	8	9	11	12	13	14	15	16
SiO_2	47.07	45.02	48.69	48.76	48.06	49.18	49.29	48.45
TiO_2	2.72	3.68	2.38	2.34	2.41	1.97	1.92	2.49
Al_2O3	5.88	7.39	4.71	4.18	5.72	3.87	4.04	4.30
Cr_2O3	0.11	0.06	0.01	0.00	0.14	0.08	0.10	0.02
FeO	6.46	7.44	6.55	6.21	6.46	5.73	6.03	6.15
MnO	0.09	0.05	0.06	0.08	0.02	0.08	0.04	0.04
MgO	13.04	11.88	12.98	13.23	12.87	14.08	13.96	13.55
CaO	23.62	23.27	23.60	23.79	23.76	23.82	23.57	23.77
Na_2O	0.40	0.51	0.43	0.43	0.52	0.40	0.49	0.38
K_2O	0.00	0.00	0.00	0.00	0.00	0.00	0.01	0.01
NiO	0.02	0.02	0.03	0.06	0.04	0.02	0.00	0.00
Total	99.42	99.32	99.43	99.08	99.99	99.21	99.44	99.16
Si	1.77	1.71	1.83	1.84	1.80	1.84	1.84	1.82
Ti	0.08	0.11	0.07	0.07	0.07	0.06	0.05	0.07
Al	0.26	0.33	0.21	0.19	0.25	0.17	0.18	0.19
Cr	0.00	0.00	0.00	0.00	0.00	0.00	0.00	0.00
Fe	0.20	0.24	0.21	0.20	0.20	0.18	0.19	0.19
Mn	0.00	0.00	0.00	0.00	0.00	0.00	0.00	0.00
Mg	0.73	0.67	0.73	0.74	0.72	0.79	0.78	0.76
Ca	0.95	0.95	0.95	0.96	0.95	0.96	0.95	0.96
Na	0.03	0.04	0.03	0.03	0.04	0.03	0.04	0.03
K	0.00	0.00	0.00	0.00	0.00	0.00	0.00	0.00
Ni	0.00	0.00	0.00	0.00	0.00	0.00	0.00	0.00
Total	4.03	4.04	4.02	4.02	4.03	4.03	4.03	4.03
Mg#	78.26	74.01	77.96	79.16	78.04	81.42	80.50	79.70
$D^{(cpx\text{-}melt)}_{H2O}$	0.0255	0.0388	0.0179	0.0167	0.0219	0.0159	0.0160	0.0182
Absorbance of cpx (cm^{-1})	0.8	0.9	0.9	0.7	1.0	0.4	0.9	0.7
Thickness of cpx (0.001mm)	92	95	110	110	104	90	101	95
Absorbance normalized to 1 cm (cm^{-1})	88	96	85	63	93	44	86	72
H_2O-cpx (ppm)	37	41	36	27	39	19	36	30
H_2O-melt (wt%)	0.15	0.10	0.20	0.16	0.18	0.12	0.23	0.17

Sample No.							MX-7
Section No.							2
Point No.	18	20	21	21.2	22	23	1
SiO_2	49.59	46.82	49.13	48.77	49.27	42.94	47.33
TiO_2	1.74	2.96	2.18	2.28	1.89	5.01	3.17
Al_2O3	5.88	5.35	4.58	4.68	4.27	8.63	5.04
Cr_2O3	0.02	0.00	0.15	0.11	0.20	0.00	0.01
FeO	6.13	6.95	5.63	6.31	5.83	7.87	7.29
MnO	0.06	0.07	0.06	0.04	0.07	0.13	0.09
MgO	13.27	12.74	13.70	13.59	13.97	10.95	12.52
CaO	22.22	23.79	23.78	23.56	23.37	23.02	23.73
Na_2O	0.71	0.41	0.47	0.37	0.53	0.47	0.64
K_2O	0.19	0.03	0.01	0.01	0.00	0.01	0.00
NiO	0.04	0.05	0.03	0.03	0.03	0.02	0.01
Total	99.85	99.17	99.71	99.76	99.42	99.06	99.81
Si	1.84	1.77	1.83	1.82	1.84	1.64	1.78
Ti	0.05	0.08	0.06	0.06	0.05	0.14	0.09
Al	0.26	0.24	0.20	0.21	0.19	0.39	0.22
Cr	0.00	0.00	0.00	0.00	0.01	0.00	0.00
Fe	0.19	0.22	0.18	0.20	0.18	0.25	0.23
Mn	0.00	0.00	0.00	0.00	0.00	0.00	0.00
Mg	0.73	0.72	0.76	0.76	0.78	0.62	0.70
Ca	0.88	0.97	0.95	0.94	0.94	0.94	0.96
Na	0.05	0.03	0.03	0.03	0.04	0.04	0.05
K	0.01	0.00	0.00	0.00	0.00	0.00	0.00
Ni	0.00	0.00	0.00	0.00	0.00	0.00	0.00
Total	4.01	4.04	4.02	4.02	4.03	4.04	4.04
Mg#	79.42	76.57	81.27	79.34	81.04	71.26	75.37
$D^{(cpx\text{-}melt)}_{H2O}$	0.0177	0.0248	0.0174	0.0186	0.0164	0.0595	0.0235
Absorbance of cpx (cm^{-1})	1.1	0.2	0.7	1.2	0.7	0.5	1.2
Thickness of cpx (0.001mm)	112	99	113	113	89	94	40
Absorbance normalized to 1 cm (cm^{-1})	96	15	62	104	83	54	288
H_2O-cpx (ppm)	41	6	26	44	35	23	122
H_2O-melt (wt%)	0.23	0.03	0.15	0.24	0.21	0.04	0.52

Sample No.								
Section No.								
Point No.	2	4 5	6	7	8	8.2	9	
SiO_2	45.67	50.49	54.38	53.54	47.43	49.58	45.54	46.44
TiO_2	4.03	1.67	0.27	0.32	3.04	1.97	3.36	3.23
Al_2O3	7.47	4.33	0.09	0.12	6.12	4.15	7.59	6.88
Cr_2O3	0.05	0.48	0.03	0.96	0.01	0.27	0.12	0.26
FeO	7.47	5.67	7.67	8.90	7.08	6.13	7.18	6.70
MnO	0.02	0.05	0.14	0.14	0.09	0.09	0.06	0.05
MgO	11.92	13.90	13.72	12.80	12.54	13.72	11.97	12.50
CaO	23.26	22.65	23.57	22.74	23.04	23.73	23.25	23.70
Na_2O	0.61	0.67	0.57	0.51	0.37	0.32	0.51	0.35
K_2O	0.00	0.02	0.01	0.01	0.00	0.00	0.00	0.01
NiO	0.00	0.00	0.00	0.02	0.01	0.03	0.00	0.05
Total	100.51	99.92	100.44	100.04	99.74	99.99	99.57	100.16
Si	1.71	1.87	2.01	2.00	1.78	1.85	1.72	1.74
Ti	0.11	0.05	0.01	0.01	0.09	0.06	0.10	0.09
Al	0.33	0.19	0.00	0.01	0.27	0.18	0.34	0.30
Cr	0.00	0.01	0.00	0.03	0.00	0.01	0.00	0.01
Fe	0.23	0.18	0.24	0.28	0.22	0.19	0.23	0.21
Mn	0.00	0.00	0.00	0.00	0.00	0.00	0.00	0.00
Mg	0.67	0.77	0.76	0.71	0.70	0.76	0.67	0.70
Ca	0.93	0.90	0.93	0.91	0.93	0.95	0.94	0.95
Na	0.04	0.05	0.04	0.04	0.03	0.02	0.04	0.03
K	0.00	0.00	0.00	0.00	0.00	0.00	0.00	0.00
Ni	0.00	0.00	0.00	0.00	0.00	0.00	0.00	0.00
Total	4.03	4.01	4.00	3.99	4.01	4.02	4.03	4.03
Mg#	73.97	81.39	76.14	71.94	75.95	79.96	74.83	76.89
$D^{(cpx\text{-}melt)}_{H2O}$	0.0388	0.0144	0.0054	0.0059	0.0251	0.0159	0.0364	0.0316
Absorbance of cpx (cm^{-1})	1.7	0.1	0.5	0.1	1.3	1.9	1.4	0.8
Thickness of cpx (0.001mm)	41	46	54	54	57	52	52	57
Absorbance normalized to 1 cm (cm^{-1})	412	22	83	19	230	369	262	144
H_2O-cpx (ppm)	174	9	35	8	97	156	111	61
H_2O-melt (wt%)	0.45	0.06	0.65	0.13	0.39	0.98	0.30	0.19

Sample No.					MX-4		
Section No.					3		
Point No.	10	11	12	13	1	2	3
SiO_2	50.40	45.88	49.75	48.35	49.69	47.71	44.38
TiO_2	1.71	3.27	0.77	2.95	2.00	2.63	4.36
Al_2O3	3.81	7.61	5.56	4.64	4.63	5.27	7.92
Cr_2O3	0.07	0.39	0.03	0.03	0.28	0.14	0.06
FeO	6.41	7.15	10.23	7.51	5.74	6.75	7.75
MnO	0.07	0.07	0.09	0.11	0.06	0.05	0.02
MgO	13.96	11.79	11.14	12.79	13.70	12.91	11.51
CaO	23.14	23.39	21.67	23.15	23.12	23.77	23.11
Na_2O	0.47	0.43	0.80	0.49	0.53	0.33	0.48
K_2O	0.00	0.00	0.00	0.01	0.01	0.00	0.00
NiO	0.03	0.00	0.04	0.03	0.04	0.01	0.00
Total	100.07	99.95	100.07	100.05	99.78	99.55	99.58
Si	1.87	1.72	1.87	1.81	1.85	1.79	1.68
Ti	0.05	0.09	0.02	0.08	0.06	0.07	0.12
Al	0.17	0.34	0.25	0.20	0.20	0.23	0.35
Cr	0.00	0.01	0.00	0.00	0.01	0.00	0.00
Fe	0.20	0.22	0.32	0.24	0.18	0.21	0.25
Mn	0.00	0.00	0.00	0.00	0.00	0.00	0.00
Mg	0.77	0.66	0.62	0.71	0.76	0.72	0.65
Ca	0.92	0.94	0.87	0.93	0.92	0.96	0.94
Na	0.03	0.03	0.06	0.04	0.04	0.02	0.04
K	0.00	0.00	0.00	0.00	0.00	0.00	0.00
Ni	0.00	0.00	0.00	0.00	0.00	0.00	0.00
Total	4.01	4.02	4.02	4.02	4.01	4.02	4.03
Mg#	79.51	74.63	66.02	75.23	80.96	77.32	72.60
$D^{(cpx\text{-}melt)}_{H2O}$	0.0139	0.0351	0.0148	0.0201	0.0162	0.0220	0.0462
Absorbance of cpx (cm^{-1})	0.6	0.6	0.4	1.1	0.8	1.3	1.5
Thickness of cpx (0.001mm)	40	57	50	59	56	62	64
Absorbance normalized to 1 cm (cm^{-1})	145	100	80	186	143	210	234
H_2O-cpx (ppm)	61	42	34	79	60	89	99
H_2O-melt (wt%)	0.44	0.12	0.23	0.39	0.37	0.40	0.21

Sample No.								
Section No.								4
Point No.	4	5	6	7	8	9	10	1
SiO_2	45.88	48.23	50.26	48.68	48.49	45.32	47.63	48.62
TiO_2	3.27	2.27	1.91	2.46	2.43	3.62	3.17	2.16
Al_2O3	6.41	5.50	3.79	5.62	5.08	7.28	5.05	5.73
Cr_2O3	0.10	0.17	0.21	0.14	0.01	0.06	0.00	0.17
FeO	7.10	6.17	5.89	6.48	6.57	7.44	7.16	6.20
MnO	0.05	0.09	0.08	0.10	0.07	0.06	0.09	0.10
MgO	12.08	13.28	13.85	12.97	13.23	11.69	12.73	12.97
CaO	23.38	23.60	23.70	23.59	23.76	23.26	23.40	23.21
Na_2O	0.50	0.49	0.38	0.44	0.36	0.46	0.41	0.52
K_2O	0.00	0.02	0.00	0.00	0.00	0.02	0.00	0.00
NiO	0.04	0.08	0.02	0.01	0.04	0.04	0.02	0.00
Total	98.80	99.90	100.10	100.48	100.02	99.24	99.65	99.69
Si	1.75	1.80	1.86	1.81	1.81	1.72	1.79	1.81
Ti	0.09	0.06	0.05	0.07	0.07	0.10	0.09	0.06
Al	0.29	0.24	0.17	0.25	0.22	0.33	0.22	0.25
Cr	0.00	0.01	0.01	0.00	0.00	0.00	0.00	0.01
Fe	0.23	0.19	0.18	0.20	0.21	0.24	0.23	0.19
Mn	0.00	0.00	0.00	0.00	0.00	0.00	0.00	0.00
Mg	0.69	0.74	0.77	0.72	0.74	0.66	0.71	0.72
Ca	0.95	0.94	0.94	0.94	0.95	0.95	0.94	0.93
Na	0.04	0.04	0.03	0.03	0.03	0.03	0.03	0.04
K	0.00	0.00	0.00	0.00	0.00	0.00	0.00	0.00
Ni	0.00	0.00	0.00	0.00	0.00	0.00	0.00	0.00
Total	4.03	4.03	4.01	4.02	4.02	4.03	4.02	4.02
Mg#	75.22	79.34	80.73	78.11	78.21	73.69	76.00	78.84
$D^{(cpx\text{-}melt)}_{H2O}$	0.0301	0.0212	0.0142	0.0207	0.0199	0.0360	0.0225	0.0198
Absorbance of cpx (cm^{-1})	0.6	0.9	0.5	1.2	1.0	0.6	0.9	0.9
Thickness of cpx (0.001mm)	58	64	60	63	71	68	72	57
Absorbance normalized to 1 cm (cm^{-1})	110	134	77	190	134	88	119	154
H_2O-cpx (ppm)	47	57	32	81	57	37	51	65
H_2O-melt (wt%)	0.15	0.27	0.23	0.39	0.28	0.10	0.22	0.33

Sample No. Section No. Point No.	2	3	5	6	7	8	9	10
SiO_2	49.90	46.71	46.17	48.18	45.82	44.27	48.77	47.69
TiO_2	2.12	2.66	3.19	2.35	2.93	3.68	2.50	2.65
Al_2O3	3.66	6.17	6.20	4.34	6.80	6.15	4.77	5.98
Cr_2O3	0.00	0.31	0.00	0.03	0.07	0.00	0.12	0.19
FeO	6.31	6.43	7.51	6.36	6.99	8.13	6.36	6.34
MnO	0.06	0.05	0.08	0.05	0.07	0.08	0.06	0.03
MgO	13.91	12.79	12.11	13.50	12.51	11.17	13.49	12.85
CaO	23.65	23.16	23.62	23.63	23.03	23.31	23.44	23.10
Na_2O	0.43	0.45	0.36	0.37	0.53	0.55	0.37	0.59
K_2O	0.01	0.00	0.00	0.00	0.00	0.01	0.00	0.02
NiO	0.06	0.05	0.00	0.04	0.00	0.02	0.07	0.10
Total	100.10	98.78	99.25	98.84	98.74	97.37	99.95	99.54
Si	1.86	1.77	1.75	1.82	1.74	1.72	1.82	1.79
Ti	0.06	0.08	0.09	0.07	0.08	0.11	0.07	0.07
Al	0.16	0.28	0.28	0.19	0.30	0.28	0.21	0.26
Cr	0.00	0.01	0.00	0.00	0.00	0.00	0.00	0.01
Fe	0.20	0.20	0.24	0.20	0.22	0.26	0.20	0.20
Mn	0.00	0.00	0.00	0.00	0.00	0.00	0.00	0.00
Mg	0.77	0.72	0.69	0.76	0.71	0.65	0.75	0.72
Ca	0.94	0.94	0.96	0.96	0.94	0.97	0.94	0.93
Na	0.03	0.03	0.03	0.03	0.04	0.04	0.03	0.04
K	0.00	0.00	0.00	0.00	0.00	0.00	0.00	0.00
Ni	0.00	0.00	0.00	0.00	0.00	0.00	0.00	0.00
Total	4.02	4.03	4.03	4.03	4.04	4.05	4.02	4.02
Mg#	79.73	78.01	74.19	79.10	76.15	71.02	79.08	78.32
$D^{(cpx\text{-}melt)}_{H2O}$	0.0149	0.0264	0.0289	0.0185	0.0316	0.0339	0.0191	0.0236
Absorbance of cpx (cm^{-1})	1.1	1.0	0.6	1.0	0.9	0.7	0.5	0.9
Thickness of cpx (0.001mm)	59	59	58	54	53	51	56	51
Absorbance normalized to 1 cm (cm^{-1})	186	169	95	185	166	131	89	171
H_2O-cpx (ppm)	79	72	40	78	70	56	38	72
H_2O-melt (wt%)	0.53	0.27	0.14	0.42	0.22	0.16	0.20	0.31

Sample No.								
Section No.								
Point No.	11	12	13	14	15	16	17	18
SiO_2	48.54	46.14	49.60	46.04	45.81	49.12	46.71	49.54
TiO_2	2.26	3.13	2.15	2.94	3.32	2.41	2.71	2.05
Al_2O3	4.94	6.66	4.18	6.41	6.73	4.08	6.32	4.27
Cr_2O3	0.25	0.01	0.15	0.15	0.07	0.04	0.34	0.10
FeO	5.97	7.41	5.96	7.06	7.06	6.38	6.39	6.19
MnO	0.11	0.06	0.07	0.04	0.05	0.09	0.06	0.06
MgO	13.47	11.82	13.78	12.45	12.24	13.72	12.71	13.65
CaO	23.40	23.36	23.37	23.11	23.25	23.80	23.43	23.77
Na_2O	0.46	0.53	0.43	0.47	0.45	0.34	0.55	0.44
K_2O	0.00	0.01	0.02	0.00	0.01	0.01	0.00	0.00
NiO	0.00	0.00	0.07	0.03	0.03	0.00	0.03	0.00
Total	99.39	99.13	99.76	98.70	99.01	99.98	99.23	100.08
Si	1.82	1.75	1.85	1.75	1.74	1.83	1.76	1.84
Ti	0.06	0.09	0.06	0.08	0.09	0.07	0.08	0.06
Al	0.22	0.30	0.18	0.29	0.30	0.18	0.28	0.19
Cr	0.01	0.00	0.00	0.00	0.00	0.00	0.01	0.00
Fe	0.19	0.24	0.19	0.22	0.22	0.20	0.20	0.19
Mn	0.00	0.00	0.00	0.00	0.00	0.00	0.00	0.00
Mg	0.75	0.67	0.77	0.71	0.69	0.76	0.71	0.76
Ca	0.94	0.95	0.93	0.94	0.94	0.95	0.95	0.95
Na	0.03	0.04	0.03	0.03	0.03	0.02	0.04	0.03
K	0.00	0.00	0.00	0.00	0.00	0.00	0.00	0.00
Ni	0.00	0.00	0.00	0.00	0.00	0.00	0.00	0.00
Total	4.02	4.03	4.01	4.04	4.03	4.02	4.04	4.02
Mg#	80.09	73.98	80.48	75.87	75.57	79.31	78.01	79.72
$D^{(cpx\text{-}melt)}_{H2O}$	0.0191	0.0294	0.0159	0.0295	0.0320	0.0172	0.0273	0.0162
Absorbance of cpx (cm^{-1})	0.4	1.0	0.6	1.4	1.6	0.7	0.5	0.2
Thickness of cpx (0.001mm)	50	58	47	47	53	50	50	57
Absorbance normalized to 1 cm (cm^{-1})	70	166	117	298	302	140	98	35
H_2O-cpx (ppm)	30	70	50	126	128	59	41	15
H_2O-melt (wt%)	0.15	0.24	0.31	0.43	0.40	0.34	0.15	0.09

Sample No.							
Section No.							
Point No.	18.2	19	20	21	22	23	25
SiO_2	47.56	46.09	47.91	47.63	47.67	47.46	47.17
TiO_2	3.04	3.40	3.13	2.91	2.37	2.78	3.09
Al_2O3	5.20	7.09	4.96	4.91	5.36	5.98	6.47
Cr_2O3	0.02	0.05	0.04	0.06	0.15	0.20	0.24
FeO	6.94	7.04	7.14	7.07	6.05	6.39	6.59
MnO	0.03	0.03	0.07	0.08	0.05	0.08	0.04
MgO	12.86	12.04	12.79	12.74	13.00	12.80	12.66
CaO	23.29	23.14	23.48	23.56	23.61	23.42	23.42
Na_2O	0.40	0.49	0.38	0.45	0.47	0.46	0.47
K_2O	0.01	0.00	0.01	0.01	0.00	0.00	0.00
NiO	0.00	0.04	0.01	0.05	0.00	0.00	0.01
Total	99.35	99.40	99.91	99.47	98.74	99.55	100.15
Si	1.79	1.74	1.80	1.80	1.80	1.78	1.76
Ti	0.09	0.10	0.09	0.08	0.07	0.08	0.09
Al	0.23	0.32	0.22	0.22	0.24	0.26	0.28
Cr	0.00	0.00	0.00	0.00	0.00	0.01	0.01
Fe	0.22	0.22	0.22	0.22	0.19	0.20	0.21
Mn	0.00	0.00	0.00	0.00	0.00	0.00	0.00
Mg	0.72	0.68	0.72	0.72	0.73	0.72	0.70
Ca	0.94	0.94	0.94	0.95	0.96	0.94	0.94
Na	0.03	0.04	0.03	0.03	0.03	0.03	0.03
K	0.00	0.00	0.00	0.00	0.00	0.00	0.00
Ni	0.00	0.00	0.00	0.00	0.00	0.00	0.00
Total	4.02	4.02	4.02	4.03	4.03	4.02	4.02
Mg#	76.76	75.31	76.17	76.26	79.31	78.13	77.41
$D^{(cpx\text{-}melt)}_{H2O}$	0.0227	0.0321	0.0218	0.0217	0.0210	0.0243	0.0277
Absorbance of cpx (cm^{-1})	0.4	0.4	0.6	0.5	0.6	0.9	0.3
Thickness of cpx (0.001mm)	57	50	49	49	49	66	49
Absorbance normalized to 1 cm (cm^{-1})	77	75	110	108	114	180	57
H_2O-cpx (ppm)	33	32	47	46	48	76	24
H_2O-melt (wt%)	0.14	0.10	0.21	0.21	0.23	0.31	0.09

Sample No.	MX-8							
Section No.	3					4		
Point No.	1	2	3	4	5	1	2	3
SiO_2	48.21	49.09	50.45	48.14	49.85	49.31	48.86	48.98
TiO_2	2.72	1.77	1.61	2.84	1.95	2.23	2.04	0.95
Al_2O3	4.74	5.82	3.49	5.81	3.84	3.98	4.38	6.52
Cr_2O3	0.05	0.88	0.12	0.02	0.00	0.05	0.01	0.02
FeO	7.21	6.26	6.30	6.71	6.68	6.58	6.83	8.01
MnO	0.06	0.08	0.09	0.06	0.05	0.10	0.09	0.18
MgO	13.01	13.15	13.93	12.60	13.43	13.45	13.58	11.64
CaO	23.44	22.18	23.31	23.53	23.45	23.53	23.52	22.44
Na_2O	0.36	0.79	0.42	0.56	0.44	0.38	0.43	0.73
K_2O	0.00	0.01	0.00	0.00	0.01	0.00	0.00	0.00
NiO	0.07	0.04	0.01	0.01	0.06	0.04	0.00	0.00
Total	99.86	100.06	99.73	100.28	99.75	99.65	99.75	99.47
Si	1.81	1.82	1.88	1.79	1.86	1.85	1.83	1.84
Ti	0.08	0.05	0.05	0.08	0.05	0.06	0.06	0.03
Al	0.21	0.25	0.15	0.26	0.17	0.18	0.19	0.29
Cr	0.00	0.03	0.00	0.00	0.00	0.00	0.00	0.00
Fe	0.23	0.19	0.20	0.21	0.21	0.21	0.21	0.25
Mn	0.00	0.00	0.00	0.00	0.00	0.00	0.00	0.01
Mg	0.73	0.73	0.77	0.70	0.75	0.75	0.76	0.65
Ca	0.94	0.88	0.93	0.94	0.94	0.94	0.94	0.90
Na	0.03	0.06	0.03	0.04	0.03	0.03	0.03	0.05
K	0.00	0.00	0.00	0.00	0.00	0.00	0.00	0.00
Ni	0.00	0.00	0.00	0.00	0.00	0.00	0.00	0.00
Total	4.02	4.02	4.01	4.02	4.02	4.02	4.03	4.02
Mg#	76.28	78.92	79.77	77.00	78.19	78.45	78.01	72.15
$D^{(cpx\text{-}melt)}_{H2O}$	0.0203	0.0197	0.0130	0.0224	0.0144	0.0159	0.0176	0.0174
Absorbance of cpx (cm^{-1})	1.4	1.1	0.6	1.4	0.6	1.3	1.0	0.6
Thickness of cpx (0.001mm)	84	96	82	93	89	64	64	73
Absorbance normalized to 1 cm (cm^{-1})	167	109	76	151	67	203	156	85
H_2O-cpx (ppm)	71	46	32	64	29	86	66	36
H_2O-melt (wt%)	0.35	0.23	0.25	0.28	0.20	0.54	0.38	0.21

Sample No.								
Section No.								
Point No.	4	5	7	8	9	10	11	12
SiO_2	50.25	47.19	45.81	44.99	47.49	52.99	50.24	47.04
TiO_2	1.63	3.14	3.47	3.77	2.50	0.18	1.87	2.56
Al_2O3	3.44	5.70	6.96	7.27	5.66	1.86	3.30	6.17
Cr_2O3	0.12	0.01	0.22	0.00	0.12	0.05	0.06	0.00
FeO	6.27	6.99	7.37	7.69	6.96	8.67	6.12	6.93
MnO	0.04	0.12	0.06	0.05	0.08	0.46	0.04	0.09
MgO	13.85	12.05	11.40	11.46	12.63	12.73	13.96	12.34
CaO	23.48	23.48	23.24	23.17	23.44	22.74	23.73	23.35
Na_2O	0.31	0.50	0.58	0.54	0.46	0.49	0.37	0.52
K_2O	0.00	0.00	0.00	0.00	0.00	0.01	0.01	0.01
NiO	0.02	0.02	0.03	0.00	0.06	0.26	0.00	0.06
Total	99.39	99.19	99.15	98.93	99.39	100.44	99.70	99.06
Si	1.88	1.78	1.74	1.72	1.79	1.97	1.87	1.78
Ti	0.05	0.09	0.10	0.11	0.07	0.00	0.05	0.07
Al	0.15	0.25	0.31	0.33	0.25	0.08	0.14	0.27
Cr	0.00	0.00	0.01	0.00	0.00	0.00	0.00	0.00
Fe	0.20	0.22	0.23	0.25	0.22	0.27	0.19	0.22
Mn	0.00	0.00	0.00	0.00	0.00	0.01	0.00	0.00
Mg	0.77	0.68	0.65	0.65	0.71	0.71	0.78	0.70
Ca	0.94	0.95	0.95	0.95	0.95	0.91	0.95	0.95
Na	0.02	0.04	0.04	0.04	0.03	0.04	0.03	0.04
K	0.00	0.00	0.00	0.00	0.00	0.00	0.00	0.00
Ni	0.00	0.00	0.00	0.00	0.00	0.01	0.00	0.00
Total	4.01	4.02	4.02	4.03	4.03	4.00	4.02	4.03
Mg#	79.77	75.45	73.40	72.65	76.39	72.36	80.28	76.04
$D^{(cpx\text{-}melt)}_{H2O}$	0.0130	0.0236	0.0319	0.0371	0.0228	0.0073	0.0133	0.0245
Absorbance of cpx (cm^{-1})	1.1	1.1	1.3	0.8	0.7	1.3	1.2	1.2
Thickness of cpx (0.001mm)	64	63	69	63	68	63	66	66
Absorbance normalized to 1 cm (cm^{-1})	178	175	181	119	104	203	177	174
H_2O-cpx (ppm)	75	74	77	50	44	86	75	74
H_2O-melt (wt%)	0.58	0.31	0.24	0.14	0.19	1.18	0.56	0.30

Sample No. Section No. Point No.	13	14	15	16	17	18	19	20
SiO_2	49.17	48.03	49.46	49.26	50.14	49.06	49.00	48.97
TiO_2	2.05	2.78	2.10	1.99	1.85	2.42	1.79	2.61
Al_2O3	3.82	4.59	3.85	4.19	3.66	4.51	5.19	4.55
Cr_2O3	0.08	0.00	0.03	0.01	0.19	0.00	0.73	0.12
FeO	6.59	6.96	6.70	6.65	5.83	7.25	5.74	6.87
MnO	0.08	0.09	0.06	0.06	0.11	0.04	0.06	0.06
MgO	13.52	12.66	12.89	13.36	14.13	13.12	13.51	13.47
CaO	23.23	23.41	23.36	23.42	23.23	23.17	22.96	23.25
Na_2O	0.42	0.44	0.40	0.47	0.38	0.32	0.51	0.48
K_2O	0.00	0.01	0.00	0.00	0.00	0.00	0.01	0.00
NiO	0.00	0.03	0.00	0.00	0.06	0.00	0.04	0.05
Total	98.95	98.99	98.84	99.41	99.56	99.89	99.52	100.42
Si	1.85	1.82	1.86	1.85	1.87	1.83	1.83	1.82
Ti	0.06	0.08	0.06	0.06	0.05	0.07	0.05	0.07
Al	0.17	0.20	0.17	0.18	0.16	0.20	0.23	0.20
Cr	0.00	0.00	0.00	0.00	0.01	0.00	0.02	0.00
Fe	0.21	0.22	0.21	0.21	0.18	0.23	0.18	0.21
Mn	0.00	0.00	0.00	0.00	0.00	0.00	0.00	0.00
Mg	0.76	0.71	0.72	0.75	0.78	0.73	0.75	0.75
Ca	0.94	0.95	0.94	0.94	0.93	0.93	0.92	0.93
Na	0.03	0.03	0.03	0.03	0.03	0.02	0.04	0.03
K	0.00	0.00	0.00	0.00	0.00	0.00	0.00	0.00
Ni	0.00	0.00	0.00	0.00	0.00	0.00	0.00	0.00
Total	4.02	4.02	4.00	4.02	4.01	4.01	4.02	4.02
Mg#	78.54	76.44	77.43	78.18	81.19	76.33	80.75	77.76
$D^{(cpx\text{-}melt)}_{H2O}$	0.0154	0.0191	0.0141	0.0158	0.0140	0.0175	0.0183	0.0190
Absorbance of cpx (cm^{-1})	1.0	0.7	0.7	1.0	0.8	1.0	0.8	1.3
Thickness of cpx (0.001mm)	69	73	71	67	63	61	62	62
Absorbance normalized to 1 cm (cm^{-1})	145	99	99	149	133	164	129	210
H_2O-cpx (ppm)	61	42	42	63	56	69	55	89
H_2O-melt (wt%)	0.40	0.22	0.30	0.40	0.40	0.40	0.30	0.47

Sample No.					MX-9			
Section No.					1			4
Point No.	21	22	23	24	2	3	4	1
SiO_2	47.97	49.43	49.49	48.53	49.01	45.19	49.74	46.95
TiO_2	2.42	2.18	1.97	2.32	1.94	3.64	1.65	2.84
Al_2O3	5.70	4.14	4.58	4.56	4.74	7.35	3.94	5.08
Cr_2O3	0.10	0.00	0.00	0.06	0.23	0.04	0.02	0.02
FeO	6.93	6.88	6.64	7.22	6.49	7.55	6.34	7.61
MnO	0.04	0.07	0.13	0.08	0.08	0.07	0.07	0.06
MgO	12.73	12.82	12.98	13.01	13.10	11.35	13.68	12.62
CaO	23.20	23.28	22.95	23.17	22.85	22.90	22.65	23.50
Na_2O	0.55	0.35	0.71	0.46	0.53	0.73	0.61	0.40
K_2O	0.02	0.00	0.01	0.00	0.01	0.00	0.00	0.00
NiO	0.05	0.02	0.01	0.00	0.00	0.01	0.03	0.02
Total	99.70	99.17	99.46	99.40	98.99	98.83	98.73	99.10
Si	1.80	1.86	1.85	1.83	1.84	1.72	1.87	1.78
Ti	0.07	0.06	0.06	0.07	0.05	0.10	0.05	0.08
Al	0.25	0.18	0.20	0.20	0.21	0.33	0.17	0.23
Cr	0.00	0.00	0.00	0.00	0.01	0.00	0.00	0.00
Fe	0.22	0.22	0.21	0.23	0.20	0.24	0.20	0.24
Mn	0.00	0.00	0.00	0.00	0.00	0.00	0.00	0.00
Mg	0.71	0.72	0.72	0.73	0.73	0.64	0.77	0.71
Ca	0.93	0.94	0.92	0.93	0.92	0.94	0.91	0.96
Na	0.04	0.03	0.05	0.03	0.04	0.05	0.04	0.03
K	0.00	0.00	0.00	0.00	0.00	0.00	0.00	0.00
Ni	0.00	0.00	0.00	0.00	0.00	0.00	0.00	0.00
Total	4.03	4.00	4.02	4.02	4.01	4.03	4.02	4.04
Mg#	76.62	76.86	77.71	76.27	78.26	72.82	79.36	74.72
$D^{(cpx\text{-}melt)}_{H2O}$	0.0219	0.0149	0.0156	0.0182	0.0167	0.0358	0.0140	0.0236
Absorbance of cpx (cm^{-1})	1.7	1.2	1.0	1.0	1.8	1.7	0.2	0.4
Thickness of cpx (0.001mm)	60	57	67	70	107	141	113	57
Absorbance normalized to 1 cm (cm^{-1})	283	211	149	143	168	121	14	67
H_2O-cpx (ppm)	120	89	63	60	71	51	6	28
H_2O-melt (wt%)	0.55	0.60	0.40	0.33	0.43	0.14	0.04	0.12

Sample No. Section No. Point No.	2	3	4	5	6	7	8	9
SiO_2	50.18	47.82	46.90	48.07	49.83	48.62	48.58	46.45
TiO_2	1.76	2.61	2.72	2.52	1.95	2.57	2.33	2.90
Al_2O3	4.56	4.45	4.81	4.46	4.02	4.14	4.13	6.40
Cr_2O3	0.49	0.00	0.05	0.01	0.26	0.02	0.02	0.20
FeO	5.46	7.46	7.42	7.08	6.48	6.92	7.07	7.99
MnO	0.07	0.10	0.08	0.08	0.09	0.06	0.05	0.07
MgO	14.14	12.94	12.80	13.03	13.59	12.93	13.55	11.86
CaO	22.96	23.36	23.56	23.20	23.37	23.43	23.08	22.82
Na_2O	0.38	0.38	0.40	0.41	0.41	0.55	0.32	0.64
K_2O	0.00	0.01	0.00	0.00	0.01	0.08	0.00	0.00
NiO	0.03	0.04	0.04	0.00	0.04	0.05	0.01	0.01
Total	100.03	99.17	98.79	98.86	100.04	99.36	99.15	99.35
Si	1.85	1.81	1.79	1.82	1.85	1.83	1.83	1.76
Ti	0.05	0.07	0.08	0.07	0.05	0.07	0.07	0.08
Al	0.20	0.20	0.22	0.20	0.18	0.18	0.18	0.29
Cr	0.01	0.00	0.00	0.00	0.01	0.00	0.00	0.01
Fe	0.17	0.24	0.24	0.22	0.20	0.22	0.22	0.25
Mn	0.00	0.00	0.00	0.00	0.00	0.00	0.00	0.00
Mg	0.78	0.73	0.73	0.74	0.75	0.73	0.76	0.67
Ca	0.91	0.95	0.96	0.94	0.93	0.95	0.93	0.93
Na	0.03	0.03	0.03	0.03	0.03	0.04	0.02	0.05
K	0.00	0.00	0.00	0.00	0.00	0.00	0.00	0.00
Ni	0.00	0.00	0.00	0.00	0.00	0.00	0.00	0.00
Total	4.00	4.03	4.04	4.02	4.01	4.03	4.02	4.03
Mg#	82.19	75.57	75.45	76.64	78.89	76.92	77.35	72.56
$D^{(cpx\text{-}melt)}_{H2O}$	0.0155	0.0199	0.0229	0.0189	0.0152	0.0174	0.0177	0.0282
Absorbance of cpx (cm^{-1})	0.4	0.0	1.3	1.1	0.8	1.0	0.1	1.0
Thickness of cpx (0.001mm)	55	42	64	47	47	51	48	52
Absorbance normalized to 1 cm (cm^{-1})	80	2	198	240	170	196	21	190
H_2O-cpx (ppm)	34	1	84	102	72	83	9	81
H_2O-melt (wt%)	0.22	0.01	0.37	0.54	0.47	0.48	0.05	0.29

Sample No.								
Section No.								5
Point No.	10	11	12	13	14	15	16	1
SiO_2	49.62	51.10	49.64	48.62	44.52	49.58	48.02	49.20
TiO_2	1.88	1.47	1.73	2.19	3.71	1.33	2.35	2.12
Al_2O3	3.87	3.15	4.27	5.31	7.59	5.59	4.30	3.93
Cr_2O3	0.07	0.00	0.72	0.37	0.08	0.87	0.03	0.02
FeO	6.82	7.74	5.45	6.50	7.64	6.15	7.25	6.88
MnO	0.09	0.12	0.05	0.02	0.08	0.07	0.09	0.06
MgO	13.55	14.32	13.81	12.94	11.34	13.43	13.11	13.25
CaO	22.91	21.12	22.60	22.90	23.23	20.88	23.39	23.36
Na_2O	0.44	0.51	0.48	0.54	0.51	0.99	0.43	0.36
K_2O	0.00	0.00	0.00	0.00	0.01	0.01	0.02	0.02
NiO	0.00	0.05	0.00	0.00	0.00	0.00	0.02	0.01
Total	99.23	99.58	98.76	99.38	98.71	98.90	99.00	99.21
Si	1.86	1.90	1.86	1.82	1.70	1.85	1.82	1.85
Ti	0.05	0.04	0.05	0.06	0.11	0.04	0.07	0.06
Al	0.17	0.14	0.19	0.23	0.34	0.25	0.19	0.17
Cr	0.00	0.00	0.02	0.01	0.00	0.03	0.00	0.00
Fe	0.21	0.24	0.17	0.20	0.24	0.19	0.23	0.22
Mn	0.00	0.00	0.00	0.00	0.00	0.00	0.00	0.00
Mg	0.76	0.80	0.77	0.72	0.65	0.75	0.74	0.74
Ca	0.92	0.84	0.91	0.92	0.95	0.84	0.95	0.94
Na	0.03	0.04	0.03	0.04	0.04	0.07	0.03	0.03
K	0.00	0.00	0.00	0.00	0.00	0.00	0.00	0.00
Ni	0.00	0.00	0.00	0.00	0.00	0.00	0.00	0.00
Total	4.01	4.00	4.00	4.01	4.04	4.01	4.03	4.02
Mg#	77.98	76.72	81.86	78.03	72.56	79.56	76.31	77.45
$D^{(cpx\text{-}melt)}_{H2O}$	0.0147	0.0121	0.0151	0.0191	0.0400	0.0170	0.0188	0.0155
Absorbance of cpx (cm^{-1})	0.6	0.7	0.7	0.3	0.2	1.0	1.8	0.1
Thickness of cpx (0.001mm)	50	55	52	50	64	64	49	40
Absorbance normalized to 1 cm (cm^{-1})	122	124	125	52	23	159	367	25
H_2O-cpx (ppm)	52	52	53	22	10	67	155	11
H_2O-melt (wt%)	0.35	0.43	0.35	0.12	0.02	0.40	0.83	0.07

Sample No.							MX-10
Section No.							1
Point No.	2	3	4	5	6	7	1
SiO_2	41.69	47.67	48.16	47.89	45.24	50.43	51.40
TiO_2	5.20	2.42	2.65	2.54	3.72	1.55	1.38
Al_2O3	8.79	5.69	4.22	5.56	6.85	3.39	2.93
Cr_2O3	0.00	0.25	0.01	0.11	0.06	0.00	0.40
FeO	8.82	6.62	7.17	7.08	7.35	6.22	5.49
MnO	0.05	0.06	0.09	0.05	0.08	0.08	0.09
MgO	10.36	12.73	13.17	12.53	11.78	13.99	14.81
CaO	23.30	23.16	23.53	23.00	23.18	23.16	23.41
Na_2O	0.56	0.47	0.43	0.52	0.61	0.48	0.39
K_2O	0.01	0.01	0.01	0.01	0.02	0.00	0.00
NiO	0.00	0.00	0.00	0.00	0.00	0.01	0.01
Total	98.77	99.07	99.43	99.27	98.89	99.31	100.31
Si	1.61	1.80	1.82	1.80	1.72	1.88	1.90
Ti	0.15	0.07	0.08	0.07	0.11	0.04	0.04
Al	0.40	0.25	0.19	0.25	0.31	0.15	0.13
Cr	0.00	0.01	0.00	0.00	0.00	0.00	0.01
Fe	0.29	0.21	0.23	0.22	0.23	0.19	0.17
Mn	0.00	0.00	0.00	0.00	0.00	0.00	0.00
Mg	0.60	0.72	0.74	0.70	0.67	0.78	0.81
Ca	0.97	0.94	0.95	0.93	0.95	0.93	0.92
Na	0.04	0.03	0.03	0.04	0.05	0.04	0.03
K	0.00	0.00	0.00	0.00	0.00	0.00	0.00
Ni	0.00	0.00	0.00	0.00	0.00	0.00	0.00
Total	4.06	4.02	4.03	4.02	4.04	4.02	4.01
Mg#	67.68	77.43	76.60	75.93	74.08	80.04	82.79
$D^{(cpx\text{-}melt)}_{H2O}$	0.0708	0.0220	0.0191	0.0213	0.0351	0.0126	0.0118
Absorbance of cpx (cm^{-1})	0.3	0.7	0.4	0.4	0.3	0.6	0.6
Thickness of cpx (0.001mm)	42	57	58	54	53	53	126
Absorbance normalized to 1 cm (cm^{-1})	71	123	69	78	51	106	48
H_2O-cpx (ppm)	30	52	29	33	22	45	20
H_2O-melt (wt%)	0.04	0.24	0.15	0.15	0.06	0.35	0.17

Sample No.								
Section No.			2			3		
Point No.	2	4	3	4	5	1	1.1	1.2
SiO_2	50.59	49.62	46.66	44.02	42.48	49.60	50.28	45.88
TiO_2	1.63	2.27	2.93	4.02	4.55	1.90	1.60	3.49
Al_2O3	3.13	3.75	6.21	7.70	8.63	3.84	3.67	7.35
Cr_2O3	0.20	0.00	0.16	0.04	0.04	0.03	0.13	0.05
FeO	5.77	6.85	7.22	8.01	8.50	6.34	6.36	7.78
MnO	0.06	0.08	0.03	0.04	0.07	0.11	0.10	0.05
MgO	14.18	13.57	12.42	11.22	10.52	13.59	13.82	11.47
CaO	23.10	23.60	23.38	23.48	23.05	23.09	22.98	22.67
Na_2O	0.41	0.40	0.46	0.46	0.50	0.46	0.54	0.60
K_2O	0.00	0.00	0.02	0.02	0.00	0.00	0.01	0.00
NiO	0.10	0.00	0.00	0.00	0.05	0.03	0.00	0.00
Total	99.16	100.14	99.49	99.00	98.39	98.97	99.48	99.34
Si	1.89	1.85	1.76	1.68	1.64	1.86	1.88	1.74
Ti	0.05	0.06	0.08	0.12	0.13	0.05	0.04	0.10
Al	0.14	0.16	0.28	0.35	0.39	0.17	0.16	0.33
Cr	0.01	0.00	0.00	0.00	0.00	0.00	0.00	0.00
Fe	0.18	0.21	0.23	0.26	0.27	0.20	0.20	0.25
Mn	0.00	0.00	0.00	0.00	0.00	0.00	0.00	0.00
Mg	0.79	0.75	0.70	0.64	0.61	0.76	0.77	0.65
Ca	0.92	0.94	0.95	0.96	0.95	0.93	0.92	0.92
Na	0.03	0.03	0.03	0.03	0.04	0.03	0.04	0.04
K	0.00	0.00	0.00	0.00	0.00	0.00	0.00	0.00
Ni	0.00	0.00	0.00	0.00	0.00	0.00	0.00	0.00
Total	4.01	4.02	4.03	4.04	4.05	4.01	4.02	4.02
Mg#	81.42	77.94	75.41	71.42	68.83	79.27	79.48	72.44
$D^{(cpx\text{-}melt)}_{H2O}$	0.0122	0.0156	0.0276	0.0446	0.0589	0.0144	0.0133	0.0333
Absorbance of cpx (cm^{-1})	1.6	2.8	1.9	1.3	0.5	0.8	0.9	1.1
Thickness of cpx (0.001mm)	118	119	113	114	117	139	139	139
Absorbance normalized to 1 cm (cm^{-1})	136	235	168	114	43	54	61	81
H_2O-cpx (ppm)	57	100	71	48	18	23	26	34
H_2O-melt (wt%)	0.47	0.64	0.26	0.11	0.03	0.16	0.19	0.10

Sample No.								
Section No.	4							
Point No.	1	1.2	2	3	4	5	6	7
SiO_2	48.63	50.27	48.66	48.76	48.16	46.40	47.12	49.89
TiO_2	2.32	1.66	2.15	2.37	2.41	3.17	2.55	1.84
Al_2O3	4.83	3.82	3.98	4.23	5.92	6.28	5.89	3.59
Cr_2O3	0.19	0.39	0.05	0.05	0.12	0.00	0.21	0.46
FeO	6.67	5.38	6.60	6.85	8.52	7.73	7.10	6.49
MnO	0.08	0.09	0.13	0.08	0.05	0.09	0.09	0.07
MgO	12.51	13.42	12.62	13.31	12.30	12.20	12.53	13.61
CaO	23.25	23.23	24.34	23.84	21.53	23.25	22.93	23.49
Na_2O	0.41	0.48	0.54	0.46	0.71	0.53	0.56	0.38
K_2O	0.00	0.00	0.02	0.00	0.02	0.00	0.01	0.01
NiO	0.00	0.01	0.00	0.00	0.00	0.00	0.00	0.00
Total	98.88	98.75	99.08	99.96	99.74	99.65	98.98	99.82
Si	1.83	1.88	1.84	1.83	1.81	1.75	1.78	1.86
Ti	0.07	0.05	0.06	0.07	0.07	0.09	0.07	0.05
Al	0.21	0.17	0.18	0.19	0.26	0.28	0.26	0.16
Cr	0.01	0.01	0.00	0.00	0.00	0.00	0.01	0.01
Fe	0.21	0.17	0.21	0.21	0.27	0.24	0.22	0.20
Mn	0.00	0.00	0.00	0.00	0.00	0.00	0.00	0.00
Mg	0.70	0.75	0.71	0.74	0.69	0.69	0.71	0.76
Ca	0.94	0.93	0.99	0.96	0.87	0.94	0.93	0.94
Na	0.03	0.04	0.04	0.03	0.05	0.04	0.04	0.03
K	0.00	0.00	0.00	0.00	0.00	0.00	0.00	0.00
Ni	0.00	0.00	0.00	0.00	0.00	0.00	0.00	0.00
Total	4.01	4.00	4.03	4.03	4.02	4.04	4.03	4.01
Mg#	76.97	81.66	77.31	77.61	72.01	73.77	75.89	78.90
$D^{(cpx\text{-}melt)}_{H2O}$	0.0173	0.0126	0.0158	0.0179	0.0220	0.0292	0.0242	0.0144
Absorbance of cpx (cm^{-1})	0.2	0.5	0.2	0.6	0.6	0.5	0.6	0.3
Thickness of cpx (0.001mm)	60	60	61	64	64	70	73	57
Absorbance normalized to 1 cm (cm^{-1})	33	83	33	94	94	71	82	53
H_2O-cpx (ppm)	14	35	14	40	40	30	35	22
H_2O-melt (wt%)	0.08	0.28	0.09	0.22	0.18	0.10	0.14	0.16

Sample No.								
Section No.								
Point No.	8	9	11	12	13	14	15	17
SiO_2	47.23	50.18	49.89	49.24	45.27	48.65	45.78	44.32
TiO_2	2.41	1.74	1.62	2.13	3.80	2.44	2.74	4.72
Al_2O3	6.51	3.59	3.94	3.91	6.39	4.22	5.84	7.40
Cr_2O3	0.15	0.02	0.13	0.08	0.01	0.02	0.00	0.00
FeO	7.60	6.64	6.71	7.18	7.85	7.19	7.50	7.20
MnO	0.13	0.06	0.07	0.09	0.04	0.12	0.09	0.04
MgO	12.31	13.67	13.41	13.11	11.86	13.38	12.98	11.11
CaO	23.30	23.11	23.26	23.58	23.35	23.43	23.30	23.44
Na_2O	0.60	0.47	0.46	0.40	0.49	0.48	0.55	0.67
K_2O	0.02	0.00	0.00	0.00	0.00	0.00	0.00	0.00
NiO	0.02	0.06	0.06	0.04	0.07	0.03	0.00	0.00
Total	100.26	99.53	99.53	99.77	99.12	99.95	98.77	98.91
Si	1.77	1.87	1.87	1.85	1.73	1.82	1.75	1.69
Ti	0.07	0.05	0.05	0.06	0.11	0.07	0.08	0.14
Al	0.29	0.16	0.17	0.17	0.29	0.19	0.26	0.33
Cr	0.00	0.00	0.00	0.00	0.00	0.00	0.00	0.00
Fe	0.24	0.21	0.21	0.23	0.25	0.23	0.24	0.23
Mn	0.00	0.00	0.00	0.00	0.00	0.00	0.00	0.00
Mg	0.69	0.76	0.75	0.73	0.67	0.75	0.74	0.63
Ca	0.94	0.93	0.93	0.95	0.95	0.94	0.95	0.96
Na	0.04	0.03	0.03	0.03	0.04	0.03	0.04	0.05
K	0.00	0.00	0.00	0.00	0.00	0.00	0.00	0.00
Ni	0.00	0.00	0.00	0.00	0.00	0.00	0.00	0.00
Total	4.04	4.01	4.02	4.02	4.04	4.03	4.06	4.03
Mg#	74.28	78.58	78.10	76.50	72.93	76.86	75.51	73.33
$D^{(cpx\text{-}melt)}_{H2O}$	0.0263	0.0134	0.0141	0.0158	0.0343	0.0185	0.0299	0.0427
Absorbance of cpx (cm^{-1})	0.8	0.3	0.2	0.5	0.8	0.9	0.5	0.3
Thickness of cpx (0.001mm)	65	65	62	59	59	63	68	66
Absorbance normalized to 1 cm (cm^{-1})	123	46	32	85	136	143	74	45
H_2O-cpx (ppm)	52	20	14	36	57	60	31	19
H_2O-melt (wt%)	0.20	0.15	0.10	0.23	0.17	0.33	0.10	0.05

Sample No.								
Section No.		5						
Point No.	18	1	3	4	5	5.2	6	8
SiO_2	49.23	48.40	51.67	47.99	48.57	49.04	46.73	48.88
TiO_2	2.25	2.61	1.31	2.58	2.20	2.07	3.00	2.40
Al_2O3	4.20	4.51	2.41	5.67	4.10	4.72	5.97	3.94
Cr_2O3	0.13	0.04	0.10	0.58	0.03	0.83	0.00	0.01
FeO	6.56	6.40	6.95	6.36	6.88	5.88	8.05	6.78
MnO	0.04	0.12	0.16	0.05	0.14	0.01	0.09	0.06
MgO	13.78	13.24	13.91	11.94	13.20	13.49	11.65	13.28
CaO	23.38	23.30	22.69	23.19	23.18	23.13	22.91	23.50
Na_2O	0.41	0.45	0.60	0.51	0.36	0.52	0.76	0.36
K_2O	0.00	0.00	0.00	0.00	0.00	0.00	0.00	0.00
NiO	0.00	0.02	0.04	0.02	0.01	0.04	0.00	0.04
Total	99.98	99.09	99.83	98.89	98.66	99.74	99.17	99.24
Si	1.84	1.82	1.92	1.81	1.84	1.83	1.77	1.84
Ti	0.06	0.07	0.04	0.07	0.06	0.06	0.09	0.07
Al	0.18	0.20	0.11	0.25	0.18	0.21	0.27	0.17
Cr	0.00	0.00	0.00	0.02	0.00	0.02	0.00	0.00
Fe	0.20	0.20	0.22	0.20	0.22	0.18	0.26	0.21
Mn	0.00	0.00	0.00	0.00	0.00	0.00	0.00	0.00
Mg	0.77	0.74	0.77	0.67	0.74	0.75	0.66	0.75
Ca	0.93	0.94	0.90	0.94	0.94	0.92	0.93	0.95
Na	0.03	0.03	0.04	0.04	0.03	0.04	0.06	0.03
K	0.00	0.00	0.00	0.00	0.00	0.00	0.00	0.00
Ni	0.00	0.00	0.00	0.00	0.00	0.00	0.00	0.00
Total	4.02	4.02	4.01	4.00	4.02	4.02	4.03	4.02
Mg#	78.93	78.67	78.11	76.99	77.38	80.35	72.08	77.74
$D^{(cpx\text{-}melt)}_{H2O}$	0.0172	0.0186	0.0101	0.0202	0.0167	0.0181	0.0255	0.0165
Absorbance of cpx (cm^{-1})	0.6	0.7	0.9	0.8	0.4	0.6	0.6	0.2
Thickness of cpx (0.001mm)	72	63	62	65	73	73	72	73
Absorbance normalized to 1 cm (cm^{-1})	81	105	137	123	49	78	78	25
H_2O-cpx (ppm)	34	44	58	52	21	33	33	10
H_2O-melt (wt%)	0.20	0.24	0.58	0.26	0.13	0.18	0.13	0.06

Sample No.					MX-12		
Section No.					1		
Point No.	9	10	10.2	11	1	2	3
SiO_2	49.14	49.02	48.69	48.88	47.25	47.67	49.00
TiO_2	2.28	2.14	2.42	2.34	2.45	2.52	2.61
Al_2O3	3.97	4.12	4.69	3.74	6.09	5.16	4.27
Cr_2O3	0.00	0.03	0.00	0.06	0.06	0.04	0.39
FeO	6.82	6.81	7.21	7.09	7.44	6.88	6.62
MnO	0.03	0.08	0.06	0.11	0.09	0.07	0.09
MgO	13.51	13.36	12.60	13.09	12.42	12.54	12.77
CaO	23.43	23.24	23.33	23.48	23.09	23.59	23.43
Na_2O	0.51	0.46	0.47	0.49	0.61	0.51	0.53
K_2O	0.00	0.00	0.00	0.00	0.00	0.00	0.00
NiO	0.00	0.00	0.03	0.02	0.06	0.00	0.05
Total	99.69	99.26	99.50	99.30	99.55	98.99	99.74
Si	1.84	1.84	1.83	1.84	1.78	1.80	1.83
Ti	0.06	0.06	0.07	0.07	0.07	0.07	0.07
Al	0.18	0.18	0.21	0.17	0.27	0.23	0.19
Cr	0.00	0.00	0.00	0.00	0.00	0.00	0.01
Fe	0.21	0.21	0.23	0.22	0.23	0.22	0.21
Mn	0.00	0.00	0.00	0.00	0.00	0.00	0.00
Mg	0.75	0.75	0.71	0.74	0.70	0.71	0.71
Ca	0.94	0.94	0.94	0.95	0.93	0.96	0.94
Na	0.04	0.03	0.03	0.04	0.04	0.04	0.04
K	0.00	0.00	0.00	0.00	0.00	0.00	0.00
Ni	0.00	0.00	0.00	0.00	0.00	0.00	0.00
Total	4.03	4.02	4.01	4.02	4.04	4.03	4.01
Mg#	77.94	77.76	75.71	76.69	74.86	76.48	77.47
$D^{(cpx\text{-}melt)}_{H2O}$	0.0165	0.0163	0.0177	0.0161	0.0245	0.0207	0.0171
Absorbance of cpx (cm^{-1})	0.3	0.3	0.6	0.6	0.8	0.1	0.6
Thickness of cpx (0.001mm)	69	63	63	51	79	65	78
Absorbance normalized to 1 cm (cm^{-1})	48	48	89	116	101	15	77
H_2O-cpx (ppm)	20	20	38	49	43	7	33
H_2O-melt (wt%)	0.12	0.12	0.21	0.30	0.17	0.03	0.19

Sample No.								
Section No.								
Point No.	4	5	6	7	8	9	9.2	10
SiO_2	49.34	46.23	49.67	49.84	48.25	50.47	47.66	49.94
TiO_2	2.23	3.30	1.60	1.87	2.48	1.80	2.27	1.74
Al_2O3	4.35	6.43	3.43	3.81	4.33	3.90	5.47	4.39
Cr_2O3	0.03	0.00	0.02	0.16	0.07	0.12	0.08	0.04
FeO	6.93	6.90	6.63	6.62	6.82	6.70	6.95	6.62
MnO	0.08	0.07	0.04	0.04	0.11	0.08	0.05	0.07
MgO	12.70	12.28	13.05	13.66	13.27	13.97	12.30	13.38
CaO	23.10	23.06	23.16	23.24	23.75	22.99	23.29	22.95
Na_2O	0.51	0.51	0.46	0.48	0.38	0.46	0.58	0.41
K_2O	0.00	0.00	0.01	0.00	0.01	0.00	0.00	0.02
NiO	0.00	0.07	0.03	0.00	0.01	0.03	0.06	0.00
Total	99.27	98.84	98.09	99.72	99.49	100.52	98.71	99.55
Si	1.85	1.75	1.88	1.86	1.82	1.87	1.81	1.86
Ti	0.06	0.09	0.05	0.05	0.07	0.05	0.06	0.05
Al	0.19	0.29	0.15	0.17	0.19	0.17	0.24	0.19
Cr	0.00	0.00	0.00	0.00	0.00	0.00	0.00	0.00
Fe	0.22	0.22	0.21	0.21	0.21	0.21	0.22	0.21
Mn	0.00	0.00	0.00	0.00	0.00	0.00	0.00	0.00
Mg	0.71	0.69	0.74	0.76	0.74	0.77	0.70	0.74
Ca	0.93	0.94	0.94	0.93	0.96	0.91	0.95	0.92
Na	0.04	0.04	0.03	0.03	0.03	0.03	0.04	0.03
K	0.00	0.00	0.00	0.00	0.00	0.00	0.00	0.00
Ni	0.00	0.00	0.00	0.00	0.00	0.00	0.00	0.00
Total	4.01	4.03	4.01	4.02	4.03	4.01	4.03	4.01
Mg#	76.56	76.03	77.82	78.62	77.63	78.79	75.93	78.27
$D^{(cpx\text{-}melt)}_{H2O}$	0.0154	0.0291	0.0124	0.0146	0.0190	0.0144	0.0204	0.0146
Absorbance of cpx (cm^{-1})	0.6	0.3	0.5	0.9	0.8	0.5	0.6	0.3
Thickness of cpx (0.001mm)	78	78	78	78	78	75	75	47
Absorbance normalized to 1 cm (cm^{-1})	77	38	64	115	103	67	80	64
H_2O-cpx (ppm)	33	16	27	49	43	28	34	27
H_2O-melt (wt%)	0.21	0.06	0.22	0.33	0.23	0.20	0.17	0.18

Sample No.								
Section No.							2	
Point No.	11	12	13	14	15	17	1	2
SiO_2	50.67	51.89	48.56	48.23	49.38	50.98	50.86	50.57
TiO_2	1.65	0.91	1.85	2.68	1.67	1.44	1.39	1.73
Al_2O3	3.35	2.30	5.20	4.14	4.84	3.23	3.05	3.09
Cr_2O3	0.25	0.00	0.32	0.00	0.60	0.14	0.40	0.34
FeO	5.88	6.51	6.42	7.05	5.87	6.17	5.51	5.76
MnO	0.08	0.14	0.07	0.08	0.02	0.08	0.06	0.07
MgO	13.77	13.63	13.20	13.25	13.70	14.23	14.72	14.41
CaO	23.31	23.47	23.16	23.47	22.97	23.35	23.84	23.46
Na_2O	0.40	0.63	0.53	0.27	0.53	0.43	0.49	0.40
K_2O	0.01	0.00	0.01	0.00	0.00	0.01	0.01	0.01
NiO	0.00	0.00	0.00	0.03	0.06	0.00	0.00	0.00
Total	99.36	99.48	99.30	99.19	99.63	100.05	100.31	99.84
Si	1.89	1.94	1.82	1.82	1.84	1.89	1.88	1.88
Ti	0.05	0.03	0.05	0.08	0.05	0.04	0.04	0.05
Al	0.15	0.10	0.23	0.18	0.21	0.14	0.13	0.14
Cr	0.01	0.00	0.01	0.00	0.02	0.00	0.01	0.01
Fe	0.18	0.20	0.20	0.22	0.18	0.19	0.17	0.18
Mn	0.00	0.00	0.00	0.00	0.00	0.00	0.00	0.00
Mg	0.77	0.76	0.74	0.75	0.76	0.79	0.81	0.80
Ca	0.93	0.94	0.93	0.95	0.92	0.93	0.94	0.93
Na	0.03	0.05	0.04	0.02	0.04	0.03	0.04	0.03
K	0.00	0.00	0.00	0.00	0.00	0.00	0.00	0.00
Ni	0.00	0.00	0.00	0.00	0.00	0.00	0.00	0.00
Total	4.00	4.01	4.03	4.02	4.02	4.01	4.03	4.02
Mg#	80.67	78.88	78.57	77.03	80.62	80.44	82.65	81.68
$D^{(cpx\text{-}melt)}_{H2O}$	0.0121	0.0089	0.0188	0.0186	0.0170	0.0122	0.0127	0.0130
Absorbance of cpx (cm^{-1})	0.7	0.1	0.4	0.6	0.5	0.7	1.3	0.9
Thickness of cpx (0.001mm)	61	45	65	49	64	75	56	56
Absorbance normalized to 1 cm (cm^{-1})	115	22	62	122	78	93	232	161
H_2O-cpx (ppm)	49	9	26	52	33	39	98	68
H_2O-melt (wt%)	0.40	0.11	0.14	0.28	0.19	0.32	0.77	0.52

Sample No. Section No. Point No.	3	4	5	6	7	8	9	10
SiO_2	49.82	45.43	50.10	49.00	48.68	48.28	45.21	46.63
TiO_2	1.40	3.75	2.20	2.14	2.36	2.60	3.85	2.78
Al_2O3	4.57	6.99	4.17	4.59	4.25	4.80	7.45	6.45
Cr_2O3	1.03	0.00	0.07	0.09	0.05	0.14	0.02	0.25
FeO	5.25	7.99	6.08	7.07	6.90	6.76	8.06	6.83
MnO	0.06	0.09	0.08	0.06	0.06	0.09	0.05	0.03
MgO	13.67	11.05	13.48	13.43	12.77	13.00	11.12	12.20
CaO	22.47	23.42	23.77	23.15	23.62	23.10	23.49	23.25
Na_2O	0.54	0.62	0.58	0.51	0.43	0.55	0.68	0.56
K_2O	0.00	0.00	0.03	0.02	0.00	0.00	0.02	0.01
NiO	0.03	0.00	0.01	0.04	0.00	0.04	0.04	0.00
Total	98.84	99.34	100.57	100.08	99.12	99.35	99.99	98.99
Si	1.86	1.73	1.85	1.83	1.84	1.82	1.71	1.76
Ti	0.04	0.11	0.06	0.06	0.07	0.07	0.11	0.08
Al	0.20	0.31	0.18	0.20	0.19	0.21	0.33	0.29
Cr	0.03	0.00	0.00	0.00	0.00	0.00	0.00	0.01
Fe	0.16	0.25	0.19	0.22	0.22	0.21	0.25	0.22
Mn	0.00	0.00	0.00	0.00	0.00	0.00	0.00	0.00
Mg	0.76	0.63	0.74	0.75	0.72	0.73	0.63	0.69
Ca	0.90	0.95	0.94	0.93	0.95	0.93	0.95	0.94
Na	0.04	0.05	0.04	0.04	0.03	0.04	0.05	0.04
K	0.00	0.00	0.00	0.00	0.00	0.00	0.00	0.00
Ni	0.00	0.00	0.00	0.00	0.00	0.00	0.00	0.00
Total	4.00	4.03	4.02	4.03	4.02	4.02	4.04	4.03
Mg#	82.29	71.15	79.81	77.21	76.73	77.41	71.09	76.12
$D^{(cpx\text{-}melt)}_{H2O}$	0.0149	0.0339	0.0153	0.0181	0.0167	0.0196	0.0381	0.0269
Absorbance of cpx (cm^{-1})	0.2	0.5	0.4	0.6	0.7	0.6	0.6	0.5
Thickness of cpx (0.001mm)	55	56	56	56	68	68	63	73
Absorbance normalized to 1 cm (cm^{-1})	36	89	71	107	103	88	95	68
H_2O-cpx (ppm)	15	38	30	45	44	37	40	29
H_2O-melt (wt%)	0.10	0.11	0.20	0.25	0.26	0.19	0.11	0.11

Sample No. Section No. Point No.	11	12	13	14	15	16	17	17.2
SiO_2	47.26	44.78	50.55	49.02	49.73	48.33	47.80	45.34
TiO_2	2.87	3.79	2.03	2.19	2.15	2.46	2.53	3.57
Al_2O3	5.76	7.33	3.51	4.58	3.86	4.12	4.31	7.54
Cr_2O3	0.00	0.03	0.01	0.05	0.09	0.00	0.01	0.05
FeO	7.31	7.74	5.93	6.30	6.61	7.09	6.96	7.78
MnO	0.09	0.10	0.13	0.10	0.09	0.09	0.10	0.06
MgO	12.09	11.31	13.39	13.38	13.56	13.18	12.96	11.45
CaO	23.19	23.24	23.61	23.16	23.37	24.04	23.97	23.13
Na_2O	0.75	0.48	0.63	0.44	0.44	0.47	0.44	0.58
K_2O	0.01	0.00	0.00	0.01	0.01	0.00	0.00	0.00
NiO	0.00	0.03	0.01	0.00	0.00	0.00	0.01	0.03
Total	99.31	98.83	99.79	99.22	99.90	99.78	99.10	99.53
Si	1.79	1.71	1.88	1.84	1.85	1.82	1.81	1.72
Ti	0.08	0.11	0.06	0.06	0.06	0.07	0.07	0.10
Al	0.26	0.33	0.15	0.20	0.17	0.18	0.19	0.34
Cr	0.00	0.00	0.00	0.00	0.00	0.00	0.00	0.00
Fe	0.23	0.25	0.18	0.20	0.21	0.22	0.22	0.25
Mn	0.00	0.00	0.00	0.00	0.00	0.00	0.00	0.00
Mg	0.68	0.64	0.74	0.75	0.75	0.74	0.73	0.65
Ca	0.94	0.95	0.94	0.93	0.93	0.97	0.97	0.94
Na	0.05	0.04	0.05	0.03	0.03	0.03	0.03	0.04
K	0.00	0.00	0.00	0.00	0.00	0.00	0.00	0.00
Ni	0.00	0.00	0.00	0.00	0.00	0.00	0.00	0.00
Total	4.03	4.03	4.01	4.01	4.02	4.04	4.04	4.03
Mg#	74.68	72.26	80.10	79.11	78.54	76.83	76.84	72.39
$D^{(cpx\text{-}melt)}_{H2O}$	0.0236	0.0380	0.0127	0.0170	0.0152	0.0186	0.0194	0.0369
Absorbance of cpx (cm^{-1})	0.8	0.4	0.4	0.5	0.3	0.5	0.5	0.4
Thickness of cpx (0.001mm)	63	69	69	64	61	57	52	52
Absorbance normalized to 1 cm (cm^{-1})	127	58	61	78	49	88	96	77
H_2O-cpx (ppm)	54	25	26	33	21	37	41	33
H_2O-melt (wt%)	0.23	0.06	0.20	0.19	0.14	0.20	0.21	0.09

Sample No.					
Section No.					
Point No.	18	19	20	21	22
SiO_2	48.77	48.93	50.30	49.70	48.04
TiO_2	2.38	2.23	1.86	2.05	3.01
Al_2O3	4.21	4.38	3.54	3.87	6.42
Cr_2O3	0.04	0.14	0.03	0.03	0.13
FeO	6.93	6.69	6.71	6.33	6.38
MnO	0.07	0.09	0.08	0.04	0.13
MgO	12.70	13.56	13.85	13.31	12.08
CaO	23.65	23.28	23.34	23.41	22.39
Na_2O	0.42	0.39	0.44	0.43	1.24
K_2O	0.00	0.02	0.01	0.00	0.68
NiO	0.02	0.05	0.05	0.07	0.13
Total	99.19	99.76	100.22	99.25	100.64
Si	1.84	1.83	1.87	1.86	1.79
Ti	0.07	0.06	0.05	0.06	0.08
Al	0.19	0.19	0.15	0.17	0.28
Cr	0.00	0.00	0.00	0.00	0.00
Fe	0.22	0.21	0.21	0.20	0.20
Mn	0.00	0.00	0.00	0.00	0.00
Mg	0.71	0.76	0.77	0.74	0.67
Ca	0.96	0.93	0.93	0.94	0.89
Na	0.03	0.03	0.03	0.03	0.09
K	0.00	0.00	0.00	0.00	0.03
Ni	0.00	0.00	0.00	0.00	0.00
Total	4.02	4.02	4.02	4.01	4.05
Mg#	76.57	78.32	78.63	78.94	77.15
$D^{(cpx\text{-}melt)}_{H2O}$	0.0165	0.0177	0.0139	0.0143	0.0245
Absorbance of cpx (cm^{-1})	1.3	0.6	0.6	1.2	0.5
Thickness of cpx (0.001mm)	50	53	61	64	65
Absorbance normalized to 1 cm (cm^{-1})	260	113	92	188	83
H_2O-cpx (ppm)	110	48	39	79	35
H_2O-melt (wt%)	0.67	0.27	0.28	0.55	0.14

Sample No.	SH-1							
Section No.	1							
Point No.	1	1.1	2	3	5	6	7	8
SiO_2	47.77	49.95	45.13	51.69	49.92	47.90	51.85	49.66
TiO_2	1.94	1.56	3.01	1.24	1.48	2.36	1.09	1.46
Al_2O3	6.85	4.78	8.12	3.43	4.88	6.43	3.55	4.35
Cr_2O3	0.14	0.52	0.04	0.34	0.35	0.42	0.18	0.77
FeO	7.29	6.43	8.53	5.30	6.37	6.81	6.27	5.62
MnO	0.01	0.00	0.00	0.30	0.00	0.00	0.03	0.00
MgO	13.37	14.35	10.73	14.66	14.19	12.14	15.40	14.17
CaO	20.89	21.67	22.61	23.10	22.40	22.81	21.37	23.26
Na_2O	0.59	0.52	0.58	0.31	0.39	0.46	0.45	0.36
K_2O	0.01	0.01	0.00	0.00	0.00	0.00	0.00	0.01
NiO	0.01	0.00	0.00	0.30	0.00	0.00	0.03	0.00
Total	98.86	99.78	98.76	100.67	99.99	99.34	100.21	99.66
Si	1.79	1.85	1.72	1.90	1.85	1.80	1.90	1.85
Ti	0.05	0.04	0.09	0.03	0.04	0.07	0.03	0.04
Al	0.30	0.21	0.37	0.15	0.21	0.28	0.15	0.19
Cr	0.00	0.02	0.00	0.01	0.01	0.01	0.01	0.02
Fe	0.23	0.20	0.27	0.16	0.20	0.21	0.19	0.17
Mn	0.00	0.00	0.00	0.01	0.00	0.00	0.00	0.00
Mg	0.75	0.79	0.61	0.80	0.78	0.68	0.84	0.79
Ca	0.84	0.86	0.92	0.91	0.89	0.92	0.84	0.93
Na	0.04	0.04	0.04	0.02	0.03	0.03	0.03	0.03
K	0.00	0.00	0.00	0.00	0.00	0.00	0.00	0.00
Ni	0.00	0.00	0.00	0.01	0.00	0.00	0.00	0.00
Total	4.02	4.01	4.03	4.00	4.01	4.01	4.00	4.02
Mg#	76.58	79.92	69.16	83.14	79.88	76.05	81.41	81.81
$D^{(cpx\text{-}melt)}_{H2O}$	0.0248	0.0166	0.0361	0.0118	0.0165	0.0225	0.0121	0.0160
Absorbance of cpx (cm^{-1})	14.5	13.9	9.5	11.0	12.0	16.0	10.8	13.0
Thickness of cpx (0.001mm)	87	87	87	83	110	110	113	110
Absorbance normalized to 1 cm (cm^{-1})	1667	1598	1092	1325	1091	1455	956	1182
H_2O-cpx (ppm)	705	676	462	561	462	615	404	500
H_2O-melt (wt%)	2.85	4.06	1.28	4.74	2.80	2.74	3.33	3.13

Sample No.								
Section No.								
Point No.	9	10	11	12	13	13.1	13.2	13.3
SiO_2	51.87	48.69	51.17	50.71	47.97	48.65	48.29	47.99
TiO_2	0.87	2.39	1.33	1.21	2.29	1.98	1.98	1.81
Al_2O3	3.66	4.80	3.58	4.72	5.31	4.56	6.60	6.67
Cr_2O3	0.13	0.10	0.14	0.57	0.10	0.07	0.35	0.60
FeO	6.51	7.54	5.96	5.37	6.99	6.43	6.56	6.47
MnO	0.07	0.05	0.02	0.07	0.00	0.05	0.02	0.04
MgO	15.54	13.36	14.64	14.92	12.97	13.63	13.33	13.53
CaO	20.68	21.79	22.55	21.78	23.45	23.67	22.06	22.10
Na_2O	0.62	0.27	0.36	0.63	0.35	0.32	0.61	0.56
K_2O	0.00	0.01	0.00	0.01	0.00	0.00	0.00	0.00
NiO	0.07	0.05	0.02	0.07	0.00	0.05	0.02	0.04
Total	100.01	99.05	99.77	100.07	99.43	99.40	99.82	99.79
Si	1.91	1.83	1.89	1.87	1.80	1.83	1.80	1.79
Ti	0.02	0.07	0.04	0.03	0.06	0.06	0.06	0.05
Al	0.16	0.21	0.16	0.20	0.24	0.20	0.29	0.29
Cr	0.00	0.00	0.00	0.02	0.00	0.00	0.01	0.02
Fe	0.20	0.24	0.18	0.17	0.22	0.20	0.20	0.20
Mn	0.00	0.00	0.00	0.00	0.00	0.00	0.00	0.00
Mg	0.85	0.75	0.81	0.82	0.73	0.76	0.74	0.75
Ca	0.81	0.88	0.89	0.86	0.94	0.95	0.88	0.88
Na	0.04	0.02	0.03	0.04	0.03	0.02	0.04	0.04
K	0.00	0.00	0.00	0.00	0.00	0.00	0.00	0.00
Ni	0.00	0.00	0.00	0.00	0.00	0.00	0.00	0.00
Total	4.01	4.00	4.00	4.01	4.03	4.03	4.02	4.03
Mg#	80.99	75.97	81.42	83.21	76.77	79.07	78.36	78.85
$D^{(cpx\text{-}melt)}_{H2O}$	0.0121	0.0187	0.0124	0.0152	0.0209	0.0179	0.0234	0.0247
Absorbance of cpx (cm^{-1})	8.0	16.0	11.0	14.0	18.0	16.0	13.0	13.0
Thickness of cpx (0.001mm)	104	114	115	118	119	119	119	119
Absorbance normalized to 1 cm (cm^{-1})	769	1404	957	1186	1513	1345	1092	1092
H_2O-cpx (ppm)	325	594	405	502	640	569	462	462
H_2O-melt (wt%)	2.69	3.17	3.27	3.31	3.07	3.17	1.98	1.87

Sample No.								
Section No.								
Point No.	15	16	17	18	19	20	22	23
SiO_2	50.91	49.97	49.82	50.07	49.74	49.94	49.49	49.34
TiO_2	1.00	1.55	1.40	1.38	1.49	1.36	1.97	1.76
Al_2O3	4.26	5.51	5.64	4.84	3.79	4.74	4.80	5.43
Cr_2O3	0.22	0.56	0.17	0.08	0.44	0.42	0.07	0.06
FeO	5.41	6.16	6.45	7.03	5.55	6.28	7.76	6.61
MnO	0.02	0.05	0.01	0.04	0.02	0.05	0.03	0.00
MgO	15.13	14.11	13.74	14.63	14.26	14.97	13.48	13.77
CaO	21.53	21.72	21.54	21.02	23.33	20.98	22.02	21.98
Na_2O	0.59	0.52	0.76	0.48	0.35	0.51	0.39	0.53
K_2O	0.03	0.01	0.00	0.00	0.00	0.00	0.00	0.00
NiO	0.02	0.05	0.01	0.04	0.02	0.05	0.03	0.00
Total	99.10	100.21	99.53	99.61	98.98	99.29	100.05	99.47
Si	1.89	1.84	1.85	1.86	1.86	1.86	1.84	1.84
Ti	0.03	0.04	0.04	0.04	0.04	0.04	0.06	0.05
Al	0.19	0.24	0.25	0.21	0.17	0.21	0.21	0.24
Cr	0.01	0.02	0.01	0.00	0.01	0.01	0.00	0.00
Fe	0.17	0.19	0.20	0.22	0.17	0.20	0.24	0.21
Mn	0.00	0.00	0.00	0.00	0.00	0.00	0.00	0.00
Mg	0.84	0.78	0.76	0.81	0.80	0.83	0.75	0.76
Ca	0.85	0.86	0.86	0.84	0.94	0.84	0.88	0.88
Na	0.04	0.04	0.05	0.03	0.03	0.04	0.03	0.04
K	0.00	0.00	0.00	0.00	0.00	0.00	0.00	0.00
Ni	0.00	0.00	0.00	0.00	0.00	0.00	0.00	0.00
Total	4.01	4.01	4.01	4.01	4.02	4.01	4.01	4.01
Mg#	83.30	80.32	79.15	78.76	82.07	80.96	75.59	78.78
$D^{(cpx\text{-}melt)}_{H2O}$	0.0133	0.0177	0.0170	0.0163	0.0143	0.0166	0.0174	0.0180
Absorbance of cpx (cm^{-1})	15.0	15.0	13.0	14.0	6.9	14.0	13.2	17.8
Thickness of cpx (0.001mm)	121	117	120	120	111	113	113	113
Absorbance normalized to 1 cm (cm^{-1})	1240	1282	1083	1167	622	1239	1168	1575
H_2O-cpx (ppm)	525	542	458	494	263	524	494	667
H_2O-melt (wt%)	3.94	3.06	2.70	3.03	1.83	3.16	2.84	3.69

Sample No.						SH-2		
Section No.						1		
Point No.	24	25	26	27	28	1	2	3
SiO_2	49.46	51.55	50.59	49.01	50.11	50.13	51.96	50.53
TiO_2	1.43	1.14	1.42	1.31	1.89	1.40	1.00	1.02
Al_2O3	5.39	3.39	3.48	6.52	4.03	4.42	3.81	4.06
Cr_2O3	0.53	0.24	0.48	0.00	0.20	0.16	0.45	0.15
FeO	5.92	6.12	5.93	8.36	6.36	7.29	5.94	6.45
MnO	0.11	0.01	0.04	0.00	0.05	0.03	0.01	0.11
MgO	14.15	15.22	14.72	11.79	13.72	14.59	15.32	14.29
CaO	21.83	21.80	22.95	21.83	22.49	20.89	20.96	22.54
Na_2O	0.53	0.44	0.29	0.85	0.27	0.43	0.47	0.35
K_2O	0.01	0.01	0.02	0.00	0.01	0.01	0.00	0.01
NiO	0.11	0.01	0.04	0.00	0.05	0.03	0.01	0.11
Total	99.47	99.92	99.96	99.66	99.17	99.37	99.93	99.61
Si	1.84	1.90	1.87	1.83	1.87	1.87	1.91	1.88
Ti	0.04	0.03	0.04	0.04	0.05	0.04	0.03	0.03
Al	0.24	0.15	0.15	0.29	0.18	0.19	0.16	0.18
Cr	0.02	0.01	0.01	0.00	0.01	0.00	0.01	0.00
Fe	0.18	0.19	0.18	0.26	0.20	0.23	0.18	0.20
Mn	0.00	0.00	0.00	0.00	0.00	0.00	0.00	0.00
Mg	0.78	0.84	0.81	0.66	0.76	0.81	0.84	0.79
Ca	0.87	0.86	0.91	0.87	0.90	0.83	0.82	0.90
Na	0.04	0.03	0.02	0.06	0.02	0.03	0.03	0.03
K	0.00	0.00	0.00	0.00	0.00	0.00	0.00	0.00
Ni	0.00	0.00	0.00	0.00	0.00	0.00	0.00	0.00
Total	4.01	4.01	4.01	4.02	3.99	4.01	3.99	4.01
Mg#	81.00	81.59	81.58	71.55	79.36	78.12	82.14	79.80
$D^{(cpx\text{-}melt)}_{H2O}$	0.0178	0.0121	0.0136	0.0184	0.0140	0.0155	0.0121	0.0133
Absorbance of cpx (cm^{-1})	8.8	15.0	14.0	12.7	13.3	3.1	1.8	3.9
Thickness of cpx (0.001mm)	111	107	98	89	97	88	88	88
Absorbance normalized to 1 cm (cm^{-1})	793	1402	1429	1427	1371	352	205	443
H_2O-cpx (ppm)	335	593	604	604	580	149	87	188
H_2O-melt (wt%)	1.88	4.89	4.44	3.27	4.13	0.96	0.72	1.41

Sample No.								
Section No.								
Point No.	4	5	6	7	8	9	10	10.2
SiO_2	49.06	49.42	50.34	45.78	51.15	45.12	51.23	50.87
TiO_2	1.97	1.76	1.27	2.93	1.28	3.08	0.93	1.30
Al_2O3	6.21	4.44	4.30	7.15	3.94	9.28	4.93	3.51
Cr_2O3	0.11	0.06	0.59	0.67	0.10	0.00	0.18	0.39
FeO	7.15	7.13	5.48	6.83	6.50	7.56	5.45	6.00
MnO	0.01	0.05	0.03	0.00	0.07	0.00	0.02	0.01
MgO	12.95	14.00	14.74	12.34	14.97	11.42	15.18	14.57
CaO	21.31	22.03	22.17	22.93	21.05	21.87	21.04	22.40
Na_2O	0.62	0.37	0.52	0.42	0.48	0.74	0.57	0.37
K_2O	0.00	0.00	0.01	0.00	0.00	0.00	0.01	0.01
NiO	0.01	0.05	0.03	0.00	0.07	0.00	0.02	0.01
Total	99.42	99.31	99.45	99.05	99.60	99.06	99.55	99.43
Si	1.83	1.85	1.87	1.73	1.89	1.70	1.88	1.89
Ti	0.06	0.05	0.04	0.08	0.04	0.09	0.03	0.04
Al	0.27	0.20	0.19	0.32	0.17	0.41	0.21	0.15
Cr	0.00	0.00	0.02	0.02	0.00	0.00	0.01	0.01
Fe	0.22	0.22	0.17	0.22	0.20	0.24	0.17	0.19
Mn	0.00	0.00	0.00	0.00	0.00	0.00	0.00	0.00
Mg	0.72	0.78	0.82	0.70	0.83	0.64	0.83	0.81
Ca	0.85	0.88	0.88	0.93	0.83	0.89	0.83	0.89
Na	0.04	0.03	0.04	0.03	0.03	0.05	0.04	0.03
K	0.00	0.00	0.00	0.00	0.00	0.00	0.00	0.00
Ni	0.00	0.00	0.00	0.00	0.00	0.00	0.00	0.00
Total	4.00	4.02	4.01	4.03	4.00	4.03	4.00	4.01
Mg#	76.35	77.78	82.76	76.31	80.41	72.93	83.24	81.23
$D^{(cpx\text{-}melt)}_{H2O}$	0.0195	0.0165	0.0147	0.0336	0.0132	0.0422	0.0139	0.0126
Absorbance of cpx (cm^{-1})	3.1	3.8	2.2	4.5	2.5	6.5	5.7	9.0
Thickness of cpx (0.001mm)	88	91	91	65	91	80	93	93
Absorbance normalized to 1 cm (cm^{-1})	352	418	242	692	275	813	613	968
H_2O-cpx (ppm)	149	177	102	293	116	344	259	409
H_2O-melt (wt%)	0.76	1.07	0.69	0.87	0.88	0.81	1.86	3.25

Sample No. Section No. Point No.	11	12	13	14	15	16	17	18
SiO_2	50.32	48.73	49.06	50.39	47.96	50.98	49.98	48.94
TiO_2	1.19	1.94	2.06	1.36	1.56	1.11	1.73	1.90
Al_2O3	4.79	4.59	4.70	3.42	7.00	3.72	4.31	6.08
Cr_2O3	0.74	0.12	0.16	0.44	0.00	0.45	0.31	0.59
FeO	5.04	7.47	7.19	5.83	9.45	5.40	5.57	6.50
MnO	0.01	0.03	0.00	0.03	0.08	0.01	0.00	0.08
MgO	14.39	13.86	13.23	14.48	11.30	15.05	13.84	12.78
CaO	22.62	21.46	22.63	22.73	21.34	21.68	23.35	22.28
Na_2O	0.55	0.41	0.32	0.33	0.80	0.45	0.35	0.47
K_2O	0.00	0.01	0.00	0.01	0.01	0.00	0.02	0.02
NiO	0.01	0.03	0.00	0.03	0.08	0.01	0.00	0.08
Total	99.65	98.65	99.34	99.06	99.58	98.85	99.44	99.72
Si	1.86	1.84	1.84	1.88	1.81	1.90	1.86	1.82
Ti	0.03	0.06	0.06	0.04	0.04	0.03	0.05	0.05
Al	0.21	0.20	0.21	0.15	0.31	0.16	0.19	0.27
Cr	0.02	0.00	0.00	0.01	0.00	0.01	0.01	0.02
Fe	0.16	0.24	0.23	0.18	0.30	0.17	0.17	0.20
Mn	0.00	0.00	0.00	0.00	0.00	0.00	0.00	0.00
Mg	0.79	0.78	0.74	0.81	0.64	0.83	0.77	0.71
Ca	0.90	0.87	0.91	0.91	0.86	0.86	0.93	0.89
Na	0.04	0.03	0.02	0.02	0.06	0.03	0.02	0.03
K	0.00	0.00	0.00	0.00	0.00	0.00	0.00	0.00
Ni	0.00	0.00	0.00	0.00	0.00	0.00	0.00	0.00
Total	4.01	4.02	4.01	4.01	4.02	4.00	4.01	4.00
Mg#	83.58	76.78	76.65	81.58	68.07	83.25	81.57	77.80
$D^{(cpx\text{-}melt)}_{H2O}$	0.0151	0.0180	0.0172	0.0130	0.0221	0.0125	0.0147	0.0196
Absorbance of cpx (cm^{-1})	3.1	4.8	5.3	3.3	3.2	4.2	3.7	8.0
Thickness of cpx (0.001mm)	99	93	85	85	85	85	108	104
Absorbance normalized to 1 cm (cm^{-1})	313	516	624	382	376	494	343	769
H_2O-cpx (ppm)	132	218	264	162	159	209	145	325
H_2O-melt (wt%)	0.88	1.21	1.53	1.25	0.72	1.67	0.98	1.66

Sample No.								
Section No.								
Point No.	19	20	21	22	23	24	25	26
SiO_2	48.64	46.60	50.79	49.77	47.25	50.16	48.99	50.57
TiO_2	1.89	2.65	0.26	1.57	2.27	1.57	2.25	1.53
Al_2O3	5.08	7.98	3.21	5.28	7.92	4.46	5.12	3.78
Cr_2O3	0.51	0.00	0.02	0.51	0.10	0.16	0.13	0.10
FeO	6.14	7.06	11.11	6.28	6.82	6.87	7.30	6.61
MnO	0.00	0.01	0.00	0.05	0.03	0.05	0.00	0.01
MgO	13.72	12.10	11.73	13.89	12.42	13.98	12.89	14.36
CaO	23.07	22.35	21.73	21.61	22.53	21.83	22.66	22.34
Na_2O	0.37	0.64	0.46	0.56	0.57	0.42	0.24	0.30
K_2O	0.00	0.01	0.00	0.02	0.01	0.00	0.00	0.00
NiO	0.00	0.01	0.00	0.05	0.03	0.05	0.00	0.01
Total	99.42	99.40	99.30	99.59	99.95	99.56	99.57	99.61
Si	1.82	1.75	1.93	1.85	1.76	1.87	1.83	1.88
Ti	0.05	0.07	0.01	0.04	0.06	0.04	0.06	0.04
Al	0.22	0.35	0.14	0.23	0.35	0.20	0.23	0.17
Cr	0.02	0.00	0.00	0.01	0.00	0.00	0.00	0.00
Fe	0.19	0.22	0.35	0.20	0.21	0.21	0.23	0.21
Mn	0.00	0.00	0.01	0.00	0.00	0.00	0.00	0.00
Mg	0.77	0.68	0.66	0.77	0.69	0.78	0.72	0.80
Ca	0.92	0.90	0.88	0.86	0.90	0.87	0.91	0.89
Na	0.03	0.05	0.03	0.04	0.04	0.03	0.02	0.02
K	0.00	0.00	0.00	0.00	0.00	0.00	0.00	0.00
Ni	0.00	0.00	0.00	0.00	0.00	0.00	0.00	0.00
Total	4.02	4.02	4.01	4.01	4.02	4.00	4.00	4.01
Mg#	79.95	75.35	65.30	79.77	76.45	78.39	75.90	79.47
$D^{(cpx\text{-}melt)}_{H2O}$	0.0193	0.0312	0.0101	0.0172	0.0289	0.0150	0.0180	0.0136
Absorbance of cpx (cm^{-1})	2.7	5.9	2.7	4.9	4.3	4.1	4.7	10.0
Thickness of cpx (0.001mm)	108	109	125	104	121	123	120	118
Absorbance normalized to 1 cm (cm^{-1})	250	248	472	260	355	333	392	847
H_2O-cpx (ppm)	106	105	200	110	150	141	166	359
H_2O-melt (wt%)	0.55	0.34	1.98	0.64	0.52	0.94	0.92	2.64

Sample No. Section No. Point No.	27	28	29	30	31	32	33	34
SiO_2	51.15	49.97	51.48	50.31	48.68	49.04	48.43	50.63
TiO_2	1.00	1.60	1.23	1.46	1.59	1.85	2.20	1.11
Al_2O3	4.28	4.51	4.13	3.72	6.25	4.91	6.20	3.68
Cr_2O3	0.56	0.94	0.22	0.18	0.00	0.76	0.30	0.22
FeO	5.48	5.75	6.13	6.34	10.04	5.92	6.85	6.40
MnO	0.00	0.06	0.02	0.00	0.01	0.00	0.04	0.03
MgO	14.62	13.91	14.70	14.87	11.60	13.96	13.23	14.48
CaO	21.65	23.25	21.11	22.26	21.21	23.19	22.66	22.24
Na_2O	0.54	0.39	0.50	0.32	0.89	0.28	0.43	0.30
K_2O	0.00	0.00	0.00	0.01	0.00	0.00	0.00	0.01
NiO	0.00	0.06	0.02	0.00	0.01	0.00	0.04	0.03
Total	99.29	100.45	99.54	99.47	100.26	99.91	100.37	99.12
Si	1.89	1.85	1.90	1.87	1.82	1.82	1.80	1.89
Ti	0.03	0.04	0.03	0.04	0.04	0.05	0.06	0.03
Al	0.19	0.20	0.18	0.16	0.28	0.22	0.27	0.16
Cr	0.02	0.03	0.01	0.01	0.00	0.02	0.01	0.01
Fe	0.17	0.18	0.19	0.20	0.31	0.18	0.21	0.20
Mn	0.00	0.00	0.00	0.00	0.00	0.00	0.00	0.00
Mg	0.81	0.77	0.81	0.82	0.65	0.77	0.73	0.81
Ca	0.86	0.92	0.83	0.89	0.85	0.92	0.90	0.89
Na	0.04	0.03	0.04	0.02	0.06	0.02	0.03	0.02
K	0.00	0.00	0.00	0.00	0.00	0.00	0.00	0.00
Ni	0.00	0.00	0.00	0.00	0.00	0.00	0.00	0.00
Total	4.00	4.01	3.99	4.02	4.03	4.02	4.02	4.01
Mg#	82.62	81.18	81.04	80.69	67.32	80.78	77.51	80.15
$D^{(cpx\text{-}melt)}_{H2O}$	0.0128	0.0162	0.0125	0.0143	0.0201	0.0187	0.0229	0.0127
Absorbance of cpx (cm^{-1})	2.6	4.2	3.0	8.2	11.0	8.0	3.9	4.5
Thickness of cpx (0.001mm)	119	123	115	118	104	116	85	107
Absorbance normalized to 1 cm (cm^{-1})	218	341	261	695	1058	690	459	421
H_2O-cpx (ppm)	92	144	110	294	448	292	194	178
H_2O-melt (wt%)	0.72	0.89	0.88	2.06	2.22	1.56	0.85	1.40

Sample No.							
Section No.							
Point No.	35	36	36.2	37	38	38.2	39
SiO_2	46.97	49.20	51.74	50.86	50.48	49.24	49.75
TiO_2	2.78	1.71	1.02	1.35	1.11	1.49	1.86
Al_2O3	6.65	6.08	3.79	3.44	5.30	5.62	4.08
Cr_2O3	0.46	0.06	0.14	0.69	0.45	0.49	0.11
FeO	6.80	7.67	7.02	5.71	5.92	6.33	6.47
MnO	0.05	0.00	0.01	0.04	0.06	0.01	0.07
MgO	12.47	13.52	15.12	14.57	14.23	14.21	14.02
CaO	23.09	20.61	20.80	22.64	21.60	21.85	23.36
Na_2O	0.41	0.52	0.40	0.30	0.59	0.55	0.22
K_2O	0.00	0.01	0.00	0.00	0.02	0.01	0.00
NiO	0.05	0.00	0.01	0.04	0.06	0.01	0.07
Total	99.74	99.37	100.04	99.64	99.80	99.80	99.99
Si	1.76	1.83	1.90	1.89	1.86	1.83	1.85
Ti	0.08	0.05	0.03	0.04	0.03	0.04	0.05
Al	0.29	0.27	0.16	0.15	0.23	0.25	0.18
Cr	0.01	0.00	0.00	0.02	0.01	0.01	0.00
Fe	0.21	0.24	0.22	0.18	0.18	0.20	0.20
Mn	0.00	0.00	0.00	0.00	0.00	0.00	0.00
Mg	0.70	0.75	0.83	0.81	0.78	0.79	0.78
Ca	0.93	0.82	0.82	0.90	0.85	0.87	0.93
Na	0.03	0.04	0.03	0.02	0.04	0.04	0.02
K	0.00	0.00	0.00	0.00	0.00	0.00	0.00
Ni	0.00	0.00	0.00	0.00	0.00	0.00	0.00
Total	4.02	4.00	4.00	4.00	4.00	4.02	4.01
Mg#	76.57	75.87	79.35	81.99	81.09	80.00	79.43
$D^{(cpx\text{-}melt)}_{H2O}$	0.0278	0.0195	0.0123	0.0128	0.0155	0.0193	0.0156
Absorbance of cpx (cm^{-1})	4.7	6.3	8.0	9.6	6.5	4.1	3.8
Thickness of cpx (0.001mm)	107	97	97	98	99	99	96
Absorbance normalized to 1 cm (cm^{-1})	439	649	825	980	657	414	396
H_2O-cpx (ppm)	186	275	349	414	278	175	167
H_2O-melt (wt%)	0.67	1.41	2.83	3.24	1.80	0.91	1.07

Sample No.	SH-3							
Section No.	1							
Point No.	1	2	3	4	5	6	7	8
SiO_2	50.99	48.00	50.52	45.86	49.73	46.18	50.40	49.83
TiO_2	1.36	2.24	1.35	3.26	1.89	2.76	1.38	2.27
Al_2O3	3.13	6.17	4.36	7.51	4.15	7.77	3.94	4.48
Cr_2O3	0.53	0.18	0.74	0.11	0.20	0.48	0.29	0.08
FeO	5.50	7.00	5.53	7.68	7.06	6.69	6.25	6.96
MnO	0.00	0.00	0.00	0.03	0.11	0.00	0.00	0.02
MgO	14.80	12.82	14.42	11.91	13.96	12.21	14.69	13.50
CaO	22.92	22.72	22.86	22.70	22.39	22.48	22.11	22.97
Na_2O	0.31	0.37	0.47	0.41	0.31	0.52	0.38	0.27
K_2O	0.00	0.00	0.00	0.01	0.00	0.01	0.01	0.00
NiO	0.00	0.00	0.00	0.03	0.11	0.00	0.00	0.02
Total	99.54	99.51	100.23	99.50	99.90	99.10	99.44	100.39
Si	1.89	1.80	1.86	1.73	1.85	1.74	1.87	1.85
Ti	0.04	0.06	0.04	0.09	0.05	0.08	0.04	0.06
Al	0.14	0.27	0.19	0.33	0.18	0.35	0.17	0.20
Cr	0.02	0.01	0.02	0.00	0.01	0.01	0.01	0.00
Fe	0.17	0.22	0.17	0.24	0.22	0.21	0.19	0.22
Mn	0.00	0.00	0.00	0.00	0.00	0.00	0.00	0.00
Mg	0.82	0.72	0.79	0.67	0.78	0.69	0.81	0.75
Ca	0.91	0.91	0.90	0.92	0.89	0.91	0.88	0.91
Na	0.02	0.03	0.03	0.03	0.02	0.04	0.03	0.02
K	0.00	0.00	0.00	0.00	0.00	0.00	0.00	0.00
Ni	0.00	0.00	0.00	0.00	0.00	0.00	0.00	0.00
Total	4.01	4.01	4.01	4.02	4.01	4.02	4.01	4.00
Mg#	82.76	76.55	82.30	73.46	77.89	76.50	80.74	77.57
$D^{(cpx\text{-}melt)}_{H2O}$	0.0122	0.0225	0.0149	0.0345	0.0160	0.0328	0.0142	0.0164
Absorbance of cpx (cm^{-1})	9.0	14.0	11.0	12.0	6.8	12.9	10.5	7.5
Thickness of cpx (0.001mm)	81	88	82	82	88	88	83	86
Absorbance normalized to 1 cm (cm^{-1})	1111	1591	1341	1463	773	1466	1265	872
H_2O-cpx (ppm)	470	673	568	619	327	620	535	369
H_2O-melt (wt%)	3.84	2.99	3.82	1.80	2.05	1.89	3.78	2.25

Sample No. Section No. Point No.	9	10	12	13	14	15	16	17
SiO_2	49.83	49.84	47.71	47.25	51.12	49.18	49.09	47.02
TiO_2	2.27	1.45	2.66	2.59	1.03	1.83	1.48	2.92
Al_2O3	4.48	5.58	5.48	6.24	4.58	4.82	5.23	6.53
Cr_2O3	0.08	0.24	0.02	0.08	0.57	0.20	0.43	0.47
FeO	6.96	6.49	7.41	7.95	5.04	7.18	6.02	7.02
MnO	0.02	0.08	0.02	0.10	0.03	0.08	0.03	0.03
MgO	13.50	14.17	12.44	12.87	14.81	14.00	13.80	12.59
CaO	22.97	21.21	22.87	21.63	21.89	21.41	22.59	22.57
Na_2O	0.27	0.54	0.49	0.46	0.50	0.43	0.42	0.40
K_2O	0.00	0.00	0.00	0.02	0.01	0.00	0.01	0.00
NiO	0.02	0.08	0.02	0.10	0.03	0.08	0.03	0.03
Total	100.39	99.67	99.12	99.28	99.61	99.20	99.11	99.59
Si	1.85	1.85	1.80	1.78	1.88	1.84	1.84	1.76
Ti	0.06	0.04	0.08	0.07	0.03	0.05	0.04	0.08
Al	0.20	0.24	0.24	0.28	0.20	0.21	0.23	0.29
Cr	0.00	0.01	0.00	0.00	0.02	0.01	0.01	0.01
Fe	0.22	0.20	0.23	0.25	0.16	0.22	0.19	0.22
Mn	0.00	0.00	0.00	0.00	0.00	0.00	0.00	0.00
Mg	0.75	0.78	0.70	0.72	0.81	0.78	0.77	0.70
Ca	0.91	0.84	0.92	0.87	0.86	0.86	0.91	0.91
Na	0.02	0.04	0.04	0.03	0.04	0.03	0.03	0.03
K	0.00	0.00	0.00	0.00	0.00	0.00	0.00	0.00
Ni	0.00	0.00	0.00	0.00	0.00	0.00	0.00	0.00
Total	4.00	4.01	4.02	4.02	4.00	4.01	4.02	4.02
Mg#	77.57	79.56	74.95	74.27	83.98	77.65	80.33	76.18
$D^{(cpx\text{-}melt)}_{H2O}$	0.0164	0.0175	0.0217	0.0260	0.0135	0.0178	0.0177	0.0279
Absorbance of cpx (cm^{-1})	13.3	13.4	13.0	18.0	13.9	13.0	16.0	9.0
Thickness of cpx (0.001mm)	86	89	96	96	98	98	96	85
Absorbance normalized to 1 cm (cm^{-1})	1547	1506	1354	1875	1418	1327	1667	1059
H_2O-cpx (ppm)	654	637	573	793	600	561	705	448
H_2O-melt (wt%)	3.98	3.64	2.64	3.06	4.44	3.16	3.99	1.60

Sample No.								
Section No.								
Point No.	18	19	20	21	22	22.1	23	24
SiO_2	51.04	47.94	49.67	50.17	49.10	50.78	48.98	50.09
TiO_2	1.39	2.25	1.46	1.45	1.89	1.38	2.11	1.52
Al_2O3	4.48	7.11	5.04	4.82	4.97	4.09	4.76	5.02
Cr_2O3	0.12	0.42	0.40	0.51	0.08	0.16	0.05	0.03
FeO	6.98	6.99	6.27	6.33	8.01	6.72	8.04	7.65
MnO	0.10	0.03	0.04	0.01	0.08	0.04	0.01	0.05
MgO	14.61	12.97	14.35	14.27	13.88	14.77	13.54	14.21
CaO	20.82	20.84	21.89	21.35	21.19	21.67	21.68	20.92
Na_2O	0.47	0.66	0.50	0.48	0.44	0.43	0.36	0.54
K_2O	0.01	0.00	0.00	0.00	0.01	0.01	0.00	0.00
NiO	0.10	0.03	0.04	0.01	0.08	0.04	0.01	0.05
Total	100.11	99.23	99.65	99.38	99.71	100.09	99.55	100.07
Si	1.88	1.79	1.84	1.86	1.83	1.88	1.83	1.86
Ti	0.04	0.06	0.04	0.04	0.05	0.04	0.06	0.04
Al	0.19	0.31	0.22	0.21	0.22	0.18	0.21	0.22
Cr	0.00	0.01	0.01	0.01	0.00	0.00	0.00	0.00
Fe	0.21	0.22	0.19	0.20	0.25	0.21	0.25	0.24
Mn	0.00	0.00	0.00	0.00	0.00	0.00	0.00	0.00
Mg	0.80	0.72	0.79	0.79	0.77	0.81	0.76	0.78
Ca	0.82	0.83	0.87	0.85	0.85	0.86	0.87	0.83
Na	0.03	0.05	0.04	0.03	0.03	0.03	0.03	0.04
K	0.00	0.00	0.00	0.00	0.00	0.00	0.00	0.00
Ni	0.00	0.00	0.00	0.00	0.00	0.00	0.00	0.00
Total	4.00	4.01	4.02	4.00	4.02	4.01	4.01	4.01
Mg#	78.88	76.79	80.33	80.06	75.56	79.68	75.02	76.81
$D^{(cpx\text{-}melt)}_{H2O}$	0.0143	0.0253	0.0172	0.0157	0.0188	0.0143	0.0184	0.0168
Absorbance of cpx (cm^{-1})	11.0	17.0	13.0	12.0	17.0	13.5	15.0	17.0
Thickness of cpx (0.001mm)	105	105	106	105	106	106	106	112
Absorbance normalized to 1 cm (cm^{-1})	1048	1619	1226	1143	1604	1274	1415	1518
H_2O-cpx (ppm)	443	685	519	484	679	539	599	642
H_2O-melt (wt%)	3.11	2.70	3.01	3.09	3.61	3.78	3.25	3.83

Sample No. Section No. Point No.	25	26	27	28	29	30	31	32
SiO_2	51.77	51.00	50.18	46.94	50.51	52.03	48.97	49.84
TiO_2	0.97	0.94	1.24	2.90	1.08	1.08	1.75	1.64
Al_2O3	3.59	4.44	4.49	5.91	3.90	3.57	5.06	4.32
Cr_2O3	0.66	0.60	0.75	0.00	0.38	0.29	0.41	0.15
FeO	5.00	5.24	5.84	7.37	5.75	5.92	6.39	6.01
MnO	0.01	0.05	0.05	0.04	0.00	0.03	0.00	0.04
MgO	15.06	15.25	14.69	12.26	15.03	15.30	13.48	13.61
CaO	22.82	21.74	21.39	22.94	21.95	21.34	23.37	23.03
Na_2O	0.38	0.59	0.56	0.48	0.46	0.40	0.35	0.33
K_2O	0.00	0.00	0.00	0.00	0.01	0.00	0.00	0.00
NiO	0.01	0.05	0.05	0.04	0.00	0.03	0.00	0.04
Total	100.25	99.90	99.23	98.89	99.08	99.99	99.77	99.00
Si	1.90	1.88	1.87	1.78	1.88	1.91	1.83	1.87
Ti	0.03	0.03	0.03	0.08	0.03	0.03	0.05	0.05
Al	0.16	0.19	0.20	0.26	0.17	0.15	0.22	0.19
Cr	0.02	0.02	0.02	0.00	0.01	0.01	0.01	0.00
Fe	0.15	0.16	0.18	0.23	0.18	0.18	0.20	0.19
Mn	0.00	0.00	0.00	0.00	0.00	0.00	0.00	0.00
Mg	0.82	0.84	0.81	0.69	0.83	0.84	0.75	0.76
Ca	0.90	0.86	0.85	0.93	0.88	0.84	0.93	0.92
Na	0.03	0.04	0.04	0.04	0.03	0.03	0.03	0.02
K	0.00	0.00	0.00	0.00	0.00	0.00	0.00	0.00
Ni	0.00	0.00	0.00	0.00	0.00	0.00	0.00	0.00
Total	4.00	4.01	4.01	4.02	4.02	3.99	4.02	4.00
Mg#	84.31	83.84	81.76	74.78	82.33	82.17	79.01	80.16
$D^{(cpx\text{-}melt)}_{H2O}$	0.0119	0.0142	0.0154	0.0248	0.0137	0.0116	0.0183	0.0143
Absorbance of cpx (cm^{-1})	14.0	14.0	16.0	12.0	13.8	11.3	14.8	14.0
Thickness of cpx (0.001mm)	108	113	113	116	114	112	116	115
Absorbance normalized to 1 cm (cm^{-1})	1296	1239	1416	1034	1211	1006	1276	1217
H_2O-cpx (ppm)	549	524	599	438	512	426	540	515
H_2O-melt (wt%)	4.62	3.69	3.90	1.76	3.75	3.66	2.95	3.60

Sample No.	SH-4						
Section No.	2						
Point No.	1	2	3	4	5	7	8
SiO_2	50.52	48.33	45.42	51.62	46.65	46.19	48.47
TiO_2	1.65	1.89	3.45	0.80	2.96	3.14	2.29
Al_2O3	3.75	6.10	7.91	3.66	7.11	7.10	4.92
Cr_2O3	0.10	0.08	0.01	0.40	0.52	0.20	0.09
FeO	6.87	6.53	8.44	6.09	6.48	6.39	7.83
MnO	0.08	0.04	0.04	0.08	0.08	0.09	0.09
MgO	14.42	13.56	10.87	15.55	11.96	12.22	13.40
CaO	21.95	22.25	22.87	20.88	22.77	23.39	22.48
Na_2O	0.37	0.59	0.53	0.53	0.42	0.41	0.33
K_2O	0.00	0.00	0.01	0.00	0.01	0.00	0.00
NiO	0.00	0.00	0.03	0.07	0.00	0.00	0.00
Total	99.69	99.36	99.56	99.69	98.96	99.15	99.89
Si	1.88	1.81	1.72	1.90	1.76	1.74	1.82
Ti	0.05	0.05	0.10	0.02	0.08	0.09	0.06
Al	0.16	0.27	0.35	0.16	0.32	0.32	0.22
Cr	0.00	0.00	0.00	0.01	0.02	0.01	0.00
Fe	0.21	0.20	0.27	0.19	0.20	0.20	0.25
Mn	0.00	0.00	0.00	0.00	0.00	0.00	0.00
Mg	0.80	0.76	0.61	0.86	0.67	0.69	0.75
Ca	0.87	0.89	0.93	0.82	0.92	0.95	0.90
Na	0.03	0.04	0.04	0.04	0.03	0.03	0.02
K	0.00	0.00	0.00	0.00	0.00	0.00	0.00
Ni	0.00	0.00	0.00	0.00	0.00	0.00	0.00
Total	4.01	4.03	4.02	4.01	4.01	4.02	4.02
Mg#	78.90	78.75	69.66	81.99	76.70	77.33	75.31
$D^{(cpx\text{-}melt)}_{H2O}$	0.0138	0.0216	0.0363	0.0123	0.0285	0.0309	0.0202
Absorbance of cpx (cm^{-1})	7.0	11.0	13.1	12.1	11.9	10.6	11.0
Thickness of cpx (0.001mm)	83	117	128	129	130	123	132
Absorbance normalized to 1 cm (cm^{-1})	842	940	1023	938	915	862	832
H_2O-cpx (ppm)	356	398	433	397	387	365	352
H_2O-melt (wt%)	2.57	1.84	1.19	3.24	1.36	1.18	1.74

Sample No. Section No. Point No.	9	10	11	13	14	15	16	17
SiO_2	50.19	51.27	45.85	49.66	50.47	49.72	50.10	47.30
TiO_2	1.63	1.00	3.26	0.61	1.30	1.58	1.43	2.64
Al_2O3	4.30	4.58	8.44	5.62	3.78	5.99	4.66	5.54
Cr_2O3	0.25	0.61	0.21	0.02	0.08	0.07	0.41	0.04
FeO	6.45	5.39	7.56	9.05	6.24	6.96	6.22	9.10
MnO	0.14	0.09	0.04	0.14	0.10	0.06	0.07	0.12
MgO	14.03	14.89	11.29	11.55	14.63	13.95	14.59	12.65
CaO	22.41	21.43	21.33	21.80	22.48	20.57	21.87	21.75
Na_2O	0.31	0.55	0.51	0.60	0.40	0.72	0.49	0.40
K_2O	0.01	0.00	0.01	0.00	0.00	0.00	0.00	0.00
NiO	0.02	0.04	0.04	0.04	0.02	0.03	0.03	0.00
Total	99.73	99.84	98.52	99.10	99.49	99.65	99.85	99.53
Si	1.86	1.89	1.74	1.87	1.88	1.84	1.86	1.79
Ti	0.05	0.03	0.09	0.02	0.04	0.04	0.04	0.08
Al	0.19	0.20	0.38	0.25	0.17	0.26	0.20	0.25
Cr	0.01	0.02	0.01	0.00	0.00	0.00	0.01	0.00
Fe	0.20	0.17	0.24	0.29	0.19	0.22	0.19	0.29
Mn	0.00	0.00	0.00	0.00	0.00	0.00	0.00	0.00
Mg	0.78	0.82	0.64	0.65	0.81	0.77	0.81	0.71
Ca	0.89	0.84	0.87	0.88	0.90	0.82	0.87	0.88
Na	0.02	0.04	0.04	0.04	0.03	0.05	0.04	0.03
K	0.00	0.00	0.00	0.00	0.00	0.00	0.00	0.00
Ni	0.00	0.00	0.00	0.00	0.00	0.00	0.00	0.00
Total	4.00	4.00	4.00	4.01	4.02	4.01	4.01	4.03
Mg#	79.49	83.12	72.69	69.46	80.71	78.13	80.71	71.24
$D^{(cpx\text{-}melt)}_{H2O}$	0.0148	0.0136	0.0347	0.0142	0.0135	0.0185	0.0161	0.0245
Absorbance of cpx (cm^{-1})	6.4	10.3	12.9	11.0	6.4	9.8	9.7	6.5
Thickness of cpx (0.001mm)	129	116	120	108	105	89	97	94
Absorbance normalized to 1 cm (cm^{-1})	492	888	1075	1021	610	1104	999	688
H_2O-cpx (ppm)	208	376	455	432	258	467	423	291
H_2O-melt (wt%)	1.41	2.77	1.31	3.05	1.90	2.53	2.63	1.19

Sample No.								SH-5
Section No.								2
Point No.	18	19	20	21	22	23	24	1
SiO_2	50.23	48.78	49.91	50.92	50.01	49.67	48.81	50.76
TiO_2	1.04	1.85	1.63	0.77	1.30	2.18	2.06	1.68
Al_2O3	5.09	5.01	4.80	3.94	5.08	4.04	5.45	3.81
Cr_2O3	0.03	0.84	0.37	0.24	0.36	0.04	0.24	0.08
FeO	6.74	5.55	6.58	6.21	6.25	7.66	6.78	6.84
MnO	0.07	0.05	0.12	0.06	0.14	0.09	0.04	0.06
MgO	13.84	13.51	14.03	15.00	14.11	13.53	13.53	14.65
CaO	21.81	23.34	21.69	21.41	21.75	22.39	22.35	21.92
Na_2O	0.70	0.38	0.48	0.49	0.51	0.35	0.48	0.35
K_2O	0.00	0.00	0.02	0.01	0.00	0.01	0.01	0.00
NiO	0.05	0.01	0.00	0.00	0.00	0.00	0.02	0.04
Total	99.60	99.31	99.62	99.05	99.51	99.94	99.76	100.18
Si	1.87	1.82	1.86	1.89	1.86	1.85	1.82	1.88
Ti	0.03	0.05	0.05	0.02	0.04	0.06	0.06	0.05
Al	0.22	0.22	0.21	0.17	0.22	0.18	0.24	0.17
Cr	0.00	0.02	0.01	0.01	0.01	0.00	0.01	0.00
Fe	0.21	0.17	0.20	0.19	0.19	0.24	0.21	0.21
Mn	0.00	0.00	0.00	0.00	0.00	0.00	0.00	0.00
Mg	0.77	0.75	0.78	0.83	0.78	0.75	0.75	0.81
Ca	0.87	0.94	0.86	0.85	0.87	0.90	0.89	0.87
Na	0.05	0.03	0.03	0.04	0.04	0.03	0.03	0.02
K	0.00	0.00	0.00	0.00	0.00	0.00	0.00	0.00
Ni	0.00	0.00	0.00	0.00	0.00	0.00	0.00	0.00
Total	4.02	4.01	4.01	4.01	4.01	4.01	4.02	4.01
Mg#	78.55	81.27	79.18	81.16	80.10	75.89	78.06	79.24
$D^{(cpx\text{-}melt)}_{H2O}$	0.0150	0.0184	0.0162	0.0127	0.0160	0.0159	0.0198	0.0141
Absorbance of cpx (cm^{-1})	10.6	9.5	8.9	8.0	11.1	10.9	9.1	3.4
Thickness of cpx (0.001mm)	94	83	107	99	110	102	93	85
Absorbance normalized to 1 cm (cm^{-1})	1128	1141	836	803	1008	1066	982	400
H_2O-cpx (ppm)	477	483	354	340	427	451	415	169
H_2O-melt (wt%)	3.18	2.63	2.18	2.68	2.67	2.84	2.10	1.20

Sample No.								
Section No.								
Point No.	2	3	4	5	6	7	8	9
SiO_2	49.89	50.17	49.79	50.13	48.86	52.96	50.33	51.99
TiO_2	1.57	1.36	1.70	1.51	1.91	0.20	1.35	0.86
Al_2O3	3.92	5.08	4.15	5.13	4.60	2.28	3.38	3.44
Cr_2O3	0.20	0.51	0.13	0.28	0.36	0.11	0.67	0.38
FeO	6.78	6.08	6.74	6.44	6.52	5.15	5.09	5.52
MnO	0.25	0.11	0.07	0.04	0.07	0.14	0.11	0.04
MgO	13.98	14.52	14.06	14.07	13.52	15.17	14.64	15.42
CaO	22.06	21.86	21.79	21.28	22.95	23.95	23.32	21.15
Na_2O	0.32	0.50	0.43	0.64	0.33	0.37	0.28	0.48
K_2O	0.00	0.00	0.01	0.00	0.02	0.00	0.00	0.00
NiO	0.19	0.00	0.02	0.05	0.01	0.07	0.03	0.08
Total	99.17	100.18	98.89	99.55	99.15	100.39	99.20	99.35
Si	1.87	1.85	1.87	1.86	1.84	1.94	1.88	1.92
Ti	0.04	0.04	0.05	0.04	0.05	0.01	0.04	0.02
Al	0.17	0.22	0.18	0.22	0.20	0.10	0.15	0.15
Cr	0.01	0.01	0.00	0.01	0.01	0.00	0.02	0.01
Fe	0.21	0.19	0.21	0.20	0.20	0.16	0.16	0.17
Mn	0.01	0.00	0.00	0.00	0.00	0.00	0.00	0.00
Mg	0.78	0.80	0.79	0.78	0.76	0.83	0.81	0.85
Ca	0.89	0.86	0.88	0.85	0.92	0.94	0.93	0.84
Na	0.02	0.04	0.03	0.05	0.02	0.03	0.02	0.03
K	0.00	0.00	0.00	0.00	0.00	0.00	0.00	0.00
Ni	0.01	0.00	0.00	0.00	0.00	0.00	0.00	0.00
Total	4.01	4.01	4.01	4.01	4.02	4.01	4.01	3.99
Mg#	78.63	80.99	78.83	79.57	78.71	84.01	83.68	83.29
$D^{(cpx\text{-}melt)}_{H2O}$	0.0145	0.0167	0.0149	0.0161	0.0174	0.0084	0.0132	0.0111
Absorbance of cpx (cm^{-1})	3.7	6.0	4.3	4.6	4.0	2.4	4.4	5.2
Thickness of cpx (0.001mm)	85	76	77	85	85	75	94	91
Absorbance normalized to 1 cm (cm^{-1})	434	788	558	538	466	320	468	569
H_2O-cpx (ppm)	184	333	236	227	197	135	198	241
H_2O-melt (wt%)	1.27	1.99	1.59	1.42	1.14	1.60	1.51	2.18

Sample No. Section No. Point No.	10	11	11.1	12	13	14	15	16
SiO_2	47.06	50.40	50.42	48.22	47.51	50.72	49.13	50.82
TiO_2	3.11	1.57	1.72	2.44	2.29	1.29	2.27	1.66
Al_2O3	6.65	3.88	3.65	6.40	6.04	4.31	4.69	3.87
Cr_2O3	0.10	0.43	0.35	0.41	1.12	0.42	0.06	0.13
FeO	7.65	5.85	6.45	6.32	6.13	5.71	6.75	6.62
MnO	0.11	0.10	0.08	0.06	0.08	0.09	0.11	0.07
MgO	11.94	14.12	14.64	12.79	13.17	14.73	13.33	14.65
CaO	22.97	22.47	22.26	22.62	22.99	21.56	23.09	22.14
Na_2O	0.57	0.36	0.28	0.40	0.40	0.47	0.28	0.35
K_2O	0.01	0.00	0.00	0.00	0.00	0.00	0.00	0.00
NiO	0.00	0.05	0.05	0.02	0.00	0.07	0.00	0.00
Total	100.18	99.22	99.90	99.69	99.71	99.37	99.72	100.30
Si	1.76	1.88	1.87	1.80	1.78	1.88	1.83	1.88
Ti	0.09	0.04	0.05	0.07	0.06	0.04	0.06	0.05
Al	0.29	0.17	0.16	0.28	0.27	0.19	0.21	0.17
Cr	0.00	0.01	0.01	0.01	0.03	0.01	0.00	0.00
Fe	0.24	0.18	0.20	0.20	0.19	0.18	0.21	0.20
Mn	0.00	0.00	0.00	0.00	0.00	0.00	0.00	0.00
Mg	0.67	0.78	0.81	0.71	0.73	0.81	0.74	0.81
Ca	0.92	0.90	0.88	0.90	0.92	0.86	0.92	0.88
Na	0.04	0.03	0.02	0.03	0.03	0.03	0.02	0.02
K	0.00	0.00	0.00	0.00	0.00	0.00	0.00	0.00
Ni	0.00	0.00	0.00	0.00	0.00	0.00	0.00	0.00
Total	4.02	4.00	4.01	4.00	4.02	4.00	4.01	4.01
Mg#	73.57	81.15	80.18	78.30	79.29	82.14	77.86	79.79
$D^{(cpx\text{-}melt)}_{H2O}$	0.0278	0.0135	0.0144	0.0227	0.0252	0.0139	0.0174	0.0141
Absorbance of cpx (cm^{-1})	2.3	3.3	3.4	3.8	4.0	2.5	3.1	3.3
Thickness of cpx (0.001mm)	80	74	74	75	74	74	74	84
Absorbance normalized to 1 cm (cm^{-1})	288	446	459	507	534	338	419	392
H_2O-cpx (ppm)	122	189	194	214	226	143	177	166
H_2O-melt (wt%)	0.44	1.40	1.35	0.94	0.90	1.03	1.02	1.18

Sample No.								
Section No.								
Point No.	17	18	19	20	21	22	23	24
SiO_2	49.87	47.59	51.26	48.20	50.48	49.60	46.39	44.09
TiO_2	1.49	2.22	1.32	2.34	1.46	1.69	2.91	4.19
Al_2O3	4.35	6.92	3.22	5.16	3.47	5.01	7.30	9.00
Cr_2O3	0.73	0.05	0.57	0.00	0.52	0.44	0.14	0.21
FeO	5.20	6.66	5.01	7.53	5.60	5.96	6.68	7.53
MnO	0.02	0.08	0.05	0.13	0.13	0.08	0.08	0.07
MgO	14.45	13.02	14.93	12.13	14.46	13.87	12.29	11.00
CaO	23.05	22.25	23.15	22.67	23.16	21.88	23.32	22.72
Na_2O	0.43	0.58	0.32	0.48	0.32	0.52	0.40	0.53
K_2O	0.00	0.00	0.00	0.00	0.01	0.01	0.00	0.00
NiO	0.07	0.02	0.00	0.04	0.00	0.03	0.00	0.01
Total	99.65	99.38	99.83	98.66	99.59	99.08	99.51	99.34
Si	1.85	1.78	1.89	1.83	1.88	1.85	1.74	1.67
Ti	0.04	0.06	0.04	0.07	0.04	0.05	0.08	0.12
Al	0.19	0.31	0.14	0.23	0.15	0.22	0.32	0.40
Cr	0.02	0.00	0.02	0.00	0.02	0.01	0.00	0.01
Fe	0.16	0.21	0.15	0.24	0.17	0.19	0.21	0.24
Mn	0.00	0.00	0.00	0.00	0.00	0.00	0.00	0.00
Mg	0.80	0.73	0.82	0.69	0.80	0.77	0.69	0.62
Ca	0.92	0.89	0.92	0.92	0.92	0.87	0.94	0.92
Na	0.03	0.04	0.02	0.04	0.02	0.04	0.03	0.04
K	0.00	0.00	0.00	0.00	0.00	0.00	0.00	0.00
Ni	0.00	0.00	0.00	0.00	0.00	0.00	0.00	0.00
Total	4.02	4.02	4.00	4.01	4.01	4.00	4.02	4.02
Mg#	83.22	77.72	84.17	74.18	82.17	80.60	76.62	72.26
$D^{(cpx\text{-}melt)}_{H2O}$	0.0157	0.0254	0.0120	0.0184	0.0133	0.0165	0.0309	0.0503
Absorbance of cpx (cm^{-1})	4.1	4.0	3.7	3.1	4.1	6.6	3.4	4.5
Thickness of cpx (0.001mm)	85	76	77	87	81	75	73	75
Absorbance normalized to 1 cm (cm^{-1})	482	526	481	356	506	880	466	600
H_2O-cpx (ppm)	204	223	203	151	214	372	197	254
H_2O-melt (wt%)	1.30	0.88	1.69	0.82	1.62	2.25	0.64	0.50

Sample No. Section No. Point No.	25	26	27	28	29	30	31	32
SiO_2	49.12	49.70	49.72	47.95	51.12	50.81	50.48	47.62
TiO_2	1.12	1.76	1.51	1.40	1.24	1.31	1.50	2.59
Al_2O3	7.81	3.90	4.51	6.57	3.18	3.33	4.50	6.79
Cr_2O3	0.09	0.19	0.49	0.02	0.32	0.33	0.27	0.09
FeO	7.68	5.90	6.16	9.26	5.29	5.81	5.36	7.12
MnO	0.08	0.06	0.06	0.10	0.07	0.12	0.11	0.05
MgO	11.36	13.82	14.44	11.73	14.84	14.88	14.39	12.67
CaO	21.50	23.40	21.61	21.74	22.98	22.52	22.42	22.00
Na_2O	1.14	0.27	0.49	0.58	0.35	0.30	0.43	0.44
K_2O	0.00	0.00	0.00	0.01	0.00	0.00	0.01	0.01
NiO	0.02	0.06	0.01	0.03	0.00	0.03	0.04	0.00
Total	99.92	99.06	99.00	99.38	99.39	99.43	99.51	99.36
Si	1.83	1.86	1.86	1.81	1.90	1.89	1.87	1.78
Ti	0.03	0.05	0.04	0.04	0.03	0.04	0.04	0.07
Al	0.34	0.17	0.20	0.29	0.14	0.15	0.20	0.30
Cr	0.00	0.01	0.01	0.00	0.01	0.01	0.01	0.00
Fe	0.24	0.18	0.19	0.29	0.16	0.18	0.17	0.22
Mn	0.00	0.00	0.00	0.00	0.00	0.00	0.00	0.00
Mg	0.63	0.77	0.80	0.66	0.82	0.82	0.79	0.71
Ca	0.86	0.94	0.86	0.88	0.91	0.90	0.89	0.88
Na	0.08	0.02	0.04	0.04	0.03	0.02	0.03	0.03
K	0.00	0.00	0.00	0.00	0.00	0.00	0.00	0.00
Ni	0.00	0.00	0.00	0.00	0.00	0.00	0.00	0.00
Total	4.01	4.01	4.01	4.02	4.01	4.01	4.00	4.01
Mg#	72.51	80.68	80.70	69.30	83.33	82.04	82.72	76.02
$D^{(cpx\text{-}melt)}_{H2O}$	0.0197	0.0144	0.0160	0.0212	0.0117	0.0126	0.0144	0.0252
Absorbance of cpx (cm^{-1})	5.5	2.7	4.4	3.7	3.4	2.7	4.7	3.8
Thickness of cpx (0.001mm)	69	72	76	72	69	70	73	77
Absorbance normalized to 1 cm (cm^{-1})	791	375	579	514	493	389	644	494
H_2O-cpx (ppm)	335	159	245	217	208	164	272	209
H_2O-melt (wt%)	1.70	1.11	1.53	1.03	1.78	1.30	1.90	0.83

Sample No.								
Section No.								
Point No.	32.1	33	34	35	36	37	38	39
SiO_2	45.77	51.22	50.79	49.87	47.53	49.76	48.94	50.45
TiO_2	3.04	0.68	1.44	1.53	2.74	2.33	1.42	1.56
Al_2O3	7.82	3.68	4.57	5.34	5.20	3.96	6.67	4.40
Cr_2O3	0.08	0.56	0.27	0.12	0.02	0.04	0.00	0.15
FeO	7.60	5.09	6.04	6.73	7.88	7.32	8.02	6.49
MnO	0.10	0.11	0.03	0.06	0.13	0.09	0.08	0.03
MgO	12.26	15.22	14.63	13.92	12.82	13.16	12.04	14.28
CaO	21.85	22.04	21.80	21.32	21.67	22.35	21.09	21.25
Na_2O	0.50	0.49	0.50	0.60	0.38	0.28	0.79	0.44
K_2O	0.01	0.00	0.01	0.05	0.01	0.00	0.01	0.01
NiO	0.00	0.06	0.02	0.03	0.02	0.00	0.00	0.03
Total	99.02	99.15	100.11	99.56	98.39	99.30	99.04	99.09
Si	1.73	1.90	1.87	1.85	1.81	1.86	1.84	1.88
Ti	0.09	0.02	0.04	0.04	0.08	0.07	0.04	0.04
Al	0.35	0.16	0.20	0.23	0.23	0.17	0.30	0.19
Cr	0.00	0.02	0.01	0.00	0.00	0.00	0.00	0.00
Fe	0.24	0.16	0.19	0.21	0.25	0.23	0.25	0.20
Mn	0.00	0.00	0.00	0.00	0.00	0.00	0.00	0.00
Mg	0.69	0.84	0.80	0.77	0.73	0.74	0.67	0.79
Ca	0.89	0.88	0.86	0.85	0.88	0.90	0.85	0.85
Na	0.04	0.04	0.04	0.04	0.03	0.02	0.06	0.03
K	0.00	0.00	0.00	0.00	0.00	0.00	0.00	0.00
Ni	0.00	0.00	0.00	0.00	0.00	0.00	0.00	0.00
Total	4.03	4.01	4.00	4.01	4.01	3.99	4.00	4.00
Mg#	74.21	84.20	81.21	78.68	74.37	76.22	72.79	79.67
$D^{(cpx\text{-}melt)}_{H2O}$	0.0355	0.0120	0.0147	0.0168	0.0217	0.0147	0.0186	0.0142
Absorbance of cpx (cm^{-1})	5.1	3.2	2.6	4.5	5.3	4.4	3.8	4.3
Thickness of cpx (0.001mm)	77	72	74	72	75	72	72	77
Absorbance normalized to 1 cm (cm^{-1})	666	444	351	625	707	614	528	562
H_2O-cpx (ppm)	282	188	149	264	299	260	223	238
H_2O-melt (wt%)	0.79	1.57	1.01	1.58	1.38	1.76	1.20	1.68

Sample No. Section No. Point No.	40	41	42	43	44	45.1	45.2	45.3
SiO_2	48.32	51.56	47.61	49.20	50.68	52.20	49.52	46.42
TiO_2	2.12	0.74	1.58	1.65	1.50	0.93	1.39	1.70
Al_2O3	5.43	3.67	6.89	4.83	4.17	3.55	4.57	8.22
Cr_2O3	0.94	0.68	0.00	0.55	0.19	0.29	0.67	0.03
FeO	5.68	4.68	9.83	5.56	6.49	5.00	5.32	7.19
MnO	0.06	0.09	0.13	0.05	0.08	0.04	0.07	0.07
MgO	12.86	14.81	10.84	13.96	14.54	15.26	14.30	11.61
CaO	23.14	22.40	21.05	22.78	21.23	22.01	23.13	23.08
Na_2O	0.38	0.46	1.14	0.44	0.47	0.55	0.39	0.50
K_2O	0.00	0.00	0.00	0.01	0.02	0.01	0.00	0.01
NiO	0.02	0.02	0.03	0.00	0.03	0.05	0.00	0.00
Total	98.95	99.10	99.10	99.02	99.39	99.89	99.37	98.82
Si	1.82	1.91	1.81	1.84	1.88	1.92	1.85	1.76
Ti	0.06	0.02	0.05	0.05	0.04	0.03	0.04	0.05
Al	0.24	0.16	0.31	0.21	0.18	0.15	0.20	0.37
Cr	0.03	0.02	0.00	0.02	0.01	0.01	0.02	0.00
Fe	0.18	0.15	0.31	0.17	0.20	0.15	0.17	0.23
Mn	0.00	0.00	0.00	0.00	0.00	0.00	0.00	0.00
Mg	0.72	0.82	0.61	0.78	0.80	0.83	0.79	0.65
Ca	0.93	0.89	0.86	0.91	0.84	0.87	0.92	0.94
Na	0.03	0.03	0.08	0.03	0.03	0.04	0.03	0.04
K	0.00	0.00	0.00	0.00	0.00	0.00	0.00	0.00
Ni	0.00	0.00	0.00	0.00	0.00	0.00	0.00	0.00
Total	4.00	4.00	4.03	4.01	4.00	4.00	4.02	4.03
Mg#	80.15	84.93	66.28	81.73	79.99	84.48	82.74	74.22
$D^{(cpx\text{-}melt)}_{H2O}$	0.0196	0.0111	0.0221	0.0170	0.0139	0.0110	0.0163	0.0286
Absorbance of cpx (cm^{-1})	3.1	4.2	5.7	3.2	3.1	5.7	6.0	6.3
Thickness of cpx (0.001mm)	74	74	77	75	75	75	75	75
Absorbance normalized to 1 cm (cm^{-1})	419	568	740	427	413	760	800	844
H_2O-cpx (ppm)	177	240	313	181	175	322	339	357
H_2O-melt (wt%)	0.90	2.16	1.42	1.06	1.26	2.94	2.08	1.25

Sample No.	BL-2							
Section No.	1							
Point No.	2	3	4	5	6	7	8	9
SiO_2	51.12	50.17	50.56	49.92	50.61	50.35	49.31	50.54
TiO_2	1.33	1.35	0.85	2.13	1.50	1.61	1.76	1.65
Al_2O3	2.69	3.28	5.84	3.47	2.30	2.32	3.42	2.51
Cr_2O3	0.17	0.18	0.21	0.00	0.00	0.00	0.06	0.00
FeO	7.94	7.66	6.69	8.11	7.77	8.66	8.08	8.62
MnO	0.13	0.12	0.12	0.11	0.08	0.13	0.14	0.13
MgO	14.70	14.43	15.54	13.29	14.37	13.41	14.00	13.13
CaO	21.35	21.47	19.47	22.41	21.88	22.09	21.84	22.18
Na_2O	0.33	0.34	0.58	0.46	0.33	0.43	0.41	0.40
K_2O	0.00	0.00	0.00	0.00	0.00	0.00	0.00	0.00
NiO	0.00	0.01	0.02	0.00	0.04	0.00	0.02	0.07
Total	99.75	99.00	99.87	99.91	98.88	98.99	99.03	99.22
Si	1.90	1.88	1.86	1.87	1.91	1.90	1.86	1.91
Ti	0.04	0.04	0.02	0.06	0.04	0.05	0.05	0.05
Al	0.12	0.15	0.25	0.15	0.10	0.10	0.15	0.11
Cr	0.00	0.01	0.01	0.00	0.00	0.00	0.00	0.00
Fe	0.25	0.24	0.21	0.25	0.24	0.27	0.26	0.27
Mn	0.00	0.00	0.00	0.00	0.00	0.00	0.00	0.00
Mg	0.82	0.81	0.85	0.74	0.81	0.76	0.79	0.74
Ca	0.85	0.86	0.77	0.90	0.88	0.90	0.88	0.90
Na	0.02	0.02	0.04	0.03	0.02	0.03	0.03	0.03
K	0.00	0.00	0.00	0.00	0.00	0.00	0.00	0.00
Ni	0.00	0.00	0.00	0.00	0.00	0.00	0.00	0.00
Total	4.01	4.01	4.01	4.01	4.01	4.01	4.03	4.01
Mg#	76.75	77.05	80.56	74.49	76.72	73.41	75.53	73.09
$D^{(cpx\text{-}melt)}_{H2O}$	0.0119	0.0134	0.0175	0.0144	0.0114	0.0114	0.0152	0.0113
Absorbance of cpx (cm^{-1})	0.9	1.0	3.4	1.2	0.6	0.4	0.8	0.9
Thickness of cpx (0.001mm)	152	162	164	164	155	147	169	169
Absorbance normalized to 1 cm (cm^{-1})	59	62	207	73	36	27	50	53
H_2O-cpx (ppm)	25	26	88	31	15	12	21	23
H_2O-melt (wt%)	0.21	0.20	0.50	0.22	0.13	0.10	0.14	0.20

Sample No.								
Section No.								
Point No.	10	11	12	13	14	16	17	18
SiO_2	50.03	52.68	49.65	48.65	50.16	49.54	50.30	49.63
TiO_2	1.86	0.73	1.95	1.94	1.33	1.75	1.49	1.91
Al_2O3	3.46	2.30	4.53	5.01	2.83	3.14	3.54	3.29
Cr_2O3	0.04	0.31	0.24	0.20	0.00	0.01	0.18	0.00
FeO	8.26	6.38	7.48	7.60	7.97	8.45	7.62	8.54
MnO	0.14	0.13	0.12	0.12	0.15	0.13	0.12	0.11
MgO	13.54	16.34	13.60	13.65	13.75	13.31	14.16	12.97
CaO	21.90	20.69	21.75	21.83	22.15	22.24	21.21	22.30
Na_2O	0.34	0.31	0.40	0.37	0.37	0.44	0.31	0.47
K_2O	0.00	0.01	0.00	0.00	0.00	0.00	0.00	0.00
NiO	0.01	0.01	0.00	0.05	0.04	0.03	0.00	0.02
Total	99.57	99.89	99.73	99.41	98.75	99.04	98.93	99.23
Si	1.88	1.94	1.85	1.83	1.90	1.87	1.89	1.87
Ti	0.05	0.02	0.05	0.05	0.04	0.05	0.04	0.05
Al	0.15	0.10	0.20	0.22	0.13	0.14	0.16	0.15
Cr	0.00	0.01	0.01	0.01	0.00	0.00	0.01	0.00
Fe	0.26	0.20	0.23	0.24	0.25	0.27	0.24	0.27
Mn	0.00	0.00	0.00	0.00	0.00	0.00	0.00	0.00
Mg	0.76	0.90	0.76	0.76	0.77	0.75	0.79	0.73
Ca	0.88	0.81	0.87	0.88	0.90	0.90	0.85	0.90
Na	0.02	0.02	0.03	0.03	0.03	0.03	0.02	0.03
K	0.00	0.00	0.00	0.00	0.00	0.00	0.00	0.00
Ni	0.00	0.00	0.00	0.00	0.00	0.00	0.00	0.00
Total	4.01	4.00	4.00	4.02	4.02	4.02	4.00	4.02
Mg#	74.51	82.03	76.41	76.19	75.48	73.73	76.82	73.04
$D^{(cpx\text{-}melt)}_{H2O}$	0.0140	0.0100	0.0164	0.0194	0.0120	0.0137	0.0133	0.0138
Absorbance of cpx (cm^{-1})	1.0	1.5	0.6	0.6	0.8	1.1	0.9	0.4
Thickness of cpx (0.001mm)	173	173	173	174	172	162	174	174
Absorbance normalized to 1 cm (cm^{-1})	58	87	35	34	47	68	52	24
H_2O-cpx (ppm)	24	37	15	15	20	29	22	10
H_2O-melt (wt%)	0.18	0.37	0.09	0.08	0.17	0.21	0.16	0.07

Sample No.				BL-5				
Section No.				1				
Point No.	19	20	21	1	2	3	4	5
SiO_2	51.85	48.96	50.61	49.39	50.28	52.64	48.85	51.67
TiO_2	0.87	2.07	1.77	1.87	0.96	0.58	2.06	0.74
Al_2O3	2.20	4.96	2.83	4.31	5.12	4.04	4.16	3.92
Cr_2O3	0.13	0.07	0.05	0.33	0.00	0.15	0.09	0.16
FeO	7.47	8.11	8.28	8.07	7.87	7.20	7.91	6.56
MnO	0.13	0.15	0.13	0.09	0.14	0.13	0.10	0.11
MgO	15.47	13.34	13.91	13.60	15.21	17.53	13.15	15.48
CaO	20.90	21.61	22.08	21.61	19.04	17.01	22.38	19.53
Na_2O	0.26	0.41	0.38	0.38	0.58	0.58	0.44	0.55
K_2O	0.00	0.00	0.00	0.00	0.01	0.00	0.00	0.00
NiO	0.05	0.00	0.01	0.04	0.03	0.06	0.04	0.03
Total	99.32	99.68	100.05	99.70	99.24	99.91	99.19	98.76
Si	1.93	1.83	1.89	1.85	1.87	1.92	1.84	1.92
Ti	0.02	0.06	0.05	0.05	0.03	0.02	0.06	0.02
Al	0.10	0.22	0.12	0.19	0.22	0.17	0.18	0.17
Cr	0.00	0.00	0.00	0.01	0.00	0.00	0.00	0.00
Fe	0.23	0.25	0.26	0.25	0.24	0.22	0.25	0.20
Mn	0.00	0.00	0.00	0.00	0.00	0.00	0.00	0.00
Mg	0.86	0.74	0.77	0.76	0.84	0.95	0.74	0.86
Ca	0.83	0.87	0.88	0.87	0.76	0.66	0.90	0.78
Na	0.02	0.03	0.03	0.03	0.04	0.04	0.03	0.04
K	0.00	0.00	0.00	0.00	0.00	0.00	0.00	0.00
Ni	0.00	0.00	0.00	0.00	0.00	0.00	0.00	0.00
Total	4.00	4.01	4.01	4.01	4.01	4.00	4.02	3.99
Mg#	78.69	74.57	74.97	75.03	77.51	81.28	74.78	80.81
$D^{(cpx\text{-}melt)}_{H2O}$	0.0102	0.0186	0.0128	0.0168	0.0165	0.0130	0.0168	0.0118
Absorbance of cpx (cm^{-1})	1.9	1.0	1.1	8.3	9.7	7.7	6.2	10.0
Thickness of cpx (0.001mm)	172	164	165	140	141	151	157	159
Absorbance normalized to 1 cm (cm^{-1})	110	61	67	593	688	510	395	629
H_2O-cpx (ppm)	47	26	28	251	291	216	167	266
H_2O-melt (wt%)	0.46	0.14	0.22	1.49	1.77	1.65	1.00	2.25

Sample No. Section No. Point No.	6	7	8	9	10	11	12	13
SiO_2	51.35	50.49	50.85	51.64	50.16	50.24	50.99	49.79
TiO_2	0.82	1.03	0.72	0.91	0.97	1.04	0.84	1.08
Al_2O3	4.05	4.66	4.78	2.01	5.52	5.71	3.84	5.87
Cr_2O3	0.18	0.42	0.27	0.17	0.35	0.25	0.15	0.24
FeO	6.78	6.63	6.52	7.91	6.32	6.45	6.45	6.54
MnO	0.08	0.10	0.10	0.10	0.08	0.11	0.06	0.14
MgO	16.42	15.39	16.40	14.94	14.72	14.86	16.26	14.74
CaO	19.55	19.78	19.24	20.47	20.50	20.32	19.65	20.13
Na_2O	0.59	0.46	0.44	0.30	0.64	0.63	0.51	0.57
K_2O	0.01	0.00	0.00	0.00	0.00	0.01	0.00	0.01
NiO	0.02	0.05	0.06	0.04	0.08	0.08	0.00	0.00
Total	99.85	99.01	99.40	98.49	99.33	99.69	98.74	99.10
Si	1.89	1.88	1.88	1.94	1.86	1.85	1.90	1.85
Ti	0.02	0.03	0.02	0.03	0.03	0.03	0.02	0.03
Al	0.18	0.20	0.21	0.09	0.24	0.25	0.17	0.26
Cr	0.01	0.01	0.01	0.01	0.01	0.01	0.00	0.01
Fe	0.21	0.21	0.20	0.25	0.20	0.20	0.20	0.20
Mn	0.00	0.00	0.00	0.00	0.00	0.00	0.00	0.00
Mg	0.90	0.85	0.90	0.84	0.81	0.82	0.90	0.82
Ca	0.77	0.79	0.76	0.82	0.81	0.80	0.78	0.80
Na	0.04	0.03	0.03	0.02	0.05	0.05	0.04	0.04
K	0.00	0.00	0.00	0.00	0.00	0.00	0.00	0.00
Ni	0.00	0.00	0.00	0.00	0.00	0.00	0.00	0.00
Total	4.02	4.00	4.01	4.00	4.01	4.01	4.01	4.01
Mg#	81.18	80.54	81.77	77.09	80.59	80.42	81.79	80.07
$D^{(cpx\text{-}melt)}_{H2O}$	0.0142	0.0153	0.0157	0.0096	0.0166	0.0172	0.0136	0.0179
Absorbance of cpx (cm^{-1})	14.0	10.0	15.5	4.9	11.8	11.9	11.5	9.6
Thickness of cpx (0.001mm)	157	154	153	140	140	147	140	152
Absorbance normalized to 1 cm (cm^{-1})	892	649	1013	350	843	810	821	632
H_2O-cpx (ppm)	377	275	429	148	357	343	348	267
H_2O-melt (wt%)	2.65	1.79	2.73	1.53	2.15	1.99	2.56	1.49

Sample No.							
Section No.							
Point No.	14	15	16	17	18	19	20
SiO_2	51.43	49.98	50.85	51.40	50.14	51.22	51.14
TiO_2	1.00	1.68	1.01	0.80	1.37	0.81	1.11
Al_2O3	3.66	3.50	4.03	4.75	3.52	2.88	2.37
Cr_2O3	0.02	0.06	0.20	0.25	0.24	0.49	0.17
FeO	7.11	7.93	7.03	6.07	7.63	5.87	8.22
MnO	0.08	0.13	0.10	0.07	0.11	0.12	0.15
MgO	15.06	13.87	15.50	15.82	14.26	15.47	15.02
CaO	20.82	22.12	19.71	20.14	21.51	21.82	20.56
Na_2O	0.42	0.46	0.47	0.69	0.38	0.35	0.35
K_2O	0.01	0.00	0.01	0.00	0.00	0.01	0.00
NiO	0.05	0.02	0.06	0.06	0.00	0.06	0.00
Total	99.64	99.75	98.96	100.05	99.17	99.08	99.09
Si	1.90	1.87	1.89	1.88	1.88	1.91	1.92
Ti	0.03	0.05	0.03	0.02	0.04	0.02	0.03
Al	0.16	0.15	0.18	0.21	0.16	0.13	0.10
Cr	0.00	0.00	0.01	0.01	0.01	0.01	0.01
Fe	0.22	0.25	0.22	0.19	0.24	0.18	0.26
Mn	0.00	0.00	0.00	0.00	0.00	0.00	0.00
Mg	0.83	0.77	0.86	0.86	0.80	0.86	0.84
Ca	0.83	0.89	0.79	0.79	0.86	0.87	0.83
Na	0.03	0.03	0.03	0.05	0.03	0.02	0.03
K	0.00	0.00	0.00	0.00	0.00	0.00	0.00
Ni	0.00	0.00	0.00	0.00	0.00	0.00	0.00
Total	4.00	4.02	4.01	4.01	4.01	4.01	4.01
Mg#	79.06	75.71	79.73	82.30	76.92	82.46	76.52
$D^{(cpx\text{-}melt)}_{H2O}$	0.0122	0.0143	0.0138	0.0145	0.0138	0.0115	0.0113
Absorbance of cpx (cm^{-1})	8.2	7.2	5.9	9.1	7.4	10.7	7.2
Thickness of cpx (0.001mm)	130	123	130	144	146	144	152
Absorbance normalized to 1 cm (cm^{-1})	631	585	454	632	507	743	474
H_2O-cpx (ppm)	267	248	192	267	214	314	200
H_2O-melt (wt%)	2.18	1.73	1.39	1.85	1.56	2.74	1.77

Sample No.		BL-6						
Section No.		1						
Point No.	21	1	2	2.1	3	3.2	4	4.2
SiO_2	49.03	49.38	52.48	49.57	49.16	51.93	51.24	52.60
TiO_2	2.15	1.57	0.80	2.28	2.32	1.20	1.47	0.77
Al_2O3	3.92	5.01	3.97	4.72	3.83	3.90	2.89	3.90
Cr_2O3	0.03	0.22	0.21	0.12	0.03	0.13	0.08	0.08
FeO	7.51	7.41	6.20	7.40	8.19	7.50	8.76	7.75
MnO	0.10	0.13	0.14	0.10	0.16	0.17	0.15	0.16
MgO	12.98	13.11	15.62	13.06	12.91	15.28	14.38	16.97
CaO	22.78	21.27	19.60	22.78	22.63	20.05	20.91	17.47
Na_2O	0.47	0.38	0.70	0.40	0.49	0.45	0.38	0.51
K_2O	0.00	0.00	0.00	0.00	0.00	0.01	0.01	0.01
NiO	0.04	0.00	0.00	0.00	0.00	0.00	0.00	0.00
Total	99.01	98.48	99.71	100.42	99.72	100.63	100.27	100.23
Si	1.85	1.86	1.92	1.84	1.85	1.90	1.90	1.92
Ti	0.06	0.04	0.02	0.06	0.07	0.03	0.04	0.02
Al	0.17	0.22	0.17	0.21	0.17	0.17	0.13	0.17
Cr	0.00	0.01	0.01	0.00	0.00	0.00	0.00	0.00
Fe	0.24	0.23	0.19	0.23	0.26	0.23	0.27	0.24
Mn	0.00	0.00	0.00	0.00	0.00	0.01	0.00	0.01
Mg	0.73	0.74	0.85	0.72	0.72	0.83	0.80	0.92
Ca	0.92	0.86	0.77	0.91	0.91	0.79	0.83	0.68
Na	0.03	0.03	0.05	0.03	0.04	0.03	0.03	0.04
K	0.00	0.00	0.00	0.00	0.00	0.00	0.00	0.00
Ni	0.00	0.00	0.00	0.00	0.00	0.00	0.00	0.00
Total	4.02	3.99	3.99	4.01	4.02	4.00	4.01	3.99
Mg#	75.49	75.94	81.80	75.87	73.76	78.41	74.53	79.61
$D^{(cpx\text{-}melt)}_{H2O}$	0.0156	0.0157	0.0114	0.0171	0.0161	0.0129	0.0123	0.0128
Absorbance of cpx (cm^{-1})	8.2	5.6	9.5	6.8	6.5	5.9	4.6	6.3
Thickness of cpx (0.001mm)	134	87	87	87	98	98	90	90
Absorbance normalized to 1 cm (cm^{-1})	612	644	1092	782	663	597	508	694
H_2O-cpx (ppm)	259	272	462	331	281	253	215	294
H_2O-melt (wt%)	1.66	1.73	4.05	1.94	1.74	1.95	1.75	2.29

Sample No.								
Section No.								
Point No.	4.3	4.4	5	5.2	7	10	11	11.3
SiO_2	52.12	48.80	53.31	49.89	48.09	51.96	50.32	52.28
TiO_2	0.93	2.46	0.67	2.11	2.55	0.83	1.85	0.75
Al_2O3	2.57	4.22	3.54	4.12	4.59	3.79	3.84	3.20
Cr_2O3	0.00	0.00	0.15	0.02	0.08	0.15	0.29	0.29
FeO	7.60	8.45	6.95	7.40	7.91	7.05	7.65	6.60
MnO	0.22	0.16	0.09	0.11	0.11	0.25	0.14	0.12
MgO	15.09	12.50	16.58	13.29	12.76	16.64	14.06	16.34
CaO	20.56	22.44	18.66	22.55	22.18	18.33	21.36	19.16
Na_2O	0.33	0.50	0.55	0.48	0.48	0.49	0.33	0.51
K_2O	0.00	0.00	0.00	0.01	0.00	0.00	0.00	0.00
NiO	0.13	0.00	0.00	0.00	0.00	0.17	0.04	0.04
Total	99.54	99.53	100.51	99.99	98.74	99.66	99.87	99.28
Si	1.93	1.84	1.94	1.86	1.82	1.91	1.87	1.93
Ti	0.03	0.07	0.02	0.06	0.07	0.02	0.05	0.02
Al	0.11	0.19	0.15	0.18	0.21	0.16	0.17	0.14
Cr	0.00	0.00	0.00	0.00	0.00	0.00	0.01	0.01
Fe	0.24	0.27	0.21	0.23	0.25	0.22	0.24	0.20
Mn	0.01	0.01	0.00	0.00	0.00	0.01	0.00	0.00
Mg	0.84	0.70	0.90	0.74	0.72	0.91	0.78	0.90
Ca	0.82	0.91	0.73	0.90	0.90	0.72	0.85	0.76
Na	0.02	0.04	0.04	0.03	0.04	0.03	0.02	0.04
K	0.00	0.00	0.00	0.00	0.00	0.00	0.00	0.00
Ni	0.00	0.00	0.00	0.00	0.00	0.00	0.00	0.00
Total	4.00	4.01	3.99	4.01	4.02	4.00	4.00	4.00
Mg#	77.97	72.50	80.95	76.19	74.21	80.80	76.60	81.53
$D^{(cpx\text{-}melt)}_{H2O}$	0.0102	0.0171	0.0110	0.0152	0.0191	0.0131	0.0147	0.0112
Absorbance of cpx (cm^{-1})	4.3	6.2	5.5	5.1	4.6	4.2	2.6	2.4
Thickness of cpx (0.001mm)	90	90	82	82	69	80	99	99
Absorbance normalized to 1 cm (cm^{-1})	478	689	671	622	667	525	263	239
H_2O-cpx (ppm)	202	291	284	263	282	222	111	101
H_2O-melt (wt%)	1.99	1.70	2.59	1.73	1.48	1.70	0.76	0.90

Sample No.				BL-7				
Section No.				1				
Point No.	22	25	25.2	1	1.2	2	3	3.2
SiO_2	49.88	49.64	50.77	51.11	48.12	52.00	52.28	48.54
TiO_2	1.79	1.26	1.96	1.37	2.62	0.75	0.75	1.94
Al_2O3	3.38	5.94	3.28	2.63	5.31	3.99	3.70	3.83
Cr_2O3	0.13	0.42	0.09	0.07	0.07	0.18	0.16	0.15
FeO	8.00	6.52	7.93	7.95	7.62	6.43	6.60	7.58
MnO	0.17	0.09	0.19	0.15	0.05	0.16	0.12	0.07
MgO	13.83	14.63	13.49	14.63	12.33	15.87	16.12	13.59
CaO	21.62	20.02	22.05	21.11	22.69	19.97	19.85	22.15
Na_2O	0.33	0.55	0.31	0.40	0.45	0.55	0.49	0.44
K_2O	0.01	0.00	0.00	0.00	0.00	0.00	0.01	0.00
NiO	0.00	0.02	0.00	0.00	0.00	0.00	0.00	0.00
Total	99.13	99.09	100.07	99.43	99.25	99.90	100.07	98.27
Si	1.88	1.84	1.89	1.91	1.81	1.91	1.91	1.85
Ti	0.05	0.04	0.05	0.04	0.07	0.02	0.02	0.06
Al	0.15	0.26	0.14	0.12	0.24	0.17	0.16	0.17
Cr	0.00	0.01	0.00	0.00	0.00	0.01	0.00	0.00
Fe	0.25	0.20	0.25	0.25	0.24	0.20	0.20	0.24
Mn	0.01	0.00	0.01	0.00	0.00	0.00	0.00	0.00
Mg	0.78	0.81	0.75	0.81	0.69	0.87	0.88	0.77
Ca	0.87	0.80	0.88	0.85	0.92	0.79	0.78	0.90
Na	0.02	0.04	0.02	0.03	0.03	0.04	0.03	0.03
K	0.00	0.00	0.00	0.00	0.00	0.00	0.00	0.00
Ni	0.00	0.00	0.00	0.00	0.00	0.00	0.00	0.00
Total	4.01	4.00	3.99	4.01	4.01	4.00	4.00	4.03
Mg#	75.50	80.02	75.21	76.63	74.26	81.48	81.33	76.17
$D^{(cpx\text{-}melt)}_{H2O}$	0.0140	0.0186	0.0128	0.0116	0.0201	0.0124	0.0120	0.0165
Absorbance of cpx (cm^{-1})	5.8	7.0	9.2	4.7	5.8	6.0	6.1	5.0
Thickness of cpx (0.001mm)	118	121	121	86	86	93	93	93
Absorbance normalized to 1 cm (cm^{-1})	492	579	760	547	679	641	656	537
H_2O-cpx (ppm)	208	245	322	231	287	271	278	227
H_2O-melt (wt%)	1.48	1.32	2.52	1.99	1.43	2.18	2.32	1.38

Sample No.								
Section No.								
Point No.	4	5	6	7	7.2	8	8.2	9
SiO_2	46.17	48.18	48.40	51.39	49.25	50.62	51.59	52.28
TiO_2	3.74	2.50	2.40	0.86	2.48	1.75	1.32	0.71
Al_2O3	6.72	4.91	5.04	3.42	5.01	2.82	2.63	3.48
Cr_2O3	0.02	0.11	0.14	0.09	0.18	0.03	0.05	0.48
FeO	8.30	7.41	7.39	6.72	7.47	8.57	8.31	6.96
MnO	0.03	0.14	0.08	0.14	0.09	0.14	0.14	0.15
MgO	11.32	12.90	12.81	15.30	12.81	13.73	14.12	16.33
CaO	22.43	22.77	22.71	20.94	22.82	21.39	21.30	18.91
Na_2O	0.53	0.42	0.45	0.55	0.42	0.39	0.36	0.49
K_2O	0.00	0.02	0.00	0.01	0.00	0.00	0.01	0.00
NiO	0.00	0.00	0.00	0.00	0.00	0.00	0.00	0.00
Total	99.26	99.34	99.41	99.41	100.52	99.43	99.83	99.79
Si	1.75	1.81	1.82	1.91	1.83	1.90	1.92	1.92
Ti	0.11	0.07	0.07	0.02	0.07	0.05	0.04	0.02
Al	0.30	0.22	0.22	0.15	0.22	0.12	0.12	0.15
Cr	0.00	0.00	0.00	0.00	0.01	0.00	0.00	0.01
Fe	0.26	0.23	0.23	0.21	0.23	0.27	0.26	0.21
Mn	0.00	0.00	0.00	0.00	0.00	0.00	0.00	0.00
Mg	0.64	0.72	0.72	0.85	0.71	0.77	0.78	0.89
Ca	0.91	0.92	0.91	0.83	0.91	0.86	0.85	0.74
Na	0.04	0.03	0.03	0.04	0.03	0.03	0.03	0.03
K	0.00	0.00	0.00	0.00	0.00	0.00	0.00	0.00
Ni	0.00	0.00	0.00	0.00	0.00	0.00	0.00	0.00
Total	4.01	4.02	4.02	4.01	4.00	4.00	4.00	4.00
Mg#	70.85	75.64	75.56	80.25	75.36	74.07	75.19	80.71
$D^{(cpx\text{-}melt)}_{H2O}$	0.0306	0.0199	0.0194	0.0120	0.0184	0.0122	0.0107	0.0120
Absorbance of cpx (cm^{-1})	7.7	5.3	5.8	5.7	6.7	3.7	6.3	5.6
Thickness of cpx (0.001mm)	93	93	87	87	87	85	85	87
Absorbance normalized to 1 cm (cm^{-1})	825	570	669	649	770	435	741	640
H_2O-cpx (ppm)	349	241	283	275	326	184	314	271
H_2O-melt (wt%)	1.14	1.21	1.46	2.29	1.77	1.51	2.92	2.26

Sample No.								
Section No.								
Point No.	10	11	11.2	12	14.2	15	17	17.2
SiO_2	49.53	51.55	48.68	50.30	47.81	50.76	51.74	51.27
TiO_2	2.36	0.88	2.15	1.91	2.27	1.75	1.19	1.49
Al_2O3	4.17	4.42	5.04	4.84	4.61	3.25	2.68	2.76
Cr_2O3	0.01	0.11	0.10	0.10	0.19	0.11	0.09	0.14
FeO	8.63	7.48	8.02	7.56	8.55	8.10	7.89	7.46
MnO	0.13	0.12	0.12	0.13	0.17	0.10	0.11	0.10
MgO	12.48	15.98	12.91	12.62	12.97	13.43	14.42	14.15
CaO	22.35	18.88	21.96	21.36	21.64	21.48	21.32	21.43
Na_2O	0.46	0.59	0.47	0.57	0.46	0.41	0.34	0.36
K_2O	0.00	0.00	0.01	0.00	0.01	0.00	0.00	0.00
NiO	0.00	0.00	0.00	0.00	0.00	0.00	0.00	0.00
Total	100.10	99.99	99.46	99.39	98.67	99.39	99.77	99.16
Si	1.85	1.89	1.83	1.88	1.82	1.90	1.92	1.92
Ti	0.07	0.02	0.06	0.05	0.06	0.05	0.03	0.04
Al	0.18	0.19	0.22	0.21	0.21	0.14	0.12	0.12
Cr	0.00	0.00	0.00	0.00	0.01	0.00	0.00	0.00
Fe	0.27	0.23	0.25	0.24	0.27	0.25	0.25	0.23
Mn	0.00	0.00	0.00	0.00	0.01	0.00	0.00	0.00
Mg	0.70	0.87	0.72	0.70	0.74	0.75	0.80	0.79
Ca	0.90	0.74	0.88	0.85	0.88	0.86	0.85	0.86
Na	0.03	0.04	0.03	0.04	0.03	0.03	0.02	0.03
K	0.00	0.00	0.00	0.00	0.00	0.00	0.00	0.00
Ni	0.00	0.00	0.00	0.00	0.00	0.00	0.00	0.00
Total	4.00	4.01	4.01	3.98	4.03	3.99	4.00	3.99
Mg#	72.06	79.21	74.17	74.86	73.00	74.72	76.51	77.17
$D^{(cpx\text{-}melt)}_{H2O}$	0.0158	0.0142	0.0188	0.0143	0.0201	0.0122	0.0106	0.0110
Absorbance of cpx (cm^{-1})	6.1	6.9	6.0	4.9	6.8	6.1	3.5	3.7
Thickness of cpx (0.001mm)	87	95	95	101	104	96	82	82
Absorbance normalized to 1 cm (cm^{-1})	701	723	627	483	654	636	427	451
H_2O-cpx (ppm)	297	306	265	204	277	269	181	191
H_2O-melt (wt%)	1.88	2.15	1.41	1.43	1.38	2.21	1.70	1.74

Sample No.					BL-8		
Section No.					1		
Point No.	18	18.2	20	20.1	1	1.2	2
SiO_2	52.78	48.55	52.32	49.72	49.63	49.60	52.32
TiO_2	0.53	2.56	0.76	2.16	2.11	1.68	0.79
Al_2O3	3.56	5.22	3.73	4.26	4.47	4.07	3.33
Cr_2O3	0.20	0.10	0.29	0.17	0.06	0.02	0.43
FeO	7.29	7.52	6.41	7.22	7.49	8.23	6.37
MnO	0.05	0.12	0.13	0.17	0.06	0.14	0.13
MgO	16.97	12.77	15.81	13.01	13.14	13.25	15.51
CaO	18.07	22.59	19.64	22.45	22.45	21.73	21.17
Na_2O	0.46	0.47	0.52	0.41	0.50	0.53	0.34
K_2O	0.00	0.00	0.02	0.00	0.00	0.01	0.02
NiO	0.00	0.00	0.00	0.00	0.00	0.00	0.00
Total	99.92	99.90	99.62	99.57	99.90	99.27	100.39
Si	1.93	1.82	1.92	1.86	1.85	1.87	1.92
Ti	0.01	0.07	0.02	0.06	0.06	0.05	0.02
Al	0.15	0.23	0.16	0.19	0.20	0.18	0.14
Cr	0.01	0.00	0.01	0.01	0.00	0.00	0.01
Fe	0.22	0.24	0.20	0.23	0.23	0.26	0.20
Mn	0.00	0.00	0.00	0.01	0.00	0.00	0.00
Mg	0.92	0.71	0.87	0.73	0.73	0.74	0.85
Ca	0.71	0.91	0.77	0.90	0.90	0.88	0.83
Na	0.03	0.03	0.04	0.03	0.04	0.04	0.02
K	0.00	0.00	0.00	0.00	0.00	0.00	0.00
Ni	0.00	0.00	0.00	0.00	0.00	0.00	0.00
Total	3.99	4.01	3.99	4.00	4.01	4.02	4.00
Mg#	80.60	75.18	81.46	76.27	75.78	74.17	81.27
$D^{(cpx\text{-}melt)}_{H2O}$	0.0117	0.0200	0.0115	0.0152	0.0161	0.0149	0.0112
Absorbance of cpx (cm^{-1})	6.4	8.2	6.1	6.1	5.6	4.0	7.7
Thickness of cpx (0.001mm)	88	88	82	82	96	96	98
Absorbance normalized to 1 cm (cm^{-1})	727	932	744	746	578	417	782
H_2O-cpx (ppm)	308	394	315	316	245	176	331
H_2O-melt (wt%)	2.63	1.97	2.74	2.07	1.52	1.18	2.94

Sample No.								
Section No.								
Point No.	2.2	3	4	4.2	5	6	7	7.2
SiO_2	48.81	48.47	52.18	50.83	49.00	48.61	50.24	53.42
TiO_2	2.47	2.23	0.62	1.72	2.53	2.68	1.95	0.60
Al_2O3	5.13	4.74	3.81	3.11	4.26	5.01	3.89	3.47
Cr_2O3	0.11	0.17	0.20	0.03	0.04	0.12	0.09	0.15
FeO	7.41	7.11	7.68	8.79	8.20	7.78	7.97	7.26
MnO	0.13	0.12	0.15	0.10	0.11	0.10	0.09	0.11
MgO	12.77	13.08	17.96	13.86	12.99	12.66	13.40	17.50
CaO	22.76	22.73	17.05	21.49	22.49	22.74	22.01	17.44
Na_2O	0.45	0.42	0.44	0.40	0.48	0.46	0.46	0.46
K_2O	0.00	0.00	0.00	0.01	0.01	0.01	0.00	0.00
NiO	0.00	0.00	0.00	0.00	0.00	0.00	0.00	0.00
Total	100.04	99.07	100.09	100.34	100.11	100.17	100.10	100.41
Si	1.82	1.83	1.91	1.89	1.83	1.82	1.87	1.94
Ti	0.07	0.06	0.02	0.05	0.07	0.08	0.05	0.02
Al	0.23	0.21	0.16	0.14	0.19	0.22	0.17	0.15
Cr	0.00	0.01	0.01	0.00	0.00	0.00	0.00	0.00
Fe	0.23	0.22	0.23	0.27	0.26	0.24	0.25	0.22
Mn	0.00	0.00	0.00	0.00	0.00	0.00	0.00	0.00
Mg	0.71	0.73	0.98	0.77	0.72	0.71	0.74	0.95
Ca	0.91	0.92	0.67	0.86	0.90	0.91	0.88	0.68
Na	0.03	0.03	0.03	0.03	0.03	0.03	0.03	0.03
K	0.00	0.00	0.00	0.00	0.00	0.00	0.00	0.00
Ni	0.00	0.00	0.00	0.00	0.00	0.00	0.00	0.00
Total	4.01	4.02	4.01	4.01	4.02	4.01	4.00	3.99
Mg#	75.44	76.64	80.65	73.76	73.84	74.36	74.98	81.12
$D^{(cpx\text{-}melt)}_{H2O}$	0.0191	0.0184	0.0142	0.0129	0.0178	0.0198	0.0144	0.0114
Absorbance of cpx (cm^{-1})	7.8	5.4	5.2	6.5	5.3	6.2	8.4	7.2
Thickness of cpx (0.001mm)	98	115	112	112	105	102	106	106
Absorbance normalized to 1 cm (cm^{-1})	796	470	464	580	505	608	789	679
H_2O-cpx (ppm)	337	199	196	246	214	257	334	287
H_2O-melt (wt%)	1.76	1.08	1.38	1.90	1.20	1.30	2.31	2.51

Sample No.								
Section No.								
Point No.	8	9	9.2	10	11	12	12.2	13
SiO_2	52.35	48.09	50.82	47.47	48.35	51.90	48.29	48.65
TiO_2	0.59	2.56	1.75	2.83	2.41	0.84	2.56	2.50
Al_2O3	3.95	5.49	3.06	5.89	4.92	3.46	4.97	4.96
Cr_2O3	0.10	0.15	0.12	0.10	0.13	0.28	0.12	0.10
FeO	7.51	7.36	7.77	8.08	7.75	7.21	7.46	7.82
MnO	0.15	0.10	0.13	0.12	0.11	0.11	0.07	0.16
MgO	17.08	12.38	13.97	12.23	12.67	15.86	12.88	12.98
CaO	17.84	22.53	21.87	22.26	22.34	19.84	22.79	22.58
Na_2O	0.51	0.47	0.38	0.42	0.50	0.40	0.43	0.45
K_2O	0.00	0.02	0.02	0.00	0.00	0.00	0.00	0.00
NiO	0.00	0.00	0.00	0.00	0.00	0.00	0.00	0.00
Total	100.07	99.15	99.89	99.39	99.19	99.90	99.56	100.21
Si	1.91	1.81	1.89	1.79	1.82	1.91	1.81	1.82
Ti	0.02	0.07	0.05	0.08	0.07	0.02	0.07	0.07
Al	0.17	0.24	0.13	0.26	0.22	0.15	0.22	0.22
Cr	0.00	0.00	0.00	0.00	0.00	0.01	0.00	0.00
Fe	0.23	0.23	0.24	0.25	0.24	0.22	0.23	0.24
Mn	0.00	0.00	0.00	0.00	0.00	0.00	0.00	0.00
Mg	0.93	0.70	0.78	0.69	0.71	0.87	0.72	0.72
Ca	0.70	0.91	0.87	0.90	0.90	0.78	0.92	0.90
Na	0.04	0.03	0.03	0.03	0.04	0.03	0.03	0.03
K	0.00	0.00	0.00	0.00	0.00	0.00	0.00	0.00
Ni	0.00	0.00	0.00	0.00	0.00	0.00	0.00	0.00
Total	4.00	4.01	4.00	4.01	4.01	4.00	4.02	4.02
Mg#	80.23	74.99	76.22	72.96	74.46	79.68	75.49	74.73
$D^{(cpx\text{-}melt)}_{H2O}$	0.0131	0.0205	0.0126	0.0238	0.0191	0.0122	0.0200	0.0199
Absorbance of cpx (cm^{-1})	7.2	6.5	4.6	6.0	8.5	8.1	7.8	6.2
Thickness of cpx (0.001mm)	104	104	104	98	93	99	99	89
Absorbance normalized to 1 cm (cm^{-1})	692	625	442	612	914	818	788	697
H_2O-cpx (ppm)	293	264	187	259	387	346	333	295
H_2O-melt (wt%)	2.24	1.29	1.49	1.09	2.02	2.84	1.67	1.48

Sample No.			BL-11				
Section No.			1				
Point No.	14	15	9	10	10.2	10.3	10.4
SiO_2	48.00	48.38	48.80	52.19	51.71	49.68	49.20
TiO_2	2.58	2.37	2.54	0.70	1.57	2.49	2.25
Al_2O3	5.07	4.74	5.02	3.86	3.34	4.43	4.98
Cr_2O3	0.15	0.14	0.11	0.12	0.07	0.00	0.10
FeO	6.97	7.38	7.53	6.95	8.01	7.94	7.44
MnO	0.13	0.12	0.06	0.16	0.10	0.10	0.10
MgO	12.80	12.73	12.81	16.01	14.00	12.71	12.87
CaO	22.48	22.51	22.70	19.56	21.51	22.72	22.82
Na_2O	0.43	0.47	0.43	0.54	0.44	0.49	0.43
K_2O	0.00	0.00	0.00	0.00	0.00	0.00	0.00
NiO	0.00	0.00	0.00	0.00	0.00	0.00	0.00
Total	98.61	98.82	100.00	100.08	100.75	100.56	100.19
Si	1.82	1.83	1.82	1.91	1.90	1.85	1.83
Ti	0.07	0.07	0.07	0.02	0.04	0.07	0.06
Al	0.23	0.21	0.22	0.17	0.15	0.19	0.22
Cr	0.00	0.00	0.00	0.00	0.00	0.00	0.00
Fe	0.22	0.23	0.24	0.21	0.25	0.25	0.23
Mn	0.00	0.00	0.00	0.01	0.00	0.00	0.00
Mg	0.72	0.72	0.71	0.87	0.77	0.70	0.71
Ca	0.91	0.91	0.91	0.77	0.85	0.90	0.91
Na	0.03	0.03	0.03	0.04	0.03	0.03	0.03
K	0.00	0.00	0.00	0.00	0.00	0.00	0.00
Ni	0.00	0.00	0.00	0.00	0.00	0.00	0.00
Total	4.01	4.01	4.01	4.00	3.99	4.00	4.01
Mg#	76.60	75.47	75.21	80.42	75.71	74.06	75.51
$D^{(cpx\text{-}melt)}_{H2O}$	0.0199	0.0183	0.0191	0.0122	0.0119	0.0165	0.0179
Absorbance of cpx (cm^{-1})	6.6	5.6	7.0	7.4	5.7	6.4	6.2
Thickness of cpx (0.001mm)	85	84	86	86	86	86	86
Absorbance normalized to 1 cm (cm^{-1})	772	667	813	860	662	744	723
H_2O-cpx (ppm)	327	282	344	364	280	315	306
H_2O-melt (wt%)	1.64	1.55	1.80	2.98	2.35	1.91	1.71

Sample No.								
Section No.								
Point No.	11	11.2	16.1	16.2	16.3	16.4	16.5	16.6
SiO_2	49.48	49.77	50.40	52.32	48.72	51.68	50.76	49.30
TiO_2	2.26	2.51	1.01	1.08	2.75	0.97	1.66	2.85
Al_2O3	5.01	3.55	5.68	8.56	4.71	3.72	3.17	4.33
Cr_2O3	0.08	0.00	0.25	0.23	0.17	0.19	0.08	0.14
FeO	7.02	8.78	7.26	5.53	7.54	6.50	7.68	7.96
MnO	0.08	0.17	0.21	0.12	0.14	0.15	0.14	0.15
MgO	12.82	11.89	16.25	12.72	12.76	16.00	14.13	12.78
CaO	22.47	22.57	17.07	17.30	22.59	20.18	21.61	22.39
Na_2O	0.47	0.49	0.64	1.23	0.44	0.53	0.37	0.50
K_2O	0.00	0.01	0.00	0.45	0.01	0.00	0.00	0.01
NiO	0.00	0.00	0.00	0.00	0.00	0.00	0.00	0.00
Total	99.69	99.74	98.77	99.54	99.81	99.91	99.59	100.40
Si	1.85	1.87	1.87	1.90	1.83	1.90	1.89	1.84
Ti	0.06	0.07	0.03	0.03	0.08	0.03	0.05	0.08
Al	0.22	0.16	0.25	0.37	0.21	0.16	0.14	0.19
Cr	0.00	0.00	0.01	0.01	0.00	0.01	0.00	0.00
Fe	0.22	0.28	0.22	0.17	0.24	0.20	0.24	0.25
Mn	0.00	0.01	0.01	0.00	0.00	0.00	0.00	0.00
Mg	0.71	0.67	0.90	0.69	0.71	0.88	0.79	0.71
Ca	0.90	0.91	0.68	0.67	0.91	0.80	0.86	0.89
Na	0.03	0.04	0.05	0.09	0.03	0.04	0.03	0.04
K	0.00	0.00	0.00	0.02	0.00	0.00	0.00	0.00
Ni	0.00	0.00	0.00	0.00	0.00	0.00	0.00	0.00
Total	4.00	4.00	4.00	3.94	4.01	4.01	4.00	4.00
Mg#	76.51	70.72	79.97	80.41	75.11	81.43	76.64	74.12
$D^{(cpx\text{-}melt)}_{H2O}$	0.0167	0.0138	0.0182	0.0148	0.0189	0.0129	0.0126	0.0177
Absorbance of cpx (cm^{-1})	6.2	7.0	7.3	7.5	5.1	6.1	4.1	5.6
Thickness of cpx (0.001mm)	86	86	83	83	83	83	83	83
Absorbance normalized to 1 cm (cm^{-1})	721	813	880	904	614	735	494	675
H_2O-cpx (ppm)	305	344	372	382	260	311	209	285
H_2O-melt (wt%)	1.83	2.49	2.05	2.58	1.38	2.40	1.66	1.61

Sample No.								
Section No.								
Point No.	17	17.2	17.3	17.4	18	19	19.2	19.3
SiO_2	50.14	50.59	48.15	48.48	50.16	49.24	45.40	49.26
TiO_2	1.14	1.06	2.97	2.51	1.65	2.44	4.52	2.48
Al_2O3	5.70	5.06	5.15	4.69	3.79	4.21	5.89	4.88
Cr_2O3	0.30	0.25	0.09	0.17	0.33	0.06	0.00	0.17
FeO	6.52	6.97	7.49	7.40	7.37	7.41	9.56	8.28
MnO	0.13	0.16	0.12	0.12	0.12	0.10	0.17	0.12
MgO	14.71	16.00	12.76	13.18	14.45	12.91	10.62	13.11
CaO	19.96	18.84	22.49	22.69	20.86	22.47	22.15	21.22
Na_2O	0.65	0.54	0.47	0.41	0.40	0.43	0.56	0.38
K_2O	0.00	0.00	0.01	0.01	0.00	0.00	0.01	0.00
NiO	0.00	0.00	0.00	0.00	0.00	0.00	0.00	0.00
Total	99.25	99.47	99.69	99.66	99.13	99.26	98.87	99.92
Si	1.86	1.87	1.81	1.82	1.88	1.85	1.74	1.84
Ti	0.03	0.03	0.08	0.07	0.05	0.07	0.13	0.07
Al	0.25	0.22	0.23	0.21	0.17	0.19	0.27	0.21
Cr	0.01	0.01	0.00	0.01	0.01	0.00	0.00	0.01
Fe	0.20	0.22	0.23	0.23	0.23	0.23	0.31	0.26
Mn	0.00	0.00	0.00	0.00	0.00	0.00	0.01	0.00
Mg	0.81	0.88	0.71	0.74	0.81	0.72	0.61	0.73
Ca	0.79	0.75	0.90	0.91	0.84	0.90	0.91	0.85
Na	0.05	0.04	0.03	0.03	0.03	0.03	0.04	0.03
K	0.00	0.00	0.00	0.00	0.00	0.00	0.00	0.00
Ni	0.00	0.00	0.00	0.00	0.00	0.00	0.00	0.00
Total	4.00	4.01	4.01	4.02	4.00	4.00	4.01	4.00
Mg#	80.09	80.36	75.23	76.04	77.77	75.63	66.45	73.85
$D^{(cpx\text{-}melt)}_{H2O}$	0.0171	0.0168	0.0213	0.0195	0.0146	0.0160	0.0319	0.0183
Absorbance of cpx (cm^{-1})	6.7	5.4	6.1	5.2	5.5	6.6	5.7	6.4
Thickness of cpx (0.001mm)	74	74	74	74	82	88	88	88
Absorbance normalized to 1 cm (cm^{-1})	905	730	824	703	671	750	648	727
H_2O-cpx (ppm)	383	309	349	297	284	317	274	308
H_2O-melt (wt%)	2.24	1.83	1.63	1.53	1.95	1.98	0.86	1.68

Sample No.								
Section No.								
Point No.	20	20.1	21	21.2	24	25	26	26.2
SiO_2	51.97	48.31	52.06	49.00	49.07	48.96	51.85	50.15
TiO_2	0.82	2.59	1.13	2.57	2.30	2.62	1.16	2.25
Al_2O3	3.67	4.39	3.60	5.00	4.72	5.21	2.59	3.39
Cr_2O3	0.22	0.04	0.09	0.11	0.19	0.07	0.10	0.00
FeO	6.49	7.73	7.22	7.52	8.43	7.17	7.71	9.19
MnO	0.14	0.13	0.13	0.12	0.14	0.07	0.13	0.14
MgO	16.34	12.87	15.24	12.86	13.15	11.99	14.82	12.14
CaO	19.17	22.33	20.69	22.62	21.76	22.85	21.07	22.34
Na_2O	0.56	0.41	0.37	0.43	0.42	0.44	0.35	0.53
K_2O	0.00	0.00	0.00	0.01	0.00	0.01	0.01	0.01
NiO	0.00	0.00	0.00	0.00	0.00	0.00	0.00	0.00
Total	99.37	98.80	100.53	100.22	100.15	99.38	99.78	100.14
Si	1.91	1.83	1.91	1.83	1.83	1.84	1.92	1.88
Ti	0.02	0.07	0.03	0.07	0.06	0.07	0.03	0.06
Al	0.16	0.20	0.16	0.22	0.21	0.23	0.11	0.15
Cr	0.01	0.00	0.00	0.00	0.01	0.00	0.00	0.00
Fe	0.20	0.24	0.22	0.23	0.26	0.22	0.24	0.29
Mn	0.00	0.00	0.00	0.00	0.00	0.00	0.00	0.00
Mg	0.90	0.73	0.83	0.71	0.73	0.67	0.82	0.68
Ca	0.76	0.91	0.81	0.90	0.87	0.92	0.84	0.90
Na	0.04	0.03	0.03	0.03	0.03	0.03	0.03	0.04
K	0.00	0.00	0.00	0.00	0.00	0.00	0.00	0.00
Ni	0.00	0.00	0.00	0.00	0.00	0.00	0.00	0.00
Total	4.00	4.01	3.99	4.01	4.01	3.99	4.00	4.00
Mg#	81.79	74.81	79.02	75.31	73.55	74.89	77.42	70.21
$D^{(cpx\text{-}melt)}_{H2O}$	0.0123	0.0183	0.0121	0.0189	0.0186	0.0174	0.0106	0.0133
Absorbance of cpx (cm^{-1})	6.0	5.6	5.6	5.8	5.1	5.8	3.4	3.7
Thickness of cpx (0.001mm)	88	88	78	78	78	58	58	58
Absorbance normalized to 1 cm (cm^{-1})	681	634	718	744	654	1000	586	641
H_2O-cpx (ppm)	288	268	304	315	277	423	248	271
H_2O-melt (wt%)	2.34	1.46	2.52	1.67	1.49	2.43	2.33	2.04

Sample No.							
Section No.							
Point No.	30	30.2	30.3	31	31.2	34	34.2
SiO_2	52.35	47.04	47.59	49.04	44.76	48.53	48.54
TiO_2	0.73	3.51	2.89	2.60	4.76	2.16	2.51
Al_2O3	3.82	6.01	5.53	5.12	7.64	5.03	5.11
Cr_2O3	0.22	0.02	0.12	0.15	0.01	0.01	0.14
FeO	6.65	9.12	7.76	7.54	9.38	7.37	7.48
MnO	0.10	0.09	0.12	0.09	0.16	0.12	0.06
MgO	15.78	11.35	12.44	12.83	9.92	13.00	12.62
CaO	19.79	22.46	22.61	22.71	22.11	22.14	22.21
Na_2O	0.54	0.45	0.52	0.45	0.66	0.46	0.42
K_2O	0.00	0.00	0.01	0.01	0.00	0.00	0.00
NiO	0.00	0.00	0.00	0.00	0.00	0.00	0.00
Total	99.98	100.05	99.58	100.53	99.40	98.83	99.10
Si	1.92	1.77	1.79	1.82	1.71	1.83	1.83
Ti	0.02	0.10	0.08	0.07	0.14	0.06	0.07
Al	0.17	0.27	0.25	0.22	0.34	0.22	0.23
Cr	0.01	0.00	0.00	0.00	0.00	0.00	0.00
Fe	0.20	0.29	0.24	0.23	0.30	0.23	0.24
Mn	0.00	0.00	0.00	0.00	0.01	0.00	0.00
Mg	0.86	0.64	0.70	0.71	0.56	0.73	0.71
Ca	0.78	0.91	0.91	0.90	0.90	0.89	0.90
Na	0.04	0.03	0.04	0.03	0.05	0.03	0.03
K	0.00	0.00	0.00	0.00	0.00	0.00	0.00
Ni	0.00	0.00	0.00	0.00	0.00	0.00	0.00
Total	3.99	4.01	4.02	4.01	4.01	4.01	4.00
Mg#	80.87	68.94	74.09	75.21	65.35	75.88	75.05
$D^{(cpx\text{-}melt)}_{H2O}$	0.0117	0.0263	0.0232	0.0193	0.0407	0.0184	0.0188
Absorbance of cpx (cm^{-1})	5.1	2.9	2.5	2.9	2.7	2.8	5.4
Thickness of cpx (0.001mm)	57	57	57	57	57	57	57
Absorbance normalized to 1 cm (cm^{-1})	895	504	439	500	465	491	947
H_2O-cpx (ppm)	379	213	186	212	197	208	401
H_2O-melt (wt%)	3.24	0.81	0.80	1.10	0.48	1.13	2.13

Table 6-3 Lithium isotope and content of CPX phenocrysts and xenocryst in the Fujian basalts.

Location	Sample No.	Anlysis No.	Account ^{7}Li/PI	cps(7)/nA/Liof standard	$\delta^{7}Li_{SIMS}$	error	Mg#	$Slop_{Mg,Li}$	$intercept_{Mg,Li}$	$\delta^{7}Li_{cor}$	Li content	error
MX	12MX-A-1-3-8	5-4-8b@1	7.66E+12	1.64E+12	21.4	0.8	82.0	1.06	-74.3	4.7	4.7	0.6
		5-4-8b@02	5.03E+12		20.2	1.5	80.9	1.06	-74.3	3.1	3.1	0.7
		5-4-8b@03	5.41E+12		19.8	1.3	79.5	1.06	-74.3	3.3	3.3	0.9
		5-4-8b@04	6.51E+12		21.5	1.5	81.0	1.06	-74.3	4.0	4.0	0.9
		5-4-8b@05	6.70E+12		20.4	1.4	79.2	1.06	-74.3	4.1	4.1	0.8
		5-4-8b@06	6.92E+12		19.8	1.3	81.9	1.06	-74.3	4.2	4.2	0.8
		5-4-8b@07	8.19E+12		19.5	1.8	82.5	1.06	-74.3	5.0	5.0	
		5-4-8b@08	7.22E+12		19.2	1.1	81.5	1.06	-74.3	4.4	4.4	
		5-4-8b@09	8.36E+12		20.7	1.9	80.6	1.06	-74.3	5.1	5.1	
		5-4-8b@10	6.59E+12		21.5	1.0	82.7	1.06	-74.3	4.0	4.0	
	12MX-A-1-3-11	5-5-11b@1	4.95E+12		27.4	1.4	83.0	1.06	-74.3	13.8	3.0	0.6
		5-5-11b@2	5.96E+12		26.7	2.0	83.0	1.06	-74.3	13.0	3.6	0.7
		5-5-11b@3	4.96E+12		24.4	1.3	83.0	1.06	-74.3	10.8	3.0	0.6
		5-5-11b@4	5.25E+12		26.0	1.1	83.0	1.06	-74.3	12.3	3.2	0.6
	12MX-A-1-3-10	5-3-10a@06	6.96E+12		29.1	0.7	79.8	1.06	-74.3	18.9	4.2	0.8
		5-3-10a@05	7.58E+12		28.7	0.6	81.3	1.06	-74.3	16.8	4.6	0.9
		5-3-10a@04	1.16E+13		27.7	0.3	83.0	1.06	-74.3	14.0	7.1	1.4
		5-3-10a@03	6.47E+12		26.1	0.8	87.8	1.06	-74.3	7.4	3.9	0.8
		5-3-10a@02	2.10E+13		27.9	0.4	88.9	1.06	-74.3	8.0	12.8	2.6
		5-3-10a@1	5.86E+13		24.9	0.3	89.6	1.06	-74.3	4.3	35.7	7.1
		5-3-10a@07	3.84E+13		29.9	0.3	89.8	1.06	-74.3	9.0	23.4	4.7
		5-3-10a@08	3.07E+13		28.6	0.4	88.9	1.06	-74.3	8.6	18.7	3.7
		5-3-10a@09	8.75E+12		28.8	0.6	85.7	1.06	-74.3	12.3	5.3	1.1
		5-3-10a@10	1.08E+13		24.9	0.5	84.9	1.06	-74.3	9.2	6.6	1.3
		5-3-10a@11	9.85E+12		24.2	0.6	79.2	1.06	-74.3	14.6	6.0	1.2
	12MX-A-1-3-9	5-3-9a@1	4.08E+13		31.8	0.4	79.8	1.06	-74.3	21.6	24.8	5.0
		5-3-9a@2	3.57E+13		36.7	0.3	79.8	1.06	-74.3	26.4	21.8	4.4
		5-3-9a@3	4.92E+13		33.3	0.5	79.8	1.06	-74.3	23.1	29.9	6.0
		5-3-9a@4	4.62E+13		30.0	0.4	79.8	1.06	-74.3	19.7	28.1	5.6
	12MX-A-1-3-6	5-2-6a@1	6.62E+12		28.8	0.5	80.9	1.06	-74.3	17.4	4.0	0.8
		5-2-6a@2	5.96E+12		29.2	0.6	80.9	1.06	-74.3	17.8	3.6	0.7
		5-2-6a@3	9.46E+12		25.3	1.4	80.9	1.06	-74.3	13.9	5.8	1.2
		5-2-6a@4	6.43E+12		27.6	0.7	80.9	1.06	-74.3	16.2	3.9	0.8
	12MX-A-1-3-7	5-4-7b@1	1.15E+13		26.2	1.4	76.8	1.06	-74.3	19.1	7.0	1.4
		5-4-7b@2	5.39E+12		24.8	0.9	75.1	1.06	-74.3	19.5	3.3	0.7
		5-4-7b@3	5.40E+12		28.6	1.3	74.9	1.06	-74.3	23.5	3.3	0.7
		5-4-7b@4	6.46E+12		27.0	1.0	78.4	1.06	-74.3	18.2	3.9	0.8
		5-4-7b@5	7.06E+12		24.0	1.2	80.0	1.06	-74.3	13.6	4.3	0.9
		5-4-7b@6	5.31E+12		25.3	1.3	78.4	1.06	-74.3	16.5	3.2	0.6
	11MX-B-1-3-7	5-11-7a@1	7.19E+12		21.7	1.4	82.2	1.06	-74.3	8.9	4.4	0.9
		5-11-7a@2	7.38E+12		21.1	1.0	79.2	1.06	-74.3	11.5	4.5	0.9
		5-11-7a@3	6.47E+12		22.5	1.1	78.1	1.06	-74.3	14.1	3.9	0.8
		5-11-7-2a@1	4.56E+13		15.8	0.8	90.7	1.06	-74.3	-6.0	27.8	5.6
		5-11-7-2a@2	4.96E+13		16.9	0.8	90.7	1.06	-74.3	-4.9	30.2	6.0
		5-11-7-2a@3	4.91E+13		15.9	0.8	91.2	1.06	-74.3	-6.5	29.9	6.0
		5-11-7-2a@4	4.89E+13		17.0	0.8	90.8	1.06	-74.3	-5.0	29.8	6.0
		5-11-7-2a@5	5.27E+13		15.9	1.4	91.2	1.06	-74.3	-6.5	32.1	6.4
	11MX-B-1-3-2	5-10-2b@1	8.14E+12		24.3	1.1	77.3	1.06	-74.3	16.6	5.0	1.0
		5-10-2b@2	6.09E+12		23.1	1.4	77.6	1.06	-74.3	15.2	3.7	0.7
		5-10-2b@3	7.91E+12		23.1	0.8	78.9	1.06	-74.3	13.8	4.8	1.0
		5-10-2b@4	7.06E+12		24.1	1.6	78.8	1.06	-74.3	14.9	4.3	0.9
		5-10-2b@5	7.35E+12		22.4	1.5	79.2	1.06	-74.3	12.8	4.5	0.9
		5-10-2b@6	7.56E+12		23.9	1.0	79.5	1.06	-74.3	14.0	4.6	0.9
		5-10-2b@7	6.50E+12		21.9	1.1	79.5	1.06	-74.3	12.0	4.0	0.8

11MX-B-1-4-24	5-13-24b@1	8.76E+12		23.1	0.9	78.0	1.06	-74.3	14.7	5.3	1.1
	5-13-24b@3	8.79E+12		23.8	1.0	79.1	1.06	-74.3	14.2	5.3	1.1
	5-13-24b@4	1.13E+13		25.3	0.9	80.8	1.06	-74.3	13.9	6.9	1.4
	5-13-24b@5	6.76E+12		21.4	1.8	76.7	1.06	-74.3	14.5	4.1	0.8
11MX-B-2-4-19	6-7-19@1	6.12E+12	1.88E+12	43.4	0.7	80.7	1.06	-74.3	32.2	3.3	0.7
	6-7-19@2	7.82E+12		38.4	0.8	80.7	1.06	-74.3	27.1	4.2	0.8
	6-7-19@3	5.21E+12		35.9	0.6	80.7	1.06	-74.3	24.6	2.8	0.6
	6-7-19-2@1	3.78E+13		32.3	0.3	90.7	1.06	-74.3	10.5	20.1	4.0
	6-7-19-2@2	4.09E+13		31.2	0.3	90.7	1.06	-74.3	9.4	21.8	4.4
	6-7-19-2@3	4.62E+13		29.9	0.3	90.7	1.06	-74.3	8.1	24.6	4.9
	6-7-19-2@4	3.70E+13		32.5	0.3	90.7	1.06	-74.3	10.7	19.7	3.9
11MX-B-2-4-17	6-7-17@1	8.32E+12		45.1	0.5	81.2	1.06	-74.3	33.4	4.4	0.9
	6-7-17@2	6.57E+12		39.3	2.0	81.2	1.06	-74.3	27.6	3.5	0.7
	6-7-17@3	8.16E+12		43.4	0.6	81.2	1.06	-74.3	31.6	4.3	0.9
11MX-B-2-4-18	6-7-18@1	6.91E+12		41.6	0.7	76.3	1.06	-74.3	35.0	3.7	0.7
	6-7-18@2	5.76E+12		41.4	0.7	76.3	1.06	-74.3	34.8	3.1	0.6
	6-7-18@3	5.46E+12		43.9	0.6	76.3	1.06	-74.3	37.3	2.9	0.6
11MX-B-2-4-7	6-2-7@1	5.41E+12		41.8	0.8	73.4	1.06	-74.3	38.3	2.9	0.6
	6-2-7@2	6.00E+12		42.4	0.5	73.4	1.06	-74.3	39.0	3.2	0.6
	6-2-7@3	7.31E+12		43.2	0.5	73.4	1.06	-74.3	39.8	3.9	0.8
	6-2-7@4	5.70E+12		42.2	0.6	73.4	1.06	-74.3	38.7	3.0	0.6
11MX-B-2-4-3	6-3-3@1	1.15E+13		28.3	1.2	72.1	1.06	-74.3	26.1	6.1	1.2
	6-3-3@2	1.48E+13		37.8	0.3	72.1	1.06	-74.3	35.6	7.9	1.6
	6-3-3@3	1.46E+13		37.7	0.4	72.1	1.06	-74.3	35.6	7.8	1.6
	6-3-3@4	1.23E+13		39.2	0.5	72.1	1.06	-74.3	37.0	6.6	1.3
11MX-B-3-5-3	6-8-3@2	1.29E+13		45.8	1.2	77.4	1.06	-74.3	38.0	6.9	1.4
	6-8-3@3	1.16E+13		40.3	1.7	77.4	1.06	-74.3	32.6	6.2	1.2
11MX-B-3-5-5	6-11-5@1	9.08E+12		45.3	0.6	75.9	1.06	-74.3	39.1	4.8	1.0
	6-11-5@2	8.45E+12		45.5	0.5	75.9	1.06	-74.3	39.3	4.5	0.9
	6-11-5@3	9.59E+12		41.2	0.7	75.9	1.06	-74.3	35.0	5.1	1.0
	6-11-5@4	1.02E+13		43.1	0.5	75.9	1.06	-74.3	36.9	5.4	1.1
11MX-B-3-5-1	6-9-1@1	9.06E+12		44.2	0.4	77.4	1.18	-71.7	24.5	4.8	1.0
	6-9-1@2	7.06E+12		42.9	0.6	77.4	1.18	-71.7	23.2	3.8	0.8
	6-9-1@3	6.32E+12		45.9	1.0	77.4	1.18	-71.7	26.2	3.4	0.7
	6-9-1@4	6.74E+12		43.8	0.6	77.4	1.18	-71.7	24.1	3.6	0.7
11MX-B-3-4-5	6-14-5@1	9.96E+12		44.6	1.3	76.6	1.18	-71.7	25.9	5.3	1.1
	6-14-5@2	8.73E+12		44.4	0.5	76.6	1.18	-71.7	25.7	4.6	0.9
	6-14-5@3	7.09E+12		45.2	0.5	76.6	1.18	-71.7	26.5	3.8	0.8
	6-14-5@4	8.60E+12		44.0	0.5	76.6	1.18	-71.7	25.3	4.6	0.9
11MX-B-3-4-6	6-14-6@1	7.07E+12		43.1	0.5	78.9	1.18	-71.7	21.8	3.8	0.8
	6-14-6@2	8.53E+12		44.8	0.4	78.9	1.18	-71.7	23.5	4.5	0.9
	6-14-6@3	5.80E+13		48.5	0.4	78.9	1.18	-71.7	27.2	30.9	6.2
11MX-B-3-4-12	6-16-12@1	7.82E+12		43.4	0.5	81.9	1.18	-71.7	18.5	4.2	0.8
	6-16-12@2	8.55E+12		44.7	0.6	81.9	1.18	-71.7	19.8	4.6	0.9
	6-16-12@3	8.81E+12		45.1	0.7	81.9	1.18	-71.7	20.2	4.7	0.9
	6-16-12@4	1.04E+13		44.9	0.6	81.9	1.18	-71.7	20.0	5.5	1.1
11MX-B-3-5-7	6-12-7@1	9.87E+12		44.8	1.4	80.0	1.18	-71.7	22.1	5.3	1.1
	6-12-7@2	1.02E+13		47.3	0.9	80.0	1.18	-71.7	24.6	5.4	1.1
	6-12-7@3	6.41E+12		44.6	0.8	80.0	1.18	-71.7	21.8	3.4	0.7
	6-12-7@4	2.02E+13		47.6	0.8	80.0	1.18	-71.7	24.9	10.8	2.2

	11MX-B-4-5-5	6-17-5@1	8.93E+12	45.3	0.5	80.4	1.18	-71.7	22.2	4.8	1.0
		6-17-5@2	8.06E+12	43.8	0.5	80.4	1.18	-71.7	20.7	4.3	0.9
		6-17-5@3	8.76E+12	45.6	0.9	80.4	1.18	-71.7	22.5	4.7	0.9
		6-17-5@4	6.91E+12	47.5	0.5	80.4	1.18	-71.7	24.4	3.7	0.7
	11MX-A-2-6-8	3-12-8@1	7.10E+12	38.2	1.1	77.8	1.18	-71.7	18.1	3.8	0.8
		3-12-8@2	1.29E+13	27.3	1.4	77.8	1.18	-71.7	7.2	6.9	1.4
		3-12-8@3	6.76E+12	42.7	0.9	77.8	1.18	-71.7	22.6	3.6	0.7
		3-12-8@4	6.72E+12	43.6	1.0	77.8	1.18	-71.7	23.5	3.6	0.7
	11MX-A-2-6-7	3-12-7@1	6.83E+12	42.3	1.1	74.1	1.18	-71.7	26.6	3.6	0.7
		3-12-7@2	9.52E+12	40.7	0.9	74.1	1.18	-71.7	25.1	5.1	1.0
		3-12-7@3	9.56E+12	41.1	1.1	74.1	1.18	-71.7	25.4	5.1	1.0
		3-12-7@4	6.46E+12	40.2	1.1	74.1	1.18	-71.7	24.5	3.4	0.7
	11MX-A-1-6-19	3-9-19@1	7.99E+12	41.8	0.9	73.9	1.18	-71.7	26.4	4.3	0.9
		3-9-19@2	8.16E+12	41.6	1.7	73.9	1.18	-71.7	26.2	4.3	0.9
		3-9-19@3	8.23E+12	41.7	0.7	73.9	1.18	-71.7	26.3	4.4	0.9
		3-9-19@4	8.74E+12	43.0	0.8	73.9	1.18	-71.7	27.5	4.7	0.9
	11MX-A-1-6-14	3-10-14-2@1	4.78E+13	36.2	0.7	90.0	1.18	-71.7	1.7	25.5	5.1
		3-10-14-2@2	4.51E+13	33.9	1.0	90.0	1.18	-71.7	-0.6	24.0	4.8
		3-10-14-2@3	4.46E+13	35.8	0.8	90.0	1.18	-71.7	1.3	23.7	4.7
		3-10-14-2@4	4.13E+13	35.5	0.7	90.0	1.18	-71.7	1.0	22.0	4.4
SH	MX-C-2-1-16	1-3-16@1	6.81E+12	48.6	1.1	83.2	1.18	-71.7	22.1	3.6	0.7
		1-3-16@2	4.62E+12	44.1	1.1	83.2	1.18	-71.7	17.5	2.5	0.5
		1-3-16@3	8.11E+12	38.3	0.8	83.2	1.18	-71.7	11.7	4.3	0.9
		1-3-16@4	6.70E+12	36.5	0.9	83.2	1.18	-71.7	10.0	3.6	0.7
	MX-C-2-1-15	1-3-15@1	1.10E+13	45.8	0.6	68.1	1.18	-71.7	37.2	5.9	1.2
		1-3-15@2	7.71E+12	44.7	1.1	68.1	1.18	-71.7	36.1	4.1	0.8
		1-3-15@3	9.78E+12	43.2	1.3	68.1	1.18	-71.7	34.6	5.2	1.0
		1-3-15@4	1.00E+13	31.6	0.8	68.1	1.18	-71.7	23.0	5.3	1.1
	MX-C-2-1-36	1-8-36@1	1.32E+13	27.9	0.9	75.9	1.18	-71.7	10.1	7.0	1.4
		1-8-36@2	1.26E+13	23.8	0.7	75.9	1.18	-71.7	6.0	6.7	1.3
		1-8-36@3	1.26E+13	26.2	0.5	75.9	1.18	-71.7	8.4	6.7	1.3
		1-8-36@4	1.40E+13	25.9	1.0	75.9	1.18	-71.7	8.1	7.5	1.5
	MX-C-4-2-22	1-11-22@1	8.30E+12	45.7	1.0	80.1	1.18	-71.7	22.9	4.4	0.9
		1-11-22@2	6.00E+12	50.4	0.8	80.1	1.18	-71.7	27.6	3.2	0.6
		1-11-22@3	3.46E+12	49.7	1.5	80.1	1.18	-71.7	26.9	1.8	0.4
		1-11-22@4	7.60E+12	46.5	1.0	80.1	1.18	-71.7	23.7	4.0	0.8
	MX-C-4-2-10	1-12-10@1	2.82E+13	37.4	0.6	83.1	1.18	-71.7	11.1	15.0	3.0
		1-12-10@2	1.85E+13	43.7	0.6	83.1	1.18	-71.7	17.4	9.8	2.0
		1-12-10@3	1.75E+13	43.5	1.1	83.1	1.18	-71.7	17.2	9.3	1.9
		1-12-10@4	5.31E+12	45.9	1.0	83.1	1.18	-71.7	19.5	2.8	0.6
	MX-C-2-1-12	1-5-12@1	1.55E+13	42.3	0.8	76.8	1.18	-71.7	23.4	8.3	1.7
		1-5-12@2	1.91E+13	37.5	0.9	76.8	1.18	-71.7	18.6	10.2	2.0
		1-5-12@3	3.13E+13	32.0	0.6	76.8	1.18	-71.7	13.1	16.7	3.3
		1-5-12@4	2.70E+13	34.4	0.6	76.8	1.18	-71.7	15.6	14.4	2.9
	MX-C-4-2-14	1-13-14@2	3.31E+12	44.2	1.6	80.7	1.18	-71.7	20.6	1.8	0.4
		1-13-14@3	9.82E+12	46.0	1.1	80.7	1.18	-71.7	22.5	5.2	1.0
		1-13-14@4	2.44E+13	18.8	1.0	80.7	1.18	-71.7	-4.7	13.0	2.6
	MX-C-4-2-23	1-10-23@2	3.06E+13	25.0	0.8	75.9	1.18	-71.7	7.2	16.3	3.3
		1-10-23@3	2.13E+13	34.4	0.6	75.9	1.18	-71.7	16.6	11.3	2.3

	MX-C-4-2-20	1-10-20@1	2.28E+13		24.6	0.5	79.2	1.18	-71.7	2.8	12.1	2.4
		1-10-20@2	2.29E+13		28.0	0.5	79.2	1.18	-71.7	6.3	12.2	2.4
		1-10-20@3	3.28E+13		34.4	1.0	79.2	1.18	-71.7	12.7	17.4	3.5
		1-10-20@4	3.48E+13		27.9	0.4	79.2	1.18	-71.7	6.2	18.5	3.7
		1-10-20@5	2.60E+13		18.4	0.5	79.2	1.18	-71.7	-3.3	13.8	2.8
		1-10-20@6	2.48E+13		17.8	0.5	79.2	1.18	-71.7	-3.9	13.2	2.6
	MX-C-4-2-21	1-10-21@1	7.40E+12		27.9	0.9	81.2	1.18	-71.7	3.9	3.9	0.8
		1-10-21@2	2.99E+13		26.0	0.6	81.2	1.18	-71.7	2.0	15.9	3.2
		1-10-21@3	2.61E+13		31.0	0.8	81.2	1.18	-71.7	6.9	13.9	2.8
		1-10-21@4	5.83E+12		40.2	1.1	81.2	1.18	-71.7	16.1	3.1	0.6
	MX-C-4-2-24	1-10-24@1	1.84E+13		45.9	0.5	78.1	1.18	-71.7	25.5	9.8	2.0
		1-10-24@2	1.21E+13		41.9	1.0	78.1	1.18	-71.7	21.5	6.4	1.3
		1-10-24@3	1.50E+13		48.3	0.7	78.1	1.18	-71.7	27.9	8.0	1.6
		1-10-24@4	1.51E+13		42.1	1.0	78.1	1.18	-71.7	21.8	8.0	1.6
		1-10-24@5	1.36E+13		49.7	0.8	78.1	1.18	-71.7	29.3	7.3	1.5
		1-10-24@6	1.41E+13		50.9	1.0	78.1	1.18	-71.7	30.5	7.5	1.5
BL	12BL-3-3-1-17	10-0-17@1	1.40E+05	2.21E+12	30.0	0.8	76.9	1.06	-74.3	22.8	4.9	1.0
		10-0-17@2	8.11E+04		29.2	0.9	78.3	1.06	-74.3	20.5	2.8	0.6
		10-0-17@3	5.26E+04		31.6	0.9	82.6	1.06	-74.3	18.4	1.8	0.4
		10-0-17@4	5.17E+04		40.6	1.1	81.5	1.06	-74.3	28.5	1.8	0.4
		10-0-17@5	4.31E+04		36.7	1.7	81.6	1.06	-74.3	24.5	1.5	0.3
		10-0-17@6	8.70E+04		31.9	1.4	79.4	1.06	-74.3	22.0	3.1	0.6
		10-0-17@7	5.16E+04		30.9	1.4	81.0	1.06	-74.3	19.3	1.9	0.4
		10-0-17@8	6.27E+04		28.4	1.9	80.2	1.06	-74.3	17.8	2.4	0.5
		10-0-17@9	6.90E+04		24.7	0.8	81.2	1.06	-74.3	12.9	3.0	0.6
		10-0-17@10	8.01E+04		31.9	1.1	78.1	1.06	-74.3	23.5	3.7	0.7
		10-0-17@11	8.62E+04		32.2	1.2	76.0	1.06	-74.3	26.0	4.1	0.8
	12BL-3-3-1-19	10-0-19-3@1	1.37E+13		29.7	1.1	66.4	1.06	-74.3	33.6	6.2	1.2
		10-0-19-3@2	1.13E+13		30.8	1.1	66.4	1.06	-74.3	34.7	5.1	1.0
		10-0-19-3@3	1.08E+13		29.9	1.6	66.4	1.06	-74.3	33.8	4.9	1.0
		10-0-19-3@4	8.39E+12		30.0	0.9	66.4	1.06	-74.3	33.9	3.8	0.8
		10-0-19-2@1	1.38E+13		35.5	1.4	73.9	1.06	-74.3	31.5	6.3	1.3
		10-0-19-2@2	1.25E+13		34.1	1.9	73.9	1.06	-74.3	30.1	5.7	1.1
	12BL-3-3-1-16	10-0-16-6@2	2.09E+12		39.3	1.7	74.1	1.06	-74.3	35.0	0.9	0.2
		10-0-16-6@3	2.38E+12		40.1	1.7	74.1	1.06	-74.3	35.8	1.1	0.2
		10-0-16-6@4	4.26E+12		39.6	1.4	74.1	1.06	-74.3	35.4	1.9	0.4
		10-0-16-6@5	3.45E+12		35.9	1.2	74.1	1.06	-74.3	31.6	1.6	0.3
		10-0-16-5@1	3.90E+12		37.4	1.5	76.6	1.06	-74.3	30.5	1.8	0.4
		10-0-16-5@2	4.11E+12		35.5	1.4	76.6	1.06	-74.3	28.5	1.9	0.4
		10-0-16-5@3	4.12E+12		37.5	1.4	76.6	1.06	-74.3	30.6	1.9	0.4
	12BL-3-3-1-18	10-0-18@1	1.46E+13		35.3	1.6	66.3	1.06	-74.3	39.3	6.6	1.3
		10-0-18@02	7.03E+12		28.5	1.2	76.7	1.06	-74.3	21.5	3.2	0.6
		10-0-18@03	6.84E+12		28.9	1.0	75.1	1.06	-74.3	23.6	3.1	0.6
		10-0-18@04	8.08E+12		32.2	1.5	76.4	1.06	-74.3	25.5	3.7	0.7
		10-0-18@05	1.01E+13		37.6	1.1	76.2	1.06	-74.3	31.1	4.6	0.9
		10-0-18@06	1.03E+13		33.8	0.9	76.6	1.06	-74.3	27.0	4.7	0.9
		10-0-18@07	8.18E+12		35.4	1.6	80.3	1.06	-74.3	24.6	3.7	0.7
		10-0-18@08	5.44E+12		22.3	1.2	80.2	1.06	-74.3	11.6	2.5	0.5
		10-0-18@09	2.68E+12		36.1	1.3	78.1	1.06	-74.3	27.6	1.2	0.2
		10-0-18@10	4.24E+12		32.9	1.4	76.9	1.06	-74.3	25.7	1.9	0.4
		10-0-18@11	6.53E+12		29.1	1.2	76.8	1.06	-74.3	22.0	3.0	0.6
		10-0-18@12	8.19E+12		28.5	1.0	76.2	1.06	-74.3	22.1	3.7	0.7
		10-0-18-2@1	1.06E+13		25.9	0.9	77.8	1.06	-74.3	17.8	4.8	1.0
		10-0-18-2@2	8.57E+12		26.4	0.8	77.8	1.06	-74.3	18.3	3.9	0.8
		10-0-18-2@3	5.04E+12		30.5	1.0	77.8	1.06	-74.3	22.4	2.3	0.5

	10-0-18-1@2	7.26E+12	29.0	0.8	78.5	1.06	-74.3	20.1	3.3	0.7
	10-0-18-1@3	7.20E+12	29.2	0.7	78.7	1.06	-74.3	20.0	3.3	0.7
12BL-1-2-1-9	8-8-9@1	2.71E+12	36.8	1.4	80.7	1.06	-74.3	25.6	1.2	0.2
	8-8-9@2	5.14E+12	33.8	1.6	80.7	1.06	-74.3	22.5	2.3	0.5
	8-8-9@3	3.47E+12	34.6	1.3	80.7	1.06	-74.3	23.4	1.6	0.3
	8-8-9@4	3.30E+12	36.0	1.3	80.7	1.06	-74.3	24.8	1.5	0.3
	8-8-9@5	4.10E+12	41.8	1.3	80.7	1.06	-74.3	30.6	1.9	0.4
	8-8-9@6	4.78E+12	37.8	1.5	80.7	1.06	-74.3	26.6	2.2	0.4
12BL-1-1-1-10	8-3-10@1	4.34E+12	35.4	1.4	80.8	1.06	-74.3	24.1	2.0	0.4
	8-3-10@2	4.45E+12	34.2	1.6	80.8	1.06	-74.3	22.9	2.0	0.4
	8-3-10@3	3.04E+12	34.6	1.9	80.8	1.06	-74.3	23.2	1.4	0.3
	8-3-10@4	4.78E+12	34.3	1.3	80.8	1.06	-74.3	23.0	2.2	0.4
12BL-1-1-1-4	8-1-4@02	6.01E+12	44.5	1.9	74.5	1.06	-74.3	39.8	2.7	0.5
	8-1-4@04	7.25E+12	30.4	1.4	74.5	1.06	-74.3	25.7	3.3	0.7
	8-1-4@05	1.06E+13	25.3	0.9	74.5	1.06	-74.3	20.6	4.8	1.0
	8-1-4@06	3.73E+12	32.5	1.6	74.5	1.06	-74.3	27.8	1.7	0.3
	8-1-4@07	3.80E+12	37.2	1.3	74.5	1.06	-74.3	32.5	1.7	0.3
	8-1-4@08	3.85E+12	35.1	1.7	74.5	1.06	-74.3	30.4	1.7	0.3
	8-1-4@09	2.76E+12	40.9	1.1	74.5	1.06	-74.3	36.2	1.2	0.2
	8-1-4@10	3.18E+12	39.9	1.5	74.5	1.06	-74.3	35.3	1.4	0.3
	8-1-4@11	2.71E+12	43.2	1.8	74.5	1.06	-74.3	38.5	1.2	0.2
	8-1-4@13	3.34E+12	48.4	1.6	74.5	1.06	-74.3	43.7	1.5	0.3
	8-1-4@14	4.21E+12	45.1	1.6	74.5	1.06	-74.3	40.5	1.9	0.4
	8-1-4-2@4	3.38E+12	28.3	1.5	79.6	1.06	-74.3	18.3	1.5	0.3
	8-1-4-2@5	3.25E+12	37.7	1.8	79.6	1.06	-74.3	27.6	1.5	0.3
	8-1-4-2@6	2.95E+12	34.7	1.6	79.6	1.06	-74.3	24.7	1.3	0.3
	8-1-4-2@7	3.28E+12	38.0	1.3	79.6	1.06	-74.3	27.9	1.5	0.3
	8-1-4-2@8	2.99E+12	40.7	2.0	79.6	1.06	-74.3	30.6	1.4	0.3

Table 6-4 Oxygen isotope of cpx phenocrysts in the Fujian basalts.

Location/Sample No.	Sample No.	Mg#	$\delta^{18}O_{SIMS}$	$Slop_{Mg,O}$	$intercept_{Mg,O}$	IMF_{ST}	IMF	Mean of $\delta^{18}O_{cor}$	SD	Si	Al	Ca	Ca/Al	Si/Al
MX-5-3-8	5-4-8@03	81.9	7.4	-0.162	13.5	0.3	-0.6	8.0	0.4	1.8	0.2	0.8	3.7	8.3
	5-4-8@04	81.5	6.7	-0.162	13.5	0.2	-0.6	7.4	0.1	1.8	0.2	0.9	4.4	8.9
	5-4-8@5	81.5	7.4	-0.162	13.5	-0.1	-1.0	7.8	0.2	1.8	0.2	0.9	4.4	8.9
MX-5-3-8	5-4-8@6	82.8	7.9	-0.162	13.5	1.7	-0.6	7.9	0.2	1.8	0.2	0.9	3.7	7.5
	5-4-8@7	82.7	6.9	-0.162	13.5	0.0	-1.1	8.1	0.3	1.8	0.2	0.8	4.3	9.3
MX-5-3-7	5-4-7@1	76.8	7.7	-0.162	13.5	0.1	-0.1	7.5	0.1	1.8	0.2	1.0	4.1	7.6
MX-5-3-10	5-3-10@1	80.5	7.4	-0.218	17.2	1.7	-0.1	7.4	0.4	1.8	0.2	0.8	3.6	7.6
MX-1-6-12	3-8-12@1	75.2	8.1	-0.2	17.8	1.4	2.0	6.0	0.1	1.8	0.2	1.0	4.1	7.6
MX-1-6-13	3-8-13@1	72.5	8.4	-0.216	17.8	1.4	2.6	5.4	0.4	1.7	0.3	1.0	2.7	4.9
MX-1-6-14	3-10-14@1	79.1	6.6	-0.085	7.4	0.8	0.8	5.9	0.1	1.8	0.2	0.9	4.9	9.4
	3-10-14@4	79.1	6.7	-0.085	7.4	0.8	0.8	5.9	0.0	1.8	0.2	0.9	4.9	9.4
	3-10-14@6	79.1	7.2	-0.085	7.4	0.8	0.8	6.5	0.1	1.8	0.2	0.9	4.9	9.4
	3-10-14@8	79.1	7.0	-0.085	7.4	0.7	0.7	6.2	0.0	1.8	0.2	0.9	4.9	9.4
	3-10-14@10	79.1	7.2	-0.085	7.4	0.7	0.7	6.5	0.0	1.8	0.2	0.9	4.9	9.4
MX-1-6-19	3-9-19@1	73.9	6.2	-0.085	7.4	1.3	1.2	6.2	0.3	1.7	0.3	1.0	2.9	5.2
MX-1-6-22	3-5-22@3	76.3	6.2	-0.216	17.8	1.4	1.8	6.2	0.0	1.7	0.3	0.9	3.0	5.5
MX-1-6-23	3-7-23@1	75.4	7.2	-0.216	17.8	1.4	2.0	7.1	0.3	1.8	0.2	0.9	3.9	7.3
MX-1-6-24	3-6-24@1	79.1	6.9	-0.085	7.4	1.4	1.2	6.9	0.1	1.8	0.3	0.9	3.6	6.8
MX-1-6-28	3-4-28@3	81.6	7.2	-0.085	7.4	1.4	0.6	7.2	0.0	1.8	0.3	0.9	3.5	6.6
MX-1-6-29	3-1-29@1	76.7	5.7	-0.216	17.8	2.1	2.3	5.5	0.1	1.8	0.3	0.9	3.5	6.6
	3-1-29@3	76.7	6.2	-0.216	17.8	1.9	2.2	6.3	0.1	1.8	0.3	0.9	3.5	6.6
	3-1-29@5	76.7	5.9	-0.216	17.8	1.8	2.1	6.1	0.2	1.8	0.3	0.9	3.5	6.6
	3-1-29@6	76.7	6.4	-0.216	17.8	1.8	2.0	6.3	0.1	1.8	0.3	0.9	3.5	6.6
MX-1-6-4	3-2-4@1	80.6	5.5	-0.216	17.8	1.7	1.1	5.5	0.1	1.8	0.2	0.9	4.9	9.6
MX-1-6-6	3-3-6@1	77.7	6.0	-0.216	17.8	1.5	1.6	6.2	0.3	1.8	0.2	0.9	4.4	8.7
MX-2-6-14	3-13-14@1	80.3	5.9	-0.216	17.8	2.6	2.0	6.2	0.2	1.9	0.2	0.9	5.3	10.7
MX-2-6-4	3-11-4@1	78.2	6.7	-0.085	7.4	1.5	0.9	6.5	0.1	1.7	0.3	1.0	3.3	6.0
MX-2-6-5	3-11-5@1	77.3	6.5	-0.085	7.4	1.4	1.0	6.5	0.2	1.8	0.3	1.0	3.5	6.4
MX-2-6-7	3-12-7@1	74.1	6.4	-0.085	7.4	1.4	1.2	6.4	0.2	1.7	0.3	1.0	2.8	5.0
MX-2-6-8	3-12-8@1	77.8	6.8	-0.085	7.4	1.4	0.9	6.7	0.1	1.8	0.3	0.9	3.4	6.4
MX-2-7-2	3-17-2@1	77.4	6.2	-0.216	17.8	2.5	2.7	6.3	0.3	1.7	0.3	0.9	3.2	5.9
MX-2-7-3	3-17-3@1	80.6	6.7	-0.216	17.8	2.5	1.9	6.6	0.0	1.8	0.2	0.9	4.2	8.3
MX-2-7-4	3-16-4@1	77.2	6.5	-0.216	17.8	2.6	2.7	6.5	0.1	1.8	0.2	1.0	4.7	8.9
MX-2-7-8	3-15-8@1	74.0	5.9	-0.216	17.8	2.6	3.4	5.7	0.2	1.7	0.3	1.0	2.9	5.1
MX-2-7-8.2	3-15-8-2@1	76.1	5.9	-0.216	17.8	2.6	3.0	5.7	0.1	1.8	0.3	1.0	3.3	6.1
MX-4-3-4	5-9-4@1	75.2	6.7	-0.162	13.5	1.4	0.7	6.7	0.4	1.7	0.3	1.0	3.3	6.1
MX-4-3-6	5-9-6@1	80.7	5.4	-0.162	13.5	1.3	-0.6	5.4	0.0	1.9	0.2	0.9	5.7	11.2
MX-4-3-7	5-11-7@1	78.1	7.0	-0.162	13.5	1.2	-0.1	7.0	0.2	1.8	0.2	0.9	3.8	7.3
MX-4-4-13	5-14-13@4	80.5	6.1	-0.162	13.5	1.0	-0.8	7.1	1.0	1.8	0.2	0.9	5.1	10.1
MX-4-4-18	5-15-18@1	79.7	6.5	-0.162	13.5	1.2	-0.5	6.5	0.0	1.8	0.2	0.9	4.1	7.8
MX-4-4-18.2	5-15-18-2@1	76.8	6.6	-0.162	13.5	1.2	0.2	6.5	0.2	1.8	0.2	0.9	4.1	7.8
MX-8-4-13	6-6-13@1	78.5	6.4	-0.216	17.8	2.6	2.4	6.4	0.0	1.9	0.2	0.9	5.5	10.9
MX-8-4-16	6-7-18@1	78.2	6.4	-0.216	17.8	1.9	1.8	6.6	0.2	1.8	0.2	0.9	5.1	10.0
MX-8-4-17	6-7-17@1	81.2	7.1	-0.216	17.8	2.0	1.3	7.0	0.1	1.9	0.2	0.9	5.8	11.6
MX-8-4-19	6-7-19@1	80.7	7.4	-0.216	17.8	1.6	1.0	7.3	0.1	1.8	0.2	0.9	4.0	8.0
MX-9-5-1	6-9-1@1	77.4	6.6	-0.216	17.8	2.2	2.4	6.3	0.3	1.9	0.2	0.9	5.4	10.6
MX-9-5-5	6-11-5@1	75.9	6.0	-0.216	17.8	2.5	2.9	5.8	0.2	1.8	0.2	0.9	3.8	7.3
MX-5-3-11	5-5-11@1	83.0	7.8	-0.162	13.5	0.7	-0.4	7.4	0.3	1.8	0.3	0.9	3.3	7.1
MX-5-4-14	3-19-14@1	81.4	5.5	-0.216	17.8	2.1	1.4	5.5	0.2	1.8	0.2	1.0	5.6	10.8
MX-5-4-21	3-18-21@1	81.3	7.2	-0.216	17.8	2.2	1.5	7.5	0.2	1.8	0.2	0.9	4.7	9.1
MX-7-2-4	14-3-4@1	81.4	8.0	-0.123	10.2	2.6	1.1	8.2	0.2	1.9	0.2	0.9	4.8	9.9
MX-7-2-7	14-4-7@1	76.0	7.7	-0.123	10.2	2.6	2.1	7.5	0.1	1.8	0.3	0.9	3.4	6.6
Mean								8.2	5.4					

Location/Sample No.	Sample No.	Mg#	$\delta^{18}O_{SIMS}$	$Slop_{Mg.O}$	$intercept_{Mg.O}$	IMF_{ST}	IMF	Mean of $\delta^{18}O_{cor}$	SD	Si	Al	Ca	Ca/Al	Si/Al
SH-1-1-1	2-9-1@1	76.6	8.5	12.970	0.9	2.4	2.8	5.7	0.1	1.8	0.3	0.8	2.8	5.9
SH-1-1-13	2-17-13@1	76.8	8.4	12.970	0.9	2.0	2.4	6.2	0.1	1.8	0.2	0.9	4.0	7.7
SH-1-1-16	2-16-16@1	80.3	9.1	12.970	0.9	2.4	2.4	6.7	0.1	1.8	0.2	0.9	3.6	7.7
SH-1-1-19	2-16-19@1	82.1	8.6	12.970	0.9	2.3	2.0	7.6	0.0	1.9	0.2	0.9	5.6	11.1
SH-1-1-3	2-10-3@1	83.1	8.3	12.970	0.9	2.0	1.6	7.0	0.2	1.9	0.1	0.9	6.1	12.8
SH-1-1-5	2-13-5@1	79.9	10.8	12.970	0.9	2.5	2.6	8.2	0.0	1.8	0.2	0.9	4.2	8.7
SH-1-1-9	2-15-9@1	81.0	8.5	12.970	0.9	1.8	1.7	7.0	0.2	1.9	0.2	0.8	5.1	12.0
SH-2-1-10.2	1-5-10@1	81.2	6.5	12.970	0.9	0.6	-0.6	7.2	0.0	1.9	0.2	0.9	5.8	12.3
SH-2-1-12	1-5-12@1	76.8	6.9	12.970	0.9	0.6	0.1	6.6	0.1	1.8	0.2	0.9	4.2	9.0
SH-2-1-22	2-7-22@1	79.8	8.6	12.970	0.9	2.6	2.6	6.0	0.0	1.8	0.2	0.9	3.7	8.0
SH-2-1-25	2-5-25@1	75.9	4.1	12.970	0.9	2.5	3.0	5.4	0.1	1.8	0.2	0.9	4.0	8.1
	2-5-25@4	75.9	8.3	12.970	0.9	2.0	2.6	5.7	0.0	1.8	0.2	0.9	4.0	8.1
SH-2-1-26	2-8-26@1	79.5	8.9	12.970	0.9	2.4	2.4	6.3	0.2	1.9	0.2	0.9	5.4	11.3
SH-2-1-27	2-8-27@1	82.6	8.7	12.970	0.9	2.3	2.0	6.8	0.1	1.9	0.2	0.9	4.6	10.1
SH-2-1-29	2-6-29@1	81.0	8.4	12.970	0.9	2.4	2.2	6.6	0.3	1.9	0.2	0.8	4.6	10.6
SH-2-1-36	1-8-36@1	75.9	6.9	12.970	0.9	0.9	0.5	6.5	0.1	1.8	0.3	0.8	3.1	6.9
SH-3-1-1	2-2-1@1	82.8	9.3	12.970	0.9	3.2	2.8	6.6	0.0	1.9	0.1	0.9	6.7	13.8
SH-3-1-10	2-2-10@1	79.6	8.7	12.970	0.9	2.0	2.1	6.3	0.3	1.8	0.2	0.8	3.5	7.6
SH-3-1-2	2-2-2@1	76.5	8.8	12.970	0.9	2.2	2.7	6.0	0.2	1.8	0.3	0.9	3.3	6.6
SH-3-1-3	2-2-3@1	82.3	9.5	12.970	0.9	2.1	1.8	6.8	0.2	1.9	0.2	0.9	4.8	9.8
SH-3-1-30	2-4-30@1	82.2	8.7	12.970	0.9	2.5	2.1	6.4	0.2	1.9	0.2	0.8	5.4	12.4
SH-3-1-32	2-3-32@1	80.2	8.7	12.970	0.9	2.5	2.4	6.3	0.0	1.9	0.2	0.9	4.8	9.8
SH-3-1-4	2-2-6@1	73.5	9.0	12.970	0.9	2.0	2.9	6.1	0.2	1.7	0.3	0.9	2.7	5.2
SH-3-1-5	2-2-5@1	77.9	8.8	12.970	0.9	1.9	2.2	6.8	0.2	1.9	0.2	0.9	4.9	10.2
SH-3-1-6	2-2-6@4	76.5	9.1	12.970	0.9	2.1	2.6	6.4	0.1	1.7	0.3	0.9	2.6	5.0
SH-4-2-10	1-12-10@1	83.1	6.1	-0.155	12.5	0.6	-0.9	7.0	0.1	1.9	0.2	0.8	4.3	9.5
SH-4-2-14	1-13-14@1	80.7	7.1	-0.155	12.5	0.7	-0.4	6.7	0.6	1.9	0.2	0.9	5.4	11.3
SH-4-2-20	1-10-20@1	79.2	5.9	-0.226	17.8	0.0	-1.1	7.1	0.3	1.9	0.2	0.9	4.1	8.8
SH-4-2-24	1-10-24@1	78.1	6.4	-0.226	17.8	0.0	-0.8	7.5	0.5	1.8	0.2	0.9	3.7	7.6
SH-4-2-4	2-2-4@1	82.0	8.1	12.970	0.9	2.2	1.9	6.6	0.4	1.9	0.2	0.8	5.2	12.0
SH-4-2-5	2-2-5@1	76.7	8.4	12.970	0.9	2.3	2.7	5.7	0.0	1.8	0.3	0.9	2.9	5.6
Mean								8.2	5.4					
BL-7-1-9	8-8-9@1	80.7	6.8	-0.081	6.2	0.3	-1.1	7.5	0.3	1.9	0.2	0.7	4.9	12.8
BL-8-1-12	9-6-12@1	74.9	8.2	11.765	1.0	2.2	2.8	5.1	0.2	1.9	0.2	0.9	4.0	8.8
BL-8-1-13	9-6-13@1	74.7	9.1	11.765	1.0	2.3	2.9	6.1	0.2	1.8	0.2	0.9	4.1	8.3
BL-8-1-4.1	9-2-4-1@1	73.8	8.3	11.765	1.0	2.2	2.9	4.7	0.1	1.9	0.1	0.9	6.3	13.9
BL-8-1-7	9-5-7@1	80.2	8.4	11.765	1.0	2.2	2.1	5.9	0.3	1.9	0.1	0.8	5.6	12.8
BL-8-1-7.2	9-5-7-2@1	75.4	7.8	11.765	1.0	2.1	2.7	5.4	0.3	1.8	0.2	0.9	4.1	8.3
BL-8-1-8	9-3-8@1	74.1	8.0	11.765	1.0	2.1	2.8	5.3	0.2	1.9	0.1	0.9	6.9	15.3
BL-11-1-10	9-8-10@1	80.4	8.2	11.765	1.0	2.3	2.2	6.0	0.1	1.9	0.2	0.8	4.6	11.5
BL-11-1-10.2	9-8-10-2@1	75.7	8.5	11.765	1.0	2.4	2.9	5.7	0.0	1.9	0.1	0.8	5.9	13.1
BL-11-1-10.3	9-8-10-3@1	74.1	8.5	11.765	1.0	2.4	3.1	5.6	0.3	1.8	0.2	0.9	4.7	9.5
BL-11-1-10.4	9-8-10-4@1	75.5	8.5	11.765	1.0	2.3	2.8	5.9	0.1	1.8	0.2	0.9	4.2	8.4
BL-11-1-16.5	10-16-5@1	76.6	6.5	-0.081	6.2	-3.1	-4.1	6.6	0.3	1.9	0.1	0.9	6.2	13.6
BL-11-1-16.4	10-16-4@1	81.4	6.5	-0.081	6.2	-3.1	-4.5	6.8	0.2	1.9	0.2	0.8	4.9	11.8
BL-11-1-16.6	10-16-4@4	74.1	7.3	-0.081	6.2	-3.1	-3.9	7.3	0.0	1.8	0.2	0.9	4.7	9.7
BL-11-1-17	10-1-17@1	80.1	6.2	-0.081	6.2	-3.1	-4.4	6.7	0.1	1.8	0.2	0.9	3.6	7.3
BL-11-1-17.2	10-1-17-2@1	80.4	6.3	-0.081	6.2	-3.1	-4.4	6.6	0.1	1.9	0.2	0.7	3.4	8.9
BL-11-1-17.3	10-1-17-3@1	75.2	7.2	-0.081	6.2	-3.1	-4.0	7.2	0.0	1.9	0.2	0.8	4.1	10.4
BL-11-1-17.4	10-1-17-4@1	76.0	7.0	-0.081	6.2	-3.1	-4.1	7.1	0.0	1.9	0.1	0.8	5.6	14.3
BL-11-1-18	10-1-18-14@1	78.5	6.5	-0.081	6.2	-3.4	-4.5	7.3	0.2	1.9	0.1	0.8	8.2	20.7
BL-11-1-18.2	10-1-18-7@1	80.3	6.5	-0.081	6.2	-3.6	-4.9	7.3	0.1	1.9	0.2	0.8	3.6	8.7
BL-11-1-19	10-1-19-3@1	76.0	6.0	-0.081	6.2	-4.0	-5.0	7.2	0.2	1.8	0.2	0.8	4.2	9.2
BL-11-1-20	9-9-20-1@1	81.8	8.4	-0.081	6.2	2.4	2.1	6.5	0.2	1.9	0.2	0.8	4.8	12.0
Mean								7.5	4.7					

Chapter 7 Hainan basalts and the spatial chemical variation of Cenozoic basalts in East China

7.1 Results

7.1.1 Bulk-rock major and trace element compositions

The major element compositions of cpx phenocrysts for the Hainan basalts are listed in Table 7-1. Zou et al. (2010) have reported three very young basalts in the Hainan Islands (the ML with an age of less than 9 ka, LH with an age of less than 9 ka, and SJY with an age of less than 77ka). The Hainan samples are plotted within a total alkali versus silica (TAS) diagram (Fig. 7-1), with less than 1.5 wt. % LOI (Table 7-1). The Hainan samples show two continuous trends in TAS diagram (Fig. 7-1): most samples from LH and all the DY and FJT samples are the alkaline rocks ranging from basalts through trachybasalts to basaltic trachyandesites, and the ML, SJY samples and one LH sample are sub-alkaline rocks ranging from basalts to basaltic andesite (Fig. 7-1). The ML, LH, and SJY major and trace element compositions are from Zou et al. (2010). The DY basalts have high Al_2O_3 (more than 13 wt. %), intermediate SiO_2 (47.9 to 51 wt. %), TiO_2 (2.2 to 2.5 wt. %), and Fe_2O_3 (about 12 wt. %), and variations in MgO (6.5 to 10.2 wt. %). Meanwhile, the FJT samples have similar MgO (7.8 to 10.1 wt. %) and Al_2O_3 (12.8 to 13.7 wt. %), higher Fe_2O_3 (>12 wt. %) and TiO_2 (>2.7 wt. %), but lower SiO_2 (46.3 to 47.2 wt. %).

In the primitive mantle-normalized extended trace element patterns (Fig. 7-2a), the Hainan basalts can be divide into three series; the two display OIBs-like patterns, including the LH samples (HIMUs-like) except HN9907, the DY and FJT samples (EM-like), while the others have lower trace element concentrations. All the Hainan samples have positive Nb (Ta) anomalies and negative Th and U anomalies except some LH samples. The Hainan samples except DY and FJT samples also share the negative Zr, Hf, and Ti anomalies. These geochemical characteristics have shared some similar points with other Cenozoic basalts in SE China (Li et al., 2015; Chapter 5 and 6). The ML and SJY samples also do not have the positive K anomalies, like the NTS and BL samples in the Fujian region (Fig. 7-2a). Most of the Hainan samples are characterized by high Ba/Th (100-160, except the LH samples), Ce/Pb (>25), and high Nb/Ta (>16),

except the HN9907, ML, and SJY samples.

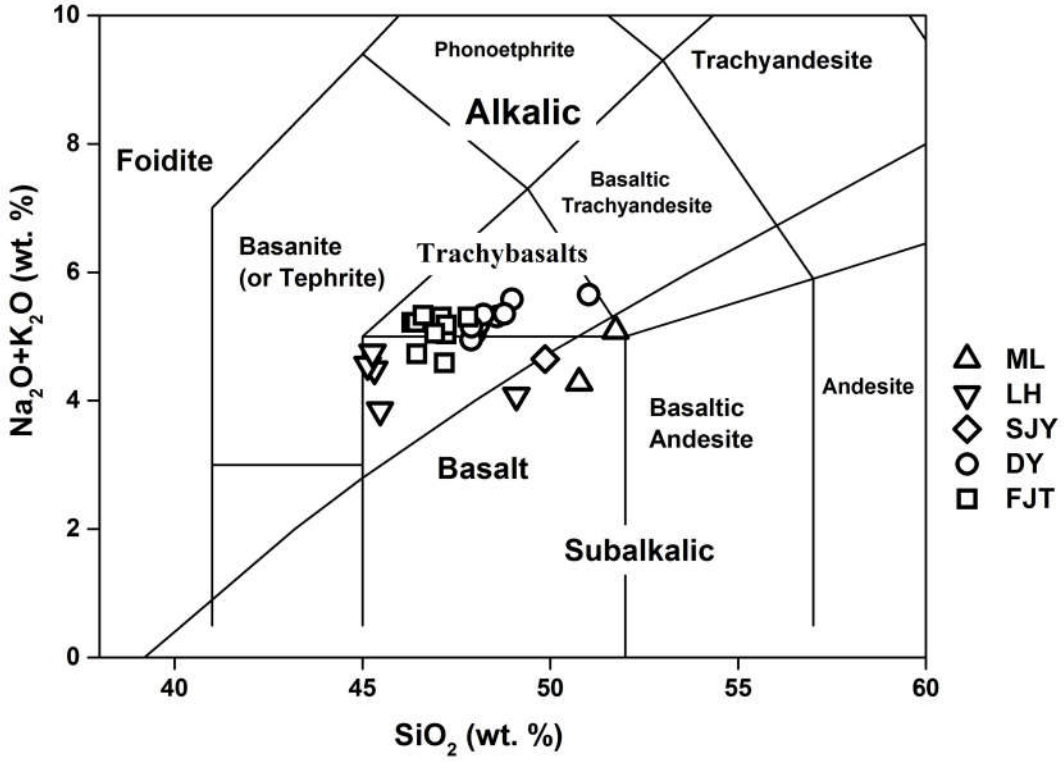

Fig. 7-1 TAS plots of the Hainan basalts. Classification of rock after Le Bas et al. (1986), and line separating the alkali basalts and tholeiites from MacDonald and Katsura (1964).

Chondrite-normalized REE patterns of the Hainan basalts show similar characteristics, with LREE enrichment and HREE depletion (Fig. 7-2b). The LH samples except HN9907 have the most REE concentrations, while the SYJ have the lowest REE concentrations. Meanwhile, the LH samples except HN9907 have almost no Eu anomaly ($Eu_N/Eu^* = Eu_N/(Sm_N * Gd_N)^{1/2}$), while, the slightly positive Eu anomalies are commonly observed for other Hainan samples.

7.1.2 Chemical and isotopic composition of cpx phenocrysts

7.1.2.1 Major elements of cpx phenocrysts

The cpx phenocrysts in the Hainan samples range from the augitic to the diopsidic, with Mg# varying from less than 60 to higher than 86. Most of the Hainan cpx phenocrysts have homogenous intra-granular composition. The Hainan cpx phenocrysts cluster in the Mg# range from 75 to 84. The cpx phenocrysts with very low

Mg# are very rare. The cpx phenocrysts show relatively low Cr_2O_3, in common, in spite of Mg#. The detailed cpx phenocryst major element compositions are listed in Table 7-2. The partition coefficient ($D^{cpx\text{-}melt}$) of H_2O between cpx phenocryst and basaltic melt can be calculated using the equation provided by O'Leary (2010) which depend on cpx phenocryst chemistry.

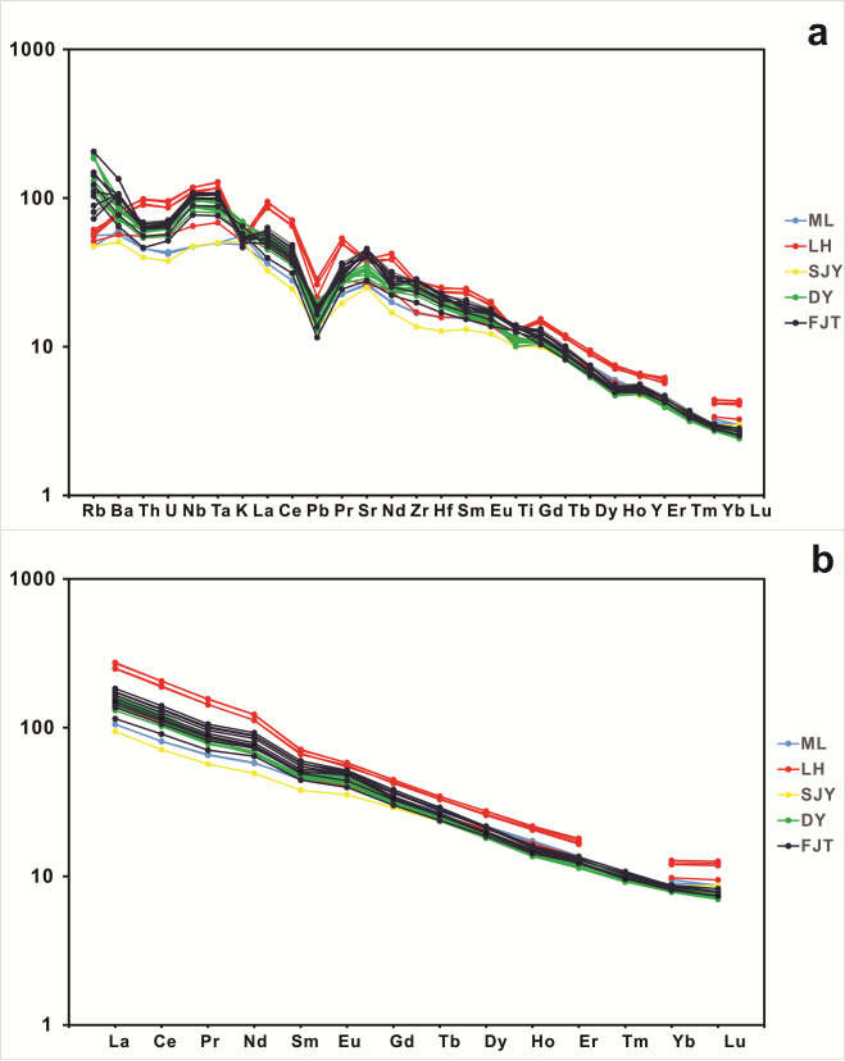

Fig. 7-2 Spider diagram of the Hainan basalt samples; REE content of the Hainan basalt samples, normalized values are from Sun and McDonough (1989), whereas $Pm^*=((Sm)_N * (Nd)_N)^{1/2}$.

7.1.2.2 Water content of cpx phenocrysts

The cpx phenocrysts of the Hainan samples have OH-typical IR absorption spectra in its stretching vibration region (3000-3800 cm^{-1}), and their IR bands are centered at 3630 cm^{-1} and 3540 cm^{-1} (Fig. 7-3), which consist with typical structural OH bands of

cpx in previous studies (Bell et al., 1995; Denis et al., 2013; Ingrin and Skogby, 2000; Kovacs et al., 2012; Li et al., 2008; Peslier et al., 2002; Skogby et al., 1990; Sundvall and Stalder, 2011; Xia et al., 2010; Xia et al., 2013; Xia et al., 2014). The ML, LH, and SJY basalts except HN9910 have almost totally dry cpx phenocrysts (Fig. 7-3a). The typical structural OH bands of HN9910, DY, and FJT samples are presented in Fig. 7-3b, c, and d, respectively. The H_2O contents of the cpx phenocrysts for the HN9910 samples range from 174 to 850 ppm, those of the DY-4 and DY-7 samples range from 36 to 588 ppm, and those of the FJT samples range from 28 to 321 ppm. Other DY and FJT samples failed to provide measurable cpx phenocryst. The detailed major element contents, absorbance of OH bands, section thicknesses, and the calculated H_2O content of the cpx phenocrysts are listed in Table 7-2. The -OH profiles in the FJT cpx phenocrysts display various absorbance from the core to the rim, as shown in Fig. 7-3d. The xenocryst core have higher water contents than those in the phenocryst rim, while the phenocryst also can be observed slight H-loss from the core the rim in FJT-6-1-5 grain. The suspected crust xenocryst with very low Mg# has different –OH absorption spectrum among different measured point in one grain.

7.1.2.3 Li and O isotopic compositions of cpx phenocrysts

The Li and O isotope of cpx phenocrysts are analyzed for the LH samples, with associated chemical composition matrix effect, as we discussed in Chapter 6.

The matrix effect in the Li analysis through SIMS with various cpx element composition are similar as the discussion in Chapter 6. The slopes of δ^7Li IMF line to Mg# for cpx phenocrysts are approximately 1.18 on IMS 1270. All the number of the measured samples are listed and presented in the Table 7-3. The IMF has been discussed in detail in the Chapter 4 and Chapter 6. The corrected δ^7Li values of the LH cpx phenocrysts range from -4 to +5.1‰, and Li content range from 0.2 to 1.5 ppm. The intra-granular Li content and δ^7Li profiles of the cpx phenocrysts are displayed in Fig. 7-4a. The Li content and δ^7Li vs. Mg# for the cpx phenocrysts are plotted in Fig. 7-4b. The detailed intra-granular profiles of these cpx phenocrysts are complex and can be divided into multiple kinds (Fig. 7-4a): a) some cpx phenocrysts display “V”-like δ^7Li, but almost homogeneous Li content. The lightest ^{7}Li are found in the core of phenocrysts; b) some cpx phenocrysts have “W”-like δ^7Li, and corresponding Li content variation. The lightest ^{7}Li are found in the mantle of phenocrysts, while the core of phenocryst have the heaviest ^{7}Li; c) some cpx phenocrysts have “M”-like δ^7Li, and

corresponding Li content variation. The rim have lighter ^{7}Li than the mantle of cpx phenocrysts with opposite trend to the “W”-like phenocrysts.

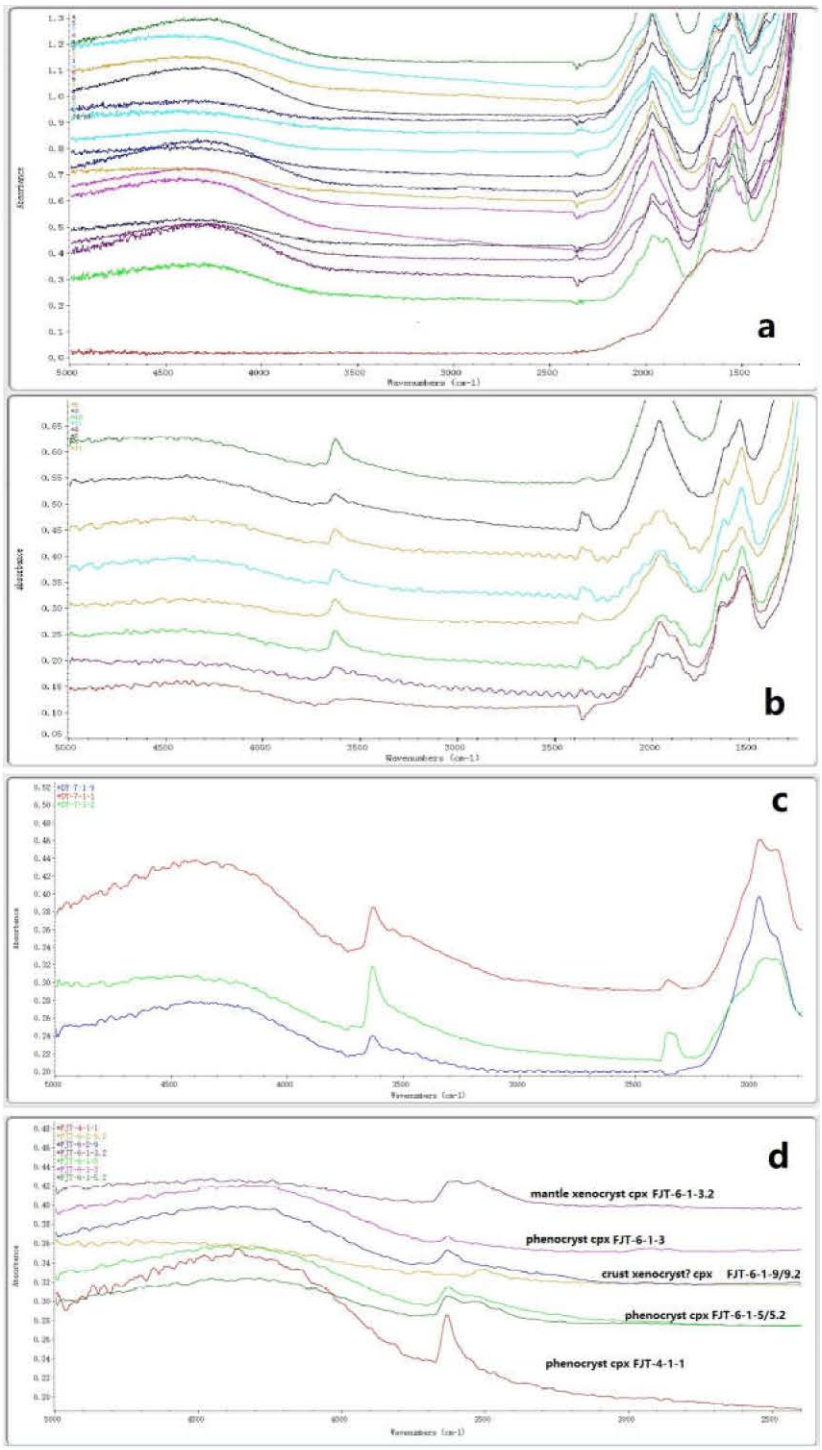

Fig. 7-3 (a) Representative OH IR absorption spectrum of the ML, LH, and SJY cpx phenocrysts, except HN9910; (b) Representative OH IR absorption spectrum of the HN9910 cpx phenocrysts; (c) Representative OH IR absorption spectrum of the DY cpx phenocrysts; and (d) OH IR absorption spectrum profiles of the FJT cpx phenocrysts.

The high Oxygen isotope cpx phenocrysts are found in the Hainan basalts (Fig. 7-4c). Unlike the Hainan basalts, the high Oxygen isotope are observed in spite of Ca/Al ratios. The Oxygen isotope ratios of cpx phenocrysts of the Hainan basalts are listed in Table 7-4. The cpx phenocrysts $\delta^{18}O$ values range from +4.5 to +8.3‰ (n=16), from which most fall within the range from +6.1 ‰ to +8.2‰ and only two are below +5.0‰, two are higher than +10.0‰ as shown in Fig. 7-4c.

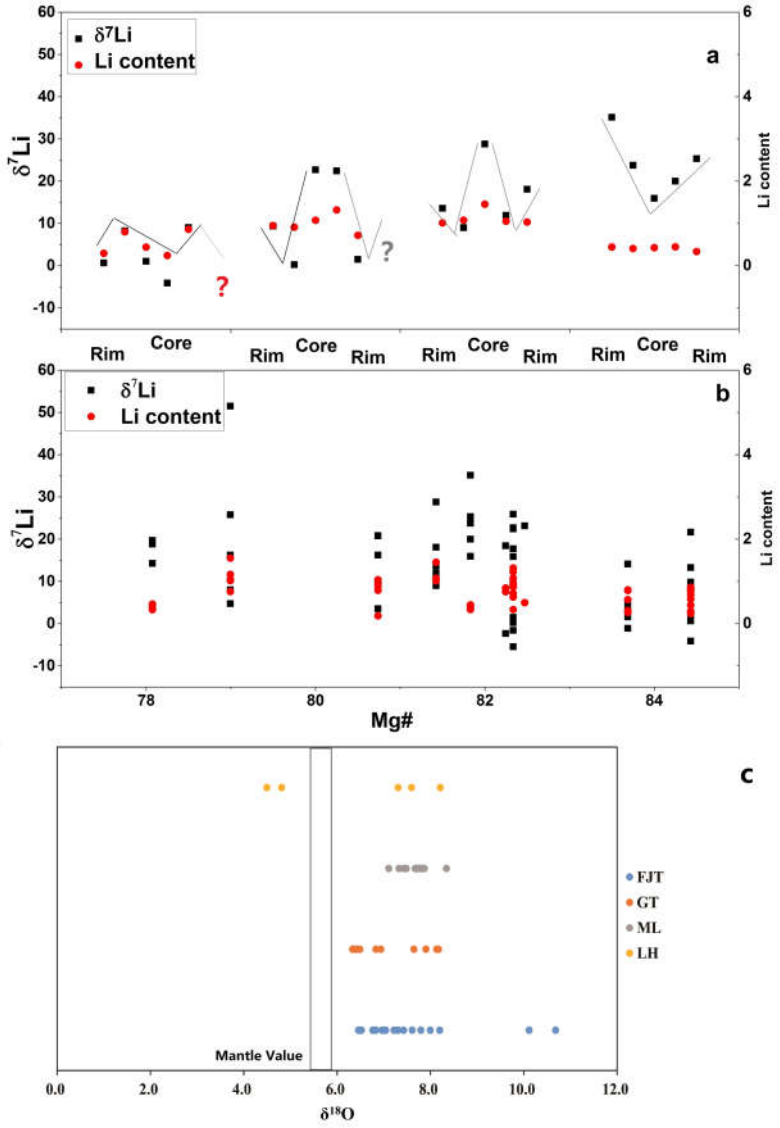

Fig. 7-4 a) Cpx phenocryst intra-grain δ^7Li and Li content profiles of the Hainan basalts; b) The plots of δ^7Li and Li vs. Mg# of the Hainan basalts; (c) The plots of $\delta^{18}O$ for the Hainan cpx phenocrysts.

7.2 Discussions

A large number of studies have been conducted on the Hainan Island basalts in the past, because of the suspicion of the mantle plume beneath the Hainan Island (Fig. 1-2). Zou et al. (2010) have discussed in detail about the existence and the low speed of the upwelling buoyant mantle plume. Meanwhile, the Nd isotopic compositions of the Hainan basalts do not indicate a highly depleted asthenospheric mantle source, but the enriched mantle source of the young Hainan basalts in the MTZ or lower mantle, caught by a plume upwelling. Zou et al. (2010) suggested the other Cenozoic basalts in SE China that might also be the result of partial melting of lower mantle materials in the rising Hainan plume, those include Cathaysia, Hainan Island, and South China Sea Basin.

7.2.1 Crust contamination and fractional crystallization

The continental crust contamination may potentially effect the chemical compositions of the Hainan basalts. The possibilities of continental crust assimilation were excluded by Zou et al. (2010), while, the DY and FJT basalts have high Nb/U (46-51 and 51-54, respectively) and Ce/Pb (23-26 except DY-3, and 21-27, respectively). The OIBs-like high Ce/Pb, and high Nb/U ratios coincide with the values for the global primary OIBs and MORBs (Ce/Pb=25±5, Nb/U=40±7, Hoffmann et al., 1986), suggesting the insignificant influence of continental crusts.

Due to enriched Ni and MgO in peridotites, the decreasing Ni with decreasing MgO in DY and FJT is considered as the result of ol fractional crystallization. While, the CaO/Al_2O_3 have limited variation in spite of Mg#, and limited cpx are found in most DY and FJT samples, suggesting limited cpx fractional crystallization. In addition, positive Ba and Eu anomalies of all the Hainan basalts (Fig. 7-2) exclude a significant fractional crystallization of pl.

7.2.2 Water contents of the Hainan basalts

All the LH, ML, and SJY cpx phenocrysts are totally “dry” (Fig. 7-3a), except the cpx phenocrysts of HN9910 (Fig. 7-3b), unlike the SC and MX samples, which still contain some water enriched cpx phenocrysts. The BL samples are actually water enriched (Chapter 6) and some cpx phenocrysts in SC samples (Chapter 5) as well as Taihang samples (Liu et al., 2015) have residue water with visible -OH IR spectrum

after H loss, disagreeing with the total dehydration. The totally "dry" water contents of cpx phenocrysts are very rare for all the basalts in East China. Three reasons are considered to lead towards the totally "dry" water contents of cpx phenocrysts: (a) the absence of water content in the source of the Hainan basalts; (b) the very intense dehydration before the crystallization of cpx phenocryst, during the Hainan basaltic magma upwelling; (c) the later H-loss after the crystallization of cpx phenocryst. The Li content and δ^7Li profiles of Hainan Island basalts are almost like those of the cpx phenocrysts from BL diabases with regular variation with Li content and δ^7Li from the core to rim (Fig. 7-4a), suggesting significant Li diffusion. If the BL samples are considered to have undergone later H re-equilibrium, these "dry" Hainan cpx phenocryst cannot survive from later H re-equilibrium. Although the samples of HN9907 in LH is really compacted, the samples of ML and some LH are actually enriched in volatiles because of vesicular texture with large number of holes after gaseous escape from magma, arguing against the intense dehydration before eruption. Therefore, the totally "dry" cpx phenocryst are caused by the H-loss of cpx phenocrysts after the crystallization of cpx phenocryst. The LH basalts are suggested to be represented by HN9910 of 2.7% (Table 7-3). The measurable cpx phenocrysts are actually rare in most DY and FJT samples. Only five samples (2 from DY, and 3 from FJT samples) have the efficient results of the H_2O content of a corresponding equilibrated melts deduced from its H_2O content and its corresponding partition coefficient ($D^{cpx\text{-}melt}$). The preliminary results of the H_2O content of corresponding equilibrated basaltic melts range from 0.7 to 1.3 wt. % for the FJT samples, and from 0.7 to 2.6 wt. % for the DY samples. The detailed calculated data of water content for cpx grains and corresponding equilibrated basaltic melts are presented in Table 7-2. The preliminary water content results of the LH, DY, and FJT basalts are similar. The water difference of corresponding equilibrated basaltic melts among cpx phenocrysts with low and high Mg# is really insignificant, relative to the measurement error. The -OH profiles in FJT-6 have slight difference of absorbance between the core and the rim (Fig. 7-3). The absorbance difference suggest the occurrence of later H-loss in FJT, which may also occur in the DY samples, like the SC samples. Therefore, the highest magma water content of 1.3 wt. % and 2.6 wt. % are suggested to represent to the water content of the DY and FJT basalts, respectively; the water content of 1.3 wt. %, 2.6 wt. %, and 2.7 wt. % are considered as the lowest estimation of the FJT, DY, and LH basalts, respectively.

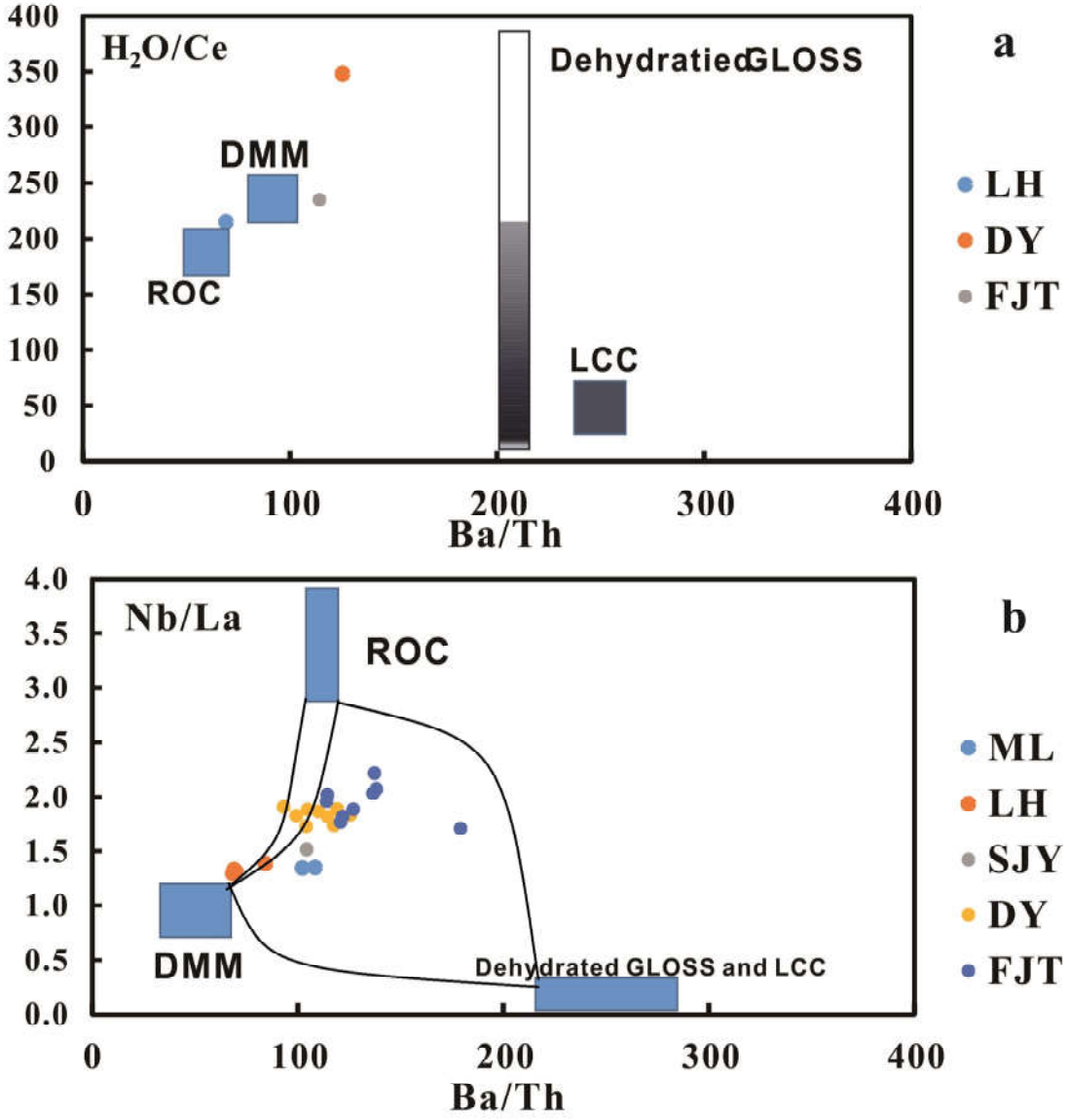

Fig. 7-5 (a) Plots of H_2O/Ce vs. Ba/Th for the Hainan basalt samples. (b) Plots of Nb/La vs. Ba/Th for the Hainan basalt samples. The error bar of H_2O/Ce is 30%. The source data are the same as in Fig. 5-13.

7.2.3 The abnormal Oxygen isotope in Hainan basalts.

The Haina cpx phenocrysts with the high $\delta^{18}O$ values can provide insights into the mixture within the magma system. The $\delta^{18}O$ values in the ML, LH, DY, and FJT cpx phenocrysts are considerably higher than the expected typical mantle values (e.g., Sheppard and Harris, 1985; Hoefs, 1996; Bindeman, 2008); the $\delta^{18}O$ values of average

Indian Ocean type MORBs is about +5.7±0.2‰ (Ito et al., 1987), while mafic arc melts have $\delta^{18}O$ from +5.2 to +6.2‰ (Eiler et al., 2000), if the difference between mineral and magma follow $\Delta_O^{cpx\text{-}melt}$= -0.1‰, as suggested in Chapter 6. The ML, LH, DY, and FJT cpx phenocryst $\delta^{18}O$ values are similar to the values previously reported by Liu et al. (2016) in the NCC Mesozoic basalts and the Merapi basalts (+5.1 to +7.2‰) reported by Gertisser and Keller, (2003). Gertisser and Keller, (2003) and Troll et al. (2013) suggested the high $\delta^{18}O$ values in Merapi cpx phenocrysts are the results of the crustal contamination due to their relative low crystallization pressure and depth. However, the ε_{Nd} and ^{230}Th excesses disagree with the significant crustal contamination during the magma upwelling (Zou et al., 2010). The high $\delta^{18}O$ values (high to +8.3‰ for cpx and +8.4‰ for the melting) cannot be the result of fractional crystallization but may be inherited from the recycled materials. If so, the $\delta^{18}O$ of cpx phenocrysts would represent the recycled material derived magma. The high $\delta^{18}O$ values but asthenosphere-like bulk rock geochemical composition suggest the involvement of recycled components occurred in their mantle source. However, four extreme $\delta^{18}O$ values of cpx phenocrysts are observed in LH and FJT basalts (Fig. 7-4c). Two cpx with extremely high $\delta^{18}O$ values have very low Mg# of 58, suggesting not phenocrysts but crustal crystals. The Two cpx with low $\delta^{18}O$ values have normal Mg# of 79 and 83, therefore these two cpx may be the phenocrysts crystallized from basalts.

7.2.4 The recycled materials in Hainan basalts

The recovered water content for the Hainan basalts is 1.3- 2.7 wt. % falling within the range of MORBs to IABs (Dixon et al., 2004), i.e. the ratios of H_2O/Ce range from 215 to 350, almost similar to the MORBs H_2O/Ce ratios. However, the Ba/Th, Ce/Pb and Nb/La of LH is about from 70 to 140, from 19 to 27, and from 1.3 to 2.2 (Fig. 7-5), respectively. The positive relationship in the plots of Ba/Th vs. Nb/La suggests the existence of recycled oceanic crust component (Fig. 7-5). The higher Nb/La ratios reveal the potential recycled oceanic crust material existence. However, the plots of H_2O/Ce and Nb/La vs. Ba/Th imply the most Ba/Th enriched sample from FJT and DY involved recycled sediments component. The recycled sediment component may have undergone various dehydration. The MORB-like H_2O/Ce ratios suggest the upwelling plume under the Hainan Island may be not a wet buoyancy plume, but a hot plume. These observations also accord with the trace patterns in Fig. 7-2a. The LH samples mainly involved the recycled oceanic crust component, whereas the DY and FJT

samples require more recycled oceanic sediment component.

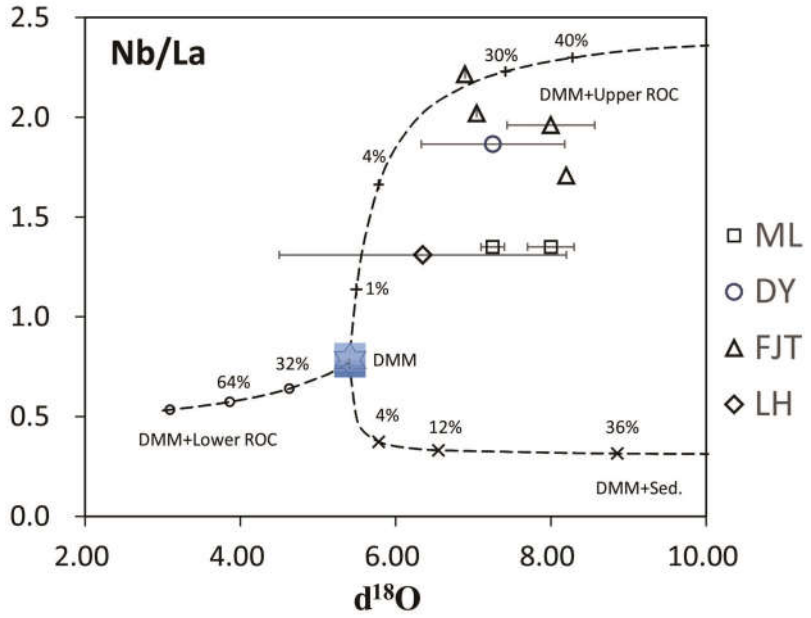

Fig. 7-6 The comparison of $\delta^{18}O$ of cpx with the bulk rock Nb/La ratios for the Hainan basalt samples. The modeled mixing are among the DMM (Workman and Hart, 2005) and GLOSS (Plank and Langmuir, 1998), partial melts of altered upper oceanic crust and altered lower oceanic crust (Gregory and Taylor's, 1981). The recycled material trace element composition are recalculated based on the mobility from Jonhson and Plank (1999) and Kessel et al. (2005).

The high $\delta^{18}O$ values may be inherited from the recycled materials undergone low-T reaction, such as low temperature water-rock altered oceanic crust or the marine limestone. Wang et al. (2013) suggest the Hainan basalts may contain as much as 20%-40% recycled oceanic crust in its mantle source, also consistent with high $\delta^{18}O$ data of Hainan samples (Fig. 7-6). Besides the high $\delta^{18}O$ cpx phenocryst grains, a few cpx phenocryst grains with the lower Oxygen isotope (<5 ‰) are observed in the Hainan basalts. Two possibilities are considered to lead towards the low $\delta^{18}O$ cpx phenocrysts, when the secondary alteration is excluded: (1) the involvement of the lower oceanic crust gabbro component with the mixture of different magma in the mantle source at the time of cpx phenocrysts crystallization which occurred before eruption; (2) the mechanical mixing of cpx from surrounding rocks in the shallow lithosphere. The low $\delta^{18}O$ cpx phenocrysts have normal TiO_2, implying the magma crystallization genesis, not the mechanical mixing. The low $\delta^{18}O$ in two LH cpx phenocrysts suggest a limited

volume of the recycled lower oceanic crust gabbro component are related to the LH magma.

Therefore, beyond considerable upper recycled oceanic crust, a small quantity of gabbros from lower recycled oceanic crust are also involved for the young LH basalts, while the additional recycled oceanic sediments were involved in the relatively older DY and FJT samples. Because the U–Th disequilibrium data and Nd isotopic compositions support for a model of deep melting in the MTZ or even in the lower mantle (plume melting) as suggested by Zou et al. (2010), these recycled materials are more likely caught by the plume from deep mantle. Large number of recycled materials are required in the plume for the high $\delta^{18}O$ values, but the varying radiogenic isotopic composition of Sr-Nd, and Pb, suggest the recycled oceanic materials are not too old, otherwise they should have much more radiogenic isotopic Sr-Nd-Pb composition. The ML and SYJ samples have less trace element concentrations (Fig. 7-2), but similar trace element ratios as of the DY and FJT samples (Fig. 7-5b), suggesting that they most likely share the similar genesis as of DY and FJT, but have larger degree of melting.

7.3 The variation of geochemistry for Cenozoic basalts depended on latitude

Although, the Cenozoic basalts in the Southeast China almost display similar geochemical feature, the variation of geochemistry with latitude can be observed in Fig. 7-7. Trace element compositions also show systematic along-arc variations (Fig. 7-8 and Fig. 7-9). As recognized in the isotopes, there is a significant change at the region of 24°N to 29°N, and some trace element ratios also change in this region. The Ba/Th, Zr/Hf, Nb/La, Nb/Zr, and Ti_n/Ti^* have the highest values at about 29°N. The highest $^{143}Nd/^{144}Nd$, and almost the lowest $^{87}Sr/^{86}Sr$ ratios are found at 29°N. However, the highest Pb radiogenic ratios are observed at 24°N. Meanwhile, the range and variation of trace element ratios from this section to the north or to the south are similar, such as Nb/Ta, Nb/La and Ba/Th. The systematics of isotope and trace element ratio variations with latitude appear to be coupled in this section. The latitude related systematics variation are also observed in the Izu-Bonin- Mariana (IBM) Trench system (Ishizuka et al., 2007; Staudigel et al., 2010). The similar vibration are displayed in Fig. 7-8 and Fig. 7-9, which are from the Ishizuka et al. (2007) and Staudigel et al. (2010), respectively. The section from 24°N to 29°N along East China coast can be found in the section from 23°N to 25°N in IBM Trench.

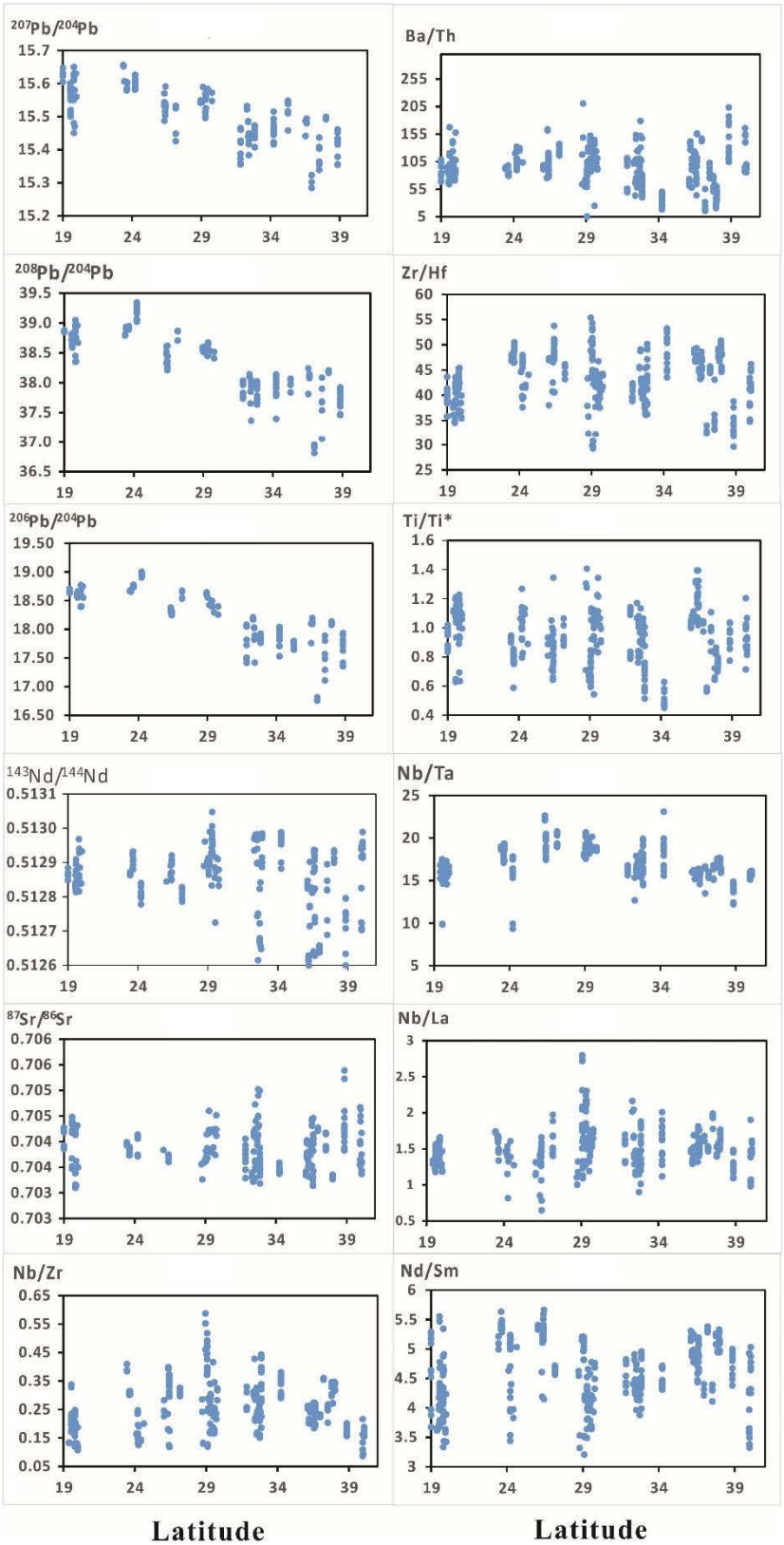

Fig. 7-7 The variation of trace element ratios and isotopic composition with latitude in East China. The data source of Cenozoic basalts are the same as in Fig. 5-5.

The systematic variations found in IBM Trench, are explained as the involvement of the HIMU-like contributions. The HIMU-like contribution are considered to inherit from the subducted Pacific slab, which enter into the IBM mantle wedge. The HIMU-like contributions should be a small scale of contribution, otherwise, it is hard to explain the lower Pb radiogenic isotopic ratios in Hainan Island. Ishizuka et al. (2007) and Staudigel et al. (2010) suggest the small scale HIMU-like contribution is the seamounts on the Pacific Plate east to the IBM Trench. These seamounts were emplaced on the ocean crust and remained on the seafloor between 100 and 120 Ma (Koppers et al., 2003). This long-lived HIMU subduction related basalts suggest that the recycling of HIMU seamount is a significant contributor to mantle evolution.

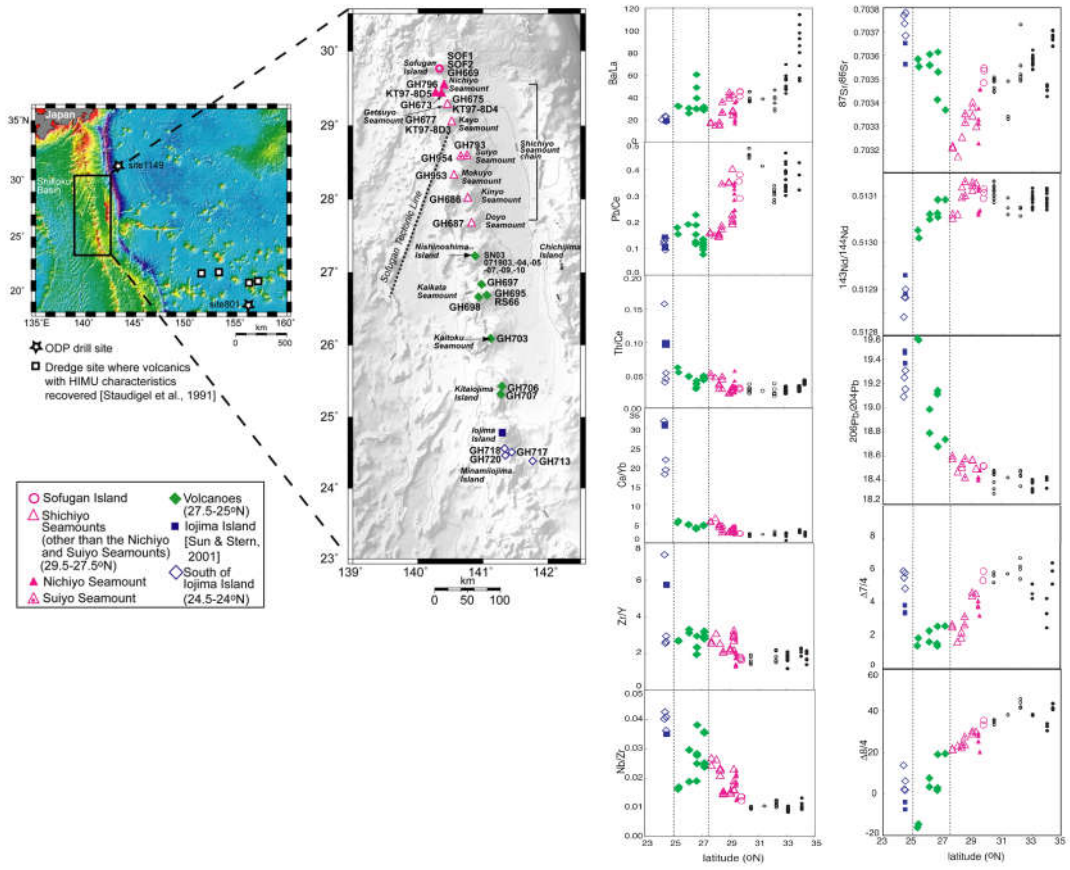

Fig. 7-8 The variation of trace element ratios and isotopic composition in IBM trench, from Ishizuka et al. (2007).

The Cenozoic basalts show similar $^{143}Nd/^{144}Nd$ and $^{87}Sr/^{86}Sr$ range in SE China, the NCC, and NE China (Fig. 7-10a). However, Cenozoic basalts in SE China and the NCC together with NE China are located at right and left side of DMM respectively, on

the plots of $^{206}Pb/^{204}Pb$ vs $^{87}Sr/^{86}Sr$ ratios (Fig. 7-10b). Relative to the NCC and NE China, Cenozoic basalts in SE China display clearer pattern of variation of geochemical feature with latitude than those of the NCC and NE China (Fig. 7-7). However, the generation of this difference between north and south are still unclear. Two possibilities are proposed to explain the difference between the Cenozoic basalts in the northern China and in southern China: 1) the indistinct geochemical feature is the result of complex geological history in Mesozoic including old subduction events and delamination of thickened lower continental crust and lithospheric mantle; 2) the lack of the HIMU-like contributions, just are similar to the northern part of the IBM trench system.

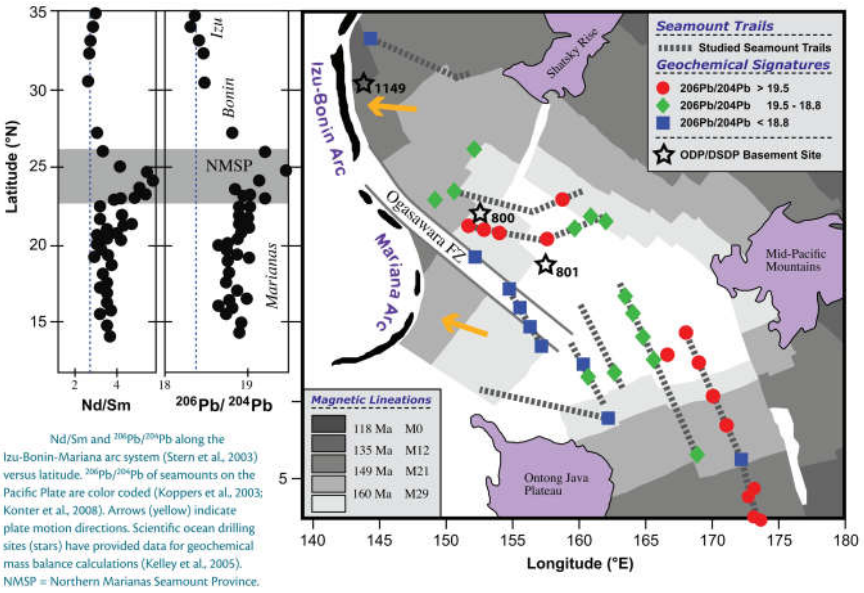

Fig. 7-9 The variation of trace element ratios and isotopic composition in IBM trench, from Staudigel et al. (2010).

Cenozoic basalts in SE China fall in the right part of DMM in Fig. 7-10b, consistent of the recent subduction event Pacific slab subduction, with slight radiogenic isotopic enrichment. However, the NCC and NE China Cenozoic basalts have scarcely any enriched Pb isotopic data, despite is enriched Sr isotopic data and depleted Nd isotopic data, unless no recycled oceanic crust component in their source, if the older than 200Ma subducted oceanic crust components are considered (Chapter 5). If the low $^{206}Pb/^{204}Pb$ are considered as the results of the successor of the northern part of the Pacific slab, they should display more enriched Pb isotope (Fig. 7-10b) like SE China basalts.

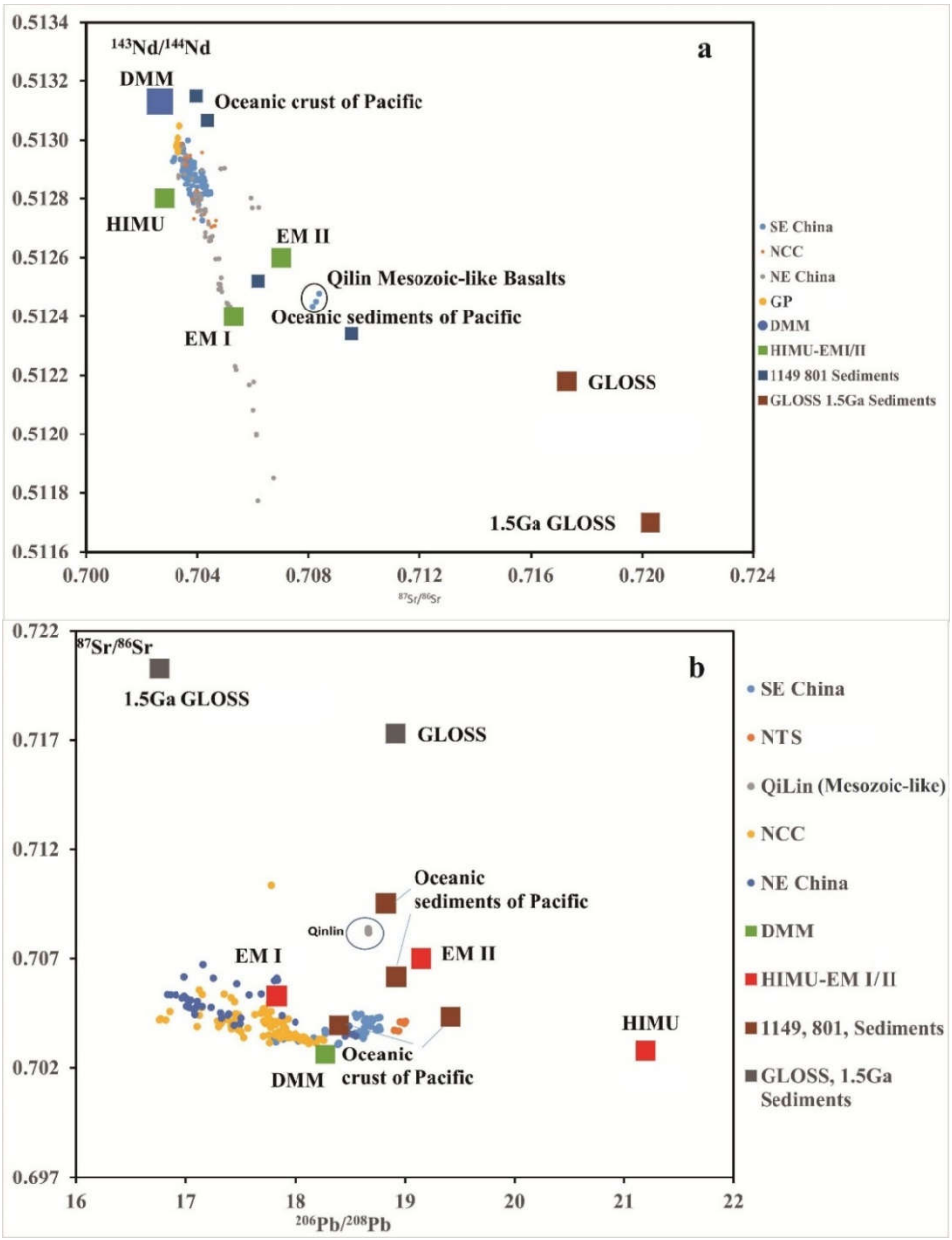

Fig. 7-10 (a) the $^{87}Sr/^{86}Sr$ vs $^{143}Nd/^{144}Nd$ for Cenozoic basalts in the East China and (b) $^{87}Sr/^{86}Sr$ vs. $^{206}Pb/^{204}Pb$ for Cenozoic basalts in the East China. The data source of Cenozoic basalts are the same as in Fig. 5-5

All the Cenozoic basalts along East China are located immediately above the western leading edge of the stagnant Pacific slab. It is noteworthy, that the north part of China had been subducted by and recorded multiple oceanic slabs from different directions (Sengör et al., 1993; Windley et al., 2010), these subduction caught lots of ascent subducted oceanic sediments and these ascent sediments may stay and be kept

in MTZ for a long time, reflected by EM I isotopic signature (Kuritani et al., 2011; Murphy et al., 2002). The older oceanic crust have relative high Pb radiogenic isotopic data, however, only the older recycled oceanic sediments or delamination of thickened lower continental crust could have served as source of the low Pb radiogenic isotope, like Kuritani et al. (2011) suggested for the Changbaishan basalts. Researchers have reported some evidences to demonstrate the occurrence of the recycled oceanic material in the MTZ beneath the NEC and NC (e.g. Kuritani et al., 2011; Chen et al., 2015; Xu et al., 2012a). However, Southeast China lacks such subduction process or record like the Cenozoic basalts in the NCC and NE China, so SE China Cenozoic basalts show relatively clear geochemical mixture feature between recent recycled oceanic material and the depleted mantle source, which are the result from the subduction effect of the Pacific Oceanic Plate.

7.4 Conclusions

(1) The low water content in some Hainan basalts are the result of later H-loss. The Hainan basalts have 2.7 wt. %, 1.3 wt. %, and 2.6 wt. % water content for the LH, DY, and FJT basalts, after the samples undergone H-loss are excluded.

(2) The Hainan basalts have higher$\delta^{18}O$ than normal mantle values. The coexistence of high and low $\delta^{18}O$ cpx phenocrysts observed in the LH basalts, combined with their trace element composition, the recycled upper oceanic crust components altered by low temperature hydrothermal reaction are dominantly required in the LH basalts, while limited recycled lower oceanic gabbro components altered by high temperature hydrothermal reaction were also involved. The DY and FJT basalts are suggested as the results of the mixture of DMM, recycled oceanic sediments and crusts. These recycled materials should not be very old and are most likely caught by upwelling plume from the deep mantle.

(3) Cenozoic basalts in East China have systematic variation of geochemical composition with the latitude; their radiogenic isotopic and trace element ratios display opposite symmetrical variation from N 25-29º section to south Hainan Island and from N 25-29º section to NE China, respectively. The spatial chemical and isotopic variation are observed both along the coast in East China and IBM trench. The consistency imply the spatial chemical variation may be caused by either the systematic varying chemical and isotopic composition of upper mantle or the influence of upper mantle by the Pacific Plate subduction.

Table 7-1 Major, trace element and water content compositions of the Hainan basalts.

Location	Maanling		Leihuling				Sanjiaoyuan
Rock type	OT[e]	OT[e]	AOB[f]	AOB[f]	AOB[f]	AOB[f]	OT[e]
Sample No.	HN9901[h]	HN9902[h]	HN9907[h]	HN9908[h]	HN9910[h]	HN9912[h]	HN9914[h]
SiO_2	51.74	50.77	49.10	45.32	45.47	45.27	49.87
TiO_2	2.34	2.37	2.30	2.81	2.76	2.75	2.17
Al_2O_3	14.32	15.12	13.36	12.83	12.98	12.76	13.86
Fe_2O_3	10.64	10.42	11.42	12.79	12.67	12.63	10.41
MnO	0.15	0.25	0.27	0.20	0.31	0.20	0.15
MgO	6.53	6.81	9.63	10.29	10.17	10.29	9.08
CaO	8.92	9.24	9.46	10.57	10.80	10.46	9.37
Na_2O	3.41	2.82	2.55	2.85	2.42	3.12	3.12
K_2O	1.68	1.46	1.53	1.64	1.43	1.63	1.53
P_2O_5	0.47	0.47	0.48	0.86	0.82	0.79	0.42
LOI（%）							
Total	100.19	99.73	100.11	100.15	99.84	99.88	99.97
Mg#[b]	59.00	60.00	66.00	65.00	65.00	65.00	67.00
Rb	36	30	32	37	35	39	30
Sr	546	559	557	817	820	811	525
Y	23.4	23.3	22.7	30.0	29.8	29.1	21.2
Zr	188	189	191	309	309	294	152
Nb	34	34	46.1	84.1	83.9	79.1	33.8
Cs	0.57	0.61	0.42	0.46	0.71	0.71	0.39
Ba	396	423	396	573	574	536	353
La	24.9	24.9	33.3	64.8	64.1	59.4	22.3
Ce	49	50	65	126	126	117	43
Pr	6.2	6.3	7.8	14.8	14.7	13.6	5.4
Nd	26.9	27.1	32.0	57.2	57.0	52.2	23.0
Sm	6.9	6.8	7.1	10.9	10.77	10.10	5.79
Eu	2.34	2.36	2.33	3.35	3.37	3.24	2.05
Gd	6.8	6.9	6.52	9.12	9.15	8.65	5.95
Tb	1.03	1.01	0.97	1.28	1.29	1.23	0.88
Dy	5.52	5.51	5.25	6.96	6.94	6.53	4.87
Ho	0.98	0.96	0.94	1.23	1.21	1.16	0.86
Er	2.26	2.20	2.23	2.97	2.87	2.72	2.07
Tm							
Yb	1.61	1.53	1.66	2.17	2.15	2.06	1.46
Lu	0.22	0.22	0.24	0.32	0.32	0.31	0.22
Hf	4.85	4.92	4.87	7.60	7.72	7.16	3.93
Ta	2.04	2.04	2.80	5.20	5.25	4.79	2.05
Pb	3.03	3.53	3.53	5.19	5.27	4.84	2.48
Th	3.87	3.9	4.70	8.36	8.29	7.76	3.38
U	0.91	0.88	1.19	2.00	1.96	1.81	0.79
H_2O[c] (wt. %)	0.0	0.0	0.0	0.0	2.5	0.0	0.0
H_2O[d] (wt. %)	0.0	0.0	0.0	0.0	2.7	0.0	0.0
Recommend H_2O (wt. %)					2.7		
$^{87}Sr/^{86}Sr$	0.703853 11	0.703919 9	0.704180 15	0.704230 14	0.704273 11	0.704182 13	
$^{143}Nd/^{144}Nd$	0.512868 10	0.512884 8	0.512848 9	0.512869 8	0.512861 10	0.512862 8	
$^{206}Pb/^{204}Pb$	18.631		18.655	18.692	18.696	18.705	
$^{207}Pb/^{204}Pb$	15.605		15.633	15.647	15.630	15.622	
$^{208}Pb/^{204}Pb$	38.846		38.874	38.881	38.872	38.853	

a	The data of Major and trace elements composition are from Huang et al. (2013)
b	$Mg\#=Mg^{2+}/(Mg^{2+}+\Sigma Fe^{2+})$(values were calculated assuming $Fe^{2+}/\Sigma Fe = 0.85$.
c	Average of H_2O content cpx with Mg# >80
d	Average of H_2O content cpx with Mg# >75
f	OT: Olivine Tholeiite
g	AOB: Alkali olivine basalt
h	The data of Major and trace elements composition are from Zou et al. (2010)

Fujitian AOB	AOB	AOB	AOB	AOB	AOB	AOB	AOB	AOB	AOB
FJT-1	FJT-2	FJT-3	FJT-4	FJT-5	FJT-6	FJT-7	FJT-8	FJT-9	FJT-10
47.11	47.23	46.45	46.32	46.43	46.62	47.81	47.24	46.92	47.18
2.88	2.88	2.86	2.77	3.03	2.72	2.90	2.94	2.88	2.66
13.69	13.60	13.36	12.75	13.43	12.88	13.64	13.37	13.64	12.84
12.50	12.20	12.42	12.30	12.73	12.29	12.11	12.34	12.44	12.19
0.15	0.14	0.15	0.15	0.15	0.15	0.14	0.14	0.14	0.14
8.34	7.84	8.75	10.11	9.04	9.65	8.02	8.34	8.17	9.30
7.48	7.51	7.50	7.81	7.60	7.87	7.39	7.39	7.39	8.12
3.90	3.61	3.45	2.86	3.39	2.79	3.71	3.67	3.66	2.98
1.40	1.57	1.60	1.73	1.65	1.94	1.51	1.66	1.64	1.84
0.65	0.55	0.61	0.47	0.63	0.49	0.51	0.54	0.62	0.41
0.96	1.15	1.00	1.04	0.96	1.52	0.92	0.53	0.94	1.03
99.05	98.29	98.16	98.30	99.04	98.91	98.65	98.16	98.45	98.69
59.99	59.09	61.29	64.88	61.48	63.83	59.81	60.30	59.61	63.16
17.3	17.7	17.7	20.8	18.0	20.3	18.6	18.3	17.2	20.3
161	164	166	178	169	172	170	168	159	122
241	234	296	374	307	321	235	295	228	244
52.5	49.3	54.3	59.1	56.0	56.2	50.4	50.6	49.4	39.1
237	206	269	338	282	310	213	231	214	205
49.8	46.2	49.7	63.8	51.2	66.7	50.8	49.1	47.7	46.7
142	134	134	119	138	129	135	134	140	85
24.2	23.6	23.5	22.2	23.3	21.4	24.2	23.7	24.1	18.5
1.46	1.40	1.44	1.51	1.45	1.49	1.46	1.42	1.44	1.11
51	46	94	65	130	78	56	90	70	58
951	934	852	586	864	852	943	944	961	543
25.4	23.4	24.6	22.4	25.1	24.1	22.8	23.0	24.8	21.0
305	314	285	221	281	259	318	308	309	152
76.6	75.4	71.1	54.8	70.3	63.4	75.5	73.5	77.1	34.5
0.75	0.77	0.83	0.37	0.84	0.70	0.59	0.55	0.61	0.43
703	742	650	450	938	537	742	722	721	356
43.3	37.1	39.1	27.1	41.2	32.3	34.1	35.5	40.9	23.8
86	73	77	55	82	65	68	70	81	44
10.0	8.7	9.1	6.7	9.6	7.8	8.1	8.3	9.5	5.9
43.1	36.8	39.4	30.0	41.4	34.1	34.7	35.4	41.0	26.4
9.14	8.04	8.39	6.79	8.80	7.54	7.66	7.75	8.73	6.15
2.99	2.87	2.81	2.30	2.86	2.55	2.87	2.78	2.95	2.15
7.84	7.07	7.44	6.17	7.59	6.70	6.79	6.88	7.53	5.66
1.09	0.99	1.04	0.89	1.05	0.96	0.96	0.96	1.05	0.83
5.49	5.05	5.36	4.72	5.45	5.08	4.92	4.93	5.45	4.41
0.91	0.85	0.88	0.81	0.88	0.85	0.82	0.83	0.89	0.75
2.23	2.05	2.16	2.04	2.17	2.13	2.02	2.02	2.16	1.92
0.27	0.25	0.26	0.25	0.26	0.27	0.25	0.24	0.26	0.24
1.47	1.37	1.43	1.44	1.45	1.48	1.38	1.40	1.46	1.37
0.20	0.19	0.20	0.20	0.20	0.21	0.19	0.19	0.20	0.19
6.84	6.89	6.52	5.23	6.28	5.93	7.00	6.79	7.03	3.58
4.36	4.38	4.09	3.11	4.02	3.59	4.38	4.31	4.44	1.96
3.22	3.46	3.04	2.13	3.19	2.52	3.25	3.37	3.23	1.59
5.82	5.43	5.33	3.93	5.23	4.70	5.40	5.22	5.67	3.58
1.48	1.44	1.39	1.08	1.33	1.20	1.43	1.37	1.47	0.71
			1.3	0.8	0.7				
			1.3		0.6				
			1.3	0.8	0.6				

Table 7-2 Major element compositions and the H_2O content of cpx phenocrysts for the Hainan basalts

Sample No.	HN99-01							
Section No.	21							
Point No.	1	2	3	4	5	6	7	8
SiO_2	51.66	51.04	49.86	48.84	51.61	50.64	50.15	48.08
TiO_2	0.88	0.81	1.53	1.91	0.83	1.20	1.27	2.03
Al_2O3	2.28	2.11	4.03	4.50	2.18	3.49	3.64	4.76
Cr_2O3	0.41	0.44	0.83	0.36	0.25	0.53	0.70	0.62
FeO	6.00	6.03	6.34	7.29	6.20	6.42	6.20	7.27
MnO	0.14	0.05	0.13	0.13	0.11	0.10	0.10	0.12
MgO	15.72	15.96	14.93	13.83	16.10	15.01	14.99	14.38
CaO	21.66	21.54	21.44	21.95	21.43	21.36	21.71	20.95
Na_2O	0.27	0.28	0.31	0.34	0.26	0.16	0.29	0.32
K_2O	0.00	0.00	0.01	0.00	0.00	0.00	0.00	0.00
NiO	0.00	0.00	0.00	0.00	0.00	0.00	0.00	0.00
Total	99.03	98.26	99.40	99.14	98.98	98.90	99.06	98.53
Si	1.92	1.92	1.86	1.84	1.92	1.89	1.87	1.82
Ti	0.02	0.02	0.04	0.05	0.02	0.03	0.04	0.06
Al	0.10	0.09	0.18	0.20	0.10	0.15	0.16	0.21
Cr	0.01	0.01	0.02	0.01	0.01	0.02	0.02	0.02
Fe	0.19	0.19	0.20	0.23	0.19	0.20	0.19	0.23
Mn	0.00	0.00	0.00	0.00	0.00	0.00	0.00	0.00
Mg	0.87	0.89	0.83	0.78	0.89	0.84	0.83	0.81
Ca	0.86	0.87	0.86	0.88	0.85	0.85	0.87	0.85
Na	0.02	0.02	0.02	0.02	0.02	0.01	0.02	0.02
K	0.00	0.00	0.00	0.00	0.00	0.00	0.00	0.00
Ni	0.00	0.00	0.00	0.00	0.00	0.00	0.00	0.00
Total	4.01	4.02	4.01	4.02	4.01	4.00	4.01	4.02
Mg#	82.36	82.51	80.76	77.18	82.23	80.65	81.16	77.89
$D^{(cpx\text{-}melt)}_{H_2O}$								
Absorbance of cpx (cm^{-1})	0.0	0.0	0.0	0.0	0.0	0.0	0.0	0.0
Thickness of cpx (0.001mm)	85	56	57	103	116	118	90	90
Absorbance normalized to 1 cm (cm^{-1})								
H_2O-cpx (ppm)								
H_2O-melt (wt%)								

s.

Sample No.								
Section No.	22							
Point No.	1	2	3	4	5	6	7	7.2
SiO_2	51.48	50.04	48.32	50.43	49.81	51.56	49.64	50.23
TiO_2	0.87	1.09	2.05	1.20	0.99	0.94	1.60	1.52
Al_2O3	2.03	3.10	4.85	3.31	3.55	1.86	4.57	4.20
Cr_2O3	0.53	0.77	0.66	0.82	0.48	0.07	0.38	0.55
FeO	6.14	6.04	6.99	5.92	6.17	7.51	6.97	7.00
MnO	0.12	0.12	0.10	0.10	0.11	0.13	0.04	0.09
MgO	16.21	15.25	13.96	15.39	15.18	15.85	14.44	14.72
CaO	21.20	21.94	21.23	21.52	21.66	20.78	21.24	21.36
Na_2O	0.24	0.29	0.31	0.29	0.33	0.24	0.30	0.32
K_2O	0.00	0.01	0.01	0.00	0.00	0.00	0.01	0.00
NiO	0.00	0.00	0.00	0.00	0.00	0.00	0.00	0.00
Total	98.81	98.65	98.47	98.99	98.28	98.94	99.18	99.99
Si	1.92	1.88	1.83	1.88	1.88	1.93	1.85	1.86
Ti	0.02	0.03	0.06	0.03	0.03	0.03	0.04	0.04
Al	0.09	0.14	0.22	0.15	0.16	0.08	0.20	0.18
Cr	0.02	0.02	0.02	0.02	0.01	0.00	0.01	0.02
Fe	0.19	0.19	0.22	0.18	0.19	0.24	0.22	0.22
Mn	0.00	0.00	0.00	0.00	0.00	0.00	0.00	0.00
Mg	0.90	0.85	0.79	0.86	0.85	0.88	0.80	0.81
Ca	0.85	0.88	0.86	0.86	0.87	0.83	0.85	0.85
Na	0.02	0.02	0.02	0.02	0.02	0.02	0.02	0.02
K	0.00	0.00	0.00	0.00	0.00	0.00	0.00	0.00
Ni	0.00	0.00	0.00	0.00	0.00	0.00	0.00	0.00
Total	4.01	4.02	4.01	4.01	4.02	4.01	4.01	4.01
Mg#	82.47	81.83	78.07	82.25	81.42	78.99	78.71	78.94
$D^{(cpx\text{-}melt)}_{H_2O}$								
Absorbance of cpx (cm^{-1})	0.0	0.0	0.0	0.0	0.0	0.0	0.0	0.0
Thickness of cpx (0.001mm)	85	56	57	103	116	118	50	50
Absorbance normalized to 1 cm (cm^{-1})								
H_2O-cpx (ppm)								
H_2O-melt (wt%)								

Sample No.	HN99-02							
Section No.	22					23		
Point No.	1	2	3	4	6	1	2	3
SiO_2	50.30	51.32	50.38	49.24	50.82	50.34	50.66	50.22
TiO_2	1.09	0.86	0.84	1.66	1.27	1.06	1.13	1.31
Al_2O3	3.34	2.05	3.10	4.02	3.50	3.66	3.29	3.64
Cr_2O3	1.00	0.58	0.96	0.49	0.87	0.51	0.96	0.33
FeO	5.89	5.65	5.95	6.78	6.15	6.30	5.86	6.46
MnO	0.09	0.11	0.10	0.13	0.08	0.12	0.11	0.10
MgO	15.32	15.95	15.27	14.56	15.21	15.31	15.33	15.19
CaO	21.71	21.79	21.95	21.82	21.94	21.75	21.88	21.82
Na_2O	0.22	0.26	0.29	0.30	0.31	0.29	0.30	0.28
K_2O	0.00	0.00	0.00	0.00	0.00	0.00	0.00	0.00
NiO	0.00	0.00	0.00	0.00	0.00	0.00	0.00	0.00
Total	98.96	98.55	98.83	98.98	100.14	99.33	99.53	99.33
Si	1.88	1.92	1.89	1.85	1.88	1.87	1.88	1.87
Ti	0.03	0.02	0.02	0.05	0.04	0.03	0.03	0.04
Al	0.15	0.09	0.14	0.18	0.15	0.16	0.14	0.16
Cr	0.03	0.02	0.03	0.01	0.03	0.01	0.03	0.01
Fe	0.18	0.18	0.19	0.21	0.19	0.20	0.18	0.20
Mn	0.00	0.00	0.00	0.00	0.00	0.00	0.00	0.00
Mg	0.85	0.89	0.85	0.82	0.84	0.85	0.85	0.84
Ca	0.87	0.87	0.88	0.88	0.87	0.87	0.87	0.87
Na	0.02	0.02	0.02	0.02	0.02	0.02	0.02	0.02
K	0.00	0.00	0.00	0.00	0.00	0.00	0.00	0.00
Ni	0.00	0.00	0.00	0.00	0.00	0.00	0.00	0.00
Total	4.01	4.01	4.02	4.02	4.01	4.02	4.01	4.02
Mg#	82.27	83.43	82.08	79.31	81.51	81.26	82.33	80.74
$D^{(cpx\text{-}melt)}_{H_2O}$								
Absorbance of cpx (cm^{-1})	0.0	0.0	0.0	0.0	0.0	0.0	0.0	0.0
Thickness of cpx (0.001mm)	58	58	58	58	52	50	50	50
Absorbance normalized to 1 cm (cm^{-1})								
H_2O-cpx (ppm)								
H_2O-melt (wt%)								

Sample No.				HN99-07		
Section No.				21		
Point No.	4	5	6	1	2	3
SiO_2	51.97	50.65	51.20	50.94	47.33	47.54
TiO_2	0.79	1.15	1.05	1.05	2.20	2.33
Al_2O3	1.93	3.37	2.32	3.32	6.76	5.87
Cr_2O3	0.51	0.81	0.37	0.10	0.38	0.26
FeO	5.95	6.08	6.64	7.48	7.27	6.98
MnO	0.11	0.10	0.13	0.13	0.12	0.10
MgO	16.27	14.74	16.46	15.87	13.29	13.37
CaO	21.45	21.70	20.38	19.91	21.21	22.09
Na_2O	0.26	0.32	0.16	0.26	0.40	0.35
K_2O	0.00	0.00	0.00	0.03	0.01	0.00
NiO	0.00	0.00	0.00	0.00	0.00	0.00
Total	99.23	98.91	98.70	99.08	98.97	98.88
Si	1.93	1.89	1.91	1.90	1.78	1.79
Ti	0.02	0.03	0.03	0.03	0.06	0.07
Al	0.08	0.15	0.10	0.15	0.30	0.26
Cr	0.01	0.02	0.01	0.00	0.01	0.01
Fe	0.18	0.19	0.21	0.23	0.23	0.22
Mn	0.00	0.00	0.00	0.00	0.00	0.00
Mg	0.90	0.82	0.92	0.88	0.75	0.75
Ca	0.85	0.87	0.82	0.79	0.85	0.89
Na	0.02	0.02	0.01	0.02	0.03	0.03
K	0.00	0.00	0.00	0.00	0.00	0.00
Ni	0.00	0.00	0.00	0.00	0.00	0.00
Total	4.01	4.00	4.01	4.01	4.02	4.02
Mg#	82.99	81.22	81.55	79.09	76.52	77.35
$D^{(cpx\text{-}melt)}_{H_2O}$						
Absorbance of cpx (cm^{-1})	0.0	0.0	0.0	0.0	0.0	0.0
Thickness of cpx (0.001mm)	49	49	40	96	96	100
Absorbance normalized to 1 cm (cm^{-1})						
H_2O-cpx (ppm)						
H_2O-melt (wt%)						

Sample No.	HN99-08		HN99-10					
Section No.	21		21					
Point No.	1	2	1	2	3	4	5	6
SiO_2	52.75	51.53	47.24	47.07	47.94	49.04	52.22	49.31
TiO_2	0.75	1.00	2.32	2.28	2.09	1.91	0.85	1.91
Al_2O3	1.75	2.95	6.03	5.92	4.93	3.81	1.62	3.80
Cr_2O3	0.49	0.50	0.47	0.80	0.03	0.14	0.20	0.14
FeO	5.23	5.29	6.11	6.61	7.60	6.89	6.46	6.30
MnO	0.13	0.07	0.08	0.05	0.13	0.13	0.18	0.12
MgO	15.90	15.22	13.39	13.04	13.32	14.30	15.98	14.27
CaO	21.90	22.69	22.72	22.82	22.57	22.10	21.75	22.46
Na_2O	0.38	0.29	0.34	0.40	0.39	0.23	0.21	0.62
K_2O	0.01	0.00	0.00	0.00	0.01	0.01	0.00	0.07
NiO	0.02	0.05	0.00	0.00	0.00	0.00	0.00	0.00
Total	99.29	99.59	98.69	98.99	99.01	98.55	99.46	99.00
Si	1.95	1.91	1.78	1.78	1.81	1.85	1.94	1.85
Ti	0.02	0.03	0.07	0.06	0.06	0.05	0.02	0.05
Al	0.08	0.13	0.27	0.26	0.22	0.17	0.07	0.17
Cr	0.01	0.01	0.01	0.02	0.00	0.00	0.01	0.00
Fe	0.16	0.16	0.19	0.21	0.24	0.22	0.20	0.20
Mn	0.00	0.00	0.00	0.00	0.00	0.00	0.01	0.00
Mg	0.88	0.84	0.75	0.73	0.75	0.81	0.88	0.80
Ca	0.87	0.90	0.92	0.92	0.91	0.89	0.86	0.90
Na	0.03	0.02	0.02	0.03	0.03	0.02	0.02	0.05
K	0.00	0.00	0.00	0.00	0.00	0.00	0.00	0.00
Ni	0.00	0.00	0.00	0.00	0.00	0.00	0.00	0.00
Total	4.00	4.00	4.02	4.03	4.03	4.02	4.01	4.03
Mg#	84.43	83.69	79.61	77.87	75.76	78.72	81.52	80.15
$D^{(cpx\text{-}melt)}_{H_2O}$			0.0245	0.0252	0.0203	0.0161	0.0095	0.0158
Absorbance of cpx (cm^{-1})	0.0	0.0	6.6	10.9	6.7	7.3	4.8	5.2
Thickness of cpx (0.001mm)	86	86	51	54	54	58	58	58
Absorbance normalized to 1 cm (cm^{-1})			1294	2019	1241	1259	828	897
H_2O-cpx (ppm)			548	854	525	533	350	379
H_2O-melt (wt%)			2.2	3.4	2.6	3.3	3.7	2.4

Sample No. Section No. Point No.	7	8	9	10	11	12	13	14
SiO_2	51.06	48.71	49.08	46.00	49.09	46.17	45.04	50.10
TiO_2	1.31	1.62	1.79	3.12	1.78	2.79	3.41	1.61
Al_2O3	3.01	4.10	4.49	7.69	4.13	6.64	7.58	3.29
Cr_2O3	0.50	0.19	0.04	0.05	0.12	0.48	0.07	0.00
FeO	5.71	6.49	7.39	7.58	7.01	7.19	8.80	8.94
MnO	0.08	0.18	0.14	0.07	0.19	0.12	0.14	0.21
MgO	15.07	14.62	13.52	11.80	14.08	12.56	11.27	12.67
CaO	22.60	22.52	22.06	22.40	22.22	22.78	22.22	22.06
Na_2O	0.26	0.50	0.37	0.44	0.24	0.39	0.44	0.29
K_2O	0.00	0.00	0.01	0.03	0.00	0.00	0.01	0.00
NiO	0.00	0.00	0.00	0.00	0.00	0.00	0.00	0.00
Total	99.60	98.93	98.88	99.16	98.85	99.12	98.98	99.15
Si	1.89	1.83	1.85	1.74	1.85	1.75	1.72	1.89
Ti	0.04	0.05	0.05	0.09	0.05	0.08	0.10	0.05
Al	0.13	0.18	0.20	0.34	0.18	0.30	0.34	0.15
Cr	0.01	0.01	0.00	0.00	0.00	0.01	0.00	0.00
Fe	0.18	0.20	0.23	0.24	0.22	0.23	0.28	0.28
Mn	0.00	0.01	0.00	0.00	0.01	0.00	0.00	0.01
Mg	0.83	0.82	0.76	0.66	0.79	0.71	0.64	0.71
Ca	0.90	0.91	0.89	0.91	0.90	0.92	0.91	0.89
Na	0.02	0.04	0.03	0.03	0.02	0.03	0.03	0.02
K	0.00	0.00	0.00	0.00	0.00	0.00	0.00	0.00
Ni	0.00	0.00	0.00	0.00	0.00	0.00	0.00	0.00
Total	4.01	4.04	4.01	4.02	4.02	4.03	4.03	4.00
Mg#	82.47	80.06	76.54	73.52	78.18	75.70	69.55	71.64
$D^{(cpx\text{-}melt)}_{H_2O}$	0.0122	0.0177	0.0164	0.0331	0.0164	0.0306	0.0376	0.0124
Absorbance of cpx (cm^{-1})	7.7	10.8	4.3	7.3	2.3	5.7	1.9	7.1
Thickness of cpx (0.001mm)	58	56	59	56	56	56	64	63
Absorbance normalized to 1 cm (cm^{-1})	1321	1932	734	1304	411	1009	297	1127
H_2O-cpx (ppm)	559	818	311	552	174	427	126	477
H_2O-melt (wt%)	4.6	4.6	1.9	1.7	1.1	1.4	0.3	3.8

Sample No.						HN99-12		
Section No.	22					21		
Point No.	1	2	3	4	5	1-0	1.1	2
SiO_2	49.22	48.83	48.37	43.84	45.41	49.05	49.05	50.75
TiO_2	1.75	1.74	1.99	3.71	3.14	1.83	1.83	1.12
Al_2O3	5.07	3.75	4.41	8.36	6.89	4.90	4.90	2.76
Cr_2O3	0.17	0.17	0.01	0.09	0.40	0.86	0.86	0.49
FeO	7.82	7.01	7.64	7.52	7.57	6.01	6.01	5.38
MnO	0.14	0.12	0.12	0.06	0.12	0.06	0.06	0.12
MgO	12.56	14.50	13.65	11.69	12.32	13.79	13.79	15.22
CaO	21.36	22.70	22.55	22.66	22.78	22.96	22.96	22.46
Na_2O	0.36	0.28	0.36	0.39	0.40	0.36	0.36	0.27
K_2O	0.05	0.02	0.00	0.02	0.00	0.00	0.00	0.01
NiO	0.00	0.00	0.00	0.00	0.00	0.00	0.00	0.00
Total	98.49	99.10	99.10	98.34	99.01	99.82	99.82	98.57
Si	1.86	1.84	1.83	1.68	1.73	1.83	1.83	1.90
Ti	0.05	0.05	0.06	0.11	0.09	0.05	0.05	0.03
Al	0.23	0.17	0.20	0.38	0.31	0.22	0.22	0.12
Cr	0.01	0.01	0.00	0.00	0.01	0.03	0.03	0.01
Fe	0.25	0.22	0.24	0.24	0.24	0.19	0.19	0.17
Mn	0.00	0.00	0.00	0.00	0.00	0.00	0.00	0.00
Mg	0.71	0.81	0.77	0.67	0.70	0.77	0.77	0.85
Ca	0.86	0.92	0.91	0.93	0.93	0.92	0.92	0.90
Na	0.03	0.02	0.03	0.03	0.03	0.03	0.03	0.02
K	0.00	0.00	0.00	0.00	0.00	0.00	0.00	0.00
Ni	0.00	0.00	0.00	0.00	0.00	0.00	0.00	0.00
Total	3.99	4.04	4.03	4.04	4.04	4.01	4.01	4.01
Mg#	74.13	78.67	76.10	73.49	74.36	80.36	80.36	83.45
$D^{(cpx\text{-}melt)}_{H_2O}$	0.0158	0.0170	0.0186	0.0473	0.0350			
Absorbance of cpx (cm^{-1})	8.3	4.6	7.2	11.2	6.2	0.0	0.0	0.0
Thickness of cpx (0.001mm)	76	70	69	79	76	78	78	78
Absorbance normalized to 1 cm (cm^{-1})	1092	660	1043	1422	818			
H_2O-cpx (ppm)	462	279	442	601	346			
H_2O-melt (wt%)	2.9	1.6	2.4	1.3	1.0			

Sample No.								
Section No.								
Point No.	3	4	5	6	7	8	9	10
SiO_2	49.57	47.59	47.68	48.55	51.86	50.24	50.77	49.13
TiO_2	1.64	2.31	2.28	1.91	0.99	1.46	1.53	2.00
Al_2O3	4.65	5.93	5.65	4.31	2.95	3.49	3.05	4.34
Cr_2O3	0.62	0.43	0.62	0.09	0.80	0.27	0.35	0.00
FeO	5.87	6.65	6.38	7.21	4.69	6.28	6.14	8.14
MnO	0.09	0.09	0.13	0.11	0.05	0.09	0.13	0.10
MgO	14.05	13.01	12.84	14.01	15.45	14.52	14.94	13.54
CaO	22.95	22.88	22.86	22.32	22.70	22.45	22.43	22.32
Na_2O	0.32	0.33	0.35	0.28	0.32	0.27	0.27	0.35
K_2O	0.02	0.01	0.01	0.00	0.00	0.00	0.00	0.00
NiO	0.07	0.00	0.00	0.00	0.00	0.00	0.00	0.00
Total	99.84	99.22	98.80	98.78	99.80	99.09	99.62	99.92
Si	1.84	1.79	1.80	1.83	1.91	1.88	1.89	1.84
Ti	0.05	0.07	0.06	0.05	0.03	0.04	0.04	0.06
Al	0.20	0.26	0.25	0.19	0.13	0.15	0.13	0.19
Cr	0.02	0.01	0.02	0.00	0.02	0.01	0.01	0.00
Fe	0.18	0.21	0.20	0.23	0.14	0.20	0.19	0.25
Mn	0.00	0.00	0.00	0.00	0.00	0.00	0.00	0.00
Mg	0.78	0.73	0.72	0.79	0.85	0.81	0.83	0.76
Ca	0.91	0.92	0.92	0.90	0.90	0.90	0.89	0.90
Na	0.02	0.02	0.03	0.02	0.02	0.02	0.02	0.03
K	0.00	0.00	0.00	0.00	0.00	0.00	0.00	0.00
Ni	0.00	0.00	0.00	0.00	0.00	0.00	0.00	0.00
Total	4.01	4.02	4.01	4.03	4.00	4.01	4.01	4.02
Mg#	81.02	77.72	78.21	77.59	85.45	80.47	81.27	74.79
$D^{(cpx\text{-}melt)}_{H_2O}$								
Absorbance of cpx (cm^{-1})	0.0	0.0	0.0	0.0	0.0	0.0	0.0	0.0
Thickness of cpx (0.001mm)	78	77	77	80	80	80	77	77
Absorbance normalized to 1 cm (cm^{-1})								
H_2O-cpx (ppm)								
H_2O-melt (wt%)								

Sample No.								
Section No.								
Point No.	11	12	13	14	15	16	17	18
SiO_2	48.09	50.59	49.19	50.69	47.90	48.98	49.85	48.71
TiO_2	2.28	1.40	2.05	1.25	2.09	1.73	1.52	1.71
Al_2O3	4.92	3.02	4.21	3.08	5.48	4.93	3.53	4.01
Cr_2O3	0.03	0.33	0.05	0.55	0.91	0.88	0.78	0.13
FeO	8.08	6.28	7.91	5.77	5.82	5.79	6.30	6.75
MnO	0.11	0.14	0.15	0.12	0.06	0.10	0.08	0.10
MgO	12.93	14.74	13.77	15.11	13.71	13.76	14.44	14.17
CaO	21.96	22.70	22.21	22.53	22.84	22.98	22.28	22.22
Na_2O	0.29	0.30	0.31	0.19	0.39	0.39	0.25	0.27
K_2O	0.00	0.03	0.00	0.01	0.00	0.01	0.00	0.00
NiO	0.00	0.00	0.00	0.00	0.00	0.00	0.00	0.00
Total	98.70	99.53	99.84	99.29	99.19	99.53	99.03	98.07
Si	1.82	1.89	1.84	1.89	1.80	1.83	1.87	1.85
Ti	0.06	0.04	0.06	0.03	0.06	0.05	0.04	0.05
Al	0.22	0.13	0.19	0.14	0.24	0.22	0.16	0.18
Cr	0.00	0.01	0.00	0.02	0.03	0.03	0.02	0.00
Fe	0.26	0.20	0.25	0.18	0.18	0.18	0.20	0.21
Mn	0.00	0.00	0.00	0.00	0.00	0.00	0.00	0.00
Mg	0.73	0.82	0.77	0.84	0.77	0.77	0.81	0.80
Ca	0.89	0.91	0.89	0.90	0.92	0.92	0.89	0.90
Na	0.02	0.02	0.02	0.01	0.03	0.03	0.02	0.02
K	0.00	0.00	0.00	0.00	0.00	0.00	0.00	0.00
Ni	0.00	0.00	0.00	0.00	0.00	0.00	0.00	0.00
Total	4.01	4.02	4.02	4.01	4.02	4.02	4.01	4.02
Mg#	74.03	80.70	75.62	82.36	80.76	80.91	80.35	78.92
$D^{(cpx\text{-}melt)}_{H_2O}$								
Absorbance of cpx (cm^{-1})	0.0	0.0	0.0	0.0	0.0	0.0	0.0	0.0
Thickness of cpx (0.001mm)	81	73	77	74	77	77	77	77
Absorbance normalized to 1 cm (cm^{-1})								
H_2O-cpx (ppm)								
H_2O-melt (wt%)								

Sample No. Section No. Point No.	19	20	21	22	23	24	25	26
SiO_2	47.63	50.09	51.01	50.99	45.44	49.35	50.89	50.92
TiO_2	2.29	1.41	0.99	1.12	3.31	1.55	1.39	1.14
Al_2O3	5.73	4.57	2.87	2.60	8.05	4.78	3.18	2.85
Cr_2O3	0.12	0.73	0.49	0.10	0.32	0.87	0.43	0.46
FeO	7.86	5.68	4.87	6.68	7.47	5.72	5.85	5.32
MnO	0.14	0.05	0.08	0.12	0.10	0.07	0.10	0.07
MgO	13.25	14.18	15.35	15.44	12.00	14.23	15.09	15.09
CaO	21.98	22.88	23.23	21.59	22.12	23.02	22.89	23.03
Na_2O	0.43	0.38	0.29	0.30	0.37	0.40	0.26	0.28
K_2O	0.00	0.02	0.01	0.00	0.01	0.00	0.00	0.01
NiO	0.00	0.00	0.00	0.00	0.00	0.00	0.00	0.00
Total	99.43	99.99	99.17	98.94	99.18	99.99	100.07	99.17
Si	1.79	1.85	1.90	1.91	1.72	1.83	1.88	1.90
Ti	0.06	0.04	0.03	0.03	0.09	0.04	0.04	0.03
Al	0.25	0.20	0.13	0.11	0.36	0.21	0.14	0.12
Cr	0.00	0.02	0.01	0.00	0.01	0.03	0.01	0.01
Fe	0.25	0.18	0.15	0.21	0.24	0.18	0.18	0.17
Mn	0.00	0.00	0.00	0.00	0.00	0.00	0.00	0.00
Mg	0.74	0.78	0.85	0.86	0.68	0.79	0.83	0.84
Ca	0.89	0.91	0.93	0.86	0.90	0.92	0.91	0.92
Na	0.03	0.03	0.02	0.02	0.03	0.03	0.02	0.02
K	0.00	0.00	0.00	0.00	0.00	0.00	0.00	0.00
Ni	0.00	0.00	0.00	0.00	0.00	0.00	0.00	0.00
Total	4.03	4.01	4.02	4.01	4.02	4.02	4.01	4.01
Mg#	75.03	81.66	84.89	80.48	74.13	81.60	82.14	83.48
$D^{(cpx\text{-}melt)}_{H_2O}$								
Absorbance of cpx (cm^{-1})	0.0	0.0	0.0	0.0	0.0	0.0	0.0	0.0
Thickness of cpx (0.001mm)	80	80	80	80	78	75	72	73
Absorbance normalized to 1 cm (cm^{-1})								
H_2O-cpx (ppm)								
H_2O-melt (wt%)								

Sample No.	HN99-14							
Section No.	21							
Point No.	1	2	3	4	5	6	7	8
SiO_2	51.62	52.12	51.25	50.21	51.47	51.87	51.39	51.77
TiO_2	0.99	0.94	1.18	1.74	1.06	1.36	1.30	1.16
Al_2O3	1.61	1.96	1.70	3.89	1.94	1.74	1.82	1.88
Cr_2O3	0.04	0.34	0.04	0.31	0.23	0.02	0.04	0.07
FeO	11.08	6.84	10.77	6.97	6.98	9.10	8.30	7.80
MnO	0.18	0.09	0.16	0.09	0.10	0.16	0.13	0.16
MgO	12.75	15.72	13.04	14.65	15.68	14.05	14.67	14.70
CaO	20.83	21.04	20.76	20.89	20.84	21.10	21.30	21.33
Na_2O	0.32	0.24	0.37	0.30	0.18	0.25	0.26	0.31
K_2O	0.02	0.01	0.01	0.00	0.02	0.02	0.00	0.01
NiO	0.01	0.04	0.01	0.06	0.00	0.00	0.04	0.04
Total	99.46	99.33	99.28	99.10	98.51	99.66	99.24	99.22
Si	1.95	1.94	1.94	1.87	1.93	1.94	1.93	1.94
Ti	0.03	0.03	0.03	0.05	0.03	0.04	0.04	0.03
Al	0.07	0.09	0.08	0.17	0.09	0.08	0.08	0.08
Cr	0.00	0.01	0.00	0.01	0.01	0.00	0.00	0.00
Fe	0.35	0.21	0.34	0.22	0.22	0.28	0.26	0.24
Mn	0.01	0.00	0.01	0.00	0.00	0.00	0.00	0.01
Mg	0.72	0.87	0.74	0.82	0.88	0.78	0.82	0.82
Ca	0.84	0.84	0.84	0.84	0.84	0.85	0.86	0.85
Na	0.02	0.02	0.03	0.02	0.01	0.02	0.02	0.02
K	0.00	0.00	0.00	0.00	0.00	0.00	0.00	0.00
Ni	0.00	0.00	0.00	0.00	0.00	0.00	0.00	0.00
Total	4.00	4.00	4.00	4.00	4.00	3.99	4.01	4.00
Mg#	67.24	80.37	68.36	78.94	80.02	73.35	75.91	77.05
$D^{(cpx\text{-}melt)}_{H_2O}$								
Absorbance of cpx (cm^{-1})	0.0	0.0	0.0	0.0	0.0	0.0	0.0	0.0
Thickness of cpx (0.001mm)	90	77	88	88	88	95	95	95
Absorbance normalized to 1 cm (cm^{-1})								
H_2O-cpx (ppm)								
H_2O-melt (wt%)								

Sample No.								
Section No.								
Point No.	9	10	11	12	13	14	15	16
SiO_2	52.54	51.35	51.80	52.32	52.73	52.31	51.06	52.78
TiO_2	0.90	1.27	1.17	1.08	0.89	0.99	0.96	1.04
Al_2O3	2.18	1.53	1.49	2.40	2.11	1.85	2.31	1.88
Cr_2O3	0.47	0.04	0.01	0.34	0.35	0.07	1.04	0.06
FeO	6.08	12.16	12.05	5.89	6.23	7.06	6.15	6.86
MnO	0.06	0.25	0.18	0.08	0.10	0.10	0.08	0.06
MgO	15.48	11.82	11.87	15.13	15.46	15.20	15.04	15.39
CaO	21.65	20.92	20.97	22.04	21.82	21.54	21.28	21.69
Na_2O	0.26	0.35	0.35	0.26	0.26	0.23	0.35	0.27
K_2O	0.00	0.00	0.00	0.00	0.00	0.00	0.02	0.00
NiO	0.07	0.01	0.01	0.05	0.04	0.00	0.01	0.06
Total	99.69	99.71	99.91	99.58	99.98	99.35	98.28	100.11
Si	1.94	1.95	1.96	1.93	1.94	1.94	1.92	1.94
Ti	0.02	0.04	0.03	0.03	0.02	0.03	0.03	0.03
Al	0.09	0.07	0.07	0.10	0.09	0.08	0.10	0.08
Cr	0.01	0.00	0.00	0.01	0.01	0.00	0.03	0.00
Fe	0.19	0.39	0.38	0.18	0.19	0.22	0.19	0.21
Mn	0.00	0.01	0.01	0.00	0.00	0.00	0.00	0.00
Mg	0.85	0.67	0.67	0.83	0.85	0.84	0.84	0.85
Ca	0.86	0.85	0.85	0.87	0.86	0.86	0.86	0.86
Na	0.02	0.03	0.03	0.02	0.02	0.02	0.03	0.02
K	0.00	0.00	0.00	0.00	0.00	0.00	0.00	0.00
Ni	0.00	0.00	0.00	0.00	0.00	0.00	0.00	0.00
Total	3.99	3.99	3.99	3.99	3.99	3.99	4.00	3.99
Mg#	81.95	63.40	63.71	82.07	81.58	79.35	81.35	80.00
$D^{(cpx\text{-}melt)}_{H_2O}$								
Absorbance of cpx (cm^{-1})	0.0	0.0	0.0	0.0	0.0	0.0	0.0	0.0
Thickness of cpx (0.001mm)	95	95	94	95	93	94	95	96
Absorbance normalized to 1 cm (cm^{-1})								
H_2O-cpx (ppm)								
H_2O-melt (wt%)								

Sample No.						DY-4	
Section No.						1	2
Point No.	17	18	19	20	21	6	4
SiO_2	52.63	49.22	51.36	52.67	51.58	50.88	49.11
TiO_2	0.82	2.60	0.64	1.00	1.04	1.10	0.95
Al_2O3	2.05	3.41	1.08	2.18	1.36	6.98	10.59
Cr_2O3	0.64	0.02	0.00	0.29	0.03	0.14	0.06
FeO	6.15	10.13	14.12	6.17	12.49	4.84	5.21
MnO	0.10	0.18	0.26	0.08	0.21	0.02	0.10
MgO	15.73	12.17	10.77	15.44	11.69	13.88	11.67
CaO	21.49	21.38	20.15	21.78	20.88	20.10	20.66
Na_2O	0.27	0.45	0.45	0.23	0.33	1.37	1.53
K_2O	0.00	0.00	0.01	0.00	0.02	0.00	0.00
NiO	0.00	0.04	0.01	0.07	0.02	0.03	0.00
Total	99.86	99.59	98.86	99.92	99.63	99.34	99.89
Si	1.94	1.86	1.98	1.94	1.96	1.87	1.80
Ti	0.02	0.07	0.02	0.03	0.03	0.03	0.03
Al	0.09	0.15	0.05	0.09	0.06	0.30	0.46
Cr	0.02	0.00	0.00	0.01	0.00	0.00	0.00
Fe	0.19	0.32	0.45	0.19	0.40	0.15	0.16
Mn	0.00	0.01	0.01	0.00	0.01	0.00	0.00
Mg	0.86	0.69	0.62	0.85	0.66	0.76	0.64
Ca	0.85	0.87	0.83	0.86	0.85	0.79	0.81
Na	0.02	0.03	0.03	0.02	0.02	0.10	0.11
K	0.00	0.00	0.00	0.00	0.00	0.00	0.00
Ni	0.00	0.00	0.00	0.00	0.00	0.00	0.00
Total	3.99	4.00	4.00	3.99	3.99	4.00	4.00
Mg#	82.02	68.16	57.63	81.69	62.52	83.64	79.98
$D^{(cpx\text{-}melt)}_{H_2O}$						0.0162	0.0248
Absorbance of cpx (cm^{-1})	0.0	0.0	0.0	0.0	0.0	2.5	4.3
Thickness of cpx (0.001mm)	90	103	86	86	93	128	99
Absorbance normalized to 1 cm (cm^{-1})						195	434
H_2O-cpx (ppm)						83	184
H_2O-melt (wt%)						0.5	0.7

Sample No.							DY-7	
Section No.	3			4			1	
Point No.	1	3.2	5	2	3.1	4.1	1	2
SiO_2	50.03	50.80	50.42	50.89	50.86	49.35	50.72	50.03
TiO_2	1.72	1.79	1.49	1.41	1.59	1.90	2.05	1.98
Al_2O3	4.15	2.87	2.77	3.95	2.79	3.33	2.88	3.57
Cr_2O3	0.16	0.07	0.06	0.31	0.08	0.03	0.07	0.12
FeO	7.91	8.04	8.34	7.38	8.27	9.39	7.92	8.33
MnO	0.11	0.14	0.10	0.12	0.14	0.14	0.12	0.13
MgO	13.44	14.14	14.02	14.49	14.00	13.50	13.86	13.43
CaO	21.62	21.30	21.13	20.15	21.18	20.45	22.02	21.57
Na_2O	0.43	0.41	0.39	0.49	0.42	0.48	0.40	0.38
K_2O	0.00	0.01	0.00	0.01	0.01	0.02	0.00	0.00
NiO	0.05	0.06	0.01	0.02	0.02	0.00	0.08	0.03
Total	99.62	99.62	98.73	99.20	99.35	98.59	100.11	99.57
Si	1.87	1.90	1.90	1.89	1.91	1.87	1.89	1.88
Ti	0.05	0.05	0.04	0.04	0.04	0.05	0.06	0.06
Al	0.18	0.13	0.12	0.17	0.12	0.15	0.13	0.16
Cr	0.00	0.00	0.00	0.01	0.00	0.00	0.00	0.00
Fe	0.25	0.25	0.26	0.23	0.26	0.30	0.25	0.26
Mn	0.00	0.00	0.00	0.00	0.00	0.00	0.00	0.00
Mg	0.75	0.79	0.79	0.80	0.78	0.76	0.77	0.75
Ca	0.87	0.85	0.85	0.80	0.85	0.83	0.88	0.87
Na	0.03	0.03	0.03	0.04	0.03	0.04	0.03	0.03
K	0.00	0.00	0.00	0.00	0.00	0.00	0.00	0.00
Ni	0.00	0.00	0.00	0.00	0.00	0.00	0.00	0.00
Total	4.00	4.00	4.01	3.99	4.00	4.01	4.00	4.00
Mg#	75.20	75.81	74.98	77.78	75.11	71.95	75.73	74.19
$D^{(cpx\text{-}melt)}_{H_2O}$	0.0147	0.0125	0.0120	0.0133	0.0118	0.0148	0.0128	0.0142
Absorbance of cpx (cm^{-1})	1.8	2.9	1.2	1.9	2.9	0.8	10.6	10.0
Thickness of cpx (0.001mm)	99	89	70	94	106	94	92	91
Absorbance normalized to 1 cm (cm^{-1})	177	326	171	202	274	85	1152	1093
H_2O-cpx (ppm)	75	138	73	86	116	36	488	463
H_2O-melt (wt%)	0.5	1.1	0.6	0.6	1.0	0.2	3.8	3.3

Sample No.								
Section No.								
Point No.	3	5	8	8.2	9	10.1	11	12
SiO_2	50.76	50.92	50.78	50.22	50.38	52.84	49.16	52.13
TiO_2	1.61	1.78	1.66	1.71	1.43	0.41	2.20	1.02
Al_2O3	2.84	3.09	2.49	3.11	2.78	4.32	4.09	1.63
Cr_2O3	0.07	0.21	0.07	0.10	0.11	0.74	0.16	0.15
FeO	7.97	7.68	7.66	7.93	8.07	4.08	8.38	9.20
MnO	0.12	0.10	0.13	0.13	0.15	0.05	0.16	0.19
MgO	13.83	13.95	14.29	13.53	14.42	15.21	13.40	14.89
CaO	21.76	21.62	21.44	21.64	21.79	21.15	21.55	19.97
Na_2O	0.46	0.42	0.46	0.39	0.39	0.82	0.40	0.21
K_2O	0.00	0.01	0.02	0.00	0.01	0.00	0.00	0.00
NiO	0.03	0.00	0.00	0.06	0.00	0.05	0.00	0.00
Total	99.44	99.78	98.99	98.81	99.53	99.66	99.51	99.38
Si	1.90	1.90	1.91	1.89	1.89	1.93	1.85	1.95
Ti	0.05	0.05	0.05	0.05	0.04	0.01	0.06	0.03
Al	0.13	0.14	0.11	0.14	0.12	0.19	0.18	0.07
Cr	0.00	0.01	0.00	0.00	0.00	0.02	0.00	0.00
Fe	0.25	0.24	0.24	0.25	0.25	0.12	0.26	0.29
Mn	0.00	0.00	0.00	0.00	0.00	0.00	0.00	0.01
Mg	0.77	0.77	0.80	0.76	0.81	0.83	0.75	0.83
Ca	0.87	0.86	0.86	0.87	0.88	0.83	0.87	0.80
Na	0.03	0.03	0.03	0.03	0.03	0.06	0.03	0.01
K	0.00	0.00	0.00	0.00	0.00	0.00	0.00	0.00
Ni	0.00	0.00	0.00	0.00	0.00	0.00	0.00	0.00
Total	4.01	4.00	4.01	4.00	4.02	3.99	4.01	3.99
Mg#	75.57	76.41	76.90	75.25	76.12	86.91	74.04	74.26
$D^{(cpx\text{-}melt)}_{H_2O}$	0.0119	0.0124	0.0116	0.0125	0.0129	0.0105	0.0170	0.0094
Absorbance of cpx (cm^{-1})	8.8	4.8	5.6	7.9	3.3	5.6	6.8	3.5
Thickness of cpx (0.001mm)	91	94	97	97	75	84	84	81
Absorbance normalized to 1 cm (cm^{-1})	966	511	577	811	444	668	810	432
H_2O-cpx (ppm)	409	216	244	343	188	283	343	183
H_2O-melt (wt%)	3.4	1.7	2.1	2.7	1.5	2.7	2.0	1.9

Sample No.								
Section No.			2					
Point No.	13	13.2	2	3	4	5	6	8
SiO_2	49.14	50.04	49.72	49.18	50.77	50.04	52.16	50.76
TiO_2	2.30	1.75	1.75	2.00	1.49	1.86	1.18	1.81
Al_2O3	4.51	3.31	3.19	3.58	3.87	3.57	2.13	2.91
Cr_2O3	0.10	0.41	0.15	0.08	0.01	0.08	0.01	0.07
FeO	8.90	8.08	8.20	8.75	7.81	8.97	9.29	8.54
MnO	0.09	0.15	0.09	0.12	0.12	0.16	0.16	0.09
MgO	12.64	13.63	13.63	13.55	12.68	13.15	13.82	13.29
CaO	21.55	21.50	21.69	21.19	22.00	21.27	20.50	21.56
Na_2O	0.46	0.39	0.39	0.41	0.59	0.41	0.34	0.43
K_2O	0.00	0.01	0.00	0.00	0.28	0.00	0.00	0.00
NiO	0.00	0.00	0.00	0.00	0.00	0.00	0.00	0.00
Total	99.69	99.26	98.81	98.87	99.60	99.51	99.58	99.47
Si	1.85	1.88	1.88	1.86	1.90	1.88	1.95	1.90
Ti	0.07	0.05	0.05	0.06	0.04	0.05	0.03	0.05
Al	0.20	0.15	0.14	0.16	0.17	0.16	0.09	0.13
Cr	0.00	0.01	0.00	0.00	0.00	0.00	0.00	0.00
Fe	0.28	0.25	0.26	0.28	0.24	0.28	0.29	0.27
Mn	0.00	0.00	0.00	0.00	0.00	0.00	0.01	0.00
Mg	0.71	0.76	0.77	0.76	0.71	0.74	0.77	0.74
Ca	0.87	0.87	0.88	0.86	0.88	0.86	0.82	0.87
Na	0.03	0.03	0.03	0.03	0.04	0.03	0.02	0.03
K	0.00	0.00	0.00	0.00	0.01	0.00	0.00	0.00
Ni	0.00	0.00	0.00	0.00	0.00	0.00	0.00	0.00
Total	4.00	4.01	4.01	4.02	4.00	4.00	3.98	4.00
Mg#	71.69	75.04	74.78	73.40	74.31	72.32	72.61	73.51
$D^{(cpx\text{-}melt)}_{H_2O}$	0.0172	0.0137	0.0137	0.0156	0.0120	0.0139	0.0093	0.0118
Absorbance of cpx (cm^{-1})	6.1	8.0	2.9	5.6	5.6	3.1	4.1	4.3
Thickness of cpx (0.001mm)	84	84	72	93	40	91	89	102
Absorbance normalized to 1 cm (cm^{-1})	726	952	403	605	1390	335	460	422
H_2O-cpx (ppm)	307	403	170	256	588	142	194	178
H_2O-melt (wt%)	1.8	2.9	1.2	1.6	4.9	1.0	2.1	1.5

Sample No.	FJT-5			FJT-6				
Section No.	1		2	1				
Point No.	1	2	1	1	2	3	4	6
SiO_2	49.60	48.60	51.36	49.82	49.92	50.19	49.85	49.28
TiO_2	1.92	2.25	1.28	1.88	0.63	1.92	1.56	2.22
Al_2O3	3.65	5.33	3.44	3.52	5.27	3.48	3.67	3.90
Cr_2O3	0.07	0.15	0.05	0.07	0.11	0.06	0.69	0.08
FeO	8.06	8.53	6.86	7.93	10.31	7.93	7.66	7.62
MnO	0.19	0.08	0.09	0.10	0.13	0.13	0.11	0.07
MgO	13.48	13.06	14.06	13.17	11.50	13.12	14.05	13.49
CaO	21.94	21.92	22.10	21.67	21.47	21.87	21.19	22.08
Na_2O	0.33	0.46	0.36	0.41	0.75	0.38	0.36	0.41
K_2O	0.00	0.00	0.06	0.00	0.01	0.01	0.01	0.00
NiO	0.02	0.01	0.00	0.01	0.07	0.01	0.00	0.00
Total	99.27	100.38	99.63	98.57	100.16	99.09	99.13	99.15
Si	1.87	1.81	1.91	1.88	1.87	1.89	1.87	1.85
Ti	0.05	0.06	0.04	0.05	0.02	0.05	0.04	0.06
Al	0.16	0.23	0.15	0.16	0.23	0.15	0.16	0.17
Cr	0.00	0.00	0.00	0.00	0.00	0.00	0.02	0.00
Fe	0.25	0.27	0.21	0.25	0.32	0.25	0.24	0.24
Mn	0.01	0.00	0.00	0.00	0.00	0.00	0.00	0.00
Mg	0.76	0.73	0.78	0.74	0.64	0.74	0.79	0.76
Ca	0.88	0.88	0.88	0.88	0.86	0.88	0.85	0.89
Na	0.02	0.03	0.03	0.03	0.05	0.03	0.03	0.03
K	0.00	0.00	0.00	0.00	0.00	0.00	0.00	0.00
Ni	0.00	0.00	0.00	0.00	0.00	0.00	0.00	0.00
Total	4.01	4.02	4.00	4.00	4.02	3.99	4.01	4.01
Mg#	74.88	73.19	78.52	74.76	66.55	74.69	76.58	75.94
$D^{(cpx\text{-}melt)}_{H_2O}$	0.0148	0.0210	0.0114	0.0133	0.0144	0.0130	0.0148	0.0159
Absorbance of cpx (cm^{-1})	2.7	3.4	1.3	3.8	1.5	1.0	2.4	1.9
Thickness of cpx (0.001mm)	92	66	97	94	83	88	99	103
Absorbance normalized to 1 cm (cm^{-1})	288	518	137	404	178	108	246	182
H_2O-cpx (ppm)	122	219	58	171	75	46	104	77
H_2O-melt (wt%)	0.8	1.0	0.5	1.3	0.5	0.4	0.7	0.5

Sample No.								
Section No.								2
Point No.	7	8	9	10	11	12	13	1
SiO_2	50.35	50.04	50.17	50.76	51.13	50.15	50.26	47.22
TiO_2	1.92	1.88	1.97	1.71	1.60	1.99	2.01	2.60
Al_2O3	3.33	3.80	3.24	3.15	2.61	3.39	3.47	4.80
Cr_2O3	0.04	0.04	0.06	0.13	0.21	0.12	0.05	0.06
FeO	8.15	7.70	7.93	7.82	7.80	7.77	7.94	8.67
MnO	0.09	0.14	0.14	0.09	0.10	0.12	0.08	0.12
MgO	13.86	13.59	13.79	14.05	13.96	13.84	13.81	12.92
CaO	21.75	22.01	22.02	21.65	21.96	21.91	21.89	21.68
Na_2O	0.40	0.42	0.44	0.38	0.45	0.42	0.39	0.45
K_2O	0.00	0.00	0.00	0.00	0.00	0.01	0.00	0.00
NiO	0.00	0.11	0.00	0.07	0.04	0.03	0.02	0.01
Total	99.89	99.74	99.75	99.80	99.85	99.75	99.93	98.51
Si	1.88	1.87	1.88	1.89	1.91	1.87	1.87	1.80
Ti	0.05	0.05	0.06	0.05	0.04	0.06	0.06	0.07
Al	0.15	0.17	0.14	0.14	0.11	0.15	0.15	0.22
Cr	0.00	0.00	0.00	0.00	0.01	0.00	0.00	0.00
Fe	0.25	0.24	0.25	0.24	0.24	0.24	0.25	0.28
Mn	0.00	0.00	0.00	0.00	0.00	0.00	0.00	0.00
Mg	0.77	0.76	0.77	0.78	0.78	0.77	0.77	0.74
Ca	0.87	0.88	0.88	0.86	0.88	0.88	0.87	0.89
Na	0.03	0.03	0.03	0.03	0.03	0.03	0.03	0.03
K	0.00	0.00	0.00	0.00	0.00	0.00	0.00	0.00
Ni	0.00	0.00	0.00	0.00	0.00	0.00	0.00	0.00
Total	4.01	4.01	4.01	4.00	4.00	4.01	4.01	4.03
Mg#	75.20	75.89	75.61	76.23	76.14	76.07	75.61	72.67
$D^{(cpx\text{-}melt)}_{H_2O}$	0.0138	0.0145	0.0138	0.0128	0.0115	0.0142	0.0141	0.0223
Absorbance of cpx (cm^{-1})	2.5	1.9	2.9	2.7	1.6	1.9	1.9	1.0
Thickness of cpx (0.001mm)	123	123	123	131	132	129	130	72
Absorbance normalized to 1 cm (cm^{-1})	203	153	233	203	121	146	147	132
H_2O-cpx (ppm)	86	65	98	86	51	62	62	56
H_2O-melt (wt%)	0.6	0.4	0.7	0.7	0.4	0.4	0.4	0.3

Sample No.								
Section No.								
Point No.	3	4	5	6	8	8.2	9	9.2
SiO_2	49.23	49.79	49.80	48.78	50.63	50.34	47.85	46.79
TiO_2	1.84	1.77	1.89	2.27	1.45	1.72	1.62	1.75
Al_2O3	3.21	3.33	3.49	3.83	2.92	2.70	6.91	7.82
Cr_2O3	0.14	0.08	0.11	0.00	0.04	0.86	0.04	0.06
FeO	7.95	8.12	7.81	8.04	7.82	7.87	11.08	10.86
MnO	0.09	0.10	0.07	0.07	0.09	0.13	0.15	0.18
MgO	13.97	14.01	13.65	13.64	13.93	13.50	8.74	8.67
CaO	21.82	22.09	21.88	21.84	21.83	21.42	23.19	23.02
Na_2O	0.40	0.42	0.37	0.42	0.42	0.41	0.36	0.43
K_2O	0.00	0.00	0.00	0.00	0.01	0.00	0.00	0.01
NiO	0.04	0.04	0.02	0.04	0.01	0.00	0.00	0.00
Total	98.68	99.74	99.07	98.92	99.13	98.96	99.94	99.58
Si	1.86	1.87	1.87	1.84	1.90	1.90	1.82	1.78
Ti	0.05	0.05	0.05	0.06	0.04	0.05	0.05	0.05
Al	0.14	0.15	0.15	0.17	0.13	0.12	0.31	0.35
Cr	0.00	0.00	0.00	0.00	0.00	0.03	0.00	0.00
Fe	0.25	0.25	0.25	0.25	0.25	0.25	0.35	0.35
Mn	0.00	0.00	0.00	0.00	0.00	0.00	0.00	0.01
Mg	0.79	0.78	0.77	0.77	0.78	0.76	0.49	0.49
Ca	0.89	0.89	0.88	0.88	0.88	0.86	0.94	0.94
Na	0.03	0.03	0.03	0.03	0.03	0.03	0.03	0.03
K	0.00	0.00	0.00	0.00	0.00	0.00	0.00	0.00
Ni	0.00	0.00	0.00	0.00	0.00	0.00	0.00	0.00
Total	4.02	4.02	4.01	4.02	4.01	4.00	3.99	4.00
Mg#	75.80	75.46	75.72	75.15	76.05	75.37	58.44	58.73
$D^{(cpx\text{-}melt)}_{H_2O}$	0.0149	0.0147	0.0141	0.0170	0.0119	0.0123	0.0192	0.0238
Absorbance of cpx (cm^{-1})	0.5	1.2	2.4	1.9	3.1	1.9	2.0	1.0
Thickness of cpx (0.001mm)	72	78	79	84	95	95	94	94
Absorbance normalized to 1 cm (cm^{-1})	67	159	308	227	327	201	214	102
H_2O-cpx (ppm)	28	67	130	96	139	85	90	43
H_2O-melt (wt%)	0.2	0.5	0.9	0.6	1.2	0.7	0.5	0.2

Sample No.		FJT-4					
Section No.		1					
Point No.	10	1	1.2	2	3	4	5
SiO_2	49.44	50.63	50.27	50.38	48.69	49.81	50.07
TiO_2	2.17	1.89	1.98	1.65	2.55	2.12	1.89
Al_2O3	3.96	3.00	3.37	3.37	4.48	3.65	3.13
Cr_2O3	0.08	0.04	0.05	0.02	0.07	0.08	0.08
FeO	7.88	7.59	7.75	8.14	8.14	7.92	7.97
MnO	0.09	0.10	0.12	0.08	0.07	0.10	0.07
MgO	12.48	14.07	13.12	13.69	13.06	13.13	13.84
CaO	22.11	22.00	21.88	21.84	21.69	22.20	22.04
Na_2O	0.32	0.44	0.40	0.42	0.49	0.45	0.42
K_2O	0.01	0.01	0.00	0.01	0.01	0.00	0.01
NiO	0.05	0.04	0.05	0.07	0.04	0.01	0.04
Total	98.59	99.83	98.99	99.68	99.29	99.47	99.56
Si	1.87	1.89	1.89	1.88	1.83	1.87	1.88
Ti	0.06	0.05	0.06	0.05	0.07	0.06	0.05
Al	0.18	0.13	0.15	0.15	0.20	0.16	0.14
Cr	0.00	0.00	0.00	0.00	0.00	0.00	0.00
Fe	0.25	0.24	0.24	0.25	0.26	0.25	0.25
Mn	0.00	0.00	0.00	0.00	0.00	0.00	0.00
Mg	0.70	0.78	0.74	0.76	0.73	0.73	0.77
Ca	0.90	0.88	0.88	0.88	0.88	0.89	0.89
Na	0.02	0.03	0.03	0.03	0.04	0.03	0.03
K	0.00	0.00	0.00	0.00	0.00	0.00	0.00
Ni	0.00	0.00	0.00	0.00	0.00	0.00	0.00
Total	3.99	4.01	3.99	4.01	4.01	4.01	4.01
Mg#	73.86	76.77	75.10	75.00	74.10	74.72	75.58
$D^{(cpx\text{-}melt)}_{H_2O}$	0.0142	0.0129	0.0127	0.0132	0.0184	0.0143	0.0137
Absorbance of cpx (cm^{-1})	4.4	3.3	5.8	6.8	4.3	5.3	4.7
Thickness of cpx (0.001mm)	97	118	118	107	110	100	113
Absorbance normalized to 1 cm (cm^{-1})	454	283	490	634	391	530	416
H_2O-cpx (ppm)	192	120	207	268	165	224	176
H_2O-melt (wt%)	1.4	0.9	1.6	2.0	0.9	1.6	1.3

Sample No.						
Section No.				2		
Point No.	6	7	8	1	2	3
SiO_2	50.68	51.00	49.68	50.57	50.74	50.95
TiO_2	1.68	1.81	1.96	1.96	1.95	2.01
Al_2O3	2.84	2.96	3.45	3.09	3.11	3.52
Cr_2O3	0.06	0.03	0.06	0.10	0.07	0.10
FeO	7.54	7.67	8.01	7.61	7.87	7.65
MnO	0.12	0.12	0.12	0.09	0.12	0.10
MgO	14.17	14.00	13.97	14.12	14.03	13.98
CaO	21.63	22.19	21.95	22.05	21.98	22.22
Na_2O	0.39	0.42	0.44	0.42	0.41	0.38
K_2O	0.00	0.00	0.01	0.00	0.00	0.00
NiO	0.03	0.03	0.10	0.09	0.01	0.00
Total	99.15	100.22	99.75	100.09	100.30	100.90
Si	1.90	1.89	1.86	1.88	1.88	1.88
Ti	0.05	0.05	0.06	0.05	0.05	0.06
Al	0.13	0.13	0.15	0.14	0.14	0.15
Cr	0.00	0.00	0.00	0.00	0.00	0.00
Fe	0.24	0.24	0.25	0.24	0.24	0.24
Mn	0.00	0.00	0.00	0.00	0.00	0.00
Mg	0.79	0.78	0.78	0.78	0.78	0.77
Ca	0.87	0.88	0.88	0.88	0.87	0.88
Na	0.03	0.03	0.03	0.03	0.03	0.03
K	0.00	0.00	0.00	0.00	0.00	0.00
Ni	0.00	0.00	0.00	0.00	0.00	0.00
Total	4.00	4.01	4.02	4.01	4.01	4.00
Mg#	77.01	76.51	75.67	76.79	76.08	76.53
$D^{(cpx\text{-}melt)}_{H_2O}$	0.0121	0.0124	0.0153	0.0134	0.0133	0.0138
Absorbance of cpx (cm^{-1})	3.6	5.2	7.2	2.1	2.5	4.3
Thickness of cpx (0.001mm)	128	127	95	97	114	107
Absorbance normalized to 1 cm (cm^{-1})	281	409	758	216	220	402
H_2O-cpx (ppm)	119	173	321	92	93	170
H_2O-melt (wt%)	1.0	1.4	2.1	0.7	0.7	1.2

Table 7-3 Lithium isotope and content of cpx phenocrysts for the Hainan basalts.

Location/Sample No.	Sample No.	PI	Account ^{7}Li	cps(7)/nA/Li of standard	$\delta^{7}Li_{SIMS}$	error	Mg#	$Slop_{Mg, Li}$	$intercept_{Mg, Li}$	$\delta^{7}Li_{cor}$	Li content	error
HN99-08-2	13-2-2@1	1.68E-08	3.62E+04	1.72E+12	32.4	1.1	83.7	1.18	-71.7	5.4	0.8	0.2
	13-2-2@2	1.64E-08	4.96E+04		25.9	0.9	83.7			-1.1	0.6	0.1
	13-2-2@3	1.55E-08	8.57E+04		31.2	1.1	83.7			4.2	0.3	0.1
	13-2-2@4	1.43E-08	3.14E+04		41.1	1.2	83.7			14.1	0.8	0.2
	13-2-2@5	1.36E-08	8.82E+04		28.6	0.8	83.7			1.6	0.3	0.1
HN99-08-1	13-2-1@1	1.30E-08	7.63E+04		28.6	0.9	84.4			0.7	0.3	0.1
	13-2-1@2	1.24E-08	2.66E+04		36.2	1.0	84.4			8.2	0.8	0.2
	13-2-1@3	1.26E-08	4.94E+04		29.0	1.0	84.4			1.0	0.4	0.1
	13-2-1@4	1.29E-08	9.31E+04		23.8	1.1	84.4			-4.1	0.2	0.0
	13-2-1@9	1.09E-08	2.18E+04		36.9	1.5	84.4			9.0	0.9	0.2
												0.0
HN99-02-23-02	13-11-2@1	1.09E-08	1.98E+04		34.8	1.6	82.3			9.3	0.9	0.2
	13-11-2@02	1.09E-08	2.06E+04		25.6	1.5	82.3			0.2	0.9	0.2
	13-11-2@03	1.10E-08	1.76E+04		48.1	1.9	82.3			22.7	1.1	0.2
	13-11-2@04	1.09E-08	1.42E+04		47.9	1.6	82.3			22.4	1.3	0.3
	13-11-2@05	1.05E-08	2.52E+04		26.9	1.8	82.3			1.5	0.7	0.1
												0.0
HN99-02-23-03	13-12-3@1	8.41E-09	1.83E+04		44.4	1.7	80.7			20.8	0.8	0.2
	13-12-3@2	8.33E-09	1.61E+04		27.1	1.2	80.7			3.5	0.9	0.2
	13-12-3@3	8.49E-09	1.41E+04		44.3	2.0	80.7			20.8	1.0	0.2
	13-12-3@4	8.66E-09	1.54E+04		39.8	2.0	80.7			16.2	1.0	0.2
	13-12-3@5	8.82E-09	8.17E+04		32.6	2.1	80.7			9.1	0.2	0.0
												0.0
HN99-01-22-01	13-15-1@1	8.76E-09	3.03E+04		48.8	1.6	82.5			23.2	0.5	0.1
												0.0
HN99-01-22-02	13-16-2@1	1.16E-08	4.52E+04		59.9	1.1	81.8			35.1	0.4	0.1
	13-16-2@2	1.16E-08	4.94E+04		48.6	1.2	81.8			23.8	0.4	0.1
	13-16-2@3	1.18E-08	4.79E+04		40.8	2.9	81.8			15.9	0.4	0.1
	13-16-2@4	1.21E-08	4.69E+04		44.8	1.2	81.8			20.0	0.4	0.1
	13-16-2@5	1.23E-08	6.37E+04		50.2	1.2	81.8			25.3	0.3	0.1
												0.0
HN99-01-22-03	13-17-3@1	1.37E-08	7.14E+04		44.5	1.1	78.1			19.7	0.3	0.1
	13-17-3@2	1.39E-08	5.16E+04		43.7	1.1	78.1			18.8	0.5	0.1
	13-17-3@3	1.41E-08	6.38E+04		39.1	0.8	78.1			14.2	0.4	0.1
												0.0
HN99-01-22-06	13-19-6@1	1.42E-08	3.22E+04		50.6	1.7	79.0			25.8	0.8	0.2
	13-19-6@2	1.42E-08	1.58E+04		76.3	2.3	79.0			51.5	1.5	0.3
	13-19-6@3	1.43E-08	2.42E+04		29.6	1.3	79.0			4.7	1.0	0.2
	13-19-6@4	1.42E-08	2.33E+04		32.9	1.4	79.0			8.0	1.0	0.2
	13-19-6@5	1.42E-08	2.10E+04		41.0	1.3	79.0			16.2	1.2	0.2
HN99-01-22-04	13-18-4@1	1.41E-08	3.21E+04		43.3	1.2	82.2			18.4	0.8	0.2
	13-18-4@2	1.40E-08	2.85E+04		22.5	1.3	82.2			-2.3	0.8	0.2
HN99-01-22-05	13-20-5@1	1.38E-08	2.34E+04		38.4	1.4	81.4			13.6	1.0	0.2
	13-20-5@2	1.36E-08	2.18E+04		33.8	1.4	81.4			9.0	1.1	0.2
	13-20-5@3	1.39E-08	1.64E+04		53.6	2.3	81.4			28.8	1.5	0.3
	13-20-5@4	1.42E-08	2.32E+04		36.7	1.2	81.4			11.9	1.1	0.2
	13-20-5@5	1.43E-08	2.38E+04		42.9	1.5	81.4			18.1	1.0	0.2

Table 7-4 Oxygen isotopic ratios of cpx phenocrysts for the Hainan basalts.

Location/Sample No.	Sample No.	Mg#	$\delta^{18}O_{SIMS}$	$Slop_{Mg,O}$	$intercept_{Mg,O}$	IMF_{ST}	IMF	Mean of $\delta^{18}O_{cor}$	SD
HN99-01-22-01	13-15-1@1	82.5	9.7	-0.100	10.6	2.9	1.8	7.7	0.3
HN99-01-22-02	13-16-2@1	81.8	9.3	-0.100	10.6	2.8	1.7	7.8	0.2
HN99-01-22-03	13-17-3@1	78.1	8.7	-0.100	10.6	2.5	1.8	7.7	0.8
HN99-01-22-03-r	13-17-3-a@1	78.1	9.0	-0.100	10.6	2.0	1.3	7.7	0.0
HN99-01-22-04	13-18-4@1	82.2	8.7	-0.100	10.6	2.3	1.1	7.8	0.3
HN99-01-22-05	13-20-5@1	81.4	9.6	-0.100	10.6	2.0	1.0	8.3	0.4
HN99-01-22-06	13-19-6@1	79.0	9.1	-0.100	10.6	2.0	1.2	7.8	0.2
HN99-02-23-01	13-10-1@1	81.3	8.7	-0.100	10.6	2.9	1.9	7.1	0.3
HN99-02-23-02	13-12-2@1	82.3	9.0	-0.100	10.6	3.0	1.8	7.5	0.3
HN99-02-23-03	13-12-3@1	80.7	9.8	-0.100	10.6	3.0	2.0	7.3	0.4
HN99-02-23-03-r	13-12-3-a@1	80.7	9.5	-0.100	10.6	3.0	2.0	7.4	0.0
HN99-10-21-12	13-5-12@1	75.7	9.7	-0.100	10.6	2.9	2.4	7.3	0.6
HN99-10-21-13	13-9-13@1	69.5	8.1	-0.100	10.6	3.0	3.2	4.8	0.1
HN99-10-21-2	13-8-2@1	77.9	7.4	-0.100	10.6	3.0	2.3	4.5	0.6
HN99-10-21-3	13-8-3@1	75.8	10.3	-0.100	10.6	3.0	2.5	7.6	0.2
HN99-10-21-7	13-6-7@1	82.5	10.2	-0.100	10.6	2.9	1.8	8.2	0.2
FJT-2-0-1	12-19-1@1	81.5	7.9	-0.195	16.3	1.9	0.2	7.8	0.1
FJT-4-1-1.2	13-28-1-2@1	75.1	9.5	-0.184	16.7	2.8	2.5	7.0	0.0
FJT-4-1-2	13-27-2@1	75.0	8.8	-0.184	16.7	2.7	2.4	6.5	0.0
FJT-4-1-3	13-26-3@1	74.1	9.5	-0.184	16.7	2.8	2.6	6.8	0.1
FJT-4-1-4	13-22-4@1	74.7	8.7	-0.184	16.7	2.3	2.0	6.8	0.1
FJT-4-1-4	13-22-4-x@1	74.7	9.0	-0.184	16.7	2.3	2.0	7.0	0.0
FJT-4-1-4	13-22-4@4	74.7	8.9	-0.184	16.7	2.3	2.0	6.8	0.0
FJT-4-1-5	13-23-5@1	75.6	9.3	-0.184	16.7	2.6	2.2	7.0	0.2
FJT-4-1-6	13-25-6@1	77.0	9.6	-0.184	16.7	2.6	1.8	7.4	0.2
FJT-4-1-7	13-24-7@1	76.5	9.2	-0.184	16.7	2.2	1.6	7.6	0.0
FJT-4-1-7	13-24-7@4	76.5	8.9	-0.184	16.7	2.3	1.7	7.2	0.0
FJT-4-1-8	13-21-8@1	75.7	9.1	-0.184	16.7	2.4	1.9	7.3	0.2
FJT-5-2-1	12-25-1@1	78.5	9.2	-0.096	10.5	2.4	1.0	8.2	0.3
FJT-6-1-4	12-32-4@1	76.6	9.8	-0.096	10.5	2.9	2.1	7.3	0.3
FJT-6-1-6	12-31-6@1	75.9	8.8	-0.096	10.5	3.3	2.7	6.5	0.5
FJT-6-2-3	12-27-3@1	75.8	9.7	-0.096	10.5	3.5	3.0	6.5	0.2
FJT-6-2-9	12-26-9@1	58.4	17.4	-0.096	10.5	2.4	7.4	10.1	0.1
FJT-6-2-9.2	12-26-9-2@1	58.7	17.9	-0.096	10.5	2.4	7.3	10.7	0.2
FJT-7-0-5	12-20-5@1	82.0	7.5	-0.096	10.5	2.5	0.0	8.0	0.4
DY-4-1-6	12-18-6@1	83.6	7.9	-0.195	16.3	1.8	-0.3	8.2	0.3
DY-4-2-2	13-35-2@1	77.8	7.1	-0.123	10.2	1.1	-0.8	8.1	0.2
DY-4-2-4	13-39-4@1	80.0	8.9	-0.184	16.7	2.7	1.4	7.6	0.1
DY-4-3-1	13-30-1@1	75.2	9.3	-0.184	16.7	2.9	2.5	6.5	0.2
DY-4-3-5	13-29-5@1	75.0	9.0	-0.184	16.7	2.9	2.5	6.4	0.0
DY-4-4-2	13-33-2@1	77.8	7.7	-0.184	16.7	2.7	1.9	6.4	0.5
DY-4-4-2.1	13-33-2-1@1	75.1	8.2	-0.184	16.7	2.8	2.4	6.9	0.3
DY-4-4-3	13-32-3@1	75.1	6.5	-0.184	16.7	0.6	-1.0	7.9	0.3
DY-4-4-3.1	13-32-3-1@1	75.1	8.9	-0.100	10.6	2.9	2.5	6.3	0.1
DY-4-4-3.1	13-32-3-1@4	75.1	9.2	-0.184	16.7	2.7	2.3	6.8	0.0
DY-4-4-4.1	13-31-4-1@1	71.9	9.3	-0.184	16.7	2.8	3.0	6.4	0.2

Chapter 8 Conclusions

(1) Water content of basaltic magma is an efficient index to identify the origin of different recycled materials in the mantle source. Most of Cenozoic basalts in SE China have kept their original water contents except the SC, BL, LH, SJY, and ML basaltic rocks. These basalts have IABs or BABBs-like water content suggesting wet enriched melting source underneath SE China. The magma water contents for the Zhejiang basalts range from 1.3 to 2.9 wt. %, for the Fujian basalts range from 0.3 to 0.5 wt. % (for "dry" basalts) and from 1.5 to 3.8 wt. % ("wet" basalts), and from 1.3 to 2.6 wt. % for the Hainan basalts. The H loss and re-equilibrium are identified from unusual low water content, OH profiles and the Li content and δ^7Li profiles of cpx grains, as well as the relationship between Mg# and the water content of corresponding magma. The BL cpx phenocrysts have re-equilibrated water content. Some cpx phenocrysts in such as SC basalts have experienced a loss of the origin water during the magma ascent or after eruption.

(2) Cenozoic basalts in SE China almost had survived from the crust contamination, while a little fractional crystallization occurred. Their chemical compositions can be used to deduce the geochemical feature of their mantle source. Cenozoic basalts in SE China display the geochemical signature of different recycled oceanic material components:

a. **The Zhejiang case:** Zhejiang Cenozoic basalts erupted in 20-27Ma (Group 1) and after 11Ma (Group 2), respectively, with distinct geochemical features. The "initial" H_2O contents of the melts, reversely calculated from the H_2O content of the cpx phenocrysts and the corresponding partition coefficients of H_2O between cpx and basaltic melts, range from 1.4 to 2.2 wt. % for the Group 1 samples and from 1.3 to 2.6 wt. % for the Group 2 samples, falling within the water content range of BABBs and IABs, and indicating wet materials in the mantle source. More alkaline, lower Si and Al contents, higher trace element concentrations, La/Yb, Ce/Pb, and Nb/La ratios, lower H_2O/Ce, Ba/La, and Ba/Th ratios, and stronger negative K, Pb, Zr, Hf and Ti anomalies are observed in the older Group 1 basalts than those in the younger Group 2 ones. The Group 1 samples are plotted on the mixing curve between DMM and recycled oceanic alkali basalt component. The Group 2 samples show higher H_2O/Ce, Ba/La and Ba/Th ratios than the Group 1 samples, reflecting enriched sources involved recycled

oceanic sediment component together with recycled oceanic crust component. The continuous change of the recycled oceanic material compositions over time in the mantle source of Zhejiang Cenozoic basalts imply that a continuous material supply in the mantle source. These recycled materials are most likely provided by the stagnant Pacific slab in the MTZ, which is the only subducted plate since 100 Ma in the Zhejiang region.

b. **The Fujian case:** Fujian Cenozoic basaltic rocks erupted after 10Ma and have similar trace element patterns to Zhejiang Cenozoic basalts. The "initial" water contents of the SH and MX basalts are 1.5-3.8 wt. % and 0.3-0.5 wt. % respectively. However, the BL samples display re-equilibrated water content of 2.1-2.5 wt. %. Li in situ analysis of cpx by SIMS and OH IR profiles of cpx are used to identify later H variation after cpx crystallization. The Li analysis of cpx by SIMS have considerable IMF associated with chemical composition. Therefore, a series of known standards with wide and similar chemical compositions to unknown samples are required for accurate measurement. The Li content and the Li isotopic component demonstrate the MX basalts have escaped intense Li diffusion, while the SH and BL samples have undergone significant later Li diffusion. The high $\delta^{18}O$ values of the cpx phenocrysts in the Fujian basalts suggest the existence of recycled material components in their mantle source. The highest $\delta^{18}O$ values are found in the cpx phenocrysts with the intermediate ratios of Si/Al and Ca/Al, and the relationship between Mg# and $\delta^{18}O$ in the MX samples, suggesting a mixture of two kinds of magmas. The SH and BL samples involved the recycled upper and lower oceanic crust components together with the recycled oceanic sediment component in their source, whereas the MX basalts involved the recycled upper oceanic crust component together with the recycled oceanic sediment component. The NTS melts dominantly generated from the residual lower oceanic crust component and some recycled oceanic sediment components after earlier melting. The low water content of the MX basalts suggest high dehydration of the enriched components than other Fujian basaltic rocks. The pronounced recycled oceanic materials are most likely the distributed residue of the previous subducted slab in the upper mantle, which have sunk to the lower mantle.

c. **The Hainan case:** Relative to Cenozoic basalts in the Fujian and Zhejiang provinces, the Hainan Cenozoic basalts have complex trace element patterns, including HIMUs-like and EM-like characters, suggesting more heterogeneous mantle sources than Zhejiang and Fujian Cenozoic basalts. The Hainan basalts have higher$\delta^{18}O$ than

normal mantle values. Combined with the more enriched Sr, Nd, and Pb isotopic ratios of Hainan Cenozoic basalts than those of the normal mantle, the recycled materials are also required in the mantle source. Most of the ML, LH, and SJY basalts have dry cpx phenocrysts, while one LH sample (HN9910) have kept its original water content of 2.7 w.t. %. The DY and FJT samples have the water content of 2.6 wt. % and 1.3 wt. %, respectively. The coexistence of high and low $\delta^{18}O$ cpx phenocrysts observed in the LH basalts, combined with their trace element composition, the recycled upper oceanic crust components are dominantly required in the LH basalts, while limited volume of recycled lower oceanic crust gabbro component was also involved. The DY and FJT basalts are suggested as the results of the mixture of DMM, recycled oceanic sediment, and crust components. These recycled materials are most likely caught by upwelling plume from the deep mantle.

(3) Cenozoic basalts, especially in SE China, have systematic variation of geochemical composition with the latitude. The radiogenic isotopic and trace element ratios display opposite symmetrical variation from N 25-29º section to south Hainan Island and from N 25-29º section to NE China, respectively. The spatial chemical and isotopic variation are observed both along the coast in East China and IBM trench. The consistency implies the spatial chemical variation may be caused by either the systematic varying chemical and isotopic composition of upper mantle or the influence of upper mantle by the Pacific subduction. The difference of radiogenic isotope between the northern part of eastern China and the southern part of eastern China may be caused by the difference of their enriched component in the mantle source; the mixture of young and old subducted crust and sediments as well as recycled continental crust might occur, due to the complex history in the northern part, however, the southern part only might involve young subducted materials in the mantle

References:

Aizawa, Y., Tatsumi, Y., Yamada, H., 1999. Element transport by dehydration of subducted sediments: Implication for arc and ocean island magmatism. Island Arc, 8, 38-46.

Asimow, P. D., Langmuir, C. H., 2003. The importance of water to oceanic mantle melting regimes. Nature, 421(6925), 815-820.

Asimow, P.D., Dixon, J.E., Langmuir, C.H., 2004. A hydrous melting and fractionation model for mid-ocean ridge basalts: application to the Mid-Atlantic Ridge near the Azores. Geochemistry, Geophysics, Geosystems, 5, http://dx.doi.org/10.1029/2003GC000568.

Auer, S., Bindecman, I., Wallace, P., Ponomareva, V. & Portnyagin, M., 2009. The origin of hydrous, high-$\delta^{18}O$ voluminous volcanism: diverse oxygen isotope values and high magmatic water contents within the volcanic record of Klyuchevskoy volcano, Kamchatka, Russia. Contributions to mineralogy and petrology, 157, 209-230.

Baker, M.B., Stolper, E.M., 1994. Determining the composition of high-pressure mantle melts using diamond aggregates. Geochimica et Cosmochimica Acta, 58, 2811-2827.

Balta, J.B., Asimow, P.D., Mosenfelder, J.L., 2011. Hydrous, Low-carbon Melting of Garnet Peridotite. Journal of Petrology, 52, 2079-2105.

Barrat, J.A., Chaussidon, M., Bohn, M., Gillet, P., Göpel, C., Lesourd, M., 2005. Lithium behavior during cooling of a dry basalt: An ion-microprobe study of the lunar meteorite Northwest Africa 479 (NWA 479). Geochimica et Cosmochimica, Acta 69, 5597-5609.

Beck, P., Barrat, J.A., Chaussidon, M., Gillet, P., Bohn, M., 2004. Li isotopic variations in single pyroxenes from the Northwest Africa 480 shergottite (NWA 480): a record of degassing of Martian magmas? Geochimica et Cosmochimica Acta, 68, 2925-2933.

Beck, P., Chaussidon, M., Barrat, J.A., Gillet, P., Bohn, M., 2006. Diffusion induced Li isotopic fractionation during the cooling of magmatic rocks: The case of pyroxene phenocrysts from nakhlite meteorites. Geochimica et Cosmochimica Acta, 70, 4813-4825.

References

Bell, D.R., Hervig, R.L., Buseck, P.R., Aulbach, S., 2009. Lithium isotope analysis of olivine by SIMS: Calibration of a matrix effect and application to magmatic phenocrysts. Chemical Geology, 258, 5-16.

Bell, D.R., Ihinger, P.D., Rossman, G.R., 1995. Quantitative analysis of trace OH in garnet and pyroxenes. American Mineralogist, 80, 465-474.

Bennett, S.L., Blundy, J., Elliott, T., 2004. The effect of sodium and titanium on crystal-melt partitioning of trace elements. Geochimica et Cosmochimica, Acta 68, 2335-2347.

Bindeman IN, Eiler JN, et al., 2005, Oxygen isotope evidence for slab melting in modern and ancient subduction zones. Earth and Planetary Science Letters, 235: 480–496

Bindeman I.N., Ponomareva V.V., Bailey J.C., Valley J.W., 2004, Volcanic arc of Kamchatka: a province with high-$\delta^{18}O$ magma sources and large scale $^{18}O/^{16}O$ depletion of the upper crust. Geochim Cosmochim Acta, 68: 841–865

Bindeman, I., 2008. Oxygen isotopes in mantle and crustal magmas as revealed by single crystal analysis. Reviews in Mineralogy and Geochemistry, 69, 445–478.

Bizimis, M., Salters, V.J.M., Dawson, J.B., 2003. The brevity of carbonatite source in the mantle: evidence from Hf isotopes. Contributions to Mineralogy and Petrology, 145, 281–300.

Blundy, J.D., Falloon, T.J., Wood, B.J., Dalton, J.A., 1995. Sodium partitioning between clinopyroxene and silicate melts. Journal of Geophysical Research, 100, 15501–15515.

Bodnar RJ, Azbej T, Becker SP. et al., 2013, Whole Earth geohydrologic cycle, from the clouds to the core: The distribution of water in the dynamic Earth system. In: Bickford ME (Ed), The web of geological sciences: Advances, impacts, and interactions. Geol Soc Am Spec Paper, 500: 431–461.

Bouman, C., Elliott, T., Vroon, P. Z., 2004. Lithium inputs to subduction zones. Chemical Geology, 212(1), 59-79.

Brenan J.M., Neroda E., Lundstrom C.C., Shaw H.F., Ryerson F.J., Phinney D.L., 1998, Behaviour of boron, beryllium, and lithium during melting and crystallization: constraints from mineral–melt partitioning experiments, Geochim. Cosmochim. Acta, 62 (12) 2129–2141.

Castillo, P.R., 2015. The recycling of marine carbonates and sources of HIMU and FOZO ocean island basalts. Lithos, 216–217, 254-263.

References

Charvet, J., Shu, L., Faure, M., Choulet, F., Wang, B., Lu, H., and Le Breton, N., 2010, Structural development of the Lower Paleozoic belt of South China: Genesis of an intra-continental orogen: Journal of Asian Earth Sciences, v. 39, n. 4, p. 309–330, http://dx.doi.org/10.1016/j.jseaes.2010.03.006.

Chan, L. H., & Kastner, M., 2000. Lithium isotopic compositions of pore fluids and sediments in the costa rica subduction zone: implications for fluid processes and sediment contribution to the arc volcanoes. Earth and Planetary Science Letters, 183(1-2), 275-290.

Chan, L. H., Alt, J. C., Teagle, D. A., 2002b. Lithium and lithium isotope profiles through the upper oceanic crust: a study of seawater–basalt exchange at ODP Sites 504B and 896A. Earth and Planetary Science Letters, 201(1), 187-201.

Chan, L. H., Edmond, J. M., 1988. Variation of lithium isotope composition in the marine environment: a preliminary report. Geochimica et Cosmochimica Acta, 52(6), 1711-1717.

Chan, L. H., Edmond, J. M., Thompson, G., Gillis, K., 1992. Lithium isotopic composition of submarine basalts: implications for the lithium cycle in the oceans. Earth and Planetary Science Letters, 108(1), 151-160.

Chan, L. H., Frey, F. A., 2003. Lithium isotope geochemistry of the Hawaiian plume: results from the Hawaii Scientific Drilling Project and Koolau volcano. Geochemistry, Geophysics, Geosystems, 4(3).

Chan, L. H., Gieskes, J. M., Chen-Feng, Y., Edmond, J. M., 1994. Lithium isotope geochemistry of sediments and hydrothermal fluids of the Guaymas Basin, Gulf of California. Geochimica et Cosmochimica Acta, 58(20), 4443-4454.

Chan, L. H., Lassiter, J. C., Hauri, E. H., Hart, S. R., Blusztajn, J., 2009. Lithium isotope systematics of lavas from the Cook–Austral Islands: constraints on the origin of HIMU mantle. Earth and Planetary Science Letters, 277(3), 433-442.

Chan, L. H., Leeman, W. P., Plank, T., 2006. Lithium isotopic composition of marine sediments. Geochemistry, Geophysics, Geosystems, 7(6).

Chan, L. H., Leeman, W. P., You, C. F., 2002a. Lithium isotopic composition of Central American volcanic arc lavas: implications for modification of subarc mantle by slab-derived fluids: correction. Chemical Geology, 182(2), 293-300.

Chen, C.-H., Lee, C.-Y., Shinjo, R., 2008. Was there Jurassic paleo-Pacific subduction in South China?: Constraints from $^{40}Ar/^{39}Ar$ dating, element and Sr–Nd–Pb isotopic geochemistry of the Mesozoic basalts. Lithos 106, 83-92.

References

Chen, F., Satir, M., Ji, J., Zhong, D., 2002. Nd-Sr-Pb isotopes of Tengchong Cenozoic volcanic rocks from western Yunnan, China: evidence for an enriched-mantle source. Journal of Asian Earth Sciences 21, 39-45.

Chen, H., Xia, Q.-K., Ingrin, J., Jia, Z.-B., Feng, M., 2015. Changing recycled oceanic components in the mantle source of the Shuangliao Cenozoic basalts, NE China: New constraints from water content. Tectonophysics 650, 113-123.

Chen, J., Inoue, T., Weidner, D. J., Wu, Y., Vaughan, M. T., 1998. Strength and water weakening of mantle minerals, olivine, wadsleyite and ringwoodite. Geophysical Research Letters, 25(4), 575-578.

Chen, L.H., Zeng, G., Jiang, S.Y., Hofmann, A.W., Xu, X.S., Pan, M.B., 2009. Sources of Anfengshan basalts: Subducted lower crust in the Sulu UHP belt, China. Earth and Planetary Science Letters 286, 426-435.

Chen, Y., Provost, A., Schiano, P., Cluzel, N,. 2011. The rate of water loss from olivine-hosted melt inclusions. Contributions to Mineralogy and Petrology, 162(3), 625-636.

Choi, S.H., Mukasa, S.B., Kwon, S.T., Andronikov, A.V., 2006. Sr, Nd, Pb and Hf isotopic compositions of late Cenozoic alkali basalts in South Korea: Evidence for mixing between the two dominant asthenospheric mantle domains beneath East Asia. Chemical Geology 232, 134-151.

Chung, S.-L., Sun, S.-s., 1992. A new genetic model for the East Taiwan Ophiolite and its implications for Dupal domains in the Northern Hemisphere. Earth and Planetary Science Letters 109, 133-145.

Class, C., Goldstein, S.L., 1997. Plume-lithosphere interactions in the ocean basins: constraints from the source mineralogy. Earth and Planetary Science Letters 150, 245-260.

Coogan, L.A., Kasemann, S.A., Chakraborty, S., 2005. Rates of hydrothermal cooling of new oceanic upper crust derived from lithium-geospeedometry. Earth and Planetary Science Letters 240, 415-424.

Cooper KM, Eiler JM, Asimov PD, Langmuir CH, 2004. Oxygen isotope evidence for the originof enriched mantle beneath the mid-Atlantic ridge. Earth and Planetary Science Letters, 220: 297–316

Costa, F., Chakraborty, S., 2008. The effect of water on Si and O diffusion rates in olivine and implications for transport properties and processes in the upper mantle. Physics of the Earth and Planetary Interiors, 166(1), 11-29.

Dai, B.-Z., Jiang, S.-Y., Jiang, Y.-H., Zhao, K.-D., Liu, D.-Y., 2008. Geochronology, geochemistry and Hf–Sr–Nd isotopic compositions of Huziyan mafic xenoliths, southern Hunan Province, South China: Petrogenesis and implications for lower crust evolution. Lithos, 102, 65-87.

Danyushevsky, L.V., Eggins, S.M., Falloon, T.J., Christie, D.M., 2000. H2O abundance in depleted to moderately enriched Mid-ocean ridge magmas; Part I: incompatible behaviour, implications for mantle storage, and origin of regional variations. Journal of Petrology, 41, 1329–1364.

Danyushevsky, L.V., Falloon, T.J., Sobolev, A.V., Crawford, A.J., Carroll, M., Price, R.C., 1993. The H2O content of basalt glasses from southwest Pacific backarc basins. Earth and Planetary Science Letters, 117, 347–362

Dasgupta, R., Hirschmann, M.M., Smith,N.D., 2007. Partial melting experiments of peridotite+CO_2 at 3 GPa and genesis of alkalic ocean island basalts. Journal of Petrology, 48, 2093–2124.

Dasgupta, R., Hirschmann, M.M., Stalker, K., 2006. Immiscible transition from carbonate-rich to silicate-rich melts in the 3 GPa melting interval of eclogite plus CO_2 and genesis of silica-undersaturated ocean island lavas. Journal of Petrology, 47, 647-671.

Dasgupta, R., Hirschmann, M.M., Withers, A.C., 2004. Deep global cycling of carbon constrained by the solidus of anhydrous, carbonated eclogite under upper mantle conditions. Earth and Planetary Science Letters, 227, 73-85.

Dasgupta, R., Jackson, M.G., Lee, C.T.A., 2010. Major element chemistry of ocean island basalts—conditions of mantle melting and heterogeneity of mantle source. Earth and Planetary Science Letters, 289, 377-392.

Decitre, S., Deloule, E., Reisberg, L., James, R., Agrinier, P., Mével, C., 2002. Behavior of Li and its isotopes during serpentinization of oceanic peridotites. Geochemistry, Geophysics, Geosystems, 3, 1-20.

Deegan, F.M., Troll, V.R., Freda, C., Misiti, V., Chadwick, J.P., McLeod, C.L., Davidson, J.P., 2010. Magma–carbonate interaction processes andassociated CO_2 release at MerapiVolcano, Indonesia: insights from experimental petrology. Journal of Petrology, 51, 1027–1051.

Dellinger, M., Gaillardet, J., Bouchez, J., Calmels, D., Louvat, P., Dosseto, A., Gorge, C., Alanoca, L., Maurice, L., 2015. Riverine Li isotope fractionation in the Amazon River basin controlled by the weathering regimes. Geochimica et Cosmochimica

Acta, 164, 71-93.

Deloule, E., Albarede, F., Alle´, P., 1992. Isotope fractionation, energy distribution and H^+ emission processes from hydroxylated minerals, in: Benninghoven, A., Janssen, K.T.F., Tumpner, J.H., Werner, W. (Eds.), Secondary Ion Mass Spectrometry SIMS VIII, Wiley, U.K., pp. 66-72.

Deloule, E., Albarede, F., Sheppard, S. M., 1991. Hydrogen isotope heterogeneities in the mantle from ion probe analysis of amphiboles from ultramafic rocks. Earth and Planetary Science Letters, 105(4), 543-553.

Demouchy, S., Mackwell, S. J., Kohlstedt, D. L., 2007. Influence of hydrogen on Fe–Mg interdiffusion in (Mg, Fe)O and implications for Earth's lower mantle. Contributions to Mineralogy and Petrology, 154(3), 279-289.

Denis, C.M.M., Demouchy, S., Shaw, C.S.J., 2013. Evidence of dehydration in peridotites from Eifel Volcanic Field and estimates of the rate of magma ascent. Journal of Volcanology and Geothermal Research, 258, 85-99.

DePaolo, D. J., Daley, E. E., 2000. Neodymium isotopes in basalts of the southwest basin and range and lithospheric thinning during continental extension. Chemical Geology, 169(1), 157-185.

Dixon, J. E., Dixon, T. H., Bell, D. R., Malservisi, R., 2004. Lateral variation in upper mantle viscosity: role of water. Earth and Planetary Science Letters, 222(2), 451-467.

Dixon, J.E., Clague, D.A., 2001. Volatiles in basaltic glasses from Loihi Seamount, Hawaii: evidence for a relatively dry plume component. Journal of Petrology, 42, 627-634.

Dixon, J.E., Clague, D.A., Wallace, P., Poreda, R., 1997. Volatiles in alkalic basalts from the North Arch Volcanic Field, Hawaii: extensive degassing of deep submarine-erupted alkalic series lavas. Journal of Petrology, 38, 911–939.

Dixon, J.E., Dixon, T.H., Bell, D.R., Malservisi, R., 2004. Lateral variation in upper mantle viscosity: role of water. Earth and Planetary Science Letters, 222, 451-467.

Dixon, J.E., Leist, L., Langmuir, C., Schilling, J.G., 2002. Recycled dehydrated lithosphere observed in plume-influenced mid-ocean-ridge basalt. Nature, 420, 385-389.

Dixon, J.E., Stolper, E., Delaney, J.R., 1988. Infrared spectroscopic measurements of CO_2 and H_2O in Juan de Fuca Ridge basaltic glasses. Earth and Planetary Science Letters, 90, 87–104.

References

Dobson, P.F., Skogby, H., Rossman, G.R., 1995. Water in boninite glass and coexisting orthopyroxene: concentration and partitioning. Contributions to Mineralogy and Petrology, 118, 414–419.

Dorendorf F., Wiechert U., Worner G., 2000. Hydrated sub-arc mantle: a source for the Kluchevskoy volcano, Kamchatka, Russia. Earth and Planetary Science Letters, 175: 69–86

Eiler J. M., 2001 Oxygen Isotope Variations of Basaltic Lavas and Upper Mantle Rocks[J]. Reviews in Mineralogy & Geochemistry, 43(1):319-364.

Eiler J.M., Farley K.A., Valley J.W., Hofmann A., Stolper E.M., 1996. Oxygen isotope constraints on the sources of Hawaiian volcanism. Earth and Planetary Science Letters, 144: 453–468

Eiler, J. M., Farley, K. A., Valley, J. W., Hauri, E., Craig, H., Hart, S. R. & Stolper, E. M., 1997. Oxygen isotope variations in ocean island basalt phenocrysts. Geochimica et Cosmochimica Acta, 61, 2281-2293.

Eiler, J.M., Crawford, A., Elliott, T., Farley, K.A., Valley, J.W., Stolper, E.M., 2000. Oxygen isotope geochemistry of oceanic arc lavas. Journal of Petrology, 41, 229–256.

Falloon, T.J., Danyushevsky, L.V., 2000. Melting of refractory mantle at 1.5, 2 and 2.5 GPa under, anhydrous and H_2O-undersaturated conditions: Implications for the petrogenesis of high-Ca boninites and the influence of subduction components on mantle melting. Journal of Petrology, 41, 257-283.

Falus, G., Tommasi, A., Ingrin, J., Szabó, C., 2008. Deformation and seismic anisotropy of the lithospheric mantle in the southeastern Carpathians inferred from the study of mantle xenoliths. Earth and Planetary Science Letters, 272(1), 50-64.

Fan Q. C., Sun Q., Li N. and Sui J. L., 2004. Periods of volcanic activity and magma evolution of Holocene in North Hainan Island. Acta Petrol. Sin. 20, 533–544 (in Chinese with English abstract).

Fan, Q.C., Chen, S.S., Zhao, Y.W., Zou, H.B., Li, N., Sui, J.L., 2014. Petrogenesis and evolution of Quaternary basaltic rocks from the Wulanhada area, North China. Lithos, 206, 289-302.

Fan, Q.C., Hooper, P.R., 1991. The Cenozoic basaltic rocks of eastern China: petrology and chemical composition. Journal of Petrology, 32, 765-810.

Fan, W.M., Zhang, H.F., Baker, J., Jarvis, K.E., Mason, P.R.D., Menzies, M.A., 2000. On and off the North China Craton: Where is the Archaean keel? Journal of

Petrology, 41, 933-950.

Faure, M., Shu, L., Wang, B., Charvet, J., Choulet, F., and Monie, P., 2009, Intracontinental subduction: a possible mechanism for the Early Palaeozoic Orogen of SE China: Terre Nova, v. 21, n. 5, p. 360–368, http://dx.doi.org/10.1111/j.1365-3121.2009.00888.X

Farver, J. R. & Giletti, B. J., 1989. Oxygen and strontium diffusion kinetics in apatite and potential applications to thermal history determinations. Geochimica et Cosmochimica Acta, 53, 1621–1631.

Flesch, G.D., Anderson, A.R., Svec, H.J., 1973. A secondary isotopic standard for 6Li/7Li determinations. International Journal of Mass Spectrometry and Ion Physics, 12, 265-272.

Flower M. F. J., Zhang M., Chen C. Y., Tu K. and Xie G. H., 1992. Magmatism in the south China basin: 2. Post-spreading Quaternary basalts from Hainan Island, south China. Chemical Geology, 97, 65–87.

Frey, F.A., Green, D.H., Roy, S.D., 1978. Integrated Models of Basalt Petrogenesis: A Study of Quartz Tholeiites to Olivine Melilitites from South Eastern Australia Utilizing Geochemical and Experimental Petrological Data. Journal of Petrology, 19, 463-513.

Fukao, Y., Obayashi, M., Inoue, H., Nenbai, M., 1992. Subducting slabs stagnant in the mantle transition zone. Journal of Geophysical Research-Solid Earth, 97, 4809-4822.

Gaeta, M., Di Rocco, T., Freda, C., 2009. Carbonate assimilation in open magmatic systems: the role of melt-bearing skarns and cumulate forming processes. Journal of Petrology, 50, 361–385.

Gaetani, G. A., Grove, T. L., 1998. The influence of water on melting of mantle peridotite. Contributions to Mineralogy and Petrology, 131(4), 323-346

Gaetani, G. A., O'Leary, J. A., Shimizu, N., Bucholz, C. E., Newville, M. 2012. Rapid reequilibration of H_2O and oxygen fugacity in olivine-hosted melt inclusions. Geology, 40(10), 915-918.

Gaetani, G.A., Kent, A.J.R., Grove, T.L., Hutcheon, I.D., Stolper, E.M., 2003. Mineral/melt partitioning of trace elements during hydrous peridotite partial melting. Contributions to Mineralogy and Petrology, 145, 391-405.

Gale, A., Dalton, C.A., Langmuir, C.H., Su, Y.J., Schilling, J.G., 2013. The mean composition of ocean ridge basalts. Geochemistry, Geophysics, Geosystems, 14,

489-518.

Gallagher, K., Elliott, T., 2009. Fractionation of lithium isotopes in magmatic systems as a natural consequence of cooling. Earth and Planetary Science Letters 278, 286–296.

Gao, S., Rudnick, R.L., Xu, W.L., Yuan, H.L., Liu, Y.S., Walker, R.J., Puchtel, I.S., Liu, X.M., Huang, H., Wang, X.R., Yang, J., 2008. Recycling deep cratonic lithosphere and generation of intraplate magmatism in the North China Craton. Earth and Planetary Science Letters, 270, 41-53.

Garth, Tom, and Andreas Rietbrock. 2014. Order of magnitude increase in subducted H_2O due to hydrated normal faults within the Wadati-Benioff zone. Geology, 42. 207-210.

Gertisser, G., Keller, J., 2003. Trace element and Sr, Nd, Pb and O isotope variations in medium-K and high-K volcanic rocks from Merapi Volcano, Central Java, Indonesia: evidence for the involvement of subducted sediments in Sunda Arc magma genesis. Journal of Petrology, 44, 457–489.

Ghosh, S., Litasov, K., Ohtani, E., 2014. Phase relations and melting of carbonated peridotite between 10 and 20 GPa: a proxy for alkali- and CO_2-rich silicate melts in the deep mantle. Contributions to Mineralogy and Petrology, 167, 964-986.

Giletti, B.J., Shanahan, T.M., 1997. Alkali diffusion in plagioclase feldspar. Chemical Geology, 139, 3–20.

Gonfiantini, R., 1978. Standards for stable isotope measurements in natural compounds. Nature, 271, 534-536.

Green, D. H., Hibberson, W. O., Kovács, I., Rosenthal, A., 2010. Water and its influence on the lithosphere-asthenosphere boundary. Nature, 467(7314), 448-451.

Green, D. H., Hibberson, W. O., Rosenthal, A., Kovács, I., Yaxley, G. M., Falloon, T. J., Brink, F., 2014. Experimental study of the influence of water on melting and phase assemblages in the upper mantle. Journal of Petrology, 55(10), 2067-2096.

Gregory R.T., Taylor H.P., 1981. An oxygen isotope profile in a section of Cretaceous oceanic crust, Samail ophiolite, Oman: evidence for $\delta^{18}O$ buffering of the oceans by deep (>5 km) seawater-hydrothermal circulation at mid-ocean ridges. Journal of Geophysical Research, 86:2737-2755

Griffin, W.L., Andi, Z., O'Reilly, S.Y., Ryan, C.G., 1998. Phanerozoic evolution of the lithosphere beneath the Sino-Korean Craton. Mantle Dynamics and Plate Interactions in East Asia, 27, 107-126.

References

Grove, T., Parman, S., Bowring, S., Price, R., & Baker, M., 2002. The role of an H2O-rich fluid component in the generation of primitive basaltic andesites and andesites from the Mt. Shasta region, N California. Contributions to Mineralogy and Petrology, 142(4), 375-396.

Grove, T.L., Chatterjee, N., Parman, S.W., Medard, E., 2006. The influence of H_2O on mantle wedge melting. Earth and Planetary Science Letters, 249, 74-89.

Guo, P.Y., Niu, Y.L., Ye, L., Liu, J.J., Sun, P., Cui, H.X., Zhang, Y., Gao, J.P., Su, L., Zhao, J.X., Feng, Y.X., 2014. Lithosphere thinning beneath west North China Craton: Evidence from geochemical and Sr-Nd-Hf isotope compositions of Jining basalts. Lithos, 202, 37-54.

Gurenko, A.A., Chaussidon, M., Schmincke, H.-U., 2001. Magma ascent and contamination beneath one intraplate volcano: evidence from S and O isotopes in glass inclusions and their host clinopyroxenes from Miocene basaltic hyaloclastites southwest of Gran Canaria (Canary Islands). Geochimica et Cosmochimica Acta, 65, 4359-4374.

Gurenko, A. A., Bindeman, I. N. & Chaussidon, M., 2011. Oxygen isotope heterogeneity of the mantle beneath the Canary Islands: insights from olivine phenocrysts. Contributions to Mineralogy and Petrology, 162, 349–363.

Hacker, B.R., Wallis, S.R., Ratschbacher, L., Grove, M., Gehrels, G., 2006. High-temperature geochronology constraints on the tectonic history and architecture of the ultrahigh-pressure Dabie-Sulu Orogen. Tectonics, 25, 17.

Halama, R., McDonough, W.F., Rudnick, R.L., Bell, K., 2008. Tracking the lithium isotopic evolution of the mantle using carbonatites. Earth and Planetary Science Letters, 265, 726–742

Halliday, A. N., Davidson, J. P., Holden, P., DeWolf, C., Lee, D. C., & Fittoni, J. G. 1990. Trace-element fractionation in plumes and the origin of HIMU mantle beneath the. Nature, 347, 11.

Halliday, A.N., Lee, D.-C., Tommasini, S., Davies, G.R., Paslick, C.R., Godfrey Fitton, J., James, D.E., 1995. Incompatible trace elements in OIB and MORB and source enrichment in the sub-oceanic mantle. Earth and Planetary Science Letters, 133, 379-395.

Hao, Y.T., Xia, Q.K., Li, Q.W., Chen, H., Feng, M., 2014. Partial melting control of water contents in the Cenozoic lithospheric mantle of the Cathaysia block of South China. Chemical Geology, 380, 7-19.

Harmon R.S., Hoefs .J, 1995. Oxygen isotope heterogeneity of the mantle deduced from global ^{18}O systematics of basalts from different geotectonic settings. Contributions to Mineralogy and Petrology, 120: 95–114

Harris, C., Pronost, J.J.M., Ashwal, L.D., Cawthorn, R.G., 2005. Oxygen and hydrogen isotope stratigraphy of the Rustenburg layered suite, Bushveld Complex: constraints on crustal contamination. Journal of Petrology, 46, 579–601.

Hart S. R., Hauri E. H., Oschmann L. A. and Whitehead J. A. (1992) Mantle plumes and entrainment—isotopic evidence. Science, 256, 517–520.

Hauff, F., Hoernle, K., Schmidt, A., 2003. Sr-Nd-Pb composition of Mesozoic Pacific oceanic crust (Site 1149 and 801, ODP Leg 185): Implications for alteration of ocean crust and the input into the Izu-Bonin-Mariana subduction system. Geochemistry, Geophysics, Geosystems, 4, 30.

Hauri, E.H., Wagner, T.P., Grove, T.L., 1994. Experimental and natural partitioning of Th, U, Pb and other trace elements between garnet, clinopyroxene and basaltic melts. Chemical Geology, 117, 149-166.

Hercule, S., Ingrin, J., 1999. Hydrogen in diopside: Diffusion, kinetics of extraction-incorporation, and solubility. American Mineralogist, 84, 1577-1587.

Hervig, R.L., Bell, D.R., Moore, G., Williams, L.B., Yamamoto, J., Buseck, P.R., 2004. SIMS analyses for Li isotope ratios: from olivine to clay minerals. Eos Trans. AGU, 85 (47), Fall Meet. Suppl., Abstract, V51C-0593.

Herzberg, C., 2011. Identification of source lithology in the Hawaiian and Canary islands: implications for origins. Journal of Petrology, 52, 113-146.

Hier-Majumder, S., Anderson, I. M., Kohlstedt, D. L., 2005b. Influence of protons on Fe-Mg interdiffusion in olivine. Journal of Geophysical Research: Solid Earth, 110(B2).

Hier-Majumder, S., Mei, S., Kohlstedt, D. L., 2005a. Water weakening of clinopyroxenite in diffusion creep. Journal of Geophysical Research: Solid Earth, 110(B7).

Hirose, K., 1997. Partial melt compositions of carbonated peridotite at 3 GPa and role of CO_2 in alkali-basalt magma generation. Geophysical Research Letters 24, 2837-2840.

Hirose, K., Kushiro, I., 1993. Partial melting of dry peridotites at high pressures: determination of compositions of melts segregated from peridotite using aggregates of diamond. Earth and Planetary Science Letters, 114, 477-489.

Hirschmann M.M., Aubaud C., Withers A.C. 2005. Storage capacity of H_2O in nominally anhydrous minerals in the upper mantle. Earth and Planetary Science Letters, 236: 167-181.

Hirschmann, M. M., Tenner, T., Aubaud, C., Withers, A. C., 2009. Dehydration melting of nominally anhydrous mantle: The primacy of partitioning. Physics of the Earth and Planetary Interiors, 176(1), 54-68.

Hirschmann, M.M., Stolper, E.M., 1996. A possible role for garnet pyroxenite in the origin of the "garnet signature" in MORB. Contributions to Mineralogy and Petrology, 124, 185-208.

Hirth, G., Kohlstedt, D. L., 1996. Water in the oceanic upper mantle: implications for rheology, melt extraction and the evolution of the lithosphere. Earth and Planetary Science Letters, 144(1), 93-108.

Ho K.S., Chen J. and Juang W., 2000. Geochronology and geochemistry of late Cenozoic basalts from the Leiqiong area, southern China. Journal of Asian Earth Sciences, 18, 307–324.

Ho, K.S., Chen, J.C., Lo, C.H., Zhao, H.L., 2003. $^{40}Ar/^{39}Ar$ dating and geochemical characteristics of late Cenozoic basaltic rocks from the Zhejiang-Fujian region, SE China: eruption ages, magma evolution and petrogenesis. Chemical Geology, 197, 287-318.

Ho, K.S., Ge, W.C., Chen, J.C., You, C.F., Yang, H.J., Zhang, Y.L., 2013. Late Cenozoic magmatic transitions in the central Great Xing'an Range, Northeast China: Geochemical and isotopic constraints on petrogenesis. Chemical Geology, 352, 1-18.

Hochstaedter, A.G., Gill, J.B., Kusakabe, M., Newman, S., Pringle, M.S., Taylor, B., Fryer, P., 1990. Volcanism in the Sumisu rift: I. Major element, volatile, and stable isotope geochemistry, the Mariana Trough. Earth and Planetary Science Letters, 100, 179–194.

Hoefs, J., 1996. Stable Isotopes. Springer Verlag, Berlin, p. 201.

Hoernle, K., Tilton, G., Le Bas, M., Duggen, S., Garbe-Schönberg, D., 2002. Geochemistry of oceanic carbonatites compared with continental carbonatites: mantle recycling of oceanic crustal carbonate. Contributions to Mineralogy and Petrology, 142, 520-542.

Hofmann, A. W., Jochum, K. P., Seufert, M., White, W. M. 1986. Nb and Pb in oceanic basalts: new constraints on mantle evolution. Earth and Planetary Science Letters,

79(1), 33-45.

Hofmann, A.W., 1988. Chemical differentiation of the Earth: the relationship between mantle, continental crust, and oceanic crust. Earth and Planetary Science Letters, 90, 297-314.

Huh, Y., Chan, L. H., Edmond, J. M., 2001. Lithium isotopes as a probe of weathering processes: Orinoco River. Earth and Planetary Science Letters, 194(1), 189-199.

Huh, Y., Chan, L. H., Zhang, L., Edmond, J. M. (1998). Lithium and its isotopes in major world rivers: implications for weathering and the oceanic budget. Geochimica et Cosmochimica Acta, 62(12), 2039-2051.

Huang, F., Li, S., Dong, F., He, Y., and Chen, F., 2008, High-Mg adakitic rocks in the Dabie orogen, central China: implications for foundering mechanism of lower continental crust: Chemical Geology, v. 255, n. 1-2, p. 1-13, doi:10.1016/j.chemgeo.2008.02.014.

Huang, J.L., Zhao, D.P., 2006. High-resolution mantle tomography of China and surrounding regions. Journal of Geophysical Research-Solid Earth, 111, B09305.

Huang, X., Xu, Y., Karato, S. I., 2005. Water content in the transition zone from electrical conductivity of wadsleyite and ringwoodite. Nature, 434(7034), 746-749.

Huang, X.L., Niu, Y.L., Xu, Y.G., Ma, J.L., Qiu, H.N., Zhong, J.W., 2013. Geochronology and geochemistry of Cenozoic basalts from eastern Guangdong, SE China: constraints on the lithosphere evolution beneath the northern margin of the South China Sea. Contributions to Mineralogy and Petrology, 165, 437-455.

Huh Y., Chan L-H, Zhang Edmond J.M., 1998. Lithium and its isotopes in major world rivers; implications for weathering and the oceanic budget. Geochim Cosmochim Acta, 62: 2039–2051

Ingrin, J., Blanchard, M., 2006. Diffusion of Hydrogen in Minerals. Reviews in Mineralogy and Geochemistry, 62, 291-320.

Ingrin, J., Skogby, H., 2000. Hydrogen in nominally anhydrous upper-mantle minerals: concentration levels and implications. European Journal of Mineralogy, 12, 543-570.

Ishizuka, O., Taylor, R.N., Yuasa, M., Milton, J.A., Nesbitt, R.W., Uto, K., Sakamoto, I., 2007. Processes controlling along-arc isotopic variation of the southern Izu-Bonin arc. Geochemistry, Geophysics, Geosystems, 8, Q06008.

Ito, E., White, W.M., Göpel, C., 1987. The O, Sr, Nd and Pb isotope geochemistry of MORB. Chemical Geology, 62, 157–176.

References

IUPAC, Compendium of Chemical Terminology, 2nd ed. (the “Gold Book”). 1997. Online corrected version: (1989) “Matrix (in analysis)”

Jackson, M. G., Kurz, M. D., Hart, S. R., Workman, R. K. 2007. New Samoan lavas from Ofu Island reveal a hemispherically heterogeneous high $^{3}He/^{4}He$ mantle. Earth and Planetary Science Letters, 264(3), 360-374.

Jackson, M.G., Hart, S.R., Koppers, A.A.P., Staudigel, H., Konter, J., Blusztajn, J., Kurz, M., Russell, J.A., 2007. The return of subducted continental crust in Samoan lavas. Nature, 448, 684-687.

Jahn, B.M., Wu, F.Y., Lo, C.H., Tsai, C.H., 1999. Crust-mantle interaction induced by deep subduction of the continental crust: Geochemical and Sr-Nd isotopic evidence from post-collisional mafic-ultramafic intrusions of the northern Dabie complex, central China. Chemical Geology, 157, 119-146.

Jeffcoate, A. B., Elliott, T., Kasemann, S. A., Ionov, D., Cooper, K., Brooker, R., 2007. Li isotope fractionation in peridotites and mafic melts. Geochimica et Cosmochimica Acta, 71(1), 202-218.

Johnson, M.C., Plank, T., 1999. Dehydration and melting experiments constrain the fate of subducted sediments. Geochemistry, Geophysics, Geosystems, 1, 26.

Jung, H., Karato, S. I., 2001. Water-induced fabric transitions in olivine. Science, 293(5534), 1460-1463.

Karato, S. I., 1990. The role of hydrogen in the electrical conductivity of the upper mantle. Nature, 347, 272.

Karato, S. I., 2010a. Rheology of the Earth's mantle: A historical review. Gondwana Research, 18(1), 17-45.

Karato, S. I., 2010b. Rheology of the deep upper mantle and its implications for the preservation of the continental roots: A review. Tectonophysics, 481(1), 82-98.

Karato, S. I., Jung, H., 1998. Water, partial melting and the origin of the seismic low velocity and high attenuation zone in the upper mantle. Earth and Planetary Science Letters, 157(3), 193-207.

Karato, S. I., Jung, H., Katayama, I., Skemer, P., 2008. Geodynamic significance of seismic anisotropy of the upper mantle: new insights from laboratory studies. Annu. Rev. Earth and Planetary Science Letters, 36, 59-95.

Karato, S. I., Paterson, M. S., FitzGerald, J. D., 1986. Rheology of synthetic olivine aggregates: influence of grain size and water. Journal of Geophysical Research: Solid Earth, 91(B8), 8151-8176.

Karato, S. I., Wu, P., 1993. Rheology of the upper mantle- A synthesis. Science, 260(5109), 771-778.

Karato, S.I., 2010. Rheology of the deep upper mantle and its implications for the preservation of the continental roots: A review. Tectonophysics, 481, 82-98.

Kasemann, S., Jeffcoate, A.B., Elliott, T., 2005. Lithium isotope composition of basalt glass reference material. Analytical Chemistry, 77, 5251–5257.

Kelemen, P. B., Hirth, G., Shimizu, N., Spiegelman, M. & Dick, H. J., 1997. A review of melt migration processes in the adiabatically upwelling mantle beneath oceanic spreading ridges. Philosophical Transactions of the Royal Society of London, Series A, 355, 283–318.

Kelley, K. A., Plank, T., Newman, S., Stolper, E. M., Grove, T. L., Parman, S., Hauri, E. H., 2010. Mantle melting as a function of water content beneath the Mariana Arc. Journal of Petrology, egq036.

Kelley, K.A., Plank, T., Ludden, J., Staudigel, H., 2003. Composition of altered oceanic crust at ODP Sites 801 and 1149. Geochemistry, Geophysics, Geosystems, 4, 21.

Keshav, S., Gudfinnsson, G.H., Sen, G., Fei, Y.W., 2004. High-pressure melting experiments on garnet clinopyroxenite and the alkalic to tholefitic transition in ocean-island basalts. Earth and Planetary Science Letters, 223, 365-379.

Kessel, R., Schmidt, M.W., Ulmer, P., Pettke, T., 2005. Trace element signature of subduction-zone fluids, melts and supercritical liquids at 120-180 km depth. Nature, 437, 724-727.

Kinzler, R.J., 1997. Melting of mantle peridotite at pressure approaching the spinel to garnet transition: application to mid-ocean ridge petrogenesis. Journal of Geophysical Research, 102, 853–874.

Klemme, S., Prowatke, S., Hametner, K., Gunther, D., 2005. Partitioning of trace elements between rutile and silicate melts: Implications for subduction zones. Geochimica et Cosmochimica Acta, 69, 2361-2371.

Kobayashi, K., Tanaka, R., Moriguti, T., Shimizu, K., Nakamura, E., 2004. Lithium, boron, and lead isotope systematics of glass inclusions in olivines from Hawaiian lavas: evidence for recycled components in the Hawaiian plume. Chemical Geology, 212(1), 143-161.

Kogiso, T., Hirschmann, M.M., 2001. Experimental study of clinopyroxenite partial melting and the origin of ultra-calcic melt inclusions. Contributions to Mineralogy and Petrology, 142, 347-360.

Kogiso, T., Hirschmann, M.M., 2006. Partial melting experiments of bimineralic eclogite and the role of recycled mafic oceanic crust in the genesis of ocean island basalts. Earth and Planetary Science Letters, 249, 188-199.

Kogiso, T., Hirschmann, M.M., Pertermann, M., 2004. High-pressure partial melting of mafic lithologies in the mantle. Journal of Petrology, 45, 2407-2422.

Kogiso, T., Tatsumi, Y., Nakano, S., 1997. Trace element transport during dehydration processes in the subducted oceanic crust: 1. Experiments and implications for the origin of ocean island basalts. Earth and Planetary Science Letters, 148, 193-205.

Koppers, A. A. P., H. Staudigel, M. S. Pringle, and J. R. Wijbrans., 2003, Short-lived and discontinuous intraplate volcanism in the South Pacific: Hot spots or extensional volcanism? Geochemistry, Geophysics, Geosystems, 4(10), 1089, doi:10.1029/2003GC000533.

Kovacs, I., Green, D.H., Rosenthal, A., Hermann, J., O'Neill, H.S., Hibberson, W.O., Udvardi, B., 2012. An Experimental Study of Water in Nominally Anhydrous Minerals in the Upper Mantle near the Water-saturated Solidus. Journal of Petrology, 53, 2067-2093.

Kovacs, I., Hermann, J., O'Neill, H.S.C., Gerald, J.F., Sambridge, M., Horvath, G., 2008. Quantitative absorbance spectroscopy with unpolarized light: Part II. Experimental evaluation and development of a protocol for quantitative analysis of mineral IR spectra. American Mineralogist, 93, 765-778.

Kuang, Y.S., Wei, X., Hong, L.B., Ma, J.L., Pang, C.J., Zhong, Y.T., Zhao, J.X., Xu, Y.G., 2012. Petrogenetic evaluation of the Laohutai basalts from North China Craton: Melting of a two-component source during lithospheric thinning in the late Cretaceous-early Cenozoic. Lithos, 154, 68-82.

Kuritani, T., Ohtani, E., Kimura, J.I., 2011. Intensive hydration of the mantle transition zone beneath China caused by ancient slab stagnation. Nature Geoscience, 4, 713-716.

Kyser, T.K., O'Neil, J.R., Carmichael, I.S.E., 1981. Oxygen isotope thermometry of basic lavas and mantle nodules. Contributions to Mineralogy and Petrology, 77, 11-23.

Langmuir, C.H., Klein, E.M., Plank, T., 1992. Petrological systematics of mid-ocean ridge basalts: constraints on melt generation beneath ocean ridges. In: Morgan, J.P., Blackman, D.K., Sinton, J.M. (Eds.), Mantle Flow and Melt Generation at Mid-Ocean Ridges, Geophys Monogr Series, vol. 71. AGU (American Geophysic

Union), Washington DC, pp. 81–180.

Laporte, D., Toplis, M.J., Seyler, M., Devidal, J.L., 2004. A new experimental technique for extracting liquids from peridotite at very low degrees of melting: application to partial melting of depleted peridotite. Contributions to Mineralogy and Petrology, 146, 463-484.

Le Bas, M.J., Le Maitre, R.W., Streckeisen, A., Zanettin, B., 1986. A Chemical Classification of Volcanic Rocks Based on the Total Alkali-Silica Diagram. Journal of Petrology, 27, 745-750.

Le Roux, V., Dasgupta, R., Lee, C.T.A., 2011. Mineralogical heterogeneities in the Earth's mantle: Constraints from Mn, Co, Ni and Zn partitioning during partial melting. Earth and Planetary Science Letters, 307, 395-408.

Leeman W.P., Tonarini S., Chan L.H., Borg L.E., 2004. Boron and lithium isotopic variations in a hot subduction zone – the southern Washington Cascades. Chemical Geology, 212: 101–124.

Leo W. R., 1994. Techniques for Nuclear and Particle Physics Experiments. Springer. pp. 122–127. ISBN 3-540-57280-5.

Lepvrier, C., Maluski, H., Van Tich, V., Leyreloup, A., Thi, P.T., Van Vuong, N., 2004. The Early Triassic Indosinian orogeny in Vietnam (Truong Son Belt and Kontum Massif); implications for the geodynamic evolution of Indochina. Tectonophysics, 393, 87-118.

Li Pei, Xia Qunke, Etienne Deloule, 2012. Anomalous Lithium Isotopic Compositions of the Cenozoic Lithospheric Mantle Beneath Penglai, Shandong Province: The ion Probe Analyses of Peridotite Xenoliths. Geological Journal of China Universities, Vol. 18, No.1, p. 62-73 (in Chinese, Abstract in English).

Li, H.Y., Huang, X.L., Guo, H., 2014. Geochemistry of Cenozoic basalts from the Bohai Bay Basin: Implications for a heterogeneous mantle source and lithospheric evolution beneath the eastern North China Craton. Lithos, 196, 54-66.

Li, J.-W., Zhao, X.-F., Zhou, M.-F., Ma, C.-Q., de Souza, Z. S., and Vasconcelos, P., 2009. Late Mesozoic magmatism from the Daye region, eastern China: U-Pb ages, petrogenesis, and geodynamic implications: Contributions to Mineralogy and Petrology, v. 157, n. 3, p. 383–409, doi:10.1007/s00410-008-0341-x.

Li, X.-H., Li, W.-X., Li, Z.-X., Lo, C.-H., Wang, J., Ye, M.-F., and Yang, Y.-H., 2009. Amalgamation between the Yangtze and Cathaysia blocks in South China: Constraints from SHRIMP U–Pb zircon ages, geochemistry and Nd–Hf isotopes of

the Shuangxiwu volcanic rocks: Precambrian Research, v. 174, n. 1-2, p. 117-128, http://dx.doi.org/10.1016/j.precamres.2009.07.004.

Li, X.H., Li, Z.X., Ge, W.C., Zhou, H.W., Li, W.X., Liu, Y., Wingate, M.T.D., 2003a. Neoproterozoic granitoids in South China: crustal melting above a mantle plume at ca. 825 Ma? Precambrian Research 122, 45-83.

Li, Y.-Q., Ma, C.-Q., Robinson, P.T., Zhou, Q., Liu, M.-L., 2015. Recycling of oceanic crust from a stagnant slab in the mantle transition zone: Evidence from Cenozoic continental basalts in Zhejiang Province, SE China. Lithos, 230, 146-165.

Li, Z.X., Li, X.H., Kinny, P.D., Wang, J., Zhang, S., Zhou, H., 2003b. Geochronology of Neoproterozoic syn-rift magmatism in the Yangtze Craton, South China and correlations with other continents: evidence for a mantle superplume that broke up Rodinia. Precambrian Research, 122, 85-109.

Li, Z.-X., Li, X.-H., Wartho, J.-A., Clark, C., Li, W.-X., Zhang, C.-L., and Bao, C., 2010. Magmatic and metamorphic events during the early Paleozoic Wuyi-Yunkai Orogeny, southeastern South China: New age constraints and pressure-temperature conditions: Geological Society of America Bulletin, v. 122, n. 5–6, p. 772–793, http://dx.doi.org/10.1130/B30021.1.

Li, C., van der Hilst, R.D., 2010. Structure of the upper mantle and transition zone beneath Southeast Asia from traveltime tomography. Journal of Geophysical Research: Solid Earth, 115, 19.

Li, Z.X.A., Lee, C.T.A., Peslier, A.H., Lenardic, A., Mackwell, S.J., 2008. Water contents in mantle xenoliths from the Colorado Plateau and vicinity: Implications for the mantle rheology and hydration-induced thinning of continental lithosphere. Journal of Geophysical Research: Solid Earth, 113, 22.

Liu, C.Z., Wu, F.Y., Sun, J., Chu, Z.Y., Qiu, Z.L., 2012. The Xinchang peridotite xenoliths reveal mantle replacement and accretion in southeastern China. Lithos, 150, 171-187.

Liu, D.Y., Nutman, A.P., Compston, W., Wu, J.S., Shen, Q.H., 1992. Remnants of 3800 Ma crust in the Chinese part of the Sino-Korean craton. Geology, 20, 339-342

Liu, J., Xia, Q.-K., Deloule, E., Chen, H., Feng, M., 2015a. Recycled oceanic crust and marine sediment in the source of alkali basalts in Shandong, eastern China: Evidence from magma water content and oxygen isotopes. Journal of Geophysical Research: Solid Earth, n/a-n/a.

Liu, J., Xia, Q.-K., Deloule, E., Ingrin, J., Chen, H., Feng, M., 2015b. Water Content

and Oxygen Isotopic Composition of Alkali Basalts from the Taihang Mountains, China: Recycled Oceanic Components in the Mantle Source. Journal of Petrology, 56, 681-702.

Liu J., Wang Z. Z., Yu H.R., Xia Q.K., Deloule E., Feng M., 2016. Dynamic contribution of recycled components from the subducted Pacific slab: oxygen isotopic composition of the basalts from 106 Ma to 60 Ma in North China Craton. Accepted by Journal of Geophysical Research.

Liu, S.F., Steel, R., Zhang, G.W., 2005. Mesozoic sedimentary basin development and tectonic implication, northern Yangtze Block, eastern China: record of continent - continent collision. Journal of Asian Earth Sciences, 25, 9-27.

Liu, Y.S., Gao, S., Kelemen, P.B., Xu, W.L., 2008. Recycled crust controls contrasting source compositions of Mesozoic and Cenozoic basalts in the North China Craton. Geochimica et Cosmochimica Acta, 72, 2349-2376.

Ma, X.Y., Wu, D.N., 1987. Cenozoic extensional tectonics in China. Tectonophysics, 133, 243-255.

MacDonald, G.A., Katsura, T., 1964. Chemical Composition of Hawaiian Lavas1. Journal of Petrology, 5, 82-133.

Mackwell, S. J., Kohlstedt, D. L., Paterson, M. S., 1985. The role of water in the deformation of olivine single crystals. Journal of Geophysical Research: Solid Earth, 90(B13), 11319-11333.

Manthilake, M. A. G. M., Miyajima, N., Heidelbach, F., Soustelle, V., Frost, D. J., 2013. The effect of aluminum and water on the development of deformation fabrics of orthopyroxene. Contributions to Mineralogy and Petrology, 165(3), 495-505.

Marschall, H. R., von Strandmann, P. A. P., Seitz, H. M., Elliott, T., Niu, Y., 2007. The lithium isotopic composition of orogenic eclogites and deep subducted slabs. Earth and Planetary Science Letters, 262(3), 563-580.

Martin, E., Bindeman, I. & Grove, T. L., 2011. The origin of high-Mg magmas in Mt Shasta and Medicine Lake volcanoes, Cascade Arc (California): higher and lower than mantle oxygen isotope signatures attributed to current and past subduction. Contributions to Mineralogy and Petrology, 162, 945–960.

Mattey, D., Lowry, D. & Macpherson, C., 1994. Oxygen isotope composition of mantle peridotite. Earth and Planetary Science Letters, 128, 231-241.

Mei, S., Kohlstedt, D. L., 2000a. Influence of water on plastic deformation of olivine aggregates: 1. Diffusion creep regime. Journal of Geophysical Research: Solid

Earth, 105(B9), 21457-21469.

Mei, S., Kohlstedt, D. L., 2000b. Influence of water on plastic deformation of olivine aggregates: 2. Dislocation creep regime. Journal of Geophysical Research: Solid Earth, 105(B9), 21471-21481.

Menzies, M., Xu, Y., Zhang, H., Fan, W., 2007. Integration of geology, geophysics and geochemistry: A key to understanding the North China Craton. Lithos, 96, 1-21.

Menzies, M.A., Fan, W.M., Zhang, M., 1993. Paleozoic and Cenozoic lithoprobes and the loss of >120 km of Archean lithosphere, Sino-Korean craton, China, in: Prichard, H.M. (Ed.), Magmatic processes and plate tectonics. Geological Society, London, pp. 71–81.

Michael, P., 1995. Regionally distinctive sources of depleted MORB: Evidence from trace elements and H_2O. Earth and Planetary Science Letters, 131, 301-320.

Michael, P.J., 1988. The concentration, behavior and storage of H_2O in the suboceanic upper mantle: implications for mantle metasomatism. Geochim. Cosmochim. Acta, 52, 555–566.

Michael, P.J., 1995. Regionally distinctive sources of depleted MORB: evidence from trace elements and H_2O. Earth and Planetary Science Letters 131, 301–320.

Millot, R., Vigier, N., Gaillardet, J., 2010. Behaviour of lithium and its isotopes during weathering in the Mackenzie Basin, Canada. Geochimica et Cosmochimica Acta, 74(14), 3897-3912.

Mironov, N., Portnyagin, M., Botcharnikov, R., Gurenko, A., Hoernle, K., Holtz, F., 2015. Quantification of the CO_2 budget and H_2O–CO_2 systematics in subduction-zone magmas through the experimental hydration of melt inclusions in olivine at high H2O pressure. Earth and Planetary Science Letters, 425, 1-11.

Misra S, Froelich P N. Lithium isotope history of Cenozoic seawater: changes in silicate weathering and reverse weathering.[J]. Science, 2012, 335(335):818-23.

Moriguti T., Nakamura E., 1998. Across-arc variation of Li-isotopes in lavas and implications for crust /mantle recycling at subduction zones. Earth and Planetary Science Letters, 163: 167–174

Morimoto N. 1988. Nomenclature of pyroxene. Mineralogical Magazine, 52:535-550

Muehlenbachs, K., 1986. Alteration of the oceanic crust and the 18O history of seawater. Reviews in Mineralogy and Geochemistry, 16(1), 425-444.

Müller, R.D., Sdrolias, M., Gaina, C., Steinberger, B., Heine, C., 2008. Long-Term Sea-Level Fluctuations Driven by Ocean Basin Dynamics. Science 319, 1357-1362.

Murphy, D.T., Collerson, K.D., Kamber, B.S., 2002. Lamproites from Gaussberg, Antarctica: Possible transition zone melts of Archaean subducted sediments. Journal of Petrology, 43, 981-1001.

Nichols, A.R.L., Carroll, M.R., Hoskuldsson, A., 1999. Is the Iceland hot spot also wet? Evidence from the water contents of undegassed submarine and subglacial pillow basalts. Earth and Planetary Science Letters, 202, 77-87.

Niida, K., Green, D.H., 1999. Stability and chemical composition of pargasitic amphibole in MORB pyrolite under upper mantle conditions. Contributions to Mineralogy and Petrology, 135, 18-40.

Nishi, M., 2015. Deep water cycle: Mantle hydration. Nature Geoscience, 8, 9-10.

Nishi, M., Irifune, T., Tsuchiya, J., Tange, Y., Nishihara, Y., Fujino, K., Higo, Y., 2014. Stability of hydrous silicate at high pressures and water transport to the deep lower mantle. Nature Geoscience, 7, 224-227.

Nishio, Y., Nakai, S. I., Kogiso, T., Barsczus, H. G., 2005. Lithium, strontium, and neodymium isotopic compositions of oceanic island basalts in the Polynesian region: constraints on a Polynesian HIMU origin. Geochemical Journal, 39(1), 91-103

Niu, Y.L., 2005. Generation and Evolution of Basaltic Magmas: Some Basic Concepts and a New View on the Origin of Mesozoic- Cenozoic Basaltic Volcanism in Eastern China. Geological Journal of China Universities, 11, 9-46.

Niu, Y.L., 2013. Subduction initiation, trench retreat and global tectonic consequences: The origin of backarc basins in the western Pacific and effect on eastern China geology since the Mesozoic, in: Zhai, M.G., Xiao, W.J. (Eds.), Plate Tectonics, Geological Events and Resources: New Advances in Geological Sciences. Science Press, Beijing, pp. 1-25.

Niu, Y.L., O'Hara, M.J., 2003. Origin of ocean island basalts: A new perspective from petrology, geochemistry, and mineral physics considerations. Journal of Geophysical Research, 108, DOI: 10.1029/2002JB002048.

Niu, Y.L., Wilson, M., Humphreys, E. R., O'Hara, M. J. 2011. The origin of intra-plate ocean island basalts (OIB): the lid effect and its geodynamic implications. Journal of Petrology, 52(7-8), 1443-1468.

Ohtani E. Hydrous minerals and the storage of water in the deep mantle. Chem Geol, 2015; 418: 6-15.

Ohtani, E., 2005a. Recent progress in experimental mineral physics: Phase relations of

hydrous systems and the role of water in slab dynamics, in: VanDerHilst, R.D., Bass, J.D., Matas, J., Trampert, J. (Eds.), Earth's Deep Mantle: Structure, Composition, and Evolution. Amer Geophysical Union, Washington, pp. 321-334.

Ohtani, E., 2005b. Water in the mantle. Elements, 1, 25-30.

O'Leary, J.A., Gaetani, G.A., Hauri, E.H., 2010. The effect of tetrahedral Al^{3+} on the partitioning of water between clinopyroxene and silicate melt. Earth and Planetary Science Letters, 297, 111-120.

O'Reilly, S.Y., Griffin, W.L., 2010. Rates of magma ascent: constraints from mantle-derived xenoliths, in: Dosseto, A., Turner, S., Van-Orman, J. (Eds.), Timescales of Magmatic Processes: From Core to Atmosphere, Oxford, pp. 116-124.

Otsuka, K., Karato, S. I., 2015. The influence of ferric iron and hydrogen on Fe–Mg inter diffusion in ferropericlase ((Mg, Fe)O) in the lower mantle. Physics and Chemistry of Minerals, 42(4), 261-273.

Panero W.R., Pigott J.S., Reaman D.M., Kabbes E.J., and Liu Z.X., 2015. Dry (Mg, Fe)SiO_3 perovskite in the Earth's lower mantle. Journal of Geophysical Research, 120: 894-908.

Parkinson, I. J., Hammond, S. J., James, R. H., Rogers, N. W., 2007. High-temperature lithium isotope fractionation: insights from lithium isotope diffusion in magmatic systems. Earth and Planetary Science Letters, 257(3), 609-621.

Parman, S.W., Grove, T.L., 2004. Harzburgite melting with and without H2O: Experimental data and predictive modeling. Journal of Geophysical Research-Solid Earth, 109, B02201.

Pearson DG, Brenker FE, Nestola F et al. Hydrous mantle transition zone indicated by ringwoodite included within diamond. Nature, 2014; 507: 221-224.

Penniston-Dorland, S. C., Sorensen, S. S., Ash, R. D., Khadke, S. V., 2010. Lithium isotopes as a tracer of fluids in a subduction zone mélange: Franciscan Complex, CA. Earth and Planetary Science Letters, 292(1), 181-190.

Pertermann, M., Hirschmann, M.M., 2003a. Anhydrous partial melting experiments on MORB-like eclogite: Phase relations, phase compositions and mineral-melt partitioning of major elements at 2-3 GPa. Journal of Petrology, 44, 2173-2201.

Pertermann, M., Hirschmann, M.M., 2003b. Partial melting experiments on a MORB-like pyroxenite between 2 and 3 GPa: Constraints on the presence of pyroxenite in basalt source regions from solidus location and melting rate. Journal of Geophysical Research-Solid Earth, 108, 2125.

Peslier, A.H., Luhr, J.F., Post, J., 2002. Low water contents in pyroxenes from spinel-peridotites of the oxidized, sub-arc mantle wedge. Earth and Planetary Science Letters, 201, 69-86.

Pilet, S., Baker, M.B., Müntener, O., Stolper, E.M., 2011. Monte Carlo Simulations of Metasomatic Enrichment in the Lithosphere and Implications for the Source of Alkaline Basalts. Journal of Petrology, 52, 1415-1442.

Pilet, S., Baker, M.B., Stolper, E.M., 2008. Metasomatized Lithosphere and the Origin of Alkaline Lavas. Science, 320, 916-919.

Pilet, S., Hernandez, J., Sylvester, P., Poujol, M., 2005. The metasomatic alternative for ocean island basalt chemical heterogeneity. Earth and Planetary Science Letters, 236, 148-166.

Pistiner, J.S., Henderson, G.M., 2003. Lithium-isotope fractionation during continental weathering processes. Earth and Planetary Science Letters, 214, 1–13.

Plank, T., Langmuir, C.H., 1998. The chemical composition of subducting sediment and its consequences for the crust and mantle. Chemical Geology, 145, 325-394.

Poli S, Franzolin E, Fumagalli P, Crottini A (2009) The transport of carbon and hydrogen in subducted oceanic crust: An experimental study to 5 GPa Earth and Planetary Science Letters, 278: 350-360 doi:http://dx.doi.org/10.1016/j.epsl.2008.12.022.

Poli S, Schmidt MW (2002) Petrology of Subducted Slabs Annu Rev Earth Pl Sc 30:207-235 doi:doi:10.1146/annurev.earth.30.091201.140550.

Putirka, K., 1999. Melting depth and mantle heterogeneity beneath Hawaii and the East Pacific Rise: constraints from Na/Ti and rare earth element ratios. Journal of Geophysical Research, 104, 2817–2829.

Putirka, K., Ryerson, F. J., Perfit, M., & Ridley, W. I. 2011. Mineralogy and composition of the oceanic mantle. Journal of Petrology, 52(2), 279-313.

Rapp, R.P., Irifune, T., Shimizu, N., Nishiyama, N., Norman, M.D., Inoue, T., 2008. Subduction recycling of continental sediments and the origin of geochemically enriched reservoirs in the deep mantle. Earth and Planetary Science Letters, 271, 14-23.

Rapp, R.P., Shimizu, N., Norman, M.D., Applegate, G.S., 1999. Reaction between slab-derived melts and peridotite in the mantle wedge: experimental constraints at 3.8 GPa. Chemical Geology, 160, 335-356.

Rapp, R.P., Watson, E.B., 1995. Dehydration melting of metabasalt at 8-32 kbar:

implications for continental growth and crust-mantle recycling. Journal of Petrology, 36, 891-931.

Rehkämper, M., Hofmann, A.W., 1997. Recycled ocean crust and sediment in Indian Ocean MORB. Earth and Planetary Science Letters, 147, 93-106.

Richter, F. M., Davis, A. M., DePaolo, D. J., Watson, E. B., 2003. Isotope fractionation by chemical diffusion between molten basalt and rhyolite. Geochimica et Cosmochimica Acta, 67(20), 3905-3923.

Richter, F., Watson, B., Chaussidon, M., Mendybaev, R., Ruscitto, D., 2014. Lithium isotope fractionation by diffusion in minerals. Part 1: Pyroxenes. Geochimica et Cosmochimica Acta, 126, 352-370.

Rudnick, R.L., Gao, S., 2003. Composition of the Continental Crust, in: Turekian, H.D.H.K. (Ed.), Treatise on Geochemistry. Pergamon, Oxford, pp. 1-64.

Rudnick, R.L., and Ionov, D.A., 2007, Lithium element and isotopic disequilibrium in minerals from peridotitic xenoliths from far-east Russia: product of recent melt-fluid/rock reaction, Earth and Planetary Science Letters, 256, 278–293, doi:10.1016/j.epsl.2007.01.035.

Ruprecht, P. & Plank, T., 2013. Feeding andesitic eruptions with a high-speed connection from the mantle. Nature, 500, 68–72.

Ryan, J. G., Kyle, P. R., 2004. Lithium abundance and lithium isotope variations in mantle sources: insights from intraplate volcanic rocks from Ross Island and Marie Byrd Land (Antarctica) and other oceanic islands. Chemical Geology, 212(1), 125-142.

Saal, A.E., Hauri, E.H., Langmuir, C.H., Perfit, M.R., 2002. Vapor undersaturation in primitive mid-ocean-ridge basalt and the volatile content of Earth's upper mantle. Nature, 419, 451–455.

Sakuyama, T., Tian, W., Kimura, J.I., Fukao, Y., Hirahara, Y., Takahashi, T., Senda, R., Chang, Q., Miyazaki, T., Obayashi, M., Kawabata, H., Tatsumi, Y., 2013. Melting of dehydrated oceanic crust from the stagnant slab and of the hydrated mantle transition zone: Constraints from Cenozoic alkaline basalts in eastern China. Chemical Geology, 359, 32-48.

Salters, V.J.M., Longhi, J., 1999. Trace element partitioning during the initial stages of melting beneath mid-ocean ridges. Earth and Planetary Science Letters, 166, 15-30.

Salters, V.J.M., Stracke, A., 2004. Composition of the depleted mantle. Geochemistry,

Geophysics, Geosystems, 5, Q05B07.

Sambridge, M., Gerald, J.F., Kovacs, I., O'Neill, H.S.C., Hermann, J., 2008. Quantitative absorbance spectroscopy with unpolarized light: Part I. Physical and mathematical development. American Mineralogist, 93, 751-764.

Schwab, B.E., Johnston, A.D., 2001. Melting systematics of modally variable, compositionally intermediate peridotites and the effects of mineral fertility. Journal of Petrology, 42, 1789-1811.

Sengör, A.M.C., Natalin, B.A., Burtman, V.S., 1993. Evolution of the Altaid tectonic collage and Palaeozoic crustal growth in Eurasia. Nature, 364, 299-307.

Shaw, A.M., Hauri, E.H., Behn, M.D., Hilton, D.R., Macpherson, C.G., Sinton, J.M., 2012. Long-term preservation of slab signatures in the mantle inferred from hydrogen isotopes. Nature Geoscience, 5, 224-228.

Sheppard, S.M.F., Harris, C., 1985. Hydrogen and oxygen isotope geochemistry of Ascension Island lavas and granites: variation with crystal fractionation and interaction with seawater. Contributions to Mineralogy and Petrology, 91, 74–81.

Simons, K., Dixon, J., Schilling, J.G., Kingsley, R., Poreda, R., 2002. Volatiles in basaltic glasses from the Easter-Salas y Gomez Seamount Chain and Easter Microplate: implications for geochemical cycling of volatile elements. Geochemistry, Geophysics, Geosystems, 3, http://dx.doi.org/10.1029/2001GC000173.

Sisson, T.W., Layne, G.D., 1993. H_2O in basalt and basaltic andesite glass inclusions from four subduction-related volcanoes. Earth and Planetary Science Letters, 117, 619–635.

Skogby, H., Bell, D.R., Rossman, G.R., 1990. Hydroxide in pyroxene: Variations in the natural-environment. American Mineralogist, 75, 764-774.

Sobolev, A.V., Chaussidon, M., 1996. H_2O concentrations in primary melts from supra-subduction zones and mid-ocean ridges: implications for H_2O storage and recycling in the mantle. Earth and Planetary Science Letters, 137, 45–55.

Sobolev, A.V., Hofmann, A.W., Kuzmin, D.V., Yaxley, G.M., Arndt, N.T., Chung, S.L., Danyushevsky, L.V., Elliott, T., Frey, F.A., Garcia, M.O., Gurenko, A.A., Kamenetsky, V.S., Kerr, A.C., Krivolutskaya, N.A., Matvienkov, V.V., Nikogosian, I.K., Rocholl, A., Sigurdsson, I.A., Sushchevskaya, N.M., Teklay, M., 2007. The amount of recycled crust in sources of mantle-derived melts. Science, 316, 412-417.

Sobolev, A.V., Hofmann, A.W., Sobolev, S.V., Nikogosian, I.K., 2005. An olivine-free mantle source of Hawaiian shield basalts. Nature, 434, 590–597.

Sobolev. A.V., Shimizu, N., 1993. Ultra-depleted primary melt included in an olivine from the Mid-Atlantic Ridge. Nature, 363, 151–154.

Spath, A., Le Roex, A.P., Opiyo-Akech, N., 2001. Plume-lithosphere interaction and the origin of continental rift-related alkaline volcanism - the Chyulu Hills Volcanic Province, southern Kenya. Journal of Petrology, 42, 765-787.

Spiegelman, M. & Kelemen, P. B., 2003. Extreme chemical variability as a consequence of channelized melt transport. Geochemistry, Geophysics, Geosystems, 4, 1055, doi:10.1029/2002GC000336.

Staudigel, H., Koppers, A.A.P., Plank, T.A., Hanan, B.B., 2010. Seamounts in the Subduction Factory. Oceanography, 23, 176-181.

Straub SM, Woodhead JD, Arculus RJ (2015) Temporal Evolution of the Mariana Arc: Mantle Wedge and Subducted Slab Controls Revealed with a Tephra Perspective. Journal of Petrology, 56:409-439 doi:10.1093/petrology/egv005.

Stolper, E., Newman, S., 1994. The role of water in the petrogenesis of Mariana trough magmas. Earth and Planetary Science Letters, 121, 293–325.

Stracke, A., Hofmann, A.W., Hart, S.R., 2005. FOZO, HIMU, and the rest of the mantle zoo. Geochemistry, Geophysics, Geosystems, 6, DOI: 10.1029/2004GC000824.

Su, B.X., Gu, X.Y., Deloule, E., Zhang, H.F., Li, Q.L., Li, X.H., Vigier, N., Tang, Y.J., Tang, G.Q., Liu, Y., Pang, K.N., Brewer, A., Mao, Q., Ma, Y.G., 2015. Potential Orthopyroxene, Clinopyroxene and Olivine Reference Materials for In Situ Lithium Isotope Determination. Geostandards and Geoanalytical Research, 39, 357-369.

Sun, S.S., McDonough, W.F., 1989. Chemical and isotopic systematics of oceanic basalts: implications for mantle composition and processes, in: Saunders, A.D., Norry, M.J. (Eds.), Magmatism in the Ocean Basins, London, pp. 313–345.

Sundvall, R., Stalder, R., 2011. Water in upper mantle pyroxene megacrysts and xenocrysts: A survey study. American Mineralogist, 96, 1215-1227.

Tang, Y.-J., Zhang, H.-F., Ying, J.-F., 2006. Asthenosphere-lithospheric mantle interaction in an extensional regime: Implication from the geochemistry of Cenozoic basalts from Taihang Mountains, North China Craton. Chemical Geology, 233, 309-327.

Tatsumi, Y., Hamilton, D. L. & Nesbitt, R. W., 1986. Chemical characteristics of fluid

phase released from a subducted lithosphere and origin of arc magmas: evidence from high-pressure experiments and natural rocks. Journal of Volcanology and Geothermal Research, 29, 293-309.

Tatsumoto, M., Basu, A.R., Huang, W.K., Wang, J.W., Xie, G.H., 1992. Sr, Nd, and Pb isotopes of ultramafic xenoliths in volcanic rocks of Eastern China: enriched components EMI and EMII in subcontinental lithosphere. Earth and Planetary Science Letters, 113, 107-128.

Taylor, H. P. & Sheppard, S. M. F., 1986. Igneous rocks; I, Processes of isotopic fractionation and isotope systematics. Reviews in Mineralogy and Geochemistry, 16, 227-271.

Taylor T.I., Urey H.C., 1938. Fractionation of the lithium and potassium isotopes by chemical exchange with zeolites. The Journal of Chemical Physics, 6: 429–438

Teng F.Z., McDonough W.F., Rudnick R.L., Dalpé C., Tomascak P.B., Chappell B.W., Gao S., 2004. Lithium isotope composition and concentration of the upper continental crust. Geochim Cosmochim Acta, 68: 4167–4178

Tenner, T. J., Hirschmann, M. M., Humayun, M., 2012a. The effect of H_2O on partial melting of garnet peridotite at 3.5 GPa. Geochemistry, Geophysics, Geosystems, 13(3).

Teng, F. Z., Rudnick, R. L., McDonough, W. F., Gao, S., Tomascak, P. B., Liu, Y., 2008. Lithium isotopic composition and concentration of the deep continental crust. Chemical Geology, 255(1), 47-59.

Thirlwall, M.F., 1991. Long-term reproducibility of multicollector Sr and Nd isotope ratio analysis. Chemical Geology, 94, 85-104.

Tomascak, P. B., Langmuir, C. H., le Roux, P. J., Shirey, S. B., 2008. Lithium isotopes in global mid-ocean ridge basalts. Geochimica et Cosmochimica Acta, 72(6), 1626-1637.

Tomascak, P. B., Tera, F., Helz, R. T., Walker, R. J., 1999. The absence of lithium isotope fractionation during basalt differentiation: new measurements by multicollector sector ICP-MS. Geochimica et Cosmochimica Acta, 63(6), 907-910.

Tomascak, P. B., Widom, E., Benton, L. D., Goldstein, S. L., Ryan, J. G., 2002. The control of lithium budgets in island arcs. Earth and Planetary Science Letters, 196(3), 227-238.

Tomaszak P.B., 2004. Lithium isotopes in earth and planetary sciences. Rev Miner Geochem, 55(1):153-195.

Troll, V.R., Deegan, F.M., Jolis, E.M., Harris, C., Chadwick, J.P., Gertisser, R., Schwarzkopf, L.M., Borisova, A.Y., Bindeman, I.N., Sumarti, S., Preece, K., 2013. Magmatic differentiation processes at Merapi Volcano: inclusion petrology and oxygen isotopes. Journal of Volcanology and Geothermal Research, 261, 38-49.

Van Orman, J. A., Grove, T. L., & Shimizu, N., 2001. Rare earth element diffusion in diopside: influence of temperature, pressure, and ionic radius, and an elastic model for diffusion in silicates. Contributions to Mineralogy and Petrology, 141(6), 687-703.

Vlastelic, I., Koga, K., Chauvel, C., Jacques, G., and Telouk, P., 2009, Survival of lithium isotopic heterogeneities in the mantle supported by HIMU-lavas from Rurutu island, Austral Chain: Earth and Planetary Science Letters, 286, 456-466, doi:10.1016/j.epsl.2009.07.013

Von Strandmann, P. A. P., Elliott, T., Marschall, H. R., Coath, C., Lai, Y. J., Jeffcoate, A. B., Ionov, D. A., 2011. Variations of Li and Mg isotope ratios in bulk chondrites and mantle xenoliths. Geochimica et Cosmochimica Acta, 75(18), 5247-5268.

Wade, J.A., Plank, T., Hauri, E.H., Kelly, K.A., Roggensack, K., Zimmer, M., 2008. Prediction of magmatic water contents via measurement of H_2O in clinopyroxene phenocrysts. Geology 36, 799-802.

Wallace, P.J., 1998. Water and partial melting in mantle plumes: inferences from the dissolved H2O concentrations of Hawaiian basaltic magmas. Geophysical Research Letters, 25, 3639–3642.

Wallace, P.J., 2005. Volatiles in subduction zone magmas: concentrations and fluxes based on melt inclusion and volcanic gas data. Journal of Volcanology and Geothermal Research, 140, 217–240

Walter, M.J., 1998. Melting of garnet peridotite and the origin of komatiite and depleted lithosphere. Journal of Petrology, 39, 29-60.

Wang, Y., Fan, W., Cawood, P.A., Li, S., 2008. Sr–Nd–Pb isotopic constraints on multiple mantle domains for Mesozoic mafic rocks beneath the South China Block hinterland. Lithos, 106, 297-308.

Wang, D., Mookherjee, M., Xu, Y., Karato, S. I., 2006. The effect of water on the electrical conductivity of olivine. Nature, 443(7114), 977-980.

Wang, X.C., Li, Z.X., Li, X.H., Li, J., Liu, Y., Long, W.G., Zhou, J.B., Wang, F., 2012. Temperature, Pressure, and Composition of the Mantle Source Region of Late Cenozoic Basalts in Hainan Island, SE Asia: a Consequence of a Young Thermal

Mantle Plume close to Subduction Zones? Journal of Petrology, 53, 177-233.

Wang, X.C., Li, Z.X., Li, X.H., Li, J., Xu, Y.G., 2013. Identification of an ancient mantle reservoir and young recycled materials in the source region of a young mantle plume: Implications for potential linkages between plume and plate tectonics. Earth and Planetary Science Letters, 377, 248-259.

Wang, X.L., Zhou, J.C., Qiu, J.S., Zhang, W.L., Liu, X.M., Zhang, G.L., 2006. LA-ICP-MS U-Pb zircon geochronology of the Neoproterozoic igneous rocks from Northern Guangxi, South China: Implications for tectonic evolution. Precambrian Research, 145, 111-130.

Wang, Y., Fan, W., Cawood, P.A., Li, S., 2008. Sr–Nd–Pb isotopic constraints on multiple mantle domains for Mesozoic mafic rocks beneath the South China Block hinterland. Lithos, 106, 297-308.

Wang, Y., Fan, W., Zhang, G., and Zhang, Y., 2013, Phanerozoic tectonics of the South China Block: Key observations and controversies: Gondwana Research, v. 23, n. 4, p. 1273–1305 http://dx.doi.org/ 10.1016/j.gr.2012.02.019

Wang, Y., Zhao, Z.F., Zheng, Y.F., Zhang, J.J., 2011. Geochemical constraints on the nature of mantle source for Cenozoic continental basalts in east-central China. Lithos, 125, 940-955.

Wang, Z., Hiraga, T., Kohlstedt, D. L., 2004. Effect of H^+ on Fe-Mg inter-diffusion in olivine, $(Fe, Mg)_2SiO_4$. Applied physics letters, 85(2), 209-211.

Wasylenki, L.E., Baker, M.B., Kent, A.J.R., Stolper, E.M., 2003. Near-solidus melting of the shallow upper mantle: Partial melting experiments on depleted peridotite. Journal of Petrology, 44, 1163-1191.

Wei, W., Xu, J.D., Zhao, D.P., Shi, Y.L., 2012. East Asia mantle tomography: New insight into plate subduction and intraplate volcanism. Journal of Asian Earth Sciences, 60, 88-103.

Weis, F.A., Skogby, H., Troll, V.R., Deegan, F.M., Dahren, B., 2015. Magmatic water contents determined through clinopyroxene: Examples from the Western Canary Islands, Spain. Geochemistry, Geophysics, Geosystems, 16(7), 2127-2146.

Weis, F.A., Stalder, R., Skogby, H., 2016. Experimental hydration of natural volcanic clinopyroxene phenocrysts under hydrothermal pressures (0.5–3 kbar). American Mineralogist, 101, 2233.

Widom, E. & Farquhar, J., 2003. Oxygen isotope signatures in olivines from Sao Miguel (Azores) basalts: implications for crustal and mantle processes. Chemical

Geology, 193, 237-255.

Willbold, M., Stracke, A., 2006. Trace element composition of mantle end-members: Implications for recycling of oceanic and upper and lower continental crust. Geochemistry, Geophysics, Geosystems, 7, doi: 10.1029/2005GC001005.

Windley, B.F., Maruyama, S., Xiao, W.J., 2010. Delamination/thinning of sub-continental lithospheric mantle under Eastern China: the role of water and multiple subduction. American Journal of Science, 310(10), 1250-1293.

Woods, S.C., Mackwell, S., Dyar, D., 2000. Hydrogen in diopside: Diffusion profiles. American Mineralogist, 85, 480-487.

Workman, R.K., Hart, S.R., 2005. Major and trace element composition of the depleted MORB mantle (DMM). Earth and Planetary Science Letters, 231, 53-72.

Workman, R.K., Hart, S.R., Jackson, M., Regelous, M., Farley, K.A., Blusztajn, J., Kurz, M., Staudigel, H., 2004. Recycled metasomatized lithosphere as the origin of the enriched mantle II (EM2) end-member: Evidence from the Samoan volcanic chain. Geochemistry, Geophysics, Geosystems, 5, Q04008.

Wu, F.Y., Walker, R.J., Ren, X.W., Sun, D.Y., Zhou, X.H., 2003. Osmium isotopic constraints on the age of lithospheric mantle beneath northeastern China. Chemical Geology, 196, 107-129.

Wu, R.X., Zheng, Y.F., Wu, Y.B., Zhao, Z.F., Zhang, S.B., Liu, X.M., Wu, F.Y., 2006. Reworking of juvenile crust: Element and isotope evidence from Neoproterozoic granodiorite in South China. Precambrian Research, 146, 179-212.

Xia, Q.K., Hao, Y.T., Li, P., Deloule, E., Coltorti, M., Dallai, L., Yang, X.Z., Feng, M., 2010. Low water content of the Cenozoic lithospheric mantle beneath the eastern part of the North China Craton. Journal of Geophysical Research-Solid Earth, 115, B07207.

Xia, Q.K., Liu, J., Liu, S.C., Kovacs, I., Feng, M., Dang, L., 2013. High water content in Mesozoic primitive basalts of the North China Craton and implications on the destruction of cratonic mantle lithosphere. Earth and Planetary Science Letters, 361, 85-97.

Xia, Q.K., Yang, X.Z., Deloule, E., Sheng, Y.M., Hao, Y.T., 2006. Water in the lower crustal granulite xenoliths from Nushan, eastern China. Journal of Geophysical Research-Solid Earth, 111, B11202.

Xia, Y., Xu, X., Zou, H., Liu, L., 2014. Early Paleozoic crust–mantle interaction and lithosphere delamination in South China Block: Evidence from geochronology,

geochemistry, and Sr–Nd–Hf isotopes of granites. Lithos, 184–187, 416-435.

Xiang, H., Zhang, L., Zhou, H., Zhong, Z., Zeng, W., Liu, R., Jin, S., 2008. U-Pb zircon geochronology and Hf isotope study of metamorphosed basic-ultrabasic rocks from metamorphic basement in southwestern Zhejiang: The response of the Cathaysia Block to Indosinian orogenic event. Science in China Series D: Earth Sciences, 51, 788-800.

Xiao, W.J., Windley, B.F., Hao, J., Zhai, M.G., 2003. Accretion leading to collision and the Permian Solonker suture, Inner Mongolia, China: Termination of the central Asian orogenic belt. Tectonics, 22, 21.

Xiao, W.J., Windley, B.F., Huang, B.C., Han, C.M., Yuan, C., Chen, H.L., Sun, M., Sun, S., Li, J.L., 2009. End-Permian to mid-Triassic termination of the accretionary processes of the southern Altaids: implications for the geodynamic evolution, Phanerozoic continental growth, and metallogeny of Central Asia. International Journal of Earth Sciences, 98, 1189-1217.

Xiao, Y., Zhang, H.F., Deloule, E., Su, B.X., Tang, Y.J., Sakyi, P.A., Hu, Y., Ying, J.F., 2015. Large Lithium Isotopic Variations in Minerals from Peridotite Xenoliths from the Eastern North China Craton. Journal of Geology, 123, 79-94.

Xie, X., Xu, X.S., Zou, H.B., Xing, G.F., 2001. Trace element and Nd-Sr-Pb isotope studies of Mesozoic and Cenozoic basalts in coastal area of SE China. Acta Petrologica Sinica, 17, 617-628.

Xiong, X.L., Adam, J., Green, T.H., 2005. Rutile stability and rutile/melt HFSE partitioning during partial melting of hydrous basalt: Implications for TTG genesis. Chemical Geology, 218, 339-359.

Xu, X.S., O'Reilly, S.Y., Griffin, W.L., Zhou, X.M., 2000. Genesis of young lithospheric mantle in southeastern China: an LAM-ICPMS trace element study. Journal of Petrology, 41, 111-148.

Xu, X.S., O'Reilly, S.Y., Griffin, W.L., Zhou, X.M., 2003. Enrichment of upper mantle peridotite: petrological, trace element and isotopic evidence in xenoliths from SE China. Chemical Geology, 198, 163-188.

Xu, Y. G., Bodinier, J. L. 2004. Contrasting enrichments in high-and low-temperature mantle xenoliths from Nushan, Eastern China: results of a single metasomatic event during lithospheric accretion? Journal of Petrology, 45(2), 321-341.

Xu, Y.G., Sun, M., Yan, W., Liu, Y., Huang, X.L., Chen, X.M., 2002. Xenolith evidence for polybaric melting and stratification of the upper mantle beneath South China.

Journal of Asian Earth Sciences, 20, 937-954.

Xu, J.-F., Castillo, P.R., 2004. Geochemical and Nd–Pb isotopic characteristics of the Tethyan asthenosphere: implications for the origin of the Indian Ocean mantle domain. Tectonophysics, 393, 9-27.

Xu, Y.G., Ma, J.L., Frey, F.A., Feigenson, M.D., Liu, J.F., 2005. Role of lithosphere-asthenosphere interaction in the genesis of Quaternary alkali and tholeiitic basalts from Datong, western North China Craton. Chemical Geology, 224, 247-271.

Xu, Y.G., Zhang, H.H., Qiu, H.N., Ge, W.C., Wu, F.Y., 2012a. Oceanic crust components in continental basalts from Shuangliao, Northeast China: Derived from the mantle transition zone? Chemical Geology, 328, 168-184.

Xu, Z., Zhao, Z.F., Zheng, Y.F., 2012b. Slab-mantle interaction for thinning of cratonic lithospheric mantle in North China: Geochemical evidence from Cenozoic continental basalts in central Shandong. Lithos, 146, 202-217.

Yakob, J. L., Feineman, M. D., Deane, J. A., Eggler, D. H., Penniston-Dorland, S. C., 2012. Lithium partitioning between olivine and diopside at upper mantle conditions: An experimental study. Earth and Planetary Science Letters, 329, 11-21.

Yan, J., Zhao, J.X., 2008. Cenozoic alkali basalts from Jingpohu, NE China: The role of lithosphere-asthenosphere interaction. Journal of Asian Earth Sciences, 33, 106-121.

Yang, H.J., Frey, F.A., Clague, D.A., 2003. Constraints on the source components of lavas forming the Hawaiian North Arch and Honolulu volcanics. Journal of Petrology, 44, 603-627.

Yang, W., & Li, S., 2008. Geochronology and geochemistry of the Mesozoic volcanic rocks in Western Liaoning: implications for lithospheric thinning of the North China Craton. Lithos, 102(1), 88-117.

Yang, X.-Z., Deloule, E., Xia, Q.-K., Fan, Q.-C., Feng, M., 2008a. Water contrast between Precambrian and Phanerozoic continental lower crust in eastern China. Journal of Geophysical Research: Solid Earth, 113, n/a-n/a.

Yang, X.Z., Xia, Q.K., Deloule, E., Dallai, L., Fan, Q.C., Feng, M., 2008b. Water in minerals of the continental lithospheric mantle and overlying lower crust: A comparative study of peridotite and granulite xenoliths from the North China Craton. Chemical Geology, 256, 33-45.

Yao, J., Shu, L., and Santosh, M., 2011. Detrital zircon U-Pb geochronology, Hf-

isotopes and geochemistry-New clues for the Precambrian crustal evolution of Cathaysia block, South China: Gondwana Research, v. 20, n. 2–3, p. 553–567, http://dx.doi.org/10.1016/j.gr.2011.01.005.

Yoshino, T., Katsura, T., 2013. Electrical conductivity of mantle minerals: role of water in conductivity anomalies. Annual review of earth and planetary sciences, 41, 605-628.

Yoshino, T., Matsuzaki, T., Yamashita, S., Katsura, T., 2006. Hydrous olivine unable to account for conductivity anomaly at the top of the asthenosphere. Nature, 443(7114), 973-976.

You, C. F., Chan, L. H., 1996. Precise determination of lithium isotopic composition in low concentration natural samples. Geochimica et Cosmochimica Acta, 60(5), 909-915.

Yu, J.H., O'Reilly, Y.S., Wang, L.J., Griffin, W.L., Jiang, S.Y., Wang, R.C., Xu, X.S., 2007. Finding of ancient materials in Cathaysia and implication for the formation of Precambrian crust. Chinese Science Bulletin, 52, 13-22.

Yu, J.H., Wang, L., O'Reilly, S.Y., Griffin, W.L., Zhang, M., Li, C., Shu, L., 2009. A Paleoproterozoic orogeny recorded in a long-lived cratonic remnant (Wuyishan terrane), eastern Cathaysia Block, China. Precambrian Research, 174, 347-363.

Yu, Y., Xu, X.S., Griffin, W.L., O'Reilly, S.Y., Xia, Q.K., 2011. H_2O contents and their modification in the Cenozoic subcontinental lithospheric mantle beneath the Cathaysia block, SE China. Lithos, 126, 182-197.

Zack, T., Tomascak, P. B., Rudnick, R. L., Dalpé, C., McDonough, W. F., 2003. Extremely light Li in orogenic eclogites: the role of isotope fractionation during dehydration in subducted oceanic crust. Earth and Planetary Science Letters, 208(3), 279-290.

Zeng, G., Chen, L.H., Hofmann, A.W., Jiang, S.Y., Xu, X.S., 2011. Crust recycling in the sources of two parallel volcanic chains in Shandong, North China. Earth and Planetary Science Letters, 302, 359-368.

Zhang, H.F., Sun, M., Zhou, X.H., Fan, W.M., Zhai, M.G., Yin, J.F., 2002a. Mesozoic lithosphere destruction beneath the North China Craton: evidence from major-, trace-element and Sr-Nd-Pb isotope studies of Fangcheng basalts. Contributions to Mineralogy and Petrology, 144, 241-253.

Zhang, J., Zhang, H. F., Ying, J. F., Tang, Y. J., & Niu, L. F., 2008. Contribution of subducted Pacific slab to Late Cretaceous mafic magmatism in Qingdao region,

China: a petrological record. Island Arc, 17(2), 231-241.

Zhang, J.J., Zheng, Y.F., Zhao, Z.F., 2009. Geochemical evidence for interaction between oceanic crust and lithospheric mantle in the origin of Cenozoic continental basalts in east-central China. Lithos, 110, 305-326.

Zhang, M., Hu, P., Niu, Y., Su, S., 2007. Chemical and stable isotopic constraints on the nature and origin of volatiles in the sub-continental lithospheric mantle beneath eastern China. Lithos, 96, 55-66.

Zhang, W.H., Zhang, H.F., Fan, W.M., Han, B.F., Zhou, M.F., 2012. The genesis of Cenozoic basalts from the Jining area, northern China: Sr-Nd-Pb-Hf isotope evidence. Journal of Asian Earth Sciences, 61, 128-142.

Zhang, Z.C., Feng, C.Y., Li, Z.N., Li, S.C., Xin, Y., Li, Z.M., Wang, X.Z., 2002b. Petrochemical study of the Jingpohu Holocene alkali basaltic rocks, northeastern China. Geochemical Journal, 36, 133-153.

Zhang B.M., Zhang X.L., Di J.R., Ye D.L., 2010, Structural OH and Hydrogen and Oxygen Isotope of Pyroxenes from Upper Mantle in Fujitian, Hainan, China. Geological Science and Technology Information, 29, (3): 1-7. (In Chinese, English abstract).

Zhao, D., Ohtani, E., 2009. Deep slab subduction and dehydration and their geodynamic consequences: Evidence from seismology and mineral physics. Gondwana Research, 16, 401-413.

Zhao, Y.W., Fan, Q.C., Zou, H.B., Li, N., 2014. Geochemistry of Quaternary basaltic lavas from the Nuomin volcanic field, Inner Mongolia: Implications for the origin of potassic volcanic rocks in Northeastern China. Lithos, 196, 169-180.

Zheng, J., O'Reilly, S. Y., Griffin, W. L., Lu, F., and Zhang, M., 1998, Nature and evolution of Cenozoic lithospheric mantle beneath Shandong peninsula, Sino-Korean craton: International Geology Review, v. 40, n. 6, p. 471–499, doi:10.1080/00206819809465220.

Zheng, Y.F., 2012, Metamorphic chemical geodynamics in continental subduction zones, Chemical Geology, 328, 5–48.

Zhou, M.F., Kennedy, A.K., Sun, M., Malpas, J., Lesher, C.M., 2002a. Neoproterozoic arc-related mafic intrusions along the northern margin of South China: Implications for the accretion of Rodinia. Journal of Geology, 110, 611-618.

Zhou, M.F., Ma, Y.X., Yan, D.P., Xia, X.P., Zhao, J.H., Sun, M., 2006. The Yanbian terrane (Southern Sichuan Province, SW China): A neoproterozoic are assemblage

in the western margin of the Yangtze block. Precambrian Research, 144, 19-38.

Zhou, M.F., Yan, D.P., Kennedy, A.K., Li, Y.Q., Ding, J., 2002b. SHRIMP U-Pb zircon geochronological and geochemical evidence for Neoproterozoic arc-magmatism along the western margin of the Yangtze Block, South China. Earth and Planetary Science Letters, 196, 51-67.

Zhou, X., Armstrong, R.L., 1982. Cenozoic volcanic rocks of eastern China: secular and geographic trends in chemistry and strontium isotopic composition. Earth and Planetary Science Letters, 58, 301-329.

Zhu B.Q., Wang H.F., Chen Y.W., Chang X.Y., Hu Y.G., Xie J., 2004. Geochronological and geochemical constraint of the Cenozoic extension of Cathaysian lithosphere and tectonic evolution of the border sea basins in East Asia. Journal of Asian Earth Sciences, 24:163–175.

Zindler, A., Hart, S.R., 1986. Chemical geodynamics. Annual Review of Earth and Planetary Sciences, 14, 493–571.

Zindler, A., Staudigel, H., Batiza, R., 1984. Isotope and trace element geochemistry of young Pacific seamounts: implications for the scale of upper mantle heterogeneity. Earth and Planetary Science Letters, 70, 175-195.

Zinner, E., Fahey, A. J., McKeegan, K. D., 1986. Characterization of electron multipliers by charge distributions. In Secondary Ion Mass Spectrometry SIMS V (pp. 170-172). Springer Berlin Heidelberg.

Zou, H.B., Fan, Q.C., 2010. U-Th isotopes in Hainan basalts: Implications for sub-asthenospheric origin of EM2 mantle endmember and the dynamics of melting beneath Hainan Island. Lithos, 116, 145-152.

Zou, H.B., Fan, Q.C., Yao, Y.P., 2008. U-Th systematics of dispersed young volcanoes in NE China: Asthenosphere upwelling caused by piling up and upward thickening of stagnant Pacific slab. Chemical Geology, 255, 134-142.

Zou, H.B., Reid, M.R., Liu, Y.S., Yao, Y.P., Xu, X.S., Fan, Q.C., 2003. Constraints on the origin of historic potassic basalts from northeast China by U-Th disequilibrium data. Chemical Geology, 200, 189-201.

Zou, H.B., Zindler, A., Xu, X.S., Qi, Q., 2000. Major, trace element, and Nd, Sr and Pb isotope studies of Cenozoic basalts in SE China: mantle sources, regional variations, and tectonic significance. Chemical Geology, 171, 33-47.

Published Papers:

Liu, S.C., Xia, Q.K., Choi, S.H., Deloule, E., Li, P., Liu, J., 2016. Continuous supply of recycled Pacific oceanic materials in the source of Cenozoic basalts in SE China: the Zhejiang case. Contributions to Mineralogy and Petrology, 171, 100.

Liu, S.C., Xia, Q.K., 2014. Water content in the early Cretaceous lithospheric mantle beneath the south-central Taihang Mountains: implications for the destruction of the North China Craton. Chinese Science Bulletin, 59, 1362-1365.

Yang, Y.B., Fang, X.M., Galy, A., Zhang, G.X., **Liu, S.C.**, Zan, J.B., Wu, F.L., Meng, Q.Q., Ye, C.C., Yang, R.S., Liu, X.M., 2015. Carbonate composition and its impact on fluvial geochemistry in the NE Tibetan Plateau region. Chemical Geology, 410, 138-148.

Xia, Q.K., Hao, Y.T., **Liu, S.C.**, Gu, X.Y., Feng, M., 2013a. Water contents of the Cenozoic lithospheric mantle beneath the western part of the North China Craton: Peridotite xenolith constraints. Gondwana Research, 23, 108-118.

Xia, Q.K., Liu, J., **Liu, S.C.**, Kovacs, I., Feng, M., Dang, L., 2013b. High water content in Mesozoic primitive basalts of the North China Craton and implications on the destruction of cratonic mantle lithosphere. Earth and Planetary Science Letters, 361, 85-97.

Hao, Y.T., Xia, Q.K., **Liu, S.C.**, Feng, M., Zhang, Y.P., 2012. Recognizing juvenile and relict lithospheric mantle beneath the North China Craton: Combined analysis of H2O, major and trace elements and Sr-Nd isotope compositions of clinopyroxenes. Lithos, 149, 136-145.

Yang, Y., Xia, Q.K., Feng, M., **Liu, S.C.**, 2012. OH in natural orthopyroxene: an in situ FTIR investigation at varying temperatures. Physics and Chemistry of Minerals, 39, 413-418.

Contrib Mineral Petrol (2016) 171:100
DOI 10.1007/s00410-016-1310-4

ORIGINAL PAPER

Continuous supply of recycled Pacific oceanic materials in the source of Cenozoic basalts in SE China: the Zhejiang case

Shao-Chen Liu[1,3] · Qun-Ke Xia[2] · Sung Hi Choi[4] · Etienne Deloule[3] · Pei Li[2] · Jia Liu[1]

Received: 4 August 2016 / Accepted: 15 October 2016

Abstract Various enriched recycled oceanic components in the source of Cenozoic intra-plate alkaline basalts from eastern China were identified by previous studies. Due to the existence of a stagnant subducted Pacific slab in the mantle transition zone beneath eastern China, it is logical to connect the stagnant slab to the recycled oceanic materials. However, the recycled oceanic materials could also result from ancient subduction events (e.g., Paleo-Tethyan, Paleo-Asian or Izanagi plate subduction) because enriched geochemical signatures of a recycled slab can be preserved in the mantle for longer than 1 Gyr. Investigating the temporal variations of the recycled oceanic materials in the mantle source is a useful way to trace the origin of the basalts. In this article, we have conducted a detailed geochemical study, including major and trace elements and Sr–Nd–Pb isotopes, on two alkaline basalt groups from Zhejiang, SE China, which erupted 26–17 Ma and after 11 Ma, respectively. In particular, we recovered the H_2O content of the initial magmas based on the H_2O content of the clinopyroxene (cpx) phenocrysts and the partition coefficients of H_2O between cpx and basaltic melts. The H_2O contents of the Zhejiang basalts range from 1.3 to 2.6 (wt.%), which fall within the range of back-arc basin or island arc basalts. The older basalts are more alkaline and have lower Si and Al contents; higher trace element concentrations; higher La/Yb, Ce/Pb and Nb/La ratios; lower H_2O/Ce and Ba/Th ratios; and stronger negative K, Pb, Hf and Ti anomalies than the younger ones. The co-relationships between Ba/La, H_2O/Ce, Nb/La, Ce/Pb and Ba/Th in the two groups of the Zhejiang basalts indicate that a recycled dehydrated oceanic alkaline basalt component is needed in the source of the older rocks, along with a depleted mantle component. Meanwhile, an additional recycled dehydrated sediment component was required in the source of the younger rocks. The temporal change in the recycled oceanic materials in the mantle sources of Zhejiang Cenozoic basalts demonstrates that the recycled components can only originate in the stagnant Pacific slab that is the only plate subducted since 100 Ma in this area.

Keywords Water content · Continental basalts · Recycled oceanic crust · Recycled oceanic sediments · Southeast China

Communicated by Hans Keppler.

Electronic supplementary material The online version of this article (doi:10.1007/s00410-016-1310-4) contains supplementary material, which is available to authorized users.

✉ Qun-Ke Xia
qkxia@zju.edu.cn

[1] School of Earth and Space Sciences, University of Science and Technology of China, Hefei 230026, China

[2] School of Earth Sciences, Zhejiang University, Hangzhou 310027, China

[3] CRPG, UMR 7358, CNRS, Université de Lorraine, BP20, 54501 Vandœuvre-lès-Nancy cedex, France

[4] Department of Geology and Earth Environmental Sciences, Chungnam National University, Daejeon 34134, Republic of Korea

Introduction

Intra-plate basalt is one of the most important windows for observing the deep earth. However, the genesis of intra-plate basalts and the constituents of their mantle sources remain poorly known. In past decades, growing numbers of experimental and natural observations have demonstrated

Published online: 19 November 2016

Chin. Sci. Bull. (2014) 59(13):1362–1365
DOI 10.1007/s11434-014-0203-z

csb.scichina.com

Letter

Geology

Water content in the early Cretaceous lithospheric mantle beneath the south-central Taihang Mountains: implications for the destruction of the North China Craton

Shaochen Liu · Qunke Xia

Received: 28 May 2013 / Accepted: 16 September 2013 / Published online: 22 February 2014

Abstract Based on studies of the water content of the early Cretaceous Feixian high-magnesium basalts in the eastern part of the North China Craton (NCC), it has been suggested that the early Cretaceous lithospheric mantle of the eastern NCC was highly hydrous (>1,000 ppm, H_2O wt.) and that this high water content had significantly reduced the viscosity of the lithospheric mantle and provided a prerequisite for the destruction of the NCC. The eastern part of the NCC had undergone multistage subduction of oceanic plates from the south, north, and east sides since the early Paleozoic, and these events may have caused the strong hydration of the NCC lithospheric mantle. To determine which subduction had contributed most to this hydration, we measured the water contents of the peridotite xenoliths hosted by the early Cretaceous high-magnesium diorites of Fushan in the south-central part of the Taihang Mountains. Our results demonstrate that the water content of the early Cretaceous lithospheric mantle beneath the south part of the Taihang Mountains was ~40 ppm and significantly lower than that of the contemporary lithospheric mantle beneath the eastern part of the NCC. Thus, the hydration of the early Cretaceous lithospheric mantle of the eastern part of the NCC can be ascribed to the subduction of the Pacific plate from the west side. Thus, the main dynamic factor in the destruction of the NCC was likely the subduction of the Pacific plate.

Keywords Water · Peridotite xenoliths · Early Cretaceous · The south-central Taihang Mountains · Destruction of the NCC

S. Liu · Q. Xia (✉)
Key Laboratory of Crust-Mantle Materials and Environments, University of Science and Technology of China, Chinese Academy of Sciences, Hefei 230026, China
e-mail: qkxia@ustc.edu.cn

Reducing the strength of the lithospheric mantle is necessary for the destruction of stable cratons, and hydration of the lithosphere mantle is one of the most effective causes of weakening of the lithospheric mantle [1–4]. The North China Craton (NCC) experienced strong destruction in the Mesozoic that peaked in the early Cretaceous [5]. Studies of the water content of the early Cretaceous (~120 Ma) high-magnesium basalts that erupted at Feixian in the Shandong Province have confirmed that the eastern part of the NCC lithospheric mantle was indeed strongly hydrated (>1,000 ppm H_2O by weight) [1]. The NCC had undergone multistage subduction of oceanic plates since the early Paleozoic— the Paleo-Pacific plate from the eastside; the oceanic plates along the Solonker and Mongol-Okhotsk sutures from the north side; and the oceanic plates along the Dabie Shan and Song Ma sutures from the south side are all subducting the NCC [6, 7], and all of these subduction events could hydrate the lithospheric mantle of the NCC. If the north and south side subductions have dominant roles in the hydration of the NCC lithospheric mantle, then the early Cretaceous lithospheric mantle beneath the southern part of the Taihang Mountains should be rich in water as is the contemporary lithospheric mantle beneath the Feixian region (~1,000 ppm). However, if the west side subduction of the Paleo-Pacific plate is the main cause of the hydration [8], then the early Cretaceous lithosphere mantle beneath the southern part of the Taihang Mountains should not be as hydrated as that of the Feixian region because the subducted Pacific plate has extended as far as the Taihang Mountains. Based on the above considerations, we analyzed the water contents of six peridotite xenoliths that are hosted by the early Cretaceous high-magnesium diorites of Fushan of the south-central part of the Taihang Mountains with Fourier transform infrared (FTIR) spectroscopy to determine the mechanism responsible for the

AGU PUBLICATIONS

JGR

Journal of Geophysical Research: Solid Earth

RESEARCH ARTICLE
10.1002/2015JB012105

Key Points:
- We report water content of peridotite xenoliths from Northeast China
- Regional heterogeneity in water content exists in Eastern China lithosphere
- Regional heterogeneity is related to distinct origins and geodynamic processes

Supporting Information:
- Tables S1–S3
- Text S1
- Text S2
- Text S3

Correspondence to:
Y.-T. Hao and Q.-K. Xia,
ythao@zju.edu.cn;
qkxia@zju.edu.cn

Citation:
Hao, Y.-T., Q.-K. Xia, Z.-B. Jia, Q.-C. Zhao, P. Li, M. Feng, and S.-C. Liu (2016), Regional heterogeneity in the water content of the Cenozoic lithospheric mantle of Eastern China, *J. Geophys. Res. Solid Earth*, *121*, 517–537, doi:10.1002/2015JB012105.

Received 8 APR 2015
Accepted 29 DEC 2015
Accepted article online 5 JAN 2016
Published online 3 FEB 2016

Regional heterogeneity in the water content of the Cenozoic lithospheric mantle of Eastern China

Yan-Tao Hao[1,2], Qun-Ke Xia[1,2], Zu-Bing Jia[2], Qi-Chao Zhao[2], Pei Li[1,2], Min Feng[2], and Shao-Chen Liu[2]

[1]School of Earth Sciences, Zhejiang University, Hangzhou, China, [2]School of Earth and Space Sciences, University of Science and Technology of China, Hefei, China

Abstract The major and trace elements and H_2O contents of minerals in peridotite xenoliths hosted by the Cenozoic basalts in Northeast China (NEC) were evaluated using electron microprobe, laser-ablation inductively coupled plasma–mass spectrometry and Fourier transform infrared spectroscopy, respectively. Although a potential loss of H during the xenoliths' ascent cannot be excluded for olivine, orthopyroxene (opx) and clinopyroxene (cpx) largely preserved the H_2O contents of their mantle source in all of the samples, as inferred from (1) the homogenous H_2O contents within single pyroxene grains and (2) the equilibrium H_2O partitioning between cpx and opx. No OH was detected for pyroxenes of peridotite xenoliths from the north part of NEC (NNEC). Combined with previously published data from the North China Craton (NCC) and the South China Block (SCB), the regional heterogeneity in the water contents in the Cenozoic lithospheric mantle beneath the whole Eastern China has been revealed. The lithospheric mantle beneath the NNEC is completely dry. The "bulk" water contents of the lithospheric mantle of the south part of NEC and the NCC have similar ranges and average values, whereas those of the SCB are much higher (12–195 ppm, average 90 ± 45 ppm for whole rock). The regional variations in the H_2O content of the Cenozoic lithospheric mantle of Eastern China cannot be caused by partial melting, mantle metasomatism, or variations in redox state. We propose that the lithospheric mantle beneath the different regions of Eastern China may have distinct origins and may have undergone distinct geodynamic processes.

1. Introduction

Peridotite xenoliths hosted by alkali basalts are direct samples of the continental lithospheric mantle. They have the potential to largely preserve the geochemical signatures of the mantle source because they generally reach the surface within 50 h after their entrainment in the host magma [*Peslier et al.*, 2002; *Demouchy et al.*, 2006; *Peslier and Luhr*, 2006; *O'Reilly and Griffin*, 2010]. Although the main minerals (olivine, orthopyroxene (opx), clinopyroxene (cpx), and garnet) of peridotite xenoliths are nominally anhydrous, they contain a trace amount of water (generally several to hundreds of ppm H_2O by weight) as OH defects and can be used to infer the amount and distribution of water in the lithospheric mantle [*Bell and Rossman*, 1992; *Ingrin and Skogby*, 2000; *Peslier et al.*, 2002, 2012; *Hirschmann et al.*, 2005; *Peslier and Luhr*, 2006; *Grant et al.*, 2007; *Bonadiman et al.*, 2009; *Xia et al.*, 2010, 2013a; *Yu et al.*, 2011; *Hao et al.*, 2012, 2014; *Mosenfelder and Rossman*, 2013a, 2013b; *Warren and Hauri*, 2014; *Demouchy et al.*, 2015]. The water content of the lithospheric mantle is closely related to the stability (longevity and destruction) of continents [*Li et al.*, 2008; *Peslier et al.*, 2010; *Xia et al.*, 2013b]. Therefore, the spatial and temporal distribution of water in the lithospheric mantle is crucial to understanding the evolution of continents.

Cenozoic volcanoes are widely distributed in Eastern China, extending from Heilongjiang province in the north to Hainan province in the south. In many localities, abundant mantle xenoliths are hosted in the alkali basalts, and they have attracted numerous studies of the characteristics of the lithospheric mantle [*Deng and Macdougall*, 1992; *Tatsumoto et al.*, 1992; *Qi et al.*, 1995; *Xu et al.*, 1996a, 1996b, 2001, X. S. *Xu et al.*, 2003, 2008; *Griffin et al.*, 1998; *Zheng et al.*, 1998, 2001, 2004, 2005a, 2005b, 2006, 2007; *Fan et al.*, 2000; *Xu et al.*, 2000, 2008; *Chen et al.*, 2001; *Gao et al.*, 2002; *Chen et al.*, 2003; *Wu et al.*, 2003, 2006; *Zhang et al.*, 2003, 2007; *Rudnick et al.*, 2004; *Xu and Bodinier*, 2004; *Reisberg et al.*, 2005; *Ying et al.*, 2006; *Yu et al.*, 2006; *Choi et al.*, 2008; *Tang et al.*, 2008, 2011, 2013; *Chu et al.*, 2009; *Yu et al.*, 2009, 2010; *J. G. Liu et al.*, 2010, 2012; *Xiao et al.*, 2010; *Zhao and Fan*, 2011; *Hong et al.*, 2012; *Liu et al.*, 2012; *Zhang et al.*, 2012; *Lu et al.*, 2013; *Pan et al.*, 2013; *Xu et al.*, 2013; *Li et al.*, 2014; *Liu et al.*, 2015]. Eastern China consists of three main blocks from

Chemical Geology 410 (2015) 138–148

Contents lists available at ScienceDirect

Chemical Geology

journal homepage: www.elsevier.com/locate/chemgeo

Carbonate composition and its impact on fluvial geochemistry in the NE Tibetan Plateau region

Yibo Yang [a,*], Xiaomin Fang [a,b], Albert Galy [c], Gengxin Zhang [a], Shaochen Liu [c], Jinbo Zan [a,b], Fuli Wu [a,b], Qingquan Meng [d], Chengcheng Ye [a], Rongsheng Yang [a], Xiaoming Liu [a]

[a] Key Laboratory of Continental Collision and Plateau Uplift, Institute of Tibetan Plateau Research, Chinese Academy of Sciences, Beijing 100101, China
[b] CAS Center for Excellence in Tibetan Plateau Earth Sciences, Beijing 100101, China
[c] Centre de Recherches Pétrographiques et Géochimiques (CRPG), UMR7358, CNRS — Université de Lorraine, 15 rue Notre Dame des Pauvres, 54501 Vandoeuvre les Nancy, Cedex, France
[d] School of Earth Sciences & Key Laboratory of Western China's Mineral Resources of Gansu Province, Lanzhou University, Lanzhou 730000, China

ARTICLE INFO

Article history:
Received 16 February 2015
Received in revised form 7 June 2015
Accepted 8 June 2015
Available online 11 June 2015

Keywords:
Carbonate weathering
Fluvial geochemistry
Calcite precipitation
Incongruent calcite dissolution
NE Tibetan Plateau

ABSTRACT

Using co-variations of Sr/Ca and Mg/Ca, we examined the carbonate compositions of various bedrocks (silicate and carbonate rocks) and sediments (eolian and fluvial sediments, sand, and topsoil) found in the NE Tibetan Plateau (TP) region. A combined carbonate composition dataset based on our results and other reported data shows that bedrock carbonate composition on the NE TP displays a much broader range of Sr/Ca and Mg/Ca ratios than restricted source carbonate endmembers reported upon in previous studies. This has clear implications for modern weathering studies in addition to paleo-reconstructions in this tectonically active and climatically variable area during the Late Cenozoic. Bedrock carbonate compositions are characterized by disseminated carbonates with higher Sr/Ca and Mg/Ca ratios, and sedimentary carbonates (mostly marine) with lower Sr/Ca, but variable Mg/Ca, ratios. The mostly authigenic carbonates found in sediments show similar trends, with a gradient ~0.97–1.00 in a plot of log (Sr/Ca) *versus* log (Mg/Ca), suggesting that 'calcite precipitation' processes – *i.e.* the sources of the dissolved cations in the water – control their chemistry. Based on observations and modeling, we conclude that the mixing of authigenic and bedrock carbonate endmembers, plus the incongruent dissolution of bedrock carbonates, accounts for the bulk carbonate composition of sediments (*e.g.* loess, sand and topsoil). A comparison of bedrock and sedimentary carbonate composition with reported fluvial water data in the NE TP suggests that weathering of carbonates in terrigenous sediments, rather than in bedrock, is mostly responsible for the changes in fluvial Sr, Mg and Ca compositions. Our study suggests that interactions between carbonates and water occur widely during the exposure, transport and deposition of sediments, significantly modifying regional carbonate compositions and fluvial geochemistry.

1. Introduction

Carbonates in bedrock and sediments can play a unique role both in the study of modern chemical processes and in paleo-reconstructions (*e.g.* Gaillardet et al., 1999; Dettman et al., 2003; Han and Liu, 2004; Yokoo et al., 2004; Wu et al., 2005; Fan et al., 2007; Jin et al., 2011; Zhang et al., 2013a; Li and Li, 2014). Soil carbonates, as typical products of the interactions between carbonates and water in eolian deposits or floodplain environments, provide a powerful tool for paleo-reconstructions (*e.g.* Cerling, 1984; Dettman et al., 2003). Proxies derived from soil carbonates, *e.g.* $^{87}Sr/^{86}Sr$, $\delta^{13}C$, $\delta^{18}O$, carbonate-clumped isotopes and trace elements, can be extensively used to explore paleoclimate, paleoenvironment and paleoelevation (*e.g.* Cerling et al., 1993; Rowley and Garzione, 2007; Quade et al., 1989, 1997, 2011, 2013; Li and Li, 2014). Unfortunately, such paleosol-based reconstructions are always hampered by the presence of detrital carbonates in sediments (Fan et al., 2007; Li et al., 2013). Isolating the authigenic and detrital carbonates in sediments has therefore long been a challenge.

Mn/Ca ratios in bulk carbonate have been proposed as discriminatory indicators of detrital carbonate signatures in Chinese loess–paleosol sequences, where a binary mixing between secondary carbonate with low Mn/Ca and Mg/Ca ratios and detrital carbonate with high Mn/Ca and Mg/Ca ratios is found (Li et al., 2013). However, an abundance of Mn oxide coating during soil development and possible Mn oxide dissolution by weak acetic acid (Chester and Hughes, 1967; Gourlan et al., 2010) complicates the valence and source of acid-exacted Mn, and thus limits the wider application of Mn/Ca ratios to carbonate analysis. Sr and Mg partition coefficients are <1 in carbonates, and the co-variation of both elements (as opposed to Mn) is generally a more robust tool for describing the interactions between carbonates and water (*e.g.* Plummer and Mackenzie, 1974; Fairchild et al., 1994; Reeve and Perry, 1994; Galy et al., 1999; Tipper et al., 2008). Sinclair

* Corresponding author.
E-mail address: yangyibo@itpcas.ac.cn (Y. Yang).

Gondwana Research 23 (2013) 108–118

Contents lists available at SciVerse ScienceDirect

Gondwana Research

journal homepage: www.elsevier.com/locate/gr

Water contents of the Cenozoic lithospheric mantle beneath the western part of the North China Craton: Peridotite xenolith constraints

Qun-Ke Xia *, Yan-Tao Hao, Shao-Chen Liu, Xiao-Yan Gu, Min Feng

CAS Key Laboratory of Crust-Mantle Materials and Environments, School of Earth and Space Sciences, University of Science and Technology of China, Hefei 230026, China

ARTICLE INFO

Article history:
Received 7 September 2011
Received in revised form 13 January 2012
Accepted 29 January 2012
Available online 4 February 2012

Keywords:
H_2O contents
Peridotite xenoliths
Beishan
Fansi
Western North China Craton

ABSTRACT

Nominally anhydrous phases (clinopyroxene (cpx), orthopyroxene (opx), and olivine (ol)) of peridotite xenoliths hosted by the Cenozoic basalts from Beishan (Hebei province), and Fansi (Shanxi province), Western part of the North China Craton (WNCC) have been investigated by Fourier transform infrared spectrometry (FTIR). The H_2O contents (wt.) of cpx, opx and ol are 30–255 ppm, 14–95 ppm and ~0 ppm, respectively. Although potential H-loss during xenolith ascent cannot be excluded for olivine, pyroxenes (cpx and opx) largely preserve the H_2O content of their mantle source inferred from (1) the homogenous H_2O content within single pyroxene grains, and (2) equilibrium H_2O partitioning between cpx and opx. Based on mineral modes and assuming a partition coefficient of 10 for H_2O between cpx and ol, the recalculated whole-rock H_2O contents range from 6 to 42 ppm. In combination with previously reported data for other two localities (Hannuoba and Yangyuan from Hebei province), the H_2O contents of cpx, opx and whole-rock of peridotite xenoliths (43 samples) hosted by the WNCC Cenozoic basalts range from 30 to 654 ppm, 14 to 225 ppm, and 6 to 262 ppm respectively. The H_2O contents of the Cenozoic lithospheric mantle represented by peridotite xenoliths fall in a similar range for both WNCC and the eastern part of the NCC (Xia et al., 2010, Journal of Geophysical Research). Clearly, the Cenozoic lithospheric mantle of the NCC is dominated by much lower water content compared to the MORB source (50–250 ppm). The low H_2O content is not caused by oxidation of the mantle domain, and likely results from mantle reheating, possibly due to an upwelling asthenospheric flow during the late Mesozoic–early Cenozoic lithospheric thinning of the NCC. If so, the present NCC lithospheric mantle mostly represents relict ancient lithospheric mantle. Some newly accreted and cooled asthenospheric mantle may exist in localities close to deep fault.

1. Introduction

Cratons are old and stable parts of the continental lithosphere, usually occurring in the interiors of tectonic plates. Because of their refractory, low-density and anhydrous keels, cratons generally lack tectonic or volcanic activities and can survive for several billion years. The presence of structurally bonded water in minerals which make up the lithospheric mantle of cratons can greatly affect the physical (rheology, electrical conductivity, seismic velocity and attenuation) and chemical (elemental diffusion, partial melting) properties of these mantle domains (Hirth and Kohlstedt, 1996; Karato and Jung, 1998; Hirschmann et al., 2009; Karato, 2010). Therefore, water may weak the stability of the cratonic lithospheric mantle.

Mantle-derived xenoliths are transported by alkali magmas to the Earth's surface during volcanic eruption in a very short time (few hours to days); they represent the "quenched" products of their mantle source and peridotite xenoliths are believed to be direct samples of the lithospheric mantle. Therefore, the H_2O contents of peridotite xenoliths may provide information about the distribution of water in the lithospheric mantle. Although the main minerals of peridotite xenoliths (olivine (ol), orthopyroxene (opx), clinopyroxene (cpx) and spinel (sp)/garnet) are nominally anhydrous, they still contain a significant amount of water as crystal defects (Bell and Rossman, 1992; Ingrin and Skogby, 2000; Peslier et al., 2010; Sundvall and Stalder, 2011).

The North China Craton (NCC) is the Chinese part of the Sino–Korean Craton. It is one of the ancient cratons on the Earth, with the oldest recorded crustal ages > 3.8 Ga (Liu et al., 1992), and it is mainly composed of early Archean and Proterozoic metamorphic rocks (Zhai and Santosh, 2011). The NCC can be divided into two topographically and tectonically different regions, the eastern part (ENCC) and the western part (WNCC), separated by the NS trending Daxing'anling–Taihangshan Gravity Lineament (DTGL) (Fig. 1). The ENCC experienced widespread lithospheric thinning from a thick (~200 km), cold (~40 mW/m^2) and highly refractory lithospheric mantle in the mid-Ordovician to a hot (60–80 mW/m^2), thin (60–80 km) and fertile lithospheric mantle after the late Mesozoic (Menzies et al., 2007, and references therein). In contrast, lithospheric removal was possibly relative limited in the

* Corresponding author. Tel.: +86 551 3607008; fax: +86 551 3607656.
E-mail address: qkxia@ustc.edu.cn (Q.-K. Xia).

1342-937X/$ – see front matter © 2012 International Association for Gondwana Research. Published by Elsevier B.V. All rights reserved.
doi:10.1016/j.gr.2012.01.010

Earth and Planetary Science Letters 361 (2013) 85–97

Contents lists available at SciVerse ScienceDirect

Earth and Planetary Science Letters

journal homepage: www.elsevier.com/locate/epsl

High water content in Mesozoic primitive basalts of the North China Craton and implications on the destruction of cratonic mantle lithosphere

Qun-Ke Xia [a,*], Jia Liu [a], Shao-Chen Liu [a], István Kovács [b], Min Feng [a], Li Dang [c]

[a] CAS Key Laboratory of Crust-Mantle Materials and Environments, School of Earth and Space Sciences, University of Science and Technology of China, Hefei 230026, China
[b] Hungarian Geological and Geophysical Institute, Stefánia Street 14, 1143 Budapest, Hungary
[c] Department of Precision Machinery and Precision Instruments, University of Science and Technology of China, Hefei 230026, China

ARTICLE INFO

Article history:
Received 19 August 2012
Received in revised form
2 November 2012
Accepted 13 November 2012
Editor: B. Marty

Keywords:
water
clinopyroxene phenocryst
basalt
lithospheric mantle
North China Craton

ABSTRACT

It has been suggested that the longevity of cratons (i.e. ancient and stable cores of continents) is related in part to the low water content of their deep mantle roots; this gives them a higher viscosity than the underlying asthenosphere. Consequently, the removal of cratonic roots is expected to be closely connected to the hydration of the lithospheric mantle, but direct evidence for this speculation has been scarce. The eastern part of the North China Craton (NCC) is a clear example of a "destroyed craton". In this study the H_2O content of clinopyroxene phenocrysts was measured in lithospheric mantle-derived high-magnesium basalts of the Feixian area, in the eastern part of the NCC. These lavas erupted in the early Cretaceous (~120 Ma), which was the peak time of the NCC destruction. Based on these data, it was estimated that the H_2O content of the lithospheric mantle source of these basalts consists of more than 1000 ppm by weight. This water content is much higher than in the source of mid-ocean-ridge basalts (50–200 ppm by weight) and also higher than in the Kaapvaal cratonic mantle in South Africa (~120 ppm by weight); the latter is still stable after >3 billion years. This study argues that a large amount of water was indeed added to the NCC's lithospheric mantle, probably due to the multi-stage subduction of oceanic plates since the early Paleozoic. This high water content significantly reduced the viscosity contrast between the lithospheric mantle and the underlying asthenosphere, and provided a prerequisite for the removal of the cratonic root of the NCC by reducing its strength.

1. Introduction

Cratons are the ancient cores (Precambrian) of continents, and their lithospheric mantle roots can extend down to more than 250 km and remain isolated from the convecting asthenosphere for more than 3 billion years (Boyd and Gurney, 1986; Boyd and Mertzman, 1987; Carlson et al., 2005; Jordan, 1978; James et al., 2001; Lee et al., 2011; O'Reilly and Griffin, 2010; Richardson et al., 2001; Walker et al., 1989). The cause for the longevity of the cratonic mantle is not fully understood, but it is generally thought to be related to its chemical buoyancy, low temperature and low water content (Carlson et al., 2005; Lee et al., 2011; O'Reilly and Griffin, 2010; Peslier et al., 2010; Sleep, 2003). In some cases, cratonic roots can be removed and this process has been linked to lithospheric thinning and tectonic/magmatic activities (Carlson et al., 2005; Lee et al., 2011; O'Reilly et al., 2001). In addition to chemical refertilization and temperature increase, water addition is also expected to promote the removal of cratonic roots. Indeed, water can significantly reduce the viscosity of the lithospheric mantle, thus reducing the viscosity contrast between the lithospheric mantle and the asthenosphere (Dixon et al., 2004; Hirth and Kohlstedt, 1996; Hyndman et al., 2005; Li et al., 2008; Mackwell et al., 1985; Karato, 2010). However, direct evidence for this longstanding theory has been scarce.

The eastern part of the North China Craton (NCC, Fig. 1) has very few relict Archean crustal rocks and is a clear example of a 'destroyed craton' (i.e. a craton in which the lithospheric root has been removed; Griffin et al., 1998; Menzies et al., 1993, 2007; Windley et al., 2010). The high-magnesium basalts of the Feixian area in the eastern part of the NCC erupted in the early Cretaceous (~120 Ma), which was the peak time of the NCC destruction (Gao et al., 2008). In addition, detailed petrological and geochemical studies have demonstrated that these basalts were derived from the lithospheric mantle without significant crustal contamination (Gao et al., 2008). Therefore, these basalts can provide information on the lithospheric mantle of the NCC at the peak time of its destruction. In this paper, the H_2O content of clinopyroxene phenocrysts (cpx) was measured in terms of OH defects. This was done using a Fourier transform infrared spectrometer (FTIR). Based on these data and the partition coefficient of H_2O between

* Corresponding author. Tel.: +86 551 3607008; fax: +86 551 3607656.
E-mail address: qkxia@ustc.edu.cn (Q.-K. Xia).

0012-821X/$ - see front matter © 2012 Elsevier B.V. All rights reserved.
http://dx.doi.org/10.1016/j.epsl.2012.11.024

Lithos 149 (2012) 136–145

Contents lists available at SciVerse ScienceDirect

Lithos

journal homepage: www.elsevier.com/locate/lithos

Recognizing juvenile and relict lithospheric mantle beneath the North China Craton: Combined analysis of H_2O, major and trace elements and Sr–Nd isotope compositions of clinopyroxenes

Yantao Hao, Qunke Xia *, Shaochen Liu, Min Feng, Yaping Zhang

CAS Key Laboratory of Crust–Mantle Materials and Environments, School of Earth and Space Sciences, University of Science and Technology of China, Hefei 230026, PR China

ARTICLE INFO

Article history:
Received 5 August 2011
Accepted 2 March 2012
Available online 13 March 2012

Keywords:
H_2O contents
Sr–Nd isotope composition
Peridotite xenolith
North China Craton

ABSTRACT

Recognizing juvenile and relict lithospheric mantle is crucial in unraveling the mechanism of lithospheric thinning (delamination vs. thermal/mechanic erosion). The H_2O contents and Sr–Nd isotopic compositions of juvenile lithospheric mantle are expected to be similar to the MORB source (asthenospheric mantle), whereas those of the relict lithospheric mantle should be of typical cratonic character. Consequently, combined analysis of H_2O contents and Sr–Nd isotope compositions could be an effective way to distinguish the juvenile and relict lithospheric mantle. Among the peridotite minerals, clinopyroxene is the major host for rare earth elements as well as H_2O contents, making it the most suitable target sample for such analyses. We collected fresh peridotite xenoliths hosted by Cenozoic basalts from Beiyan, Shandong province and Yangyuan, Hebei province to carry out combined analyses of major elements, trace elements, Sr–Nd isotopes and H_2O contents for clinopyroxene. At both Beiyan and Yangyuan, pyroxene from peridotite xenoliths shows homogenous H_2O contents within individual grains, and equilibrium distribution of H_2O contents between clinopyroxene and orthopyroxene has been achieved. There is a positive correlation between H_2O contents and Al contents in clinopyroxene and orthopyroxene, these features imply that the pyroxenes largely preserve the H_2O contents of their mantle source. The variations of H_2O contents in clinopyroxene are controlled by partial melting rather than the later episode of mantle metasomatism, because there is a correlation between H_2O contents of clinopyroxene and degree of partial melting index (Yb content of clinopyroxene and Mg# of olivine).

Based on the correlation between H_2O contents and Sr isotope ratios of clinopyroxene, the estimated H_2O contents and $^{87}Sr/^{86}Sr$ ratios of mantle source of peridotites in Beiyan (450 to less than 600 ppm, and ~0.7028 respectively) are similar to the MORB source, thereby implying that the lithospheric mantle beneath Beiyan is juvenile. In contrast, the variation of H_2O contents and Sr–Nd isotope compositions of clinopyroxene from the Yangyuan peridotites is best explained as relict mantle (H_2O contents less than 300 ppm and EM1-type Sr–Nd isotope ratios) coexisting with juvenile lithospheric mantle (H_2O contents more than 600 ppm and $^{87}Sr/^{86}Sr$ about 0.7030). These conclusions are in agreement with previous studies which have demonstrated that the lithospheric mantle beneath Beiyan is made up of juvenile material accreted from the asthenosphere after the North China Craton had undergone thinning.

1. Introduction

The North China Craton (NCC) is one of the major cratons in eastern Eurasia with crustal remnants older than 3.8 Ga (Liu et al., 1992). The eastern NCC experienced widespread lithospheric extension and dramatic changes of mantle characteristics. A thick (~200 km), cold (~40 mW/m^2) and highly refractory lithospheric mantle was in place until the mid-Ordovician, but was replaced by a hot (60–80 mW/m^2), thin (80–60 km) and fertile lithospheric mantle during the late Mesozoic period (Menzies et al., 2007, and references therein). The timing, spatial and temporal variation as well as mechanism for lithospheric thinning are hotly debated. Delineating the juvenile (e.g., newly accreted materials from upwelling asthenosphere after the NCC thinning) versus relict lithospheric mantle is crucial to unravel the mechanism of lithospheric thinning (delamination vs. thermal/mechanic erosion). The H_2O contents and Sr–Nd isotopic compositions of the juvenile lithospheric mantle are expected to be similar to Mid-Ocean Ridge Basalt (MORB) source, whereas the relict lithospheric mantle should be more like typical cratonic mantle. Therefore, combined analyses of H_2O contents and Sr–Nd isotope compositions of mantle-derived xenoliths could be an effective way to distinguish between the juvenile and relict lithospheric mantle.

* Corresponding author at: No. 96, Jinzhai Road, 230026, Hefei, Anhui, PR China. Tel.: +86 551 3607008; fax: +86 551 3607386.
E-mail address: qkxia@ustc.edu.cn (Q. Xia).

0024-4937/$ – see front matter © 2012 Elsevier B.V. All rights reserved.
doi:10.1016/j.lithos.2012.03.013

Phys Chem Minerals (2012) 39:413–418
DOI 10.1007/s00269-012-0496-x

ORIGINAL PAPER

OH in natural orthopyroxene: an in situ FTIR investigation at varying temperatures

Y. Yang · Q. K. Xia · M. Feng · S. C. Liu

Received: 19 October 2011 / Accepted: 24 February 2012 / Published online: 11 March 2012

Abstract In situ unpolarized and polarized Fourier transform infrared spectra of a natural orthopyroxene at varying temperatures were obtained using a heating stage attached on an Infrared microscope. The three main bands (3,595, 3,520 and 3,410 cm^{-1}) at room temperature are ascribed to OH fundamental stretching bands. With increasing temperature from room temperature to 500 °C, the 3,595 cm^{-1} band shifts 20 cm^{-1} to lower frequency. The total integral absorbance decreases with increasing temperature. These changes are reversible. Excluding the influences of dehydration, proton migration, thermal expansion, and changes in OH dipole direction, the change of integral absorbance with temperature reflects the temperature dependence of absorption coefficient due to the anharmonicity of OH vibration. Based on the integral absorption coefficient at room temperature (14.84 ppm^{-1} cm^{-2}) from Bell et al. (Am Mineral 80:463–474, 1995), the integral absorption coefficients at other temperatures are calculated. The variation of integral absorption coefficient between room temperature and 500 °C obtained in this study is about 18.5 % and may be greater at higher temperature according to the proposed linear relationship.

Keywords OH · IR · Varying temperatures · Orthopyroxene

Y. Yang · Q. K. Xia (✉) · M. Feng · S. C. Liu
CAS Key Laboratory of Crust-Mantle Materials and Environments, School of Earth and Space Sciences, University of Science and Technology of China, Hefei 230026, China
e-mail: qkxia@ustc.edu.cn

Introduction

Numerous investigations have demonstrated that water can be stored in nominally anhydrous minerals (NAMs) as hydrogen structurally bound to specific oxygen sites. NAMs cover a wide range of common rock-forming minerals from the Earth's crust (e.g., quartz and feldspars) and upper mantle (e.g., olivine, pyroxenes, and garnet) to the mantle transition zone (e.g., wadsleyite, ringwoodite, and majoritic garnet). H incorporation into NAMs has a significant influence on physical properties such as viscosity and electric conductivity as well as on melting, mantle convection, and the stabilization of cratonic roots (e.g., Karato 1990; Thompson 1992; Hirose and Kawamoto 1995; Hirth and Kohlstedt 1996; Asimow and Langmuir 2003; Yang et al. 2008; Peslier et al. 2010; Green et al. 2010).

Orthopyroxene is the second most abundant mineral in the upper mantle above the transition zone and may contain a trace water component in the form of OH defects (Bell and Rossman 1992). The water content in orthopyroxene is lower than in clinopyroxene, but far higher than in the coexisting olivine (Skogby 2006; Tenner et al. 2009; Green et al. 2010; Xia et al. 2010). So, based on its great abundance, orthopyroxene may be a major repository for water in the upper mantle. Fourier transform infrared (FTIR) spectroscopy is a widely used method for investigating H in NAMs. The hydrous components in minerals are mobile, so their speciation, physicochemical properties, and sites in the crystal structures may vary with temperature. However, the previous FTIR studies on OH in orthopyroxene were mainly undertaken at room temperature, providing a limited insight into the properties of minerals. Moreover, IR absorption coefficients of OH in some NAMs decrease with increasing temperature (Suzuki and Nakashima 1999; Zhang et al. 2007; Yang et al. 2010). The aim of this study

Resume:

Titre:

Teneur en eau et géochimie des basaltes cénozoïques SE chinois: implication pour l'enrichissement de la source des basaltes continentaux

Mots-clefs:

Teneur en eau;

Basaltes continentaux;

Roûte océanique recyclés;

édiment océanique recyclés;

Sud Est Chinois

Resume:

Les teneurs en éléments majeurs et trace, les isotopes Sr-Nd-Pb, les teneurs en H_2O et la isotope de l'O des phénocristaux de cpx des basaltes cénozoïques de 11 sites du Sud Est Chinois situés dans des contextes géodynamiques variables ont été mesurés pour identifier les différents composants faisant partie de leur source. Les basaltes Cénozoïques de Zhejiang se sont mi en place durant deux périodes, 20-27Ma et après 11Ma. Leurs teneurs en H_2O varient de 1.3-2.6%. Les basaltes Cénozoïques du Fujian ont fait éruption il y a moins de 10 Ma. Le teneurs en H_2O initial des basaltes de Shiheng s'étend de 1.3-2.4%; les diabases de Bailin ont des teneurs s en eau estimés de 1.9-2.1%, et ceux de Mingxi des teneurs es initiaux de 0.3-0.5%. Les teneurs en H_2O des basaltes de sont de 1.3-2.6%. Les basaltes de Xilong (Zhejiang), Mingxi (Fujian) et Leihuling (Hainan) ont des sources mantelliques contaminées par de la croûte océanique recyclée, ceux de Gaoping et Shuangcai (Zhejiang), Shiheng, Bailin et Niutuoshan (Fujian) et Maanling, Dayang et Fujitian (Hainan) voient leur sources mantelliques contaminées par à la fois des sédiments et la croûte océanique recyclés. Les matériaux recyclés diffèrent suivant l'âge et la localisation. En résumé, les basaltes cénozoïques SE chinois ont des signatures élémentaires et isotopiques marquées par la présence de matériaux océaniques recyclés dans leurs sources mantelliques. Les matériauxl recyclés varient entre les différentes localités, tant dans leurs proportions que leur degré d'évolution. Nos résultats montrent que la plaque subductée Ouest Pacifique affecte probablement la composition du manteau sous continentale du Sud Est Chinois.

Resume

Title:

Water content and geochemistry of the Cenozoic basalts in SE China: implications for enrichment in the mantle source of intra-plate basalts

Key Word:

Water content;

Continental basalts;

Recycled oceanic crust;

Recycled oceanic sediments;

Southeast China

Abstract:

The major and trace element contents, Sr-Nd-Pb isotope, H_2O contents and the cpx phenocryst O isotope of Cenozoic basalts from 11 places with distinct geological backgrounds in SE China have been measured to decipher the relationship between the possible recycled components and mantle geochemical heterogeneities. Zhejiang basalts erupted in two stages, 20-27Ma and after 11Ma. Their H_2O contents range from 1.3-2.6%. The estimated H_2O contents of initial basaltic melts for the Shiheng basalts range from 1.3-2.4%; the Bailin diabases have “fake” basaltic melt water contents from 1.9-2.1%; and the Mingxi basalts have initial H_2O contents of 0.3-0.5%, in Fujian. H_2O content the basalts from Leihuling (LH), Dayang (DY) and Fujitian (FJT) areas in Hainan are 2.7 wt. %, 1.3 wt. %, and 2.6 wt. %. The Xilong basalts from Zhejiang, Mingxi basalts from Fujian and Leihuling basalts from Hainan involved recycled oceanic crust components in the mantle source, while the Gaoping and Shuangcai basalts from Zhejiang, Shiheng, Bailin, and Niutoushan basalts from Fujian as well as the Maanling, Dayang and Fujitian basalts from Hainan involved recycled oceanic sediments and crust components in their mantle source. Overall, the SE China Cenozoic basalts have involved the recycled oceanic materials in their mantle source. The recycled oceanic materials have different existential state and locations, when the geological history of SE China are considered. The subducted Pacific slab most likely effect the composition of mantle in SE China.